AFASES 2014

ISSN, ISSN-L: 2247-3173

Volume I

"HENRI COANDA"
AIR FORCE ACADEMY
ROMANIA

"GENERAL M.R. STEFANIK"
ARMED FORCES ACADEMY
SLOVAK REPUBLIC

INTERNATIONAL CONFERENCE of SCIENTIFIC PAPER
AFASES 2014
Brasov, 22-24 May 2014

INTERNATIONAL SCIENTIFIC COMMITTEE

Presidents ship:

Commander **Vasile BUCINSCHI**, PhD

Brigadier General **Boris ĎURKECH**, PhD

Members:

Professor **Răzvan - Lucian ANDRONIC,** PhD

Colonel **Mihail ANTON**, PhD

Professor **Hamid R. ARABNIA**, PhD

Brigadier General **Ghiţă BÂRSAN**, PhD

Commander **Mircea BOŞCOIANU**, PhD

Professor **Gavrila CALEFARIU**, PhD

Professor **Ivan Menes CAMEJO**, Doc

Associate Professor **Sergiu CATARANCIUC**, PhD

Professor **Constantin -Edmond CRACSNER,** PhD

Professor **Aurel CRIŞAN**, PhD

Researcher **Maria DINESCU**, PhD

Professor **Philippe DONDON**, PhD

Professor **Constantin DUGULEANĂ**, PhD

Professor **Cătălin Marius GHERASIM,** PhD

Lecturer **Mihaela GURANDA**,PhD

Professor **Vladimir HORAK, CSc**

"HENRI COANDA"
AIR FORCE ACADEMY
ROMANIA

"GENERAL M.R. STEFANIK"
ARMED FORCES ACADEMY
SLOVAK REPUBLIC

INTERNATIONAL CONFERENCE of SCIENTIFIC PAPER
AFASES 2014
Brasov, 22-24 May 2014

ORGANIZING COMMITTEE

President:
   LTC **Laurian GHERMAN**,PhD

Members:
   Prof. **Ion DINESCU**, PhD
   Capt. Cmd. **Ionica CÎRCIU**, PhD
   Maj. **Cornel ARAMĂ**, PhD
   Lt.col. **Danut BĂLOS**
   Lt.col. **Cristian ENE**
   WO. **Vasile PRISACARIU**
   Assist. Prof. **Liliana MIRON**, PhD
   Assist. Prof. **Constantin STRÎMBU**, PhD
   Assist. Prof. **Cristian CONSTANTINESCU**, PhD
   Maj. **Cătălin CIOACĂ,** PhD
   Math. **Carmen URSOIU**
   Assist. Prof. Math. **Gheorghe RADU**, PhD
   Assist. Prof **Mihaela GURANDA**, PhD
   Assist. Prof **Mihaela SMEADA**, PhD
   Assoc. Prof. **Diana ILIŞOI**, PhD
   Assist. **Bogdan Gheorghe MUNTEANU**
   Assist. **Daniela NAGY**

Logistics:
   Maj **Ionel FEROIU**
   Lt.col. **Bogdan CHIOSEAUA**
   Lt **Cosmin TĂTULESCU**
   WO **Marian MIHALACHE**

Secretariat:
   Maj **Criste RĂU**
   Eng.Capt. **Mariana GHINDĂOANU**

INTERNATIONAL CONFERENCE of SCIENTIFIC PAPER
AFASES 2014
Brasov, 22-24 May 2014

CONTENTS

Volum I

ELECTRICAL AND ELECTRONICAL ENGINEERING

MECHANICAL ENGINEERING. MATERIALS AND TECHNOLOGY

"HENRI COANDA"
AIR FORCE ACADEMY
ROMANIA

"GENERAL M.R. STEFANIK"
ARMED FORCES ACADEMY
SLOVAK REPUBLIC

INTERNATIONAL CONFERENCE of SCIENTIFIC PAPER
AFASES 2014
Brasov, 22-24 May 2014

RENEWABLE ENERGY AND ENVIRONMENT

APPLIED MATHEMATICS, COMPUTER SCIENCE, IT&C

"HENRI COANDA"
AIR FORCE ACADEMY
ROMANIA

"GENERAL M.R. STEFANIK"
ARMED FORCES ACADEMY
SLOVAK REPUBLIC

INTERNATIONAL CONFERENCE of SCIENTIFIC PAPER
AFASES 2014
Brasov, 22-24 May 2014

Volum II

MANAGEMENT

SOCIO AND HUMANITIES

"HENRI COANDA"
AIR FORCE ACADEMY
ROMANIA

"GENERAL M.R. STEFANIK"
ARMED FORCES ACADEMY
SLOVAK REPUBLIC

INTERNATIONAL CONFERENCE of SCIENTIFIC PAPER
AFASES 2014
Brasov, 22-24 May 2014

"HENRI COANDA"
AIR FORCE ACADEMY
ROMANIA

"GENERAL M.R. STEFANIK"
ARMED FORCES ACADEMY
SLOVAK REPUBLIC

PHASES ANALYSIS AND STRUCTURAL CHARACTERIZATION OF CuAlMnFe ALLOY

Dragoş Cristian ACHIŢEI*, Petrică VIZUREANU*, Mirabela Georgiana MINCIUNĂ*, Bogdan ISTRATE**, Andrei Victor SANDU*

*Faculty of Materials Science and Engineering, Gheorghe Asachi Technical University, Iaşi, Romania, ** Faculty of Mechanical Engineering, Gheorghe Asachi Technical University, Iaşi, Romania,

Abstract: The paper presents a study on alloy CuAlMnFe, analyzed in terms of phases and structural aspects and physical and mechanical properties, after some heat treatments like annealing, quenching and tempering.

Keywords: aluminum bronzes, micro-hardness, constituents

1. INTRODUCTION

The properties of cast alloys are dependent on the chemical composition and structure.

The introduction of one or more alloying elements in the metal alloy can be obtained for various compositions, structures and properties that will be suitable for technical purposes.

Forming the non-ferrous alloys is influenced by development conditions and the configuration of the parts and on the casting and cooling thereof.

The most important copper alloys are brasses, bronzes and copper alloys - nickel - zinc.

Bronzes are characterized by good mechanical properties, superior castability and good corrosion resistance.

Alloying elements contained in a bronze may have influence on the properties:

- Aluminum - improves castability and plasticity.
- Silicon - increases the fluidity.
- Manganese - improves elasticity and electrical resistance.
- Lead - improves plasticity and anti-friction properties.
- Nickel - increases the mechanical strength and electrical resistivity.
- Beryllium and titanium - add further strength.

Table 1

Applications of aluminum bronzes

Valve case for
railway industry
[3]

Bearing pivoting
for medical
applications[3]

Clutch
components for
ship winch system
[4]

Rough-cast wheel
gearbox [4]

Fittings [7]

Spare parts [5]

Valve case for
railway machines
[3]
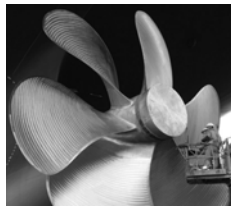
Six propeller
blades used to
propel the ship. It
weighs 107 tons
and is 9.1 meters
in diameter [6].

Aluminum bronze are alloys of copper -
aluminum containing up to 15 % Al , which
may also contain other added materials (iron ,
silicon , lead , manganese , nickel) in order to
improve certain physico - chemical properties
[1,8] .

According to the Cu- Al equilibrium
diagram (fig. 1), the structure of aluminum
bronzes can be found:

- Phase α - solid solution of aluminum in
copper substitution, with face-centered cubic
lattice. The solid solubility limit is 7.4 % Al to
1037°C and is increased to 9.4 % at 570°C,
remains approximately constant up to the
normal temperature;

- β phase - intermediate solid solution based
on electronic compound Cu_3Al, report

$n_e/n_a = 3/2$;

- phase γ - is formed on the basis of a novel
compound of formula $Cu_{32}Al_{19}$ electronic and
electronic concentration and the changes in the
ordering phenomena due to solid state at
780...870°C [1,9] .

β phase stable at high temperature
undergoes eutectoid decomposition
temperature of 570 ° C and 11.8 % Al :

$$\beta \overset{570°C}{\Longleftrightarrow} \alpha + \gamma'.$$
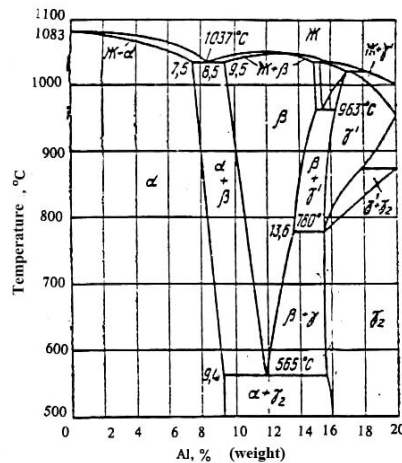
Fig.1. Cu-Al equilibrium diagram [2].

The structural constituents of the
aluminum bronzes [1] according to the
composition and the cooling rate are shown in
table 2.

Table 2

Composition % weight		Equilibrium constituents after slow cooling – annealing	Equilibrium constituents after rapid cooling – quenching
Cu	Al		
100 … 92.5	0 … 7.5	α	α
92.5 … 91	7.5 … 9	α	α + β
91 … 88.2	9 … 11.8	α + γ'	β → α + β
88.2 … 84	11 … 16	α + γ'	β → β + γ'

2. EXPERIMENTAL TESTS

a. **Chemical compositions determination**

Chemical composition determinate by
spectral analysis, made on Foundry Masters
optical spectrometer, is presented in table 3.

Table 3

Cu	Zn	Sn	Mn	Fe
88.8	0.0985	0.0053	1.97	0.741

"HENRI COANDA"
AIR FORCE ACADEMY
ROMANIA

"GENERAL M.R. STEFANIK"
ARMED FORCES ACADEMY
SLOVAK REPUBLIC

INTERNATIONAL CONFERENCE of SCIENTIFIC PAPER
AFASES 2014
Brasov, 22-24 May 2014

Si	Cr	Al	As	Co
0.0637	0.0265	8.19	0.0097	0.015

Based on analysis bulletin, was establish that the studied alloy was from aluminum bronzes classes, type $CuAl_8Mn_2Fe_1$.

b. Optimum heat treatment applied to studied aluminum bronze

Heat treatments parameters recommended to studied bronze are the following:

- Annealing:
- heating 850…950°C
- cooling in air or once furnace.
- Quenching:
- heating 850…900°C
- maintaining 6…8 min/mm thickness sample
- rapid cooling in water or oil.
- Tempering:
- heating 380…420°C
- maintaining 2…3 min/mm thickness sample
- cooling in air

c. Investigation using X-ray diffraction

X-ray diffraction is a non -destructive analytical technique versatile, and with the help they can get information on the identification and quantification of various crystalline compounds known as "phase" compounds that are present in the material.

We analyzed and characterized, and structural roentgeno method based on X-ray diffraction crystallographic planes of the structure, the alloy CuAlMnFe.

Determination of structural constituents is by diffraction is the dependence of the diffracted radiation intensity and double diffraction angle.

Determination of the compositional phases was carried out by qualitative analysis by X - ray diffraction, X -ray diffraction carried out to Panalytical X'Pert PRO MPD.

Scope of analysis was between $2\theta = 20-120°$, step size being 0.0010, and the time step is 3 seconds / step.

It was used a proportional detector with a single channel, the analysis is performed as Gonio.

The analysis of copper alloys by X-ray diffractometry, the samples will be obtained from the system alloy, Cu-Al-Mn-Fe section having Ø15 mm and sample length 20 mm.

Figure 2 shows the diffraction pattern obtained for alloy CuAlMnFe - after annealing.
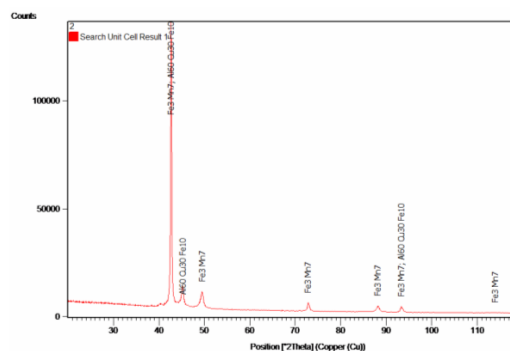
Fig.2. X-ray diffractogram (indexed)
obtained for alloy CuAlMnFe - annealed

X-ray diffraction is the process by which the radiation, to wave lengths without change, is converted by interfering with the crystal lattice of a large number of "reflection" of the observable characteristic spatial directions.

Indexing diffractometry is the association of maximum - diffraction peak and a plan. Indexing diffractogram reveals the following: The test phases are present as majority: Fe_3Mn_7 with cubic crystal lattice, with the main peak at $2\theta = 42.6430$ and $Al_{60}Cu_{30}Fe_{10}$ angle with cubic crystal lattice, with the main peak at $2\theta = 42.8920$ angle.

Figure 3 shows the diffraction pattern obtained for new alloy CuAlMnFe - after quenching heat treatment.

Fig.3. X-ray diffractogram (indexed) obtained on the sample CuAlMnFe - quenched condition.

Indexing X-ray diffraction pattern reveals the following:

The test phases are present as majority: Fe_3Mn_7 with cubic crystal lattice, with the main peak at 2θ angle $= 42.54540$ and Cu_3Fe_4 with cubic crystal lattice, with the main peak at $2\theta = 42.1160$ angle.

As a minor phase present $AlCu_3$ compound crystallized in the orthorhombic system, with the main maximum at the angle $2\theta = 44.7910$.

Figure 4 shows the diffraction pattern obtained for sample CuAlMnFe - after heat treatment tempered.

Fig.4. X-ray diffractogram (indexed) obtained for sample CuAlMnFe - tempered condition.

X-ray structural analysis is the method by which the direction and intensity of these reflections is measured and deducted order atoms.

The sample CuAlMnFe tempered condition is present as majority phases: Fe_3Mn_7 with cubic crystal lattice, with the main peak at $2\theta = 42.6430$ and Cu_3Fe_4 angle with cubic crystal lattice, with the main maximum at the angle $2\theta = 42.59770$.

d. **Dilatometric analysis**

The purpose of the experiments is the record length (Δl) that a sample undergoes when subjected to a certain temperature.

Dilatometer L75 is suitable for both the expansion and the contraction of the sample. Dilatometer analysis in this paper was performed using differential dilatometer L75H/1400 LINSEIS type (fig. 5).

Using large samples promotes good accuracy for determining elongation, instead using small samples ensures a good temperature control precision and repeatability of results.

To obtain accurate and repeatable experimental data is recommended that the dilatometer to work with relatively low speeds of approx. 5 to 10 °C/min.

The heating rate was required for the experiment at 10 °C/min.

Fig.5. Linseis L75H / 1400 dilatometer.

After applying heat treatment, the samples with specific size dilatometer tests were carried out dialatograme heating from ambient temperature to 900 °C.

The dilatograms, obtained for CuAlMnFe alloy, have the shape of the specific of alloy shown in figures 6, 7, 8.

Fig.6. Dilatogram of alloy after annealing.

“HENRI COANDA”
AIR FORCE ACADEMY
ROMANIA

“GENERAL M.R. STEFANIK”
ARMED FORCES ACADEMY
SLOVAK REPUBLIC

INTERNATIONAL CONFERENCE of SCIENTIFIC PAPER
AFASES 2014
Brasov, 22-24 May 2014

Fig.7. Dilatogram of alloy after quenching.

Fig.8. Dilatogram of alloy after tempering.

It was found that the samples were small oscillations of length, elongation is approximately 200μm, in any state of heat treatments that the samples are.

e. **Micro-hardness measurements**

To highlight the efficiency of heat treatments, applied to CuAlMnFe bronze, was made HV100 micro-hardness measurements on heat treated samples.

The measured values of micro-hardness are presented in table 4.

Table 4

Heat treatment	Measured micro-hardness in points / sample	Average value / sample
Annealing	181.40	175.84
	174.68	
	171.46	

Quenching	328.73	301.32
	304.83	
	270.41	
Tempering	217.02	203.39
	184.91	
	208.24	

All the measurements of micro-hardness for studied aluminum bronze were in the specific values to the heat treatments applied. The quenching effect to hardness is visible, but the decrease of hardness after high tempering is specific to mechanical parts used in industry.

f. **Microscopic analysis by optic microscopy**

100X   200X
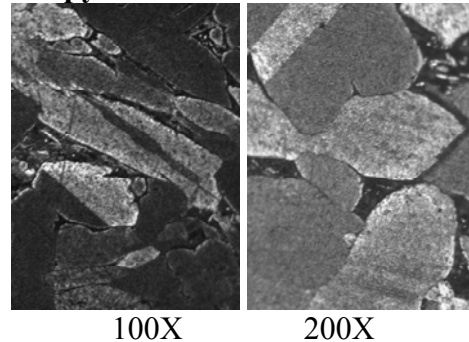
Fig.9. Alloy microstructure, annealing state, ammonium persulfate attack.

100X   200X
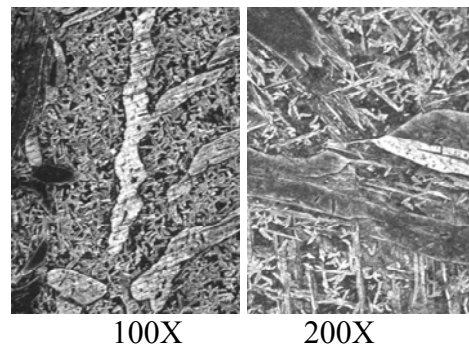
Fig.10. Alloy microstructure, quenching state, ammonium persulfate attack.

100X   200X
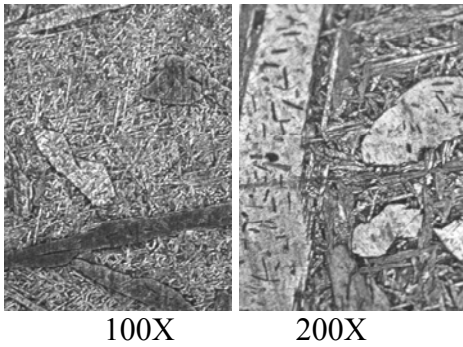
Fig.11. Alloy microstructure, tempering state, ammonium persulfate attack.

In annealing state, the studied bronze has a homogeneous structure composed by α solid solution, recrystallized in the form of polyhedral grains with macles and γ' phase, in smaller quantity and uniformly distributed.

After quenching and tempering heat treatments application, in the structure in addition to α Solid solution phase, appear and β phase, which improve the mechanical characteristics of alloy.

3. CONCLUSIONS

Phases composition of the unit cell structure and characteristics of each phase identified were determined by X-ray diffraction, and the main objective was to determine the phase composition, microstructure and of alloy composition CuAlMnFe after applying heat treatments annealing, quenching and tempering.

Physical and structural characteristics analyzed in the paper falls within the specific parameters of the alloy and can guarantee a good lifetime for industrial applications based on aluminum bronze.

4. REFERENCES

1. Gâdea Suzana, s.a., *Îndrumar de laborator pentru metalurgie fizică – structura materialelor metalice,* Editura Didactică şi Pedagogică, Bucureşti (1967).
2.http://pwatlas.mt.umist.ac.uk/internetmicroscope/index.html
3.http://www.piad.com/aluminum-bronze-alloys.html
4.http://www.copper.org/publications/newsletters/innovations/2002/08/aluminum1.html
5.http://www.indiamart.com/mamahamaya-engineering/products.html
6.http://images.businessweek.com/ss/06/05/supership/source/6.htm
7.http://www.sabtek.co.uk/aluminium.asp
8. Cimpoesu, N., s.a., *Behavior simulation of a cooper shape memory alloy under an external solicitation*, Journal of optoelectronics and advanced materials, ISSN 1772-1776, (2010).
9. Achitei, D.C.; Vizureanu, P.; Stanciu, S.; et al., *Studies concerning thermal conductivity for some copper base memory shape alloys,* Conference: 14th International Conference on Modern Technologies, Quality and Innovation - ModTech 2010, NEW FACE OF TMCR, PROCEEDINGS Book Series: Proceedings of the International Conference ModTech, pages: 15-18, (2010).

"HENRI COANDA"
AIR FORCE ACADEMY
ROMANIA

"GENERAL M.R. STEFANIK"
ARMED FORCES ACADEMY
SLOVAK REPUBLIC

INTERNATIONAL CONFERENCE of SCIENTIFIC PAPER
AFASES 2014
Brasov, 22-24 May 2014

UNMANNED COMBAT AIR VEHICLE: MQ-9 REAPER

Vladimír BEŇO*, František ADAMČÍK Jr.**,

* Kosice, Slovakia, ** Faculty of Aeronautics, Technical University Kosice, Kosice, Slovakia,

Abstract: *Currently are increasingly we meet with the term flying unmanned aerial vehicles or also drones. Also gets are into the awareness of the notion unmanned combat air vehicles, also known as UCAV. Among the best known means of unmanned aerial vehicles in categories UCAV include MQ-9 Reaper, also known as the Predator B.*

Keywords: *Unmanned Combat Air Vehicle, UCAV, MQ-9 Reaper, Predator, Aircraft*

1. INTRODUCTION

Unmanned combat air vehicle MQ-9 Reaper belongs to a group of defense systems and its primary purpose is finding, tracking and destruction of land and sea targets. This flying unmanned combat aerial vehicle has a wingspan of 20 meters and a length of 11 meters. Maximum weight of take-off is 4,763 kg, can carry 1361 kg load externally, ie. in underslung and 386 kg load internally in the fuselage.
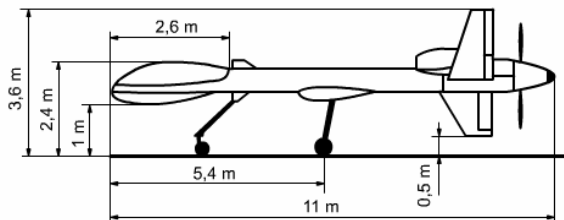
Fig.1 The Dimensions of MQ-9 Reaper

Drive provides turboprop unit from Honeywell TPE331-10, which allows this air vehicle achieve of maximum speed of 240 KTAS (445 km/h), has endurance in the air 36 hours and altitude ceiling maximum 50 000 ft (15 240 m).
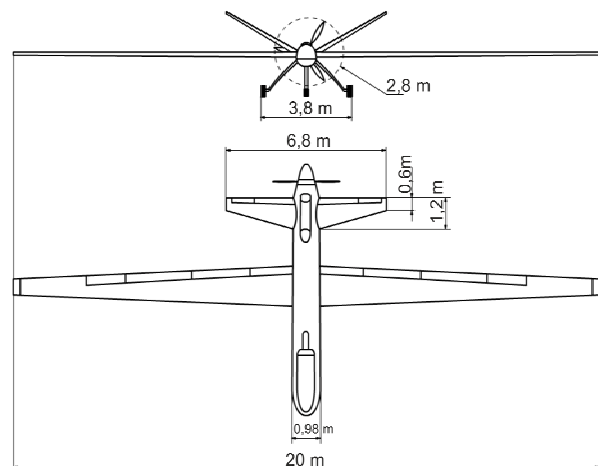
Fig.2 Drawing MQ-9 Reaper from above and from the front

The aircraft is equipped with a 6-bearing pylons for the possibility carrying of weapons and weapons systems, as well as underslung fuel tanks for increase its range. MQ-9 Reaper carries on its board 1769 kg of fuel (without underslung fuel tanks). On board there is also a multi-functional anti-ground radar LYNX ER, Multi-mode maritime radar, transmission system, electro-optical infrared system MTS-B EO/IR, laser designator of targets, electronic

support systems SIGINT/ ESM, electronic jammers, various probes and sensors. The aircraft has the developed system for the automatic take-off and automatic landing. It also contains multi-spectral tracking and targeting system (MTS-B) AN/AAS-52. Communication link is provided via SATCOM, via single channel, C-band (LOS), Ku-band SATCOM bandwidth is 1.6/3.2 Mbps. For the operation and management of the MQ-9 Reaper are required at least 2 people, 1 pilot and 1 operator.

2. CONSTRUCTION

Aircraft structure is composed primarily of advanced materials. It is a composite materials made mostly up of carbon fiber, these materials constitute up to 89% of the airframe structure. Such a high percentage of these materials contribute to the low weight of the aircraft and the prolongation of its range.

Fig.3 MQ-9 Reaper with underslung armament

Overall the construction, the shape and the materials are developed to contribute to the reduction of detectability by a radar, as well as human senses. MQ-9 Reaper is in the basic configuration 11 meters long, 3.6 meters tall and its wingspan is 20 meters, what allowing of this UCAV high ratio of buoyancy/weight.

3. DRIVE

Drive of unmanned combat air vehicle MQ-9 Reaper provides turboprop engine unit TPE331-10 from company Honeywell, which provides maximum power 944 hp (712 kW) and allows the air vehicle to reach maximum speed of 240 KTAS (445 km/h). Maximum

turbine speed is 41730 rpm, the maximum limit of speed propeller is 2000 rpm.
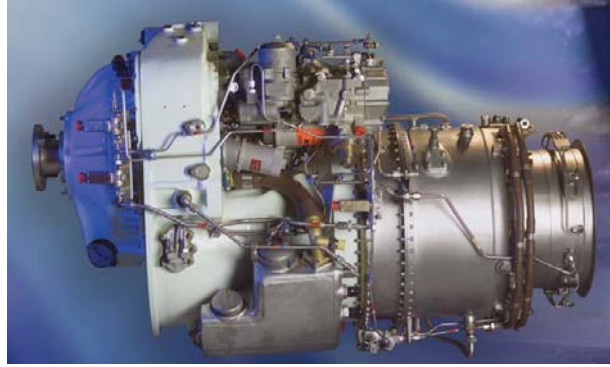
Fig.4 Turboprop engine TPE331-10 of Honeywell company

As fuel for this power unit is most commonly used fuel JP-8 or also JP-4. Weight of the entire power unit is 174,63 kg.
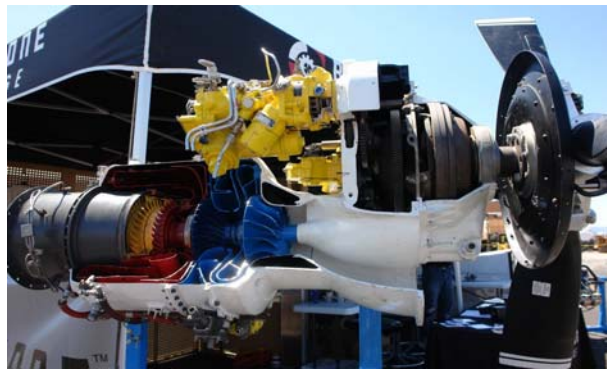
Fig.5 Showing power unit TPE331-10 with propeller in the cut

4. ARMAMENT

The primary armament which are uses for unmanned combat air vehicle MQ-9 Reaper is constituted of missiles AGM-114R known as Hellfire II which weighing 100 pounds and are designed to destroy armored objects on land and sea. Using modern semi-active laser head allows the launch also from great heights, which is for the unmanned aerial vehicles very important in view of their higher operational flight levels. Due to higher flight levels is reached even higher angle of impact of the missile to target which increases her effectiveness and thanks to the new navigation unit is more accurate. Another frequently used armament in MQ-9 Reaper are laser-guided 500-pounds aerial bomb termed as GBU-12 Paveway II. These bombs using modern advanced semi-active laser-guidance warhead

"HENRI COANDA"
AIR FORCE ACADEMY
ROMANIA

"GENERAL M.R. STEFANIK"
ARMED FORCES ACADEMY
SLOVAK REPUBLIC

INTERNATIONAL CONFERENCE of SCIENTIFIC PAPER
AFASES 2014
Brasov, 22-24 May 2014

to the effective destruction of solid-static targets, mobile targets and moving targets. With the new dual navigation units INS/GPS are accurate and destruction of targets is more efficient with reduced collateral damage.
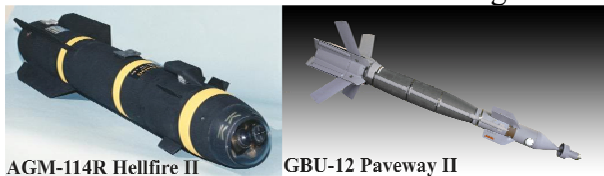
Fig.6 Demonstration of a possible armament MQ-9 Reaper

Between the further armament may be included bombs GBU-38 JDAM and GBU-49 laser-JDAM. Aerial bomb GBU-38 JDAM and its design is based on the Mk-82 bomb, but has JDAM guidance system. Thanks tail part bombs, which contains navigation system with GPS/INS is becomes accurate guided weapon, the which of accuracy is approximately 9.6 m. Weight GBU-38 JDAM is 500 pounds (227 kg), it may be drain her up to 28 km from the selected target, through day and night and in all weather conditions. Construction of GBU-49 laser-JDAM is based at bomb GBU-12 with JDAM guidance system that includes dual guidance system with laser and GPS-guidance (Bomb GBU-12 was also developed from the Mk-82).

Fig.7 Munition GBU-38 JDAM

The accuracy of the bomb is about six meters, the maximum launch is 15,000 m from the target, this aerial bomb can also be found under designation EGBU-12 Paveway II.

5. SYSTEMS

5.1 AN/AAS-52 System

Multi-spectral surveillance and targeting system (MTS-B) AN/AAS-52 includes electro-optical, laser and infrared sensors for detecting, tracking and labeling of objects and targets. Allows remote monitoring of targets in high resolution, determine their distance, coordinates and label for Hellfire missiles, as well as for all laser-guided munitions NATO. The whole system is composed of two main parts and namely from rotating tower unit, which is located in the inferior front part of the MQ-9 Reaper and electronic optical unit, which is located in fuselage UCAV. This system also allows for lighting targets, is designed to be modular and can be complemented with various optical sensors for different wavelengths, as well as additional electronic circuitry, allowing wide-spectral use of the system and as well its development.
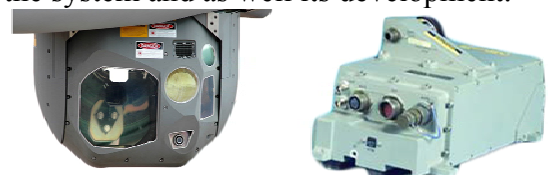
Fig.8 Turret unit WRA-1 with electronic unit WRA-2 of system AN/AAS-52 (MTS)

5.1 SIGINT/ESM System

System SIGINT / ESM allows conducting radio-electronic warfare and supports the distribution of actions at capture, identify and locate sources of electromagnetic energy. ESM system provides information you how to avoid menace, targeting and guiding of potential missiles. Information on electronics systems

can be used for creating signal intelligence - SIGINT.

5.2 Radar LYNX ER

Multifunction radar Lynx ER provides selectable resolution, operation in all weather conditions, day and night. This radar has to the fight certificate, the ability to change detection and as well can capture images SAR in high resolution. Thanks to the latest electronics and sensor delivers images of photographic quality of objectives through the clouds, dust, smoke, fog and total darkness. These its features are crucial for detecting and tracking targets at greater distances and poor visibility when it is not possible to use electro-optical and infrared sensors. Radar is composed of the two systems, namely from the radar antenna and the electronics module. Also allows to work in maritime search mode, also in mode the search ground moving targets and is able to work in so called mode of indication of movement on the ground (GMTI).

Electronics module of radar LYNX
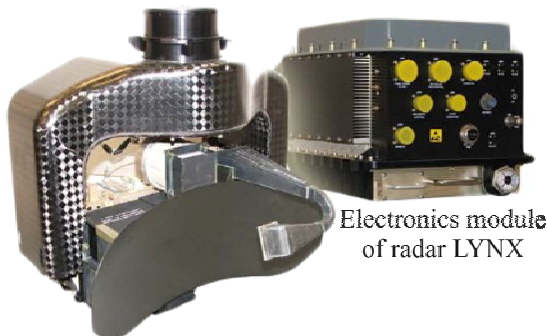
Radar antenna LYNX

Fig.9 Radar Lynx ER with antenna and with electronics module

Radar range is 80 km, and its resolution is in the range 0,1 to 0,3 m for mapping images - objects at surface depending on the mode selected. Can detect the even small vehicles moving with speed up to 70 km/h. At maximum airspeed MQ-9 Reaper 445 km/h can this radar to map the surface from a altitude of 13700 m land area of approximately 60 square kilometers per minute. In mode SPOT is capable radar to map in detail the area 300x170m from a distance of 40 km. On these images may view objects smaller than 10 cm. AN/DPY-1 Block 30 radar may detected of the car movement in real-time (system weight <85kg).

6. Control

Drone MQ-9 Reaper disposes a modern management system and autopilot. The aircraft can operate fully autonomously without pilot-operator during the entire mission, so as can take off, fly to the target of the mission, go back and land safely without human-pilot intervention to control. Such management requires careful programming of the entire mission of the aircraft to be able to fly fully autonomous.

Fig.10 Control panel of MQ-9 Reaper

Pilot-operator, however may intervene at any time into control and take control. In the event that the aircraft is in autonomous mode, command signals are received from ground control stations. Control of the aircraft is possible with using multiple systems, such as direct management (LOS) using small portable stations consisting of laptops and antennas that may use ground troops, also is possible to control UCAV using small mobile control stations (OSRVT/ ROVER). For full control of the aircraft and the manage of operations, it is necessary in most cases uses of the system SATCOM respectively Wideband Global SATCOM (WGS).

5. Communication

Unmanned combat air vehicle MQ-9 Reaper uses blos C2 data lines in the range of ultra high frequency UHF (300MHz) for the Ku band (15 GHz). Data lines Ku band of system SATCOM are often used blos C2 system (system of indirect command and control), this band is used for UAV means,

"HENRI COANDA"
AIR FORCE ACADEMY
ROMANIA

"GENERAL M.R. STEFANIK"
ARMED FORCES ACADEMY
SLOVAK REPUBLIC

INTERNATIONAL CONFERENCE of SCIENTIFIC PAPER
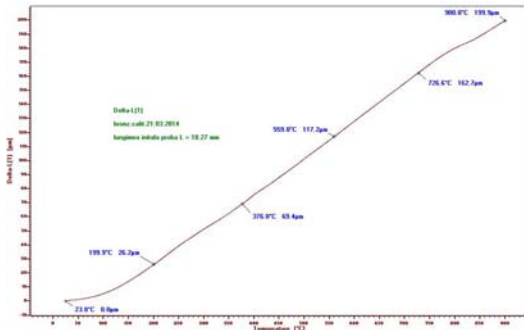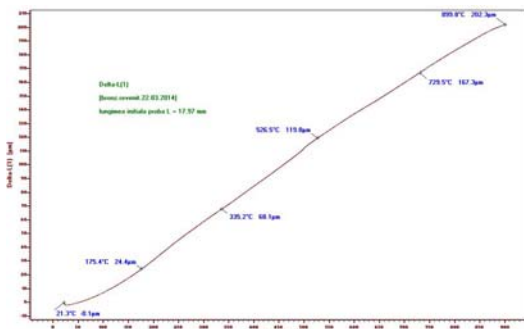AFASES 2014
Brasov, 22-24 May 2014

because has of the high resistance to interference. Uses the frequency range from 11,7 to 12,7 GHz for downlink and 14-14,5 GHz for uplink. For maintaining domination in the conflict is needs to be effectively command and control (C2). Blos C2 system is designed to build own network management and control, capable of self-interference suppression and encryption.

For this aircraft can also be used so called Common data line (CDL) and also tactical CDL (T-CDL). There are two technologies for CDL lines, the first data line uses the I-band SATCOM second data line uses Ku-band at frequencies from 14,5 to 15,38 GHz for to increase the available bandwidth.

6. CONCLUSIONS

Unmanned combat air vehicle MQ-9 Reaper represents in many aspects of the revolution in military aviation. This aircraft was among of the first unmanned flying means which were armed and used in real conflicts.

These experiences and information helped at develop unmanned combat air vehicles (UCAV) in the world and also UAV systems. Properties of this UCAV, as well his stamina in the air, modern tracking systems, the option to equip it exactly abetting ammunition as well as its price predetermine it for use in military conflicts in various regions of the world. It is thanks to the fact that this system is managed automatically or remotely and eliminates the risk of losing the crew in case of shooting down, as well as other potential costs and risks associated with the tracing actions intended to rescue the crew. Also provides support to ground and naval forces, is an excellent tool for guarding the border on land, and at sea, in day or night, in all weather conditions. With a wide range of uses, its accuracy destruction of

targets, makes it from unmanned combat air vehicle MQ-9 Reaper one of the most sophisticated aviation weapons systems of 21st century, which is able to attack anywhere in the world without finding was its presence. Development and modernization of systems this UCAV are will expand the already so wide range of uses, as well as the possibility of using other weapons systems. Aircraft MQ-9 Reaper has in currently been stable place in the several armed forces different countries of the world and its use, as well as reports of him even more rise.

REFERENCES

1. Bréda, R. – Čižmár, J. – Soták, M. – Beňo V.: *Letecké prístroje*, Vysokoškolská učebnica, Technická Univerzita Košice, Letecká Fakulta, ISBN: 987-80-553-0626-1. (2011)
2. Adamčík, F. – Adamčík, F. jr: *Spacecrafts electrical power systems*,. Acta Avionica 2010. ISSN 1335-9479. – Roč. 12, č. 20, S. 76-78. (2010)
3. Adamčík, F. : *Artificial Intelligence Technology on Board of Aircraft*, Advances in Military Technology, Vol. 1, No. 1, pp.137-142, (November 2006)
4. Valavanis, K. P. - Oh, P. - Piegl L.A.: *Unmanned Aircraft Systems*, International Symposium on Unmanned Aerial Vehicles, UAV '08. Springer, USA. ISBN 978-1-4020-9136-0. (2008)
5. General Atomics Aeronautical Systems, Inc.: *MQ-9 REAPER/PREDATOR B*, Persistent Multi-mission ISR and Strike Aircraft: Brochure. Poway, California, USA. Available: http://www.ga-asi.com/products/aircraft/pdf/Predator_B.pdf (2012)

6. Austin, R: *Unmanned Aircraft Systems, UAVS DESIGN, DEVELOPMENT AND DEPLOYMENT*, Wiley, USA**,** ISBN 978-0-470-05819-0. (2010)

7. Cullen M, T.: *The MQ-9 Reaper remotely piloted aircraft: Humans and machines in action*. Massachusetts Institute of Technology, USA. (2011)

8. Raytheon Company, Missile Systems: *Enhanced Paveway™II Dual Mode GPS/Laser Guided Bombs: Dual-Mode Precision-Guided Weapon*. Tucson, Arizona, USA. Available: www.raytheon.com (2009)

PLAYING WITH THE SAFETY DUE TO LACK OF RESOURCES

Oliver CIUICĂ*, Marcel PREDESCU**, Eduard MIHAI***

*Air Foce Academy, Braşov, Romania, ** Flight Safety Officer, Kabul International Airport, Afghanistan, *** Air Foce Academy, Bra ov, Romania

Abstract: This paper deals with one of the common issue of the flight safety organization: limited resources for Air Forces. Is it better to look forward for next days or for the next years? That is the question. The article shows how the safety has to be, which are the steps of flight safety in aviation history, and why the defense area from "Swiss cheese model" of J. Reason has to start from the top management of organization. The paper argues that a collective understanding of these issues is essential for those systems seeking to achieve an optimal safety culture to be able to maintain the requested level of capabilities, with minimum resources, in the actual worldwide context.

Keywords: safety culture, Air Force, resources, management, capabilities, training.

1. INTRODUCTION

Flight safety. Two words. In fact it is a condition for airmen. Flight safety will never be just a task in aviation. It should be a way of life from the beginning until the end of "story" for each and any individual linked to aviation (pilots, air traffic controllers, maintenance personnel, managers...).

It's main goal is to prevent the loss of aviation resources.

Flight safety is the desired condition gained by organizations through their individuals in order to be able to forecast air operations risks and produce a positive attitude for safe use of the resources using the right procedures, services, skills and knowledge to reduce to a minimum level the risks to air operations.

Basically, it is a puzzle built by each member of an organization and everyone having their own personality, behavior, and temperament.

2. SAFETY CULTURE

Risks in aviation vary depending on the stage of aviation development. The history of progress in aviation safety can be divided into three eras [1].

Technical era - from the early 1900s until the late 1960s

First attempts to build, fly, and control an object heavier than the air had its tribute. In the beginnings, identified safety deficiencies were initially related to technical factors and technological failures due to the lack of knowledge. The focus of safety was on the investigation and improvement of technical factors. During the two World Wars, aviation was seen as a very effective tool in the battle field and also an important element of the transportation industry that was constantly growing. Technological improvements starting in the early 1950s, were the first step in decreasing the frequency of accidents and the flight safety process started to be upgraded.

Human Factors era - from the early 1970s until the mid-1990s

The 1970s improved technology and materials used in aircraft construction. Despite the progress in aviation, new flight safety threats started to show up after the introduction of many new revolutionary design solutions and the new theories led for researching human factors and issues including the man/machine interface. An example of these types of risks can be found in the causes of events connected with new aircraft automation, or in the increased maneuverability of combat aircraft resulting in frequent incidences of high G-loads which affect the pilot. Despite the investment of resources in error mitigation, human performance continued to be cited as a recurring factor in accidents. The application of the Human Factors science, tends to focus on the individual without fully considering the operational and organizational context. But individuals operate in a complex environment, which includes multiple factors having the potential to affect behavior.

Organizational era - from the mid-1990s to the present day

The research until the early 1990s put first place the human factor as an individual even if this is strongly related with other individuals from the organization. The theories that followed began to highlight that those individuals operate in a fully complex environment which includes multiple factors having the potential to affect behavior, life style, or even knowledge acquisition. As a result, the notion of "organizational accident" was introduced and since then it has gained widespread acceptance and use in many service domains including the aviation safety industry. Many of them focus on so-called "the cumulative act effects". A new proactive approach to safety was introduced in aviation organizations based on routine collection. Analysis and diffusion of data using proactive and reactive methodologies to monitor known safety risks and to guide all levels of organizations to aim one safety environment.

SAFETY ORGANIZATION

An organization is known as a social entity, such as an institution or an association, which has a collective goal and is linked to an external environment. Members of an organization usually share a common vision, mission, values, and goals.

Members of an air organization have to be seen as a system that includes product and service providers. It is a complex system that requires an assessment of the human contribution to safety and an understanding of how human performance may be affected by its multiple and interrelated components.

Safety is a dynamic characteristic of the aviation system, whereby safety risks must be continuously mitigated in response to the social and technical request. Acceptability of safety performance is often influenced by domestic and international norms and culture. [2] "Being in a situation where the risks of an aircraft accident or air safety incident are reduced to a level as low as reasonably practicable" [3]

As long as safety risks are kept under an appropriate level of control, a system as open and dynamic as aviation can still be managed to maintain the appropriate balance between production and protection. [2]

So, as we see, all definitions of safety include risk management and a solid culture that is supposed to be able to maintain and focus on acceptable level of risk aimed by organization.

Culture is characterized by the beliefs, values, biases and their resultant behavior that are shared among the members of the organization.

Safety management is actually the understanding of these cultural components, and the interactions among them.
Linking the two definitions another concept is defined: "safety culture".

AIR FORCE SAFETY CULTURE – SOMEWHERE IN THE WORLD

There is no system fully safe. "If you are convinced that your organization has a good safety culture, you are almost certainly mistaken...a safety culture is something that is striven for but rarely attained. The virtue – and the reward – lies in the struggle rather than the outcome" James Reason said.

"HENRI COANDA"
AIR FORCE ACADEMY
ROMANIA

"GENERAL M.R. STEFANIK"
ARMED FORCES ACADEMY
SLOVAK REPUBLIC

INTERNATIONAL CONFERENCE of SCIENTIFIC PAPER
AFASES 2014
Brasov, 22-24 May 2014

Is this organization safe? Does it have a proper "safety culture"? Is there something to improve? If yes, which can be the starting point?

Somewhere, time ago it was a country, NATO member, that had a vast history of aviation; their predecessors were the pioneer of the flight, inventors of the jet plane. Due to the limited resources, in last 20 years, its air power decrease so much and in our days the total number of hour of flight and training for entire fleet per one year is about at the same level where only one single air base was years ago. Despite of that it is still able to maintain, with a minimum number of forces, the Aerial Police for the nation and for NATO. It is still able to maintain minimum of capabilities for air lift. But for how long?! Its pilots who are doing these kinds of missions have an average of 40-45 years old. And now some questions come around. Who will be their replacements? What level of training do they have now? How many hours of flight and training do they need to be fully capable for the kinds of missions their aircraft where designed for? Is it able to respond to NATO request?

The wings men for tomorrow will be the actual 25-30 years old pilots, but the actual culture, from this Air Force organization, said that being young is not an advantage but contrary, it's quite inadequate (it is redundant to remind that the spike of combat pilots in World War II had an average of 25-30 years old), and even it will not be like this, the few resources that it has are used only to accomplish operational needs and to keep the actual level for CMR (Combat Mission Ready) pilots. With a minimum (unacceptable) hours of flight and training it is impossible to maintain a safety environment, and that not only for flying personnel but also for maintenance department, air traffic controllers, ground operations and all elements linked to aeronautical activities due to lack of practice,

absence of lessons learned, premature aging of planes, materials and systems used in aviation activities.

James Reason found that most of the accidents happened because of the weaknesses in all levels of the system, including the decision makers' level: organizational influences, working conditions, unsafe acts (errors and violations) and the (improper) defense layers. The system as a whole produces failures when the weakness barriers align, permitting to the latent condition trajectory (hazard) passes through the holes in all of the defenses leading to a failure [4].
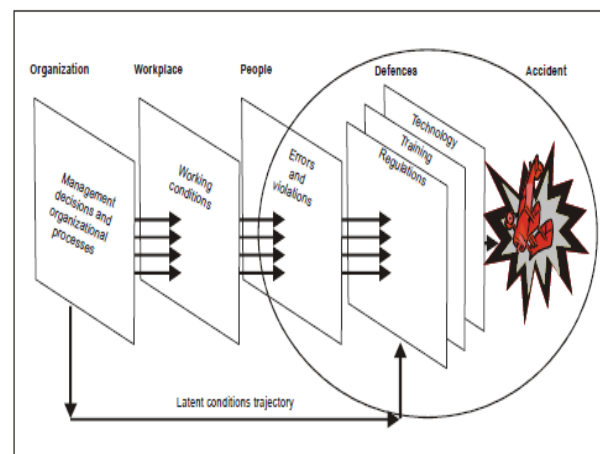
Fig. nr. 1 Swiss cheese model (ICAO)

Main target of this article is the organization by itself mainly focusing on the top level where the management decisions and organizational processes are making according to risk perception in order to reduce the possible accidents. A healthy safety culture relies on a high degree of trust and respect between personnel and management and must therefore be created and supported first at the senior management levels. As you see in the defense area the training and regulations are present but just for one single reason: to be upgraded and improved for a better product of entire members work. Often, regulations and

training are strongly related regarding the objectives, the requests of the actual national or international context and not finally, the necessary level of practice training. We all know that training costs money, but often simple calculations suggest that failing to be safe, or at least having incidents, costs more. Because of the strongly budgetary restrictions, the present training regulations have to be changed to be able to aim the main objectives. How can that be done?! Using the same people that have themselves the necessary skills, knowledge and training; grounding the others, making the youngest an inexperienced next victim. So, in that way, the Air Forces can maintain its priorities, its engagements and objectives. But for how long can it do that? There will be a hole in human resources management. When can be fill that gap and how? Nobody belongs forever to organization and when those who now are ready for mission will be retired, next generation (if there will still be one) will start to learn again without a proper training, by doing mistakes, teaching one each other. It makes no sense to remind that the actual laws will never give the opportunity to the ex-members to come back for teaching from their experience the remaining "future Air Force". Despite of that, more resources will be spent in a short period of time for getting the requested level of capabilities, not mentioning that during this time frame the air power level will be as lowest as it could be or it will not even exists. According to Reason, the elements of safety culture include: learning, informed, just, flexible and reporting culture. [5]

Fig. nr. 2 [6]

The most suggestive representation of Reason's definition is the fig. nr.2. According to this figure, the mentioned organization risk perception is the same at all its management levels, but attitudes to safety and safety related behavior is completely understood on individual scale and pretty accurate at the tactical level of management. Speaking about that and the Swiss cheese model, in the defense area where regulations, training and technology of organization is supposed to close the existing holes, these will become larger and larger and the hazard passes easier through all of these defensing walls and leads to a failure.

Does it need that? No! A real country air power should always be ready to respond to its duties. It has to be prepared at any times, in any weather conditions even if the attack threat is minimum; it exists. "If we lose the war in the air we lose the war and we lose it quickly" [7] . Don't wait to learn from your mistakes, it is better to learn from the others.

The elements of safety culture have to be the guidance within every organization.

a) learning culture – for implementing the major reforms an organization have to have the competence and the willingness to learn from mistakes, so named lessons learned. Flight debriefings, reports even safety issues between the members must be visible at any level.

b) informed culture – if the management understands the hazards and the risks of its members, (and this is the best way), they will be encouraged to identify the safety threat streams and to seek real solutions for overcome them.

c) just culture – people are able to define and clearly understand where must be the line between acceptable and unacceptable behavior. Also there has to be a better understanding that the punishment is not always a solution to improve the safety environment. All is related to circumstances (no blame culture).

d) flexible culture – the ability to reconfigure and take different forms but is characterized as shifting from the conventional hierarchical mode to a flatter professional structure.

e) reporting culture – sharing safety information. This element depend on how the

"HENRI COANDA"
AIR FORCE ACADEMY
ROMANIA

"GENERAL M.R. STEFANIK"
ARMED FORCES ACADEMY
SLOVAK REPUBLIC

INTERNATIONAL CONFERENCE of SCIENTIFIC PAPER
AFASES 2014
Brasov, 22-24 May 2014

organization is able to handle the report, blame and punishment. Having a strong reporting culture is one of the success keys.

It is well known why something have to be changed regarding that organization. Because it has to be efficient for maintaining its capabilities and to increase the safety status. That can only be done by understanding the short chart of safety culture. What should be changed?

One underlying reason why cultural change often fails to succeed is that the new situation is unknown to the participants. If this is added to existing beliefs, such as the belief that the current situation is as good as it gets, then there is little real need to change and failure is almost certain. If these failures are at the level of the workforce, then strong management commitment may save the day. If the problems lie with management, then there is little hope because they will enforce the old situation, which feels most comfortable, on the most proactive of workforces [8]

3. CONCLUSION

"To invent an airplane is nothing. To build one is something. To fly is everything"[9].

Starting from that statement and from the airplane history it's easy to remark and to understand the three steps of the progress in aviation safety. Beside the technical and human factor the most complex one is organization with all its concepts, behavior and cultural values. The first maneuver for improving the safety culture is the quality of communication (reports, briefings, requests, human needs...) inside the company between management and the rest of the members. For a better understanding of communication every part of the command chain has to be familiar with the conceptual environment regarding cultural background, people

behavior, needs and last but not least the top management level has to be filled with airmen. It is easy to say that the most safety stage of Air Force is not to fly. If somebody we'll think like this he will have the most safest air organization in the world, but this should not be the only goal. The leaders must try to maintain the balance between safety and air power. Take a look around the actual political status. Try to act like NATO not only be a part of NATO.

REFERENCES

[1,2] International Civil Aeronautical Organization, *Safety Management Manual Doc. 9859 AN/474 T*hird Edition – 2012 p. 12, 13.

[3] Airservices Australia *2001, AA-Safe-001,* p. 1.

[4] Reason, James T, *Human Error,* New York Cambridge University Press 1990, p. 203

[5] James Reason, *Safety paradoxes and safety culture,* Department of Psychology, University of Manchester, U.K. *Injury Control & Safety promotion – 2000,* p. 12.

[6] Civil Air Navigation Services Organization, *Safety culture; definition and enhancement process,* p. 3.

[7] Bernard Law Montgomery.

[8] Patrick Hudson, S*afety Culture – Theory and Practice,* Center for Safety Science Universiteit Leiden p. 11 Paper presented at the RTO HFM Workshop on "The Human Factor in System Reliability – Is Human Performance Predictable?", held in Siena, Italy,1-2 December 1999, and published in RTO MP-032.)

[9] Otto Lilienthal (1848-1896), early inventor of mono-plane and bi-plane gliders .

1. A-GA-135-001/AA-01, *Flight safety for the Canadian Forces,* (2013).

2.   European Organization for Safety of Air Navigation – *Revisiting the "Swiss cheese" model of accidents*, EEC Note 13/06, (2006).

3.   IFATCA, *A just culture in safety reporting*, paper presented at the 43rd annual Conference, Hong Kong, China MAR (2004)

4.   Panagopoulost, I., *Flight Safety in Combat Training: A revised pilot's error framework for EU Air Forces,* 5th Biennial Hellenic Observatory PhD Symposium, LSE, (2-3 Jun 2011).

5.   Reason, J., *"Human error"*. New York: Cambridge University Press, (1990).

6.   Reason J., *Managing the risk of organizational accidents*, Burlington: Ashgate Publishing Company, (2000).

7.   Roughton, E. J., Mercurio, J. J., *Developing an effective safety culture: a leadership approach*, Woburn: Butterworth-Heinemann, (2002).

“HENRI COANDA”
AIR FORCE ACADEMY
ROMANIA

“GENERAL M.R. STEFANIK”
ARMED FORCES ACADEMY
SLOVAK REPUBLIC

THEORETICAL ASPECTS RELATED TO FLIGHT SAFETY SYSTEMS IN EARLY WARNING AIR TRAFFIC CONFLICT

Ionică CÎRCIU *, Andrei LUCHIAN **

* “Henri Coanda” Air Force Academy, Brasov,Romania,
**University of Bucharest, Romania

Abstract: The quick evolution of global demographic component and the intense increase in the number of aircrafts of all types, resulted a significant congestion of air routes especially in areas near large airports. To meet the new demands of air traffic services we must modernize and implement new systems for flight safety. Air collision risk is still present and therefore is remarket the idea and concept of accepting a standardized and effective warning system.

1. INTRODUCTION

Since the 1950s, international civil aviation forums discussed the concept and development of a system to avoid collisions. ICAO (International Civil Aviation Organization) has developed standards for ACAS (Airborne Collision Avoidance Systems).

ACAS is designed to operate independent of both the navigation systems of the aircraft and ground equipment used for the provision of air traffic services [1,2]. Airborne Collision Avoidance System (ACAS) is the ultimate method accepted at global level regarding search and solve critical situations of air traffic between aircrafts.

The system mainly consists of the implementation of ACAS equipment onboard

TCAS (Traffic Alert and Collision Avoidance System) and pilot procedures regarding the use of these systems [2,3,4]. The alerts provided by ACAS depend on how sensitive is the aircraft transponder in the considered area:
• There can be no warning if the transponder is not working or is not compatible with ICAO standards;
• TA (Traffic Advisory), intended to help the pilot to visually identify aircraft in the area considered sensitive;
• RA (Resolution Advisory) are recommended pilot maneuvers, if the transponder reports the altitude (Figure 1).
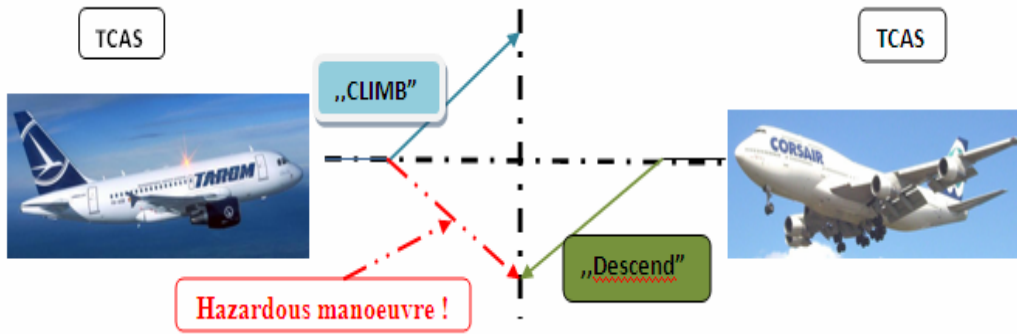
Fig.1 RA coordination example

2. ROLE

The functionality of TCAS is based on the transponder on board. The level of protection provided by TCAS equipment depends on the type of transponder which operates with the nearby aircrafts. So it is obvious that TCAS can provide protection against an aircraft not equipped with a transponder or is not operating [3,4,5, 6].

There are three types of standardized ACAS:
-ACAS I provides only TA;
-ACAS II provides TA and RA vertically;
-ACAS III provides TA and RA both vertically and horizontally.
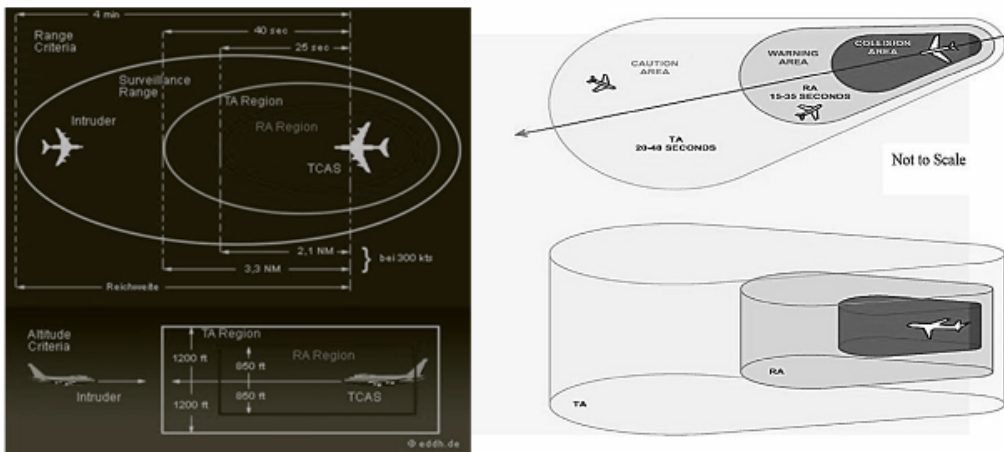
fig.2 The volume of ACAS protection between 5000 and 10000 feet

The protected volume (Fig. 2) is the represented by the airspace volume surrounding each aircraft equipped with TCAS. As shown in FIG. 2, τ is a threshold value expressed as the mean length up to the point of maximum proximity between the aircrafts or till it reaches the same altitude on both aircrafts [4, 5, 10].

In order to determine the distance and altitude, the aircraft is identified in a Cartesian coordinate system.

$$(a_n)_t = \left[(a_n)_{x,t}; (a_n)_{y,t}; (a_n)_{z,t} \right]^T \ (1),$$

3D position of the aircraft equations of n and

$$(v_n)_t = \left[(v_n)_{x,t}; (a v_n)_{y,t}; (v_n)_{z,t} \right]^T \ (2),$$

3D expression rates where the indices x, y axes are horizontal coordinate system and z is the altitude.

On the horizontal dimension the amount of protection is not defined only by the distance threshold, but also for a estimated buffer τ . However it depends on the size and speed of the aircraft head intruder. The first implementation of a mandatory collision avoidance system, TCAS II, was requested in the airspace of the United States starting with30 December 1993. All civil

"HENRI COANDA"
AIR FORCE ACADEMY
ROMANIA

"GENERAL M.R. STEFANIK"
ARMED FORCES ACADEMY
SLOVAK REPUBLIC

INTERNATIONAL CONFERENCE of SCIENTIFIC PAPER
AFASES 2014
Brasov, 22-24 May 2014

aircrafts with turbine engine having on board more than 30 passengers flying in American airspace must be equipped with TCAS II.

In 1995, EUROCONTROL *Comitee of Management* has approved a policy implementing a mandatory program of ACAS II equipment in Europe. It was ratified by the Council of the European Air Traffic Control Projects Harmonisation and Integration Programme (EATCHIP) [6, 7, 8]. The approved policy requires that:

- starting from January 1, 2000, all civil fixed-wing aircraft and turbine engine having a maximum take-off over 15,000 kg or a maximum approved configuration for passenger seats more than 30, will have to equip themselves with ACAS II and

- starting from January 1, 2005, all civil fixed-wing aircraft and turbine engine having a maximum take-off over 5700 kg, or a maximum approved configuration for passenger seats more than 19, will have to equip themselves with ACAS II , [7, 8, 9].

3. COMPOSITION

TCAS II system components
A TCAS II (Figure 3) [1, 4, 11, 12].
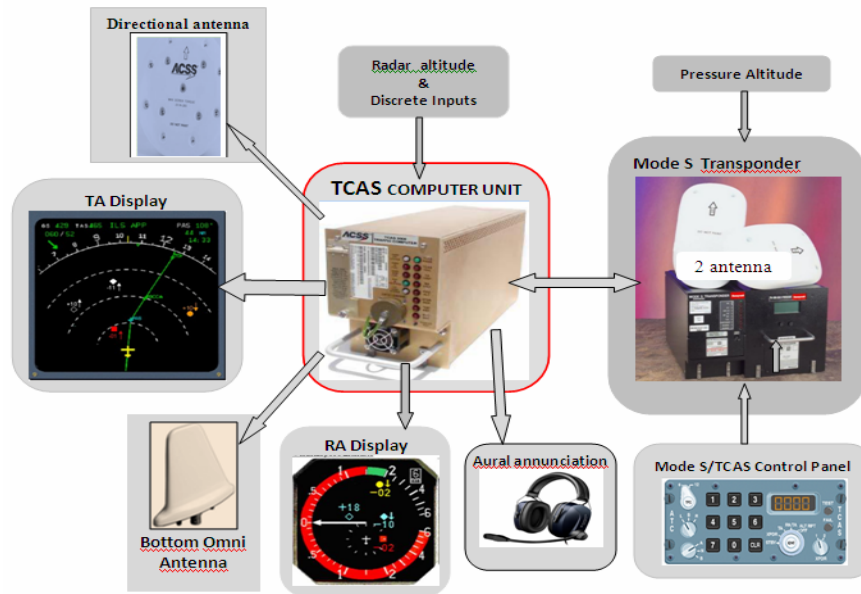
Fig.3 TCAS II system block diagram

Is composed of:

• a computer - which processes information regarding airspace surveillance, coordinates and tracking potential dangerous aircrafts, detect potential threats, calculate and determine avoidance maneuvers and making

recommendations on avoiding collisions. Dual microprocessors are used to introduce surveillance system algorithms and collision avoidance to decide if a transponder response should be considered a threat and then to calculate the appropriate climb speed to avoid

the collisions. In addition data is transmitted to the screens of the pilots to inform them that they should be able to avoid the collision.

• TCAS control panel - built into the transponder. It is a 3-position selector: - Stand-by - TCAS off - TA Only - are issued only TA - Automatic or TA / RA - TCAS operation.

• two antennas - one mounted on top of the airframe, and the second at the bottom. Above is a directional antenna to increase surveillance aircraft in the sensitive area. These antennas are separated by the transponder antenna. Queries are transmitted on 1030 MHz and the responses are received on 1090 MHz, the same frequency used by SSR (Secondary Surveillance Radar).

• Connections that make it possible to receive information from other navigation systems of the aircraft:

• Mode S transponder connection - to generate complementary and coordinated RA when both aircraft are equipped with TCAS;

• Connection with altimeter - to provide pressure altitude, and / or ADC (Air Data Computer) if it is equipped with it;

• A radar altimeter connection - on one hand to restrict RA when the aircraft is near the ground, and on the other hand to determine whether the aircraft followed by TCAS is on the ground;

• Speakers - for warning sound. The speakers which are in the cockpit alert the crew by acoustic means, and are recommended by TCAS. Acoustic messages are detailed in the table below according to the type of recommendation: Traffic Advisory (TA) and Resolution Advisory (RA)

• Displays - to display relevant data.

4. CONCLUSIONS

• The implement of TCAS system on aircrafts has led to significant air safety, event which will require that all aircrafts around the globe to be equipped with these systems

• The operating characteristics of the system provides a significant improvement in the safety of flight, however, ACAS is not perfect. ACAS can not eliminate all risks of a collision.

• It was established the fact that the use of the information on the TCAS display, by pilots, as a aerial surveillance equipment is misinterpreted due to the fact that the shown information is approximate regarding the aircraft position relative to others around him.

5. REFERENCES

1. James K. Kuchar and Ann C. Drumm, 2007 - The Traffic Alert and Collision Avoidance System, Volume 16, Number 2, 2007 Lincoln Laboratory Journal
2. PANS-ATM(ICAO Doc 4444) and in PANS-OPS (ICAO Doc 8168)
3. *** PANS-OPS (PROCEDURES FOR AIR NAVIGATION SERVICES - AIRCRAFT OPERATIONS - VOLUME I FLIGHT PROCEDURES - ICAO DOC. 8168 OPS/611), FIFTH EDITION – 2006 PLUS AMENDMENT 3
4. *** ICAO ANNEX 10, VOL. IV (AERONAUTICAL TELECOMMUNICATIONS - SURVEILLANCE AND COLLISION AVOIDANCE SYSTEMS), FOURTH EDITION, JULY 2007 – DEFINITIONS
5. *** PANS-ATM (PROCEDURES FOR AIR NAVIGATION SERVICES - ICAO DOC. 4444 FIFTEENTH EDITION 2007-ATM/501)
6. *** ICAO Doc. 7030/4 (Region Supplementary Procedures), Fifth Edition, 2008
7. *** AIRBORNE COLLISION AVOIDANCE SYSTEM (ACAS) MANUAL (DOC. 9863)
8. *** T S O C119B (TECHNICAL STANDARD ORDER) - TRAFFIC ALERT AND COLLISION AVOIDANCE SYSTEM AIRBORNE EQUIPMENT
9. *** EUROCONTROL BROCHURE ACAS TRAINING VERSION 2.0
10. Fedja Netjasov, Andrija Vidosavljevic, Vojin Tosic, Henk Blom, 2011 - Systematic Validation of a Mathematical Model of ACAS Operations for Safety Assessment Purposes, Ninth USA/Europe Air Traffic Management Research and Development Seminar (ATM2011);
11. http://www.eurocontrol.int/msa/public/standard_page/ACAS
12. http://www.eurocontrol.int/msa/gallery/content/public/documents/ACAS_guide71.pdf .

EXPERIMENTAL RESEARCH REGARDING THE MANUFACTURING OF THE ANTI FRICTION MATERIALS USED IN AERONAUTIC CONSTRUCTIONS

Ion DINESCU*, Gabi MOLDOVAN**, Ovidiu MOSOIU*

* "Henri Coandă" Air Force Academy Brasov, Romania,
** "Transilvania" University of Brasov, Romania

Abstract: The designing of a product which must be fulfilled by the product, thus it is worth to mention the issue of selecting the material out of which that particular product will be made.

The experimental researches are those concerning the assurance of high mechanical and physical characteristics under special regimes, where as the weight of the finished product must be minimized by diminishing the density of the samples.

This paper presents a few characteristics of materials used in the production of friction materials used in the aeronautic constructions.

Keywords: manufacturing, material, friction bearings, aeronautic, construction.

1. INTRODUCTION

The paper present some aspects regarding the experimental researches of the antifriction materials used in the aeronautic constructions:

AS20 – Steel Support Plated with Anti-Friction Material: 20% Tin, 1% Copper, the rest - Aluminum

and

CP10S10 – Steel Support with Anti-Friction Material Sintered from: 23% Lead, 10% Tin, the rest - Copper).

The anti-friction sample based on Cooper, Tin, Lead, sintered powders end not sintered, has a metallic structure, the relations established during the sintering process between the granules powders can be explained by the inter-atomic forces from the microstructure.

2. MATERIALS USED

At present, the main categories of metallic materials used in the production of friction (radial, axial and hydrostatic) are the following ones: [2, 4]

- alloy from the Lead-Tin system;
- cast piece or sintered Cooper-based alloy;
- Aluminium-based alloy;
- other alloys etc.

The tin based alloys (babbit – the composition 88% Sn, 8% Sb and 4% Cu). This alloy has rapidly become the most frequently used in the production of anti-friction

materials. The white metals have capacity of incorporating the particles, which conferred them certain clear advantages in comparison with other anti-friction materials. But the white materials have lost ground in the production of friction materials because of the reduced mechanical resistance, especially at high temperatures.

Pb based alloys (especially the alloys with as content) are used in the world because of the advantages offered by the Pb which replaced Sn, the Pb which is not short. The hardness and the mechanical resistance, they are similar to the Tin-based alloys. These materials are inferior from the point of view of the fatigue strength.

Bronze alloy with Lead, on steel support – is applied by casting or sintering. The Cooper-Lead alloys sintered on steel support are more modern than those directly cast on steel strip or support. These materials have a charging capacity and a strength resistance which are 3-5 bigger, the high hardness of the copper-based alloys requires a higher pin hardness.

The Aluminium-based alloys – anti-friction materials have been cast, because are obtaining an alloy having a structure similar to the babbit, that is a hard stage alloy in a soft basal mass.

An disadvantage at the Al-Si alloys is the fact that, having constituents with high melting points, they do not present the advantages of those with low hardness. In order to replace the lack of conformability, other companies use the method of working surface galvanic coating of the Al-Si layer or the AlSn6 with an extra Pb-Sn layer thick of about 0.25 mm. This layer achieves a micro-conformability of the bushing working surface during exploitation, thus intertwining the qualities of the Al-Si and AlSn6 alloys (high buoying force lift, chemical stability etc.).

3. TECHNOLOGIES USED IN THE PRODUCTION

3.1. The Production Technology of the **AS20** material (Aluminium – Tin 20%) is made in the following stages:

- the preparation of the pre-alloys of Al-Ni, Al-Cu and raw material;
- the melting of the charging;

- the transfer of the material, degasification, de-oxidation and maintenance at the casting temperature;
- the casting.

The properties of the anti-friction material are greatly determined by its chemical composition. It decides the good behaviour following lamination operations in which the material suffers structural transformations. Except the basic elements Sn, Cu, Al, Ni, the other two elements Fe and Si are undesired impurities, thus they must be limited at the minimum value. [1, 4]

The temperature must reach 750-760°C. The temperature plays an important role must be transferred into the soaking furnace, period of time in which the temperature decreases.

This is followed by a heating over the best casting temperature leading to the excessive burning of Sn.

The casting of the anti-friction material represents a important operation which greatly determines the quality of the cast material.

The appreciation of the quality of the cast material is made according to the standards. There are rejected presenting gaseous inclusions, faults as "metallic beads", cold welding or other casting faults. In order to get an ingot with great properties, deprived of casting faults, the ingot butt must be removed, that is the crop end proper.

The Production Technology of the Al-Sn material requires the use of the pre-alloy made up of Aluminium-Nickel and Aluminium-Cooper. Because of the huge differences between the melting temperatures of the alloying elements, the nickel and copper will not be introduced directly, he form of the pre-alloy Al-Cu and Al-Ni, respectively, which have low melting points.

The pre-alloy casting temperature is of 850-860°C.

The main operations for obtaining the double strips of Aluminium-Tin based anti-friction material are the following ones:

- pre-lamination of the AS20;
- annealing of the pre-laminated;
- plating the alloy ingots with Al foil;
- lamination of the plated;
- plating the steel strips with alloy strip;
- annealing the double strips.

"HENRI COANDA"
AIR FORCE ACADEMY
ROMANIA

"GENERAL M.R. STEFANIK"
ARMED FORCES ACADEMY
SLOVAK REPUBLIC

INTERNATIONAL CONFERENCE of SCIENTIFIC PAPER
AFASES 2014
Brasov, 22-24 May 2014

The pre-lamination thicknesses of the alloy ingots are chosen according to the final thickness of the alloy from the double strip.

The annealing temperature of the pre-laminated ingots is made at the best of 355-360°C, and the best annealing time duration is of 150 minutes.

After plating the alloy ingot with the Al foil and laminating the plated ingots, after a series of secondary operations, the shift is towards plating the steel (support) strips with alloy strips, thus obtaining the double strips.

3.2. The stages of the Production Technology of the CP10S10 are the following ones:
- production of alloy powder;
- sintering of the powder on the steel support (obtaining the double strip based on sintered Cu-Pb).

The technological process of obtaining the alloy powder consists of the following operations: the preparation of the cold charging, melting, casting and production of powder. [2]

The best melting temperature ranges in between 1200°C and 1280°C.

The casting, the mode of action of the atomizers and which will form the powder from the melted alloy is monitored.

The powder should be highlighted certain parameters: the pressure of the filtered water, the water softening degree, the regeneration of the de-ionized water, the pressure of the de-ionized water at the atomizers, the moisture of the powder at the entrance of the drier, the temperature at the exit of the drier, neutral air supply in the drier, powder sieving manner, the sieve quality and in the end it can be noticed if the powder corresponds to the requirements. [3, 4]

The technological process of obtaining the double strip based on sintered Cooper-Lead consists of the following:
- the preparation of the strips for sintering;
- depositing the powder on the steel strip having in view the sintering;
- the sintering of the powder on the steel strip;
- lamination of the double strip.

The preparation of the steel coils on which the Cooper-Lead powder is sintered consists in executing certain operations aiming at assuring a continuous technological process: butt welding of the strips, straightening the curvatures and unevenness resulted after welding, washing at the 77-88°C with water mixed with a degreasing and washing, drying at the 95°C through infrared rays heating.

Depositing the powder for sintering on the steel strip is made by means of a complex plant: the plant for the strip speed control and adjustment, the depositing plant proper and the suction hood.

To avoid the oxidation the powder and the steel, a neutral atmosphere is in the furnace and the sintering speed will be established according to the heating curve of the furnace.

The sintering process ends with the strip cooling. The cooling takes place in a complex and closed plant, the same neutral atmosphere being maintained, just like in the sintering furnace.

The lamination of the sintered aims obtaining the density of the deposited powder.

The Cu-Pb based powder sintering on the steel support is made in the sintering furnace ($t_{sint.}$=900-950°C).

According to the hardness of the alloy layer as well as to the tolerance of the double strip thickness, it is recommended to deal with:
- a final sintering and lamination;

- two sinterings and two laminations (a lamination in between the sinterings and a final lamination).

The lamination reduction will be made so that not to appear the melting of the lead from the alloy.

4. EXPERIMENTAL RESEARCH

The materials used in the production of the friction pieces for which there have been used samples and have been carried out studies and experimental research are the following ones: [1, 3, 4]

- Al-Sn plated on the steel support;
- Cu-Pb sintered powders on steel support.

AS20 (Steel Support Plated with Anti-Friction Material: 20% Tin, 1% Copper, the rest - Aluminum).

CP10S10 (Steel Support with Anti-Friction Material Sintered from: 23% Lead, 10% Tin, the rest - Copper).

These samples are presented in Figure 1.
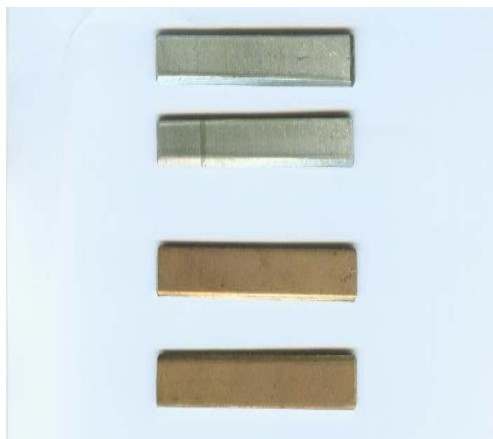
Fig. 1. Samples of Materials Used

Concerning these materials, there have been studied the following properties: chemical composition, micro-structure, resistance (hardness, stretching resistance, shearing, bending, adherence of the anti-friction layer), values of friction static quotients.

Experimental research studies have been made on a six couplings made out of different materials used when making the anti-friction materials: anti-friction material based on Aluminium-Tin (AS20) and steel OLC 45, anti friction material based on synthesized powders

Cu-Pb (CP10S10) and steel OLC 45. These are presented in the figures 2 and 3.

Fig.2. The mobile semi coupling (steel OLC 45)

In figure 2 there are presented the four mobile semicuplings made out of steel OLC 45.
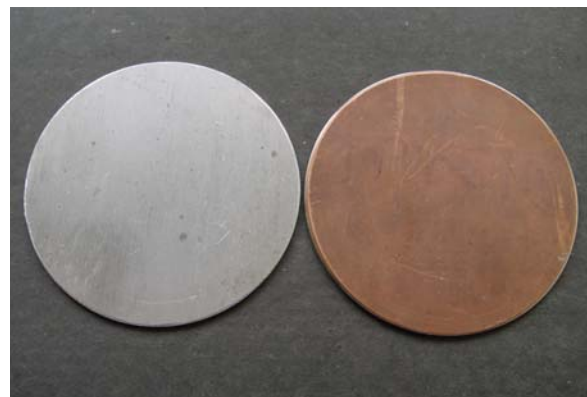
a
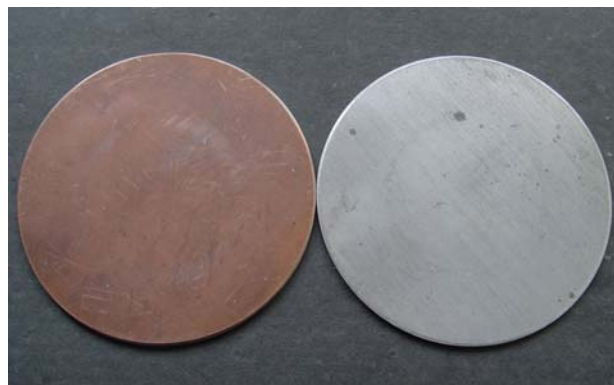
b

Fig.3. Fixed semi couplings (sintering materials)

"HENRI COANDA"
AIR FORCE ACADEMY
ROMANIA

"GENERAL M.R. STEFANIK"
ARMED FORCES ACADEMY
SLOVAK REPUBLIC

INTERNATIONAL CONFERENCE of SCIENTIFIC PAPER
AFASES 2014
Brasov, 22-24 May 2014

In figure 3 (a, b) are presented the four fixed semi couplings (sintering antifriction material.

3. CONCLUSIONS

The anti friction material based on Cooper-Lead sintered powders has a metallic microstructure. During the sintering process between the granules can be explained the inter-atomic forces.

There is a metallic contact between the powder granules. This contact is seldom realized due to an oxide coating at the surface of the granules. The concentration of oxide cannot exceed the imposed value of 0.55% in the case of the powder under research, in order to preserve the metallic structure.

At the heat temperature from the sintering, the powder deposited on the steel suffers the phenomenon of surface and volume diffusion (in solid phase). This is explained by the fact that the atoms situated on the prominences of the powder granules move on the surface of the other granules, concentrating themselves in the surface unevenness. At the heat temperatures, the diffusion between the powder granules and those of the steel takes place. [4]

The factors which influence the Cooper-Lead powder sintering on the steel are: the sintering temperature, the heating speed, the cooling speed, the atmosphere, the size of the granules, diffusion, the powder.

The mixture of alumina and tin oxide is accepted only if the surface occupied by them doesn't exceed 80% of the interface length.

The sulphide inclusions, the foreign bodies inclusions and small cracks are accepted according to the adherence tests (chiselling, peeling).

The structures with superficial corrosion of tin melt at the alloy surface during annealing and inter-crystalline corrosion are unappropriate.

The double strips must not present a series of faults, such as: overlaps, surface slag imprints, oxide traces after pickling, foreign bodies inclusions, cracks.

REFERENCES

1. Bardocz, G., Dinescu, I. *Cercetări experimentale privind proprietăţilor de rezistenţă ale materialelor bimetal pe bază de Cu-Pb şi Al-Sn*. Sesiunea de comunicări ştiinţifice cu participare internaţională „Educaţie şi cercetare ştiinţifică la standarde europene", 11-12 mai, Editura Academiei Forţelor Aeriene "Henri Coandă" (mai 2007).
2. Dinescu, I., Bardocz G. *Materials for the Bushings*, REVIEW of the Air Force Academy, The Scientific Informative Review No. 1/2007, The Air Force Academy "Henri Coandă" Printed House, ISSN 1842-9238, p. 19-22 (May 2007).
3. Dinescu, I., Bardocz, G. *Remarks Regarding the Friction within the Bushings*, Bulletin of the "Transilvania" University of Brasov, Supliment BRAMAT 2007, "Transilvania" University Press, ISSN 1223-9631, p. 503-508 (2007).
4. Dinescu, I., Bardocz G. *Technologies of Obtaining the Materials Used in the Production of Bushings (Friction Bearings)*, The 21st International Conference NAV-MAR-EDU 2009, 12th-14th, "MIRCEA CEL BATRAN" Naval Academy, Constanta, Romania, ISSN 1843-6749, p. 494-501(November, 2009).

AIR FORCE

"HENRI COANDA"
AIR FORCE ACADEMY
ROMANIA

"GENERAL M.R. STEFANIK"
ARMED FORCES ACADEMY
SLOVAK REPUBLIC

INTERNATIONAL CONFERENCE of SCIENTIFIC PAPER
AFASES 2014
Brasov, 22-24 May 2014

FLIGHT SIMULATOR AS AN ESSENTIAL DEVICE SUPPORTING THE PROCESS OF SHAPING PILOT'S SITUATIONAL AWARENESS

Jarosław KOZUBA*, Adam BONDARUK**

* Eng. pil. Jarosław KOZUBA, Phd; Faculty of National Defence and Logistic, Polish Air Force Academy, aabuzo@wp.pl, ** Eng. pil. Adam Bondaruk, Phd; Faculty of Avaiation, Polish Air Foirce Academy abond2@poczta.onet.pl

INTRODUCTION

Flight simulators[1] play a significant role both in pilot training and in sustaining pilot currency. The safety level of modern general, commercial and public aviation depends largely on simulation technologies, used not only for training purposes, but also in air accident investigations, studies of aircraft design or air traffic simulation and on a better understanding of the interactions present in the pilot-aircraft-mission environment system. Conclusions drawn from the analysis of the reference literature[2] suggest that the role of flight simulators increases with the growing complexity of modern aircraft systems, which means that simulator training is now an integral part of the processes of pilot training and professional development, or conducting the research studies related to adapting aircraft design to human capabilities and limitations. Ever increasing degree of fidelity of representing the pilot natural work environment by the simulator makes flight simulators an invaluable tool used in the process of air accident investigations.

---

[1] Simulation (Latin *simulato* – pretending, imitating). In the dictionary of contemporary Polish language the term simulation is defined as creating appearances, pretending something, appearance, feigning sickness, artificial reconstruction of a phenomenon occurring in nature: aircraft flight simulation. In colloquial language, this term has adopted a negative sense and means the act of pretending or feigning something to put someone in error, or achieve benefits. The simulator should not be, however, solely with negative or harmful acts. From the beginning of the 20th century, this word began to acquire a positive meaning. The immediate cause of the change in the approach to the concept of simulation, was the emergence of the concept of simulation as a research method for determining the specific phenomena of human activities, machinery operation, etc. This method is applied whenever there is the need of the repetition, testing or detailed preparation of a detailed, complex process without the involvement of the assets usually participating in it. The success of research carried out using this method amounts to the creation of a model of environmental conditions and the device under test in a manner as close to the reality as possible. Multi-author work, *Słownik współczesnego języka polskiego*, PWN, Warszawa 1996, p. 1080.

[2] G. Lintern, S.N. Roscoe, J.M. Koncoe, L.D. Segal, *Transfer of landing skills i beginning flight training.* Human Factor № 32/1990; R.T. Hays, J. Jacobs, C. Prince, E. Salas, *Fligcht Simulator training effectiveness. A-meta-analysis,* Military psychology № 4/1992; R. Leszczyński, *System selekcji kandydatów do Sił Powietrznych,* Praca badawcza, WSOSP, Dęblin 2000; W. Bezdek, R. Powell, D. Mays, *The history and future of military flights simulators,* AIAA modeling and simualation technologies conference and exhibit – 2004, Providence, RI, AIAA Paper 2004 – 5148; N.D. Macharella, P.K. Arban, S. M. Doherty, *Transfer of training from flight training devices to flight for ab initio pilots*, International Journal of Applied Aviation Studies № 5/2005; A.T. Lee, Flight Simulation, ASHGATE, Burlington 2005.

FLIGHT SIMULATORS – GENERAL CHARACTARESTIC

How complex has been the development of simulators can be seen from the example of the first flight simulator "Aeronautical Link Trainer", which consisted only of a basic set of cockpit flight instruments and a very basic platform for simulating the aircraft movement. It did not support the function of displaying the external mission environment for the pilot[3]. Modern flight simulators apart from the faithful reproduction of the internal and external mission environment can also be equipped with motion simulation platform. Modern flight simulator has become the essential type of ground equipment for pilot training and professional development[4]. Currently, it is difficult to imagine modern flight training without the use of flight simulators. The effectiveness of practical training using flight simulators is determined by a number of factors, including, among other things, such as: safety, economic, technical, methodological, etc. Due to the desired level of simulator training efficiency and flight simulator versatility these devices must fulfill a number of functions. The essential, desired functions of a flight simulator designed for pilot training and professional development can include:

• Demonstration function – it relates to the enrichment of the theoretical training process with demonstrating the trainee the elements of specific procedures, methods and the uses of aircraft instruments, controls and systems.

• Education function – it relates to such elements as: developing/perfecting trainee's skills and habits with regard to practical implementation of operations in the cockpit, the use of operational procedures, onboard emergency procedures, improving multi-crew cooperation, and the skills in the use of aviation phraseology, developing /perfecting training skills of flight instructors, etc.

• Personality function – it is associated with the formation and development of the desired personality and professional traits of the pilot (trainee), preparing him for it, among others, for air mission execution under high workload and/or time deficit, and in new situations (onboard and in the mission environment) from the point of view of the current pilot (trainee) experience, etc.

• Adaptive function – it amounts to improving the pilot (trainee) "recurring" actions on board the aircraft, including actions related to complex and emergency situations. Exercises performed within this function are particularly important with regard to the preparation for the execution of the mission which is new from the point of view of the pilot's current experience.

• Research function – it is related to checking the behavior of the pilot (trainee) at different stages of the planned mission execution, taking into account the specific solutions relating to the design, ergonomics, and automation of a particular aircraft type. It also amounts to verifying the validity of theoretical assumptions related to the way of solving problems onboard the aircraft by the crew, for example, the validity of assumptions concerning the crew actions in the event of certain onboard emergencies. This function is also applied when it is necessary to confirm the conclusions of the air accident investigation board's proceedings, relating to the causes of undesirable flight-related events.

• Selection function – it consists in eliminating permanently or temporarily from further aviation training those candidates who have no predispositions (competencies, knowledge, skills) to work as a pilot/perform specific flight tasks.

• Control-examination function – it allows to carry out control/examination

---

[3] W. Bezdek, R. Powell, D. Mays, *The history and future of military flights simulators,* AIAA Modeling and simulation technologies conference and exhibit – 2004, Providence RI, AIAA Paper 2004–5148.

[4] In the present work, the author refers mainly to simulators applied in the process of training and professional development of pilots. It should also be emphasized that at present simulators are an essential tool applied in the process of training and professional development of the remaining air personnel (aircraft technicians, air traffic controllers, etc.).

"HENRI COANDA"
AIR FORCE ACADEMY
ROMANIA

"GENERAL M.R. STEFANIK"
ARMED FORCES ACADEMY
SLOVAK REPUBLIC

INTERNATIONAL CONFERENCE of SCIENTIFIC PAPER
AFASES 2014
Brasov, 22-24 May 2014

exercises in relation to the specific license or aviation rating[5].

It should be noted that the effectiveness of the use of flight simulators in the recruitment, selection, training and professional development of pilots, air accident investigations, or research is dependent on an understanding of their capabilities and limitations that apply to specific areas of aviation. On the other hand, in the process of the flight simulator design, it is very important that the designer, apart from applying specific, high-tech aviation technologies, should also strive to create a mission environment model as close to the reality as possible, and take into consideration the knowledge of human capabilities and limitations, including those relating to the ability to perceive and process information, as well as the cognitive factor concerning the operational capabilities of the simulator. Modern flight simulators are also treated as an essential tool for developing the pilot's ability to "automate" the actions in the cockpit and for the efficient reception and selection of signals related to the aircraft status. Many psychologists hold the view[6], that in relatively simple situations habits can replace thinking – automatic execution of tasks. In complex, unexpected situations – non-routine air incidents – an important role is played by the quick assessment of the situation and the appropriate action programming. From the point of view of situational awareness, the pilot's ability to automatically perform actions on board the aircraft is of primary importance to the perception, selection and analysis of large amounts of information within the time limit and to the construction of the aircraft status mental images. One of the simplest examples of such actions is the cockpit pre-flight check. Research conducted by the author shows that the time differences between a trainee pilot and a pilot in continuous training[7], can range from tens of seconds to several minutes, depending on the aircraft type. Too frequently, especially in the initial stage of flight training, the preparation of a future pilot amounts to learning specific definitions and points of instruction during the theoretical training course, and learning to control certain actions (often without understanding the phenomena of e.g. aerodynamics and flight mechanics) during the practical training.

Meanwhile, with the development of aircraft design, including the more recent introduction of the solutions relating to the areas concerning the aircraft management, pilot's initiative and independent thinking based on vast general and specific knowledge and practical skills, including the skills relating to performing certain actions automatically, become more and more important for the safety and efficiency of air mission execution.

In addition to socialization techniques and teaching techniques, such as brainstorming, decision-making exercises with a limited amount of information and in time deficit, an increasing role is played by flight simulator exercises. A good example of such activities

---

[5] Author's own work, taking into account the specific functions identified in R. Pielacha, *Imitatory kierowania samolotami w kształtowaniu nawigatorów wojskowych*, Research Study, PAFA, Dęblin 1994, (in:) Op.cit. R. Leszczyński, *System selekcji kandydatów…*, p. 58.

[6] J. Terelak, *Higiena psychiczna i pilot*, MON, Warszawa 1975, p. 237.

[7] Continuous training – a term applied to fully trained air force pilots participating annually in a training program aimed at maintaining/improving pilot currency with regard to handling a particular aircraft type.

are exercises in acquiring habits relating to pilot conduct in the event of an onboard emergency. By modern flight simulator we mean a flight training device characterized by a faithful simulation of both the internal (aircraft cockpit with instrumentation and indicators) and the external mission environment (everything that the pilot observes during the flight outside the cockpit), sound and air services, events changes that occur during aircraft position in three planes of reference - pitch, roll and yaw, simulation of mechanical and functional control system that allows the aircraft to acquire and consolidate skills to effective decision-making and the efficient and secure management of aircraft, especially in the situation of a heavy workload and with a time limit. Very important in terms of forming correct situational awareness habits is to enable the participation of the pilot in a training covering receiving and processing the data to be used in order to create a status image for particularly complex situations which may be encountered when executing a specific air mission.

Therefore, it should be considered particularly important that the engineer-designer should understand how big an impact on the effectiveness of the simulator is its degree of reality representation in relation to the type of aircraft operated. The simulator designer should then apply the technology which is the most useful from the point of view of the user to re-create the functional and physical characteristics of the aircraft and external mission environment.

Today's flight simulators, regardless of the nature and extent of their use in flight training, prove that their designers are well aware of the fact that a flight simulator is not just a machine equipped with modern computer software. Flight simulator designers also understand that in the design of the flight simulator particular attention should be given to adapting the newly created equipment to the capabilities and limitations of the pilot and his tasks conducted on a specific aircraft type in a particular mission environment.

Until the second half of the 1970s, flight simulators had often been perceived by the majority of the civil aviation community as a kind of attraction. Taking into account the

economic factors and impracticality, many airlines and smaller aviation organizations had rejected the use of flight simulators for training purposes. However, with more and more evidence of the simulator training effectiveness, commercial aviation sector became increasingly interested in those devices. The final breakthrough came during the oil crisis in the 1970s, when flight simulators became a widely used training tool in commercial aviation. In fact, flight simulators were regarded as a low-cost training tool, used as an alternative to flight training. Over the years and with the development of aviation technology, flight simulators have become a commonly used training tool which is also used for basic flight training of young aviation adepts. Today, we can say that flight simulators are an essential element of pilot training and professional development, regardless of the kind of aviation and aircraft type taken into consideration.

USEFULLNES OF THE FLIGHT SIMULATORS IN THE GENERAL AVIATION PILOTS TRAINING

However, due to the economic aspects related to the purchase and operation of a flight simulator, there are still some restrictions on its use, particularly in relation to *general aviation* where trainer aircraft still remain a major tool used in instruction and training[8]. The exception is the PPL (Private Pilot Licence) training, where simulator training (simulator or FNPT BITD Class)[9] may be substituted for 5 hours of practical training, and procedural training for IFR

---

[8] The authors have not addressed the training of helicopter pilots, due to the fact that in Poland, as of 1st July, 2012, only Polish Medical Air Rescue had a certified FNPT II helicopter simulator. The remaining helicopter pilot training organizations in Poland did not use flight simulators. This is primarily due to the relatively high purchase price (approx. € 650,000) and maintenance costs of the simulator with a small number of trainees – several people each year. Such a small number of trainees is primarily due the fact that the cost of training one candidate for professional license CPL(H) is approximately € 125,000–170,000, depending on the training organization and the helicopter type used in the training.

[9] Section 1 Part-FCL 1.120 Practise and credits.

"HENRI COANDA"
AIR FORCE ACADEMY
ROMANIA

"GENERAL M.R. STEFANIK"
ARMED FORCES ACADEMY
SLOVAK REPUBLIC

INTERNATIONAL CONFERENCE of SCIENTIFIC PAPER
AFASES 2014
Brasov, 22-24 May 2014

flights, where 55 hours of flight training may be conducted as: 40 hours of practical Simulator training (FNPT II class simulator) and 15 hours of training on a trainer aircraft[10]. To sum up, in accordance with the current regulations, *20% of the total* practical air training *time* of the pilot trained for *CPL licence and IFR rating,* can be assigned to simulator training. However, it is not only because of regulations that, despite its number of advantages, simulator training, is rarely used in daily flight training. The second limitation is the fact that the vast majority of training can be conducted using the FNPT-II class simulator, whose purchase price is approx. € 400,000. In addition, the decreasing number of air training candidates each year makes the purchase, operation and maintenance of such equipment in general aviation become increasingly irrational in economic terms. Because of this barrier, as of 1st July, 2012, only 7 Flight Training Organizations in Poland possessed FNPT-II class, and 3 centers BITD class simulators. Bearing in mind that as of 1st July, 2012, there were more than 50 accredited Flight Training organizations, the above-mentioned number of flight simulators seems to be very modest. On the other hand, the results of comparative analysis of the training costs for IFR flights with and without the simulator use shows that the first variant is cheaper by more than 50%[11].

The main argument in favor of a wider use of simulators in flight training are the results of studies related to the transfer of knowledge and skills from the flight simulator to the aircraft with regard to basic flight training. Studies carried out so far clearly confirm the usefulness of flight simulators, including the simplest (BITD), in the basic aviation training process. Lintern et.al.[12] in their research studies analyzed the degree of transferring the landing skills from the simulator training to the trainer aircraft at the beginning of the pilot flight training. The first group of trained pilots held two simulator training sessions covering the landing skills prior to the commencement of practical training in the air. The second group – the controls – did not receive this kind of training before the start of practical training in the air. The investigators demonstrated that the first group of trainees needed approx. 1.5 hours of training flights less before the first solo flight, as compared with the second group, which had not undergone the simulator training. In this case, we refer to only one, particularly important and difficult element of air training – learning to land[13].

---

[10] Annex 1 to Part-FCL 1.205, pt. 10.

[11] Assuming the cost of one hour of the Cessna-172 flight to be € 225 and one hour of the FNPT II simulator use to be € 60, at 40 hrs. of simulator training and 15 hrs. of practical training conducted on the Cessna-172, the total cost of the training would be € 5,775. If the whole training were conducted on The Cessna-172, the total cost of the training would be € 12.375. The analysis was based on the average price of 1 hour of the Cessna-172

aircraft flight and 1 hour of the FNPT-II simulator use as of 1st July, 2012 – author's own analysis.

[12] G. Lintern, S.N. Roscoe, J.M. Koncoe, L.D. Segal, *Transfer of landing skills in beginning flight training.* Human Factor Nº 32/1990, pp. 319-327.

[13] Usefulness of the simulator training for basic training of pilots was also confirmed by the study team of N.D. Macharella – for further details, see N.D. Macharella, P.K. Arban, S. M. Doherty, *Transfer of training from flight training devices to flight for ab initio pilots*, International Journal of Applied Aviation Studies Nº 5/2005, pp. 25-39.

Dennis and Harris[14] examined the impact of the simulator training on the practical flight training using Microsoft Flight Simulator (v4.0) – a PC computer-based game program. Each trainees performed straight and level flight and coordinated turns for 1 hour. Then, the trainees commenced practical training in the air. The results of the comparative analyses concerning the performance demonstrated by the trainees who had received a simulator training session with those who had not explicitly confirmed that it was easier for the first group to assimilate the elements of the exercises which had been carried out before on the flight simulator. Furthermore, these studies confirmed the view that simple PC simulators are an effective tool in the development of flight skills in the initial phase of flight training.

On the other hand, the results of the research study conducted by Vaden and Hall[15] pointed to the fact that the platform imitating the motion of an aircraft does not serve an important role in the acquisition of skills by the pilot. Using the method of meta-analysis they examined the impact of the aircraft's plane of motion, which is an integral part of the aviation simulator, on the development of the pilot's skills. The study showed little effect of the use of such devices on increasing the flight training effects in cargo aircraft pilots . They also pointed to the fact that the cost of upgrading the simulator with this feature, as well as additional physical load experienced by the pilot during the exercises on a Full Flight type simulator, do not have a significant impact on reducing the number of hours of practical training carried out by the crew in the air. The authors do not comment on the impact of this training on enhancing the crew's skills in the use of the available resources during the flight.

The interviews conducted by the author with a group of instructors from flight training organizations in Poland[16] indicate that FNPT-2 simulators provide highly effective training and selection, particularly in relation to the exercises concerning: IFR flights, emergency procedures, maneuvers performed by the aircraft during mission execution, and cockpit pre-flight check.

Given the above findings, it is possible to formulate a thesis that modern flight simulators ensure a high degree of basic flight training efficiency[17]. Other air training equipment, due to its purpose and specific use is not used by general flight training organizations.

USEFULLNES OF THE FLICHT SIMULATORS IN THE COMMERCIAL AVIATION PILOTS TRAINING

Commercial aviation organizations following the current regulations conduct the simulator training within the scope of training for certain aircraft type, MCC, CRM, and mandatory periodic training. The main document regulating the air operator's duties regarding the preparation and professional development training of the crews belonging to commercial aviation organizations is OPS-1, and Part-FCL1 in relation to the training for particular aircraft type. As is the case with general aviation, each flight simulator or air training equipment item replacing the aircraft for training and testing purposes must be certified in accordance with the requirements applicable to air training equipment[18]. Under the current regulations, any member of the flight crew prior to commencing flight operations below the standard set for Cat. I, operations outside the standard of Cat. II and operations within Category II and III[19] must

---

[16] The author conducted research by interviewing a group of 10 instructors representing the leading fligcht training organizations which conduct simulator training.

[17] Training up to CPL (A) license and IFR (A) rating.

[18] In relation to simulators, these requirements are set by JAR-FSTD A: Aeroplane flight simulation training devices.

[19] These categories refer to the categories of ILS (Instrumental Landing System) applicable to certain airports. The basis of category allocation is the possibility of making a safe landing at a minimum cloud ceiling and visibility: Cat. I – DH (Decision Height) no less than 200 ft (60 m) and RVR

---

[14] K.A. Harris, D. Harris, Computer-based simulation as an adjunct to ab initio flight training, International Journal of Aviation Psychology N° 8/1998, pp. 261–276.

[15] E.A. Vaden, S. Hall, *The effect of simulation platform motion on pilot training transfer: A meta-analysis*, International Journal of Aviation Psychology N° 15/2005, pp. 375–393.

"HENRI COANDA"
AIR FORCE ACADEMY
ROMANIA

"GENERAL M.R. STEFANIK"
ARMED FORCES ACADEMY
SLOVAK REPUBLIC

INTERNATIONAL CONFERENCE of SCIENTIFIC PAPER
AFASES 2014
Brasov, 22-24 May 2014

complete the training courses and tests which use flight simulators. These courses include reduced visibility operations, including multi crew cooperation. It is emphasized that MCC and CRM trainings[20] ought to be conducted with The maximum use of flight simulators. In the case of aircraft for which the flight simulator has not been produced, the operator must ensure that the phase of simulator training specific to the visual scenarios of Category II operations is conducted in a specifically approved flight simulator[21]. Moreover, each crew member shall undergo periodic training and testing appropriate to the type or variant of aircraft in which he operates flights. Those trainings are usually conducted using the flight simulator which corresponds to a given aircraft type[22]. As part of ongoing operations the operator must ensure that:

− the pilot is not assigned to operate an aircraft as a member of the minimum approved crew, either as pilot flying or pilot non-flying, if during the past 90 days he has not performed three take-offs and three landings as pilot flying in an aircraft or in a flight simulator of the same type/class;

− the pilot who does not have a valid IFR rating is not assigned to perform night flights as a crew commander, if during the past 90 days he has not performed at least one

landing at night, as pilot flying in an aircraft or in a flight simulator of the same type/class[23].

− Moreover, each operator is required to provide transition training involving such elements as:

− ground training and tests concerning aircraft systems, routine, non-routine and emergency procedures;

− trainings and tests in order to familiarize trainees with emergency and safety equipment, which must be completed before the commencement of the practical air training. It should be noted that an important element of these courses are exercises and tests performed with the use of flight simulators[24].

Importance attached to the simulator training of commercial aviation aircrews in the above-cited regulations as well as the results of analyzes relating to the opinions of pilots from commercial aviation organizations clearly show that simulator training is an essential element of professional development training in this type of organizations. Flight simulators used in the training described above facilitate, on the one hand, a continuous improvement of the flight crew skills, and, on the other hand, they are a valuable tool to determine the level of flight crew preparedness for the tasks facing them. Moreover, taking into consideration the scale and frequency of training it is difficult to imagine a commercial aviation organization capable of affording to conduct the training in full using only the aircraft.

USEFULLNES OF THE FLIGHT SIMULATORS IN THE MILITARY AVIATION PILOTS TRAINING

(Runway Visual Range) no less than 2040 ft (800 m). Cat. II – DH no less than 100 ft (30 m) and RVR no less than 1,050 ft (350 m). Cat. III has been subdivided into three subcategories: - IIIa – DH = 0-100 ft, RVR no less than 600 ft (200 m); IIIb – DH= 0–50 ft, RVR no less than 150 ft (50 m); IIIc – DH = 0, RVR = 0 – Developed on the basis of: T. Compa, J. Rajchel, *Podstawy nawigacji lotniczej*, WSOSP, Dęblin 2011, p. 297.

[20] MCC – Multi Crew Cooperation; CRM – Crew Resource Management.
[21] Developed on the basis of: Appendix 1 OPS 1.450.
[22] Further details, see Appendix 1 OPS 1.950.

[23] Developed on the basis of: Appendix 1 OPS 1.970.
[24] Developed on the basis of: Appendix 1 OPS 1.945.

In Military aviation, which is less dependent on the financial factor, flight simulators are widely used in daily operations and training relating to the acquiring/maintaining pilot currency. Flight simulators used in military aviation can be divided into two main groups, according to the tasks performed with them:

1. Simulators for schools and military pilot training organizations. Their use is associated with familiarization of beginner pilots with the aircraft, its handling, navigation and basic combat missions. They are used for the selection and training of pilot candidates, advanced flight training, training of all flight phases, assessing the implementation of specific air missions, and crew training and coordination within the scope of MCC and CRM training. The syllabus of pilot training for Polish Air Force Academy (PAFA) officer cadets includes 120 hours of specialized simulator training during the four years of study. The situation is somewhat different in the case of training/professional development of jet pilots in the units of the Polish Armed Forces. Simulators of this aircraft type alongside handling and navigation functions support the functions related to performing combat missions. The number of simulator training hours depends on the intensity and the type of tasks performed by the pilot. Apart from the above-mentioned applications, flight simulators are treated in air force units as a valuable tool for preparing to resume pilot currency and skills in the event of long time break between flights.

2. Simulators of the Polish Armed Forces units, where the main emphasis is placed on improving aircraft handling skills associated with aerial combat techniques.[25] Individual training tasks carried out in the air are generally preceded by the training on a flight simulator which is an exact copy of the aircraft operated. As a rule, the trainee is allowed to conduct the tasks in the air after successfully conducting them on a simulator. Simulators are used for a variety of reasons, including those related to the low unit cost of

simulator training hours compared to the cost of flight hours. U.S. Air Force estimates that the cost of one hour of training on the C-5 aircraft is approximately $ 10,000, while one hour of training on the C-5 simulator is $ 500[26]. Especially with regard to military pilots and airline pilots the key advantage of simulators is the fact that they allow pilots to perform simulated flight tasks and train the behavior in non-routine situations, which if performed on the trainer aircraft would involve too high risk of undesirable flight-related events.

Another reason for the use of simulators in the Air Force is the knowledge transfer degree, which is comparable with that acquired during practical training in the air. The results of research concerning the aspects related to the effectiveness of simulator training clearly show that the knowledge, skills and habits acquired during such training exert a direct influence on the pilot's readiness to perform air missions in the air. R. Moorman et al. conducted research relating to knowledge transfer involving flight simulator. Their study covered the period 1957–1986[27]. The authors conducted a study using the meta-analysis method[28] and the results allowed them to

---

[25] The division of simulators used in military aviation was made on the basis of: C. Szczepański, *Symulatory lotnicze, stan i perspektywy* – raport , Warszawa 1998, p. 4.

[26] T.R. Moorman, *The civilian looping military*, MS&T Magazine, N° 6/2002, p. 16-20.

[27] R.T, Hays, J. Jacobs, C. Prince, E. Salas, *Flight simulator training effectiveness. A-meta-analysis,* Military psychology N° 4/1992, pp. 63-74 .

[28] Meta-analysis is a research method which involves the use of statistical techniques for connecting the results of several tests in order to find an answer to one research problem. This method comprises several phases, i.e.: formulation of the research problem, identification of the research area (person, location), encoding the test (preparation of test material, e.g. surveys), meta-analysis - analysis of results and their presentation. For example: The investigator is interested in carrying out research in order to find out whether the psychological test that measures the level of the candidate's spatial intelligence can be a tool used for the selection of pilot candidates. In this case, first of all, the test is administered to the pilot candidates, and then its results are compared with their flight training performance. The results obtained constitute the material which allows making comparisons in order to determine the correctness of the construction of the test and its questions (tasks), and therefore, they are a measure of its usefulness in the selection process of pilot candidates. Developed on the basis of: M. Marlinussen, D.R. Hunter, *Aviation*

"HENRI COANDA"
AIR FORCE ACADEMY
ROMANIA

"GENERAL M.R. STEFANIK"
ARMED FORCES ACADEMY
SLOVAK REPUBLIC

INTERNATIONAL CONFERENCE of SCIENTIFIC PAPER
AFASES 2014
Brasov, 22-24 May 2014

conclude that simulator training contributed to a permanent increase of the training effects in jet pilots, which are equal to those of practical training carried out on the specific aircraft type. However, this regularity was not confirmed for helicopter pilots.

In another study, Corveta and Dunlap[29] focused the research on the effectiveness of simulator training involving jet pilots, with respect to such items as landing maneuver, IFR flights and tasks performed at the firing ground (*aerial bombardment*). In all of the above areas of research, the results clearly indicate a *high degree of usefulness of* flight simulators for pilots' skill development.

From the situational awareness perspective, flight simulator plays a particularly important role in military aviation. Despite the high level of automation of modern combat aircraft, because of the complex character of air mission environment – unknown flight zone, limited possibility of using radio navigation instruments, low and very high altitudes, high speeds and G-loads, unpredictable enemy, conducting missions in radio silence, often as a member or head of the combat group, the pilot conducts air missions under heavy psychophysical load. Therefore, the degree of pilot mastery concerning cockpit actions, or the degree of "automation" of these actions has a major impact on the pilot's ability to maintain the desired level of situational awareness at various stages of air mission execution. The results of the analysis

of serious air incidents which concerned combat aircraft of the Polish Armed Forces in the years 1970–2004 show that the vast majority of them was caused by insufficient situational awareness of the pilot – approx. 70%[30].

The growing complexity of technical systems increases the burden on the operators. Mastering operator actions is a long and costly process which is dependent on technological advancement and the complexity of actuating devices. The essential feature of operators is the necessity of receiving, analyzing, and responding to information which is frequently acquired from several different sources. The pilot is a special type of an operator since he is constantly subjected to pressure affecting his psychomotor (operator's) skills because of the work environment, and is facing the serious consequences of errors committed during reception (interpretation) of stimuli and responding to them.

Forming pilot's habits confirmed by research studies points out to the desirability of using flight simulators in aviation training.

From the data obtained during the tests performed on the simulator and on the aircraft, it is clear that the number of errors is similar in both cases. The above ensures the suitability and necessity of using flight simulators for training pilots.

The effectiveness of the training is verified by the practical performance of air missions, and it constitutes a basis for changing the contents, methods and forms of the simulation training.

Simulator training can be divided into three areas[31]:

psychology and human factors, CRC Press, New York 2010, p. 43.

29 T.R. Carreta, *Transfer of training effectiveness in flight simulation: 1986 –1997* (technical report AFRL-HE-AZ-TR-1998-0078), Mesa, AZ: U.S. Air Force Research Laboratory, Human Effectiveness Directorate, (in:) Op.cit., M. Martinussen, D.R. Hunter, *Aviation Psychology and Human Factors…*, p. 114.

30 The analysis has been conducted on the basis of the available post-accident materials.

31 A. Bondaruk, *Metodyczne uwarunkowania konstruowanina programów szkolenia symulatorowego*

- flight maneuver training;
    - procedural training (IFR);
    - tactical training;

[Methodological considerations of designing simulator training syllabi] , Conference on "The Instructor Preparing Trainees for Difficult and Dangerous Professions", Dęblin, February, 2014.
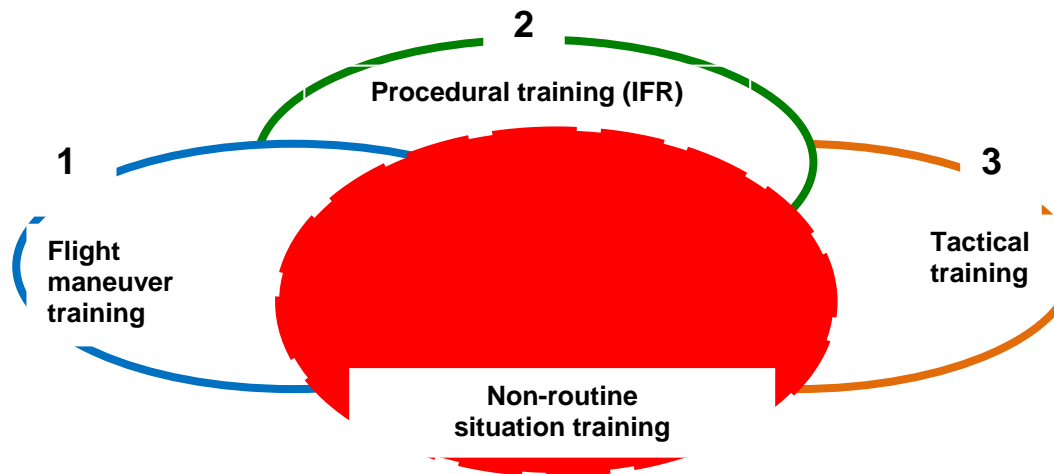
Fig. 1. Simulator training areas.

It is advisable that simulator training program should include elements of subsequent training areas that prepare the trainee for more difficult tasks, but are not the main training objective. To sum up, the areas of training overlap at particular stages. The degree of their implementation depends on the main objective and complexity of training, as well as on the level of training of a particular pilot. Training of emergency flight procedures is implemented throughout the entire flight training program.

In 2012, a research study was conducted taking into account the above considerations, with the use of an FFS (Full Flight Simulator) simulator. The purpose of the research was to determine the training susceptibility of pilots and the appropriateness of the applied simulator training program.[32].

The number of pilots tested accounted for approximately 20% of the population of F-16 pilots in the Polish Armed Forces, who have completed the basic training (acquired a minimum wingman rating).

For the purpose of the analysis, a set of "measurable" data was determined, i.e. those which have been obtained by means of measurements. This data set included the pilots' time before reaction to deviation from the prescribed (standard) flight parameter values, and the "countable" data - the number of errors made when performing certain tasks on the simulator.

The study included the completion of four sessions on the multi-role F-16 aircraft simulator by every pilot. Each session was carried out according to identical profile consisting of two scenarios (missions). The study was divided into two phases. In the first phase, the pilot being tested performed three sessions at intervals that allowed for discussion, and the analysis of errors having been made when executing the task, as well as for the preparation for the subsequent flight. Before the commencement of the first session, the pilot was briefed only on the tactical background and the task to be accomplished. The element of a non-routine situation remained unknown for the pilot until its occurrence. The second phase included the execution of the last, fourth, flight after at least one month from the completion of phase 1

Elements being assessed in scenario 1:

-    making the decision to abort the mission in a particular non-routine situation;

-    maintaining the IFR flight parameters;

-    maintaining the preparatory procedures for landing at the alternate airport;

-    maintaining the prescribed heading during the vectoring;

-    descending to the final approach point (FAP), maintaining the

[32] A. Bondaruk, *Badanie wpływu uszkodzeń i niesprawności samolotu wielozadaniowego na bezpieczeństwo lotów [Study of failure and malfunction effect in multi-role aircraft on flight safety]"*, Doctoral Dissertation, Air Force Institute of Technology (ITWL), Warsaw 2011.

minimum flight altitude H in accordance with the approach chart;
- maintaining flight parameters during descent;
- maintaining flight parameters at decision height/altitude (DH/DA);
- maintaining the missed approach procedures (MAP);
- performing the landing.

Elements being assessed in scenario No. 2:
- making the decision to abort the mission;
- maintaining flight parameters during emergency procedure execution;
- recognition of a subsequent emergency situation (observation of engine control instruments during emergency procedure execution);
- making the decision to perform the simulated flameout (SFO) landing procedure;
- if made:
- maintaining flight parameters during SFO approach in accordance with the standards of the appropriate procedure;
- performing the landing;
- if not made:
- recognition of turbine stoppage;
- performing the procedure of preparation for the ejection.
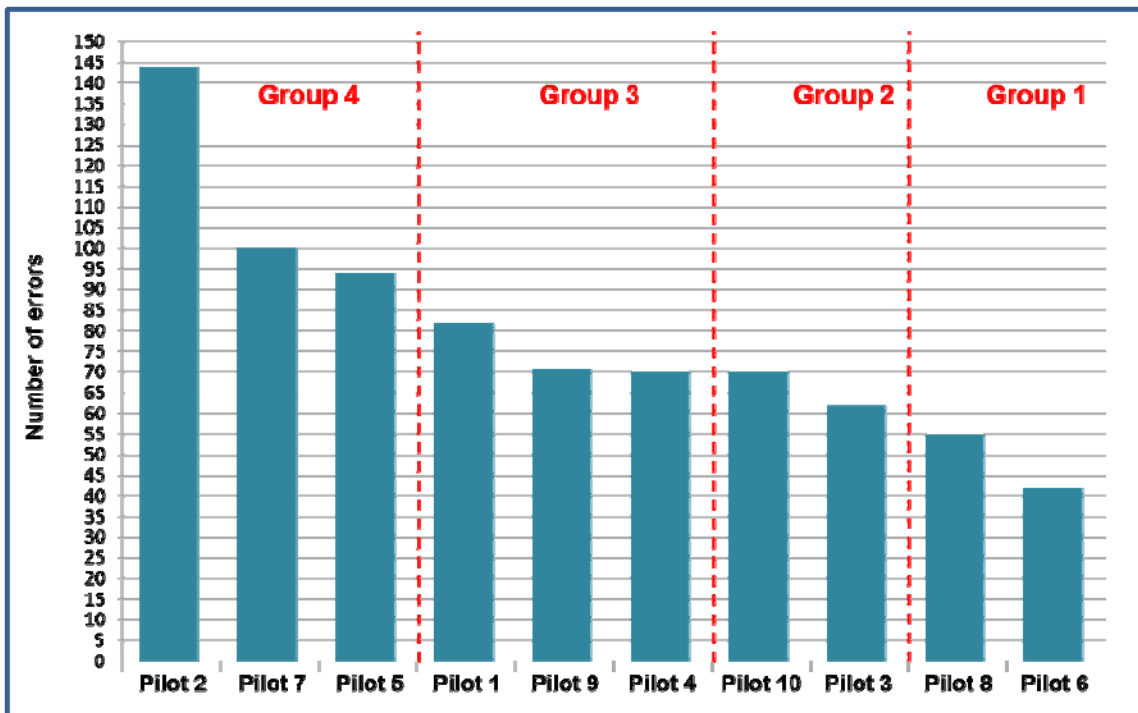
Fig. 2. The total number (sum) of errors committed by pilots during the execution of tasks in accordance with scenario No. 1

“HENRI COANDA”
AIR FORCE ACADEMY
ROMANIA

“GENERAL M.R. STEFANIK”
ARMED FORCES ACADEMY
SLOVAK REPUBLIC

INTERNATIONAL CONFERENCE of SCIENTIFIC PAPER
AFASES 2014
Brasov, 22-24 May 2014
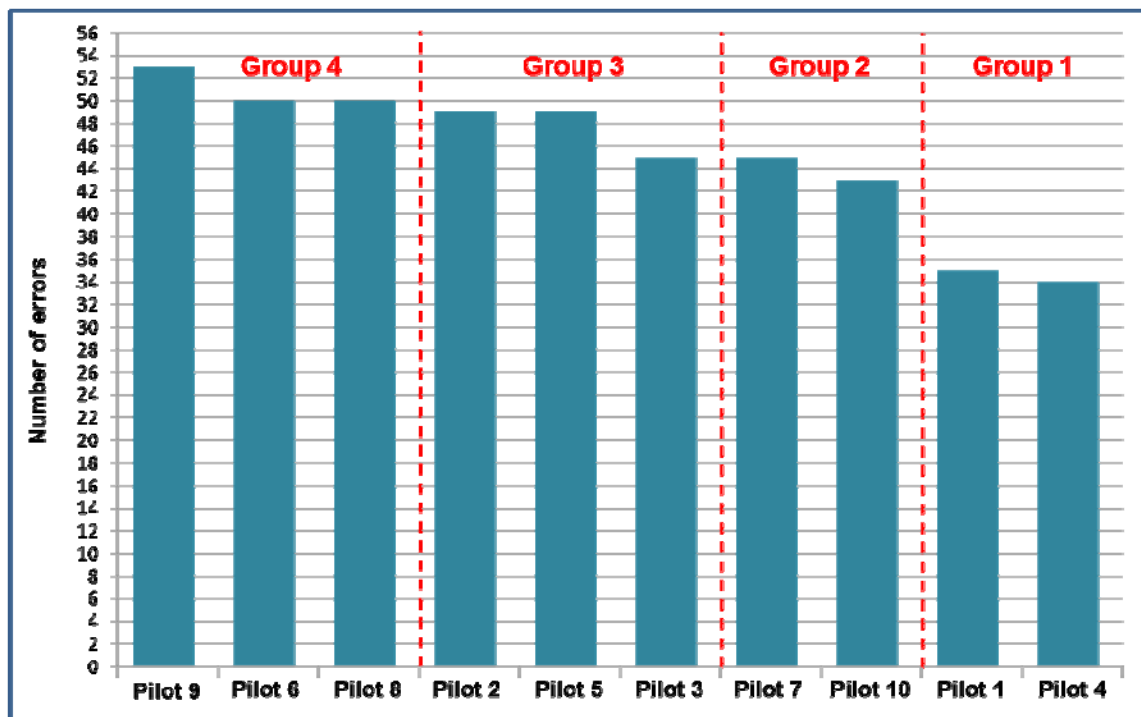
Fig. 3. The total number (sum) of errors committed by pilots during the execution of tasks in accordance with scenario No. 2
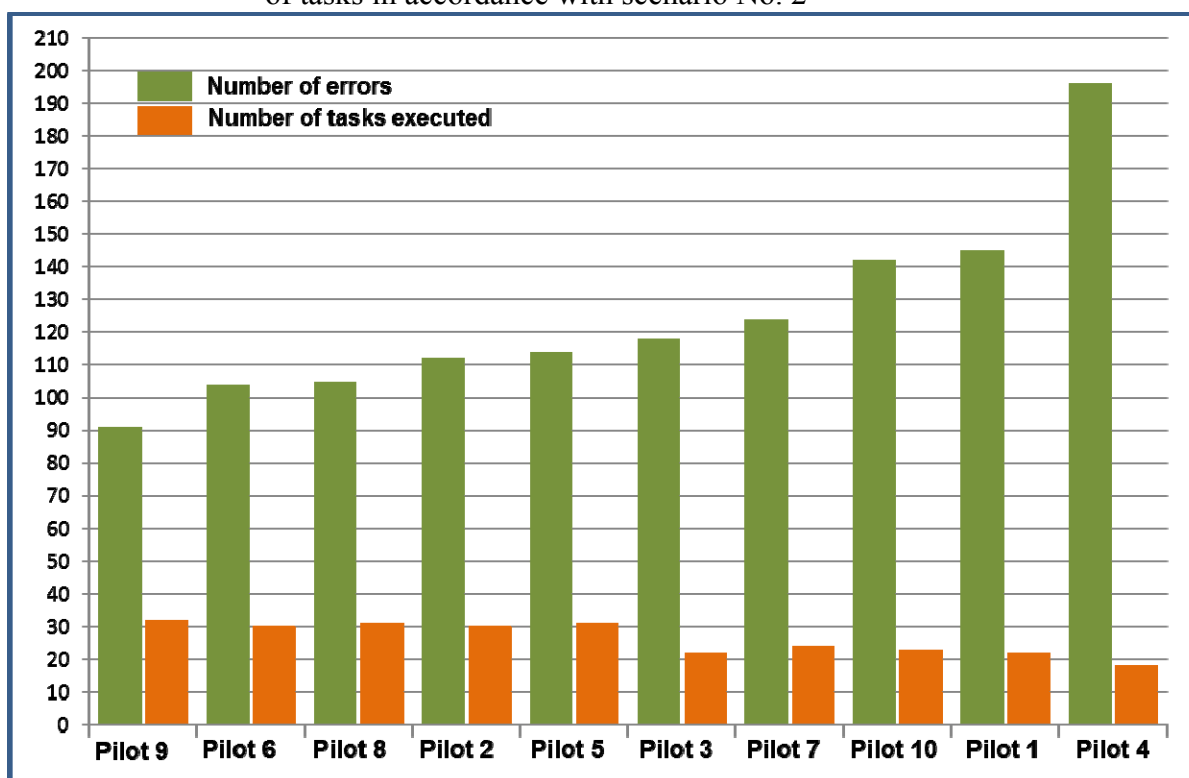
Fig. 4 Sums of the numbers characterizing the errors made during the task execution by the pilots, and the execution of tasks during an emergency situation according to the developed scenarios No. 1 and No. 2 (▬ number of errors ▬ number of tasks executed)

Analyzing the number of errors made and the tasks executed, one can conclude that during the execution of tasks in accordance with scenario No. 1 and No. 2, pilot No. 6 was best prepared for the emerging situations, whereas pilot No. 2 was the worst.

Acting in accordance with the presented scheme does not allow one to draw definite conclusions concerning the proper way of approaching the problem of pilot training. The characteristics under analysis are different in their nature, and it cannot be decided unequivocally which pilot has to undergo additional training and which does not, and what number of additional flights will allow a given pilot to acquire the appropriate responses to simulated specific situations in

the air. At the same time, there is a noticeable decrease in the number of errors as a function of the number of repetitions of a given scenario.

Basic statistics, including mean values and standard deviation, were calculated on the basis of the data obtained during the simulation of specific situations that characterized the level of training of a particular group of pilots who executed tasks using an F-16 aircraft simulator.

Presentation of these values in a scatter graph [Figure 5] allows for the disclosure of the four basic structures of meeting the requirements by pilots involved in the training system. Those structures have been defined on the basis of an analysis of the number of errors made in emergency situations.
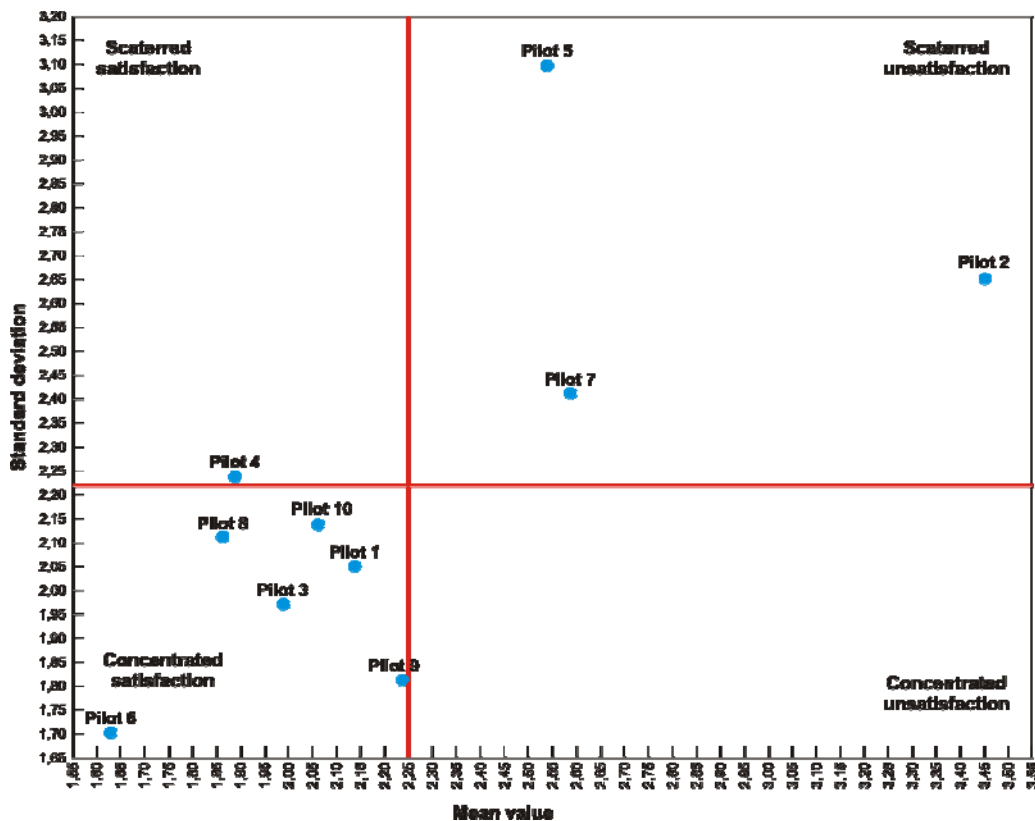
Fig. 5 Distribution of meeting the requirements by pilots, obtained on the basis of error analysis results.

The system is characterized by concentrated satisfaction with the results

achieved by pilots, No. 1, 3, 6, 8, 9, and 10. Scattered satisfaction relates to pilot No. 4.

Scattered dissatisfaction relates to pilots No 2, 5, and 7.

"HENRI COANDA"
AIR FORCE ACADEMY
ROMANIA

"GENERAL M.R. STEFANIK"
ARMED FORCES ACADEMY
SLOVAK REPUBLIC

INTERNATIONAL CONFERENCE of SCIENTIFIC PAPER
AFASES 2014
Brasov, 22-24 May 2014

Basic statistics, including mean values and standard deviation, were calculated on the basis of the data obtained from the analysis of information characterizing the level of pilot training, and on the basis of numbers characterizing the execution of specific tasks for a specific group of pilots, who were assessed using an F-16 simulator. Presentation of these values in the scatter graph [Figure 6] allows for the disclosure of the four basic structures of meeting the requirements by pilots involved in the training system. Those structures have been defined on the basis of an analysis of the number of errors committed during the execution of specific tasks.
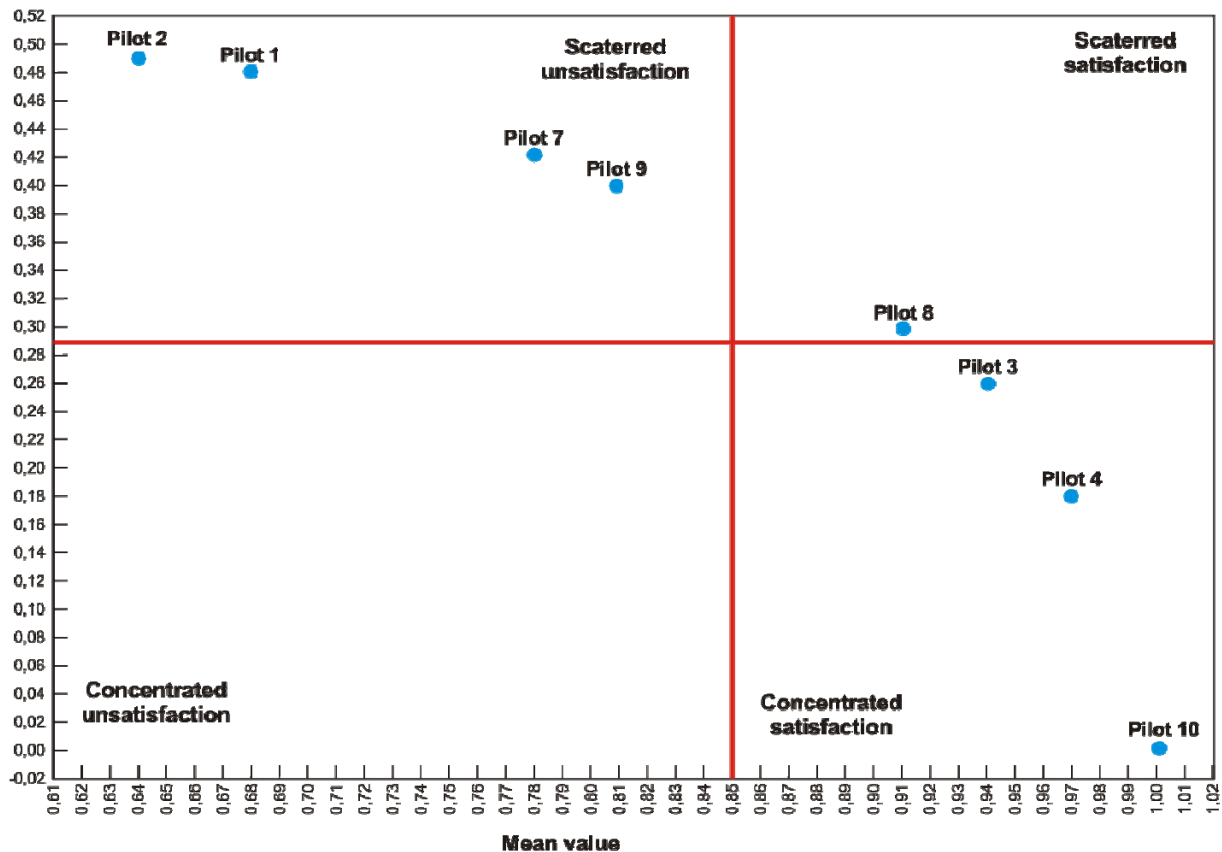
Fig. 6. Distribution of meeting the requirements by pilots, obtained on the basis of the number of executed tasks

.

The system is characterized by concentrated satisfaction with the results achieved by pilots, No. 3, 4, 6, and 10. Such a situation is perceived by the training system in a coherent and consistent manner.

Scattered satisfaction relates to pilot No. 8. Scattered dissatisfaction relates to pilots No. 1, 2, 5, 7, and 9.

Scattered dissatisfaction frequently results from errors in the adaptation of pilots to the specific requirements of the training system.

The training system is characterized by a lack of concentrated dissatisfaction with the results obtained by the pilots in the simulator training, and determined on the basis of the number of errors made during emergency situations and the execution of specific tasks. It can, therefore, be concluded that the training system is functioning properly and there is not a single pilot who would not have achieved any results within the framework of a functioning training system

The analysis conducted in this manner does not allow for a holistic approach to the problem of assessing the level of training of the pilots on the basis of the results obtained in the simulator tests. However, it was possible to identify the elements common to the number of errors committed and the number of tasks executed. Pilots were divided into training groups in accordance with the analysis conducted in this manner. Group 1 (achieving the best results) includes pilots No. 6 and 10, group 2 includes pilots No. 4 and 3, group 3 consists of pilots, No. 1, 5, and 8, whereas group 4 consists of pilots, No. 7, 2, and 9.

The advantages of using flight simulators in daily professional development training of military pilots which have been presented in this chapter point to the fact that flight simulators are an effective tool for the development of the essential elements that affect the level of air mission execution safety tasks, including the desired degree of situational awareness The confirmation of this thesis may be made by the recommendations of the UK Royal Air Force (RAF) following a large number of air accidents which resulted from the introduction of jet aircraft in 1960's. One of the key corrective actions aimed at preventing the similar events in the future was the decision to purchase flight simulators and intensify simulator training of jet pilots.

CONCLUSION

Regardless of the type of aviation and the stage of flight training/professional development, flight simulators are a widely used pilot training tool. The results of reference literature analysis, expert opinions, flight simulation studies, and the author's own air permit the conclusion that the essential benefits of the flight simulator, including those relevant to the pilot's situational awareness can include the following:

1. *High training effectiveness*. The tests related to measuring the effectiveness of flight simulation training demonstrated that the trainees develop knowledge and skills at a level similar to that achieved in a real flight. During simulator training, due to lack of necessity to physically control the aircraft, the instructor can fully focus on the student and the activities that the student performs. Modern simulators support the function of recording and collecting data from simulated air operations carried out during the training. This facilitates multiple analyses of the compatibility of flight parameters as defined in the exercise scenario with the values registered during the training flight.

2. *Maintaining high standards of training safety*. Due to the necessity of maintaining a certain level of safety during training, simulators sometimes provide the only way to learn some maneuvers, the elements of air operations performed in the event of dangerous weather conditions (wind shear, turbulence, icing, jet streams, etc.). Performing the above-mentioned maneuvers in a real flight would involve putting the trained crew at high risk. A similar situation occurs in the event of critical aircraft component failure, including, among other things, failures concerning the engine, flight instruments, or control systems, etc.

3. *Availability*. The fact that the use of the flight simulator in flight training is not dependent on the current ambient weather conditions, the state of the airport, or the good working condition of ground navigation equipment allows for a more methodical approach to the training from the human factor perspective. Moreover, it is possible to simulate non-routine in-flight situations without the necessity to wait for their occurrence in the real air mission execution environment.

4. *Repeatability*. The simulator does not require the implementation of the full cycle of a given air operation (pre-flight check,

"HENRI COANDA"
AIR FORCE ACADEMY
ROMANIA

"GENERAL M.R. STEFANIK"
ARMED FORCES ACADEMY
SLOVAK REPUBLIC

INTERNATIONAL CONFERENCE of SCIENTIFIC PAPER
AFASES 2014
Brasov, 22-24 May 2014

take-off, mission execution, landing, psot-flight check) to discuss and repeat a specific part of the exercise by the trainee. It facilitates the repetition of each flight element and making breaks for an exchange of views between the trainee and the instructor.

5. *Predictability*. Simulator training prevents the occurrence of such dangerous phenomena as air traffic collision, wind shear, icing, weather deterioration, turbulence, closure of airports, etc. Of course, all of these situations are possible to simulate, but the exercise of this kind are carried out by the trainee at the time specified by the instructor, according to the trainee's progress made in the training.

6. *"Learning from mistakes"* – with unlimited possibilities of applying a number of ways to solve an in-flight operational problem with "zero" risk level, the simulator allows the student to select the solution which is the most optimal from his perspective and to test it. This capability allows the trainee to physically "prove to himself" that some solutions considered by him to be more useful and safer than those recommended by the instructor or the instruction manuals are not a good option in operational reality and, consequently, they are eliminated by the trainee once and for all.

7. *Maintaining pilot currency and proper attention allocation*. Systematic training exercises on the flight simulator allows the trainee to consolidate the desired habits (maintain pilot currency) and, what is equally important, allows him to permanently master the optimal attention allocation in various phases of the air mission execution. It allows the beginner pilot, on the other hand, to adequately master the basic elements of cockpit preflight check and such actions as

starting up the engine and other aircraft equipment. This allows both to save the time and reduce the costs of practical training.

8. *Credibility as a tool applied in air accident investigation*. Flight simulators ensure accurate *reconstruction* of flight conditions, the situation onboard, and the evaluation of the actions taken by the crew of the aircraft in the event of an undesirable flight-related event. The conclusions of these analyses and corrective actions taken in the aspects related to the event – the pilot-operator, the aviation organization, the environment, the aircraft allow to avoid or safely respond to undesirable flight-related events in the future.

9. *Simulators can be used for training for the prototype aircraft under design, or aircraft employing new solutions (systems)*. Performing this task in practice, without the prior simulation and practice of selected flight maneuvers could be associated with a high level of risk and, in extreme situations, with high probability of undesirable flight-related event.

10. *High comfort of performing the training tasks by the instructor*. An undoubted advantage of the flight simulator in comparison with the aircraft is the fact that the instructor can focus his attention fully on the trainee and the task performed. Equipping the simulator with a module recording the operating parameters, including the correspondence between the instructor and the trainee, allows for deep analysis of multiple elements of the flight in order to draw the appropriate conclusions and facilitates methodological development of corrective

actions to be taken in relation to the trainee[33]. In contrast to a training flight conducted in the real mission environment, the instructor may but does not have to immediately correct to the trainee's errors. The instructor's actions may only amount to monitoring the situation on board the aircraft in a particular mission execution environment, and assessing the trainee's response time to committed errors. Such a situation is favorable in that the trainee can fully see the effects of his improper actions on board the aircraft. In real flights allowing such a situation could lead to an excessive risk of an undesirable flight-related event.

11. *OPTIMIZING THE USE OF financial RESOURCES*. THE USE OF THE SIMULATOR CAN SIGNIFICANTLY REDUCE THE TRAINING COSTS as COMPARED TO THOSE INCURRED FOR THE USE OF THE AIRCRAFT. FURTHERMORE, SIMULATOR TRAINING IMPLEMENTED INSTEAD OF THE TRAINING ON THE AIRCRAFT ALLOWS FOR SIGNIFICANT SAVINGS RESULTING FROM THE extended *service life* OF THE AIRCRAFT. TAKING INTO ACCOUNT the DETAILED ANALYSIS OF THE COST vs. EFFECTIVENESS RELATIONSHIP, ORLANSKY AND STRING PROVED THAT THE COSTS OF APPLYING FLIGHT SIMULATORS IN THE TRAINING OF MILITARY FLIGHT PERSONNEL ACCOUNT FOR 5%–20% of the cost OF THE SAME OPERATION PERFORMED ON trainer AIRCRAFT. THIS ALLOWS FOR the

REDUCTION OF THE FLIGHT TRAINING COST ON AVERAGE by approximately 12%. THEY ALSO FOUND THAT COMMERCIAL AVIATION ORGANIZATIONS CAN EXPECT A RETURN OF THE TOTAL PURCHASE PRICE OF THE SIMULATOR WITHIN APPROXIMATELY 9 MONTHS, AND THE RETURN OF THE COSTS OF THE NECESSARY TRAINING FACILITIES WITHIN ABOUT two years.

12. *The use of simulators significantly reduces the number of hours flown by the trainee,* which is beneficial for aircraft operating costs, and the costs resulting from the use of airspace and airports, both controlled and uncontrolled.

Despite the advantages mentioned above, no simulator can currently be defined as a device that can replace the hands-on training in the air. It is still considered as a very important form of preparing or supplementing practical training in the air.

The use of flight training simulator, like any other training device, has a number of disadvantages, which can include:

1. *Purchase price of the* simulator. The most important barrier resulting in a limited number of simulators available in our country is their purchase price.

2. Insufficient levels of environmental impact on the trainee which is present in real air operations. In a simulated emergency (dangerous weather phenomenon, onboard system failure), the trainee does not experience the same degree of stress as in the case of the same situation enocuntered in the air. However, mastering the proper execution of actions related to a specific emergency situation using the simulator makes it easier to take appropriate action in the event of encountering a similar phenomenon in the air. On the other hand, because of too strict adherence to procedures and not allowing the trainee to experiment and learn from mistakes in preventing dangerous situations during simulator training, the trainee is not able to move beyond the learned schema, and thus is often not able to properly respond to a non-routine situation in the air. This usually leads to an undesirable flight-related event. The proof of that is provided by the results of

---

[33] The simulator facilitates collecting the flight data related to the level of compliance. As a part of the diagnostic process, the instructor-pilot can compare the established criteria of conducting a given exercise with those defined by the recorded flight parameters. In addition, the instructor can make a comparative analysis of the quality of performing the tasks by trainees who are at the same stage of training (the diagnosis of the state). Having the results of progress made by the trainee during the training, the instructor can understand more deeply the causes of mistakes made by the trainee, and offer him a new approach to an element of the exercise, which will allow him to achieve acceptable results. The instructor may also evaluate the feasibility – measurability of the quality of performing various elements of the exercise can be used to enhance the effectiveness of training by changing the approach to the training of selected elements of the exercise.

"HENRI COANDA"
AIR FORCE ACADEMY
ROMANIA

"GENERAL M.R. STEFANIK"
ARMED FORCES ACADEMY
SLOVAK REPUBLIC

INTERNATIONAL CONFERENCE of SCIENTIFIC PAPER
AFASES 2014
Brasov, 22-24 May 2014

studies conducted by a NASA research team who used the data from the Aviation Safety Reporting System (ASRS).

3. Shorter flight duration in comparison with real flights. Too frequently, selective treatment of certain flight elements causes the effect of mental fatigue and weariness to occur during simulator training with less severity than in a real flight. As a result, it is difficult to assess the resistance of the trainee to weariness or mental fatigue usually present in *long lasting flights*.

4. No faithful reproduction of "radio traffic reality" of the real mission environment. While conducting simulator training, instructors often place less importance on the so-called "radio traffic reality". Because of that, the trainees with less operational experience have difficulty in understanding the radiotelephony communication and performing air operations in the "congested" areas of controlled aerodromes.

Currently, flight simulators, in addition to aircraft are considered as one of the essential tools for selection, training, and developing/maintaining currency of flight crews. They are also viewed as a reliable tool for testing pilot knowledge and skills in specific aspects of aircraft operation and air mission execution. Because of the above-mentioned advantages of these devices, simulator training, in addition to theoretical and practical training in the air, plays a crucial role in shaping the competencies needed to achieve the desired level of situational awareness by the pilot at various stages of air mission execution. Therefore, the use of these devices for forming and consolidating the pilot capabilities necessary, among others, for the efficient execution of the situational awareness process should be considered as justified.

BIBLIOGRAPHY

1. A. Bondaruk, *Badanie wpływu uszkodzeń i niesprawności samolotu wielozadaniowego na bezpieczeństwo lotów"*, Praca doktorska, ITWL, Warszawa 2011.
2. A. Bondaruk, *Metodyczne uwarunkowania konstruowania programów szkolenia symulatorowego*, Konferencja naukowa "Instruktor przygotowujący do zawodów trudnych I niebezpiecznych", Dęblin II. 2014.
3. Bezdek W., Powell R., Mays D., *The history and future of military flights simulators,* AIAA modeling and simualation technologies conference and exhibit – 2004, Providence, RI, AIAA Paper 2004 – 5148
4. Compa T., Rajchel J., *Podstawy nawigacji lotniczej,* WSOSP, Dęblin 2011
5. Harris K.A., Harris D., Computer-based simulation as an adjunct to ab initio flight training, International Journal of Aviation Psychology N° 8/1998
6. Hays R.T., Jacobs J., Prince C., Salas E., *Fligcht Simulator training effectiveness. A-meta-analysis,* Military psychology N° 4/1992
7. Leszczyński R., *System selekcji kandydatów do Sił Powietrznych,* Praca badawcza, WSOSP, Dęblin 2000
8. Lintern G., Roscoe S.N., Koncoe J.M., Segal L.D., *Transfer of landing skills i beginning flight training.* Human Factor N° 32/1990

9. Macharella N.D., Arban P.K., Doherty S.M., *Transfer of training from flight training devices to flight for ab initio pilots*, International Journal of Applied Aviation Studies N° 5/2005; A.T. Lee, Flight Simulation, ASHGATE, Burlington 2005
10. Marlinussen M., Hunter D.R., *Aviation psychology and human factors*, CRC Press, New York 2010
11. Moorman T.R., *The civilian looping military*, MS&T Magazine, N° 6/2002
12. Multi-author work, *Słownik współczesnego języka polskiego*, PWN, Warszawa 1996
13. Pielacha R., *Imitatory kierowania samolotami w kształtowaniu nawigatorów wojskowych*, Research Study, PAFA, Dęblin 1994
14. Szczepański C., *Symulatory lotnicze, stan i perspektywy* – report , Warszawa 1998
15. Terelak J., *Higiena psychiczna i pilot*, MON, Warszawa 1975
16. Vaden E.A., Hall S., *The effect of simulation platform motion on pilot training transfer: A meta-analysis*, International Journal of Aviation Psychology N° 15/2005

THE DRIVELINE ANALYSIS OF
HYPER SUSTENTATION DEVICES

Doru LUCULESCU

Air Force Academy "Henri Coandă" Braşov

Summary: *The flaps is a device used for the expansion of the hyper sustentation flight envelope. The flaps kinematics driveline control mechanisms require a dimensional study by dimensional parameterization kinematic rods and bearings used. This paper presents an optimized driveline analysis of the flaps control.*

Key words: *flaps, driveline, kinematics analysis, depending on the position.*

1. INTRODUCTION

The flaps is a hyper sustentation device placed usually at edge of the wing (aerodynamic surface) which works on the voucher principle, see Figure 1.1. The flaps role is to increase the coefficient lift by changing the local geometry. The flap actuation leads to a change in curvature of the wing that will produce an increase in lift at the same speed or a reduction in the constant incidence rate.

Fig. 1.2 Types of flaps placed on the edge of the wing

Fig.1.1 The effect of operating flaps

A series of papers [3, 5, 11] presenting the type of flaps highlighted in Figure 1.2.

Fig. 1.3. Flaps down Cessna 172

Fig. 1.4. Flaps down L-29 Delfin [4]

According to the papers [8, 9, 10] the introduction of smart materials and system drive control surfaces define the concept of morphing (biologically inspired) which deleted the joints, the structure of the bearing surfaces being flexible.

2. KINEMATIC ANALISYS

2.1. Defining the components

The kinematics of mechanisms from command driveline of the flaps requires a rigorously dimensional study to prevent buckling phenomena and reduce the friction and the kinematic parameterization games in the rods and bearings.

The flaps actuator transmits force and motion in the powertrain, which includes sticks scenes and kinematic coupling elements with different degrees of freedom [1].

The voucher command includes a number of constructive landmarks, such as the control lever assembly, support for indexing, control rods, bearing assembly, lever assembly, damper, fasteners (screws, nuts, washers, split pins), [2]. In Figure 2.1 is shown a rigid driveline (plan) for actuating the flap, where B is the retracted position of the flap (0^0) and the flap position is removed (25^0).

Fig. 2.1 The kinematic mechanism for operating the rigid flaps
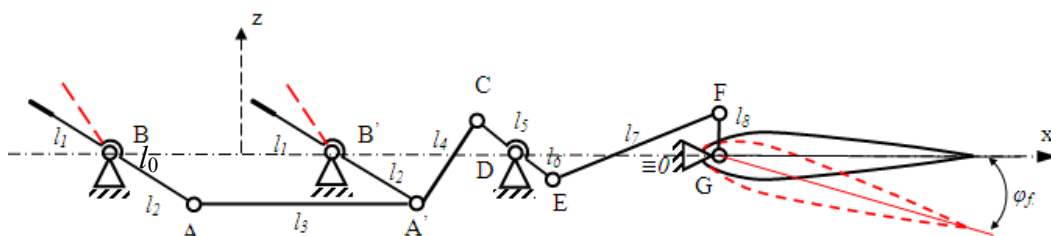
Fig. 2.2 Rigid kinematic mechanism for actuating the flaps (CAD solution)

2.2.Theoretical considerations.

The kinematic analysis of the articulated plan mechanism analyzed previously assumed structural analysis of kinematic couplings resulting connectivity, the number of independent contours, namely mobility mechanism. Based on kinematic scheme and the law of motion it is necessary to determine the intrinsic kinematic

"HENRI COANDA"
AIR FORCE ACADEMY
ROMANIA

"GENERAL M.R. STEFANIK"
ARMED FORCES ACADEMY
SLOVAK REPUBLIC

INTERNATIONAL CONFERENCE of SCIENTIFIC PAPER
AFASES 2014
Brasov, 22-24 May 2014

parameters mechanism (defining parameters) and the independent coordinates (input data).

The necessary reference system is adopted and the flap actuator relations between the unit vectors of the reference relatively to the base. In every contour considered a independent mechanism we each attach our own verse and fixed unit vector establish our own basic expressions for reference system. The stated problem for the analyzed case, is the vector equations which is written for each of the independent contours closing mechanism.

The equations reveal the unknown vector and closing through appropriate algebraic operations, we determined the necessary scalars and most importantly the law of motion transmission. We can determine successive derivations which require angular velocity and acceleration kinematics torso writing (reduced appropriately to chosen points). To control the flaps mechanism in the embodiment shown in Figure 2.2 it is necessary to determine the speed and acceleration functions.

We took into consideration the geometry mechanism in Figure 2.2 and Table 2.1 data analysis.

Tabel 1. Data analisys

Element antrenare $l_1 l_2$	500 mm
Element execuție l_9	500 mm
Timp de analiză	3s

Unghi levier φ_1	40^0
Unghi flaps φ_9	45^0

According to [7] we can define the kinematic mechanism function:

Conform [7] putem defini funcția cinematică ale mecanismului:

$$\varphi_{nj} = \varphi_{nj} \cdot (\varphi_{li}, l_k, \alpha_k) \qquad (1)$$

Depending on the position of the mechanism it is analyzed as:

$$\varphi_f = \varphi_l(\varphi_i, l_1, l_2, l_3, l_4, l_5, l_6, l_7, l_8) \qquad (2)$$

where φ – parameter position

2.3. The kinematics analysis of the control mechanism of the flaps.

For the kinematic analysis, we used a software tool called Artas SAM 6.1. This is an interactive software environment for the design, analysis, synthesis and optimization of planar mechanisms. SAM integrates a numeric preprocessor and post-processing analysis of animation and graphic display of parameters. The mathematical model is based on finite elements with a large number of characteristics allowing a unified approach for a number of highly complex mechanisms (ex. planetary gears). SAM 6.1 has a number of tools such as: design and modeling mechanisms, CAD interface, optimization mechanisms, post-processing and analysis of results [6].
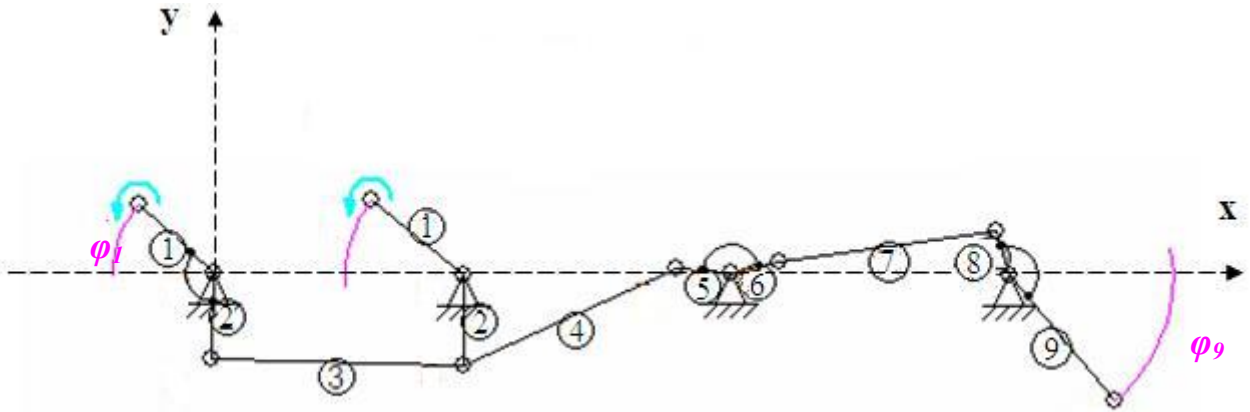
Fig. 2.3 The kinematic representation of a optimized rigid flap actuator SAM 6.1

Element 1/2 – control levers   *Element 5/6 şi 8 – sticks*
Element 3, 4 şi 7 – link connections   *Element 9 – flaps*

Fig. 2.4 Kinematic characteristics

Fig. 2.5 Flaps coordonates

Tabel 2.1. Kinematic characteristics

Time [s]	x(1) [m]	y(1) [m]	x(9) [m]	y(9) [m]
0	0.576	1.187	3.7	0.272
0.5	0.545	1.157	3.703	0.276
1	0.519	1.124	3.744	0.33
1.5	0.497	1.088	3.799	0.416
2	0.479	1.05	3.857	0.536
2.5	0.467	1.009	3.907	0.703
3	0.461	0.967	3.926	0.949

3. CONCLUSIONS & ACKNOWLEDGMENT

3.1. Conclusions

The kinematic analysis of the mechanism can build a driveline of dimensional design commands for a simple type of damper flap.

We analyze the kinematic mobility (l_1, l_2) and a kinematic running element (l_9) separately and have the characteristics shown in Figure 2.4 and 2.5, values in Table 2

"HENRI COANDA"
AIR FORCE ACADEMY
ROMANIA

"GENERAL M.R. STEFANIK"
ARMED FORCES ACADEMY
SLOVAK REPUBLIC

INTERNATIONAL CONFERENCE of SCIENTIFIC PAPER
AFASES 2014
Brasov, 22-24 May 2014

3.2. Acknowledgment

The authors wish to thank the "Henri Coandă" Air Force Academy of Braşov for supporting the research necessary for writing this article.

BIBLIOGRAPHY

1   Creţu Mariana-Simona, *Mecanisme, Analiză structurală – teorie şi aplicaţii,* Editura Sitech, Craiova, 2010, ISBN 978-606-11-0760-5, 160p

2   ICA Braşov, *Catalog piese de schimb, comandă volet, avion IAR 28MA*, 1984, 41p

3   McCormick, B. W., 1994, "Aerodynamics, Aeronautics, and Flight Mechanics", 2nd Edition, Wiley

4   http://www.airliners.net/photo/Aero-L-29-Delfin/1887338/L/

5   Rebbello da Silva B.M., Mattos B., and others, *Flap Optimization for Take-off and Landing*, Proceedings of the 10th Brazilian Congress of Thermal Sciences and Engineering, ENCIT 2004, Rio de Janeiro, Brazil, Paper CIT04-0229, 10p

6   Artas, *SAM 6.1 The ultimate mechanism designer, manual* 2010, 160p.

7   Luculescu, D., Lazăr, I. (2008) - *Cinematica mecanismelor plane*, Editura Academiei Forţelor Aeriene "Henri Coandă" din Braşov, ISBN 978-973-8415-65-2, 2008, 218p

8   Cîrciu I., Prisacariu V., *Commnad and control of the flying wing in the morphing concept,* Review of the Air Force Academy, no.1(23)/2013, ISSN 1842-9238, p13-18

9   Prisacariu V., Sandru V., Rău C., *Introduction morphing technology in unmanned aircraft vehicles (UAV),* International Conference of Scientific Paper, AFASES 2011, Brasov, 26-28 May 2011, Romania, available at http://www.afahc.ro/site_nou/ro/afases/2011/uav/Prisacaru_SANDRU_RAU.pdf

10 Prisacariu V., Cîrciu I., Boşcoianu M., *Morphing concept of UAVs of the swept flying wing*, Recent journal, ISSN 1582-0246, vol.15, 1(41) march 2014, p.26-33

AIR FORCE

PRECISION APROACH SYSTEM BASED ON GLOBAL NAVIGATION SATELLITE SYSTEM

Eduard MIHAI

"Henri Coandă" Air Force Academy, Brasov, Romania

Abstract: This paper will present an intelligent system for high precision approach. The current core satellite constellation is unable to provide accuracy and integrity to achieve precision approach. This system uses the concept of differential corrections to augment satellites signal in order to meet these requirements.

Keywords: navigation, satellite, augmentation, approach, GLS

1. INTRODUCTION

Unfortunately, typical, ground-based navigation aids failed to keep up with the global navigation requirements and modern aircraft. The old method of navigation through the use of a sextant and dead reckoning is just not adequate for modern day systems. The development, initially by the United States, of a global system providing positioning and timing services allowed the introduction of an alternative to those conventional navigation and approach aids with the possibility of using new concepts in air navigation capable of satisfying the new needs of the aeronautical community.

The International Civil Aviation Organization (ICAO) had actively promoted the use of Global Navigation Satellite System (GNSS). A wide area of applications have already demonstrated the enormous benefits to be gain from onboard Global Positionong System (GPS) receivers, including safety enhancements. In air operations, GPS accuracy streamlines enroute and terminal navigation, thereby reducing flight times and ultimately fuel consumption. Since it is a three-dimensional system, descent, approach, and landing operations can be monitored more closely.

Today, GPS is used on land, sea, and in the sky to provide life saving information to navigation systems around the earth.

2. GROUND-BASED AUGMENTATION SYSTEM

For precision approach, standard GPS information alone does not offer the required quality level. The Ground-Based Augmentation System (GBAS) is a system that provides enhanced GPS positioning to aircraft with the accuracy, integrity, continuity and availability that precision approaches demand.

The GBAS principle relies on differential corrections of the GPS signal. A ground station is fitted with a number of GPS receivers. Given the pin pointed position of the receivers, errors in the received signal can be measured and corrections calculated. Together

with final approach information this corrections are transmitted to the aircraft via Very High Frequency Data Broadcast (VDB). The aircraft benefits from accurate lateral and vertical positioning enabling procedure approach and landing operations.

GBAS works based on three segments: satellites constellation, ground station and aircraft receiver, as shown in Figure 1.
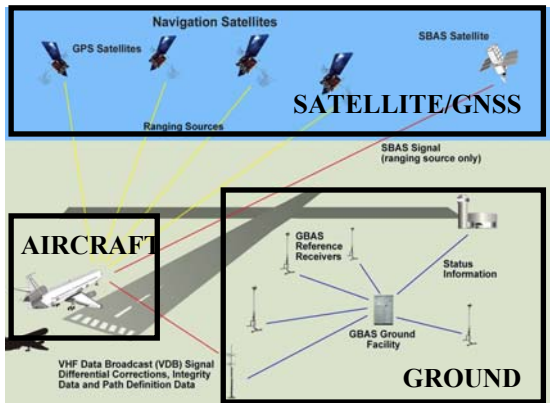
Figure 1 – GBAS architecture

• **Satellite subsystem:**
 – provides satellite status, position and timing signal;
 – has sufficient number of satellites to determine user position.
• **Ground subsystem provides:**
 – pseudorange corrections for each satellite in view;
 – integrity of aircraft subsystems (protects against satellite signal errors, ground subsystem errors and anomalous ionospheric errors);
 – approach paths (Final Approach Segment – FAS – for all runway ends);
 – local tropospheric parameters, necessary to adjustment;
 – predicted availability for precision approaches and estimates aircraft protection levels against alert limits.
• **Aircraft Subsystem:**
 – applies broadcast pseudorange corrections (PRC's);
 – computes position using corrected PRC's only;
 – computes deviations from broadcast approach path;
 – determines if GBAS Landing System (GLS) approach is safe;

 – follows desired approach path to decision height – continue with GLS approach or execute missed approach.

3. GBAS BENEFITS

Why is GBAS such a good system? It allows to fly very accurately approaches to airfields or towards runways, but with a ground installation which is more simpler, more cheaper and more flexible than the Instrumental Landing System (ILS).

One GBAS station can support multiple runway ends and reduce the total number of systems at an airport. With one ground station on an airfield you can feed all the runways and fly GLS approaches to all those fields with just one station which is located inside the airfield. A GBAS is sited to minimize critical areas which place fewer restrictions on aircraft movement during ground taxi and air operations. ILS requires one frequency per system and GBAS requires one VHF assignment for up to 48 individual approach procedures. This reduces the Very High Frequency (VHF) requirements and simplifies airport infrastructure. Also, GBAS requires less frequent flight inspections compared to those required of ILS systems.

From a pilot's point of view, GBAS has been architected to work identically to ILS (figure 2). The only difference is the nomenclature the pilot sees on the display and, instead of tuning into a frequency, they now tune a channel to select a specific procedure. From a flying perspective, it is identical to ILS, which simplifies training. No specific simulator training or checking is required as pilots.

Figure 2 – GLS and ILS flight display

"HENRI COANDA"
AIR FORCE ACADEMY
ROMANIA

"GENERAL M.R. STEFANIK"
ARMED FORCES ACADEMY
SLOVAK REPUBLIC

INTERNATIONAL CONFERENCE of SCIENTIFIC PAPER
AFASES 2014
Brasov, 22-24 May 2014

"You fly the same, you have the same signals you have the same information instead of reading ILS here you read GLS here, instead having here a frequency you read what we call a channel, but for the rest, is exactly the same thing. You fly exactly the same way".[8]

3. CONCLUSIONS

The future of GNSS appears to be virtually unlimited. The aviation industry is developing the GBAS, a new positioning and landing system that integrates satellite and ground-based navigation information.

In conclusion, potential benefits of the GLS include significantly improved takeoff and landing capability at airports worldwide at reduced cost, instrument approach service at additional airports and runways, and eventual replacement of the ILS.

REFERENCES

1. Article. *Source.* [online]. Available: http://instrument.landing-system.com (accessed at March,2014)

2. BONNOR, A. C. N., A Brief History of Global Navigation Satellite Systems, *The Journal of Navigation,* Volume 65 (2012)

3. EUROCAE ED-114 - *Minimum Operational Performance Specification for Global Navigation Satellite Ground Based Augmentation System Ground Equipment to Support Category I Operations* – EUROCA

4. ICAO, *Annex 10 to the Convention on International Civil Aviation,* Volume I Radio Navigation Aids', International Civil Aviation Organization, Sixth Edition (2006);

5. ICAO, *Annex 14 to the Convention on International Civil Aviation* International Civil Aviation Organization, Sixth Edition (2006);

6. ICAO, Doc 8071, Vol. II - *Manual on Testing of Radio Navigation Aids, Testing of Satellite-based Radio Navigation Systems*, Fifth Edition, 2007

7. ICAO, *Guide for Ground Based Augmentation System Implementation,* 2013

8. Tarnowski, E. Airbus Indsutrie Engineering Test Pilot. *Source.* [online]. Available: https://www.youtube.com (accessed at March,2014)

AIR FORCE

GAS SENSORS FABRICATED BY LASER-INDUCED FORWARD TRANSFER

Alexandra PALLA PAPAVLU*, Fabio DI PIETRANTONIO**, Domenico CANNATÀ**, Massimiliano BENETTI**, Enrico VERONA**, Valentina DINCA*, Thomas LIPPERT***, Maria DINESCU*

*Lasers Department, National Institute for Lasers, Plasma and Radiation Physics, 077125 Magurele, Romania, **"O.M. Corbino" Institute of Acoustics, Italian National Research Council–CNR, Via del Fosso del Cavaliere 100, 00133 Rome, Italy, ***General Energy Research Department, Paul Scherrer Institut, 5232 Villigen PSI, Switzerland

Abstract: This work summarizes the developments in dynamic release layer (DRL) assisted LIFT of complex materials such as polymers, biomolecules, or carbon nanotubes for applications as recognizing elements in miniaturized surface acoustic wave (SAW) resonators and chemiresistor devices.
As the functionality of such sensors depends on the applied laser source, target material, and transfer geometry, first an optimization of the process parameters is reported.
Following a morphological and structural characterization of the active material, the performance, i.e. the sensitivity, resolution, and response time of the laser-printed devices was evaluated by exposure of the sensor arrays to different toxic vapors. Different sensitivities and selectivity to the selected chemical agents i.e. dimethyl methylphosphonate, dichloromethane, dichloropentyhane, ethyl acetate, etc. have been measured thus proving the feasibility of LIFT for applications in sensors and biosensors.

Keywords: laser-induced forward transfer, surface acoustic wave, sensors, chemiresistors

1. INTRODUCTION

Environmental m onitoring due to air pollution is a problem of current interest both for the industry, i.e. automotive (d etection of polluting gases from cars) as well as for m any research groups. Since sensors are the m ain components in products and system s used to detect volatile organi c com pounds (VOCs) in air, there are always new and innovative sensor technologies em erging. Several key requirements for sensors include sensitivity, the m inimum concentration of target gases

they can detect, respon se speed, re versibility, energy consumption, and fabrication costs [1].

A wide variety of natural occurring substances (such as cells, enzym es, receptors, and antibodies) are commonly used as sensing elements in sensor technology. Besides these biological m aterials, polym ers and carbon nanotubes (CNTs) are used as active m aterials in gas sensors.

Polymers are used as recognition elem ents in sensor structures, due to their wide range of capabilities [2]:

1. Polymers can collect and concentrate vapor m olecules on sensor s urfaces by reversible sorption.

2. They can be applied on device s urfaces as thin adherent films.

3. Their chemical sele ctivity is d etermined by the chemical s tructure, which can be varied easily through synthetic design.

4. They can yield sensors with rapid, reversible, and reproducible responses.

5. Diverse sets of polym ers can be assembled rationally for sensor arrays.

In addition to polymers, single walled carbon nanotubes (SWCNT) are prom ising chemical sensing materials, due to their hollow structure, one-dim ensional nanoscale morphology, and high specific surface area that benefits physical adsorption or chem ical reaction with targ et molecules f or signal transformations with h igher efficiency and speed [3,4].

The applicability of devices based on polymer or SW CNT systems has been lim ited by the complexity as sociated with the dev ice fabrication. An inter esting a lternative to conventional printing techniques is laser-induced forward transfer (LIFT). LIFT is free from clogging problem s, which are characteristic for inkj et printing, and avoids the use of expensive ph otolithographic masks. LIFT presents also a higher potential for integration than ano ther possible deposition methods, e.g. microspotting.

This techn iques is versatile and allows printing a wide class of m aterials i.e. inorganic inks and pastes, m etals, oxides, polym ers and biological materials in solid or liquid phase [5-15]. In LIFT the mater ial of inte rest is transferred by the laser beam from a transparent support (donor substrate) onto an appropriate substrate (receiver). For improving the process efficiency and reducing the risk of damaging the layer to be transferred, the donor substrate can be previously coated with a polymeric layer, which is ca lled sacrif icial dynamic release layer (DRL) [16-18].

The aim of this work is to contr ibute to the study of applying a clean and versatile fabrication m ethod, i.e. DRL-LIFT of polymers and SWCNT based sensors for gas detection.

The microstructure of the active material in a gas sensor is a key pa rameter influencing the sensitivity o f the m aterial [19]. Therefore, th e morphology and structure of the transferred pixels is established. This work is complemented by m easuring the response to different gas exposure. Based on the requirements of National Institute for Occupational Saf ety an d Health (NIOSH), a test range of 10-200 ppm of gas was considered in this work.

2. EXPERIMENTAL

2.1 Laser-induced forward transfer

The LIFT s etup used in this work c onsists of the pulsed UV XeCl laser beam (308 nm emission wavelength, 30 ns pulse length, 1 Hz repetition rate) which is guided and im aged with an optical system onto the donor substrate to transfer m icropixels from t he donor substrate to the r eceiving surface [1, 20]. The laser fluence is varied from 100 mJ/cm^2 to 700 mJ/cm^2. A c omputer-controlled *xyz* translation stage allows the disp lacement of both donor and re ceptor subs trates with respe ct to th e laser beam . The donor and the receiver are kept in con tact while the laser irradiates the donor from the backside. For each laser pulse single m icropixels are obtained. All experiments were perform ed under am bient pressure at room temperature. A scheme of the LIFT setup is shown in Figure 1.
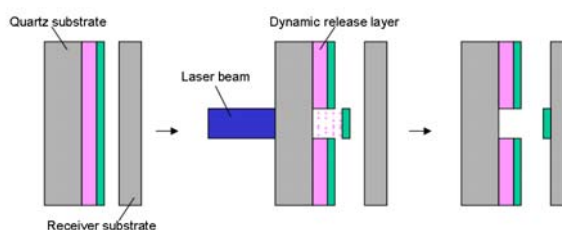
Figure 1. Scheme of the LIFT setup.

2.2 Donor and receiving substrates

The donor substrates are prepared by spin coating the triazene p olymer (TP) (with a thickness of 60 nm, 100 nm, and 300 nm) onto fused silica plates (area 5 cm ^{2}, thickness 1 mm) and then spin co ating the m aterials to transfer: polym ers and carbon nanotubes. The TP is synthesized as described by N agel *et al.* in [16] and is then pr epared by sp in coatin g from a solution in chloroben zene and

"HENRI COANDA"
AIR FORCE ACADEMY
ROMANIA

"GENERAL M.R. STEFANIK"
ARMED FORCES ACADEMY
SLOVAK REPUBLIC

INTERNATIONAL CONFERENCE of SCIENTIFIC PAPER
AFASES 2014
Brasov, 22-24 May 2014

cyclohexanone (1:1, w/w). TP is chosen as DRL layer, due to the f act tha t the em ission wavelength of the las er used in this work matches the absorption maxima of the TP.

The chem oselective polym ers, polyepichlorhydrine (P ECH), polyisobutylene (PIB), poly ethilenimine (PEI), poly(styrene-co-maleic acid) (PScMA), and hydroxypropylmethyl cellulose (HPMC) are chosen to be deposited by laser based m ethods as chemical interactive membranes on surface acoustic wave (SAW) resonators due to their ability to sp ecifically and sele ctively iden tify target gases.

As previously reported in [1, 20] t he first step in the sensor ar ray production process is to deposit the five polym ers as individual thin films onto the sam e substrate plate by m atrix-assisted pu lsed lase r evaporation (MAPLE). The aim is to create m ulti-ribbon targets, which would allow sin gle step tra nsfer (by LIFT) of m ultiple polym er layers o nto different sensors arranged in a matrix.

Single walled carbon nanotubes (S WCNT, HiPco) are purchased from Nanointegris (as a dry powder) and used without further purification.

In order to obtain SW CNT thin film s, 10 mg CNT are d ispersed in water (15 m l) containing the nonionic surfactant Triton X (100 mg), and the dispersion is bath sonicated for 40 m in. The dispersion is then spin coated onto TP coated fused silica plates under different conditions i.e. rotation speed 1500 – 2500, ram p of 1000 – 2000 rpm , and spin coating duration of 30 s and 60 s. In order to remove any trace of solvent from the donor films, the spin coated SW CNT were then left to dry on a hot plate fo r 2 hours at 50 °C. In Figure 2 an atom ic for ce m icroscopy (AFM) image of the SW CNT donor film deposited onto a TP film is shown.
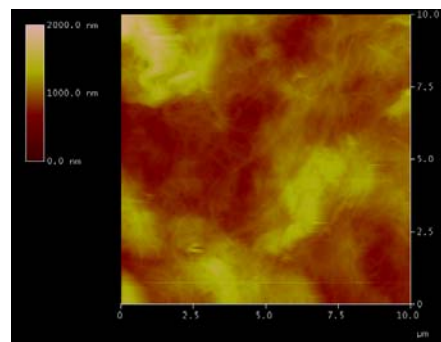
Figure 2. Atomic force microscopy image of a SWCNT donor film.

As receiver substrates, either SAW resonators (f or polym er dep osition) o r chemiresistor structures are used.

2.3 Morphological and structural investigation

The deposited features as well as the target prior to ablation are in vestigated b y optic al microscopy. The i mages are acquired with an Axiovert 200 Microscope coupled to a Carl Zeiss AxioCam MRm camera.

Raman m icroscopy is used to check for any chem ical changes in the structure of the SWCNT prior and af ter the ir dep osition by LIFT. The Ra man spectra of SWCNT are recorded on a Labram confoca l Ra man microscopy system from Jobin Yvon. The 633 nm line from a HeNe laser is u sed as an excitation s ource for th e Ram an spectra. The laser power at the sample surface is typically 20 mW . For each m easurement, the exposure time and th e accum ulation were 2 0 s and 5 times, respectiv ely. Ram an spectra are collected over the range of 200–3000 cm^{-1}. All spectra are recorded at room temperature.

2.4 Sensitivity tests

In orde r to test the SAW sensor arrays, a custom sealed ch amber equ ipped with electronic oscillato rs, one for each SAW resonator, is designed . The sensor arrays, composed of five polym er coated sensors and one reference device (uncoated devices), fabricated o n the sam e quartz sub strate, are placed ins ide the sealed cham ber and connected to the co nditioning elec tronic circuits. In order to obtain different concentrations of VOCs in N_2, the sensor array was exposed to a total flux of 1000 sccm , controlled b y two f low m eters: the m ain f or the gas carrier (N_2) an d the secon d for the analyte. The vapor conc entrations are obtained fluxing N_2 in the liqu id analy te b y using a bubbler. The oscillation of the reference sensors is m easured and the influence of humidity, tem perature, pressure, etc. in th e oscillation frequency is quantified by using the reference S AW devices. This inform ation is subtracted from the m easurement of the polymer coated sensors, allowing thus a precise measurement.

In order to carry ou t th e sensitiv ity tests , the SW CNT pixels are transferred onto Pt electrodes. They are then m ounted on a holder and electrically contac ted with Ag paste. Resistance is m onitored continuo usly with time by a com puter controlled setup using a Keithley 2400 source m eter. The holder is placed in a closed chamber with a constant gas supply and the baselin e resistance is monitored. In order to test the sensors for their gas detection ability, different ammonia concentrations were in troduced in the te st chamber us ing a chrom atography syringe. Once the s ensor reach ed satu ration, the test chamber is purged with N_2 gas until the signal recovers the original baseline value.

3. RESULTS & DISCUSSION

3.1 Polymer SAW sensors

The SAW sensors consis t either of 2-port SAW resonators obtained by two IDTs arranged between reflecting g ratings an d operating at approximately 392 MHz or solidly mounted resonators (SMRs) operating at approximately 2 GHz [1, 20].

As reported previously [1, 20-22], the performances of the SAW sensors are m ainly affected by the physical properties of the polymer coatings. Therefore in the process of applying polymer layers onto SAW devices by LIFT, param eters such as i) the la ser f luence applied for the transfer, ii) the thickn ess of the polymer layer, iii) the laser wavelength, or iii) transfer with DRL and without D RL, are of paramount importance.

Optical m icroscopy im ages of continuous, debris free and with regular edges polym er pixels transferred onto th e resonating cavity of SAW devices at laser fluences between 400 and 500 m J/cm^2 is shown in Fig. 3 a)-f). The red square in Figure 3 a indicates the activ e area of the SAW sensor.

As shown i n [1, 20-22], the laser fluence plays an importan t ro le in obtaining regular, debris free polym er coatings. As the im age reveals (F igure 3), only between 400 and 500 mJ/cm^2 the transfer is clean and well defined. Below 400 m J/cm^2, the polym er doesn't reach the surface of the SAW device, or only debris from the po lymer reach es the SAW surface, most probably due to the lim ited available mechanical force from the DRL decomposition. In contra st, at too high laser fluences, debris from polym er, and destroyed IDTs are noticed.
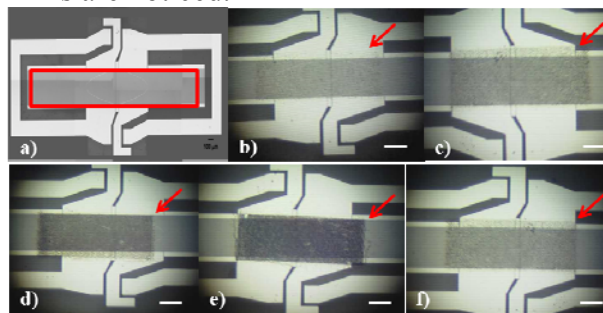
Figure 3. a) Reference SAW sensor; SAW sensor coated with b) PSCMA polymer; c) PEI polymer; d) PECH polymer; e) HPMC polymer; f) PIB polymer. The polymers are transferred at different laser fluences (from 400 to 500 mJ/cm^2). The scale bar is 100 μm.

Similarly, polym er pixels are LIFT printed onto SMR de vices. The transfer is carried out in contact between the donor and the receiver subs trate, as it was shown previously that the tran sfer across a gap is not possible [23] at ambient conditions.

"HENRI COANDA"
AIR FORCE ACADEMY
ROMANIA

"GENERAL M.R. STEFANIK"
ARMED FORCES ACADEMY
SLOVAK REPUBLIC

INTERNATIONAL CONFERENCE of SCIENTIFIC PAPER
AFASES 2014
Brasov, 22-24 May 2014
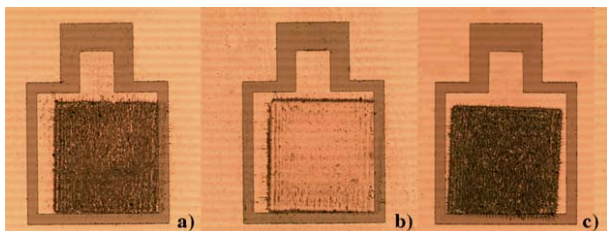
Figure 4. Optical microscopy images of SMR devices coated with PEI, PECH, AND PIB polymers deposited at a) 400 mJ/cm^2 laser fluence (adopted from Ref. 20)

Furthermore it is shown that not only the polymer pixels are regularly transferred onto the active area of sen sor devices, but th e sensors are functional after LIFT. In Figure 5 the respon se curves for thre e different polymers upon exposure to different concentration of dim ethyl m ethylphosphonate (DMMP), i.e. from 2.5 to 40 ppm, are shown.
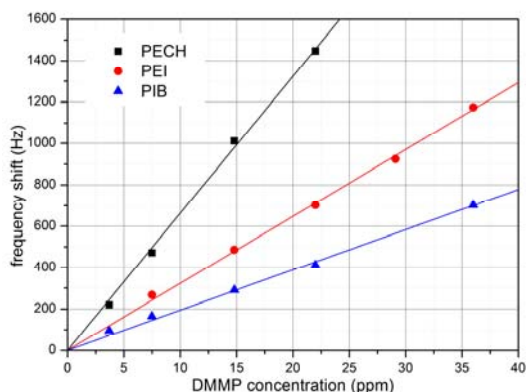
Figure 5. Response curves for PECH, PEI, and PIB sensors upon exposure to different concentration of DMMP. (adopted from Ref. 1)

The response curves for the three polym ers (PECH, PEI, and PIB) to DMMP, DCM, and EtOAc show a linear behaviour in the tested concentration ranges. For PIB, a s ensitivity of 19.45 Hz/ppm is obtained with a calculated detection limit of 0.51 ppm. In the case of PEI, the sen sitivity and the detec tion lim it of the sensor are, 32.34 Hz/ppm and 0.3 ppm , respectively. Finally, f or the PECH a

sensitivity of 66.23 Hz/ppm and a detection limit of 0.15 ppm are achieved. F or all the sensors, th e detec tion lim it is calcu lated considering a m aximum noise level of 10 Hz. As expected, the response curve behaviours of the three sensors dem onstrate that PECH has a higher sensitivity to D MMP vapour than PIB and PEI [24].

3.2 Chemiresistors based on single walled carbon nanotubes

The investigation of LIFT aim ing applications such as the fabrication of chemiresistor senso rs requires a s ystematic variation of different process param eters and an analysis of the resulting m orphological and chemical features of the transferred materials.

As shown previously in [25] the triazene polymer thickness is an i mportant param eter for obtaining a regular, "clean " transfer. TP as DRL absorbs the laser radiation and subsequently decom poses into gaseous fragments which are used to transfor m the energy into required m echanical push . Therefore, the transfer of SWCNT with 300 and 100 nm TP release layer are investigated. It has been seen in [25] that for 300 nm TP layers and all applied conditions never results in a transfer of unifor mly distributed pixels, i.e. never a CNT array, on the receiver substrate. Thus only 100 nm TP layer thicknesses are used.

Another im portant param eter which is investigated is the tr ansfer of SWCNT onto different flexible substr ates, appropriate in the fabrication of intellig ent clothing. An optical microscopy im age of SWCNT transferred by LIFT onto different flexile substrates is shown in Figure 6. As it can be seen in Figure 6, it is possible to achieve a rela tively "clean " transfer, i.e. pixels wi th well-defined contours onto all the substrates investigated.
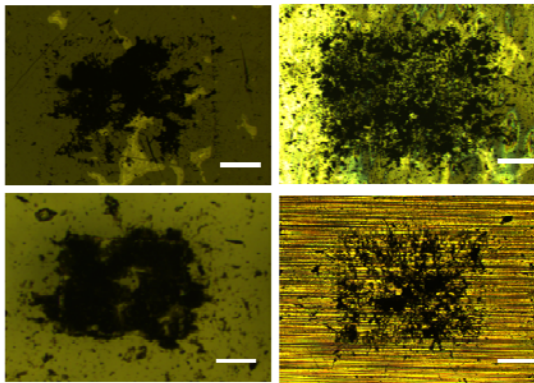
Figure 6. Optical microscopy images of SWCNT deposited onto flexible substrates (from left to right and top to bottom): Kapton, polystyrene, PDMS, Al foil. Scale bar is 100 μm.

In add ition, f or the f abrication of a chemiresistor sensor it is im portant to contro l the laser flu ence. The laser fluen ce is varied over a broad range, i.e. from conditions insufficient to break the donor layer to high irradiation fluences ($0.1 - 1$ J/c m^2), in order to optimize th e shape of th e transferred pixels without any chem ical m odification of the SWCNTs. The optim um laser fluence value s are found in the range 200-400 mJ/cm^2.

The transferred pixels are inves tigated from a structural point of view to check for possible heat dam age af ter the tr ansfer. The Raman spectra of the SW CNTs onto the receiver substrate are shown in Figure 7.
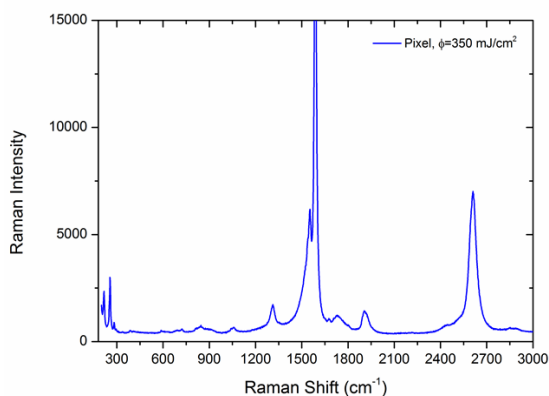
Figure 7. Raman spectra of a SWCNT pixel transferred at 350 mJ/cm^2.

The Ram an spectra presents the typical Raman bands of SWCNTs: weak bands located between 100 and 300 cm^{-1} attributed to the radial breathing m ode (RBM); the peak near 1330 cm^{-1} (D-band) ind icates d isorder in the graphitic layer of the CNTs; while the peak near 1580 c m^{-1} (G- band) is due to the tangential modes of the graphitic planes in the

CNTs. This indicate s that af ter LIFT the SWCNT do not suffer any decom position, and can be therefore further used in sensors applications.

The last ste p in orde r to dete rmine the sensing ability of the SWCNT transferred by LIFT is to carry ou t measurem ents with ppm concentrations of ammonia (an electron-withdrawing vapor). In Figure 8 an example of a typical sensor response to 100 ppm ammonia is shown (adopted from Ref. 25).
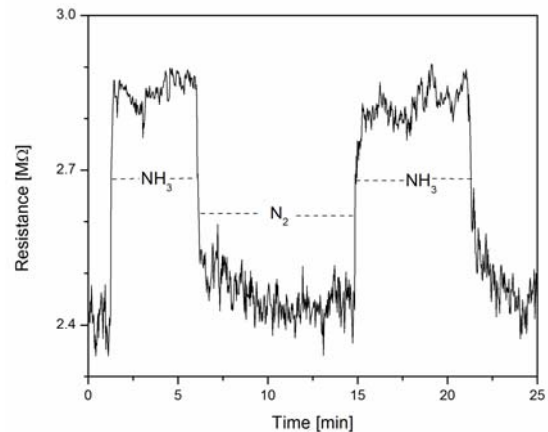
Figure 8. Sensor response upon exposure to 100 ppm of ammonia. (adopted from Ref. 25)

The LIFT-ed sensors show a repeatable response and recovery. The resistance increases sh arply in the f irst m inute, then th e response begins to satu rate in the next 10 minutes. The test chamber is then purged using N_2 gas and a spontaneous signal recovery is observed. The resist ance spontaneously recovers up to 80 % of its signal response within the first $1 - 2$ m inutes from the removal of the ammonia vapors. Th is behavior of these sensors can therefore be explained in term s of p-type characteristics.

3. CONCLUSIONS & ACKNOWLEDGMENT

The results shown above clearly reveal that laser-induced f orward transf er is a suitab le technique to fabricate functional SAW sensors and chemiresistors. The deposition param eters were optim ized in order to m inimize scattering, diffraction a nd attenuation of the SAWs. In addition, si ngle walled carbon nanotube were successfully (with no structura l

"HENRI COANDA"
AIR FORCE ACADEMY
ROMANIA

"GENERAL M.R. STEFANIK"
ARMED FORCES ACADEMY
SLOVAK REPUBLIC

INTERNATIONAL CONFERENCE of SCIENTIFIC PAPER
AFASES 2014
Brasov, 22-24 May 2014

damage) transferred by LIFT onto m etal electrodes to fabricate chemiresistor sensors.

REFERENCES

1. Di Pietrantonio F., Benetti M., Cannatà D., Verona E., Palla-Papavlu A., V. Dinca, M. Dinescu, T. Mattle, Lippert T., Volatile toxic compound detec tion by surface acoustic wave sensor arrays coated with chemoselective polym ers deposited by laser induced forward transfer: app lication to sarin, *Sens. Actuators B* 174: 158-167 (2012).
2. Porter T. L., East man M. P., Pace D. L., Bradley M., Sensor based on piezoresistive microcantilever technology, *Sens. Actuators A*, 88(1), 45-51 (2001).
3. Wu Z., Chen Z., Du X., Logan J.M., Sippel J., Nikolou M., Ka maras K., Reynolds J.R., Tanner D.B., Heba rd A.F., Rinzler A. G., Transparent conducting nanotube fil m, *Science* 305, 1273-1276 (2004).
4. Garrett M.P., Ivanov I.N., Gerhardt R.A., Puretzky A.A., Geohega n D.B., Separation of junction and bundle re sistance in singl e wall carbon nanotube pe rcolation networks by im pedance spectroscopy, *Appl. Phys. Lett. 97,* 163105 (2010).
5. Shaw-Stewart J.R.H., Mattle T., Lippert T.K., Nagel M., Nuesch F.A., W okaun, The fabrication of sm all m olecule organic light-emitting diode pixels by lase r-induced forward transf er, *J. Appl. Phys.* 113, 043104 (2013).
6. Palla P apavlu A., Patrascioiu A., Di Pietrantonio F., Fernadez-Pradas J.M., Cannata D., Benetti M., D'Auria S., Verona E., Serra P., Preparation of surface acoustic wave odor sensors by laser-induced forward transf er, *Sens. Actuators B* 192, 369–377 (2014).
7. Rapp L., Serein-Spirau F., Lère-Porte J.-P., Alloncle A .P., Delaporte P., Fages F., Videlot-Ackermann C., Laser Printing of Air-Stable High Perform ing Organic Thin Film Transistors, *Org. Electron.* 13, 2035–2041 (2012).
8. Palla-Papavlu A., Córdoba C., Patrascioiu A., Fernández-Pradas J.M., Morenza J.L., Serra P., Deposition and characterization of lines printed th rough laser-induced forward tran sfer, *Appl. Phys. A* 110, 751–755 (2013).
9. Hopp B., Sm ausz T., Kresz N., Barna N., Bor Z., Kolozsvári L., Chrisey D.B., Szabó A., Nógrádi A., Survival and proliferative ability of various livin g cell typ es af ter laser-induced forward transfer, *Tissue Eng.* 11(11–12), 1817–1823 (2005).
10. Palla Papavlu A., Dinca V., Paraico I., Moldovan A., Shaw-Stewart J., Schneider C.W., Kova cs E., Lippe rt T., Dinescu M., *J. Appl. Phys. 108 033111 (2010).*
11. Arnold C.B., Serra P., Piqué A., Laser direct-write of com plex m aterials, *Mater. Res. Soc. Bull.* 32, 23–31 (2007).
12. Serra P., Colina M ., Fernández-Pradas J.M., Sevilla L., Morenza J.L., DNA deposition through laser-induced forward transfer, *Appl. Phys. Lett.* 85 (9), 1639-1641 (2004).

13. Fardel R., Nagel M., Nüesch F., Lippert T., Wokaun A., Fabrication of organic light-emitting diode pixe ls by la ser-assisted forward transfer, *Appl. Phys. Lett.* 91, 061103 (2007).

14. Chang-Jian S.K., Ho J.R., Cheng J.-W .J., Sung C.K., Fabricati on of carbon nanotube field em ission cathodes in patterns by a laser transfer m ethod, *Nanotechnology* 17: 1184-1187 (2006).

15. Boutopoulos C., Pandis C., Giannakopoulos K., Pissis P., Zergioti I., Polymer/carbon nanotube composite patterns via laser induced forward transfer, *Appl. Phys. Lett.* 96, 041104 (2010).

16. Nagel M., Fardel R., Feurer P., Häberli M., Nüesch F.A., Lippert T., W okaun A., Aryltriazene photopoly mer thin film s as sacrificial r elease laye rs f or laser- assisted forward transfer system s: Study of photoablative decom position and transfer behaviour", *Appl. Phys. A* 92, 781–789 (2008).

17. Lippert T., Laser app lications of polymers, *Adv. Polym. Sci.* 168, 51–246 (2004).

18. Kattam is N.T., Pur nick P.E., Weiss R., Arnold C.B., Thick-film laser induced forward transfer for deposition of thermally and m echanically d elicate materials, *Appl. Phys. Lett.* 91, 171120 (2007).

19. Franke M.E., Koplin T.J., Sim on U., Metal and m etal oxide nanoparticles in chemiresistors: does the nanoscale matter?, *Small* 2, 36-50 (2006).

20. Cannatà D., Benetti M., Di Pietrantonio F., Verona E., Palla-Papavlu A., Dinca V., Dinescu M., Lippert T., Nerve agent simulant detection by solidly mounted resonators (SMRs) polym er coated using laser induced forward transfer (LIFT) technique, *Sens. Actuators B* 173, 32–39 (2012).

21. Dinca V., Palla Papavlu A., Matei A., Luculescu C., Dinescu M., Lippert T., Di Pietrantonio F., Canna ta D., Benetti M., Verona E., A com parative study of DRL-LIFT and LIFT on integrated polyisobutylene polym er m atrices, Appl. Phys. A 101:429-434 (2010).

22. Dinca V., Palla P apavlu A., Shaw-Stewart J., Dinescu M., Lippert T., Di Pietrantonio F., Cannata D., Benetti M., Verona E., Polymer pixel enhancem ent by laser induced forward transfer for sensor applications, *Appl. Phys. A* 101(3): 559-565 (2010).

23. Palla-Papavlu A., Dinca V., Luculescu C., Shaw-Stewart J., Nagel M., Lippert T., Dinescu M., Laser induced forward transfer of soft m aterials**,** *J. Opt.* 12, 124014 (2010).

24. Ballantine D.S., Rose S.L., Grate J.W ., Wohltjen H., Correlation of surf ace acoustic wave device coating responses with solub ility prope rties and ch emical structure using pa ttern recognition, *Anal. Chem.* 58 (1986).

25. Palla Papavlu A., Di nescu M., Wokaun A., Lippert T., Laser-induced forward transfer of single walled carbon nanotubes, accepted for publication in *Applied Physics A* (2014).

"HENRI COANDA"
AIR FORCE ACADEMY
ROMANIA

"GENERAL M.R. STEFANIK"
ARMED FORCES ACADEMY
SLOVAK REPUBLIC

INTERNATIONAL CONFERENCE of SCIENTIFIC PAPER
AFASES 2014
Brasov, 22-24 May 2014

THE STUDY OF ENERGY TRANSFER ON THIN LAYERS ACHIEVED BY ELECTRO-SPARK DEPOSITION WITH TiC ELECTRODE

Manuela-Cristina PERJU *, Petrică VIZUREANU *, Carmen NEJNERU *

*Faculty of Materials Science and Engineering, "Gheorghe Asachi" Technical University from Iaşi, România

Abstract: The paper aims to register tension, intensity, and time at the precise moment of mono pulse deposition, with electrode of TiC used to achieve hard-alloyed layers by electro-spark deposition method. Ferrite-pearlitic iron used as base material. An assembly used for determinations, which attached to Elitron 22A spark installation. This installation consists in an electric resistance of 0,5 Ω inserted within work system and an oscilloscope with two spots. By means of oscilloscope, intensity, tension and period of mono pulse deposition measured. Diagrams achieved by using the software Statistica 5.5.

Keywords: electro-spark method, deposition regimes, vibration amplitude, current, electrode

1. INTRODUCTION

Electro-spark deposition method is a current research method, used for coating by deposition on installation components, which works in hard conditions, abrasive wear, in moist or dry environment, in order to obtain superficial layers of superior tribological qualities. Obtaining thin layers with special properties (wear resistance, corrosion resistance and shock resistance) requires a proper choice of filler material, in strict correlation with the physical and mechanical properties of the material support, [1,2,3,6,7].

Discharge parameters regimes (voltage, current and pulse time), depends on the physico-chemical properties of the electric and working circuit (device-electrode-piece).

In this context, we can say that the parameters depend on the type of electrode deposition, and its melting temperature, the thermal conductivity, chemical reactivity of the anode elements, diffusivity, density, electrical resistance, thermal inertia, flowability and parameters temperature dependence.

Equally important is the base material, meaning the discharging cathode, because the arch character depends by the two electric poles of the discharge. Base material influences the technological and electric parameters by its conductivity, affinity absorption for discharge gases, melting point, boiling point, carbon potential, (comparing to the carbon potential for the plasma atmosphere may lead to carburizing or decarburizing of the base material), oxygen potential (comparing to oxygen potential from discharge may lead to oxidation or dezoxidation of the metal bath for the deposition drop). When changing the discharge parameters, a significant importance is the interaction between the cathode (base material) and anode (electrode) as a working couple, meaning the alloying intensity, the

melting temperature of the creating alloy, heat capacity of the metal bath, electrical resistance of the metal bath, electrical conductance of the chemical combinations, layer porosity, affinity of the melted material to the plasma gases (oxygen, hydrogen, nitrogen, CO_2, CO).

Another key factor is the existing state of tension during work, which is the surface tension of the droplet deposition, heat stresses and also stresses caused by the rapid cooling, which creates cracks on the layer due to the different expansion coefficients of piece-layer system (depends on the plasticity and elasticity of deposited layer), [4,5].

The multitude of factors that influence the electrical parameters of the discharge regimes (voltage, current, time, power and energy) led to the conclusion that they should be measured in terms of specific experimental work, meaning the ferrite-pearlitic iron cast base material TiC (titanium carbide) electrode deposition at regimes and scales according to the working range of the device Elitron 22A.

2. METHOD

For experiments, an assembly was attached to the Elitron 22A installation, [8], in order to record the current pulses during work (Fig. 1). Elitron 22A presents 9 amplitude steps and 6 working regimes. The installation parameters, taken from the technical handbook are: consumed power (kVA) – 0,5; productivity (cm^2/min) – 4; working voltage (V) – 220; working regimes (r), vibration amplitude (A) – (A1=0,04 mm, A2=0,06 mm, A3=0,08 mm, A4=0,1 mm, A5=0,12 mm, A6=0,14 mm, A7=0,16 mm, A8=0,18 mm, A9=0,2 mm); mass (kg) – 21, [4,5].

For recording the electrical signals characteristics to the established working regimes an assembly consisting of an electrical resistance of 0,5 Ω inserted into the working system and a two spots oscilloscope was used.

By measuring the resistor voltage the work current was set. Time variation diagrams for voltage and spark current was recorded using the two spots oscilloscope.

For each experimental determination, from the oscilloscope screen were taken the following values: impulse time (10^{-4} [s]), current (A), voltage (V). Power was calculated (with formula P=U·I [W]) and single-pulse energy (with formula P=U·I [W]), [4,5].
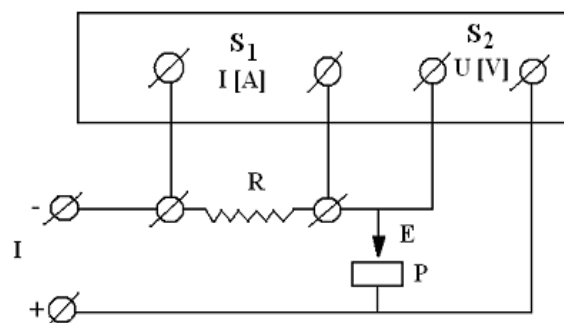
Fig. 1. Wiring diagram of installation: S1 – spot 1 for intensity of the discharge measurement; S2 – spot 2 for discharge voltage measurement; E – electrode; P – part; I – source; R – electrical resistance 0,5 Ω.

The total duration of a pulse is between 5 ÷ 14 ms. Each electrode has a different ionization capacity, according with the established working regimes, the control device positions. Power and pulse energy are different, depending on the physical properties and the quality of each electrode.

3. RESULTS AND DISCUSSIONS

Depending on the values obtained by calculation, power and energy were rendered using spatial graphs obtained with the Statistica 5.5 software.

“HENRI COANDA”
AIR FORCE ACADEMY
ROMANIA

“GENERAL M.R. STEFANIK”
ARMED FORCES ACADEMY
SLOVAK REPUBLIC

INTERNATIONAL CONFERENCE of SCIENTIFIC PAPER
AFASES 2014
Brasov, 22-24 May 2014

3.1. Deposition regimes for TiC. Single-pulse energy deposition of titanium carbide electrode has large fluctuations, ranging from $45 \cdot 10^{-3}$ J (r1, A4) and $492,8 \cdot 10^{-3}$ J (r4, A4). Energy increases and decreases randomly with regime change and amplitude of vibration. The mean value for the 48 experiments is $E_{medium}= 161,83 \cdot 10^{-3}$ J, (Fig. 2).

Power single-pulse discharge electrode of titanium carbide varies between 145 W values (r2, A4) and 448 W (r4, A2), but with much uniformity as of 48 schemes 32 values between $180 \div 270$ W. The high values, above 400 W are schemes 3 and 4, and the amplitude of between 2 and 6, (Fig. 3).

Table 1. Unipuls discharge modes for cast iron electrode TiC

Nr crt	A	r	I [A]	U [V]	t [x10⁻⁶s]	P [W]	E [x10⁻³J]	Nr crt	A	r	I [A]	U [V]	t [x10⁻⁶s]	P [W]	E [x10⁻³J]
1	2	1	15	22	6	330	198	25	2	4	14	32	11	448	492,8
2	3	1	17	10	3	170	51	26	3	4	15	12	4	180	72
3	4	1	15	10	3	150	45	27	4	4	16	22	7	352	246,4
4	5	1	14	12	4	168	67,2	28	5	4	15,5	18	5	279	139,5
5	6	1	15	20	7	300	210	29	6	4	15	14	4	210	84
6	7	1	15	16	7	240	168	30	7	4	16	15	5	240	120
7	8	1	14	14	6	196	117,6	31	8	4	13	16	5	208	104
8	9	1	15,5	18	6	279	167,4	32	9	4	13	14	4	182	72,8
9	2	2	17	14	5	238	119	33	2	5	13	16	8	208	166,4
10	3	2	13,5	12	6	162	97,2	34	3	5	17	12	4	204	81,6
11	4	2	14,5	10	4	145	58	35	4	5	16	12	5	192	96
12	5	2	16,5	14	8	231	184,8	36	5	5	15	14	8	210	168
13	6	2	15	18	7	270	189	37	6	5	18	10	5	180	90
14	7	2	17	16	8	272	217,6	38	7	5	15	12	5	180	90
15	8	2	15	18	8	270	216	39	8	5	17	12	6	204	122,4
16	9	2	13	16	8	208	166,4	40	9	5	16	12	5	192	96
17	2	3	12	36	10	432	432	41	2	6	14,5	20	8	290	232
18	3	3	12	22	7	264	184,8	42	3	6	14	14	5	196	98
19	4	3	17	26	8	442	353,6	43	4	6	16	14	5	224	112
20	5	3	15	28	9	420	378	44	5	6	18	12	4	216	86,4
21	6	3	14,5	20	7	290	203	45	6	6	12	22	6	264	158,4
22	7	3	14	24	6	336	201,6	46	7	6	16	10	5	160	80
23	8	3	15	18	5	270	135	47	8	6	18	16	7	288	201,6
24	9	3	16	20	5	320	160	48	9	6	23	18	6	414	248,4
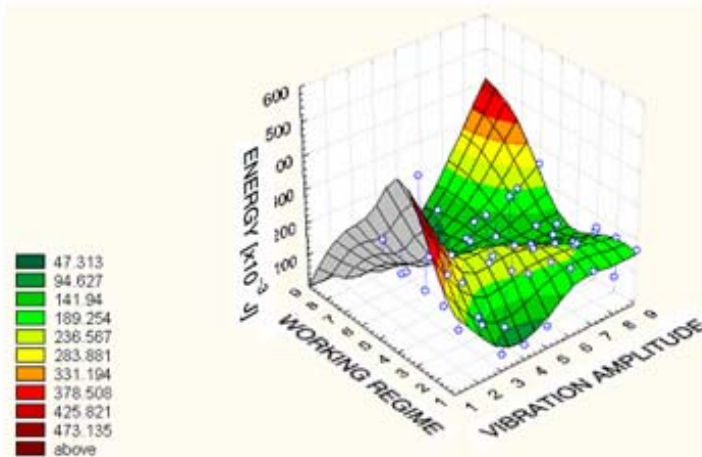
Fig. 2. Energy variation depending on the amplitude operating mode and working regime for TiC electrode.

"HENRI COANDA"
AIR FORCE ACADEMY
ROMANIA

"GENERAL M.R. STEFANIK"
ARMED FORCES ACADEMY
SLOVAK REPUBLIC

INTERNATIONAL CONFERENCE of SCIENTIFIC PAPER
AFASES 2014
Brasov, 22-24 May 2014
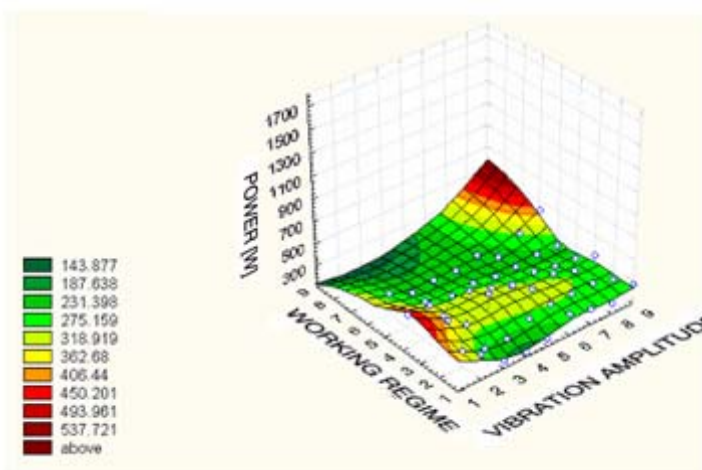
Fig. 3. Power variation depending on the amplitude operating mode and working regime for TiC electrode.

4. CONCLUSIONS

Correlation amplitude regime and deposition electrode and the base material type is important, both in terms of energy consumption and in terms of technology in order to achieve uniform deposition without burning achieve, pores or overlapping material. Energy analysis of deposits reveals that the energy deposit is inversely proportional to the size of electrical discharge pulse resistance.

REFERENCES

1. S. Frangini, A. Masci, *A study on the effect of a dynamic contact force control for improving electrospark coating properties*, Surface & Coatings Technology 204, pp. 2613–2623, (2010).

2. Liu Dongyan, Gao Wei, Li Zhengwei, Zhang Haifeng, Hu Zhuangqi, *Electro-spark deposition of Fe-based amorphous alloy coatings*, Materials Letters 61, pp. 165–167, (2007).

3. Liu Jun, Wang Ruijun, Qian Yiyu, *The formation of a single-pulse electrospark deposition spot*, Surface & Coatings Technology 200, pp. 2433–2437, (2005).

4. Perju Manuela Cristina, Găluşcă Dan Gelu, Nejneru Carmen, Ştefănică Roxana Gabriela, Răileanu Tudor, *The study of energy transfer on thin layers achieved by impulse discharge with wolfram carbide electrode*, Buletinul Institutului Politehnic, Iaşi, pg.69-76, (2010).

5. Perju Manuela Cristina, Găluşcă Dan Gelu, Nejneru Carmen, Agop Maricel, *Straturi subţiri: descărcări în impuls*, Editura Ars Longa, ISBN 978-973-148-049-7, pagini 339, (2010).

6. Reynolds, J.L., Holdren, R.L., and Brown L.E., *Electro-spark deposition*, Advanced Materials and Process, 161 (3), pp. 35-37, (2003).

7. Vermeşan, G., Vermeşan, E., Jichisan-Matiesan, D., Cretu, A., Negrea, G., Vermeşan, H., Vlad M., *Introducere în ingineria suprafeţelor*, Editura Dacia, Cluj-Napoca, (1999).

8. ******* *Instalaţie Elitron 22*, Academia de Ştiinţe, Republica Moldova, Chişinău, (1992).

THE AERODYNAMIC ANALYSIS OF HIGH LIFT DEVICES

Vasile PRISACARIU[1], Andrei LUCHIAN[2]

[1]Universitatea Transilvania Braşov, [2]Universitatea Politehnica Bucureşti

Abstract: High lift devices (DHS) are designed to expand the flight envelope by changing the local geometry (mechanization wing), they generally camber changes depending on the phase of flight (landing, take-off). As controls, the aircraft they developed aeromechanical has effects with implications for the resistance structure of the wings, and the most important effect is the twisting of the wing. The article desires a analysis of the 2D aerodynamic profile with changes in curvature at trailing edge.

Keywords: high lift devices (HLD), Clark Y, Javafoil 2.20, XFLR5 6.09, Profili 2.21

1.INTRODUCTION

High lift devices used for bearing surfaces are designed to expand the flight envelope by changing the local geometry (wing mechanization) according to phases of flight of the aircraft. Figure 1.1 is an example of this general concept
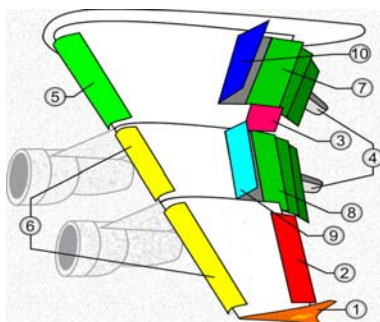
1.winglet, 2.low speed aileron, 3.high speed aileron, 4.flap track fairing, 5.Krüger flaps, 6.slats, 7.three slotted inner flaps, 8.three slotted outer flaps, 9.spoilers, 10.spoilers-air brakes
Fig. 1.1 High lift devices (HLD) [1]

Figure 1.2 presents flaps at Cessna 172.
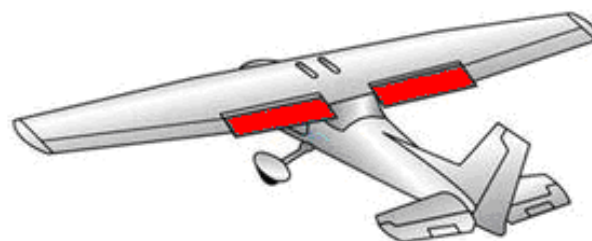
Fig. 1.2 Flaps of Cessna 172,

The use of high lift modern aircraft derived from the need for speed with low values (equation 1) for takeoff and landing phases.

$$V_{at} = \mu_{at} \cdot \sqrt{\frac{2 \cdot G}{\rho \cdot S \cdot c_{z \cdot at}}} \qquad (1)$$

$$F_{z \cdot at} = \frac{\rho \cdot V_{\infty}^2}{2} \cdot S \cdot c_{z \cdot at} \qquad (2)$$

where:
μ_{at} - *factor influencing soil landing, (0.94 – 0.96);*
ρ – *Air density;*
G – *Weight of airplane;*
S – *Lifting surface;*
C_{zat} – *lift coefficient in landing configuration*

V_∞ - *speed*
$F_{z\,at}$ – *lifting in landing configuration*

In Figure 1.3 the most common types of flaps lifting surfaces.

Plain flap   Split flap

Slotted flap   Fowler flap
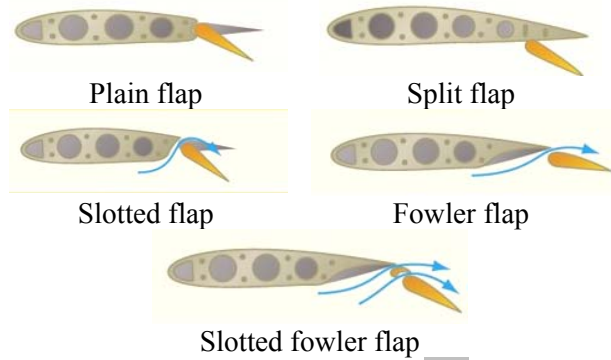
Slotted fowler flap
Fig. 1.3 Types of flaps [2, 3]

The methods used to increase the maximum lift coefficient C_{zmax} rely on either modifying the profile geometry (passive systems) or boundary layer control (active systems) or the combination of both methods. High lift studies systems based solely on increasing the bearing surface (type wing folding or telescoping wing), [14]. In carrying devices high lift continuity conditions are imposed to the lifting surfaces produces by the drag increase when high lift is un-prancing and keeping balance during turning to avoid decoupling aerodynamic moments.

Flaps effects
The operation of the wing flaps of curvature increase will cause an increase in lift at the same speed and the ratio T / F_x F_x is changed due to the change value. In this case C_p (pressure center) moves downstream as the steering angle of the flaps increases, thus changing the ratio Fz / G, so it induces a dive time, see figure 1.5.
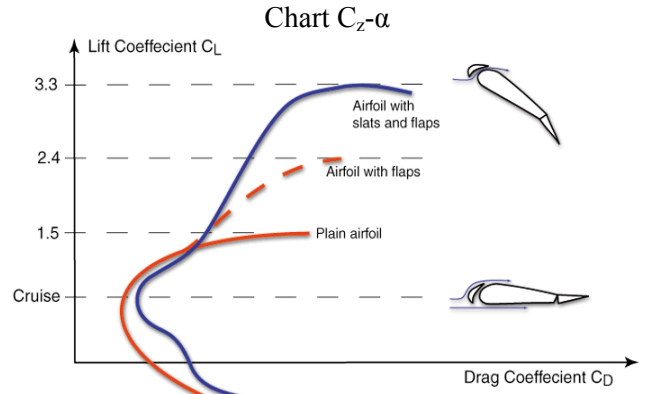
Chart C_z-α

Fig. 1.4 Chart C_z-C_x [4]

When using flaps for negative cycle (up to 50, 100) we have increased cruise by about 5% (transport planes) or better maneuverability for aerobatic maneuvers (aerobatics aircraft).
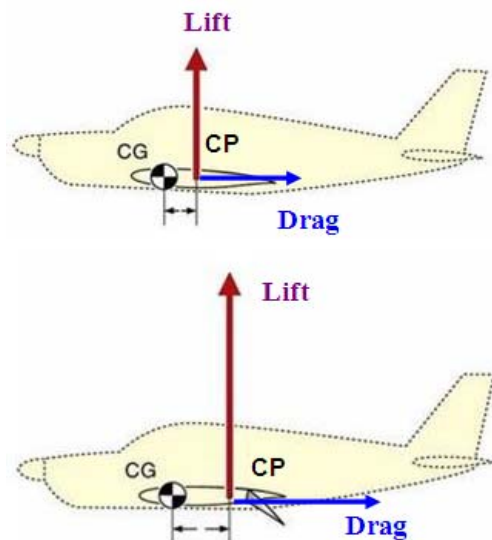
Fig. 1.5 Flaps effects

To increase the effectiveness of flaps we are using some constructive solutions and methods (operational or concept stage):
- Flaps with multiple sections, (Figure 1.6);
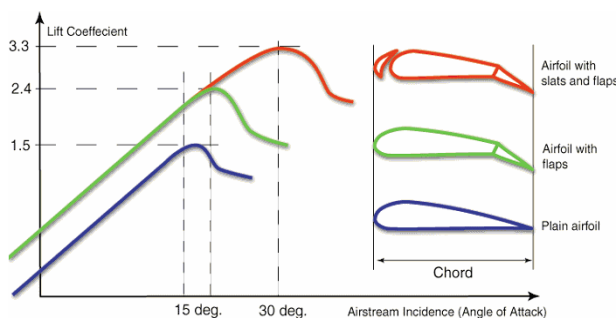
Fig. 1.6 Multiple slotted flaps - Boeing 747, [5]

"HENRI COANDA"
AIR FORCE ACADEMY
ROMANIA

"GENERAL M.R. STEFANIK"
ARMED FORCES ACADEMY
SLOVAK REPUBLIC

INTERNATIONAL CONFERENCE of SCIENTIFIC PAPER
AFASES 2014
Brasov, 22-24 May 2014

- Spoiler on the upper side in front flaps, figure 1.7;

Fig. 1.7 Spoilers - DC 9, [5]

- slotted flaps rolling extrados surfaces, see figure 1.8, drive / slot Δ_x;
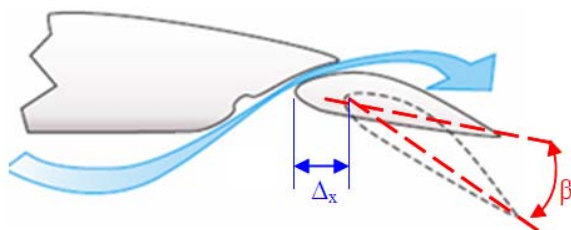
Fig.1.8 Slotted flaps

- blowing boundary layer flow on laminating flap by applying the Coanda effect, the jet flap, [15, 16, 17, 18, 19];
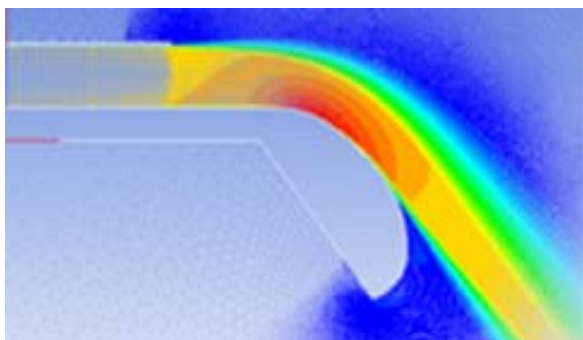
Fig. 1.9 Coandă effect [19]

- Usage of partially morphing to remove pressure jumps in the joints (morphing - no joints, offering a seamless active continuous

curvature), or the morphing trailing edge, see figure 1.10, [6, 7, 8];

Fig. 1.10 Morphing concept [6]

- command and control sequences during takeoff / landing fully automated, which eliminates discontinuities maneuver the pilot (autopilot assisted steering gear intervals);
- implementation of the concept "full stall", the landing sequence that leads to a landing speed almost zero;

- flap actuation-correlation with other commands such as thrust vectoring aircraft (aircraft V / STOL), see Figure 1.11.
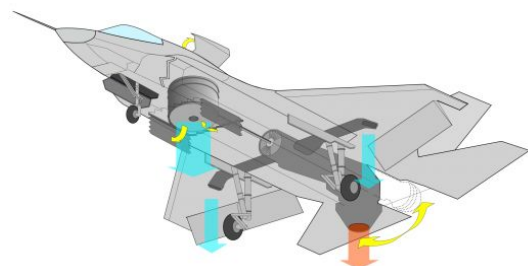
Fig. 1.11 Sukhoi VSTOL (flaps and vectoring traction), [9]

2. THE 2D FLAPS ANALYSIS

We propose to analyze a Clark Y profile with simple flaps with different steering angles, by using four 2D analysis software tools (Javafoil 2.20, Profili 2.20, XFLR5 6.06 and web Airfoil tolls) that are based on Xfoil code. [10, 11, 12, 13].
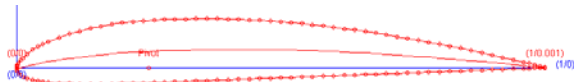
Fig. 2.1 Clark Y airfoil

The study aims to analyze the variation of drag coefficient (Cx, Cz, Cm) depending on the angle of incidence (α), the pressure coefficient (Cp) along the I chord in different positions of the flap deflection. Conditions of the analysis are presented in Table 2.1.

Table 2.1 Conditions of analysis

Definition	121 pct	Viscosity	$1{,}46 \times 10^{-5}$
Reynolds	100000	Air density	$1.221 \ kg/m^3$

2.1. The 2D analysis with flaps 0^0

Viewing the three graphs (Fig. 2.2, 2.3, 2.4) the drag coefficient data depends on the angle of incidence where we can observe the differences in values of the code provided Javafoil and for the three other software environments (profile, XFLR, Xfoil web code) which revealed close values. [11, 12, 13].

	-4	0	4	8	12
Cz Java	-0.048	0.422	0.894	1.305	1.246
Cz Profili	-0.072	0.441	0.832	1.192	1.388
Cz XFLR	-0.055	0.442	0.832	1.191	1.388
Cz web	-0.061	0.442	0.832	1.192	1.386

Fig. 2.2 Chart C_z-α (flaps 0^0)

	-4	0	4	8	12
Cx Java	0.041	0.015	0.015	0.027	0.091
Cx Profili	0.019	0.011	0.011	0.017	0.031
Cx XFLR	0.011	0.008	0.011	0.018	0.032
Cx web	0.018	0.011	0.012	0.017	0.031

Fig. 2.3 Chart C_x-α (flaps 0^0)

	-4	0	4	8	12
Cm Java	-0.036	-0.081	-0.086	-0.091	-0.032
Cm Profili	-0.087	-0.094	-0.081	-0.065	-0.031
Cm XFLR	-0.09	-0.095	-0.081	-0.066	-0.036
Cm web	-0.089	-0.095	-0.081	-0.066	-0.035
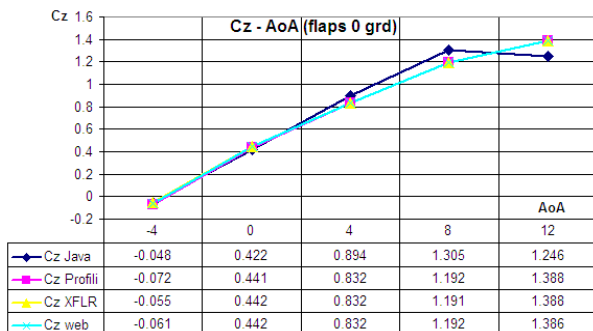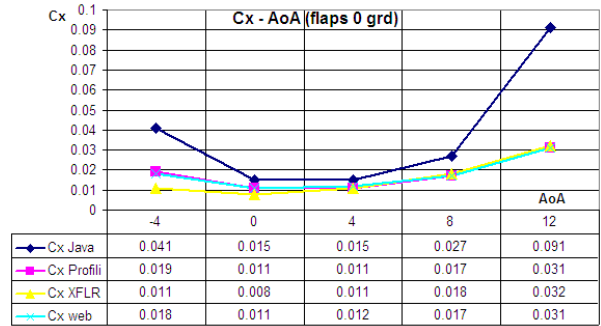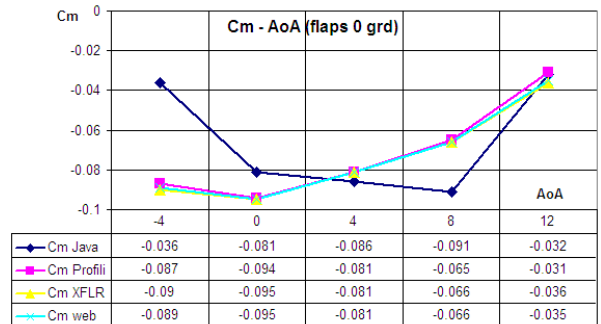
Fig. 2.4 Chart C_m-α (flaps 0^0)

2.2. The 2D analysis with flaps 15^0.

We perform a comparative analysis on 2D flow profile at different angles of deflection with the same software tools.
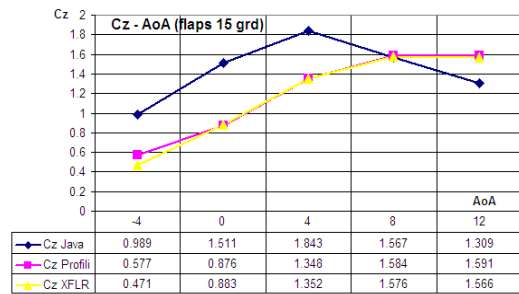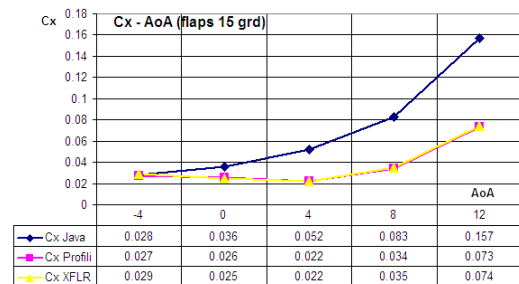
	-4	0	4	8	12
Cz Java	0.989	1.511	1.843	1.567	1.309
Cz Profili	0.577	0.876	1.348	1.584	1.591
Cz XFLR	0.471	0.883	1.352	1.576	1.566

Fig. 2.5 Chart C_z-α (flaps 15^0)

	-4	0	4	8	12
Cx Java	0.028	0.036	0.052	0.083	0.157
Cx Profili	0.027	0.026	0.022	0.034	0.073
Cx XFLR	0.029	0.025	0.022	0.035	0.074

Fig. 2.6 Chart C_x-α (flaps 15^0)

“HENRI COANDA”
AIR FORCE ACADEMY
ROMANIA

“GENERAL M.R. STEFANIK”
ARMED FORCES ACADEMY
SLOVAK REPUBLIC

INTERNATIONAL CONFERENCE of SCIENTIFIC PAPER
AFASES 2014
Brasov, 22-24 May 2014

Fig. 2.7 Chart C_m-α (flaps 15^0)

Cm - AoA (flaps 15 grd)	-4	0	4	8	12
Cm Java	-0.215	-0.223	-0.227	-0.075	-0.067
Cm Profili	-0.163	-0.169	-0.167	-0.135	-0.097
Cm XFLR	-0.177	-0.166	-0.164	-0.129	-0.091

2.3. The 2D analysis with flaps 30^0

Fig. 2.8 Chart C_z-α (flaps 30^0)

Cz - AoA (flaps 30 grd)	-4	0	4	8	12
Cz Java	1.887	2.382	1.842	1.464	1.041
Cz Profili	0.912	1.334	1.692	1.798	1.701
Cz XFLR	0.867	1.287	1.643	1.742	1.662

Fig. 2.9 Chart C_x-α (flaps 30^0)

Cx - AoA (flaps 30 grd)	-4	0	4	8	12
Cx Java	0.037	0.012	0.059	0.114	0.204
Cx Profili	0.079	0.064	0.063	0.089	0.139
Cx XFLR	0.075	0.063	0.061	0.086	0.142

Fig. 2.10 Chart C_m-α (flaps 30^0)

Cm - AoA (flaps 30 grd)	-4	0	4	8	12
Cm Java	-0.341	-0.141	-0.112	-0.101	-0.098
Cm Profili	-0.252	-0.233	-0.216	-0.174	-0.159
Cm XFLR	-0.216	-0.203	-0.185	-0.146	-0.133

The flap turning effect from 0^0 to 15^0 and 30^0 is illustrated in the graphs in Figures 2.11, 2.12. and 2.13 in the three coefficients

compare (Cz, Cx and Cm) using the software environment XFLR5 6.09.

Fig. 2.11 Chart C_z-α (flaps)

Cz - AoA	-4	0	4	8	12
flaps 0 grd	-0.055	0.442	0.832	1.191	1.388
flaps 15 grd	0.471	0.883	1.352	1.576	1.566
flaps 30 grd	0.867	1.287	1.643	1.742	1.662

Fig. 2.12 Chart C_x-α (flaps)

Cx - AoA	-4	0	4	8	12
flaps 0 grd	0.011	0.008	0.011	0.018	0.032
flaps 15 grd	0.029	0.025	0.022	0.035	0.074
flaps 30 grd	0.075	0.063	0.061	0.086	0.142

Fig. 2.12 C_m-α (flaps)

Cm - AoA	-4	0	4	8	12
flaps 0 grd	-0.09	-0.095	-0.081	-0.066	-0.036
flaps 15 grd	-0.177	-0.166	-0.164	-0.129	-0.091
flaps 30 grd	-0.216	-0.203	-0.185	-0.146	-0.133
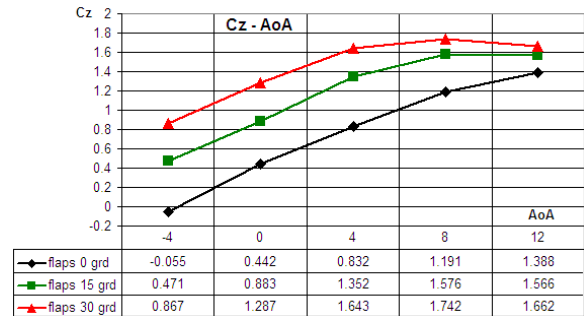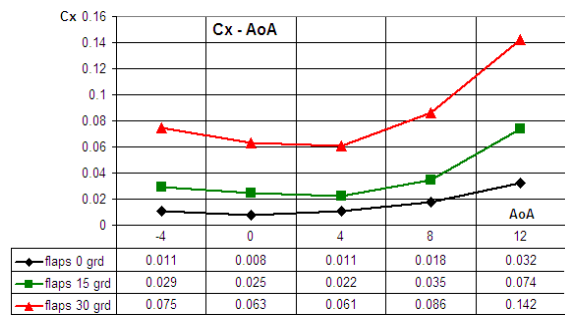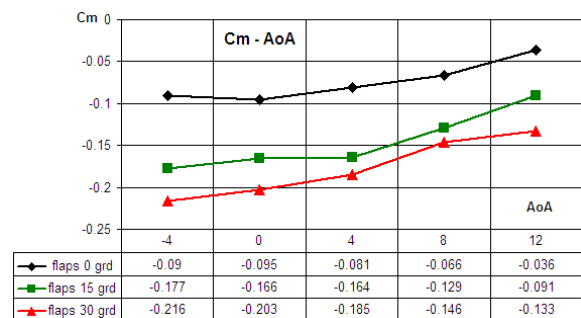
The 2D analysis reveals differences in the values provided by the software tools used, but similar numerical developments.

Java foil 2D shows an evaluation tool for highlighting ratio V / V (xfoil code), Figure x shows changes in flow velocity profile
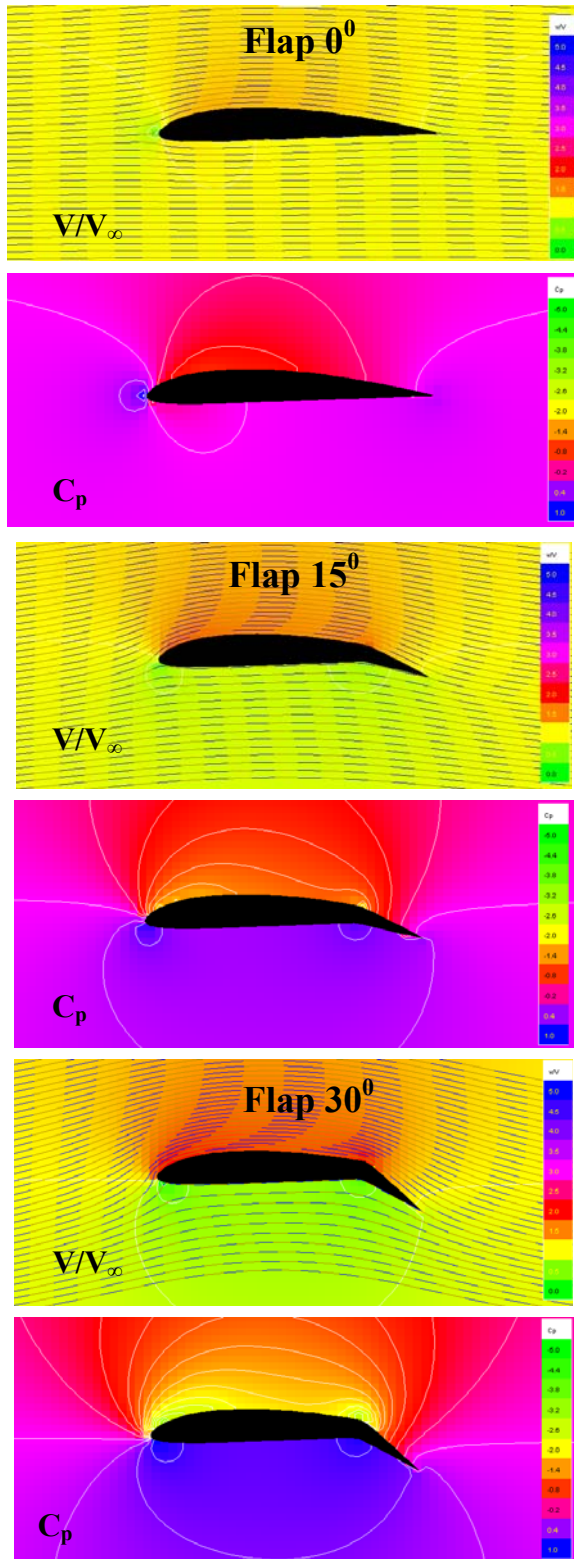
Fig. 2.13 Flow velocity distribution

turbulence. Their drive and side effects such as increased dive time decrease the horizontal speed, increasing speed descension, so intervention is required to prevent these effects by correlating flight control (throttle and stick). Aircraft flight control systems Coandă effect can make 3D maneuvers throughout the flight envelope. Next Generation on HDL is morphing concepts combined with smart materials that will increase the efficiency reaction rate of HDL.

3.2. Acknowledgment

BIBLIOGRAFIE

1 http://aviationknowledge.wikidot.com/aviation:wing
2 http://herschlogbook.blogspot.ro/2012/07/aerodynamics-flight-controls.html
3 Young A.D., *The aerodynamic characteristics of flaps*, RAE technical report Aero no. 2622, London, 1953, 56p.
4 http://www.zenithair.com/stolch801/design/design.html,
5 http://www.airliners.net/aviation-forums/tech_ops /read.main/281872/
6 Weisshaar, T.A. (2006) Morphing Aircraft Technology – New Shapes for Aircraft Design. In *Multifunctional Structures / Integration of Sensors and Antennas*. Meeting Proceedings RTO-MP-AVT-141, Neuilly-sur-Seine, France: available at : http ://www.rto.nato.int/abstracts.asp,
7 Prisacariu V., Răo C., Introduction morphing technology in unmanned aircraft vehicles (UAV), AFASES 2011: The 13th International Conference of Scientific Papers "SCIENTIFIC RESEARCH AND EDUCATION IN THE AIR FORCE", mai 2011, Braşov, Romania, , 6p
8 Barbarino S., Bilgen O., and others, *A review of morphing aircraft,* Journal of intelligent material systems and structures, Vol.22/2011, DOI:10.1177/1045389X11414084, p55.

3. CONCLUSIONS & ACKNOWLEDGMENT

3.1. Conclusions

The main effect of flaps is a generating flow vortex separation on the upper side especially in areas of the surface with air

"HENRI COANDA"
AIR FORCE ACADEMY
ROMANIA

"GENERAL M.R. STEFANIK"
ARMED FORCES ACADEMY
SLOVAK REPUBLIC

INTERNATIONAL CONFERENCE of SCIENTIFIC PAPER
AFASES 2014
Brasov, 22-24 May 2014

9   http://soni2006.hubpages.com/hub/Thrust-Vectoring-Sukhoi,

10 Hepperle M., JavaFoil 2.20, JAVAFOIL User's Guide, 2014, 44p., disponibil la http://www.mh-aerotools.de/airfoils/javafoil.htm

11 Duranti S. *Profili 2.21 software*, 2012, Feltre-Italia, www.profili2.com, consulted at 12.02.2014

12 Drela M., Yungren H., *Guidelines for XFLR5 v6.03 (Analysis of foils and wings operating at low Reynolds numbers),* 2011, http://sourceforge.net/projects /xflr5/files;

13 Airfoils database, consulted at 10.02.2014, http://airfoiltools.com/airfoil/details?airfoil= clarky-il

14 Mestrinho J.R.C., Felicio J.M.I., and others, *Design optimization of variable-span morphing wing*, 2nd International Conference on Engineering Optimization, September 2010, Lisbon, Portugal, 11p.

15 Williams J., Butler S.F.J., Wood M.N., The aerodynamics of jet flaps, no. 3304, London, 1963, 35p., dsiponibil la http://naca.central.cranfield.ac.uk/

16 Rudolf P.K.C., *High-Lift Systems on Commercial Subsonic Airliners*, NASA contractor report 4746, 1996, 166p

17 Cîrciu I, Dinea S., *Review of application on Coandă effect, history, theories, new trends,* Review of the Air Force Academy, no.2(17)/2010, p14-20, ISSN 1842-9238

18 Cîrciu I., Boşcoianu M., *An analysis of the efficiency of Coandă – NOTAR anti-torque system for small helicopters,* INCAS Bulletin, vol.2, no. 4/2010, ISSN 2066-8201, p.81-88.

19 Dumitrache A., Frunzulica F. , Ionescu T.C., *Mathematical Modelling and Numerical Investigations on the Coanda Effect*, Nonlinearity, Bifurcation and Chaos - Theory and Applications, ISBN 978-953-51-0816-0, http://dx.doi.org/10.5772/50403, , 2012, p101-132,

AIR FORCE

CONSIDERATIONS ABOUT THE LIFE EXTENSION PROGRAMS BY TECHNICAL RESOURCE RENEWAL APPLIED TO THE SURFACE-TO-AIR MISSILES

Marius RADULESCU*, Vasile SANDRU**

*Electromecanica Ploiesti, Romania, ** „Henri Coanda" Air Force Academy, Brasov, Romania

Abstract: *The work-paper presents few considerations regarding the opportunity that a life extension program to be applied in the case of a ground-to-air missile as an Air Defense Missile System (ADMS) component. A model of a hypothetical AD missile is built and serves as a base for the technical and economical reasons for the extension life decision. Using some market data for the missile's components, the authors try to balances the life-extension costs with those of the complete replacement ones. The scientific, technical and technological support needed for applying such a program is set also. The conclusions refer to the multitude of the factors which are involved in the life extension program management.*

Keywords: *missile, lifecycle, efficacy, program, costs*

1. INTRODUCTION

The air power represents the main force multiplier of an armed force. This assertion allows the huge efforts make by the owners to maintain the advance of the aerial features in the endowment. Any military organization must be able to counter the aerial menace at an appropriate technological level. This level is done today by the Air Defense Missile Systems (ADMS) using the air defense (AD) missile or SAM's. If the aerial means evolves for increasing survivability and efficacy, the ADMS's and the SAM's default must keep the same trend [3].

This implies the quickly change the SAM generation every time when the aerial threat significantly change the characteristics or the continuously up-grade of the existing ADMS until the consumption of their operational life.

The frequently replacement of the whole ADMS involves great expenses, and requires the access to the ultimate state-of-art in branch. Only the major scientific and military powers can practice this way and with corresponding costs.

The majority of other ADMS keepers may take in account the possibility of the extension system's life cycle using the life extension processes as the technical resources carry-over, the technical resource renewal and the improving up-grade.

2. THE OPERATIONAL LIFE OF THE SAM SYSTEM

2.1 The main ADMS composition

An ADMS is a complex assembly, assuring not only the battle engagement, but also the

learning [2], the training and the maintenance functions as a base for the integration into the armed forces architecture [6], generally composed by:

- Self-propelled launcher
- Missile
- Mobile summary checking station
- Maintenance checking station
- Replacement vehicle
- Mobile Command Post
- Field training equipment
- Class simulator
- Descriptive documentation
- Flight employment documentation
- Maintenance documentation
- Teaching complete (pads, sliced inert missile, system elements)

Every component of the ADMS has his own active life date, depending of some operational factors, like:

- Complexity
- Using regime
- Critical and expendable elements
- Availability of sub-components on market
- Morale usage

Figure 1 – A view of a SHORAD type ADMS

Basically three life extension processes creates the technological base to maintain in endowment a certain ADMS [4]. These processes are:

- The technical resources carry-over
- The technical resource renewal
- The up-grade

This work-paper analyses the second process, having a medium complexity and in this way being more accessible for a medium technological industrial support, and applied for the main ADMS component – the SAM only.

2.2 AD missile (SAM) – the most perishable system element

Between the ADMS components, the missile represents one of the most dynamic elements, direct connected with the potential target performance evolution. The main hardware and software aspects including in the missile structure that are relatively quickly affected in time are the following:

- The fuel and the igniters of the propulsion unit
- The explosive of the warhead
- The thermal battery (or/and other power sources)
- The guidance and control algorithm
- The command and accord function of the proximity fuse

Generally a short / medium range SAM has an operational technical resource of 10 years, while other ADMS's components has 15 to 20 years of resource. Furthermore a system operates 2 to 3 versions of the missile until complete replacement.

By the technical resource renewal process a system regains a new operational life period, but without the increasing performances.

2.3 The principle SAM organization

Generally a missile destined to an ADMS has an organization like the following schedule:
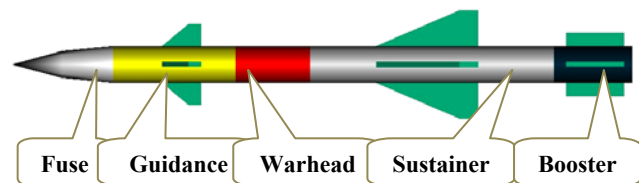
Figure 2 – General missile organization

According with its type, the missile could have some differences in organization. For the work-paper purpose we can suppose an assembly composes from a succession of compartments comprising an electro-magnetic fuse, a guidance section a warhead and a propulsion unit with a booster and a sustainer, alongside three aerodynamically sets.

Even from the initial project, a relatively complex technical system like a missile disposes of the interfaces that permits to change a compartment when a new equipment generation will be ready or for the same type replacement only.

3. THE TECHNICAL RESOURCE RENEWAL PROGRAM CRITERIA

3.1 Missile's components lending to replacement

The main components that the program will be applied are shown in the figure 3:
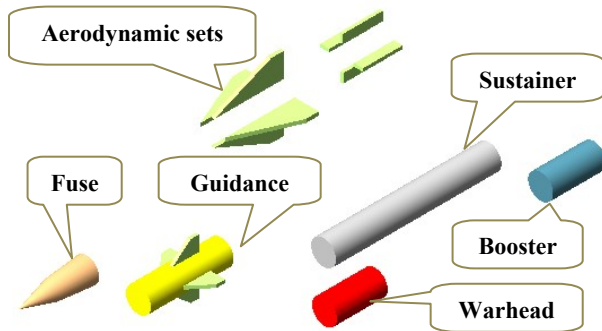
Figure 3 – The main SAM compartments

For the purpose of concept here exposed, a real close price data can be identified in the specialized literature [9], like the follows:

* rounded

#	Component	Weight [kg]	Cost indicator [USD/lb]	Estimated price * [USD]
1	Guidance Unit	12	10400	275500
2	Proximity fuse	8	7400	130500
3	Warhead	15	4800	159000
4	Sustainer rocket motor	67	4200	621000
5	Booster rocket motor	18	3600	143000
	Sum	**120**		**1329000**

3.2 The volume of the means that the program will be applied

In order to have an economical reason to develop a technical resource renewal program, a number of systems and a number of missiles respectively must be the subject of the process.

However, for the accounting necessity, we can hypothetical consider a limited number of systems in endowment like follows:
- 18 ADMS in three battalion type units, having 4 missiles each and another 4 in the unit depot
- 1 ADMS belonging to an application school unit
- 1 reserve ADMS as forces generally reserve
- 2 ammunition fire units as forces reserve for each ADMS

This account a total of: $144 + 8 + 8 + 160 = 320$ of missiles.

For the calculus necessity we consider the price for a new missile as 1.33 USD millions that climb the affair value to a total of about 425 USD millions.

3.3 The resource renewal program

Considering the entirely 320 pcs missile batch into the resource renewal program, and 10 pcs of this will be lost in partial/final tests for 310 remaining missiles we can evaluate the financial effort needed to accomplish the task.

Section	Operation	Material cost [USD]	Labor hours [25USD/hr]	Estimated price [USD]
0	1	2	3	4
Guidance (cost / pcs)	Battery replacement Interfaces refit Checking on stands	600	80	13900
Fuse	Checking on stands	200	64	10150

0	1	2	3	4
Warhead (cost / pcs)	Dismantle Cleaning Destroy of the old charge Recharging with new explosives Replacement of igniters Assembly	1500	16	5400
Sustainer (cost / pcs)	Dismantle Cleaning Destroys of the old fuel Recharging with fuel Replacement of igniters and squibs Assembly	4800	88	22750
Booster (cost / pcs)	Dismantle Cleaning Destroys of the old fuel Recharging with fuel Replacement of igniters and squibs Assembly	1600	48	10900
Airframe (cost / pcs)	Missile general checking Sections dismantle Interfaces refit Compartments checking Assembly	300	64	12100
Sub-Assembly tests (cost / batch)	Capacity tests after refitting	4200 for 310	420 missiles	290
Delivery (cost / pcs)	Boxes including at USD 2200 third-part co-work	100	16	6390
Final test (cost / batch)	Missile general checking, including 2 targets at USD 38000 third-part co-work	6600 for 310	420 missiles	660
Technological documentation (cost / batch)		1200 for 310	3240 missiles	1600

0	1	2	3	4
Technological devices	Including USD 66000 third-part co-work	7700 for 310	2160 missiles	1420
Cote	10 missile of 1,33 USD million each of batch destroyed	13.3 USD mill for 310	0 missiles	42900
Total				**128460**

This approximated result shows that for a medium-size air-defense missile [5], the resource renewal program involve a cost at less than 10% of the new one.

In the same time, the cost of the TRR program rejoins at approximately:

310 missiles x 128.460 USD each ≈

40 USD millions.

3.4 The restored value of the missile

The restored value of the missile will be calculated with the formula:

$$V_a = (V_i + V_{TRR}) * T_{LC}/(T_{LC} + T_{RL})$$

where V_a - actual value

      V_i - initial value

      V_{TRR} - technical resource renewal program value

      T_{LC} - time of lifecycle

      T_{RL} - time of restored life

Supposing an operational resource of 12 years for a missile and a restored period of 10 years by applying the resource renewal program, the value of the missile becomes:

$$V_a = (1329000 + 128460) * 12/(12 + 10)$$
$$\approx 795.000 \text{ USD}$$

i.e. approx. 60% of the new product value.

3.5 The program implementing technical and scientific support

In order to be capable to develop a missile life extension program by renewal of the technical resource, an industrial organization must disposes of the following facilities:

- Research and development capacity, including the tactical support doctrine
- Maintenance technological base
- Production capacities, partially in cooperation
- Access on the branch technology market
- Access on the branch materials and equipment market
- Financial support
- Testing infrastructure

"HENRI COANDA"
AIR FORCE ACADEMY
ROMANIA

"GENERAL M.R. STEFANIK"
ARMED FORCES ACADEMY
SLOVAK REPUBLIC

INTERNATIONAL CONFERENCE of SCIENTIFIC PAPER
AFASES 2014
Brasov, 22-24 May 2014

A continuously attention must be allowed to the scientific, technical and industrial infrastructure and personnel in order to assures the possibility of life extension programs applied to missiles and missile systems [7].

3.6 Financial risk of the program

Considering the budgetary year allocation at a cash flow of a half of the needed amount, with a 25% growth expectation and 20% of a discount factor, the NPV (Net Present Value) method can be used [1] to verify the financial risk of the project:

$$NPV = -I_0 + \sum_{i=1}^{N} \frac{E(FCF_i)}{(1 + WACC)^i}$$

where

WACC - weighted average cost of capital

I_0 - initial investment

i - numbers of years before cash flow occurs

NPV must be > 0 in order to consider the project feasible.

If some uncertainty of budgetary cash flow is considered, respectively did exist 50 – 50 percent chance to have in the second year an allowance of 25 USD millions or down at 20 USD millions, according [8] we can calculate the NPV as:

$$NPV = 0.5\max\left[\frac{-20}{1.2} + \frac{25}{1.2^2}, 0\right] + 0.5\max\left[\frac{-20}{1.2} + \frac{20}{1.2^2}, 0\right]$$

= 0.5max[-16.666+17.361, 0]+ 0.5max [-16.666+13.888, 0]= 0.3475 + 0 = 0.35 > 0

4. CONCLUSIONS & ACKNOWLEDGMENT

A superior process aiming to an extended life cycle of a technical system – a missile peculiarly is represented by the up-grade program, which can be applied to few or all the system components. But such a process is most expensive and in many cases requires unavailable know-how type technical data.

Using the available information, we look for few widespread missile models concerning their up-grade programs and costs. Using an inflation calculator [11] we has aligned the costs at the Fiscal Year (FY) 2013, in order to calculate the growth of the costs by applying the modernization program.

System Version	Previous*		Following*
	USD / FY	USD FY13	USD FY13
AIM-9 Sidewinder	AIM-9L 84,000 / 1999	185,500	AIM-9X 664,900
AIM-120 AMRAAM	AIM-120C 400,000 / 1998	567,700	AIM-120D 1,492,000
RIM-67/174 Standard	SM-2ER 409,000 / 1981	1,032,470	SM-6ERAM 4,284,000

*data from [10], [12], [13], [14]

For the studied models, the costs growth is balanced for a medium value of 245%.

System	Growth
AIM-9 Sidewinder	258 %
AIM-120 AMRAAM	163 %
RIM-67/174 Standard	315 %
Media	**245 %**

Regarding in terms of costs to all the three technological way for extend the life cycle of a missile (presented at #2.1) easily can be observed that the TRR program represent an intermediary solution.

Type of life cycle extension program	Approx. Costs *
Technical resources carry-over	10 %
Technical resource renewal	60 %
Up-grade	250 %

* reported to the acquisitions unitary cost

The technical resource renewal (TRR) solution is recommended when the assured performance of the system have an acceptable level alongside of hole system life gained by program.

The TRR is a process that aims to refits the operational life of an expired system replacing some pieces and sub-assemblies olds with the

new made ones. The TRR supposes the technologies and equipments destined to:
- dismantling of the systems
- replacement of the pieces and sub-assemblies
- mechanical and electric assemblies
- adjustments and repairs
- coating and watermark
- general and specific tests

The TRR is a process similar to fabrication, executed in a technical-skilled entity, equipped with adequate production and testing facilities.

After the TRR program the system resource is refitted at the nominal value and can be extended in the future. In the TRR process a higher number of products from the application batch are destroyed, so the new certified batch is smaller than the initial number.

An essential aspect regarding the TRR program is the access to the pieces and sub-assemblies that will be replaced, these or equivalent ones must exist on market. That means if the TRR impose the replacement of equipment or pieces which is no longer produces, the program cannot be executed.

The TRR refits the system use capability at the initial values and parameters, but don't correct the morale usage of the equipment.

REFERENCES

[1] Luenberger,D.G., (1998), *Investment Science*, Oxford University Press

[2] Rădulescu, M., Şandru, V., (2014), *Advanced use of the e-resources in the research activities regarding to missile integrated systems development*, the 10th International Scientific Conference eLearning and Software for Education, April 24-25, Bucharest, Romania

[3] Rădulescu, M., Mihăilescu, C., Marinescu, M., (2013), *Some aspects of the air defense missiles up- grading*, Proceedings of 1st International Conference New Challenges in Aerospace Sciences, ISSN 2344-4762, NCAS 2013, pp.129-133, 7-8 November, Bucharest, Romania

[4] Rădulescu, M., Şandru, V., (2013), *Prelungire de resursa, revitalizare si modernizare pentru complexele de rachete antiaeriene*, Revista Gandirea Militara Romaneasca Nr. 5, pp. 70 – 79, ISSN 1454-0460, Bucuresti, Romania

[5] Rădulescu, M., Calefariu, E., (2012), *Aspects Regarding Technical and Economic Upgrade Elements in the Case of an A.D. Missile System*, Proceedings of the 14th WSEAS International Conference on Mathematical and Computational Methods in Science and Engineering, pp. 236-242, ISSN: 2227-4588, ISBN: 978-1-61804-117-3, Sliema, Malta

[6] Şandru, V., (2013), *The current stage of air defense systems' structure and performances. SAM systems comparative analysis in Romanian inventory*, Review of the "Henri Coandă" Air Force Academy, No 1 (23), pp. 107 – 112, ISSN 1842-9238, Brasov, Romania

[7] Şandru, V., Rădulescu, M., Ciufudean, C., Boşcoianu, E.C., (2012), *Critical Aspects Regarding the Integration of a Low-Cost Up-grade Architecture in High-technology Assets for Defense*, Proceedings of the 17th WSEAS International Conference on Applied Mathematics, pp. 89-94, ISBN: 978-1-61804-148-7, Montreux, Switzerland

[8] Shao Rong Song, (2006), *Real Option Approach to R&D Project Valuation*, Dissertation for the degree of MA in Finance and Investments, p.26

[9] ***, *Cost estimating for air-to-air missiles*, (1983), The Congress of the United States – Congressional Budget Office, January, Table 1, p.11

[10] ***, GAO-13-294SP Defense Acquisitions Assessments of Selected Weapon Programs, US Government Accountability Office, March 2013, p. 43

[11] ***, The inflation calculator, http://www.westegg.com/inflation/infl.cgi

[12] ***, Aerospace & Defense Intelligence Report, US missile/munitions program, Raytheon AIM-120 AMRAAM, http://www.bga-aeroweb.com/ Defense/AMRAAM.html#DoD-Spending

[13] ***, RIM-67 Standard, http://en.wikipedia.org/wiki/RIM_67_Standard

[14] ***, RIM-174 Standard ERAM, http://en.wikipedia.org/wiki/RIM-174_Standard_ERAM

UNSTEADY AERODYNAMIC MODEL FOR AN AIRFOIL WITH TIME DEPENDENT BOUNDARY CONDITIONS

**Constantin ROTARU*, Pericle Gabriel MATEI*, Raluca Ioana EDU*,
Mihai ANDRES-MIHĂILĂ***

*Faculty of Mechatronics and Armament Integrated Systems, Military Technical Academy, Bucharest, Romania

Abstract: This paper presents a mathematical model of an unsteady fluid flow around an airfoil where the time dependency is introduced through the boundary conditions. The methods of solution that were developed for these models included the treatment of the zero normal flow on a solid surface and the use of the unsteady Bernoulli equation. As a result of the nonuniform motion, the wake becomes more complex than in the corresponding steady flow case and therefore the path along which the airfoil moves was assumed to be prescribed. One of the more difficult aspects of the unsteady problem is the modeling of the vortex wake's shape and strength, which depend on the time history of the motion. In the paper the wake shed from the trailing edge of the lifting surfaces was modeled by vortex distributions.

Keywords: unsteady aerodynamics, vortex flow, airfoil circulation

1. INTRODUCTION

In an incompressible and irrotational fluid flow, the velocity field can be obtained by solving the continuity equation. However, the incompressible continuity equation does not directly include time-dependent terms and the time dependency is introduced through the boundary conditions. The methods of solution for steady flows can be used with only small modifications that include the treatment of the zero normal flow on a solid surface boundary conditions and the use of the unsteady Bernoulli equation. As a result of the nonuniform motion, the wake becomes more complex than in the corresponding steady flow case and it should be properly accounted for.

The unsteady motion of the surface on which the "zero normal flow" boundary condition is applied, is described in a body-fixed coordinate system (x, y, z) and the motion of the origin of this coordinate system (Fig. 1) is then prescribed in an inertial frame of reference (X, Y, Z).
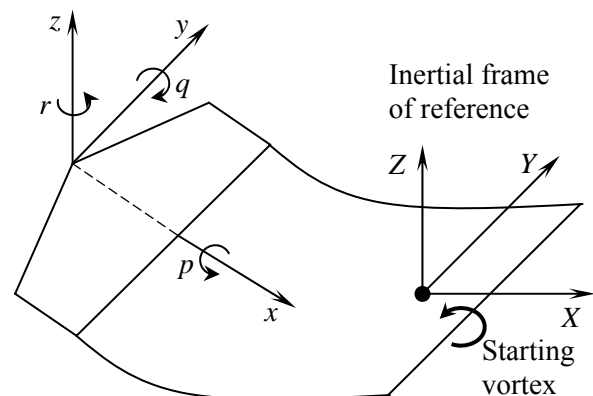
Fig. 1. Coordinate systems

At the $t > 0$, the relative motion of the origin of the body fixed frame of reference is prescribed by its location $R_0(t) = (X_0, Y_0, Z_0)$ and the instantaneous orientation $\Theta(t) = (\varphi, \theta, \psi)$, where (φ, θ, ψ) are the Euler rotation angles [1].

The fluid surrounding the body is assumed to be inviscid, irrotational and incompressible over entire flow field, excluding the body's solid boundaries and its wake. Therefore, a velocity potential $\Phi(X, Y, Z)$ can be defined in the inertial frame and the continuity equation in this frame of reference becomes $\nabla^2\Phi = 0$ and the boundary condition requiring zero normal velocity across the body's solid boundaries is

$$(\nabla\Phi + \vec{v}) \cdot n = 0 \tag{1}$$

where $\vec{v}$ is the surface velocity and $\vec{n}(x, y, z, t)$ is the unity vector normal to this moving surface (v is defined with minus sign so that the undisturbed flow velocity will be positive in the body's frame of reference).

The location and orientation of $\vec{n}$ can vary with time, so, the time dependency of equation $\nabla^2\Phi = 0$ is introduced through the boundary condition. The second boundary condition requires that the flow disturbance due to the body's motion through the fluid, should diminish far from the body,

$$\lim_{|R - R_0| \to \infty} \nabla\Phi = 0 \tag{2}$$

where $R = (X, Y, Z)$.

On the other hand, the Kelvin equation could be an additional condition for the unsteady flow, that can be used to determine the stream wise strength of the vorticity shed into a wake, so, the circulation Γ around a fluid curve enclosing the body and its wake is conserved,

$$d\Gamma / dt = 0 \tag{3}$$

Because of the boundary condition this problem becomes time dependent and it could be solved easier in the body-fixed coordinate system [2]. A transformation from (X, Y, Z) coordinate system to (x, y, z) coordinate system should include the translation and the rotation of the (x, y, z) system and may have the following form

$$
\begin{pmatrix} x \\ y \\ z \end{pmatrix} =
\begin{pmatrix} 1 & 0 & 0 \\ 0 & \cos(\varphi t) & \sin(\varphi t) \\ 0 & -\sin(\varphi t) & \cos(\varphi t) \end{pmatrix}
$$

$$
\times \begin{pmatrix} \cos(\varphi t) & 0 & -\sin(\varphi t) \\ 0 & 1 & 0 \\ \sin(\varphi t) & 0 & \cos(\varphi t) \end{pmatrix}
$$

$$
\times \begin{pmatrix} \cos(\varphi t) & \sin(\varphi t) & 0 \\ -\sin(\varphi t) & \cos(\varphi t) & 0 \\ 0 & 0 & 1 \end{pmatrix}
$$

$$
\times \begin{pmatrix} X - X_0 \\ Y - Y_0 \\ Z - Z_0 \end{pmatrix}
$$

The kinematic velocity $\vec{v}$ of the undisturbed fluid due to the motion of the airfoil as viewed in the body frame of reference is given by

$$\vec{v} = -\left(\vec{V}_0 + \vec{v}_{rel} + \vec{\Omega} \times \vec{r}\right) \tag{4}$$

where

$$
\begin{cases}
\vec{V}_0 = (\dot{X}_0, \dot{Y}_0, \dot{Z}_0) \\
\vec{v}_{rel} = (\dot{x}, \dot{y}, \dot{z}) \\
\vec{\Omega} = (p, q, r) \\
\vec{r} = (x, y, z)
\end{cases}
\tag{5}
$$

At any moment the continuity equation is independent of the coordinate system orientation and the mass is conserved [3]. Therefore, the quantity $\nabla^2\Phi$ is independent of the instantaneous coordinate system and the continuity equation in terms of (x, y, z) remains unchanged, $\nabla^2\Phi = 0$.

2. WAKE SHAPE

The zero velocity normal to the solid surface boundary condition in the body frame is

$$\left(\nabla\Phi - \vec{V}_0 - \vec{v}_{rel} - \vec{\Omega} \times \vec{r}\right) \cdot \vec{n} = 0 \tag{6}$$

in (x, y, z) coordinates.

In the case of more complex flow field, when the modeling of nonzero velocity components across the boundaries is desired, a

"HENRI COANDA"
AIR FORCE ACADEMY
ROMANIA

"GENERAL M.R. STEFANIK"
ARMED FORCES ACADEMY
SLOVAK REPUBLIC

INTERNATIONAL CONFERENCE of SCIENTIFIC PAPER
AFASES 2014
Brasov, 22-24 May 2014

transpiration velocity, V_n can be added, so, the above equation becomes

$$\left(\nabla\Phi - \vec{V}_0 - \vec{v}_{rel} - \vec{\Omega}\times\vec{r}\right)\cdot\vec{n} = V_n \qquad (7)$$

For incompressible flows the instantaneous solution is independent of time derivatives, therefore the steady-state solution techniques can be used to approach the time dependent problem by substituting at each moment, the instantaneous boundary condition

$$\left(\nabla\Phi + \vec{v}\right)\cdot n = 0 \qquad (8)$$

For lifting flow conditions, the magnitude of circulation depends on the wake shape and on the location of the wake shedding line [4]. Taking into consideration that the wake is force free, the Kutta-Jukovski theorem states that

$$V_\infty \times \gamma_w = 0 \qquad (9)$$

so, when the wake is modeled by a vortex distribution of strength γ_w the velocity V_∞ should be parallel to the circulation vector γ_w.

Solution of the equation $\nabla^2\Phi = 0$ in (x, y, z) coordinates, provides the velocity potential and the velocity components [5]

$$\begin{cases} u = \partial\Phi/\partial X \\ v = \partial\Phi/\partial Y \\ w = \partial\Phi/\partial Z \end{cases} \qquad (10)$$

The resulting pressure can be computed by the Bernoulli equation

$$\frac{p_\infty - p}{\rho} = \frac{1}{2}(\nabla\Phi)^2 + \frac{\partial\Phi}{\partial t} =$$
$$= \frac{1}{2}\left[\left(\frac{\partial\Phi}{\partial X}\right)^2 + \left(\frac{\partial\Phi}{\partial Y}\right)^2 + \left(\frac{\partial\Phi}{\partial Z}\right)^2\right] + \frac{\partial\Phi}{\partial t} \qquad (11)$$

The time derivative in the (x, y, z) system is

$$\left(\frac{\partial}{\partial t}\right)_{inertial} =$$
$$-\left(\vec{V}_0 + \vec{\Omega}\times\vec{r}\right)\cdot\left(\frac{\partial}{\partial x}, \frac{\partial}{\partial y}, \frac{\partial}{\partial z},\right) + \left(\frac{\partial}{\partial t}\right)_{body} \qquad (12)$$

therefore, the pressure difference $(p_\infty - p)/\rho$ has the form

$$\frac{p_\infty - p}{\rho} = \frac{1}{2}\left[\left(\frac{\partial\Phi}{\partial x}\right)^2 + \left(\frac{\partial\Phi}{\partial y}\right)^2 + \left(\frac{\partial\Phi}{\partial z}\right)^2\right] -$$
$$- \left(\vec{V}_0 + \vec{\Omega}\times\vec{r}\right)\cdot\nabla\Phi + \frac{\partial\Phi}{\partial t}$$

The magnitude of the velocity $\nabla\Phi$ is independent of the frame of reference.

3. PLAT PLATE MODEL

For a flat plate at an angle of attack α moving at a constant velocity U_∞ in the negative X direction (Fig. 2) the translation of the origin $\vec{V}_0$, the rotation $\vec{\Omega}$ and the normal vector $\vec{n}$, are

$$\vec{V}_0 = \left(\dot{X}_0, \dot{Y}_0, \dot{Z}_0\right) = \left(-U_\infty, 0, 0\right)$$
$$\vec{\Omega} = \left(0, 0, 0\right) \qquad (13)$$
$$\vec{n} = \left(\sin\alpha, 0, \cos\alpha\right)$$
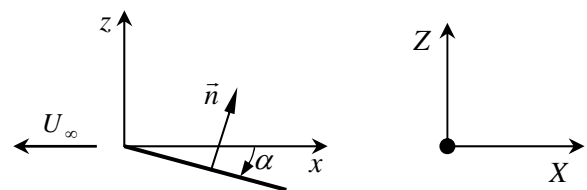
Fig. 2. Translation of a flat plate

The boundary condition requiring zero normal velocity across the plate is

$$\left(\nabla\Phi - \vec{V}_0 - \vec{\Omega}\times\vec{r}\right)\cdot\vec{n} = 0 \qquad (14)$$

or

$$\left(\frac{\partial \Phi}{\partial x} + U_\infty, \, 0, \, \frac{\partial \Phi}{\partial z}\right) \cdot (\sin\alpha, \, 0, \, \cos\alpha) = 0$$

The above scalar product has the form

$$\left(\frac{\partial \Phi}{\partial x} + U_\infty\right)\sin\alpha + \frac{\partial \Phi}{\partial z}\cos\alpha = 0 \qquad (15)$$

therefore

$$\frac{\partial \Phi}{\partial z} = -\left(\frac{\partial \Phi}{\partial x} + U_\infty\right)\tan\alpha \qquad (16)$$

If the airfoil (plate) is represented by a lumped-vortex element with the vortex placed at the quarter chord (Fig. 3), the Kutta condition is satisfied.
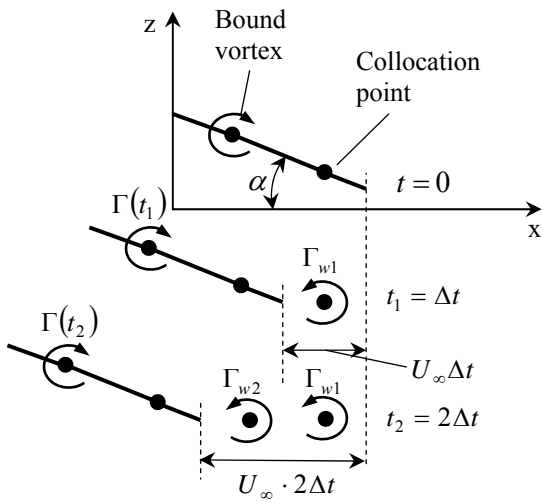
Fig. 3. Development of the wake vortex

The concentrated wake vortex has to be placed along the path traveled by the trailing edge [6].

If the wake vortex is placed at the middle of this path, then the zero normal flow boundary condition at the plate's three-quarter point is

$$-\frac{\Gamma(t_1)}{2\pi\frac{c}{2}} + \frac{T_{w1}}{2\pi\left(\frac{c}{4} + \frac{U_\infty\Delta t}{2}\right)} = -U_\infty\sin\alpha \quad (17)$$

This equation can be rewritten in the form

$$w_{body} + w_{wake} + U_\infty\sin\alpha = 0 \qquad (18)$$

which indicates that the sum of the normal velocity induced by the airfoil, w_{body}, by the wake, w_{wake}, and by the free stream must be zero.

On the other hand, an additional equation could be obtained from the Kelvin condition $(d\Gamma/dt = 0)$, namely

$$\Gamma(t_1) + \Gamma_{w1} = 0 \qquad (19)$$

The above set of equations with the unknowns $\Gamma(t_1)$ and Γ_{w1} gives the following solution

$$\begin{cases} \Gamma(t_1) = \dfrac{U_\infty\sin\alpha}{\dfrac{1}{2\pi}\left(\dfrac{1}{\frac{c}{2}} + \dfrac{1}{\frac{c}{4} + \frac{1}{2}U_\infty\Delta t}\right)} \\[4mm] \Gamma_{w1} = -\dfrac{U_\infty\sin\alpha}{\dfrac{1}{2\pi}\left(\dfrac{1}{\frac{c}{2}} + \dfrac{1}{\frac{c}{4} + \frac{1}{2}U_\infty\Delta t}\right)} \end{cases} \quad (20)$$

After the second time step, $t_2 = 2\Delta t$, the airfoil is in a new location. For high Reynolds number flows, vortex decay is negligible and therefore the strength Γ_{w1} will not change with time. At $t_2 = 2\Delta t$ the two equations describing the zero normal flow boundary condition and the Kelvin condition are:

$$\begin{cases} -\dfrac{\Gamma(t_2)}{2\pi\frac{c}{2}} + \dfrac{\Gamma_{w2}}{2\pi\left(\frac{c}{4} + \frac{1}{2}U_\infty\Delta t\right)} + \\[4mm] +\dfrac{\Gamma_{w2}}{2\pi\left(\frac{c}{4} + \frac{1}{2}U_\infty\Delta t + U_\infty\Delta t\right)} = -U_\infty\sin\alpha \\[4mm] \Gamma(t_2) + \Gamma_{w2} + \Gamma_{w2} = 0 \end{cases}$$

This set is solved for $\Gamma(t_2)$ and Γ_{w2}, while Γ_{w1} is known from the previous calculation at $t = t_1$. At $t = 3\Delta t$ the two equations can be written in a similar manner

$$\begin{cases} -\dfrac{\Gamma(t_3)}{2\pi\frac{c}{2}} + \dfrac{\Gamma_{w3}}{2\pi\left(\frac{c}{4} + \frac{1}{2}U_\infty\Delta t\right)} + \\[4mm] \dfrac{\Gamma_{w2}}{2\pi\left(\frac{c}{4} + \frac{3}{2}U_\infty\Delta t\right)} + \dfrac{\Gamma_{w1}}{2\pi\left(\frac{c}{4} + \frac{5}{2}U_\infty\Delta t\right)} = \\[4mm] = -U_\infty\sin\alpha \\[4mm] \Gamma(t_3) + \Gamma_{w3} + \Gamma_{w2} + \Gamma_{w1} = 0 \end{cases}$$

“HENRI COANDA”
AIR FORCE ACADEMY
ROMANIA

“GENERAL M.R. STEFANIK”
ARMED FORCES ACADEMY
SLOVAK REPUBLIC

INTERNATIONAL CONFERENCE of SCIENTIFIC PAPER
AFASES 2014
Brasov, 22-24 May 2014

This set is solved for $\Gamma(t_3)$ and Γ_{w3}, while Γ_{w2} and Γ_{w1} are known from the previous calculation at $t = t_2$.

The values of $\Gamma(t_i)$ and Γ_{wi} are found from the following set of equations written in the matrix form

$$\begin{bmatrix} -\dfrac{1}{2\pi\dfrac{c}{2}} & \dfrac{1}{2\pi\left(\dfrac{c}{4}+\dfrac{1}{2}U_\infty\Delta t\right)} \\ 1 & 1 \end{bmatrix} \cdot \begin{bmatrix} \Gamma(t_i) \\ \Gamma_{wi} \end{bmatrix} =$$

$$\begin{bmatrix} -U_\infty\sin\alpha - \displaystyle\sum_{j=1}^{i-1}\dfrac{\Gamma_{w(i-j)}}{2\pi\left[\dfrac{c}{4}+(2j+1)\dfrac{U_\infty\Delta t}{2}\right]} \\ -\displaystyle\sum_{j=1}^{i-1}\Gamma_{wj} \end{bmatrix}$$

4. WORTEX DISTRIBUTION

The wake shed from the trailing edge of the lifting surfaces can be modeled by doublet or vortex distributions (Fig. 4).

If the airfoil circulation is varying continuously, then a continuous vortex sheet is shed at the trailing edge and can be approximated by a discrete vortex model where the strength of each vortex Γ_{wi} is equal

to the vorticity shed during the corresponding time step Δt, such that

$$\Gamma_{wi} = \int_{t-\Delta t}^{t}\gamma_{wi}(t)U_\infty dt \qquad (21)$$

The distance and relative angle to the trailing edge are important numerical parameters and the wake vortex location should be closer to the position of the trailing edge (Fig. 5).
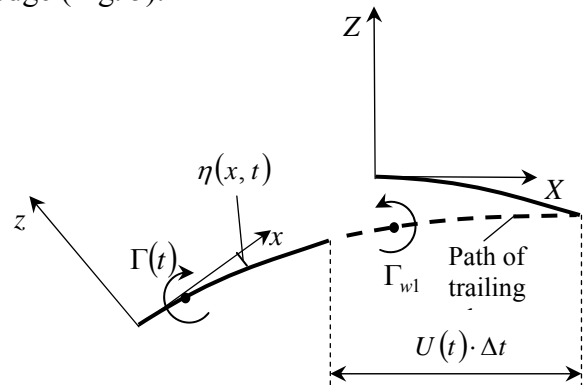
Fig. 5. Position of the discrete vortex

The placement of the discrete vortex at the middle of the interval $U(t)\Delta t$ is an approximation that underestimates the induced velocity when compared with the continuous wake vortex sheet result. A numerical approach to correct for this wake discretization error is to place the latest vortex closer to the trailing edge.

Fig. 4. Discretization of the wake's vortex distribution

The Helmholtz theorem implies that there is no vortex decay, that is if a wake vortex element is shed from the trailing edge, its strength is conserved. At each time step the combined airfoil and wake induced velocity $(u, w)_i$ is calculated and the vortex elements are moved by $(\Delta x, \Delta y) = (u, w)_i \Delta t$. The system coordinate (x, z) is selected such that the origin is placed on the path and the x coordinate axis is tangent to the path. The airfoil camberline is given in this coordinate system by $\eta(x, t)$, which is considered to be small $(\eta/c \ll 1)$ and the path radius of curvature is also much larger than the chord c.

5. MATHEMATICAL FORMULATION

The time-dependent version of the boundary condition requiring no normal flow across the surface is

$$\left(\nabla\Phi - \vec{V}_0 - \vec{v}_{rel} - \vec{\Omega} \times \vec{r}\right) \cdot \vec{n} = 0 \qquad (22)$$

where $\Phi = \Phi_B + \Phi_w$ is the equivalent of the steady-state velocity potential, divided into airfoil potential Φ_B and to a wake potential Φ_w, $\vec{V}_0$ is the instantaneous velocity of the coordinate system origin, $V_0 = \left[-U(t), 0, 0\right]$, $\vec{v}_{rel}$ is the relative velocity of the chordline within coordinate system (x, y, z), $v_{rel} = \left[0, 0, \dfrac{\partial\eta}{\partial t}\right]$, $\vec{\Omega}$ is the instantaneous rotation, $\Omega = \left[0, \dot{\theta}(t), 0\right]$ and $\vec{n}$ is the normal vector to the surface

$$n = \frac{\left[-\dfrac{\partial\eta}{\partial x}, 0, 1\right]}{\sqrt{\left(\dfrac{\partial\eta}{\partial x}\right)^2 + 1}} \qquad (23)$$

If the wake potential is known from the previous time steps then

$$\frac{\partial\Phi_B}{\partial z} = \left(\frac{\partial\Phi_B}{\partial x} + \frac{\partial\Phi_w}{\partial x} + U - \dot{\theta}z\right)\frac{\partial\eta}{\partial x} - \\ - \frac{\partial\Phi_w}{\partial z} - \dot{\theta}x + \frac{\partial\eta}{\partial t} \qquad (24)$$

On the other hand, the downwash induced by the airfoil bound circulation $\gamma(x, t)$ with assumptions presented above is

$$\frac{\partial\Phi_B}{\partial z} = -\frac{1}{2\pi}\int_0^c \frac{\varphi(x_0, t)}{x - x_0} dx_0 \qquad (25)$$

so, the time dependent equivalent of the steady-state boundary condition becomes

$$-\frac{1}{2\pi}\int_0^c \frac{\varphi(x_0, t)}{x - x_0} dx_0 = U(t)\frac{\partial\eta(x, t)}{\partial x} - \\ -\frac{\partial\Phi_w}{\partial z} - \dot{\theta}(t)\cdot x\frac{\partial\eta(x, t)}{\partial t} \qquad (26)$$

with the Kutta condition $\gamma(c, t) = 0$.

Based on the classical approach of Glauert, a similar solution to the vortex distribution is

$$\gamma(\theta, t) = 2U(t)\left[A_0(t)\frac{1 + \cos\theta}{\sin\theta} + \sum_{n=1}^{\infty} A_n(t)\sin n\theta\right]$$

where

$$A_0(t) = -\frac{1}{\pi}\int_0^\pi \frac{w(x, t)}{U(t)} d\theta$$

$$A_n(t) = \frac{2}{\pi}\int_0^\pi \frac{w(x, t)}{U(t)}\cos n\theta\, d\theta$$

The lift force per unit span L' and the pitching moment about the airfoil's leading edge M_0 are

$$L'(t) = \pi\rho c\left\{\left[U^2 A_0 + \frac{3c}{4}\frac{\partial}{\partial t}(U A_0)\right] + \\ \left[+ U^2\frac{A_1}{2} + \frac{c}{4}\frac{\partial}{\partial t}(U A_1) + \frac{c}{8}\frac{\partial}{\partial t}(U A_2)\right]\right\}$$

$$M_0(t) = -\rho c^2\frac{\pi}{2}\left[\frac{U^2}{2}A_0 + \frac{7c}{8}\frac{\partial}{\partial t}(U A_0) + \\ + \frac{U^2}{2}A_1 + \frac{3c}{8}\frac{\partial}{\partial t}(U A_1)\right] - \\ -\rho c^2\frac{\pi}{2}\left[-\frac{U^2}{4}A_2 + \frac{c}{8}\frac{\partial}{\partial t}(U A_2) - \\ -\frac{c}{32}\frac{\partial}{\partial t}(U A_3)\right]$$

6. NUMERICAL RESULTS

The results of the computations for a number of steps of 200, a velocity $U = 50\, \text{m/s}$ an angle of attack $\alpha = 5\cdot\pi/180\, \text{rad}$ and a time step $\Delta t = 1/(4\cdot U)$ are presented in fig. 6. The circulation at $t = 0$ is zero since the airfoil is still at rest. At $t > 0$ the circulation increases

"HENRI COANDA"
AIR FORCE ACADEMY
ROMANIA

"GENERAL M.R. STEFANIK"
ARMED FORCES ACADEMY
SLOVAK REPUBLIC

INTERNATIONAL CONFERENCE of SCIENTIFIC PAPER
AFASES 2014
Brasov, 22-24 May 2014

but is far less than the steady-state value due to the downwash of the starting vortex.
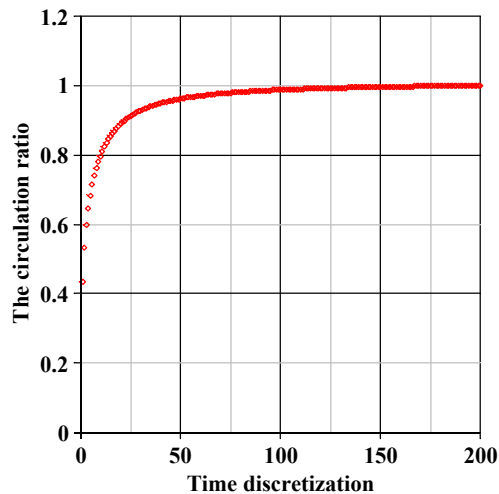
Fig. 6. The circulation ratio $\Gamma(t)/\Gamma(200)$

In the above figure was represented the ratio between $\Gamma(t)/\Gamma(200)$, where the number of time steps was 200. After approximately 200 steps this ratio reaches the value equals with the unity. To compute the lift , the small disturbance approximation $(U_\infty >> \nabla\Phi)$ is applied to the unsteady Bernoulli equation

$$\frac{p_\infty - p}{\rho} = (U_\infty, 0, 0)\cdot\nabla\Phi + \frac{\partial\Phi}{\partial t} \tag{27}$$

Taking into account that

$$\frac{\partial\Phi}{\partial x}(x, 0, \pm 0) = \pm\frac{\gamma(x)}{2} \tag{28}$$

the pressure difference between the airfoil's lower and upper surface is

$$\Delta p = p_l - p_u = 2\rho\left[U_\infty\frac{\gamma(x)}{2} + \frac{\partial\Phi}{\partial t}\right] =$$
$$= \rho U_\infty\gamma(x) + \rho\frac{\partial}{\partial t}\int_0^x\gamma(x)dx \tag{29}$$

For the lumped-vortex method there is only one airfoil vortex and therefore the lift and drag per unit span are

$$\begin{cases} L' = \rho\left[U_\infty\Gamma(t) + \frac{\partial}{\partial t}\Gamma(t)c\right] \\ D' = \rho\left[w_w(x, t)\Gamma(t) + \frac{\partial}{\partial t}\Gamma(t)c\,\alpha\right] \end{cases} \tag{30}$$

One important parameter used in the description of unsteady aerodynamics und unsteady airfoil behavior is the reduced frequency, k, defined as $k = \omega\cdot c/(2V)$, where ω is the angular frequency, c is the chord of the airfoil and V is the flow velocity. According to the dimensional analysis, the resultant force, F, on the airfoil of chord c, can be written in functional form as $F/(\rho V^2 c^2) = f(Re, M, k)$. For $k = 0$ the flow is steady and for $0 \le k \le 0.05$ the flow can be considered quasi-steady, that is, unsteady effects are generally small. Flows with characteristic reduced frequencies above of 0.05 are considered unsteady [1].

The lift amplitude and phase of lift for pure angle of attack oscillations are presented in Fig. 7 and Fig. 8, where the significance of the apparent mass contribution to both the amplitude and phase can be appreciated.
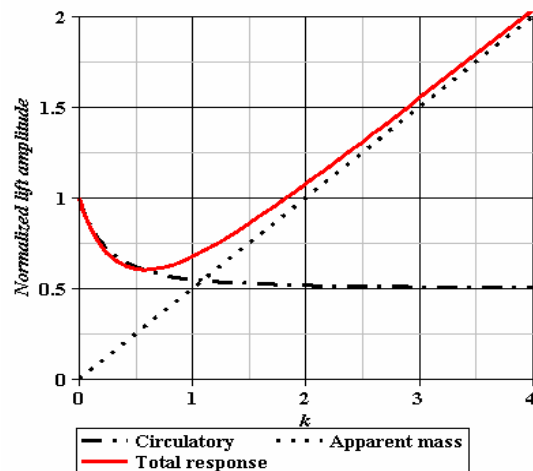
Fig. 7. Normalized lift amplitude
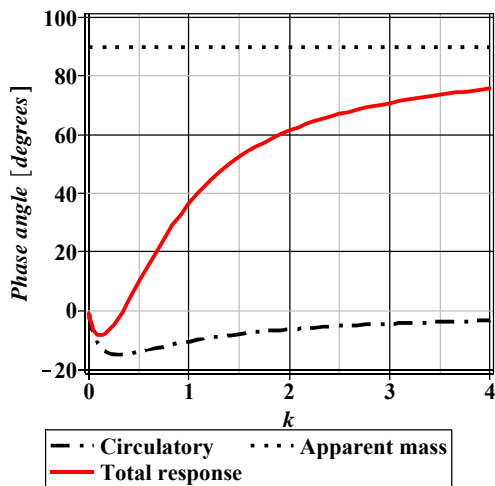
Fig. 8. Phase angle

At lower values of reduced frequency, the circulatory terms dominate the solution. At higher values of reduced frequency, the apparent mass forces dominate.

6. CONCLUSIONS

The lift at $t = 0_+$ is exactly half of the steady-state lift due to the acceleration portion of the lift that results from the change in the upwash, not due to the airfoil circulation.

The drag force has two components, one due to the wake-induced downwash which rotates the circulatory lift term by an induced angle w_w / U_∞ and other due to the fluid acceleration $\partial\Phi / \partial t$ which acts normal to the flat plate, and its contribution to the drag is the second lift term times α. One of the more difficult aspects of the unsteady problem is the modeling of the vortex wake's shape and strength, which depend on the time history of the motion.

The unsteady forces produced on a rotor blade arise primarily because of the vertical velocity between the wake disturbance and the airfoil surface. In linear theory, this is treated as an imposed unsteady upwash field, which must be used to satisfy the boundary conditions of flow tangency on the airfoil surface.

The airfoil can generate high lift as a result of a vortex that is shed at the leading edge at the instant of stall. The vortex travels back over the top of the airfoil carrying with it a low pressure wave that accounts for the very large lift coefficient.

REFERENCES

1. Gareth, D. P., *Helicopter Flight Dynamics,* AIAA Education Series (2007).
2. Gordon L., *Principles of Helicopter Aerodynamics,* Cambridge University Press (2007).
3. Katz, J., Plotkin, A., *Low Speed Aerodynamics,* Second Edition, Cambridge University Press, (2010).
4. Rotaru, C., Circiu, I., Boscoianu M. *Computational Methods for the Aerodynamic Design*, Review of the Air Force Academy, No 2(17), pp. 43-48 (2010).
5. Rotaru, C., Mihăilă M., Matei, P., Stefan, A., *Computing Nonlinear Characteristics of Helicopter Rotor Blades,* Review of the Airforce Academy, Vol. XI, No I(23), ISSN 2069-4733, pp.5-12 (2013).
6. Rotaru, C., Arghiropol A., *Maple soft solutions for nonlifting flows over arbitrary bodies,* Proceedings of the 3rd WSEAS international conference on FINITE DIFFERENCES - FINITE ELEMENTS - FINITE VOLUMES - BOUNDARY ELEMENTS, ISSN 1970-2769, pp. 270-274 (2010).
7. Maple soft documentation

ELECTRONIC WAR AND MODERNIZATION OF AIR DEFENCE MEANS

Prof. Ing. Milan SOPÓCI, PhD.* Col. Eng. Ľubomír MATTA *

*Department of Management, The Armed Forces Academy of General Milan Rastislav Štefánik in Liptovský Mikuláš

Abstract: This article deals with current problems of evalution of the effectivity of radars protection against electroning jamming. The first part examines experience with electronic warfare in local conflicts and electronic countermeasures. The paper presents basic notions and division of electronic jamming.

The second part describes a new method of evaluating effectivity of influence of electronic jamming on radars activity. Using Saaty method of multifunctional evaluation in computer environment gives distinctioned values to differcut sorts of jamming. The example of Air Defence missiles system SA – 6 Gainfull shows the possibility of using this methodic.

Introduction

A plane has gone missing. Not a small one, but a large Boening, Malaysia Aerlines with more than two hundred people on board and nobody can find it. It is just China that admit they have more than 20 satellites in that region monitoring the area. Nobody knows how many satellites do the USA, Russia, Great Britain and France have, but we can assume that it might be far more. And in spite of that, a plane goes missing. Could this be caused by Martians? Or are we witnessing another electronic war, the results of which will be known in 20 or 30 years? We should remember what the electronic war is and when it arose. As a consequence, smaller countries like us should modernize radar and missile machinery, different approaches, evaluations and policy of solving problems.

1. Electronic war

Electronic war – a term not many people know today. They do not know it first occured in 1967 in relation to the Third Arab-Israeli War also called Six-Day War due to its short duration and rapid progress. The author of the term is major Edgar Ballance, the later Chief of Intelligence service of the British Air Force. He relates the usage of this term with appointing gen. Bar-Lev the Chief of Staff of Israeli army on 3rd December 1967. The general, who later became famous for creating the so-called Bar-Lev Line along the Suez Canal on the occupied Siani Peninsula, has

probably for the first time realised what electronics meanins especially within combat aviation and air defence. At the beginning of the year 1968 Israel took action that is part of the electronic fight even today(1):

- equipping all planes (Phantom) with radiation warning receivers NRL and launched missiles warning system,
- equipping planes with jammers– especially with active narrowband ones,
- equipping diverse groups deployed to the Egyptian coast of Suez Canal with simple radiolocation jammers – active and passive, while until this time they had been focused on direct elimination o fair defence units (in the first part of the war up to 70% of air defence units were eliminated by diverse groups),
- determining special groups for seizing radiolocation means or their parts (this was the way the special comando on 27th of December 1969 seized antenna set and parts of radiolocation devices of a P-12 telemeter, the predecessor of P-18),
- elektronic monitoring of the representatives of Arab forces and their elimination (9th March 1969 the Chief of Staff of the Egyptian Armed Forces gen. Riad was killed, 9th September 1969 chief military advisor of USSR in Egypt killed).

Egypt reacted to these measures adequately:

- enhancing and equipping all aviation resources and air defence with unified identification device (at the beginning of the war the ratio of shootdowns was 1:1),
- deploying air and underwater diverse groups to the other bank of Suez Canal,
- equipping with the modernized PLRK SA-2M and SA-3M,
- arrival of soviet pilots and new MiG-21 Js in Egypt and their deployment in direct air defence of Nile road from Aswan to the Mediterranean sea,
- creating a system of early warning,
- creating systems of anti-aircraft missile defence around objects of state importance.

After the adoption of Rogers peace plan in 1970 it was time for analyzing and evaluating the mentioned measurements with a definite result – electronic warfare is becoming an integral part of any operation. The concept of **electronic war** was born.

At present, there is probably nobody who would doubt the importance of electronic measures related to the success of an operation or combat. Essential elements are (2):

- obtaining information superiority in the desired region,
- obtaining electromagnetic superiority in the field of electronic reconnaissance and electronic warfare.

Elektronic war, as a military activity in which the electromagnetic spectrum is used to obtain information about the enemy, performs organizational and technical measures for preventing, disrupting or impeding the enemy and protect one´s own electronic resources.

With the development of electronics the means of electronic warfare develop rapidly. Various forms and types of lighting weapons, laser weapons and high-frequency weapons are becoming a bigger and bigger threat for air defence, radiolocators and anti-aircraft launchers. For the most types of radiolocators, especially the older ones, the biggest threat is active, passive, broad-band or narrow-band, modulation or non-modulation jamming and all types reduce reconnaissance and firing options of launchers.
The second part of this article deals with fighting the enemy.

The division and effect of individual types of radiolocator, evaluation of radiolocators resistance and the effect of jamming on firing options of units, formations o fair defence were and continue to be current questions.

2. Air defence measures within the electronic war

Basic division of radiolocation jamming can be found in many sources (3). To evaluate the effect of individual types of jamming on the activities of radiolocators we can use the method of multicriteria evaluation. A group of

"HENRI COANDA"
AIR FORCE ACADEMY
ROMANIA

"GENERAL M.R. STEFANIK"
ARMED FORCES ACADEMY
SLOVAK REPUBLIC

INTERNATIONAL CONFERENCE of SCIENTIFIC PAPER
AFASES 2014
Brasov, 22-24 May 2014

evaluation experts has been chosen from teachers with rich experience from practice and lots of theoretical knowledge. Six types of jamming with a significant effect on activities of radiolocators were compared:

- active noise nawwor-band jamming,
- active noise broad-band jamming,
- nonsynchronous pulse jamming,
- synchronous pulse jamming, response,
- synchronous pulse jamming, non-response,
- passive jamming.

According to the Chart No 1, of comparing the significance of individual types of solutions we get a reciprocal matrix of pairwise comparison - Chart 2.

Chart 1

A1	9	8	7	6	5	4	3	2	x1	1	2	3	4	5	6	7	8	9	A2
A1	X																		A3
A1														X					A4
A1					X														A5
A1	X																		A6
A2	X																		A3
A2							X												A4
A2								X											A5
A2	X																		A6
A3																		X	A4
A3														X					A5
A3													X						A6
A4					X														A5
A4							X												A6
A5								X											A6

Chart 2

	E1	E2	E3	E4	E5	ΣE_i
A1	24	21	11	26	33	115
A2	23	18	24	19	27	111
A3	0	13	5	3	3	24
A4	22	13	20	13	5	73
A5	7	5	0	7	0	19
A6	3	0	5	0	6	14

After determining the maximum eigenvalue of matrix and determinant of the matrix,
$$6 \leq \lambda_{max} \leq 23 \qquad det = 0,000381$$
eigenvector of matrix will be the solution of homogenous set of linear equations, that will after modification be as follows:

$$w_1 - 0,1985\ w_2 - 0,3971\ w_3 - 0,9927\ w_4 - 1,1919\ w_5 - 1,5883\ w_6 = 0$$
$$w_2 - 0,4955\ w_3 - 1,2386\ w_4 - 1,4864\ w_5 - 1,9819\ w_6 = 0$$
$$w_3 - 0,9334\ w_4 - 1,2081\ w_5 - 1,5375\ w_6 = 0$$
$$w_4 - 0,4010\ w_5 - 0,8071\ w_6 = 0$$
$$w_5 - 1,1310\ w_6 = 0$$

Values of eigenvector after solving the equation:

$w_1 = w_2 = 0,3299$, $w_3 = 0,0574$, $w_4 = 0,1857$, $w_5 = 0,0515$, $w_6 = 0,0455$

$w_6 = 1$, $w_5 = 1,1310$, $w_4 = 1,2607$
$w_3 = 4,0806$, $w_2 = 7,2464$, $w_1 = 7,2464$
$\Sigma E_i = 21,9651$

The mentioned values can be used when evaluating the quality of radiolocator devices. For better understanding there is an example in Chart 3.

and after the modification of normalized eigenvector representing the value of individual types of jamming are as follows:

Chart 3

type of jamming	weight	protection device in RNRL 1S91
1.noise active narrow-band jamming	0,33	RRL 1S11M1 uses: - manual regulation of amplification of receivers; - realignment of transmitter frequency; - turning off the channel of the receiver, in which jamminghas been detected; NRL 1S31M1 uses: - manual regulation of amplification of receivers; - realignment of frequency; - switching on the „jamming 1S31M1" regime; - semiautomatic monitoring c in D; - using inertial tracking
2.noise active broad-band jamming	0,33	RRL 1S11M1 uses: - manual regulation of amplification of receivers; - realignment of transmitter frequency; - turning off the channel of the receiver, in which jamminghas been detected; NRL 1S31M1 uses: - manual regulation of amplification of receivers; - realignment of carrier frequency; - switching on the „jamming 1S31M1" regime; - semiautomatic monitoring c in D; - using inertial tracking
3.non-synchronous pulse jamming	0,057	- VNIS circuit - SMT circuit (selection of moving targets) - reducing amplification of jammed channel using the „RRU" knob.

“HENRI COANDA”
AIR FORCE ACADEMY
ROMANIA

“GENERAL M.R. STEFANIK”
ARMED FORCES ACADEMY
SLOVAK REPUBLIC

INTERNATIONAL CONFERENCE of SCIENTIFIC PAPER
AFASES 2014
Brasov, 22-24 May 2014

4. synchronous response pulse jamming	0,186	- VNIS circuit - SMT circuit (selection of moving targets) - reducing amplification of jammed channel using the „RRU“ knob.
5. synchronous pulse non-response jamming	0,051	- realignment of carrier frequency;
6.passive jamming	0,045	both RRL 1S11M1 and NRL 1S31M1 - next periodic compensation -2x or 4x subtraction; - wind compensation circuit (internal phasing); - SPC - with internal phasing; - with external phasing.

For individual types of jamming the mentioned circuits are used for RNRL 1S91, PLRK 2K-12 KUB. To determine the quality of radiolocator we can use the following formula:

$$K_{KV} = \frac{\sum\limits_{i=1}^{n} W_I}{\sum\limits_{j=1}^{n} W_J}$$

where: i – is the number of protection devices in radiolocator,

j – is the number of types of jamming affecting the radiolocator,

w – is the weight of individual types of jamming.

With proof we can confirm the effectivity of protection listed under numbers 1, 3 and 6,

then value $K_{KV} = \dfrac{0{,}427}{1} = 0{,}427$

The bigger the K_{KV} value, the better the quality of radiolocator regarding jamming protection. The coefficient value in last generation radar technology will be close to one.

Similarly we can apporach when counting the coefficient of jamming that affects the reduction of firing options, especially for determining the probability of eliminating the target and mathematical hope of the number of eliminated targets. Professional literature offers the relation to calculate the probability of eliminating target regarding the coefficient of jamming resistance – P_{CR} (3).

$$P_{CR} = \left[1 - \prod\limits_{i=1}^{n} (1 - P_i) \right] K_{KV}$$

or eventually $P_1 = P_2 = P_i$

$$P_{CR} = K_{KV} \cdot \left[1 - (1 - P_1)^n \right]$$

The calculation itself or the way of defining $k_{ru\ has}$ has never been stated and in practice various values k_{ru} have been used depending on individual literature. However, if

we have defined norstandardized weigh coefficients characterizing the relation between individual types of jamming and the coefficient characterizing the quality (resistance) of radiolocator, we can also determine the coefficient of jamming, which determines the value P_{CR}.

To calculaze K_{RU} we can use the following formula:

$$K_{RU} = \frac{1}{1 + \sum_{i=1}^{m} w_i}$$

where:

m – number of protection device agens radiolocator jamming,

w_j – weigh of individual type sof jamming.

For the example of calculating the quality of radiolocator the value P_{CR} provided $P_1 = 0,7$, when launching two rockets will be determined by following values.

$$P_{CR} = 0,7\left[1 - (1 - 0,7)^2\right] = 0,63$$

The credibility of the calculations will be higher the higher the quality of experts participating in input data of the multicriteria decision-making for the calculation of weights of individual types of jammings.

Conclusion

The above stated calculation of radiolocator coefficient and jamming coefficient is not a definite solution of the given issue. The methodology represents just one of the possible ways of solutions. It can be a stimulus for a discussion, as well as serve other researchers as one of the criteria for the evaluation of radiolocators and anti-aircraft launchers, for the selection of machinery necessary for the AF of SR. It can also allow to evaluate our own firing options in air combat more wisely in the phase of planning or operation.

Bibliography
1. BALLANCE, E.: *Electronic War in the Middle East* 1968 - 1970. London: Faber and Faber, 1974, 148 p.
2. Commander EW, Air Force Headquarters: *EW in present days*. Nitra, 2011.
3. *Manual rules of fire*. Praha, 1976.

THE ANALYSIS OF THE ALLOY $AlCu_4Mg_{1,5}Mn$ USED IN THE CONSTRUCTION OF UTILITY AIRCRAFTS

Cătălin-Andrei ȚUGUI[1,a], Petrică VIZUREANU[1,b], Dragoş Cristian ACHIȚEI[1], Ion PALAMARCIUC[1], Andrei-Victor SANDU[1]

[1] Faculty of Materials Science and Engineering, Technical University "Gheorghe Asachi" of Iasi-Romania, Department of Technologies and Equipments for Materials Processing, Blvd. Mangeron, No. 51, 700050, Iasi, Romania
[a]tzugui.andrei@yahoo.com, [b]peviz2002@yahoo.com,

Abstract: *In this paper we conducted a physic-chemical analysis for a $AlCu_4Mg_{1,5}Mn$ alloy propeller, from a small utility aircraft. Regarding the mechanical properties of the alloy, they are very good, especially machinability. Thus, if to an aluminium alloy a heat treatment for tempering is applied, it becomes more pliable and can be easily machined. After the processing operations, the alloy may be subjected to ageing, such treatment leads to an hardening, thereby improving the hardness thereof.*

Keywords: *aluminium, SEM, dilatometry, plane, propeller.*

1. INTRODUCTION

Aluminium is the most common metal in the earth's crust and in the chemical elements ranks third after oxygen and silicon. It has a high chemical activity and therefore, is found in nature only as compounds.

The first attempt of aluminium separation dates from 1810 and belongs to Davy, an english physicist who achieved electrolysis for aluminium hydroxide. Following this experience was not achieved aluminium but a Al-Fe alloy [1].

In 1854 Saint-Clair-Deville, used the Wohler method to obtain the aluminium in industry, replacing potassium with sodium and aluminium chloride, unstable and hygroscopic with double aluminium chloride solution [1].

2. ALUMINIUM IN THE AIRCRAFT INDUSTRY

To the evolution of metallic and non-metallic materials and building airplanes was observed a close connection. The development of this field, industry aircraft manufacturing was the collaboration result between metallurgists specialist's and aircraft manufacturers. From this collaboration has resulted efficient equipment and materials used to improve characteristics.

Aluminium alloys are numerous, with different and various properties. For example, Al-Zn-Mg-Cu alloy has a low weight and that is why it had been used with success in the aircraft manufacturing industry. This is highlighted in figure 1.

Figure 1. Highlighting construction aluminium alloy features from a commercial aircraft [2].

Alloys of Al-Zn-Mg-Cu may be used on some resistance elements which are loaded with compression stress due to high values of yield strength of the alloy.

The components made from 7075 are: aluminium fuselage, upper wing panels and sustaining pillars.

Also from the Al-Cu-Mg alloy, which is a hard aluminium, can be constructed elements which requires higher hardness such as the exterior case and the front of the wings [3].

3. SPECTROMETRIC ANALYSIS OF THE AlCu$_4$Mg$_{1,5}$Mn ALLOY

Spectrometic analysis on our aluminium sample was performed using Foundry Master 01J0013 optical spectrometer.

Following the three aluminium sample tests, came out the following results as shown in Table 1.

Table 1. Spectrometry analysis results of the aluminium alloy.

No test	Al	Si	Fe	Cu	Mn	Mg	Zn
1.	91,7	0,294	0,522	4,85	0,683	1,38	0,0768
2.	92,2	0,269	0,562	4,68	0,65	1,44	0,0356
3.	92,2	0,269	0,565	4,59	0,664	1,46	0,417
Average	92,0	0,277	0,55	4,71	0,666	1,43	0,517

After spectrometry analysis we found an aluminium alloy which is AlCu$_4$Mg$_{1,5}$Mn. Aluminium alloys are divided into two categories: foundry alloys and plastic alloy deformation.

AlCu$_4$Mg$_{1,5}$Mn is an aluminium alloy plastic deformation. This alloy is part of those who can be processed by hot or cold rolled, by drawing, by extrusion, by stamping or forging. Deformable alloys are divided into two

categories, depending on the possibility of heat treatment hardening by quenching and aging: treatable and untreatable [4].

Propeller is a high strength 2024 aluminium alloy which is a commonly used material in aviation, due to its advantages of resistance to crack growth, good reparability, and perfect damage tolerance properties [5].

Magnesium added to the Al-Cu alloy, improves its properties. Magnesium plays an important role in reducing the weight and increasing the hardness by heat treatment.

Figure 3. Image of the studied propeller.

4. HEAT TREATMENTS AND MICRO-STRUCTURE ANALYSIS

The heat treatment is the technological process comprising in heating and maintaining the metal or the alloy at a given temperature, usually followed by cooling with a certain speed, in an environment. The heat treatment may be applied to such semi-finished and finished parts in order to obtain superior operating characteristics and properties of the material, by modifying the structure.

After performing spectral analysis and determining the chemical composition of the material, thermal quenching and ageing treatments was applied. These treatments were applied to highlight hardened aluminium structure and ageing.

4.1. SEM analysis. After applying quenching and ageing thermal treatments, microstructural analysis was performed on a scanning electron microscope SEM VEGA II LSH, model shown in figure 4.

Using this electron microscope we may determine material surface properties, based on the study of its structure, i.e. based on the constituent's present and possible structural defects, cracks and inhomogeneities.

"HENRI COANDA"
AIR FORCE ACADEMY
ROMANIA

"GENERAL M.R. STEFANIK"
ARMED FORCES ACADEMY
SLOVAK REPUBLIC

INTERNATIONAL CONFERENCE of SCIENTIFIC PAPER
AFASES 2014
Brasov, 22-24 May 2014

Figure 4. Scanning electron microscope VEGA II LSH SEM

4.2. SEM analysis of the hardened alloy. Tempering is the most critical step in heat treatment operations. The purpose of hardening is to maintain the solid solution formed at solubilization temperature after the

heat treatment by rapid cooling close to 20℃.
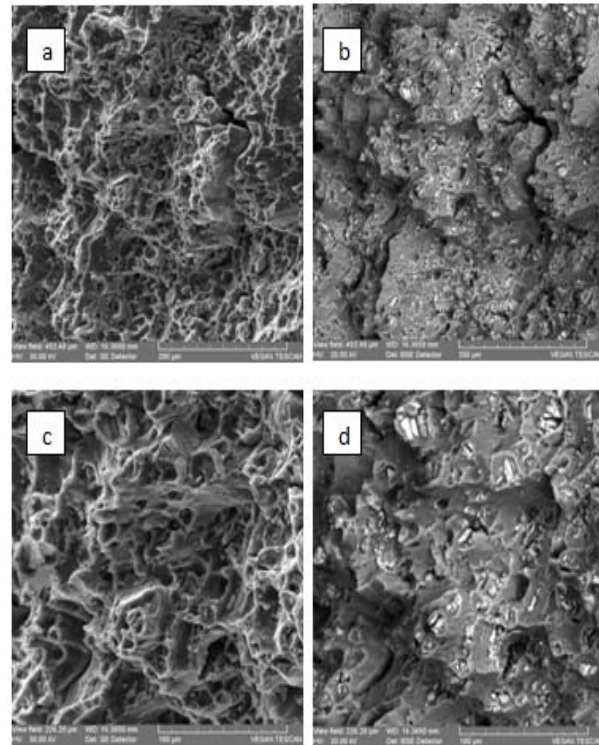
Figure 5. Fracture SEM image of a hardened structure: a)500x SE; b)500x BSE; c)1000x SE; d)1000x BSE.

When the alloy is subjected to solution treatment for hardening, a partial or complete dissolution of precipitates occurs, and the alloy will have a good cold workability.

The SEM uses two types of detectors: SE - secondary electrons and respectively BSE - back scattered electrons.

Elongated grains are observed in the fracture, also it is observed that fracture occurs inter and intra crystalline. Grain elongation occurs due to hardening thermo chemical treatment, figure 5.

4.3. SEM analysis of the aged alloy. Martensitic quenching heat treatment or solution treatment is followed by tempering, respectively ageing for increasing machinability properties.

Aluminium alloy ageing leads to hardening by precipitation of the second phase. These are highlighted in the SEM fracture, in figure 6.

Also in figure 6 we noted the particularly fragile structure, characteristic for biphasic alloys. For the aged aluminium alloys inter-granular fracture is observed.
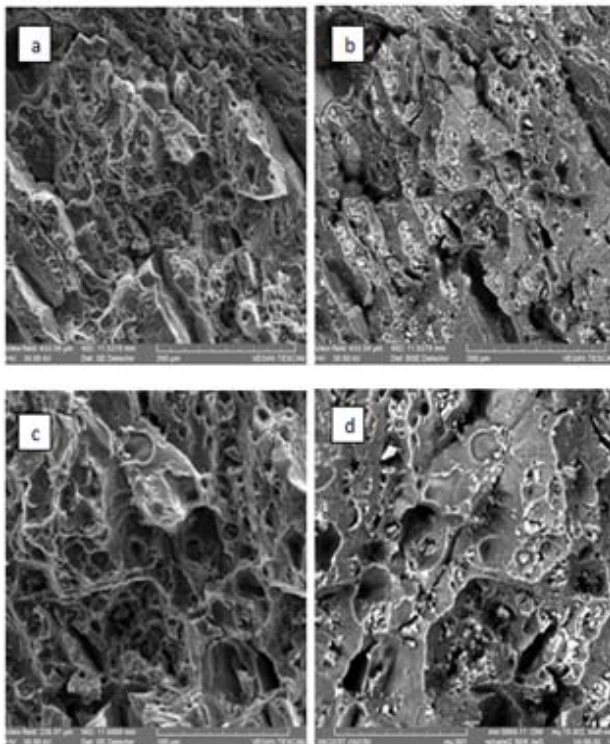
Figure 6. Fracture SEM image of the aging structure: a) 500x SE ;b) 500x BSE; c)1000x SE; d)1000x BSE.

5. DILATOMETER ANALYSIS

In this work we performed the analysis using a differential dilatometer type LINSEIS L75H/1400.

Figure 7. General Presentation: a) dilatometer measurement system; b) furnace; c) command and control system;

On this differential dilatometer can be studied in the solid state phase transformations.

When a phase transformation in the material occurs, because the new phase occupies a different volume, a discontinuity will occur on the variation curve of the thermal expansion coefficient with the temperature [6].
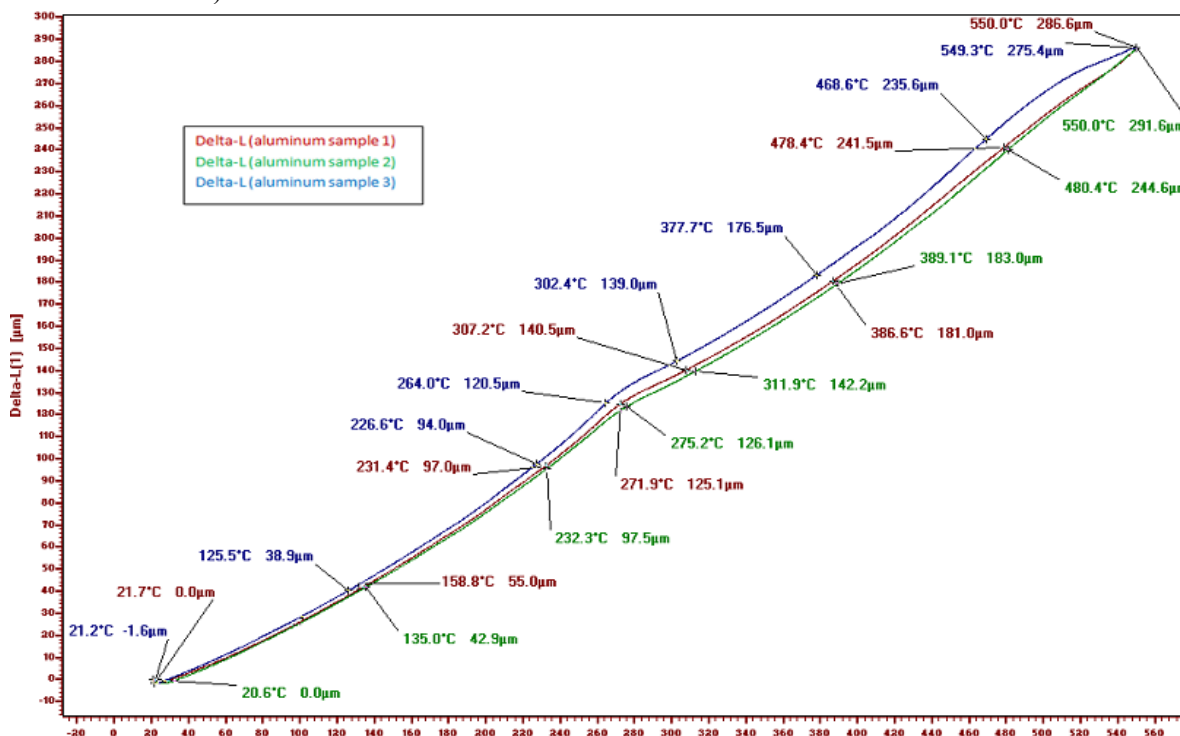
"HENRI COANDA"
AIR FORCE ACADEMY
ROMANIA

"GENERAL M.R. STEFANIK"
ARMED FORCES ACADEMY
SLOVAK REPUBLIC

INTERNATIONAL CONFERENCE of SCIENTIFIC PAPER
AFASES 2014
Brasov, 22-24 May 2014

Figure 8. Dilatometer curve for alloy AlCu$_4$ Mg$_{1,5}$Mn.

Table 2. Elongation of the three samples according to the temperature.

Aluminium Sample 1		Aluminium Sample 2		Aluminium Sample 3	
Temperature	Elongation	Temperature	Elongation	Temperature	Elongation
°C	µm	°C	µm	°C	µm
21,5	0	20,6	0	21,2	1,6
158,8	55	135	42,9	125,5	38,9
231,4	97	232,3	97,5	226,6	94
271,9	125,1	275,2	126,1	264	120,5
307,2	140,5	311,9	142,2	302,4	139
386,6	181	389,1	183	377,7	176,5
478,4	241,5	480,4	244	468,6	235,6
550	286,6	550	291,6	549,3	275,4

Dilatometer diagram of the alloy studied is shown in figure 8. From the chart we can see that at 275 °C the alloy presents a state variation passing from structure α+C'' by dissolution of C'' in a state of α saturation.

This is important in finding the heating temperature in order to achieve heating solution treatment at the variable solubility line for the alloy system.

Solution quenching treatment leads to a solution out the equilibrium, becoming more easily processed by cold plastic deformation.

CONCLUSIONS

From our research we conclude the followings:
1. The studied propeller is made from hard deformable aluminium alloy AlCu$_4$Mg$_{1,5}$Mn.
2. This propeller was made by plastic deformation, previously solution treated, and after deformation aged, in order to offer the necessary functioning hardness.
3. From the dilatometry analysis is observed that between 26 °C and 550 °C there are no phase transformations but only state transformation, due to the Mn percent.

REFERENCES

1. Minea, A., *Aliaje de aluminium - Tratamente termice și echipamente de încălzire* (Aluminium alloy heat treatments of heating), Ed.CERMI Iași, (2006).

2. http://www.donmaxwell.com/masters

3. Carabet, R.G., Nejneru, C., Comaneci, A., *Researches regarding aluminium alloys hardening through cyclic ageing* (Buletinul Institutului Politehnic din Iași, Tomul LIV,Fasc. 3-4, Secția Știința și Ingineria Materialelor, (2008).

4. Grămescu, T., Slatineanu, L. Braha, V., Sarbu I., *Prelucrabilitatea materialelor* (Material processing), Ed. Tehnica-Info, Chișinău, (2000).

5. Kushan MC, Zafer N. *Structure materials of aeroplanes* (in Turkish), I. Ulusal Metalurji ve Malzeme Günleri (Prod. Conf.), Eskişehir, Turkey; May 27-28, (2004).

6. Rusu, I., *Tehnici de analiză în ingineria materialelor - Aplicații practice* (Analysis techniques in engineering materials - Practical Applications), Ed. PIM, Iași, (2011).

ENGINEERING SCIENCES

MOBILE APPLICATION FOR BUSINESS CONTROL
OF TELECOMMUNICATION SERVICES

Alexandru BALICA*, Mihai MIJEA*, Florin SANDU*

* "Transilvania" University,
Bd. Eroilor nr. 29, Brasov, 500036, ROMANIA

Abstract: The expanding telecommunication networks start to support services closer to business control. Covering by default air-time account information management, they are extending to monetary operations: bank transactions, accounts' interrogations, recharge control. Thanks to smartphones proliferation the user interface is done via applications (apps) built for Android, iOS, Windows Mobile, etc. We propose Unstructured Supplementary Service Data (USSD) integration – a reliable and universally available control medium – for enhancing Business control via apps. By doing this we are implementing a Service Creation Environment (SCE) available to the operators in emerging economies and also for establishing immediate control in the new Internet of Things (IoT) environment.

Keywords: App, m-Business, electronic recharge, USSD, Android, Eclipse, IoT, SCE

1. INTRODUCTION

The growth in m obile applic ations (*apps*) will represent a 77 b illion m arket in 2017, each user p roviding cu stomized infor mation via 100 apps per day, according to Gardner [1].

The apps offer to the us ers an unres tricted access to services. T his interactive m odel represents the new *apps paradigm*, where the capabilities are lim ited only by the ability to imagine and develop a serv ice. This m eans expanding the apps towards *m-Business* a nd mobile devices and even *wearable* devices. In 2014 we are in the firs t stages of apps (*infotainment*) and we are exp ecting to continue with monetary services control (*m-Business*) and cloud integration. The apps would control a m yriad of electronic devices in the new Internet of Things (IoT)

environment, becom ing the access & contro l medium towards domotics (Home IoT).

Currently there are over 100 developm ent media for a pps. A very high num ber are free. The financial objective is not strong; som e apps are developed just for product placem ent or are pu rely inf otainment-oriented. Because of this, only 0.01% ar e going to generate money [2] in a highly competitive market.

Our applica tion is in tended f or telecom operators in order to an swer specific dem ands related to recharge cap abilities an d can b e extended to support interrogation and control requests for future Smart Grid and machine-to-machine (M2M) im plementations. W e are detailing the application developm ent and business case for im plementation in production environment and suggest new approaches related to the SCE (Service Creation Environment).

2. CONTEXT

2.1 Current usage an d risks. Telecom operators are relying on USSD fra mes or IVR (Interactive Voice Res ponse) to im plement queries from subscribers (e.g. balance query) or to allow various operations from authorized agents (e.g. the sales network geographically distributed).

Using specialized Value Added Service (VAS) solutions the op erator will in crease its local presence by allowing selected individuals (commercial agents) to take the burden of distributing voucher and recharge to subscribers. This m odel, highly su ccessful in emerging and developing m arkets (e.g. India, Pakistan, Algeria) is a llowing a fast and direct interaction with th e cu stomer in the la ck of banking and financial infr astructure available, very often ahead of the grid (power infrastructure is not yet ava ilable). The situation we have encoun tered is that physical vouchers cannot be transported on the ground (e.g. conflict zone or inaccessible due to natural disasters). For this reason, the electronic distribution of vouchers is needed, and was implem ented via USSD fra me or WEB interface. Considering th at W EB interface is available to only a selected number of m ain agents (dealers) we are noticing th at the bulk of operations is going to be done via USSD, by unspecialized individuals. Mitigating the access to the serv ice is the main concern in this case.

Any USSD fra me is starting with '*' and ending with '#'. The interm ediary fields are also s eparated with '*'. The first field in the frame represents the sho rt code (SC) allocated to this type of service and it is conf igured along the core network in the Public L and Mobile Network (PLMN). An USSD fra me example for voucher recharge is `*123*123456789012#` where `123` represents the SC followed by a 12 digit hidden recharge number (HRN) of a voucher.

Used mainly in the developing markets, the USSD fram es are especially useful in managing the *m-Business* in electronic recharge (i.e. top-up subscriber's balance). However, in som e cases, like the one we have encountered, the USSD fram es are becom ing too cumbersome for eas y and rapid utilization.

One of the reasons is that alongside direct recharge, we can have ot her type of operations possible that can exte nd dram atically th e number of USSD fram es available to th e agents in their interactions with the subscribers or with other agents. US SD frames, especially for voucher distribution, are too difficult to remember (e.g. the example for sending 500 vouchers of 100 units to agent 07712345678 is `*123*321*12345*07712345678*100*500#` with SCs and USSD password pr esent in the str ing `(123,321,12345)`, alongside the voucher quantity `(500)` and face value `(100)` of the voucher).

In addition to that, account control is needed for an agent (e.g. password change, transfers to and from another agen t, transaction view). This leads to a lengthy list of USSD operations av ailable to th e agents – both f or initia ting m onetary transa ctions an d for managing the account.

Because of these issues, there is a high risk that the agents will get discouraged from using the service.

2.2 Opportunity and our goal. USSD can also be regarded as an opportunity, since it is a reliable, tested m edium for control. USSD, much like Short Mess age Service (SMS), is transmitted bi-direc tionally and alternatively between subscriber and service, along core network on the signaliza tion channels used by Mobile Application Part (MAP) protocol. Available since 1993, it was developed in two stages [1],[2] and i t was fi nalized i n 1999, making it a tested and universally available service. Our proposition is that US SD should not be discarded from future im plementations in the context of the ne w app parad igm as it is available *by default* in the telecom network of all oper ators, it is secure and light. Furthermore, the subscribers are used with this service. The USSD offers:

- stability in exploitation (standardized and in production for over 15 years);
- functional s implicity (transmitted v ia th e signaling channel);
- ease of im plementation, regard less of the service provided;
- global area of distribution, supported by all mobile terminals and all mobile operators;
- provides in creased interaction co mpared with SMS

"HENRI COANDA"
AIR FORCE ACADEMY
ROMANIA

"GENERAL M.R. STEFANIK"
ARMED FORCES ACADEMY
SLOVAK REPUBLIC

INTERNATIONAL CONFERENCE of SCIENTIFIC PAPER
AFASES 2014
Brasov, 22-24 May 2014

For this reasons w e are proposing integrating the USSD f unctionality v ia m obile apps, in this case, Android OS.

2.3 Development environment. We are using for developm ent the Android Eclipse Service Delivery Kit (SDK) [5] that includes:

- Eclipse + Android Developm ent Tools (ADT) plugin
- Android SDK Tools
- Android Platform-tools
- The latest Android platform
- The lates t Android sys tem i mage for th e emulator
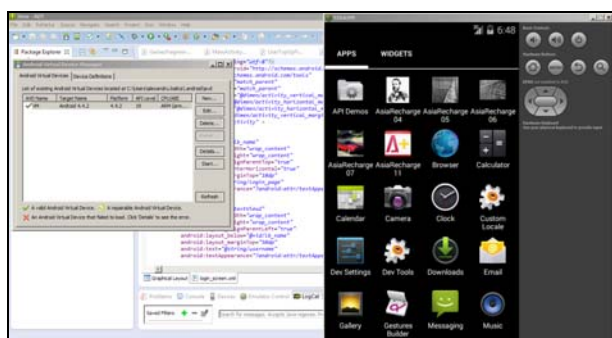
Fig. 1. Eclipse development and testing environment with the virtual machine (VM) opened

Developing in Android Eclipse is d one in Java programm ing language and XML integration for visual app content. The available simulator (*fig. 1, right*) is helping the design and validation, before deploying on real equipment.

3. BUSINESS CASE

3.1 Advantages and previous implementations. Our goal is a mobile app th at will use visual g raphical interf ace (GUI) to store and collect data and then format it, transparently to the user, into valid USSD fram es. There ar e several obvious advantages from this point of view: r educing tr ansaction tim e, mainta ining

the app interface paradig m, providing a secure channel.

Formatting USSD fr ames via apps is available through other applications (e.g. *Easy USSD Lite*, *USSD Dialer*, *USSD Management*, *Mobile Balance Checker*, *cluBalance*, *checkBalance*, *dBalance*) [6]. Howe ver, none of them is dedicated to lim ited experience commercial agents and they are no t capable to support all the functions needed.

Via our implementation, it is also possible to integrate special branding elements into the application, like logos or corporate on-screen messages. The application icon, m enus, color scheme, can all be custom ized in o rder to b e consistent with the operator's brand image.

Vendors and VAS suppliers are already seizing the opportunity, but m ost of the implementations are done using application programming interfaces (API) and require an Internet connection. Using USSD r equests is simpler and more reliab le, especially given the rough conditions av ailable in em erging markets. This approach will allow operato rs to seize the app paradigm opportunity withou t investing in PLMN inf rastructure f or Inte rnet access and it would not limit the service.

3.2 SWOT analysis. To validate our app we are lis ting the st rengths, w eaknesses, opportunities and threats (S WOT) related to it. Using the S WOT analysis we c an identify the internal factors – the strengths and weaknesses internal to the organization and the externa l factors – the opportunities and threats presented by the environm ent external to th e organization.

Internal
Strengths
- easy to use graphical interface
- rapid triggering of requests that, if done via USSD fram e, would require separate training

- the oper ator has com plete control o ver the application access m edium and over the functionalities as it is built *in-house*:
  - USSD frames via the VAS provider
  - additional functionalities like lock/unlock can be supported
  - application f low a nd logic correspond exactly to local market demands

  Weaknesses
- the current version is only available on Android OS

  External
  Opportunities
- channeling the new app paradigm
- no other operator, currently, provides this tool to own commercial agents
- Android based sm artphones have a large market share in Middle East and developing economies.
  Threats
- As the app is us ing USSD channel fo r triggering the requests, there is no additional risk. Password storage and login via the app are done via Android OS's `sharedpreferences` function.

The SW OT m atrix is im portant to late r steps in planning to achieve th e objective and in this case it validates our proposal.

3.3 M2M applications. M2M applications using the apps are possi ble, providing there is a databas e with inf ormation availab le f or query and control. One opportunity is represented by the comm on share of the records by the Sm art Grid adm inistrator with the Teleco m operator. This is part of the vertical network integration schem e (power transmission network, m etering network and transmission network). One can see sim ple applications being possible using already available USSD string s, even in em erging economies, where power scarcity is still a major issue (for exa mple, balance query for power consum ption, tariff plan interrogation and management).

4. APPLICATION

4.1 Solution design. The functions needed to be implemented are as follows:
- Register and login (store usernam e and USSD password, *fig. 2*)

- Recharge subscriber
- Send voucher to subscriber
- Transfer credit to another agent
- Transfer vouchers to another agent
- Check balance for credit or vouchers
- Account settings (account update)

Other possible m anagement operations include:
- Frequent errors (e.g. via search in Action Bar after Error ID)
- Mobile number selection from Contacts
- Guide (screens with instructions, app Help)

Implementing these operations m ust be done so that the user is able to select easily and fast the desired option. We are proposing drop-down m enus for imm ediate selection and usage of large fonts and select buttons. In order to eas e the access , we are implem enting a *3 touch maximum* s election criterion (i.e. from any point of the applica tion to reach another one in maximum three steps).
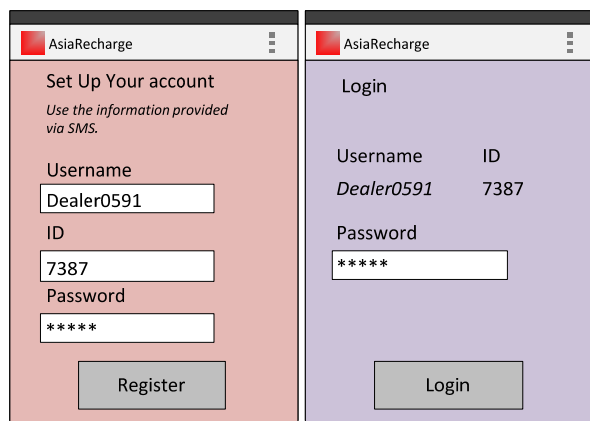
Fig. 2. Proposed schemes for registration and login screens

4.2 Implementation. From programming point of view, we are using already defined Android functions and schem es in order to implement the f unctionality (i. e. r egistering, saving the personal d ata, accep ting selection s via drop-down m enus `(spinners)` and formatting the USSD string and sending them accordingly). Apart from the functional side an equally challenging ta sk is devising an interface that can be trusted and easily used.

Since the revenue expected from the sales network is vita l, th e u sers m ust b e able to select and work in a familiar way.

For this reason we are adopting a standardized graphical interface, th e *drawer,*

"HENRI COANDA"
AIR FORCE ACADEMY
ROMANIA

"GENERAL M.R. STEFANIK"
ARMED FORCES ACADEMY
SLOVAK REPUBLIC

INTERNATIONAL CONFERENCE of SCIENTIFIC PAPER
AFASES 2014
Brasov, 22-24 May 2014

that is available in Google applications like *Google Play* (*fig. 3*), *Google +* or *YouTube* and also *Facebook* and others.
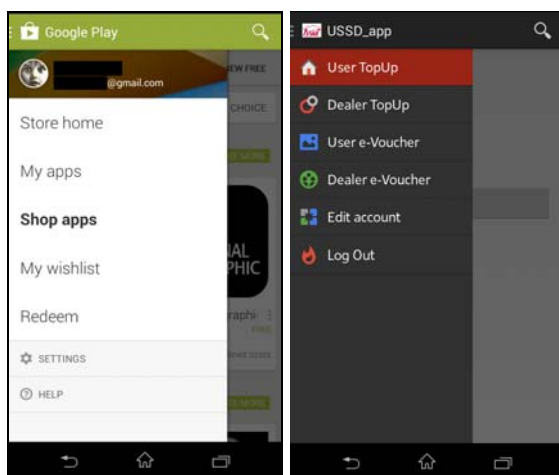
Fig. 3. Standardized, open source drawer menu design (Google Play) and the implemented one

Each screen from t he drawer m enu selection will con tain `fragment` type screens according to our guidelines. In th e recharg e screen, for exam ple (*fig. 4*), th e user is presented with an `editfield` to enter the destination mobile number and a selection for the value to be recharged (via a `spinner` drop-box). The keyboard is used to input the number in the exact location.

4.3 Security. As the app will only use USSD fram es to communicate with th e system, there is no ad ditional ind uced risk. The USSD fram es are validated in advance and are part of the delivered package for electronic recharge sys tem (licens e, security , acceptance). An additio nal secu rity restric tion can be im plemented on the PLMN side: the subscribers can be barred from accessing the USSD frames based on their mobile number.

Any commercial ag ent will have his/he r own USSD password and th is can be used in parallel to trigger manually the USSD requests or can be stored in the application.

An additio nal f unctionality allo ws the agent to set his/her ow n USSD password, also. This does not introdu ce any addition al r isk other than norm al operation with USSD frames.
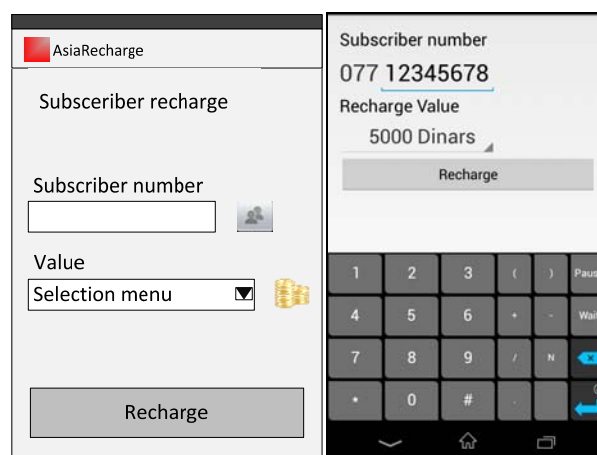
Fig. 4. Proposed scheme for direct recharge screen and implementation via Android app

5. CONCLUSIONS & FURTHER DEVELOPMENT

The advantages in developing and using apps com e from reduced developm ent costs and use of already delivered platfor ms for distribution (e.g. Google Play, App Store).

The apps, even after delivery and installation in the m arket, remain available for corrections and updates using the open development environm ent we presented hereby as a SCE (Service Creatio n Environment).

This is com pliant with the persp ective of IN (In telligent Networ ks) where individual users (e.g. juridical persons like comm ercial agents) and not only network infrastructure manufacturers/ owners/ operators can develop/ deploy/ configure/ administrate the services.

These features reduce maintenance costs as well.

ENGINEERING SCIENCES

CODE ACQUISITION WITH DOUBLE CORRELATOR IN DSSS RECEIVERS

Otilia CROITORU

Electrical Engineering and Computer Science, Transilania University of Brasov, Romania

***Abstract:** The spread spectrum (SS) communications system, use a pseudo-noise (PN) code to spread the initial bandwidth occupied by data over a bandwidth much wider. In receiver, the SS signal is despread using the same PN code. The most difficult task to achieve in receiver is to synchronize the locally generated PN code with the code existing in the received signal. The purpose of this paper is to present a receiver model for code acquisition that uses two active correlators, method derived from acquisition with active correlator. The method proposes that, in some circumstance, the synchronization of signals to be done by delaying the received signal, not the local PN code,with the advantages in reducing the acquisition time and signal recovery.*

***Keywords:** communications, spread spectrum, direct sequence, code acquisition,correlator.*

1. INTRODUCTION

The **spread spectrum** (SS) communication technique use a **pseudo-noise** (PN) code as a waveform to spread the initial bandwidth occupied by data over a bandwidth much wider. In receiver, the SS signal is **despread** using the same PN code used in transmitter.

Direct Sequence Spread Spectrum **DSSS** is a method commonly used for spreading spectrum where the PN code is multiplied with input data [1,2,3].

The most difficult task to achieve in DSSS receiver is to synchronize the locally generated PN code with the code existing in the received signal. This synchronization process is carried out in two stages [1]:

- **Code acquisition** – coarse acquisition process which beings the two PN sequences in the same range of chip;

- **Tracking code** – fine–tune process in order to maintain the synchronization.

In code acquisition, one of the critical elements is during this process.

In order to reduce time acquisition, have been developed various methods, starting from fundamental techniques (with active correlator, with matched filter, serial or parallel search, etc.) to advanced code acquisition techniques [1,6,8].

The purpose of this paper is to present a receiver model for code acquisition that uses two active correlators, method derived from acquisition with active correlator.

2. COMMUNICATION SYSTEM MODEL

2.1 The work environment. Given the complexity of a SS communication system, it is preferable that the experiments for

development of new tyle of schem es to be made initia lly, in a sof tware sim ulation. For this study, as a working environm ent for modeling and experiments was used Matlab & Simulink software package.

2.2 System description. The stru cture of the proposed system is shown in Fig. 1 and consists of:

- The tran smitter with : D ata Gene rator, PN Sequence Generator and BPSK modulator;
- Communication channel with AWGN;
- The receiver with double correlator.
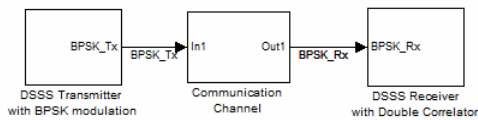
Fig. 1 Block diagram for communication system structure proposed.

Proposed s tructure for th e tran smitter shown in Fig. 2 is a sim plified version of DSSS transm itter usin g a Gold Sequence Generator (as PN generator) for spreadin g spectrum and a BPSK m odulator achieved with product operator.
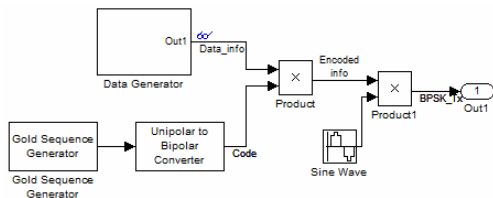
Fig. 2 Block diagram proposed for transmitter with DSSS and BPSK modulation.

For DSSS receiver was designed a m odel Pentru receptor a fost creat un m odel whose scheme is shown in Fig. 3. The main blocks of the designed receiver are:

- **BPSK Demod** – a coh erent demodulator that extract the signal *Encoded info_Rx* from t he BP SK modulated signal present at its input.
- **PN Sequence Gen erator** wh ich generates local replic a of the spreading code used in transmission.
- Two blocks with active correlator, **Delay Cou nter_LateRx** and **Delay Counter_EarlierRx**.

- Two blocks for delay, one for received signal and one for local code.
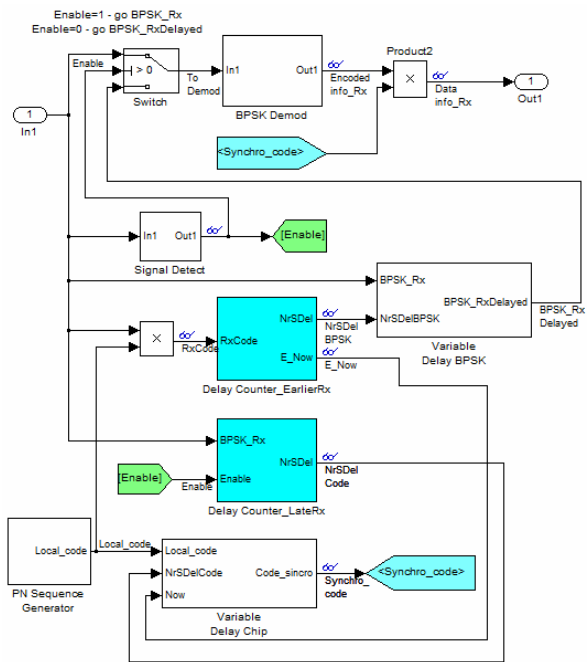
Fig. 3 Block diagram for receiver structure proposed.

The basic idea is to u se two correlato r blocks that have the role to calculate the phase shift between the rec eived signal an d the loca l code, phase shift counted in num ber of code bits (chips).

Delay Cou nter_LateRx calculates th e number of chips, *NrSDelCode*, t hat ha ve delayed the code to alig n it with th e received signal.

Delay Counter_EarlierRx calculates the number of chips, *NrSDelBPSK*, that have delayed the received signal to align it with th e code.

Through this m echanism, at the demodulator input is brought or th e receiv ed signal *BPSK_Rx*, or the received signal delayed with *NrSDelBPSK* chips. There are two possible cases:

1. If the tran smitter is turned on later than the receiver (the re ceiver waiting f or the arrival of the signal from the transmitter), becom es operational the **Delay Counter_LateRx** block and is commanded local code delay with *NrSDelCode* chips. On enter ing the demodulator block is allowed access for the received signal *BPSK_Rx*. The delayed code, *Synchro_code*, is used to

"HENRI COANDA"
AIR FORCE ACADEMY
ROMANIA

"GENERAL M.R. STEFANIK"
ARMED FORCES ACADEMY
SLOVAK REPUBLIC

INTERNATIONAL CONFERENCE of SCIENTIFIC PAPER
AFASES 2014
Brasov, 22-24 May 2014

extract the data signa l *Data info_Rx* from the *Encoded info_Rx* signal.

2. If the trans mitter is tu rned on ear lier than the receiver (b egins receivin g a signal th at it is not known when it started), becom es operational **Delay Counter_EarlierRx** block and the other op eration is inh ibited with the signal Enable = 0. Is comm anded the delay of the received s ignal *BPSK_Rx* with *NrSDelBPSK* chips and on entering the de modulator block is allowed access for the s ignal *BPSK_RxDelayed*. In this cas e, the local code delay is zero, so that the *Synchro_code* signa l is in p hase (identical) with *Local_code*.

2.3 Experimental studies. The experiments are in tended to tes t th e rece iver operation in the two cases above described:

1. The later transmission.
2. The earlier transmission.

The structu re of th e designed receiver allows:

- Delay setting for any of the two signals (*BPSK_Rx* and *Local_code*);
- Pursuit of signal processing at important points;
- Comparing the transm itted da ta s ignal to that recovered in the receiver;
- Delay analysis for recovered date signal in reception, d ue to prop osed method.

2.4 The bas ic parameters of the system. To m ake visible repres entation of signal in time diagram s measured at various points, were chos en for sy stem para meters the folowing values:

- The length of a data bit for signal information, $T_b = 0.01$ s;
- The length of PN code obtained from Gold Sequence Generator, $L_c = 63T_{chip}$

(shortened notation used in this paper: $L_c = 63$ chips);

- The length of a chip, $T_{chip} = 1/6300$ s;
- Carrier frequency, $f_c = 18900$ Hz, so that $T_c = T_{chip}/3$ (3 sinusoids/chip);
- Time s imulation $T_{sim} = 0.04$ s, corresponding to 4 data bits.

3. EXPERIMENTAL RESULTS

For each of the two cas es (as described in 2.2) were chosen two values of delay to be within:

a. $\Delta t < \frac{1}{2} L_c$
b. $\Delta t > \frac{1}{2} L_c$

In this way it may reveal to what amount of delay it is good to m ake signals alignm ent by delaying th e PN local code or th e received signal. PN code length being $L_c = 63$ chips, were chosen $\Delta t = 20T_{chip}$ and $\Delta t = 50T_{chip}$ (shortened notations used in this paper: $\Delta t = 20$ chips and $\Delta t = 50$).

3.1 Ideal case. Its shows diagram s of signals in ideal situ ation, when the re a re n o delay and th e receiv ed signal *BPSK_Rx* and *Local_code* are perfectly synchronized.
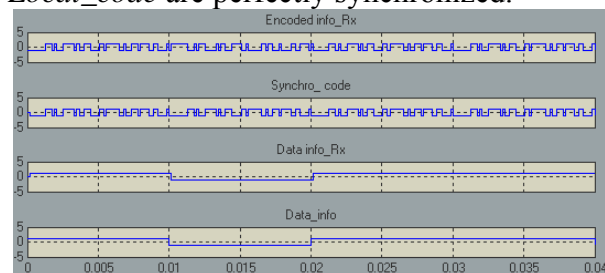
Fig. 4 Waveforms for *Encoded info_Rx*, *Synchro_code* and *Data info_Rx* compared to *Data_info* for ideal case.

If it m ake a zoom in the diagram of Fig. 4 around to t = 0 (see Fig. 5), can be observe a delay (marked with red) of 1 chip of *Encoded info_Rx* signal, due to si gnal processing in

BPSK De mod block. This delay has to be compensated by local code delay, in order to correct alig nment of bot h signals. The effect: extract data signal is delayed by one chip towards the transmission.
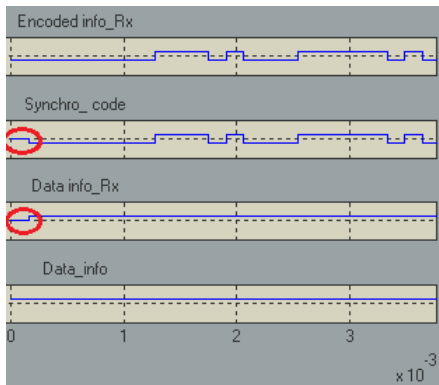
Fig. 5 The delay (of extracted data signal) by one chip towards the transmitted data signal, for ideal case.

3.2 The later transmission.

a. For a delay $\Delta t = 20$ chips of *BPSK_Rx* signal tow ards the local c ode, **Delay Counter_LateRx** block calculates the delay value and generates the signal *NrSDelCode =* 21, as show n in Fig. 6. The block **Variable Delay Chips** perform s local code delay, thus achieving the synchronization of the two signals, *Encoded info_Rx* and *Synchro_code* from which it is recovered *Data info_Rx*.
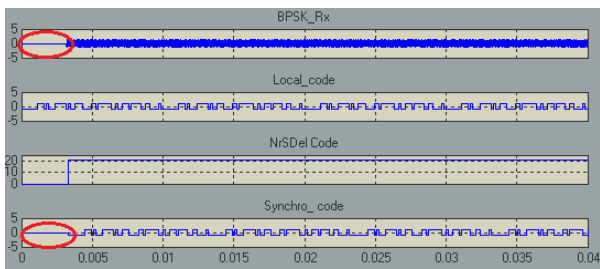
Fig. 6 Waveforms for received signal with 20 chips delay, *Local_code* and *Synchro_code* delayed with *NrSDelCode* chips for later transmission with $\Delta t = 20$.

On the wavefor ms shown in Fig. 7 can be seen synchronization of the two signals and a dealy with $\Delta t + 1 = 21$ chips of the signal *Data info_Rx*.
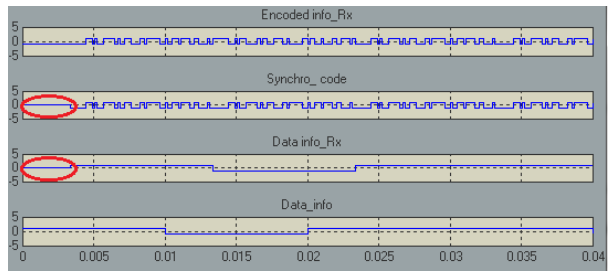
Fig. 7 Waveforms for *Encoded info_Rx*, *Synchro_code* and *Data info_Rx* compared to *Data_info* for later transmission with $\Delta t = 20$.

b. For a delay $\Delta t = 50$ chips of *BPSK_Rx* signal towar ds the lo cal code, the behavior is similar, **Variable Delay Chips** block performs local cod e delay with $\Delta t + 1 = 51$ chips, to synchronize the signals *Encoded info_Rx* and *Synchro_code*. The wavefor ms obtained are shown in Fig. 8 and Fig. 9.
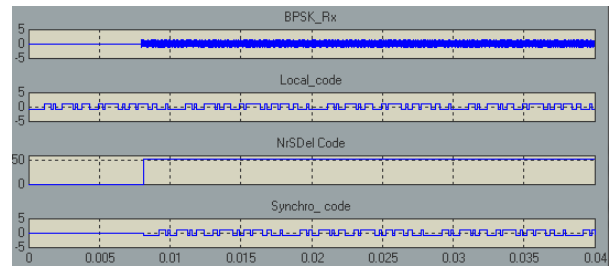
Fig. 8 Waveforms for received signal with 50 chips delay, *Local_code* and *Synchro_code* delayed with *NrSDelCode* chips for later transmission with $\Delta t = 50$.

In Fig. 9 can be seen synchronization of the two signals and a delay with $\Delta t + 1 = 51$ chips for *Data info_Rx* signal.
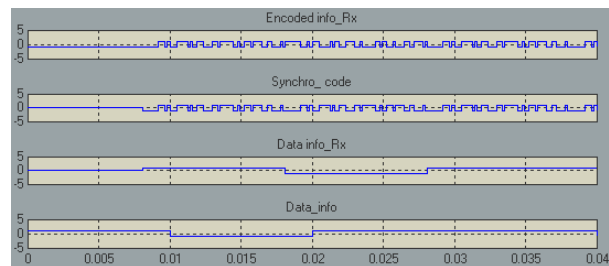
Fig. 9 Waveforms for *Encoded info_Rx*, *Synchro_code* and *Data info_Rx* compared to *Data_info* for later transmission with $\Delta t = 50$.

"HENRI COANDA"
AIR FORCE ACADEMY
ROMANIA

"GENERAL M.R. STEFANIK"
ARMED FORCES ACADEMY
SLOVAK REPUBLIC

INTERNATIONAL CONFERENCE of SCIENTIFIC PAPER
AFASES 2014
Brasov, 22-24 May 2014

3.3 The earlier transmission.

a. For t he case of a si gnal *BPSK_Rx* arrieved earlier with Δt = 20 chips towards the local code, **Delay Counter_LateRx** block calculates the offset value and gen erates th e signal *NrSDelBPSK* = 20 - 1, as shown in Fig. 11. The block **Variable Delay BPSK** performs received sign al delay with 19 chip s since turning on the re ceiver (obviously, the part arrived in advance is lost, can not be processed). The m ovement of the received signal *BPSK_Rx* on the tim e axis and the los s due to late turning on th e receiver are outlined in Fig.10.
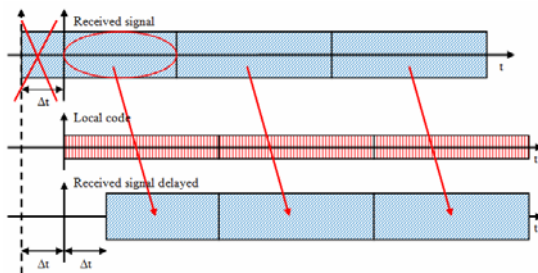
Fig. 10 The delay imposed to received signal to align it with the local code.

When the signal *Enable* = 0 ar e t wo effects:

- Is comm anded the signal *BPSK_RxDelayed* access to demodulator;
- Is inhibited operation of **Delay Counter_LateRx** block.

The signal *Synchro_code* is, in th is case, the same as *Local_code*, because the **Variable Delay Chips block** receives from **Delay Counter_LateRx** block the inf ormation *NrSDelCode* = 0.
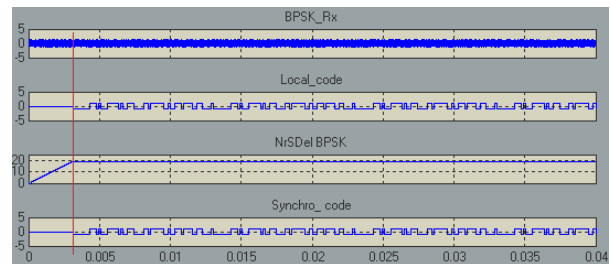
Fig. 11 Waveforms for *BPSK_Rx*, *Local_code*, *Synchro_code* and *NrSDelBPSK* for earlier transmission with **Δt = 20**.

On the wavefor ms shown in Fig. 11 it can be seen th at the sig nal *Synchro_code* is identical to *Local_code* signal.
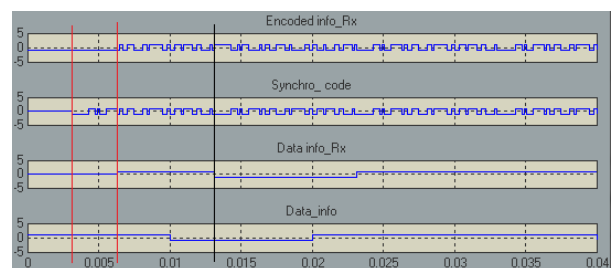
Fig. 12 Waveforms for *Encoded info_Rx*, *Synchro_code* and *Data info_Rx* compared to *Data_info* for earlier transmission with **Δt = 20**.

On the diagram in Fig. 12 was marked with a red line (first from le ft to right) the m oment when the receiver is turned on. The second red line m arks the m oment until which th e receiver de lays th e rece ived signal to synchronize it with local code. Can be observed the signal *Encoded info_Rx* delay with 2 Δt towards tim e of initia ting transmission, nam ely Δt towards tim e of turning on the receiver, m anner shown in Fig. 10. From the received signal was fully recovered everything that has been received from the receiver turning on. T he sectio n between the second red line and the black line is the area of received signal which would be

lost with a conventiona l receiver structure, using code acquisition with active correlator.

Fig. 13 shows the delay of the received signal by $\Delta t = 20$ chips towards time of turning on the receiver, respectively 2 Δt towards time of initiatind transm ission, to the demodulator input being allowed the access for *BPSK_Rx Delayed* signal.
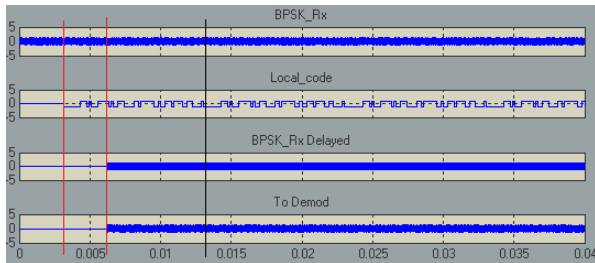
Fig. 13 The delay of the received signal towards time of turning on the receiver, for earlier transmission with $\Delta t = 20$.

b. If the s ignal *BPSK_Rx* arrives earlier with $\Delta t = 50$ chips towards the local code, the **Delay Counter_EarlierRx** block calcu lates the offset value and generates the signal *NrSDelBPSK* = 50 - 1, as shown in Fig. 14. The block **Variable Delay BPSK** perform s received s ignal delay *BPSK_Rx* with 49 chips to synchronize the signals *Encoded info_Rx* and *Synchro_code*. The wavefor ms are shown in Fig. 14 , Fig. 15 and Fig. 16.
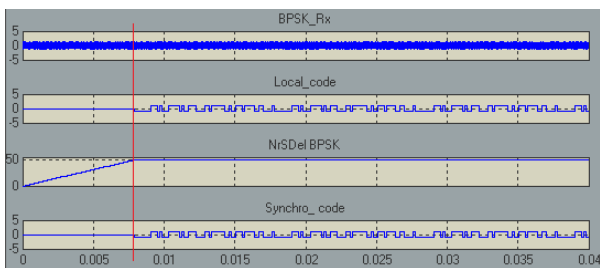
Fig. 14 Waveforms for *BPSK_Rx*, *Local_code*, *Synchro_code* and *NrSDelBPSK* chips for earlier transmission with $\Delta t = 50$.

On the wavefor ms shown in Fig. 14 it can be seen tha t the signa l *Synchro_code* is again identical to *Local_code* signal.
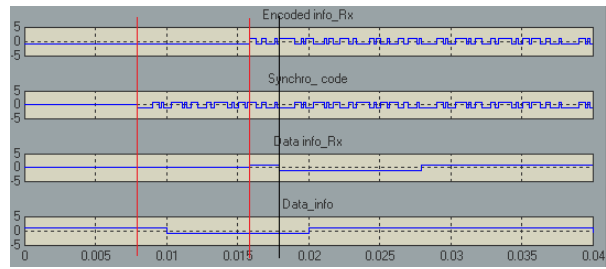
Fig. 15 Waveforms for *Encoded info_Rx*, *Synchro_code* and *Data info_Rx* compared to *Data_info* for earlier transmission with $\Delta t = 50$.

In Fig. 16 can be seen the delay caused to the received signal, to the dem odulator input being allowed the access for *BPSK_Rx Delayed* signal.

Keeping marking convention described above, it can be seen that, area between the second red line and the black line, (representing the firs t portion of the recev ed signal reco vered) is lo wer than th e case of earlier transmission with $\Delta t = 20$.
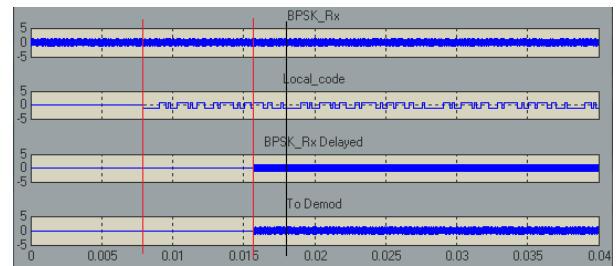
Fig. 16 The delay of the received signal towards time of turning on the receiver, for earlier transmission with $\Delta t = 50$.

3. CONCLUSIONS

From these experim ents it can be deduce some conclusions.

In the case of late r transm ission, signals synchronization is m ade by local code delaying and, regardless of the tim e of initiating th e transm ission, if the receiver is already turned on, do not lose anything from the received signal. This behavior is identical to the rec eivers that m ake code a cquisition by one of the m ethods brief presented in introduction.

The proposed m ethod is advantageous in earlier transm ission case, when the synchronization is made by delaying the received signal and not the code. In this way is possible to recover the inform ation contained

"HENRI COANDA"
AIR FORCE ACADEMY
ROMANIA

"GENERAL M.R. STEFANIK"
ARMED FORCES ACADEMY
SLOVAK REPUBLIC

INTERNATIONAL CONFERENCE of SCIENTIFIC PAPER
AFASES 2014
Brasov, 22-24 May 2014

in the received signal s tarting righ t from the moment of turning on the receiver.

The alignment take s Δt chips f rom the turning on the receiver (interval between the two marks with red line).

If $\Delta t < \frac{1}{2} L_c$, the time taken for signals alignment is:

- $t_{synchro} = \Delta t$, in case of proposed method in this paper;
- $t_{synchro} = L_c - \Delta t$, in case of code acquisition în cazul ach iziției by b asic method, where is m ade local code delay.

In other words, propo sed m ethod shortens time acquisition if the delay Δt is less than half of length of PN code.

A possibility of extending this benefit is to combine the two methods as follows:

- delaying th e received signal, if $\Delta t < \frac{1}{2} L_c$;
- delaying the local code, if $\Delta t > \frac{1}{2} L_c$.

With the model receiver proposed in Fig. 3, combining those two methods can be done by:

- Using the blocks **Delay Counter_EarlierRx** and **Variable Delay BPSK** for delaying received signal (as in experi ments described in 3.3 a.) if $\Delta t < \frac{1}{2} L_c$;
- Reactivation of bl ocks **Delay Counter_LateRx** and **Variable Delay Chips** for delaying local code (as in experiments described in 3.2 a), if $\Delta t > \frac{1}{2} L_c$.

This is poss ible becaus e both b locks with correlator, and **Delay Counter_EarlierRx** and

Delay Counter_LateRx, counts the necessary delay to align the signals.

REFERENCES

1. Byeong Gy Lee, Byoung-Hoon Ki m, *Scrambling techniques for CDMA communications*, Kluwer Academic Publishers (2002).
2. Gibson, J., D., *The communications handbook,* Southern Methodist University, Dallas, Texas, CRC Press (2002), www.crcpress.com.
3. Haykin, S., *Communication systems*, 4 th Edition, John Wiley&Sons, Inc., (2001).
4. Ibnkahla, M., *Signal Processing For Mobile Communications Handbook*. Kingston, Ontario, Canada: CRC Press (2005).
5. Madhow, U., *Fundamentals of Digital Communication*, Cam bridge University Press (2008).
6. Rappaport, T.S., *Wireless Commu-nications - Principles and Practice*, Prentice Hall (2002).
7. Sarwate, D. V., Pursley, M. B. Crosscorrelation properties of pseudorandom and related sequences, *Proc. IEEE*, vol. 68, no. 5, pp. 593–619, May 1980.
8. Yong - Hwan Lee, Sawasd Tantaratana, Sequential Acquisition of PN Sequences for DS/SS Comm unications: Design and Performance, *Proc. IEEE*, vol. 10, no. 4, May 1992.

ENGINEERING SCIENCES

HIGH POWER ELECTROMAGNETIC SYSTEMS FOR MILITARY APPLICATIONS

Vasile DOBREF, Alexandru SOTIR, Octavian TĂRĂBUȚĂ, Cătălin CLINCI

*Marine Engineering Faculty, "Mircea cel Bătrân" Naval Academy, Constanța, Romania,

Abstract:
Generation of a high energy magnetic pulse with a flux compression generator requires first of all a good mathematical approach followed by simulations of the theoretical model in laboratory and in the field. The authors above have been members of a research team that developed an electromagnetic pulse device started by a conventional explosion. This paper describes the main steps in simulating and testing the compression of the magnetic flux needed to achieve the high energy magnetic pulse.

Keywords: *electromagnetic, pulse, generator, compression*

1. INTRODUCTION

Among the military applications of the electromagnetic pulse (EMP), the most common and used method is the flux compression generation (FCG) which was the path the project followed. The first experiences involving the so called "E-bomb" of the FCG type were conducted by the U.S.A. and the U.S.S.R. in the late '50s (Bykov et al., 2001).

2. FLUX COMPRESSION SIMULATION

2.1 The simulation of the flux compression has been undertaken in a high voltage laboratory in order to check the actual flux compression development. The goal of this activity was to put into evidence the flux compression through the progressive mechanical short-circuiting of the coil's rings, according to the electrical scheme of the experimental flux compression generator (FCG) presented in Figure 1.

Two types of coils have been used. The first one was smaller and made up of off- the-shelf components (Fowler et al., 1993). The second solenoid was manufactured as a prototype in the Romanian Naval Academy's workshop according to some specific required dimensions. Eventually, the actual measurements in the experimentation facility have been done on this second variant.

2.2 The oscilloscope diagrams of the experiments using the first coil are presented in Figure 2. There have been recorded the current in the coil by using the current shunt (first two graphs) and the magnetic flux, received by the frame-type antenna.
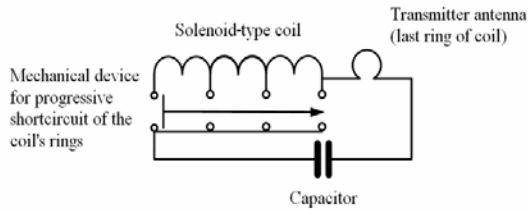
Fig. 1. The electrical principles of the experimental FCG

However, these experiments had been considered as irrelevant because, as it can be easily noticed, the vibrations of the contacts, during the mechanical short-circuiting, determine signals that have amplitudes comparable to the surge of the current and magnetic flux due to the progressive short-circuit of the coil's rings. The second experiment of the flux compression simulation used a second coil, identical to those tested in the range. This time the shunt has been removed from the circuit and only the resultant magnetic flux has been recorded by the means of the frame-type antenna (Dobref et al., 2008). We could consequently put in evidence very clearly the flux compression during the short-circuiting of the coil's rings, as presented in the oscilloscope diagrams from Figure 3.
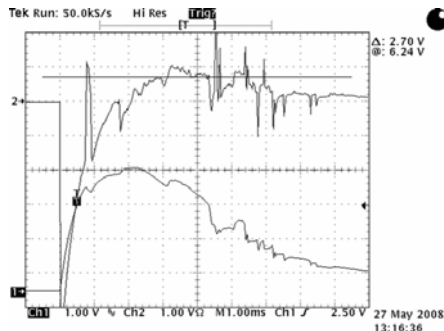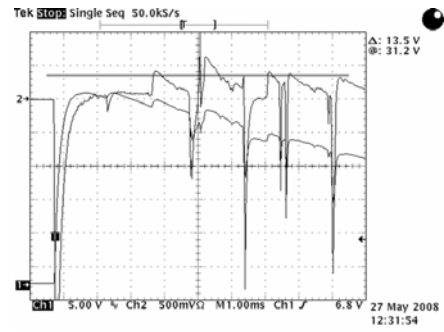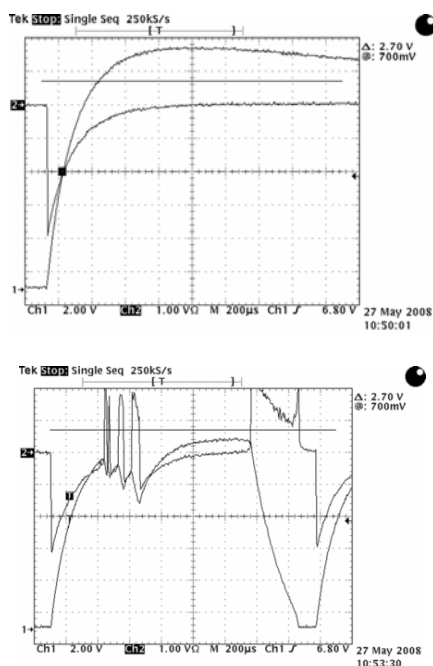
Fig. 2. Currents and magnetic fluxes in coil no.1.
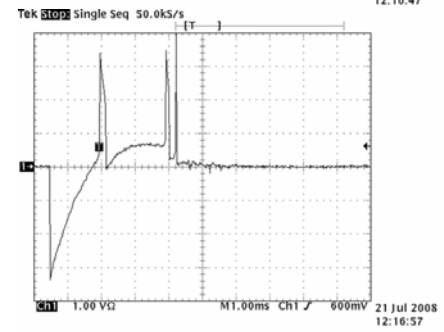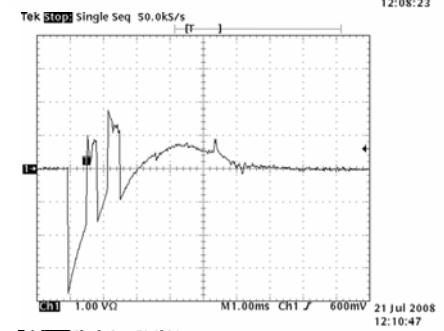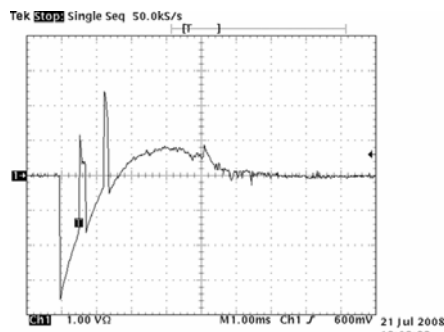
“HENRI COANDA”
AIR FORCE ACADEMY
ROMANIA

“GENERAL M.R. STEFANIK”
ARMED FORCES ACADEMY
SLOVAK REPUBLIC

INTERNATIONAL CONFERENCE of SCIENTIFIC PAPER
AFASES 2014
Brasov, 22-24 May 2014
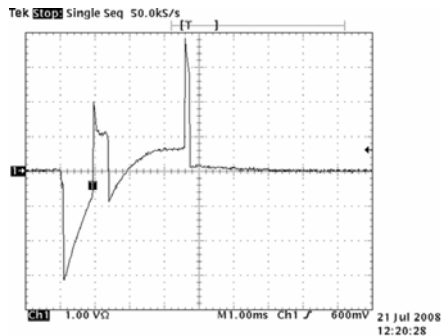
Fig. 3. Currents and magnetic fluxes in coil no.2.

2.3 EXPERIMENTAL RESULTS

During the final stage of this project – the experiments conducted in the range – the coil rings have been continuously shorcircuited at a very high speed (approximately 7200 m/s) by the means of the explosive charge. The explosive charge consisted of a mix of RDX (hexogen) and TNT. The building principles of the FCG are shown in Figure 4 (Johns, 2004).
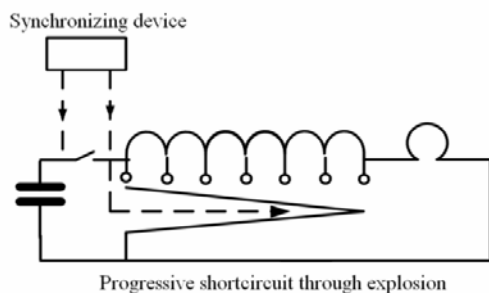
Fig. 4. FCG building principles

The actual arrangement of the experimental device was the following: the coil with the explosive charge inside was put in the first bunker. The two identical receiving antennas were mounted on the walls, simetrically with respect to the coil, on the same axis of the emitter antenna (the last ring of the coil). The coaxial cables needed to transport the signal from the antennas have been connected to two

Tektronix (TDS 724 D and TDS 5052) oscilloscopes, placed in the second bunker. The recordings were done in the same time. The two coils used for the experiments were identical.

Figure 5 presents the pulse recordings corresponding to the first and second blast, respectively
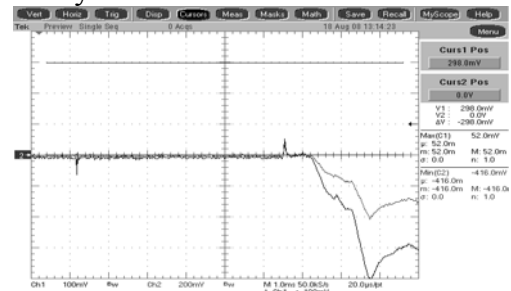
Fig. 5. The experimental recordings of the magnetic pulse

3. CONCLUSIONS

The authors take full responsibility for the contents and scientific correctness of the paper. The main conclusion rests in the compression of the flux generated by the two coils. We noticed that the signal in the receiving antenna is much greater for the second detonation, which is possible thanks to a greater starting coil current (different timing) but also to a different evolution of the explosion (Dobref et al., 2008). For establishing the maximum value of the magnetic pulse we took in account the second diagram in Figure 5. Then, the magnetic pulse size has been calculated in laboratory, after calibration. The tests in the own facilities confirmed the simulation results

REFERENCES

1. Abrams, M. (2003). The dawn of the e-bomb, IEEE Spectrum

2. Bykov, A.I.; Dolotenko, M.I. & Kolokol'chikov, N.P. (2001). Achievements on Ultra-High Magnetic Fields Generation, Physica B, 294-295, p.574-578

3. Dobref, V. et al., (2008). Research report: Modeling and design of a conventional payload for an electromagnetic pulse generation destined to block C4I systems, "Mircea cel Batran" Naval Academy, Constanta, Romania

4. Fowler, C.M.; Caird, R.S. & Garn, B. (1993). An introduction to explosive magnetic flux compression generators. Abstract, Los Alamos

5. Johns, D. (2004). Analysis of EMI/E3 Problems in Defense Applications, Flomerics

6. Knoepfel, H. (1970), Pulsed High Magnetic Fields, Nord-Holland

MULTIPROCESSOR SYSTEM DEDICATED TO MULTI-ROTOR MINI-UAV CAPABLE OF 3D FLYING

Adrian-Ioan LIȚĂ*, Ioan PLOTOG*, Lidia DOBRESCU*

*Faculty of Electronics, Telecommunications and Information Technology, POLITEHNICA University of Bucharest, Romania

Abstract: The paper describes an electronic multiprocessor system that assures functionality of a miniature UAV capable of 3D flying. The apparatus consists of six independently controlled brushless DC motors, each having a propeller attached to it. Since the brushless motor requires complex algorithms in order to achieve maximum torque, efficiency and response time a DSP must be used. All the motors are then controlled by a main microprocessor which is capable of reading sensors (Inertial Measurement Unit (IMU)-orientation and GPS), receiving input commands (remote controller or trajectory plan) and sending independent commands to each of the six motors. The apparatus contains a total of eight microcontrollers: the main unit, the IMU mathematical processor and one microcontroller for each of the six brushless DC motors. Applications for such an apparatus could include not only military, but also search-and-rescue, geodetics, aerial photography and aerial assistance.
.
Keywords: hexacopter, brushless, IMU, search-and-rescue, BLDC

1. INTRODUCTION

Vertical take-off and landing (VTOL) vehicles have been developed in the past century starting with the helicopter. The main advantages between VTOL vehicles and airplanes is hovering over a small area and being able to operate in areas with no runway. Comparing to a helicopter, having six propellers instead of two highly increases the useful payload, the stability and maneuverability. Multi-rotor systems (with 4, 6 or 8 propellers) can run faster, maintain stability in tougher winds and execute turns much faster (also used in aerobatics) than a traditional helicopter [1]. The main drawback of such systems is that building gas-powered multi-rotor systems is much harder than a classic helicopter.

The apparatus presented by the authors is an electrical powered small-sized vehicle with six vertical propellers.

The applications that can be developed on such a vehicle are of two types: imagery and transportation of small payload. From conception and design point of view, the transportation no needs extra processing. Imagery on the other hand introduces a whole new set of applications, especially when the image can be sent back to base in real time for more complex analysis, according to the mission requests.

2. THE MULTIPROCESSOR SYSTEM PROOF OF CONCEPT

2.1. The multiprocessor system solution. The authors have chosen brushless DC motors (*BLDC*) as solution for electrical powered of multi-rotor apparatus in order to assure capability to operate with a payload of 4 Kg. The reason for this requirement is that imagery applications demand high-resolution cameras, which are usually heavy.

Taking into account the necessity to implement a complex algorithm capable to achieve maximum torque, efficiency and response time for the motor, a digital signal processor (DSP) type controller was chosen. All the *BLDC* controllers are then controlled by a main microprocessor which is capable of reading sensors (Inertial Measurement Unit (IMU)-orientation and GPS), receiving input commands (remote controller or trajectory plan) and sending independent commands to each of the six motors. The apparatus (Fig. 1) contains a total of eight microcontrollers: the main unit, the IMU mathematical processor and one microcontroller for each of the six *BLDC*.
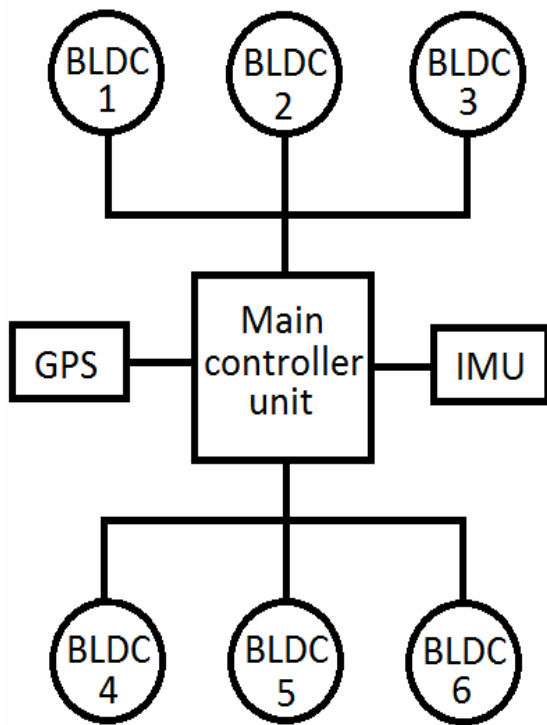
Fig. 1. Block schematic.

All the movements are combined and calculated by the main controller unit in order to achieve 3D flying. In (Fig. 2) the scale drawing of the apparatus is presented, noting the fact that the red leg represents the front direction. Also drawn with a circle around each motor is the propeller occupied area. The small arrow on the circle indicates the spinning direction of the propeller.
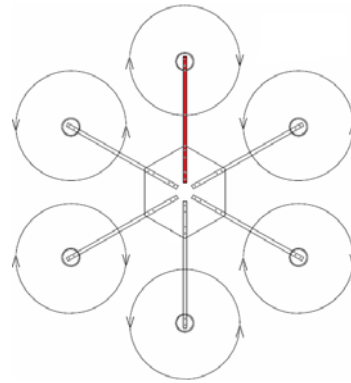
Fig. 2. Six propellers apparatus general view.

2.2. Design of movement control. While designing the apparatus (next referred as "hexacopter"), in order for it to be able to fully execute three-dimensional maneuvers each movement axis was considered, resulting in three separate moves: roll, pitch and yaw.

For maximum efficiency, all the propellers push air down.
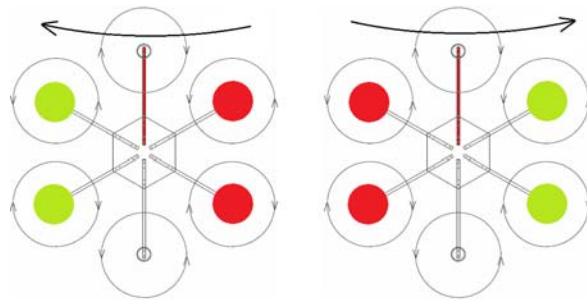
Fig. 1. Movement on Y axis – Roll.

The roll and pitch maneuvers are obtainable just by modifying the push force on some of the propellers. In order for the hexacopter to be able to modify the yaw angle and in order for it not to keep spinning at all times due to added momentum, half of the propellers need to spin in one direction and the others in the opposite direction. For best

"HENRI COANDA"
AIR FORCE ACADEMY
ROMANIA

"GENERAL M.R. STEFANIK"
ARMED FORCES ACADEMY
SLOVAK REPUBLIC

INTERNATIONAL CONFERENCE of SCIENTIFIC PAPER
AFASES 2014
Brasov, 22-24 May 2014

response time, the propellers spin is alternated clockwise and counter clockwise.

Considering the red motor-propeller pair as the front of the hexacopter (parallel to Y Cartesian axis), we can define the roll and pitch movements as following: roll moves the apparatus left and right, while pitch moves it forward or backward. (Fig. 3, 4, 6, 7) depict the propellers spinning speed as follows: transparent – normal spin, red – faster spin, more thrust and green – slower, less thrust. This makes the hexacopter modify its angle and execute the maneuver.

Fig. 2. Movement on X axis – Pitch.

It is worth noticing that the roll is done using only 4 out of 6 propellers, while pitch uses all. The reason behind this is that the pitch maneuver dictates the maximum forward speed of the apparatus, which is used more often. (Fig. 5) presents the forward movement of the UAV: red – faster spin, pink – faster spin, but slower than red.
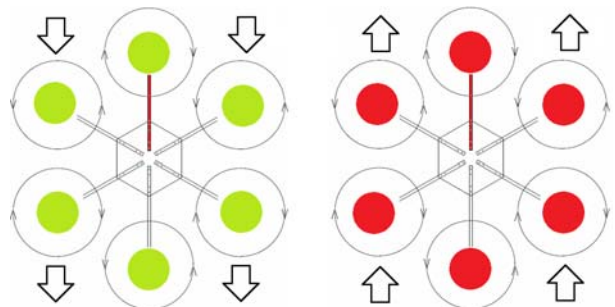
The yaw maneuver is illustrated in (Fig. 6), using all 6 propellers. Fewer propellers may be used for steadier control, with the condition that the total yaw momentum remains constant.

The last described movement is represented by the take-off and landing. Basically all propellers have the same speed, which is either higher (take-off) or lower (landing) than the steady altitude speed. There can be more than one variation, but the fastest is the one illustrated in (Fig. 7).

Fig. 3. Forward Movement.

Fig. 4. Movement on Z axis – Yaw.

Fig. 5. Take-off and Landing.

2.3 The motor controllers. The authors have chosen *BLDC* motors NX-4006-530 having speed constant Kv = 530 rpm/v, maxim current = 10A, phase resistance = 75mΩ, phase inductance = 10uH, power = 150W and

weight = 67g [7]. While using brushless motors without any sensor, the usage of a microcontroller with is mandatory. The microcontroller contains a sensorless trapezoidal six-step algorithm which drives six MOS-FET transistors in a three half-bridge configuration used to connect the three phases of the brushless motor.

Six-step trapezoidal commutation (Fig. 8) requires the use of PWM channels. Two half bridges drives two of the phases while the third remains floating and is measured by the ADC module of the microcontroller.
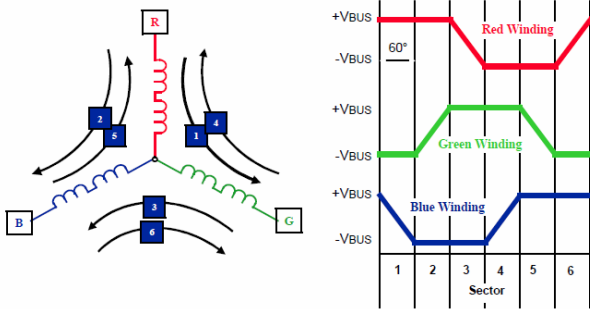
Fig. 6. Six-step trapezoidal commutation.

The floating phase is used to compute when the next commutation occurs. This can be usually implemented by two methods, both requiring prior filtering: comparing it either to half the DC voltage or to the reconstructed motor neutral point. The algorithm used in this paper uses the first method as it requires fewer electronic components and makes full use of the microcontroller's DSP functions.

Comparing the floating phase voltage (also known as back electro-magnetic force – *BEMF*) to half the DC voltage will result in finding the zero-crossing point (Fig. 9) of the voltage. The zero-crossing point is the exact moment at which the floating phase voltage is equal to DC bus voltage divided by two, and is the exact moment at which the rotor moved 30° out of 60° of a sector. By measuring the time between the sector change and zero crossing moment (30°), the algorithm then waits this exact amount of time before changing the sector again. This approach is used to replace the sensor by using the floating phase as a sensor. By using PWM modulation to control the MOS-FET transistors, the motor speed is controlled by increasing or decreasing the duty-cycle. In order for the commutation

not to create acoustical disturbance, the PWM frequency used is 20 KHz. High frequency require more expensive MOS-FET transistors to keep the losses to minimum. The duty-cycle is set by a PI (proportional integral) controller, which receives the speed as the measured parameter and the desired speed from the main controller unit as the input parameter.

The communication between the main controller unit and the motor controllers is done via I2C protocol.
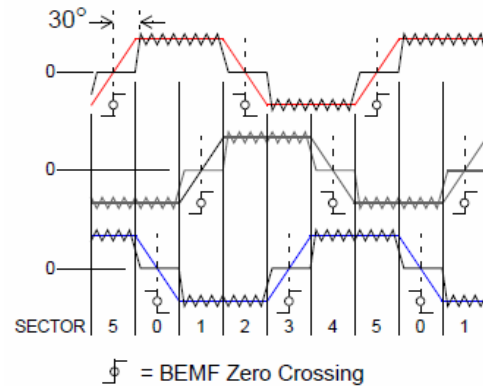
Fig. 7. Zero-Crossing detection.

The microcontroller used in this case is the dsPIC33EP64MC502 made by Microchip, for its motor control dedicated PWM channels, its 10-bit ADC module and its communication protocols (I2C and also CAN, leaving room for further implementation) [2]. The devices consume less than 100 mW of power, which minimizes the losses.

2.4 The main controller unit. The main controller unit is responsible for sensor data acquisition, wireless communications with the base station, communication with the motor controllers and for the main movement computations. It contains a 32 bit microcontroller capable of making all the calculations required in order for the apparatus to be stable and to have a fast response. The main controller unit also has access to the GPS sensor. The main controller unit has the possibility of sending all its data to another system (faster, such as a PC) via wireless link or directly via UART or SPI. This was designed to allow running of higher complexity applications such as automatic search and rescue, or monitoring. They require a color camera and image analysis software, which is very demanding and can't be ran on

"HENRI COANDA"
AIR FORCE ACADEMY
ROMANIA

"GENERAL M.R. STEFANIK"
ARMED FORCES ACADEMY
SLOVAK REPUBLIC

INTERNATIONAL CONFERENCE of SCIENTIFIC PAPER
AFASES 2014
Brasov, 22-24 May 2014

the main controller unit. The interface allows full control of the hexacopter by the 3rd party computer, but still allowing for manual override of the commands if needed. The processor used for the main controller unit is the PIC32MX795F512L made by Microchip. It offers a lot of communication protocols, 4 UART modules, 4 I2C modules, and over 100 MIPS of processing power on 32 bits mathematical sets, while requiring less than 400 mW of power [2].

The main sensor is the inertial measurement unit (IMU) which uses a three-axis accelerometer, a three-axis gyroscope and a three-axis magnetometer in order to compute the angles of roll, pitch and yaw. Initially, when the hexacopter is not started, all angles are reset in order to set the forward direction. The sensor uses UART communication to send the data back to the main controller unit.

3. THE EXPERIMENTAL RESULTS AND DISCUSSIONS

3.1. Build. As seen in (Fig. 10), the six motor-propeller pairs are connected to the main unit through carbon-fiber tubes to a central aluminum hexagonal plate. Carbon-fiber and aluminum were chosen for being very lightweight materials with increased durability and strength. The total weight of the apparatus is 1.8 Kg. The central plate was chosen to be hexagonal instead of round in order to provide higher contact to carbon-fiber tubes. Also, for increased strength, the carbon-fiber tube profile is square instead of round. The tube houses the wiring needed to provide power and commands to the motor controllers.

3.2. Lift and power consumption tests. Tests have shown that each motor-propeller pair is capable of pushing air up to a thrust capable of lifting 1 Kg / pair. Having 6 pairs

and a 1.8 Kg apparatus gives us a total of about 4 Kg of useful payload, exactly as designed.

Fig. 8. Hexacopter.

The brushless DC motor controllers provides very fast response, low commutation noise and excellent performance (Fig. 11). New speed information is fed to the motor controller with a frequency of 500 Hz.
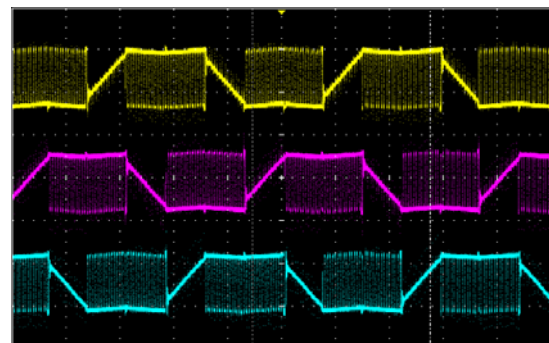
Fig. 9. Motor BEMF and driving voltage.

The total power consumption of the hexacopter while standing, with no motors running was of 850 mW, which, with a battery of 16.8V and 5800 mAh (a total of 97.4 Wh) is less than 1%.

Each of the motors running in full thrust (when able to lift approximately 1 Kg each) had a current consumption of 9.8 A at 16.8V. With the hexacopter running in full thrust, this

would give about 6 minutes of flight time. However, while hovering (keeping a steady altitude in no-wind conditions) with no payload, the total power consumption is 170W, giving a total flight time of over 30 minutes. The exact case is somewhere between 6 and 30 minutes, depending on the payload: when the apparatus is required to have extra payload (1 Kg), it is still fast in response, but the total consumption is 290W, which means about 18-20 minutes of flight. When maximum load is applied, the response time is slow, since there isn't a lot of reserve power to make the fast movements: all the power is consumed to lift and keep the payload.

The BLDC controller (Fig. 12) was designed in respect of Design for Manufacturing concept [8], so it would fit below the motor, in order to save space and increase efficiency.
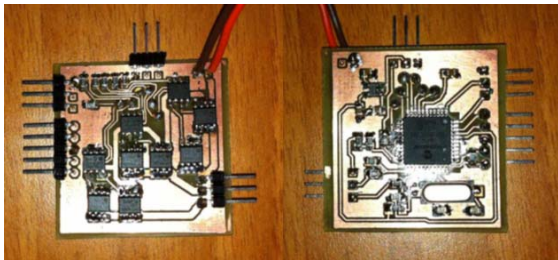
Fig. 10. BLDC controller board – all layers

Further development require designing new algorithms which can be applied to the hexacopter in order to automatically perform complex tasks, most in the field of digital image processing: automatic search for certain objects on an area, monitoring perimeter, etc.

4. CONCLUSIONS & ACKNOWLEDGMENT

4.1. Conclusions. The main controller unit initially has a simple PID controller to feed the output for the motor controllers. Though the response time is good, some oscillations are present. Tuning the PID loop parameters is mandatory, and the PID was added complexity by adding an auto-tuning sequence to be executed on every start of the hexacopter.

The ability to execute 3D maneuvers gives virtually any possibility to any application which requires 3D flight. More complex algorithms can be implemented when using more than one hexacopter to perform a collaborative work. Other example would be that the estimated flight time is around 20 minutes, and the charge time is around 1.5-2 hours, meaning that in order to fully monitor a perimeter, at least four are needed, one to be operational and the others to charge.

REFERENCES

1. Gablehouse C. Helicopters and autogiros: a chronicle of rotating-wing aircraft Lippincott (1967)
2. Lita, A., Cheles M. *AN1160 Sensorless BLDC Control with Back-EMF Filtering Using a Majority Function* [online]. Available: http://www.microchip.com
3. Alamio A., Artale V., et all. PID Controller Applied to Hexacopter Flight *Journal of Intelligent & Robotic Systems.* Issue 1-4 (Jan 2014).
4. Oursland J., The design and implementation of a quadrotor flight controller using the QUEST algorithm *South Dakota School of Mines and Technology* (2010)
5. Markley, F. L., Mortari D. Quaternion altitude estimation using vector observations *The Journal of the Astronautical Sciences* (2000)
6. Erginer B., Altug E. Modeling and PD control of a quadrotor VTOL vehicle *IEEE Intelligent Vehicles Symposium* (2007)
7. NX-4006-530kv Brushless Quadcopter Motor. Source. [online]. Available: http://www.hobbyking.com/hobbyking/store/__17923__NX_4006_530kv_Brushless_Quadcopter_Motor.html.
8. Plotog I., Marin A., Boanta L., Model of assembling process for electronic parts integrated in mechatronic products, The Romanian Review Precision Mechanics, Optics & Mechatronics, 2013, No. 44, ISSN 1584 – 5982.

FRACTAL SECTOR ANTENNA WITH RESONATORS ARRANGED IN A SQUARE SHAPE

Gheorghe MORARIU*, **Ecaterina Liliana MIRON****

*Electronics & Computers Department, "Transilvania" University, Brasov, Romania,
**Air Defense Department, Air Force Academy, Brasov, Romania

Abstract: This paper presents a model of stripline fractal antenna having resonant elements in the form of a square shape. The model is presented in two versions, one with compact resonators and second with frontier resonators, highlighting technical similarities and differences through electrical parameters. In the same time, the paper emphasizes the concordance between theoretical and experimental results.

Keywords: fractal, stripline, antenna, directivity, field intensity.

1. INTRODUCTION

Development of mobile telephony and portable phones miniaturization has imposed dimensions reduction of the radiant elements (emission-receiver antenna), keeping as much as possible their gain and efficiency at an optimum level. In the same time, it is necessary to ensure a wide frequency range, directivity and a large aperture. These requirements are best satisfied by fractal sector antennas with different geometric shapes of resonators. This paper presents two versions of a fractal antenna model with resonant elements arranged in a square shape, with three levels of demultiplication. In a radiant field resonators arranged in a square shape behaves simultaneously as a magnetic antenna (loop antenna) and closed dipole.

2. ANTENNA DESIGN

The two variations of the antenna model are shown in Figure 1 - frontier resonators, respectively Figure 2 - compact resonators.

The frontier resonators are pairs, having dimensions and ecart between them as specified in Table 1 (from the edge inwards).
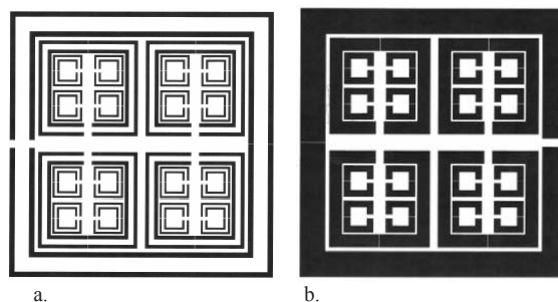
Fig. 1. Fractal sector antenna: a. with frontier resonators; b. with compact resonators

Table 1. Lengths of the frontier resonators and ecart between them

Length [cm]	Ecart [mm]
$L_{11} = 15$	10
$L_{12} = 13$	
$L_{21} = 5$	5
$L_{22} = 4$	
$L_{31} = 3$	5
$L_{31} = 2$	

Table 2. Lengths of the compact resonators and ecart between them

Length [cm]	Ecart [mm]
$L_1 = 14$	10
$L_2 = 4,5$	5
$L_3 = 2,5$	5

Compact resonator lengths were chosen as the average length of the frontier resonators to maintain the same central resonance frequency.

Figure 3 shows the resonators phasing and the feeder adaptation circuit.
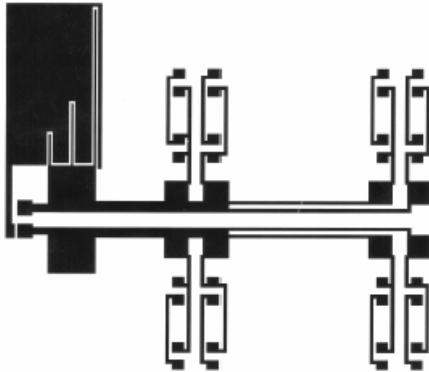
Fig. 3. Feeder adaptation circuit.

Fractal series of the radiating surface is in division with 4^n.

$$S = S_0 \sum_{n=0}^{2} \frac{1}{4^n} \quad (1)$$

where S_0 is the surface of the biggest contour.

A. *Analytical calculation of the resonator for magnetic antenna regime* (***, 2013)

$$\lambda = (4 + 10) \cdot 4 \cdot L \quad (2)$$

where L is edge length in meters.

$$h_e = \frac{2\pi NA \cos \theta}{\lambda} \quad (3)$$

where: h_e - effective height of antenna;
N – contours number;
A - surface area [m^2];
θ - the angle of incidence of the wave relative to antenna plane [°].

$$R_{rad} = Z_0 \frac{2}{8} \pi \left(\frac{h_e}{\lambda}\right)^2 \quad (4)$$

where Z_0 - impedance of free space.

$$U_{ef} = h_e E \quad (5)$$

where E - electric field intensity.
For stripline resonators, according to (2)

$\lambda = 16L$, and bandwidth is

$$\Delta B = (\pm 25\%) f_c \quad (6)$$

where f_c – central frequency.
According to (2), (3) $N=1$, $A=L^2$ and

$$h_e = \frac{2\pi A \cos \theta}{\lambda} = \frac{\pi L \cos \theta}{8} \quad (7)$$

In case of frontier resonators the lengths are given by

$$L_i = \frac{L_{i1} + L_{i2}}{2} \quad (8)$$

It is resulting in

$$h_{e1} = \frac{\pi \cos \theta}{8} \cdot 14 = \frac{7\pi}{4} \cos \theta \quad (9)$$

$$h_{e2} = 4, \frac{5\pi}{8} \cos \theta \quad (10)$$

$$h_{e3} = 2, \frac{5\pi}{8} \cos \theta \quad (11)$$

According to (4), radiation resistance is

$$R_{rad} = Z_0 \frac{2}{3} \pi^3 \frac{\cos^2 \theta}{128^2} \quad (12)$$

Resonance frequencies of the resonators are:

"HENRI COANDA"
AIR FORCE ACADEMY
ROMANIA

"GENERAL M.R. STEFANIK"
ARMED FORCES ACADEMY
SLOVAK REPUBLIC

INTERNATIONAL CONFERENCE of SCIENTIFIC PAPER
AFASES 2014
Brasov, 22-24 May 2014

$$f_{c1} = \frac{c}{\lambda_1} = \frac{3 \cdot 10^8}{16 L_1} = 135 \text{MHz} \tag{13}$$

$$f_{c2} = \frac{c}{\lambda_2} = \frac{3 \cdot 10^8}{16 L_2} = 420 \text{MHz} \tag{14}$$

$$f_{c3} = \frac{c}{\lambda_3} = \frac{3 \cdot 10^8}{16 L_3} = 750 \text{MHz} \tag{15}$$

Taking into consideration (8) bandwidth of frontier resonators is given by

$$\Delta B = (\pm 30\%) f_c \tag{16}$$

Calculation methodology presented is valid also for compact resonators with the observation that the bandwidth is different – eq. (6).

B. Analytical calculation of the resonator

for closed dipole ($\lambda/2$) regime

$$\lambda = 2 \cdot L \tag{17}$$

$$h_e = \frac{2}{\pi} h_d \tag{18}$$

where h_d – height of the dipole.

For $h_d = \lambda/2$,

$$h_e = \frac{\lambda}{\pi} \tag{19}$$

$$R_{rad} = Z_0 \frac{2}{3} \pi \frac{h_e}{\lambda} = Z_0 \frac{2}{3\pi} \tag{20}$$

Central resonant frequencies are:

$$f_{c1} = \frac{c}{\lambda_1} = \frac{3 \cdot 10^8}{0}, 3 = 1 \text{GHz} \tag{21}$$

$$f_{c2} = \frac{c}{\lambda_2} = \frac{3 \cdot 10^8}{0}, 09 = 3,4 \text{GHz} \tag{22}$$

$$f_{c3} = \frac{c}{\lambda_3} = \frac{3 \cdot 10^8}{0}, 05 = 6 \text{GHz} \tag{23}$$

3. EXPERIMENTAL RESULTS

Experimental data obtained by spectral analysis (scalar) and vector analysis (with VNA) are shown in Fig. 4 – 8 (experimental diagrams).

Fig. 4 and 5 are shown the directivity diagrams.
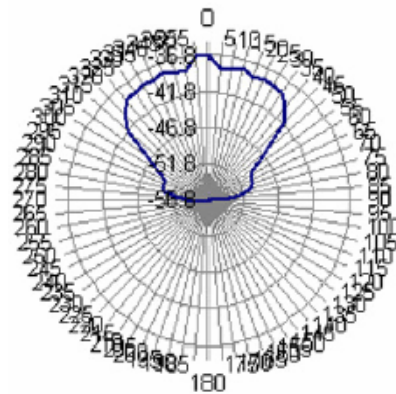
Fig. 4. Fractal sector antenna with compact resonators: Directivity diagram – E field.
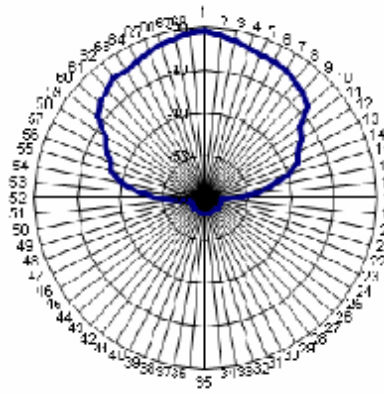
Fig. 5. Fractal sector antenna with frontier resonators: Directivity diagram – E field.
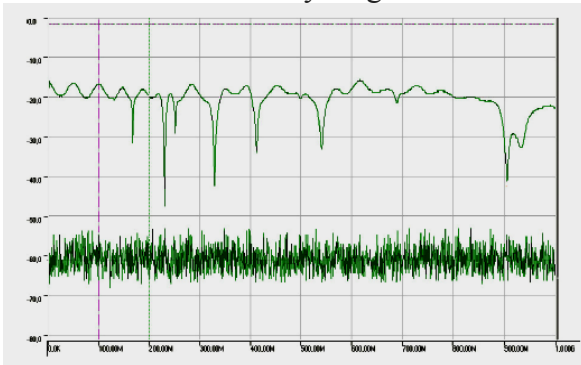
Fig. 6. Fractal sector antenna with frontier resonators: The reflection coefficient.
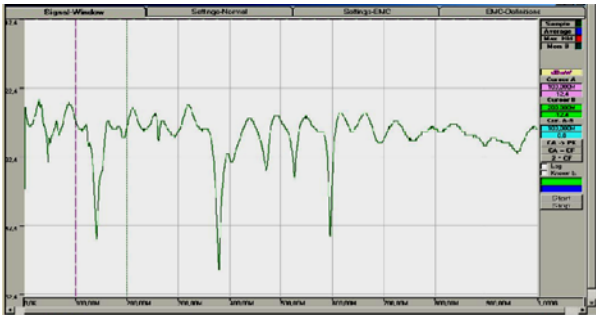
Fig. 7. Fractal sector antenna with compact resonators: The reflection coefficient.
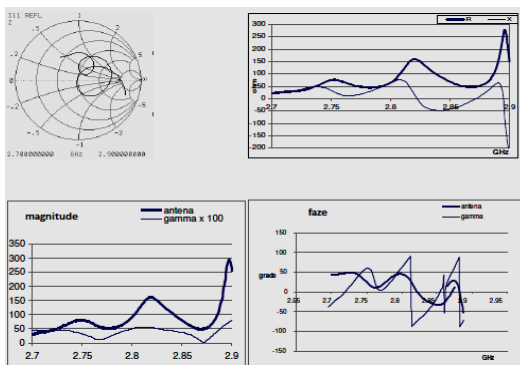
Fig. 8. Fractal sector antenna – VNA analysis in the frequency band 2.7-2.9 GHz.
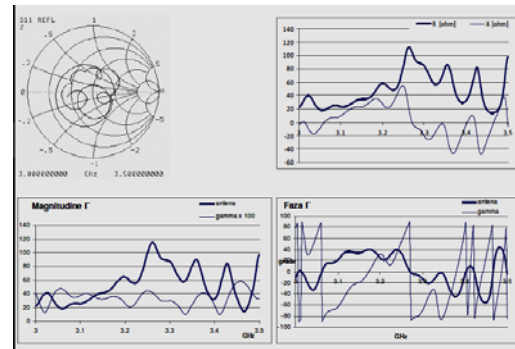
Fig. 9. Fractal sector antenna – VNA analysis in the frequency band 3-3.5 GHz.
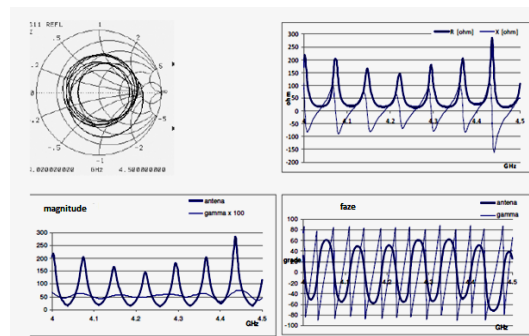
Fig. 10. Fractal sector antenna – VNA analysis in the frequency band 4-4.5 GHz.
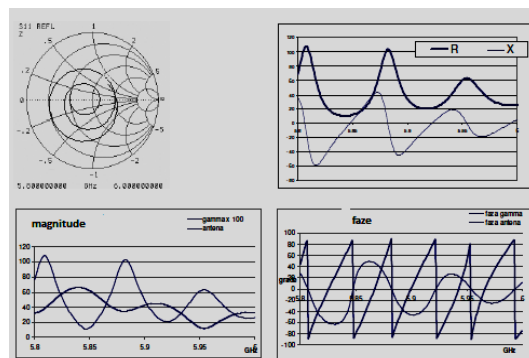
Fig. 11. Fractal sector antenna – VNA analysis in the frequency band 5.8-6 GHz.

4. CONCLUSIONS

Due to the dual behavior, both the magnetic resonator and closed dipole ($\lambda/2$), fractal sector antenna allows operation in a very wide frequency band with a gain around 10dB.

The small size and relatively simple technical realization, it is recommended for 4G and 5G mobile telephony.

Through a judicious choice of fractal dimensions, antenna can cover frequency

"HENRI COANDA"
AIR FORCE ACADEMY
ROMANIA

"GENERAL M.R. STEFANIK"
ARMED FORCES ACADEMY
SLOVAK REPUBLIC

INTERNATIONAL CONFERENCE of SCIENTIFIC PAPER
AFASES 2014
Brasov, 22-24 May 2014

bands with quasi-constant gain for the entire spectrum of mobile telephony.

REFERENCES

1. Best, S. (2003). *A Comparison of the Resonant Properties of Small Space-Filling Fractal Antennas*. IEEE Antennas and Wireless Propagation Letters **2** (1): 197–200.
2. Bogdan, I. (2008). *Antene microstrip, îndrumar de proiectare*. http://staff.etc.tuiasi.ro/bogdani/Antene/PrAntMstrip.pdf
3. Dutca, M., Morariu, G., Croitoru, O., Machedon-Pisu, M. (2012*). Logarithmic Fractal Segment Antenna.* Brasov, OPTIM 2012, ISSN 1842-0133, p.1266-1273
4. Hephzibah Lincy, B., Srinivasan, A., Rajalakshmi, B. (2013). *Wideband Fractal Microstrip Antenna for Wireless Application.* ICT Journal, Volume 3 No. 3, ISSN 2223-4985
5. Morariu, G., Zara, M.M. (2013). *Fundamente si aplicatii ale structurilor fractale in antene pentru microunde.* Brasov, Editura Universitatii TRANSILVANIA
*** (2013). Magnetic Loop Antenna Theory-*SID Monitoring Station.* http://sidstation.loudet.org/antenna-theory-en.xhtml [11.06.2013]

,

ENGINEERING SCIENCES

"HENRI COANDA"
AIR FORCE ACADEMY
ROMANIA

"GENERAL M.R. STEFANIK"
ARMED FORCES ACADEMY
SLOVAK REPUBLIC

INTERNATIONAL CONFERENCE of SCIENTIFIC PAPER
AFASES 2014
Brasov, 22-24 May 2014

THE ANALISYS OF NAVAL ELECTROMAGNETIC SYSTEMS USING SOFTWARE PROGRAMS

Gheorghe SAMOILESCU, Serghei RADU, Florentiu DELIU, Raluca MATES

*Academia Navală Mircea cel Bătrân,Constanța,România,** Stena Group,
*** Academia Navală Mircea cel Bătrân,Constanța,România, ****Academia Navală Mircea cel Bătrân,Constanța,România

Abstract: *Modernization strategy of the naval power system is based on the following: high efficiency, high flexibility with low emissions using combined systems consisting of multiple components and various generators. In order to simulate electro-energetic processes in the naval system and reduce fuel consumption, we built an application that performs the energy balance in each functioning regime of a ship by charging each consumer. The program also optimizes underway regimes, offering alternative changes in the system and thereby reducing electricity consumption on board. The optimization provided by the program will be made by passing the consumers in a particular type of operation in various modes so as the total energy consumption to be the lowest.*

Keywords: *power system, software program, maritime ship, underway and stationary regime*

1. INTRODUCTION

In order to optimize electricity consumption correlated with increased reliability of power systems aims in ships all equipment and facilities to be implemented on board must be updated along with marine propulsion development so as a greater efficiency and a reduced environmental impact to be achieved. [18, 6, 17, 14]

The aim is to develop and use digital tools to achieve combined energy production systems. [19,15] Developing component models at different levels of complexity, methods for their assembly into powerful software simulators, the use of such simulators to analyze both the dynamic and operational behavior while identifying limitations are very important in developing the next generation of naval electro-energetic power systems [8, 21,16, 10, 5, 22, 9, 1].

The program starts with the specifications of a LPG (liquefied petroleum gas) carrier: Maersk LPG/NH3 Glory. The program can be used for any other type of vessel by introducing a new set of characteristic parameters, can achieve a theoretical calculation for a ship proposed for construction in any shipyard [11,20]. The program was developed using Microsoft Visual Studio C # 2008, Microsoft Excel and MathCAD 15. [2,3,4] The strengths of the proposed program: it can be applied to all categories of ships, requiring only the introduction of the manufacturing nominal parameters of the generator and consumers

(which can be found in the technical documentation of the vessel) [13,7], it includes a study mode according to experimental data measured onboard while underway, it takes into consideration weather conditions (humidity air salinity of sea and air) in the calculation of the power system losses, it also deals with time- damage of electrical consumers caused by harsh conditions on board usage (overload, mains transient), resulting in direct decreased efficiency of the generator [1,12] . The program was tested on board for the movement of the ship between two ports, leaving open the opportunity of using the program for the entire voyage. Weak points of the program: the format of the given parameters is not checked , bowing program on the premise that users are familiar with the way the program can be used; the program is not applicable to the short-circuit protection of NPS.

2. COMPONENTS OF THE PROGRAM

The program is a Windows-Form application built in C # (Fig.1). The menu bar contains seven submenus with functions to determine the energy balance in standard underway regimes and to select the consumers according to the type of vessel.
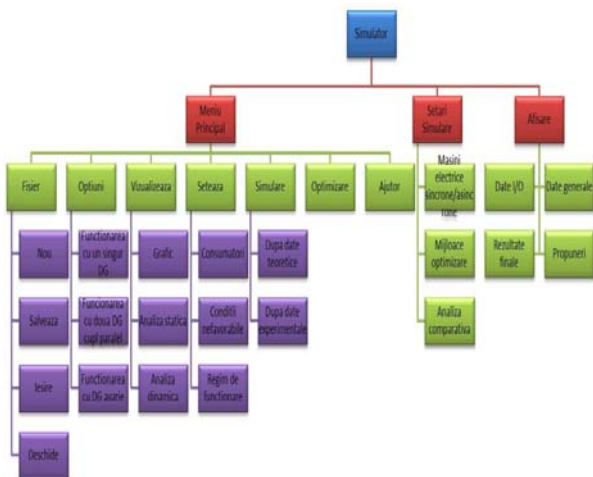
Figure 1. Block diagram of the program

3. MODEL SIMULATION

To exemplify the developed program usage, we present an optimization algorithm for a set of experimental values measured on board the reference carrier Maersk LPG/NH3 Glory. This simulation model comprises a series of steps, as follows: select the "After experimental data" from the "Simulation" submenu of the menu. The selected option appears in the "Show data I/O" window of the display;

a) In the display window select the option "Show data". Here the user can become familiar with the components and operating parameters of the power system on board (the main features of the diesel engine used for inducting the generator, the generator characteristics and high power electrical consumers features). Figure 2.

b) Access submenu "Options" from the menu. This sets the number of generators (connected to the board net). During this simulation the following underway regimes will be used: Underway regime at sea / at anchor - one DG, manoeuvre regime - 2DGs; stationary regime when loading or unloading - 2 DGs .

If the emergency generator is the only one connected to the network, it is considered that the ship operates in an emergency regime. Further on, a study on the startup behavior of generators and large consumers is performed. This particular step aims to analyze the transient process of starting the generator with all the steps that are involved (starting the diesel engine, generator excitation and coupling to the network).
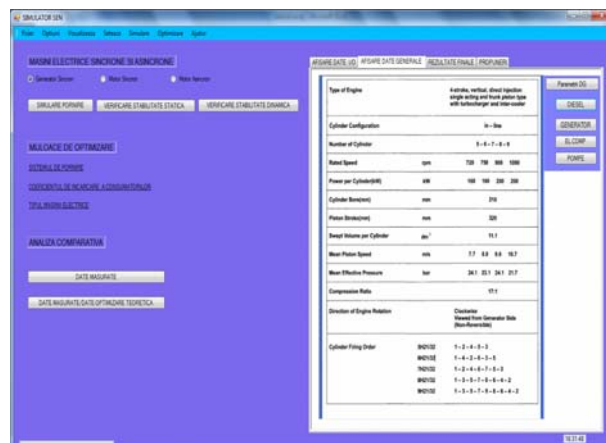
Figure 2. General data display

c) From "Settings simulation" of the parent window select the option "Synchronous Generator", then click "Start simulation". A new window with two modules will open: "The rated parameters of the chosen electric generator" and "The rated parameters of the chosen electric engine";

"HENRI COANDA"
AIR FORCE ACADEMY
ROMANIA

"GENERAL M.R. STEFANIK"
ARMED FORCES ACADEMY
SLOVAK REPUBLIC

INTERNATIONAL CONFERENCE of SCIENTIFIC PAPER
AFASES 2014
Brasov, 22-24 May 2014
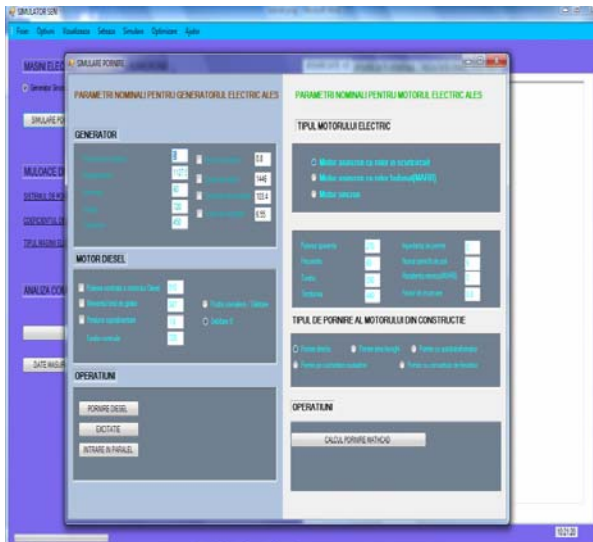
Figure 3. DG starting simulation
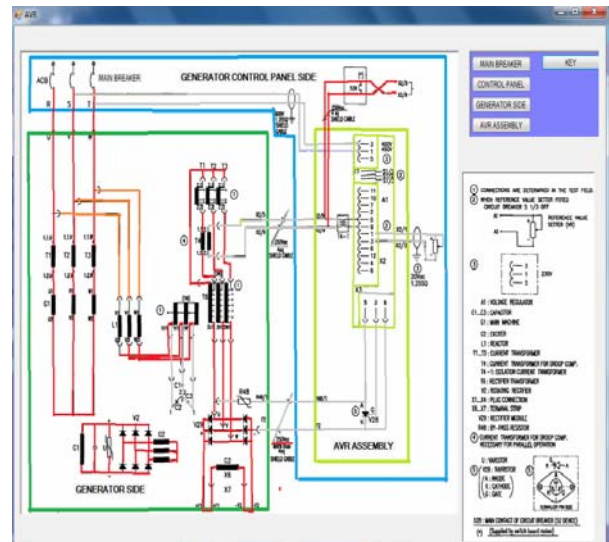
Figure 4. Generator excitation scheme

We will only work with the first module introducing the generator's features (apparent power, active power, frequency, speed and type of electric machinery, voltage to bars, power factor, power generator, excitation current, and voltage excitation).

d) In the "Diesel" section special features needed to run the engine are filled in (diesel engine rated power, total yaw moment, boost pressure, rated speed); select the "Position rack / cutting" to ensure engine start and its operation at rated parameters.

e) In the "Operations" section we will simulate the startup, excitation and parallel coupling for the parameters already introduced. Push the "Start Diesel Engine". A text box with the message "Engine started successfully" will appear.

f) Click "Excitation" from the "Start Simulation". A new form opens. It contains the excitation of the generator. In the new window a set of buttons that separate parts of the excitation scheme appears. After pressing each of the 5 buttons, the AVR window will look like in Figure 4.

g) Close "AVR "window and click "Join in parallel" from the "Start Simulation". A new form containing in parallel connection of the main generators opens.

h) Close all windows except the parent window. Select the option "Induction motor" from the section "Synchronous and induction electric machineries" in the parent window, then click "Start Simulation". A new window will appear ("Start Simulation").

i) We will apply the necessary settings to simulate the induction motor start in the following sections: electric engine type, original engine starting mode, operations. For this simulation, we consider the default option "Rotor fault induction motor", specific to the electric motor of the reference vessel. In this section there are also the main parameters of the electric motor: active power, apparent power, frequency, speed work, voltage, impedance startup, number of pole pairs, the rotor resistance, load factor. For this simulation, we will work with default values specific to the electric motor of the reference vessel. We will fill in the "Rotor Resistance"

and "Choke start" only if the engine is a coil winding rotor one. Otherwise we will fill in the indicated fields with zero. In the section "Original engine starting mode" the following options are available: direct start, star start/triangle, autotransformer start, start with features given by the rheostat, frequency converter start.

j) In the "Operations" section with the settings given above, click "MathCAD Starting Calculus". A new form will open [Figure 5].
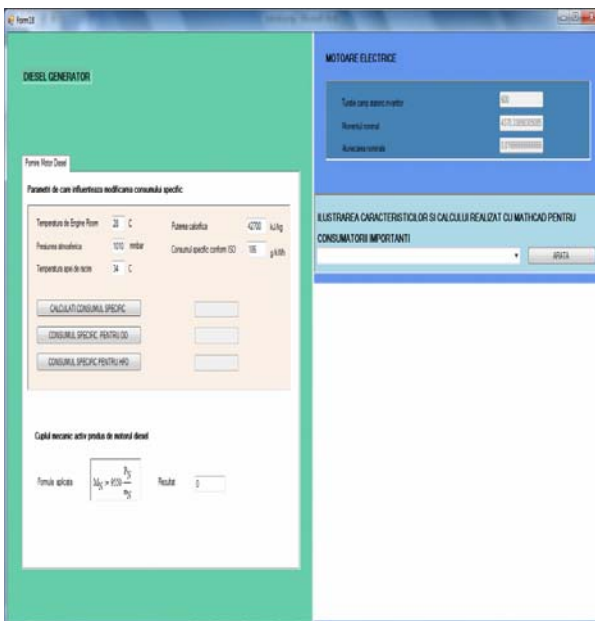
Figure 5. MathCAD Starting Calculus for the analyzed Electric motor

In the section "Illustration of MathCAD characteristics and calculus for major consumers" calculations are available for the following consumers: 270kW Compressor Motor, Deep Well Pump Motor, Booster Pump Motor, Water Pump Spray Motor, Fire and General Service Pump Motor Bilge, Ballast Pump Motor, Fire Pump Emergency generators Motor. We continue with the generators stability study. To do this, click "Check static and dynamic stability". A form that contains a number of options to illustrate the different types of system stability will appear. Press the button "Show complete MathCAD calculus" to illustrate the generator stability calculation considered in the current simulation, and then press the four buttons. Compare the result with the three already shown systems [Figure 6].
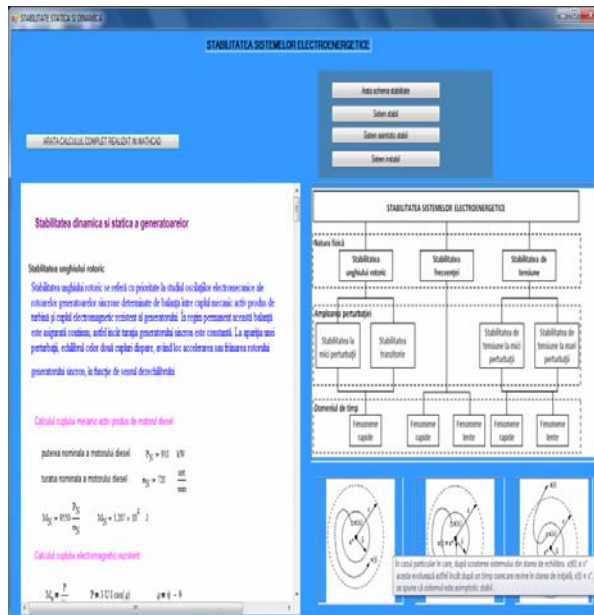
Figure 6. Comparing MathCAD calculus with illustrated systems

We will do three tests, the first for the underway regime, the second for the manoeuvre regime, and the third one for loading and unloading arrangements regime. Underway regime analysis – we use consumers that work continuously. We set up the main distribution panel like in figure 7. We obtain a power consumption of 507.44 kW. Therefore it is only necessary to connect one generator (507.44 kW represents 56% of the power generator of 910 kW). Manoeuvre regime analysis - we use consumers that work continuously. We will also add the consumers used in manoeuvring: bow winches, stern winches, and other deck installations that can be required. The necessary power will be 763.04 kW which is more than 75% of the power generator. We will also add automatic mode consumers and get a 906.64 kW power. So, for this particular regime we will have two generators connected in parallel for the network.

"HENRI COANDA"
AIR FORCE ACADEMY
ROMANIA

"GENERAL M.R. STEFANIK"
ARMED FORCES ACADEMY
SLOVAK REPUBLIC

INTERNATIONAL CONFERENCE of SCIENTIFIC PAPER
AFASES 2014
Brasov, 22-24 May 2014

Figure 7. Main distribution panel for underway regime

Loading and unloading arrangements regime analysis – we have the following configuration of the main panel, Figure 8:

Figure 8. Main panel for loading / unloading regime

We obtain a total of 1206.96 kW power consumption, having two generators connected in parallel.
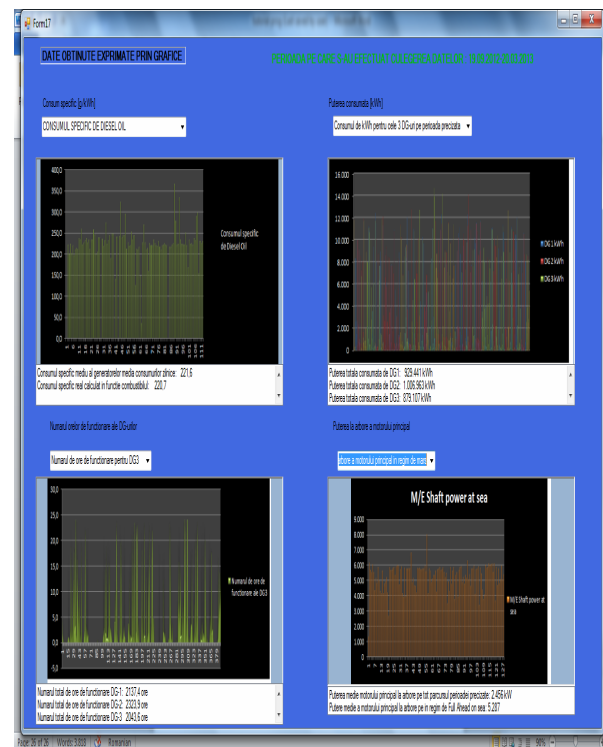
Figure 9. Statistics for considered ranges and regimes

Display the final data – we can observe all steps of this simulation. From the Display Mode window conclusions and proposals of the analyzed ship power system are accessed.

Figure 10 . Final results of the simulation

4. CONCLUSIONS

The program will do the initial analysis of the existing energy system and then will optimize each regime and seek alternatives for reducing electricity consumption thus lowering fuel consumption of internal combustion engines. The optimization made by the program allows the passage of consumers from a given running curve on another due to regime and charge changes, therefore, considering the calculated energy balance, the total power consumption to be the lowest. It also allows choosing the best alternative for the consumers as to achieve better system reliability and to launch windows illustrating energy balance for standard regimes. Particular regimes could be created as needed by selecting the consumers. Physical and functional integration of the power system and automation system, optimal allocation and power control for all subsystems are important criteria in optimizing power consumption. The aim was to use methods of analysis and optimization of energy consumption so as to realize the analysis of dynamic behavior of the equipment with the support control and energy management. In order to optimize electricity consumption in correlation with the increased reliability of power systems all equipment and

facilities that are to be implemented on board so as to achieve greater efficiency and reduced environmental impact. The control and management of electricity consumption are integral parts of achieving naval power system monitoring functionality of the system. The efficiency of electricity consumption has been charted. It has also been made a selection of marine equipment focusing on low power consumption, high efficiency and low pollution. The quality of power supply is determined by the following factors: the operational safety of the plant, power quality at the point of separation between the consumer and the supplier, the electromagnetic compatibility of systems with the works.

REFERENCES

1. ***, *Electric Ship Research and Development Consortium.* Available: www.esrdc.com.
2. ***, MathCAD 14 - Software.
3. ***, Microsoft Excel – Software (2008).
4. ***, Microsoft Visual Studio C # - Software (2008).
5. ***, *The Frontrunner - A new era in ship propulsion : The first large size (154K) LNG carrier with electric propulsion is now in operation* - ABB Marine (2007).
6. Badea, Eugene, *Contributions to the optimization of electrical and automation.* Bucharest: Technical University of Civil Engineering (2010).
7. Chalfant, J.S., Chryssostomidis, C., *Analysis of Various All - Electric Ship Electrical Distribution System topologies.* Institute of Electrical and Electronics Engineers, pp. 72 -77 (2011) Available:http://dx.doi.org/10.1109/ESTS.2011.5770844
8. Dan, Florin, *Contributions to identify, optimize and forecast electricity consumption.* Oradea: Oradea University (2011).
9. Doerry, N., *Next Generation Integrated Power System (NGIPS) Technology Development Roadmap.* Washington: - Naval Sea Systems Command, Navy Yard, DC , Ser 05D/349 (2007).

"HENRI COANDA"
AIR FORCE ACADEMY
ROMANIA

"GENERAL M.R. STEFANIK"
ARMED FORCES ACADEMY
SLOVAK REPUBLIC

INTERNATIONAL CONFERENCE of SCIENTIFIC PAPER
AFASES 2014
Brasov, 22-24 May 2014

10. Eremia , M., Cartin G. , et al , *Artificial Intelligence Techniques In Power Systems Management.* Bucharest: AGIR (2006).

11. Hawbaker, Benjamin Forrest, *Analyzing the effects of component reliability on Naval Integrated Power System quality service.* Massachusetts: Institute of Technology, Dept. of Mechanical Engineering, System Design and Management Program (2008). Available: http://hdl.handle.net/1721.1/44844

12. Mamoh, J. A., Zhu, J.Z., Kaddah, S. S., *Optimal load shedding study of naval -ship power system using the Everett optimization technique.* Original Research Article, Electric Power System Research, Volume 60 , Issue 3 , Pages : 142-152, (2002).

13. Mitronikas, E.D., Tatakis, E.C., *Migrating the experience of industrial electrical systems to ships:propulsion motors and foul detection.* "Proceedings of the International Workshop on Electric 1st Marinlive Machines and Power Converters" (2012).

14. Nemțeanu, Florin, *Review ITS & S.* (2010).

15. Rusinaru, D., Mircea, I. Mircea, P.M., *Use of dynamic simulation in the training process in power systems.* Craiova: Universitaria Publishing House (2004).

16. Samoilescu, G., Spiridon, B., *Numerical methods in electrical engineering.* Constanta: "Mircea cel Batran" Naval Academy Publishing House (2011).

17. Sarchiz, Dorin, *Electric System Reliability Optimization.* Publishing MatrixRom (2012).

18. Scutaru, Gheorghe, *Advanced Electric Systems.* Brasov: Transilvania University (2012).

19. Sohrab, A., Mohamad, D., *A Maintenance Optimization Program for Utilities ' Transmission and Distribution Systems.* Lincoln: Department of Electrical Engineering Principal Research Engineer University of Nebraska, Omaha Public Power District.

20. Spyropoulos, Dionysios V., Mitronikas, Epamindas D., *A Review on the Faults of Electric Machines Used in Electric Ships.* Hindawi Publishing Corporation, Advances in Power Electronics, Volume 2013,Article ID 216870, Available:http://dx.doi.org/10.1155/2013/216870

21. Stănciulescu, Florin, *Highly Complex Systems Modeling Applications (Modelling of high complexity systems with applications).* Boston: WIT Press, Southampton (2005).

22. Zhou, W., Habetler, T.G., Harley, R.G., *Bearing condition monitoring methods for electric machines: a general review.* "Proceedings of the IEEE International Symposium on Diagnostics for Electric Machines , Power Electronics and Drives" (SDEMPED ' 07) , pp. 3-6 (2007).

ENGINEERING SCIENCES

"HENRI COANDA"
AIR FORCE ACADEMY
ROMANIA

"GENERAL M.R. STEFANIK"
ARMED FORCES ACADEMY
SLOVAK REPUBLIC

INTERNATIONAL CONFERENCE of SCIENTIFIC PAPER
AFASES 2014
Brasov, 22-24 May 2014

RULES FOR LIMITING RISK EXPOSURE OF THE HUMAN BODY TO ELECTROMAGNETIC FIELDS

Gheorghe SAMOILESCU*, Radu SERGHEI**, Florențiu DELIU*, Laura CIZER*

* Mircea cel Bătrân Naval Academy, Constanța, România, ** Barklav Company, Constanța, România

Abstract: *This paper provides an analysis of the risk exposure of the human body to electromagnetic fields based on the European and American reference exposure levels for the general population, in controlled and uncontrolled environments, which are corroborated with our national documents regarding technical norms for ship equipment and products, stipulated by the international conventions to which Romania has adhered.*

1. INTRODUCTION

In order to interpret the data measured both with and without protective equipment, a comprehensive documentation was carried out based on [1, 2, 3,4, 5, 6, 7, 8, 9, 11, 12, 13, 14].

a) recommendations by Specific Directive 96/98/EC on the "maritime equipment", implemented in Romania by Law no. 582/2003 of the Minister of Public Works, Transport and Housing approving technical type norms regarding marine equipment and products, stipulated by international conventions to which Romania has adhered, MLPLTL.ANR-EM 2003 code;

b) SREN 55011:2001 Romanian standard provisions – industrial radio-frequency, scientific and medical equipment (ISM). Radio and electrical disturbance characteristics. Limits and methods of measurement;

c) SREN 60945:2001 Romanian standard provisions – Navigation equipment and systems, and maritime radiocommunication. General rules. Testing methods and outcomes;

d) comparative analysis of European and American norms regarding limits of human body exposure to the electromagnetic field within in a frequency range from *0 Hz* to *300GHz* ("Radio-Frequency Radiation for Transmitters: A Comparison of U.S. and European Requirements"- paper authors: Steve Dillingham and Nick Cobb);

e) recommendations by 1999/519/EC European document - Council Recommandation on the Limitation of Exposure of the General Public to Electromagnetic Fields (*0 Hz* to *300 GHz*);

f) provisions of FCC American standard: Radio-Frequency Radiation Exposure Limits. Rule Parts 1.1310, 2.1091, and 2.1036 (frequency range from *3 GHz* to *300 GHz*);

g) provisions of "General safety rules" no. 880/06.12.2002, Sections 4 and 5, Annexes 72, 73, 74 and 75;

h) provisions of 50166-1 and 50166-2 SREN standards regarding the permissible limits of induced current density and the biological effects associated, the specific absorption rate – SAR, the permissible limits of the electric field and magnet intensities, of the peak power density in the human body in controlled and uncontrolled environments within the frequency range *3kHz - 300GHz*;

i) Government Decision HG no. 59 of 06.09.2006 on the minimum health and safety requirements regarding the exposure of workers to electromagnetic field hazards - Annex: Exposure limits and activation values for electromagnetic fields;

j) rules for limiting general public exposure to electromagnetic fields ranging from *0 Hz* to *300 GHz*, passed by the Ministry of Public Health and published in the Official Gazette of Romania, Part I, no. 895/03.11.2006;

k) NATO standard: Evaluation and Control of Personnel Exposure To Radio Frequency Fields - *3 kHz* to *300 GHz*, promulgated in February 13th, 2003;

l) ICNIRP recommendations – International Commission On Non – Ionizing Radiation Protection: Guidelines for Limiting Exposure to Time – Varying Electric, Magnetic and Electromagnetic Fields (up to *300 GHz*);

m) recommendations by 2004/40/EC Directive of the European Parliament and the European Council, as of 29 April 2004, with regard to minimum safety requirements for workers' exposure to electromagnetic fields;

n) restrictions regarding "specific norms on labor protection", Volume 6, 1977, ch. NSSM for non-ionizing radiations, DoD, Occupational Safety and Health Inspectorate.

International organizations recommend taking measures to reduce the risk of human body exposure to electromagnetic fields. The standard values regarding the limits of both electric and magnetic fields with a frequency of *50/60 Hz* to which the human body may be exposed are: the electric field (exposure time = *8/24 hrs.*): *10kV/m* - professional areas; *5kV/m* - public domain, the magnetic field (exposure time = *8/24hrs.*): *500μT* - professional areas; *100 μT* – public domain.

At the industrial frequency of *50/60Hz*, the criterion for exposure limits is the induced current density since the well-established effects such as interactions with excitable membranes of nerve and muscle cells depend on this factor [10].

In this respect, the SR EN 50166 1 standard stipulates the following ranges of values of the induced current density and the associated biological effects [8]: under

1mA/m² - lack of effects; between *1-10mA/m²* - minor biological effects; between *10mA/m²* and *100mA/m²* –biological effects that are already known such as: visual (magnetophosphenes) and possible effects on the nervous system; between *100-1000 mA/m²* - changes in the excitability in the central nervous system; stimulation thresholds; possible health risks; over *1000 mA/m²* - potential extrasystoles and ventricular fibrillation, imminent health risks.

In case of permanent exposure to electric and magnetic fields of *50 Hz*, the norm requires limitation of induced current density in the head and trunk to less than *10 mA/m²*.

In defining the standard values for the average current density, the following limits of magnetic induction – B – have been taken into consideration: ranging from *5 mT* – for 12 hours of daily exposure to *150 mT* - for one second of daily exposure; the limits of the electric field strength – *E* – have also been considered: *50 V/m*, for all times of daily exposure.

$$t \le 80/E, \qquad (1)$$

where t (hours/day) is the exposure time limit, and *E (kV/m)* is the electric field strength. Normally the induced current density in the body is a resulting vector expressed by:

$$\overline{J} = \overline{J}_B + \overline{J}_E, \qquad (2)$$

where JB is the density corresponding to the magnetic flux while JE - the one corresponding to the unperturbed electric field. Thus, the basic restriction has to be interpreted as follows:

$$J_B + J_E \le 10mA/m^2. \qquad (3)$$

Normally the summation of the two densities is a vector product, acknowledging this simplification involves a significant safety margin.

Current densities are calculated by the following relations:

$$J_E = k_E \cdot E; \quad k_E = 0,2; \qquad (4)$$

$$J_B = k_B \cdot B; \quad k_B = 2, \qquad (5)$$

considering that the fields through the bodies are homogeneous. [14, 17]

The current density limit for *f = 10 kHz* will be *0.1 A/m²* and it will linearly increase, proportional to frequency as expressed by the relation: *f/100 A/m²*; these values are valid for controlled environments. In uncontrolled environments, a new additional factor of 2.5 is applied, so that the new relation will be *f/250 A/m²*.

For frequencies of the electromagnetic field ranging from a few *MHz* or *GHz*, the Specific Absorption Rate – SAR – is used as a significant size in order to establish the exposure limits of the human body.

An increased risk to health was reported at the threshold value of the SAR ranging between *1* and *4W/ body kg*, depending on the climate area (temperature, humidity), people's health, their clothing, etc.

Establishing the basic derivative limits is done by entering a safety factor of *10* compared to *4W/kg* (the threshold value), so that the whole body will accept an average SAR of *0.4 W/kg* - in controlled environments, and of *0.08 W/kg* – in uncontrolled environments (in uncontrolled environments an additional safety factor of *5* is entered).

The EN 50166-2 Standard stipulates the allowed limits of the electric field strength as well as the ones of the magnetic field in the human body, starting from the basic restrictions *f/100 A/m²* and *f/250 A/m²*.

When exposed to pulses of the electromagnetic fields in the microwave range (over *300 MHz*), the Specific absorption - SA - represents a significant measure, its basic limit is *10 mJ /kg*, in controlled environments, and *2mJ/kg* in uncontrolled environments [15,16].

Table no. 1. Limits of field strength and power density in controlled environments, in case of continuous exposure

Field Frequency (MHz)	Value of Electric Field Strength (V/m)	Value of Magnetic Field Strength (A/m)	Power Density, average value (W/m²)
0.01-0.045	614	35.6	-
0.045-1.000	614	1.6/f	-
1.000-10.000	614/f	1.6/f	-
10,000-400,000	61,4	0.16	10
400-2000	$3.07 \times f^{1/2}$	$8.14 \times 10^{-3} \times f^{1/2}$	f/40
2000-300,000	137	0.364	50

Table no. 2. Limits of field strength and power density in uncontrolled environments, in case of continuous exposure

Field Frequency (MHz)	Value of Electric Field Strength (V/m)	Value of Magnetic Field Strength (A/m)	Power Density, average value (W/m²)
0.01-0.045	275	15,6	-
0.045-1	275	0.7/f	-
1-10	275/f	0.7/f	-
10-400	27.5	0.07	2

Field Frequency (MHz)	Value of Electric Field Strength (V/m)	Value of Magnetic Field Strength (A/m)	Power Density, average value (W/m^2)
400-2000	1.37 x f$^{1/2}$	3.64 x 10^{-3} x f$^{1/2}$	f/200
2000-300,000	61.4	0.163	10

Table no. 3. Limits of field strength and peak power density in controlled environments

Field Frequency (MHz)	Value of Electric Field Strength (V/m)	Value of Magnetic Field Strength (A/m)	Peak Power Density (W/m^2)
0.01-1	20,000 x f^{0,675}	50	-
1-10	20,000/f	50/f	-
10-400	2000	5	10, 000
400-2000	100 x f$^{1/2}$	0.25 x f$^{1/2}$	25 x f
2000-300,000	4500	11.5	50, 000

Table no. 4. Limits of field strength and peak power density in uncontrolled environments

Field Frequency (MHz)	Value of Electric Field Strength (V/m)	Value of Magnetic Field Strength (A/m)	Peak Power Density (W/m^2)
0.01-1	8700 x f^{0,675}	22	-
1-10	8700/f	22/f	-
10-400	900	2.24	2000
400-2000	45 x f$^{1/2}$	0.112 x f$^{1/2}$	5 x f
2000-300,000	2000	5	10.000

In case of simultaneous exposure of the body to multiple independent sources of field of various frequencies, the assessment of actual reference levels was made on the principle of the accumulation of heat effects or electrical stimulation effects on the body.

Table no. 5. A comparison between the European and American reference exposure levels for the general public in controlled and uncontrolled environments

Frequency Range	Magnetic Flux Density (mT)	Current Density (mA/m^2) (rms)	Whole Body Average SAR (W/kg)	Localized SAR (Head and Trunk) (W/kg)	Localized SAR (limbs) (W/kg)	Power Density, S (W/m^2)
0 Hz	40	—	—	—	—	—
0–>1 Hz	—	8	—	—	—	—
1–4 Hz	—	8/f	—	—	—	—
4–1000 Hz	—	2	—	—	—	—
1.0–100 kHz	—	f/500	—	—	—	—
0.1–10 MHz	—	f/500	0.08	2	4	—
0.01–10 GHz	—	—	0.08	2	4	—
10–300 GHz	—	—	—	—	—	10

E-field Strength (V/m)	H-field Strength (A/m)	B-field (µT)	Frequency Range	Equivalent Plane-Wave Power Density S_{eq}(W/m²)
0–1 Hz	—	3.2×10^4	4×10^4	—
1–8 Hz	10,000	$3.2 \times 10^4/f^2$	$4 \times 10^4/f^2$	—
8–25 Hz	10,000	4000/f	5000/f	—
25–800 Hz	250/f	4/f	5/f	—
0.8–3 kHz	250/f	5	6.25	—
3–150 kHz	87	5	6.25	—
0.15–1 MHz	87	0.73/f	0.92/f	—
1–10 MHz	$87/f^{1/2}$	0.73/f	0.92/f	—
10–400 MHz	28	0.073	0.092	2
0.4–2 GHz	$1375\ f^{1/2}$	$0.0037\ f^{1/2}$	$0.0046\ f^{1/2}$	f/200
2–300 GHz	61	0.16	0.20	10

2. COMPARATIVE ANALYSIS OF THE RESULTS OF FIELD MEASUREMENTS, WITH AND WITHOUT PROTECTIVE EQUIPMENT

Following a well-documented research work, our choice for comparison was "The reference levels for occupational exposure to electric and magnetic fields and time varying electromagnetic fields (unperturbed RMS values)" drawn up by ICNIRP - International Commission on Non-Ionizing Radiation Protection, also mentioned in the Romanian Labor Protection Rules no. 880 as well as the NATO - STANAG standard regulations - Evaluation And Control of Personnel Exposure to Radio Frequency Fields - *3 kHz to 300 GHz*.

Table no. 6. Reference levels for occupational exposure to time varying electric and magnetic fields, and electromagnetic fields (unperturbed RMS values)

Frequency Range	E - Electric Field Strength (V/m)	H- Magnetic Field Strength (A/m)	B- Magnetic Flux Density (µT)	Equivalent Plane Wave Power Density - Sech (W/m²)
Up to 1 Hz	-	$1.63 \cdot 10^5$	2×10^5	-
1 – 8 Hz	20,000	$1.63 \cdot 10^5/f^2$		-
8 – 25 Hz	20.000	$2 \times 10^4/f$	$2 \times 10^5/f^2$	-
0.025 – 0.82 kHz	500/f	20/f	25/f	-
0.82 – 65 kHz	610	24,4	30.7	-
0.065 – 1 MHz	610	1.6/f	2.0/f	-
1 – 10 MHz	610/f	1.6/f	2.0/f	-
10 – 400 MHz	61	0.16	0.2	10
400 – 2000 MHz	$3f^{1/2}$	$0.008f^{1/2}$	$0.001f^{1/2}$	f/40
2 – 300 GHz	137	0.36	0.45	50

Table no. 7. Permissible levels of RF field exposure, uncontrolled environments

Frequency Range (MHz)	E - Electric Field (V/m)	H- Magnetic Field (A/m)	Power Density, S (mW/cm^2)	Medium Time, Tmed (min) E^2, S sau H^2	
0.003 – 0.1	614	163	$(10^2; 10^6)$	6	6
0.1 – 1.34	614	16.3/f	$(10^2; 10^4/f^2)$	6	6
1,34 - 3	823,8/f	16.3/f	$(180/f^2; 10^4/f^2)$	$f^2/3$	6
3 - 30	823,8/f	16,3/f	$(180/f^2; 10^4/f^2)$	30	6
30 – 100	27.5	$158.3/f^{1,668}$	$(0.2; 9,4 \times 10^5/f^{3,336})$	30 $0.0636f^{1,337}$	
100 - 300	27.5	0.0729	0,2	30	30
300 - 3000	-	-	f/1500	30	-
3000 – 15,000	-	-	f/1500	90,000/f	
15,000 – 300,000	-	-	10	$616,000/f^{1/2}$	

With reference to the above tables the foolowing remarks are to be pointed out:

1. At a mains frequency of *50/60 Hz*, the reference level of the electric field strength is *10 kV/m* (according to the table) and *0.5 mT* for the magnetic field.;

2. For frequencies (occupational exposure) of up to *100 kHz*, the limit for the electric fields may be exceeded by a factor of 2.

The data resulted from measurements reveal that within the considered frequency ranges (*88-200 MHz* and *200 MHz - 2.2 GHz*) the electric field strengths and radiated power densities do not exceed the basic restrictions for the health protection according to both the European norms and the U.S. standards due to the fact that the power strengths of the radio stations working in the frequency ranges covered by the measurements are of small values. The power standard of stations working in the range of *156-174 MHz* (maritime VHF) is *1W* in ports, and *25 W* outside them.

Thus, the maximum values measured for the electric field strength do not exceed 1 V/m, whereas for the electromagnetic power density they do not exceed *0,02 μW/cm^2*.

The European Standard stipulates levels of: *28-61 V/m* - for the electric field, *0.073 - 0.16 A/m* – for the magnetic field and *2-10W/m^2* – for the power density in the range

of *10-400 MHz*, and respectively a level of *1.375·f$^{1/2}$ - 3·f$^{1/2}$ V/m* - for the electric field, *0.0037·f$^{1/2}$ – 0.08·f^{½} A/m* - for the magnetic field and *f/200 – f/40 W/m^2* - for the power density in the range of *400 - 2000 MHz*. The NATO - STANAG standard regulations stipulate levels of: *27.5-61.4 V/m* - for the electric field, *0.0729-0.163 A/m* - for the magnetic field and *2-10W/m^2* - for the power density in the range of *100 - 300 MHz*, and respectively a level of *f/1500 – f/300 mW/cm^2*, or *f/150 – f/30 W/m^2* for the power density in the range of *300 - 3000 MHz* .

3. CONCLUSIONS

Due to the lack of measurement sensors in the analyzer used in frequency ranges below *80 MHz* and above *2 GHz*, no measurements were taken for the frequency ranges with powerful signal sources (radio and radar) onboard the ship, which are the main risk factors for the onboard personnel. For certain radio stations in the range of *4-30 MHz* (marine HF) the power strength ranges between *400-750 W*, while for other stations, strengths of up to *1.5 kW* are used. For some radar stations, the *9 GHz*- range transmission strengths are *15* and *25 kW*.

Due to the fact that both the constitutive parameters of the propagation medium (ε, μ)

and the air wave impedance (Z_0)are practically constant, in the absence of suitable sensors the measured values can be linearly extrapolated to other frequency ranges in order to see the exact values that can be reached by the field strengths and power density. Thus, by extrapolating the electric field strength radiated by the radio station at the power of *100 W* (*0.2509 V m* - value measured on the bridge), at *25 kW* (the value of the transmission strength power), a value of the radiated electric field strength of *62 725 V / m* is obtained. This value is particularly dangerous for the human factor onboard the ship and exceeds by far the permissible levels for the human body, according to both European and American standards.

The standard values of the electric field strength allowed are *27 V/m* in the frequency range of *100-300 MHz*.

Since all regulations in force stipulate the limitation of emission power in VHF range to 1 W when in port, the power densities measured on deck have small values. In order to obtain conclusive values of the radiated power density, onboard measurements are required in all frequency ranges of stations outside the port as well, while sailing in formation.

REFERENCES

1. Directiva Specifică 96/98/EC, referitoare la „Echipamentul maritim", obligatorie de la 1 ianuarie 1999, transpusă în România prin Ordinul ministrului lucrărilor publice, transporturilor şi locuinţei nr. 582/2003, pentru aprobarea normelor tehnice de tip a echipamentelor şi produselor pentru nave maritime, prevăzute de convenţiile internaţionale la care România este parte, cod MLPLTL.ANR-EM 2003;
2. Standardul românesc SREN 55011:2001 – Echipamente de radiofrecvenţă industriale, ştiinţifice şi medicale (ISM). Caracteristici de perturbaţii radioelectrice. Limite şi metode de măsurare;
3. Standardul românesc SREN 60945:2001 – Echipamente şi sisteme de navigaţie şi radiocomunicaţii maritime. Reguli generale. Metode de încercare şi rezultate impuse;
4. Analiza comparativă a normelor europene şi americane cu privire la limitele de expunere la câmp electromagnetic a organismului uman în gama de frecvenţa O Hz la 300 GHz, lucrarea „Radio-Freqnency Radiation for Transmitters: A Comparison of U.S. and European Requirements", autori: Steve Dillingham şi Nick Cobb);
5. Documentul european 1999/519/EC – Council Recommandation, of 12 Iuly 1999, on the Limitation of Exposure of the General Public to Electromagnetic Fields (OHz to 300 GHz);
6. Standardul american FCC Radio-Frequency Radiation Exposure Limits. Rule Parts 1.1310, 2.1091, and 2.1036 (gama de frecvenţă 3 GHz – 300 GHz);
7. Normele generale de protecţia muncii nr. 880/06.12.2002, Secţiunile 4 şi 5, Anexele nr. 72, 73, 74 şi 75;
8. Standardele româneşti SREN 50166-1 şi SREN 50166-2, referitoare la limitele admise ale densităţii curentului indus şi efectele biologice asociate, limitele ratei specifice de absorbţie – SAR, limitele admise ale intensităţii câmpului electric ale celui magnetic şi ale densităţii de putere de vârf în corpul omenesc, pentru medii controlate şi necontrolate, în gama de frecvenţă 3kHz - 300GHz;
9. Hotărârea Guvernului României, HG nr. 59, din 06.09.2006, privind cerinţele minime de securitate şi sănătate referitoare la expunerea lucrătorilor la riscuri generate de câmpurile electromagnetice – Anexă: Valori limită de expunere şi valori de declanşare a acţiunii pentru câmpurile electromagnetice;
10. Normele privind limitarea expunerii populaţiei generale la câmpuri electromagnetice de la 0Hz la 300GHz, elaborate de Ministerul Sănătăţii Publice şi publicate în Monitorul Oficial al României, Partea I, Nr. 895/03.11.2006;
11. Standardul NATO: Evaluation and Control of Personnel Exposure To Radio Frequency Fields – 3 KHz to 300 GHz, promulgat la 13 febr.2003;

12. Recomandările ICNIRP – International Commission On Non – Ionizing Radiation Protection: Guidelines for Limiting Exposure to Time – Varying Electric, Magnetic and Electromagnetic Fields (up to 300 GHz);

13. Directiva 2004/40/EC a Parlamentului European şi a Consiliului European, din 29 aprilie 2004, privind cerinţele minime de siguranţă a lucrătorilor la expunerea în câmpuri electromagnetice;

14. Radu, S., *Introducere în Compatibilitate Electromagnetică*, vol.I, *Ecranarea aparaturii electronice*, Editura Gheorghe Asachi, Iaşi, 1995

15. Hortopan, G., *Principii şi tehnici de COMPATIBILITATE ELECTROMAGNETICĂ*, Editura Tehnică, Bucureşti, 1998

16. Ignea, A., *Măsurări şi teste în Compatibilitatea Electromagnetică*, Editura Waldpress, Timişoara, 1996

17. Schwab, J.A., *Compatibilitatea Electromagnetică*, Editura Tehnică, Bucureşti, 1996

18. Sotir, A., Moşoiu, T., *Compatibilitate Electromagnetică*, Editura Militară, Bucureşti, 1997

ABOUT SINGLE-PHASE VOLTAGE RECTIFIERS OPERATION

Constantin STRIMBU*

*Faculty of Aeronautic Management, "Henri Coanda" Air Force Academy, Brasov, Romania

Abstract: *Some issues regarding the analysis of single-phase voltage rectifier operation will be presented in this paper. The switch is an uncontrolled-type, a diode in this case, which is considered as an ideal one. The expressions of the parameters characterizing the rectifier operation are computed in the paper. Their variations depending on load are also discussed.*

Keywords: *rectifier, diode, single-phase*

1. INTRODUCTION

The schematic of an angle-phase voltage rectifier is presented in figure 1.
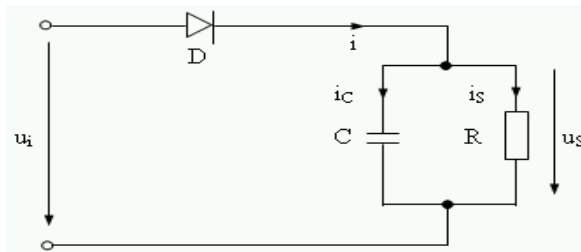
Fig.1. Single-phase voltage rectifier with diode

The steady-state signals expressions are the following [1]:

The diode is "on": $\omega t \in \left(\alpha_p, \beta \right)$

$$\begin{cases} i_S = \dfrac{U_M}{R}\sin\omega t = I_M \sin\omega t \\ i_C = \omega C\, U_M \cos\omega t \\ i = U_M \sqrt{\dfrac{1}{R^2} + (\omega C)^2}\ \sin(\omega t + \xi) = \\ = I_m \sin(\omega t + \xi) \end{cases} \quad (1)$$

The diode is "off": $\omega t \in \left(\beta, \ 2\pi + \alpha_p \right)$

$$\begin{cases} i_S = -i_C = I_{S\beta}\ e^{-(\omega t - \beta)\mathrm{ctg}\,\xi} \\ u_S = R\,i_S = U_M \sin\xi\ e^{-(\omega t - \beta)\mathrm{ctg}\,\xi} \end{cases} \quad (2)$$

where:

$$\begin{cases} \beta = \pi - \xi \\ I_{S\beta} = \dfrac{U_M}{R}\sin\beta = I_M \sin\xi \\ \sin\alpha_p = \sin\xi\, e^{-(\pi + \alpha_p + \xi)\mathrm{ctg}\,\xi} \end{cases} \quad (3)$$

The following notations were used:

$$\mathrm{tg}\,\xi = \omega RC$$
$$Z = \dfrac{R}{\sqrt{1 + (\omega RC)^2}}$$
$$I_M = \dfrac{U_M}{R}$$
$$I_m = \dfrac{U_M}{Z} = \dfrac{I_M}{\cos\xi}$$

(4)

2. CIRCUIT ANALISIS

2.1 The Voltages and Currents Average Values

According to [2], the expressions of the average values of the circuit signals are the following:

$(U_m)_{\alpha_p}$ - average value of the output voltage:

$$(U_m)_{\alpha_p} = \frac{U_M}{2\pi}\left[\cos\alpha_p + \frac{1}{\cos\xi}*\right.$$
$$\left.*\left[1-\sin^2\xi\, e^{-(\alpha_p+\pi+\xi)ctg\xi}\right]\right] \qquad (5)$$

$(U_{def})_{\alpha_p}$ - RMS value of the output voltage:

$$(U_{def})_{\alpha_p} = \frac{U_M}{\sqrt{2\pi}}*$$
$$*\sqrt{\pi-\xi-\alpha_p+\sin(\alpha_p+\xi)\cos(\alpha_p-\xi)+A} \qquad (6)$$

where

$$A = \frac{\sin^3\xi}{\cos\xi}\left[1-e^{-2(\alpha+\pi+\xi)ctg\xi}\right]$$

$(I)_{\alpha_p}$ - average value of the current flowing through the diode:

$$(I)_{\alpha_p} = \frac{1}{2\pi}\frac{U_M}{R}\left[\cos(\alpha_p+\xi)+1\right] \qquad (7)$$

$(I_S)_{\alpha_p}$ - average value of the load (R) current:

$$(I_S)_{\alpha_p} = \frac{I_M}{2\pi}\left[\cos\alpha_p + \frac{1}{\cos\xi}*\right.$$
$$\left.*\left[1-\sin^2\xi\, e^{-(\alpha_p+\pi+\xi)ctg\xi}\right]\right] \qquad (8)$$

Limit cases:

For pure resistive load, $\omega RC = 0, \xi = 0$ it results:

$$\alpha_p = 0^0, \quad \beta = 90^0 \qquad (9)$$

$$(U_m)_{\alpha_p} = \frac{U_M}{\pi}$$

$$(U_{def})_{\alpha_p} = \frac{U_M}{2}$$

$$(I)_{\alpha_p} = \frac{1}{\pi}\frac{U_M}{R} = \frac{I_M}{\pi} \qquad (10)$$

$$(I_S)_{\alpha_p} = \frac{I_M}{\pi}$$

For pure capacitive load, $\omega RC = \infty, \xi = \frac{\pi}{2}$ it results:

$$\alpha_p \approx 90^0, \beta \approx 180^0 \qquad (11)$$

$$(U_m)_{\alpha_p} = U_M$$

$$(U_{def})_{\alpha_p} = U_M$$

$$(I)_{\alpha_p} = 0 \qquad (12)$$

$$(I_S)_{\alpha_p} = 0$$

2.2 Rectifier Parameters

According to [2], the following parameters are defined:

The periodicity factor:

$$k_m = \frac{(U_m)_{\alpha_p}}{U_M} = \frac{1}{2\pi}\left[\cos\alpha_p + \frac{1}{\cos\xi}*\right.$$
$$\left.*\left[1-\sin^2\xi\, e^{-(\alpha_p+\pi+\xi)ctg\xi}\right]\right] \qquad (13)$$

The k_e factor:

$$k_e = \frac{(U_{def})_{\alpha_p}}{U_M} = \frac{1}{\sqrt{2\pi}}*$$
$$\sqrt{\pi-\xi-\alpha_p+\sin(\alpha_p+\xi)\cos(\alpha_p-\xi)+A} \qquad (14)$$

unde

$$A = \frac{\sin^3\xi}{\cos\xi}\left[1-e^{-2(\alpha+\pi+\xi)ctg\xi}\right]$$

The shape factor:

$$k_f = \frac{k_e}{k_m} \qquad (15)$$

The wave factor:

$$k_u = \sqrt{k_f^2 - 1} \qquad (16)$$

The graphic representations of the four parameters variation as functions of load

"HENRI COANDA"
AIR FORCE ACADEMY
ROMANIA

"GENERAL M.R. STEFANIK"
ARMED FORCES ACADEMY
SLOVAK REPUBLIC

INTERNATIONAL CONFERENCE of SCIENTIFIC PAPER
AFASES 2014
Brasov, 22-24 May 2014

$\xi = \operatorname{arctg}(\omega RC)$ are shown in the figures below.

The graphing was performed by using Mathcad.

The periodicity factor, k_m
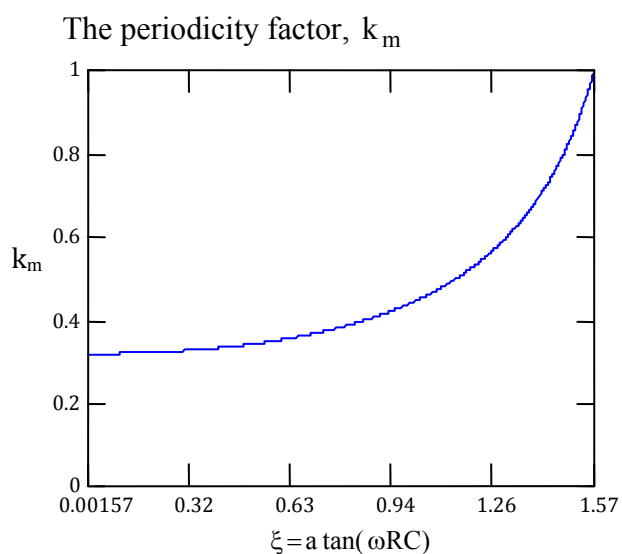
Fig.2 k_m factor variation as function of load, $\xi = \operatorname{arctg}(\omega RC)$
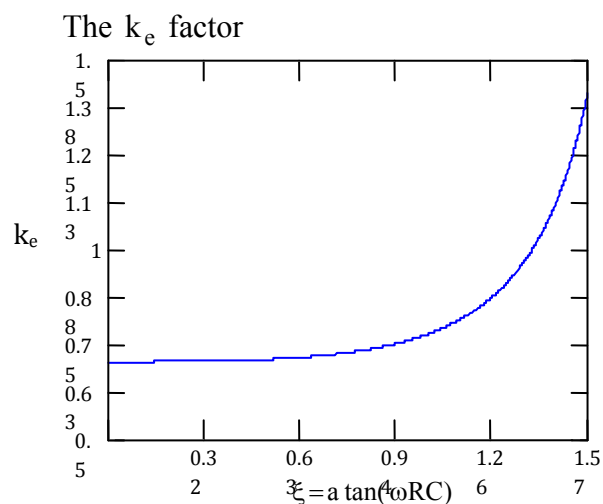
The k_e factor

Fig.3. k_e factor variation as function of load, $\xi = \operatorname{arctg}(\omega RC)$

The shape factor, k_f
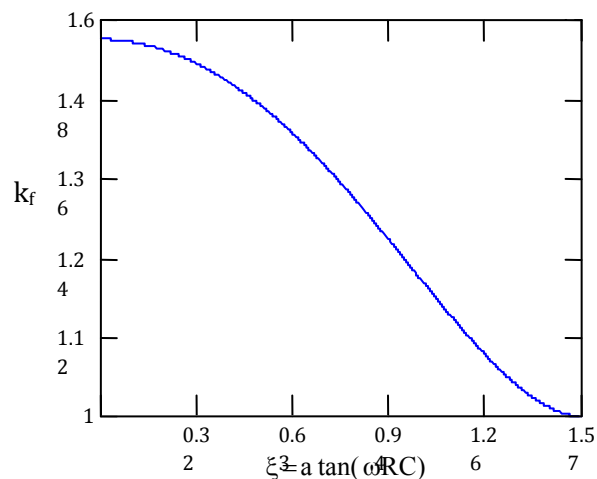
Fig.4 k_f factor variation as function of load, $\xi = \operatorname{arctg}(\omega RC)$

The wave factor, k_u
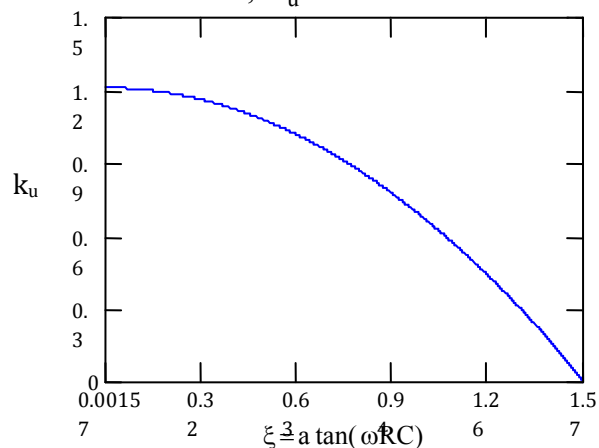
Fig.5 k_u factor variation as function of load, $\xi = \operatorname{arctg}(\omega RC)$

Considering the limit cases, the following values of the rectifier parameters are computed:

For the pure resistive load,

$\omega RC = 0$,

$\alpha_p = 0^0$

it results:

$$k_m = 0.318 = \frac{1}{\pi}$$

$$k_e = 0.707 = \frac{1}{\sqrt{2}} \tag{17}$$

$$k_f = 1.571$$

$$k_u = 1.21$$

For pure capacitive load,

$\omega RC = \infty$,

$\alpha_p \approx 90^0$,

it results:

$$k_m = 1$$

$$k_e = \sqrt{2} \tag{18}$$

$$k_f = 1$$

$$k_u \to \infty$$

3. CONCLUSIONS & ACKNOWLEDGMENT

The following conclusions are deriving from the study of the half-wave voltage rectifiers equipped with uncontrolled electrical valves:

The diode turn-on angle α_p has an increasing variation of load (R);

The diode turn-off angle β has an decreasing variation of load (R);

The periodicity factor k_m is an increasing function of load (R);

The k_e factor is an increasing function of load (R) too;

The shape factor k_f is a decreasing function of load (R);

The wave factor k_u is also a decreasing function of load (R).

REFERENCES

1. Cerbulescu, D. *Convertoare statice de putere: Redresoare* Craiova: Editura Scrisul Românesc (1995).
2. Matlac, I. *Convertoare electroenergetice* Timişoara: Editura Facla (1987).

SOME ASPECTS ABOUT AIRCRAFT STRUCTURES RELIABILITY

Daniel BOSNICEANU*, Marian VATAVU*

* PhD students, Faculty of Mechatronics and Integrated Armament Systems,
Military Technical Academy, Bucharest, Romania

Abstract: Based on the main factors which alter the durability of a structure (the loading range, the mechanical features of the materials, the environmental and technological factors, etc.) the present paper presents a way for assessing the aircraft structure durability. In this respect, there has been endorsed the linear cumulative damage criterion Palmgren-Miner results, used in the assessment of average damage level attained by the end of operating period.

Keywords: fatigue life, durability, failure, reliability

1. INTRODUCTION

Take into consideration the main factors which dete rmine the servic e lif etime of an item or an aircraft structure (the loading range, she m echanical featu res of the m aterials, th e environmental and technological factors etc). There has b een estim ated the structural life - based on a sam ple group of representative structures o f a sam e ki nd - accord ing to the romanian current standards.

There has also been considered the influence of fatigue phenom ena (reiterated loads) upon the structures regarded.

Prediction of the fatigue performance is a simple process but one beset by several complexities. Load m agnitude and sequenc e are very important features of the process.

The need to increase by 3-4 tim es the landing ge ars durab ility to the f act tha t th e problem of choosing th e m aterial brand, the designing solution and the adm issible stresse s is solved by reasons of fatigue strength and not static strength, as well using fracture mechanics principles.

2. THEORETICAL BACKGROUND

Although m any techniques have been devised to satisfy sp ecific cond itions, th e simplest and the m ost practical technique is Palmgrcn-Miner.

This method merely proposes that the fraction of fatigue life used up in se rvice is the ratio of the applied numbe r of load cycles at a given level divided by the allowable num ber of load cycles to failure at the s ame variable stress lev el. If severa l levels of variable stresses arc applied to a detail, then the sum of the respective cycle ratios is th e f raction of fatigue life used up.

When the cycle ratio sum equals unity a ll of the potential service life has been used. It is important to notice tha t there is ju st so m uch potential fatigue life available for operational utilization.

The landing gear's load range can be expressed through working cycles ground-air-ground (GAG) because within the landing

gear is used up the   biggest part of the structure's durability.

The durability fraction used up through iterated loads (fatigue) by one GAG cycle is called wear cycle (relative damage) (1).

$$N = \frac{1}{D_t}$$

(1)

N - Total number of landings

D_t -damage produced by iterated loads during one GAG cycle: $D_t \in (0,11]$.

For instance, a relative damage of $D_t = 0.5$ means that the land   ing gear sho   uld face a double number of GAG cycles, thus for a resource of 3000 landings, the structure should resist up to 6000 GAG cycles.

$$D = PREDICTED\_LIFE = \sum (\frac{n_1}{N_1} + \frac{n_2}{N_2} + ... + \frac{n_K}{N_K}) = 1.0$$

(2)

where:

n_K - num ber of loading cycles at the Kth stress level;

N_K - number of loading cycles to failure for the Kth stress level based on constant amplitude $\sigma - N$ for the app   licable m aterial and stress concentration factor.

K - number of stress levels considered.

Fatigue crack initiation is assumed to occur when the predicted life is equal to 1.0 (2). There are three parameters   which alter th   e magnitude of the summ   ation of the cycle ratios:

1.First, there is th   e effect cau   sed by the order of load applic   ations. Consider, for example, two different stress levels, f $_1$ and f $_2$ and their cyclic lives. N_2 and N_2. respectively. If f_1 is greater than f $_2$ and if it is app lied first, the life will be shorter than if f_2 is applied first.

2.The second effect on summ ation of cycle ratios is due to the am   ount of da mage caused by continuous loading at th e sam e leve l. Th e summation of cycle ratios   for di fferent st ress levels is a   ccurate on ly if the n umber of continuous cycles at each stress level is small.

For the most aircraft structures, the loading is random and the stress   level is constantly changing.

3.The third param eter which af fects the summation of the cycle ratios is whether the fatigued part is notched or not.

The fatigue strength evaluation m ust show by analysis and/or testing that the structure can withstand the typica   l load ing spec   trum expected in service.

With respect to   f atigue lif e ve rification testing of safe-life structures, the aviation regulation (FAR) adheres to the use of the following scatter factors:

Table 1

Number of test specimens	Scatter factor
1	3.00
2	2.58
3	2.43
4	2.36

This m eans that the test shou   ld verif y the safe-life times the factor without failure, or, if, failure occurs earlier the safe-life is designated as test life divided by the scatter factor.

The above short review of the theoretical notions and of the nowad ays settlements in the field of aircraft structures durability has used, for the accomplishment of the testing program, a chosen structure of th e landing gear m ade of D.16 AT aluminium alloy.

The stress (daN/mm^2) spe ctrum to be applied locally to the part consists of 5 loading sequences arranged as shown in table 2.

Table 2

Mean stress (1)	Varying Stress (2)	Number of Cycles (n) (3)	Max. Stress (4)=(1)+(2)	Min. Stress (5)=(1)-(2)
13.0	8.7	70	21.7	4.3
	12.0	10	25.0	1.0
	13.3	150	26.3	-0.3
	14.1	30	27.1	-1.1
14.5	6.1	50	20.6	7.4
	12.9	140	27.4	1.6
	18.0	150	32.5	-3.5
	18.8	40	32.8	-4.3
7.5	17.5	70	25.0	-10.0
	18.5	60	26.0	-11.0
	20.1	40	27.6	-12.6
	20.8	40	28.3	-13.3
19.0	12.0	150	31.0	7.0
	12.8	70	31.8	6.2
10.0	14.6	180	24.6	-4.6
	15.3	120	25.3	-5.3
	15.9	50	25.9	-5.9
	16.7	30	26.7	-6.7
Total : 1450 cycles				

“HENRI COANDA”
AIR FORCE ACADEMY
ROMANIA

“GENERAL M.R. STEFANIK”
ARMED FORCES ACADEMY
SLOVAK REPUBLIC

INTERNATIONAL CONFERENCE of SCIENTIFIC PAPER
AFASES 2014
Brasov, 22-24 May 2014

3. EXPERIMENTAL RESULTS AND CONCLUSIONS

For the tested structure, after 1000 cycles (landings) there has been determined cumulative damage of D = 0.05751.
   The calculated life.

$$N_C = \frac{1000}{0.05751} = 17388 cycles \tag{3}$$

The best estimate of predicted fatigue life:

$$N_{cb} = \frac{17388}{3.0} = 5796 cycles \tag{4}$$

The bottom line is that by adopting the Palmgren-Mincr cumulative damage criterion, corrected with the s tresses interaction factor, there can b e es timated the averag e dam age level reached at the en d of the operational period and also, can be established technological m eans for designing and repair in orde r to incr ease the durab ility of the analyzed structures.

REFERENCES

1. Cioclov. D., *Rezistenta si fiabilitatea la solicitari variabile*. T imisoara: Ed. Facia (1975).
2. Draghici. I.. *Indrumar de proiectare in constuctia de masini.* Bucuresti: Ed. Tehnica (1982).
3. Iordache. M., *Aspects concerning the durability of aircraft structures with regard to the landing gear.* Conferinta Nationala OPROTEH-95, Bacau (1995).
4. Kumar, R., Dash, P.K., *Design and analyses of main landing gear structure of a transport aircraft and fatique life estimation for the critical LUG,* International Journal of Mechanical and Producti on Engineering (Oct. 2013)
5. Niu C.Y. *Airframe Structural Design.* Technical Book Company, Los Angeles (1988).

ENGINEERING SCIENCES

COMPUTER SIMULATION BASED COMPARATIVE STUDY ON THE SOLIDIFICATION OF A CAST IRON AND STEEL CASTING

Aurel CRIŞAN*, Ioan CIOBANU*, Daniela IONESCU*, Maria STOICĂNESCU*

*Transilvania University of Braşov, Romania

Abstract: The authors conducted a comparative study on the solidification of a part cast from three different alloys. The study was achieved by computer simulation and concerned the solidification of a stepped casting. The analysed cases were of castings from 0.1% C steel, 0.5%C steel and eutectic spheroidal graphite cast iron, respectively. The alloys differ by their casting temperature and their solidification temperature interval. Analysis included the influence of the alloy type on macrosolidification parameters like solidification time, hot spot position, temperature distribution in the casting at the end of solidification, map of the solidus front displacement, extent of the two-phase area (solidus + liquidus) in the casting, aspect of the cooling curves, etc.

Keywords: alloys, steel, solidification

1. INTRODUCTION

A comparative study was carried out on the solidification of stepped parts cast from two steels of different chemical compositions, and from eutectic grey cast iron. In the three studied cases both the casting temperature of the liquid alloy and the solidification time interval differ.

2. AIM OF THE PAPER AND WORKING METHOD

The solidification of the casting (test piece) from eutectic cast iron was simulated at equilibrium (constant temperature solidification without reproducing the undercooling and the recalescence occurring during solidification). The aim was to reveal the extent to which the solidification interval influences the solidification parameters of a casting (solidification time, hot spot position, etc.). Figure 1

shows the part studied by simulation. Figure 2 shows the studied casting – mould subassembly. The mould is made from sand hardened with sodium silicate and CO_2. Solidification was simulated for parts cast from the following alloys:

- carbon steel with 0.1%C;
- carbon steel with 0.53%C;
- eutectic spheroidal graphite cast iron with 4.2 % CE (equivalent carbon).
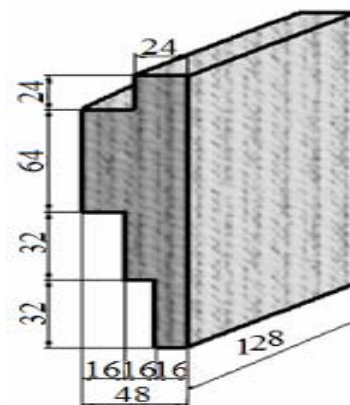
Figure 1 Casting
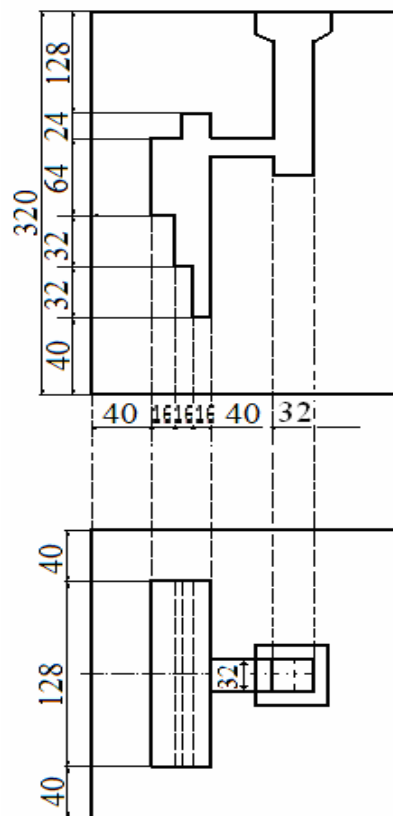
Figure 2 Casting – mould assembly used in simulation.

for the mould sand: density ρ_{FO}=1550Kg/m^3, specific heat c_{FO}=1050J/KgK; λ_{FO}=0.65W/mK.

3. RESULTS

The influence of the solidification interval (T_L-T_S) on the following solidification parameters was analysed:

- the total solidification time (related to the initial moment, tsol);

- the total actual duration of the solidification of the hot spot (the time elapsed between the beginning and the end of solidification: t_{ES}= tsol – tstart sol);

- the position (coordinates) of the ending point of solidification (x_{NOD}; y_{NOD}, z_{NOD});

- the distribution of the isotherms in the casting at the end of solidification;

- the map of the solidus front displacement;

- the extent of the two-phase area (solidus + liquidus) at a given time, in the case of steels;

- the aspect of the cooling curves (temperature variation) in the hot spot;

- the variation in time of the solidus fraction (kinetics of solidification) in the hot spot;

- the evolution of the instantaneous cooling rate in the hot spot versus time;

- the distribution of temperature along a line/row and a column, respectively in the casting-mould assembly at a given time.

Table 2 and figures 3 to 10 feature the obtained results.

In all cases simulation maintained the same overheating of the liquid alloy in relation to the liquidus temperature. The overheating related to T_L was ΔT= T_{0ME} - T_L – 155^{0}C.

Table 1 shows the values for the thermo-physical characteristics of the alloys considered in simulation. The following values were used

Table 1 Values of the thermo-physical quantities used in simulation

No.	Type of alloy	Solidus temperature	Liquidus temperature	Initial temperature	Overheating of the alloy in relation to T_L	Overheating of the alloy in relation to T_S
Symbol	-	T_S	T_L	T_{0ME}	ΔT	ΔT
u.m.	-	^{0}C	^{0}C	^{0}C	^{0}C	^{0}C
1	0.1%C steel	1495	1530	1685	155	190
2	0.53%C steel	1430	1495	1650	155	220
3	Eutectic spheroidal graphite cast iron	1150	1150	1305	155	155

"HENRI COANDA"
AIR FORCE ACADEMY
ROMANIA

"GENERAL M.R. STEFANIK"
ARMED FORCES ACADEMY
SLOVAK REPUBLIC

INTERNATIONAL CONFERENCE of SCIENTIFIC PAPER
AFASES 2014
Brasov, 22-24 May 2014

No.	Liquid alloy density	Specific heat in solid state	Specific heat in liquid state	Thermal conductibility in solid state	Thermal conductibility in liquid state	Latent solidification heat
Symbol	ρ	C_S	C_L	λ_S	λ_L	L
u.m.	Kg/m^3	J/kg/K	J/kg/K	W/m/K	W/m/K	J/Kg
1	7200	750	850	30	28	270000
2	7200	750	850	29	27	270000
3	6800	750	850	35	30	250000

Table 2 Results on the influence of the solidification interval on the parameters of solidification

No.	Type of alloy	Start time of solidification	End time of solidification	Actual solidification time of hot spot	Coordinates of the hot spot
Symbol	-	$T_{START\ SOL}$	T_{SOL}	$t_{EF\ SOL}$	x_{NOD}; y_{NOD}; z_{NOD}
u.m.	-	s	s	s	mm
1	0.1%C steel	166.5	589.5	423.0	68,132,104
2	0.53%C steel	166.5	684.0	517.5	60;132,104
4	Eutectic spheroidal graphite cast iron	573.0	718.75	145.75	68,132,104
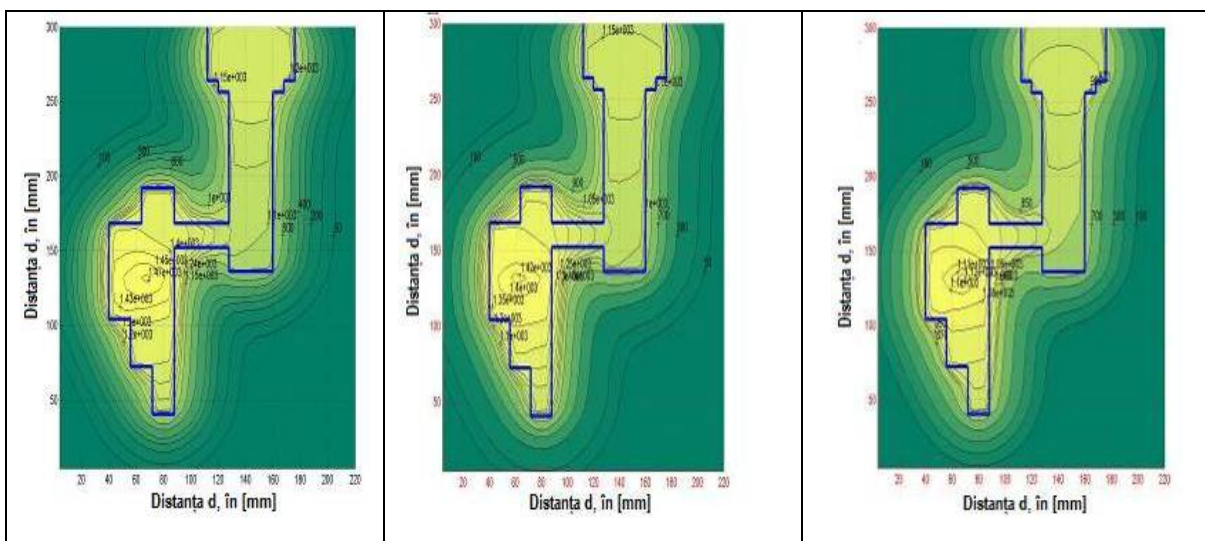
a.) 0.1%C steel   b.) 0.53%C steel   c.) Eutectic spheroidal graphite cast iron

Figure 3 Isotherms at the end of hot spot solidification

| a.) 0.1 %C steel | b.) 0.53 %C steel | c.) Eutectic spheroidal graphite cast iron |
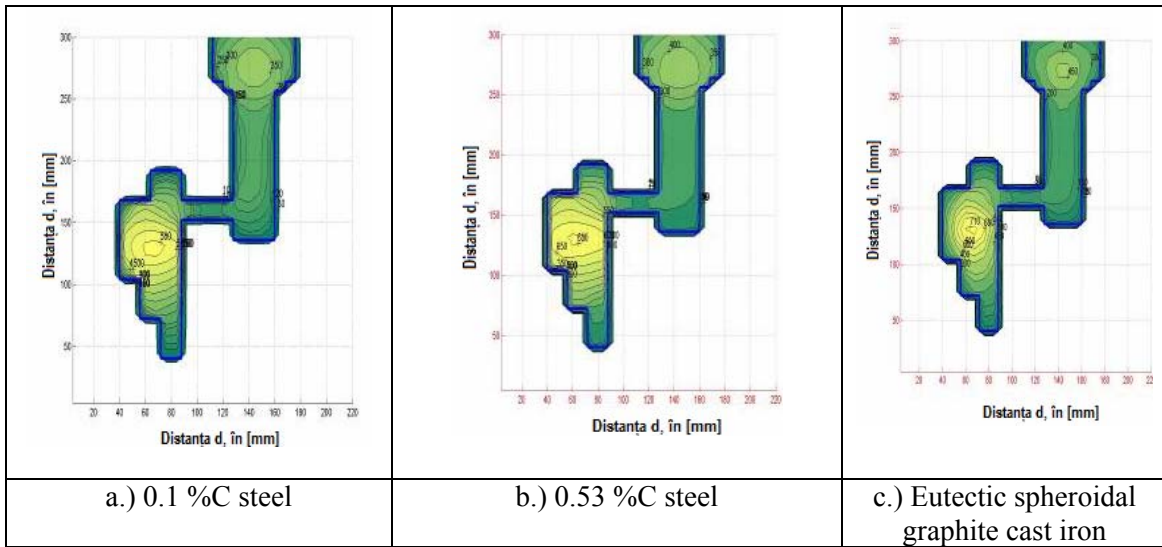
Figure 4 Map of the displacement of the solidification front

a.) 0.1%C steel   b.) 0.53%C steel   c.) Eutectic spheroidal graphite cast iron
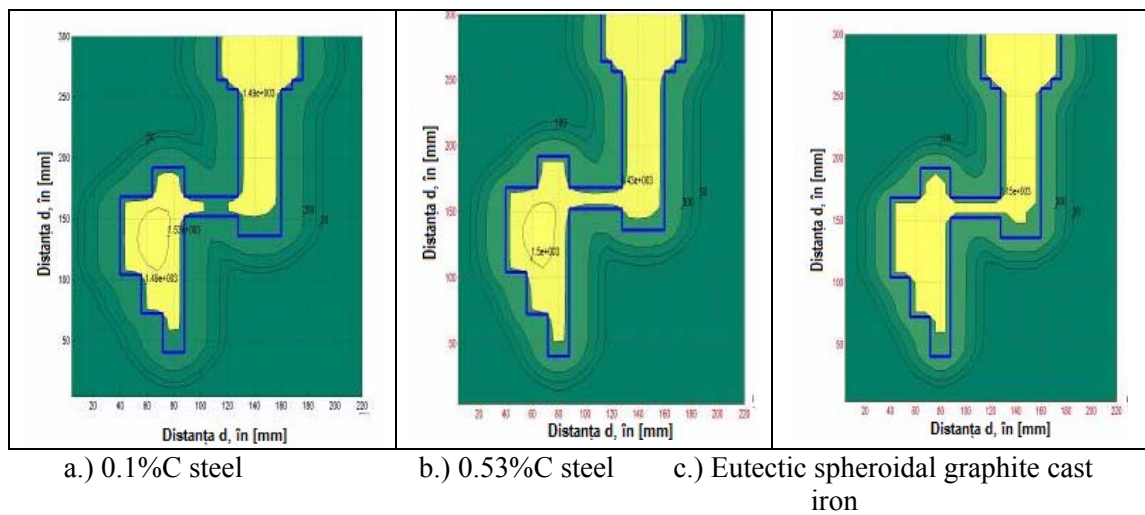
Figure 5 Distribution of the two-phase area (solidus + liquidus) at time t = 150s

| a.) 0.1%C steel | b.) 0.53%C steel | c.) Eutectic cast iron |
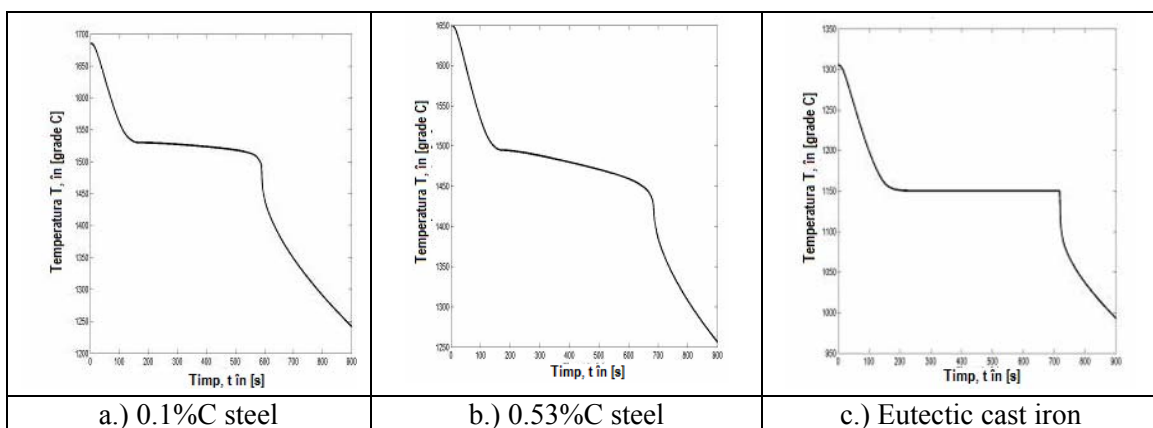
Figure 6 Variation of temperature in the hot spot

"HENRI COANDA"
AIR FORCE ACADEMY
ROMANIA

"GENERAL M.R. STEFANIK"
ARMED FORCES ACADEMY
SLOVAK REPUBLIC

INTERNATIONAL CONFERENCE of SCIENTIFIC PAPER
AFASES 2014
Brasov, 22-24 May 2014

a.) 0.1%C steel	b.) 0.53%C steel	c.) Eutectic cast iron
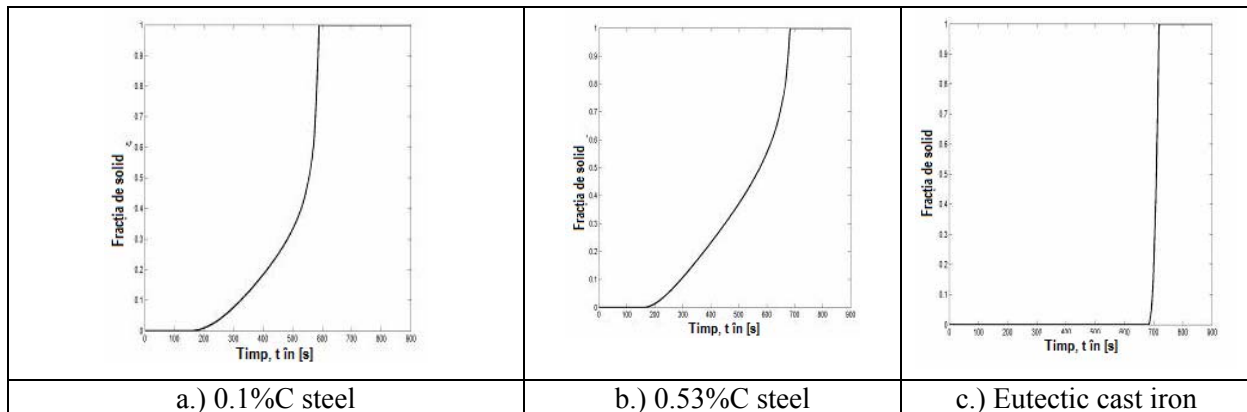
Figure 7 Variation of the solidus fraction in the hot spot

a.) 0.1%C steel	b.) 0.53%C steel	c.) Eutectic cast iron
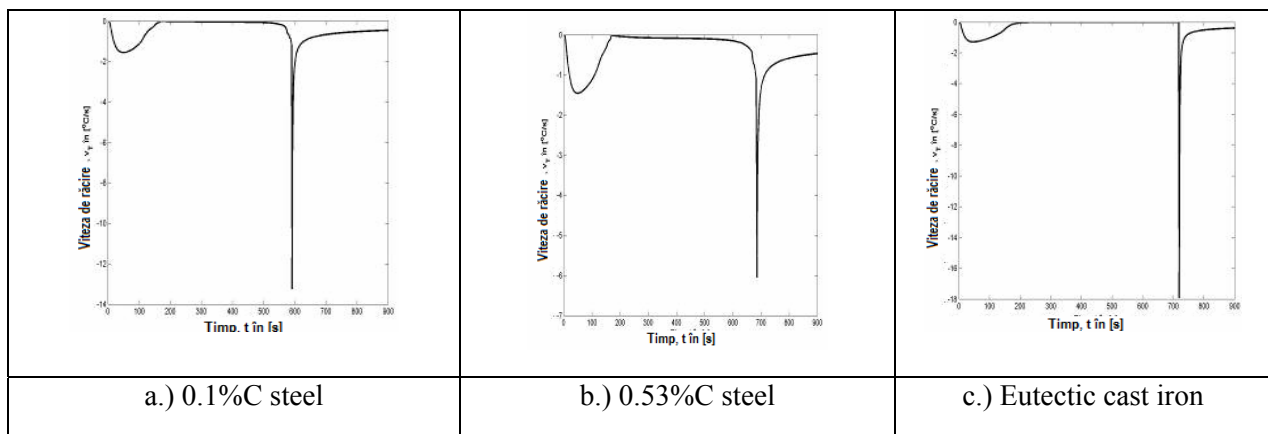
Figure 8 Cooling rate in the hot spot

a.) 0.1%C steel	b.) 0.53%C steel	c.) Eutectic cast iron
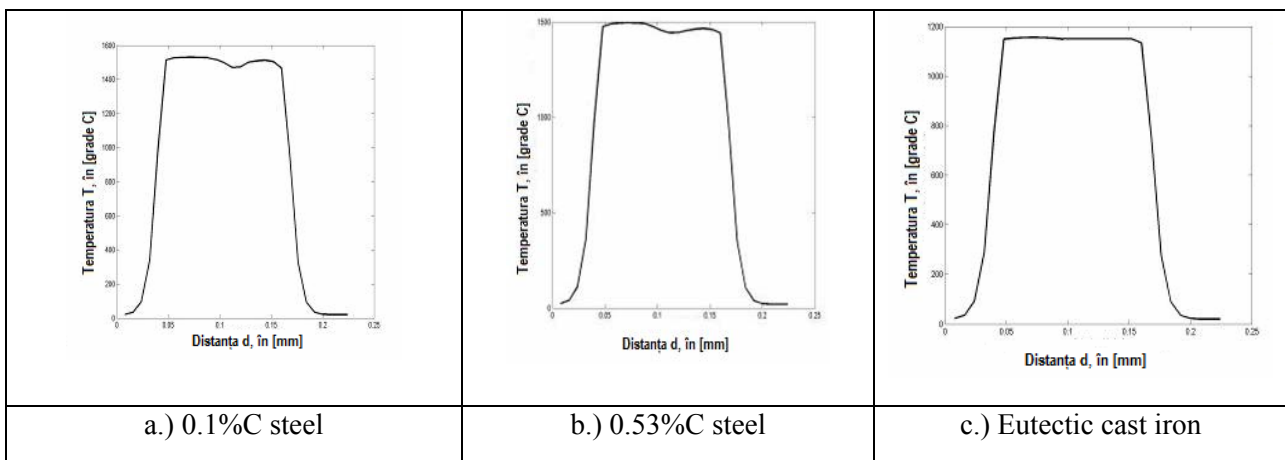
Figure 9 Distribution of temperature along line L= 19 at time t = 150s

| a.) 0.1%C steel | b.) 0.53%C steel | c.) Eutectic cast iron |
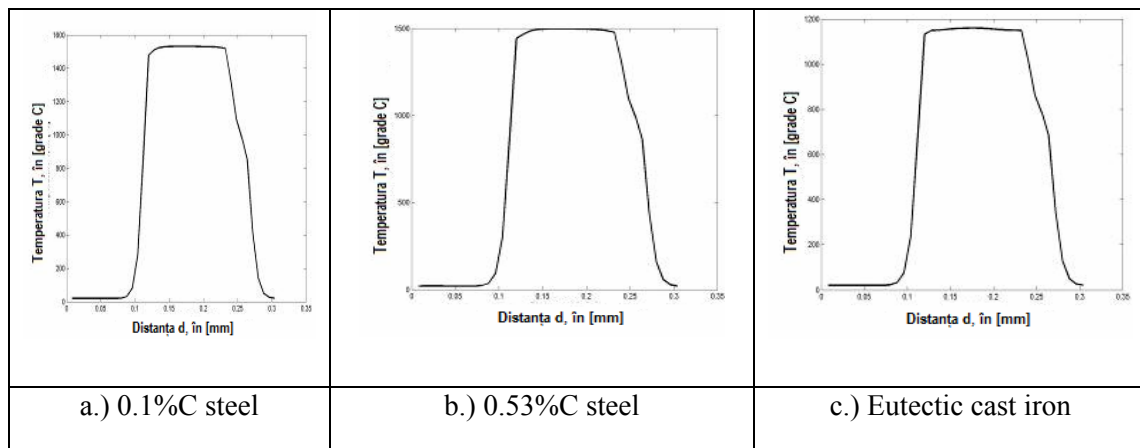
Figure 10 Distribution of temperature along column C=9 at time t=1500s

4. CONCLUSIONS

The results presented in table 2 and in figures 6 to 10 yield the following conclusions:

- the position of the hot spot is identical in all three studied cases, what shows that the solidification interval does not influence this solidification parameter at all; this can be explained by the fact that the dynamics of heat transmission from the casting to the mould is not influenced by the solidification interval, but only by the geometry of the casting and of the mould.

- for the same overheating in relation to the liquidus temperature (which in this case was $\Delta T = T_{0M} - T_L = 155^0 C$) the solidification time of the hot spot (in steels of different chemical compositions and different solidus and liquidus temperatures and in eutectic cast iron) is influenced to a relatively great extent. This influence can be. explained by the different amounts of thermal energy (heat) discharged by the alloy during solidification;

- in the case of steels solidification starts at a significantly higher rate than in the part cast from eutectic cast iron. (Table 2, $t_{START\ SOL\ OTEL} = 166.5s$ while $t_{START\ SOL\ FONTA} = 573.0s$); this can be explained by the temperature difference at the initial moment between the liquid alloy and the casting mould $(T_{0ME} - T_{FO})$, which is significantly greater for steels that are cast at a higher temperature; for this reason the heat transfer from the liquid steel to the mould immediately after filling of the mould is much more intensive for steels, what determines a higher cooling rate of the alloy at the beginning of cooling in liquid state;

- for steel parts the actual solidification takes longer (t_{SOL} - $t_{START\ SOL}$) than for the eutectic cast iron part; this can be explained by the larger overheating of steels in relation to the solidus temperature, as the overheating in relation to the solidus temperature is equal to the overheating in liquid state plus the solidification interval. Thus during solidification the steel parts have to discharge a larger quantity of heat – the latent heat plus the heat corresponding to the solidification interval;

- the start time of solidification ($t_{START\ SOL}$) and the end time of solidification (t_{SOL}) for the eutectic cast iron part are higher than those for the steel parts; this is explained by the smaller casting temperature of cast iron; thus the intensity of heat transfer to the mould is smaller for cast iron parts and the solidification time is greater;

- in the case of the two studied steels, at the same overheating in relation to the liquidus temperature, the magnitude of the solidification interval $\Delta T = T_L - T_S$, (i.e. the liquidus and solidus temperatures) has little influence on the extent of the liquidus area. For the same filling time of the mould (for example at t = 1250s) the position of the liquidus front is approximately the same (figure 5).

- in the case of the two studied steels, at the same overheating in relation to the liquidus temperature, the magnitude of the solidification interval $\Delta T = T_L - T_S$, (i.e. the liquidus and solidus temperatures) influences the magnitude of the two-phase area (solidus + liquidus) and its evolution in time in the section of the casting. This is caused by the modification of the position of the solidus front. For the same

"HENRI COANDA"
AIR FORCE ACADEMY
ROMANIA

"GENERAL M.R. STEFANIK"
ARMED FORCES ACADEMY
SLOVAK REPUBLIC

INTERNATIONAL CONFERENCE of SCIENTIFIC PAPER
AFASES 2014
Brasov, 22-24 May 2014

filling time of the mould (for example at t = 1250s) the two-phase area is smaller in the steel with a smaller solidification interval (0.1%C steel) and a higher casting temperature, the solidified area being more extended (figure 5).

- a two-phase area does not occur in the eutectic cast iron, only a liquidus area, and at the same time (a-150s since the filling of the mould) its extent is comparable to the extent of the two-phase + liquidus areas in steels with a solidification interval (for the same initial overheating) (figure 5);

- in the case of the two studied steels no differences occur as to the start time of solidification ($t_{START\ SOL}$); differences occur, however, related to the end of solidification (t_{SOL}) and the actual duration of hot spot solidification (t_{SOL} - $t_{START\ SOL}$); the 0.53%C steel has a greater end of solidification time than the 0.1%C steel, due to the larger solidification interval;

- in the studied steels (alloys with a solidification interval) the obtained evolution curves of temperature in the hot spot are influenced by the casting temperature (by the magnitude of the solidification interval and the liquidus temperature), as well as by the fact that during solidification temperature is no longer constant; the slope of the variation curve of temperature within the solidification interval is greater when the casting temperature (liquidus temperature) is smaller;

- in the studied alloys with a solidification interval (steels) the evolution curves of the solidus fraction in the hot spot (kinetics of solidification) differ significantly from the solidification curve of the eutectic cast iron; in the latter the evolution curve of the solid fraction is significantly more abrupt, what reveal s a slower solidification kinetics in steels (alloys with a solidification interval); the greater the solidification interval is, the kinetic curves (the variation of the solidus fraction) have a smaller slope, what shows that the actual solidification of the hot spot occurs within a greater

time interval; alloys solidifying at constant temperature (eutectic cast iron) have significantly swifter solidification kinetics.

- the general aspect of the variation curves of the cooling rates for the three studied alloys is similar, given the presence of peaks of the cooling rates in the first stage of cooling and immediately after completed solidification of each volume element;

- in the studied steels and cast iron the aspect of the evolution curves of the cooling rate in the hot spot differs as regards the cooling rate peaks, occurring prior to the beginning of solidification and at the end of solidification;

- the temperature distribution curves along a line/row or column of the casting-mould system, at a given time, are of similar shape, but differ by the values of the temperatures; the different values are explained by the different casting temperatures of the studied alloys.

5. REFERENCES

1. Ionescu D., Ionescu I., Ciobanu I., Monescu V. - *3D mathematical modelling of solidification of castings from alloys solidifying within a temperature interval*, in: Metalurgia International, Special issue no.6, 2013, pp. 105 - 110, ISSN 1582-2214
2. Ciobanu I., Ionescu D., Monescu V., Varga B., Munteanu I. S., Bedo T., Crişan A., Pop M. Alin – *Simulation of Solidification of Parts Cast from Alloys Solidifying within a Temperature Interval*, Editura Universităţii Transilvania din Braşov, Brasov, 2014, ISBN 978-606-19-0337-5
3. Ciobanu I., Monescu V., Munteanu S.I., Crişan A. *3D Simulation of the Solidification of Castings*, Editura Universităţii Transilvania din Braşov, Braşov (RO), 2010, ISBN 978-973-598-678-0.
4. Ionescu D. **-** *Research Concerning the Mathematical Modelling and Computer Simulation of the Solidification of Castings from Alloys Solidifying within a Temperature Interval*, Teză de doctorat [PhD Thesis], Universitatea Transilvania din Braşov, Braşov, 2014

ENGINEERING SCIENCES

A NOVEL APPROACH FOR ARMOR APPLICATIONS OF SHEAR THICKENING FLUIDS IN AVIATION AND DEFENSE INDUSTRY

Melih Cemal KUŞHAN*, Selim GÜRGEN*, Tolga ÜNALIR**, Sinem ÇEVİK***

* Department of Mechanical Engineering, ESOGU, Eskişehir, Turkey
** Payra Design Co. Inc., Eskişehir, Turkey
*** Department of Materials Science and Engineering, Ondokuz Mayis University, Samsun, Turkey

Abstract: At the beginning of 2000s, armor technology introduced to a new material: shear thickening fluid (STF). Due to the thickening behavior of this fluid under the stress, liquid state of the material turns into a solid-like state in a very limited time interval. This unique behavior of STF is intended to be used in armor systems. This paper offers an overview of STF properties and armor applications using the STF technology.

Keywords: Shear Thickening Fluids, Armors, Aviation, Defense Industry

1. INTRODUCTION

Armor systems have a remarkable importance for the area of security and military. From past to present there have been different kinds of personal armor systems used to eliminate the attacking threats. Early applications used bulk layers of leathers covering around the body as the personal armor systems. By the emerging of advance weapons, metal armor systems came into prominence such as steel shields. Metal armors were safe but unfortunately heavy to act freely during the combats. For this reason, recent studies have been focused on ceramic composites and light ballistic fabrics such as aramid based fabrics.

At the beginning of 2000s, shear thickening fluids (STF) were thought to be used as armor materials then inevitable development in the defense industry started. Usage of these fluids merely or combined with the other armor systems not only provides protection also flexible motion for the users.

2. SHEAR THICKENING FLUIDS

Shear thickening fluids are an example of non-Newtonian fluids which have increasing viscosities since shear stress is applied. Even the shear stress reaches the upper levels, fluid shows solid-like behavior for a split second. After removing the stress from the medium, fluids turn to the initial liquid behavior [1-9]. STFs are seen as appropriate armor materials with their unique characteristics.

History of STFs in the investigation area is quite new and not more than 50 years. Improvement of the research techniques such as latest rheometers, scanning methods, rheo-optical devices and Stokesian dynamics, gave us a chance to understand the STF mechanism profoundly [10]. Because discontinuous characteristics may be seen at the critical shear rates, stress controlled rheometers are more convenient than conventional type rheometers.

Beside Stokesian dynamics simulation is used widely to simulate the behavior of many-body interactions in the suspension [11].

Plenty of non-Newtonian fluids can be found in the nature, but STFs are very rare. The most common example is wet sand at the beaches. Another easily accessible example is cornstarch in water suspension whose rheological behavior is given in Figure 1.
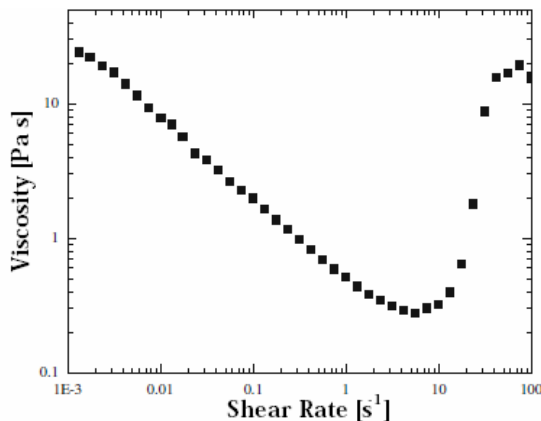
Figure 1. Rheological behavior of 55 wt% cornstarch in water suspension [9]

2.1 Mechanism of STFs.
There are two main theories explaining the mechanism of STFs: order-disorder and hydroclustering.

Hoffman made the pioneering study about the micromechanical of shear thickening. This study became the basis of order-disorder theory. He proposed that below the critical shear rate, particles in the suspension are in a hexagonally packed order. After the critical shear rate, this packed particles disorder and particles aggregate. This transition from order to disorder causes a drastic increase in the viscosity [12].

Hydrocluster theory was first introduced by Bardy with Stokesian dynamics simulations [13]. This theory was supported by neutron scattering, rheological and rheo-optical tests as well as computer simulations [14-17]. Hydrocluster mechanism arises from particle interactions in the liquid suspension. Under the high level stress, particles have contacts each other. This effect yields an increase in the hydrodynamic forces. Then hydroclustering emerges which is defined as aggregation of the particles with increased viscosity and jammed behavior of the fluid [16, 17].

Behavior of the particles in the suspension is seen in Figure 2. In the shear thickening zone, dark particles indicate the hydroclusters in the suspension.
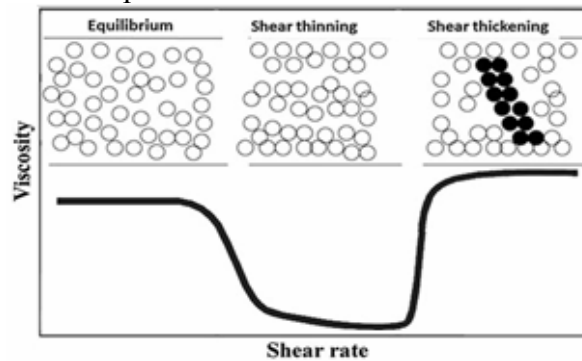
Figure 2. Particles in suspension [18]

2.2 Particle effects in suspensions.
STFs are obtained by constituting suspensions with solid particles in appropriate liquids. These suspensions can be prepared in many different ways. Since the mechanism of STF depends on particles behavior, particles have strong influence in the suspension characteristics.

Particle effects can be defined in terms of particle volume fraction, particle shape, particle size, particle size distribution, and particle interactions [1, 18-21].

Particle volume fraction is defined as the fraction of total volume by particle volume and said to be the most important parameter in the thickening mechanism. A lower limit value is reported for the thickening behavior by Barnes *et al*. [20]. It is stated that above the volume fraction of 0.5, behavior of fluid changes drastically with the change in shear rate. Critical shear rate, which is defined as at which the shear thickening begins, decreases with the increase of particle volume fraction. Figure 3 shows the effect of the particle volume in the suspensions.

"HENRI COANDA"
AIR FORCE ACADEMY
ROMANIA

"GENERAL M.R. STEFANIK"
ARMED FORCES ACADEMY
SLOVAK REPUBLIC

INTERNATIONAL CONFERENCE of SCIENTIFIC PAPER
AFASES 2014
Brasov, 22-24 May 2014
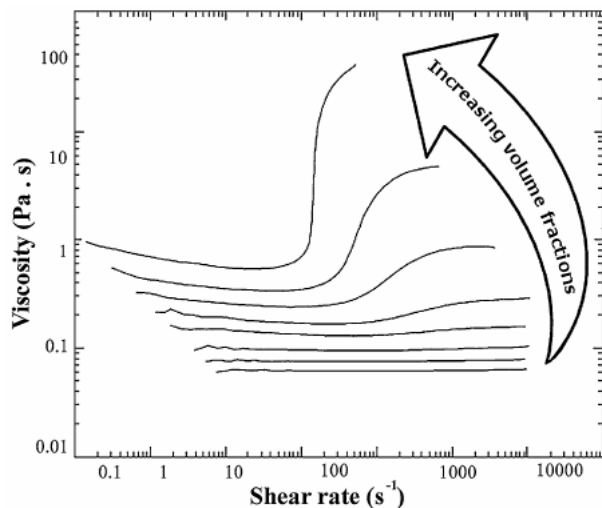
Figure 3. Effect of particle volume fraction [23]

Particle shape is another parameter having effect on the characteristics of the suspensions. Sharp edged particles in the suspension cause quick thickening as seen in Figure 4. Suspension with rod particles has the critical shear rate of $100s^{-1}$ whereas with sphere particles this rate is about $300s^{-1}$ [20].

Beazley [24] also states that particle rotation during flow may result in particle interlocking and jamming. With the high aspect ratio particles such interlockings will be seen more easily at lower particle volume fractions. Therefore, suspensions with high aspect ratio particles require lower critical volume fraction to achieve shear thickening.
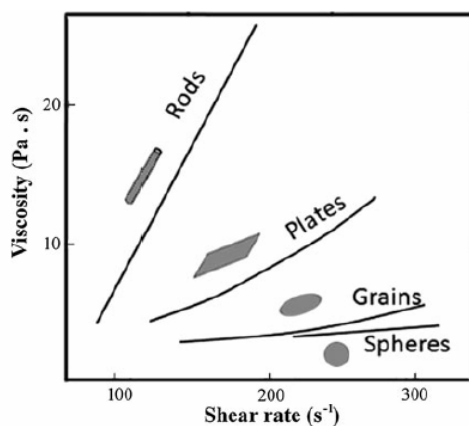
Figure 4. Effect of particle shapes in the suspension [20]

Particle size is another important parameter in STF behavior. It is known that as the particle size increases, critical shear rate decreases [20]. Figure 5 shows the relation between particle size and critical shear rate.

Particle size distribution affects the critical shear rate in the suspension. It is noted that critical shear rate increases when the particle size distribution becomes wider. Shear thickening can be achieved at lower shear rates by eliminating the small particles from the suspensions [20].
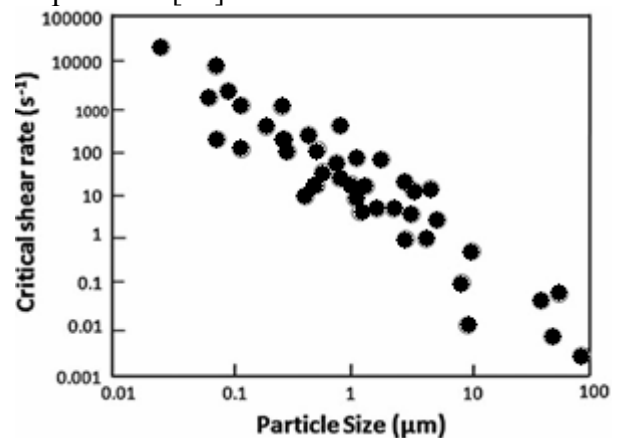
Figure 5. Effect of particle size in suspension [20]

Particle interactions have an influence on the shear thickening behavior. Particles in the suspensions may be neutral or repulsive to another by the effects of electrostatic, entropic, or steric interactions. It is stated that viscosities of deflocculated suspensions are lower at low shear rates. Shear thickening of these fluids occurs at high shear rates. On the other hand, viscosities of flocculated suspensions are higher at low shear rates. These fluids show shear thinning at high shear rates [1, 20]. Figure 6 shows the effect of chemically induced flocculation.
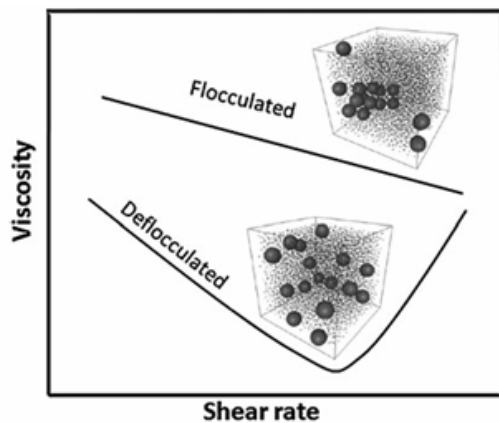
Figure 6. Effect of chemically induced flocculation [20]

Beside the parameters given above, additional parameters can be shown as examples. Hardness of the particles is one of these parameters. Shear thickening behavior increases with increase in hardness of the particles [21]. Another parameter is temperature which improves the shear thickening behavior by decreasing [25].

Some studies focus on the methods for improving the shear thickening behavior. For example, nano fillers are used to improve the shear thickening. In this method, nano fillers increase the dispersibility of nano particles which enhances the interaction between the particles and results in a better particle clustering. To achieve this, carbon nano tubes (CNTs) are applied into silica-poly ethylene glycol suspension. It is noted that CNT reinforcement improves the dispersibility of nano particles in the suspension [19].

3. ARMOR APPLICATIONS

Armor technology has been continuously improved like weapon technology. These two terms always keep up with each other. Ballistic protection has to be actual to overcome the attacking threats. Therefore, every kind of material has been considered as armor materials such as aluminum, steel, leather and silk. Principally, the method of protection uses a hard rigid material for resisting the penetration of missiles. But, after the debut of synthetic textiles, better ballistic armors have been developed [26].

3.1 Fabrics in protection. Ballistic fabrics are made of high strength fibers and chosen due to their high energy absorption capacity and proper tenacity/weight ratio. Furthermore, ballistic fabrics provide easy motion for users with their flexible structures [27-29].

Energy absorption and propagation capacity of fabric layers are related to the tensile modulus of fibers. Fibers having high tenacity and high elastic modulus are chosen for production of ballistic fabrics. In addition to this, construction of the fabrics has an intense effect on ballistic performance. In the construction of these fabrics, warp and weft yarns are woven by using different weaving types such as plain and basket types. Generally, warp and weft yarns are selected with identical strengths to achieve the same properties in all directions [30]. Then, woven layers are piled on each other to obtain laminated fabrics. Laminated fabrics are called 2D fabrics and the major problem is delamination. Latest studies focus on 3D fabrics in ballistic protection. 3D fabrics have yarns running in three directions therefore, delamination problem is decreased by the reinforcement of yarns along the third direction [31-41]. Figure 7 shows fabrics in 2D and 3D forms schematically.
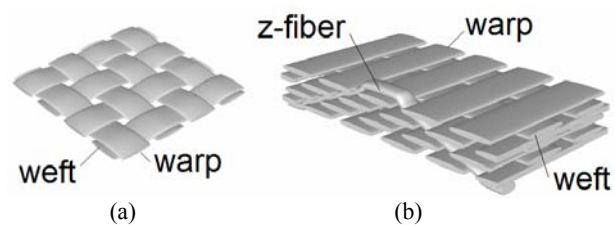
Figure 7. Fabrics in (a) 2D form (b) 3D form

3.2 Application of STFs in ballistic protection. Although STFs are worldwide known, application of these materials in ballistic protection is quite novel. First studies were started at the University of Delaware in mid 1990s. Considerable results were attained at the beginning of the 2000s. Composites of Kevlar® and STFs were introduced as armor systems in the publications. This technology was also supported by Army Research Laboratory. In 2004, a patent application [42] was filed with the cooperation of University of Delaware and Army Research Laboratory [1].

"HENRI COANDA"
AIR FORCE ACADEMY
ROMANIA

"GENERAL M.R. STEFANIK"
ARMED FORCES ACADEMY
SLOVAK REPUBLIC

INTERNATIONAL CONFERENCE of SCIENTIFIC PAPER
AFASES 2014
Brasov, 22-24 May 2014

The most important gains in STF based armors are reduced weight and flexible motion. In the combat zones, conditions are already crucial. In additions to these difficulties, struggling with the equipment and the armor makes the soldiers daunted. Average combat loads for U.S Army soldiers in Afghanistan 2003 are given in Table 1.

Table 1. Average combat loads for U.S Army soldiers in Afghanistan, 2003[43]

Duty Position	Average Fighting Load	
	Weight (kg)	Percentage of Body Weight
Rifleman	28	36
Automatic rifleman	36	45
60mm mortar gunner	29	38

In 2001, U.S Army Chief of Staff expressed a goal that the combat load of the individual soldier was not to exceed 23kg [44].

Wagner *et al.* [45] studied characteristics of STF impregnated Kevlar®. It is noted that starting shear rate values of thickening behavior are between $10s^{-1}$ and $300s^{-1}$ whereas the shear rates estimated in the ballistic shootings are at $45x10^3s^{-1}$ based on the projectile velocity. Therefore, the STFs used in the study are ready to exhibit thickening behavior in the ballistic tests. In the conclusion of the study, it is stated that STF impregnated Kevlar® has the highest energy dissipation value with respect to the neat Kevlar® and ethylene glycol (EG) impregnated Kevlar®. EG impregnated Kevlar® has the worst protection level because EG is Newtonian fluid and serves as lubricant between the yarns and the projectile. Figure 8 shows the energy dissipation percentages of armor constructions by considering the armor weights.
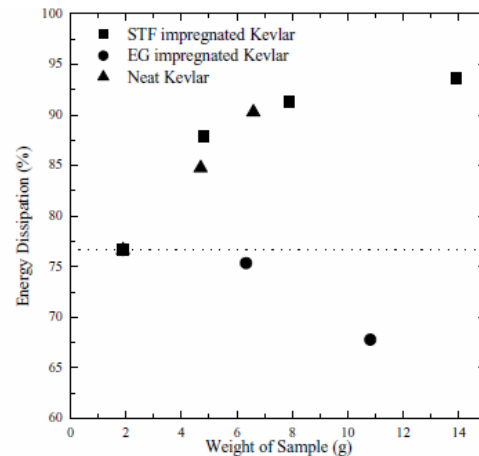
Figure 8. Energy dissipations of targets [45]

In another study using STF-Kevlar® composites, particle volume fraction of STF is investigated. As in the pure STF, thickening mechanism is more intense on fabrics with high volume fractions of particles. Furthermore, at low particle loadings, ballistic performance is less than neat Kevlar® while at high loadings is better than neat Kevlar® [23].

Tan *et al.* [50] studied single, double, quadruple and six ply Twaron® fabric systems with different percentages of STFs. Ballistic tests showed that the best protective system is double ply fabric impregnated by 40wt% STF. This system improves the ballistic limit by 65% compared to the neat double ply system.

In the studies, finite element method is preferred for modeling the STFs on fabrics. But, it is quite complicated to define the properties of STF in the model. To overcome this problem, Kim *et al.* [51] modeled the STF impregnated Kevlar® without modeling the liquid STF. Since STF increases the friction between the yarns, a friction function dependent to velocity was obtained by conducting yarn pull-out energy tests. In the conclusion, good agreements between simulation and ballistic tests were achieved in terms of residual velocities.

3.3 Application of STFs in stab protection.

STF reinforced fabrics can also be considered as protective armors against stab attacks. In the literature, studies investigating this issue are available.

Protection of STF impregnated ballistic fabrics is determined by conducted some tests. These tests are generally performed in two ways: drop stab test and quasistatic test. It is proven that STFs reinforce the Kevlar® significantly for spike impacts while slight improvement is seen for knife impacts. Also in the quasistatic tests, for puncturing the same thick armors, STF-Kevlar® composites require two times more load by knife and five times more load by spike with respect to the neat Kevlar® armors [19, 46, 47].

Decker *et al.* [48] and Gong *et al.* [49] studied the stab resistance of the armors at the fiber level. Deformation of ballistic fabric fibers were investigated by SEM imaging. It is noted that STF restricts the fiber mobility which prevents the sharp tip of the spike from pushing aside fibers and penetrating between them (windowing effect). This effect is also seen in knife stabs but since cutting takes place in knife stabs, fiber mobility cannot be restricted effectively. This mechanism explains that protection of STF impregnated fabrics is higher in spike stabs than in knife stabs. Figure 9 shows the load-displacement curves for quasistatic loading of Kevlar® and STF-Kevlar® targets against both spike and knife impactors.
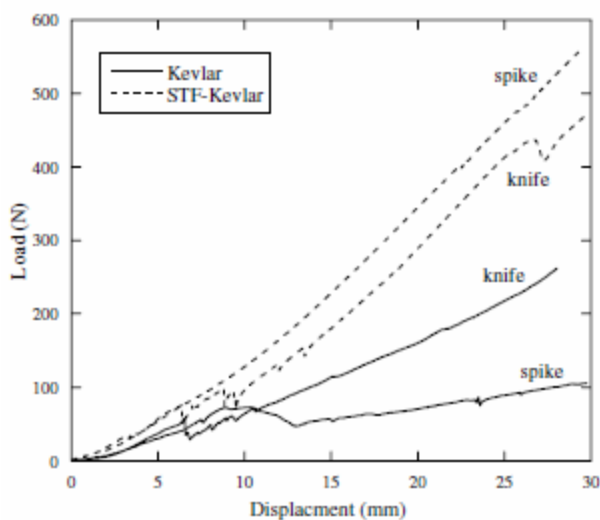
Figure 9. Load-displacement curves for quasistatic loading [47]

4. FUTURE DEVELOPMENT

STFs in armor systems are very new technology and open to developments. This technology provides two main improvements: reduced weight and flexible motion. Whenever reduction in weight comes into question, any relation with aerospace industry may take place. Thus, STFs can be applied to aerial vehicles such as helicopters beside the personal protection. Today it is just an idea however, in the near future it might be possible that this technology can protect the aerial vehicles.

REFERENCES

1. A.Srivastava, A.Majumdar, B.S.Butola, Improving the Impact Resistance of Textile Structures by using Shear Thickening Fluids: A Review, *Crit Rev Solid State Mater Sci*, 37, 115-129, (2012)
2. L.Chang, K.Friedrich, A.K.Schlarb, R.Tanner and L.Ye, Shear-Thickening Behavior of Concentrated Polymer Dispersions Under Steady and Oscillatory Shear, *J Mater Sci*, 46, 339-346, (2011)
3. W.H.Boersma, J.Laven, H.N.Stein, Shear Thickening (Dilatancy) in Concentrated Dispersions, *AIChE J*, 36, 321-332, (1990)
4. S.R.Raghavan, J.Hou, G.L.Baker, S.A.Khan, Colloidal interactions between particles with tethered nonpolar chains dispersed in polar media: direct correlation between dynamic rheology and interaction parameters, *Langmuir,* 16, 1066-1077, (2000)
5. R.L.Hoffman, Discontinuous and dilatant viscosity behavior in concentrated suspensions. II. Theory and experimental tests, *J Colloid Interface Sci,* 46, 3, 491-506, (1974)
6. R.L.Hoffman, Explanations for the cause of shear thickening in concentrated colloidal suspensions, *J Rheol,* 42, 1, 111-123, (1998)
7. B.R.Munson, D.F.Young and T.H.Okiishi, *Fundamentals of Fluid Mechanics*, 5th Edition, John Wiley & Sons, (2006)
8. R.G.Egres and N.J.Wagner, The Rheology and Microstructure of Acicular Precipitated Calcium Carbonate Colloidal Suspensions

"HENRI COANDA"
AIR FORCE ACADEMY
ROMANIA

"GENERAL M.R. STEFANIK"
ARMED FORCES ACADEMY
SLOVAK REPUBLIC

INTERNATIONAL CONFERENCE of SCIENTIFIC PAPER
AFASES 2014
Brasov, 22-24 May 2014

Through The Shear Thickening Transition, *J Rheol*, 49, 3, 719-746, (2005)

9. E.E.B.White, M.Chellamuthu, and J.P.Rothstein, Extensional Rheology of a Shear-Thickening Cornstarch and Water Suspension, *Rheol Acta*, 49, 119-129, (2010)

10. F.J.G.Rosales, F.J.R.Hernández and J.F.V.Navarro, Shear-thickening behavior of Aerosil® R816 nanoparticles suspensions in polar organic liquids, *Rheol Acta*, 48, 699-708, (2009)

11. D.R.Foss, J.F.Brady, Structure, diffusion and rheology of Brownian suspensions by Stokesian dynamics simulation, *J Fluid Mech*, 407, 167-200, (2000)

12. R.L.Hoffman, Discontinuous and dilatant viscosity behavior in concentrated suspensions. I.Observation of flow instability, *J Rheo*, 16, 1, 155-173, (1972)

13. G.Bossis, and J.F.Brady, The rheology of Brownian suspensions, *J Chem Phys*, 91, 3, 1866-1874, (1989)

14. J.W.Bender and N.J.Wagner, Optical measurement of the contribution of colloidal forces to the rheology of concentrated suspensions, *J Colloid and Interface Science*, 172, 171-184, (1995)

15. P.D'Haene, J.Mewis and G.G.Fuller, Scattering dichroism measurements of flow-induced structure of a shear thickening suspension, *J Colloid and Interface Science*, 156, 2, 350-358, (1993)

16. N.J.Wagner and J.F.Brady, Shear Thickening in Colloidal Dispersions, *Physics Today*, 62, 27-32, (2009)

17. B.J.Maranzano and N.J.Wagner, Flow-Small Angle Neutron Scattering Measurements of Colloidal Dispersion Microstructure Evolution Through The Shear Thickening Transition, *J Chem Phys*, 117, 22, 10291-10302, (2008)

18. B.J.Maranzano and N.J. Wagner, The Effects of Interparticle Interactions and Particle Size on Reversible Shear Thickening: Hard-Sphere Colloidal Dispersions, *J Rheol*, 45, 1205-1222, (2001)

19. M.Hasanzadeh, V.Mottaghitalab, The Role of Shear-Thickening Fluids (STFs) in Ballistic and Stab-Resistance Improvement of Flexible Armor, *JMEPEG*, 23, 4, 1182-1196, (2014)

20. H.A.Barnes, Shear Thickening (Dilatancy) in Suspensions of Nonaggregating Solid Particles Dispersed in Newtonian Liquids, *J Rheol*, 33, 329-366, (1989)

21. D.P.Kalman, R.L.Merrill, N.J.Wagner and E.D.Wetzel, Effect of Particle Hardness on the Penetration Behavior of Fabrics Intercalated with Dry Particles and Concentrated Particle-Fluid Suspensions, *Appl Mater Interfaces*, 1, 11, 2602-2612, (2009)

22. B.J.Maranzano and N.J.Wagner, The Effects of Particle Size on Reversible Shear Thickening of Concentrated Colloidal Dispersions, *J Chem Phys*, 114, 10514-10527, (2001)

23. E.D.Wetzel, Y.S.Lee, R.G.Egres, K.M.Kirkwood, J.E.Kirkwood and N.J.Wagner, The Effect of Rheological Parameters on the Ballistic Properties of Shear Thickening Fluid (STF)-Kevlar Composites, *Proceedings of NUMIFORM, AIP Conference Proceedings*, 712, 288-293, (2004)

24. K.M.Beazley, Industrial aqueous suspensions, Rheometry: Industrial Applications, K.Walters (ed.), *Research Studies Press*, Chichester, 339, (1980)

25. T.J.Kang, C.Y.Kim and K.H.Hong, Rheological Behavior of Concentrated Silica Suspension and Its Application to Soft Armor, *J Appl Polym Sci*, 124, 1534-1541, (2012)

26. P.Bajaj, Sriram, Ballistic Protective Clothing: An Overview, *Indian J Fibre & Textile Research*, 22, 274-291, (1997)

27. J.W.Simons, D.C.Erlich and D.A.Shockey, Finite element design model for ballistic response of woven fabrics, *Proceedings of the 19th international symposium on ballistics*, 1415-1422, (2001)

28. C.T.Lim, V.P.W.Shim and Y.H.Ng, Finite-element modeling of the ballistic impact of fabric armor, *Int J Impact Eng,* 28, 13-31, (2003)

29. V.B.C.Tan, C.T.Lim and C.H.Cheong, Perforation of high-strength fabric by projectiles of different geometry, *Int J Impact Eng*, 28, 207-222, (2003)

30. M.Karahan, A.Kus, R.Eren, An investigation into ballistic performance and energy absorption capabilities of woven aramid fabrics, *Int J Impact Eng*, 35, 499-510, (2008)

31. Y.Hou, B.Sun and B.Gu, An analytical model for the ballistic impact of three dimensional angle-interlock woven fabric penetrated by a rigid cylindro-spherical projectile, *Textile Research J*, 81, 1287-1303, (2011)

32. S.V.Lomov, A.E.Bogdanovich, D.S.Ivanov, D.Mungalov, M.Karahan and I.Verpoest, A comparative study of tensile properties of non-crimp 3D orthogonal weave and multi-layer plain weave E-glass composites. Part 1: Materials, methods and principal results, *Composites Part A: Applied Science and Manufacturing,* 40, 1134-1143, (2009)

33. G.D.Clercq, G.Haezebrouck, F.Ghekiere, L.V.Langenhove, S.Vasile, T.Gries, Y.S.Gloy and B.Wendland, Ballistic Behaviour of 3D Multilayered Fabrics Woven on Multirapier Looms, *The Third International Conference on 3D Fabrics and Their Applications*, 1-6, (2011)

34. M.P.Rao, B.V.Sankar and G.Subhash, Effect of Z-yarns on the stiffness and strength of three-dimensional woven composites, *Composites Part B: Applied Science and Manufacturing,* 40, 540-551, (2009)

35. A.Mahmood, Elastic analysis of 3D woven orthogonal composites, *Grey Systems: Theory and Application,* 1, 228-239, (2011)

36. K.Bilisik, Experimental determination of ballistic performance of newly developed multiaxis non-interlaced/non-Z E-glass/polyester and 3D woven carbon/epoxy composites with soft backing aramid fabric structures, *Textile Research J,* 81, 520-537, (2010)

37. X.Chen, L.W.Taylor and L.J.Tsai, An overview on fabrication of three-dimensional woven textile preforms for composites, *Textile Research J,* 81, 932-944, (2011)

38. X.Jia, B.Sun and B.Gu, Ballistic penetration of conically cylindrical steel projectile into 3D orthogonal woven composite: a finite element study at microstructure level, *J Comp Mat*, 45, 965-987, (2010)

39. Y.Tang, B.Sun and B.Gu, Impact Damage of 3D Cellular Woven Composite from Unit-cell Level Analysis, *Int J Damage Mech*, 20, 323-346, (2011)

40. X.Jia, B.Sun and B.Gu, A Numerical Simulation on Ballistic Penetration Damage of 3D Orthogonal Woven Fabric at Microstructure Level, *Int J Damage Mech*, 21, 237-266, (2012)

41. F.Boussu, The use of warp interlock fabric inside textile composite protection against ballistic impact, *Textile Research J*, 81, 344-354, (2010)

42. N.Wagner and E.D.Wetzel, Advanced body armor utilizing shear thickening fluids, US Patent 20060234577A1, (2006)

43. Task Force Devil Combined Arms Assessment Team (Devil CAAT), The Modern Warrior's Combat Load: Dismounted Operations in Afghanistan, April–May 2003, *Ft. Leavenworth, Kan.: U.S. Army Center for Army Lessons Learned*, (2003)

44. K.Horn, K.Biever, K.Burkman, P.D.Luca, L.Jamison, M.Kolb and A.Sheikh, *Lightening Body Armor*, RAND, (2012)

45. Y.S.Lee, E.D.Wetzel and N.J.Wagner, Ballistic impact characteristics of Kevlar® woven fabrics impregnated with a colloidal shear thickening fluid, *J Mat Sci*, 38, 2825-2833, (2003)

46. R.G.Egres Jr, Y.S.Lee, J.E.Kirkwood, K.M.Kirkwood, E.D.Wetzel and N.J.Wagner, "Liquid armor": Protective fabrics utilizing shear thickening fluids, *The 4th Int Conf on Safety and Protective Fabrics,* (2004)

47. R.G.Egres, M.J.Decker, C.J.Halbach, Y.S.Lee, J.E.Kirkwood, K.M.Kirkwood, N.J.Wagner and E.D.Wetzel, Stab Resistance of Shear Thickening Fluid (STF)-Kevlar Composites for Body Armor Applications, *Proceedings for the 24th Army Science Conference*, (2005)

48. M.J.Decker, C.J.Halbach, C.H.Nam, N.J.Wagner and E.D.Wetzel, Stab resistance

“HENRI COANDA”
AIR FORCE ACADEMY
ROMANIA

“GENERAL M.R. STEFANIK”
ARMED FORCES ACADEMY
SLOVAK REPUBLIC

INTERNATIONAL CONFERENCE of SCIENTIFIC PAPER
AFASES 2014
Brasov, 22-24 May 2014

of shear thickening fluid (STF) treated fabrics, *Composites Science and Technology*, 67, 565-578, (2007)

49. X.Gong, Y.Xu, W.Zhu, S.Xuan, W.Jiang and Wa.Jiang, Study of the knife stab and puncture-resistant performance for shear thickening fluid enhanced fabric, *J Comp Mat*, 0, 1-17, (2013)

50. V.B.C.Tan, T.E.Tay and W.K.Teo, Strengthening fabric armour with silica colloidal suspensions, *Int J Solids and Structures*, 42, 1561-1576, (2005)

51. B.W.Lee and C.G.Kim, Computational analysis of shear thickening fluid impregnated fabrics subjected to ballistic impacts, *Adv Comp Mat*, 21, 177-192, (2012)

ENGINEERING SCIENCES

"HENRI COANDA"
AIR FORCE ACADEMY
ROMANIA

"GENERAL M.R. STEFANIK"
ARMED FORCES ACADEMY
SLOVAK REPUBLIC

INTERNATIONAL CONFERENCE of SCIENTIFIC PAPER
AFASES 2014
Brasov, 22-24 May 2014

AN APPROACH FOR STATIC CALIBRATION OF ACCELEROMETER MMA8451Q

Marin MARINOV*, Zhivo PETROV*

*Aviation Faculty, NVU "V. Levski", Dolna Mitropolia, Bulgaria

Abstract: In this paper an approach for low-cost MEMS accelerometer static calibration is proposed. The approach is applied to estimate the MEMS accelerometer mathematical model, including scale factors and bias. The method does not require a three-axis rotary platform to perform perfect alignment to the Earth gravity. The measurement is easy to perform, the calculation is simple, and the proposed approach provides a different choice for accelerometer calibration. Experimental data is analyzed to prove that the bias and scale factors are eliminated.

Keywords: accelerometer, bias, calibration, scale factors.

1. INTRODUCTION

By analyzing MEMS accelerometer measurement principle and environment, it could be proved that the main errors include three gain factors and three biases [4, 5].

The manufacturers of the MEMS accelerometers usually apply a calibration. The original factory accelerometer calibration becomes less accurate once the accelerometer is soldered, by the end users, onto its circuit board as a result of thermal stresses during the soldering process.

Different approaches for recalibration are used. Some of them require measurements in only one or two positions of the accelerometer [3] but only bias can be estimated. Other approaches estimate more than 10 parameters [1, 6]. The approaches computing six calibration parameters are most widely used [1, 3]. Most of these approaches require precise orientation of the accelerometer.

In this paper an approach for low-cost MEMS accelerometer static calibration without precise orientation is proposed.

2. ACCELEROMETER CALIBRATION METHOD

According to the characteristics of the measurement error, the MEMS accelerometer error model is defined as:

$$\begin{bmatrix} a_x \\ a_y \\ a_z \end{bmatrix} = \begin{bmatrix} S_x & -k_4 S_y & -k_5 S_z \\ k_1 S_x & S_y & -k_6 S_z \\ -k_2 S_x & k_3 S_y & S_z \end{bmatrix} \begin{bmatrix} g_x \\ g_y \\ g_z \end{bmatrix} + \begin{bmatrix} b_x \\ b_y \\ b_z \end{bmatrix} + \begin{bmatrix} n_x \\ n_y \\ n_z \end{bmatrix}, (1)$$

where: b_x, b_y, b_z are accelerometer bias; S_x, S_y, S_z are scale factors for the accelerometer; n_x, n_y, n_z are random measurement noises; $k_1, k_2, k_3, k_4, k_5, k_6$ are installation error coefficients.

For an application demanding lower accuracy it could be assumed that the scale

factors are equal to on e and the equation (1) becomes:

$$\begin{bmatrix} a_x \\ a_y \\ a_z \end{bmatrix} = \begin{bmatrix} S_x & 0 & 0 \\ 0 & S_y & 0 \\ 0 & 0 & S_z \end{bmatrix} \begin{bmatrix} g_x \\ g_y \\ g_z \end{bmatrix} + \begin{bmatrix} b_x \\ b_y \\ b_z \end{bmatrix} + \begin{bmatrix} n_x \\ n_y \\ n_z \end{bmatrix}. \quad (2)$$

To determ ine the accelerom eter bias and scale f actors six dif ferent sta tic po sitions ar e used. In ea ch position one of the axes is directed along or opposite Earth gravity.

The instantaneous outputs of the accelerometer in on e of the positions a_{px}, a_{py}, a_{pz} are given by:

$$a_{px} = S_x g_{px} + b_x + n_{1x}$$
$$a_{py} = S_y g_{py} + b_y + n_y \ , \quad (3)$$
$$a_{pz} = S_z g_{pz} + b_z + n_z$$

where $p = 1 \div 6$ is the position number.

Multiple measurements in each position are done and output data is averaged to decrease the im pact of noi se. The averaged accelerations are described by:

$$A_{px} = S_x g_{px} + b_x$$
$$A_{py} = S_y g_{py} + b_y \ \Rightarrow$$
$$A_{pz} = S_z g_{pz} + b_z$$

$$\frac{1}{S_x}\left(A_{px} - b_x\right) = g_{px}$$

$$\Rightarrow \frac{1}{S_y}\left(A_{py} - b_y\right) = g_{py} \ . \quad (4)$$

$$\frac{1}{S_z}\left(A_{pz} - b_z\right) = g_{pz}$$

Both sides of each equation in (4) are raised to the second power and then the equations are summed to obtain:

$$A_p^2 + 2A_{px}C_x - 2A_{py}C_y - 2A_{pz}C_z + b^2 +$$
$$+ A_{px}\Delta_x + A_{py}\Delta_y + A_{pz}\Delta_z + \qquad , \quad (5)$$
$$+ \Delta_x a_x^2 + \Delta_y a_y^2 + \Delta_z a_z^2 = 1$$

where: $A_p^2 = A_{px}^2 + A_{py}^2 + A_{pz}^2$;

$b^2 = b_x^2 + b_y^2 + b_z^2$; $\qquad C_x = \left(1+\Delta_x\right)b_x$;

$Cy = \left(1+\Delta_y\right)b_y$; $\qquad C_z = \left(1+\Delta_z\right)b_z$;

$\Delta_x = \frac{1}{S_x^2} - 1$; $\Delta_y = \frac{1}{S_y^2} - 1$; $\Delta_z = \frac{1}{S_z^2} - 1$.

In this way six equation s are form ed. Each equation is com bined with other five and the result is fifteen co uples of equation s. Equations in every cou ple are sub tracted and system of linear equations is created. The matrix form of the system is:

$$\mathbf{H\lambda = A}, \quad (6)$$

where:

$$\mathbf{H_j} = [A_{px} - A_{qx}, A_{py} - A_{qy}, A_{pz} - A_{qz}, \ ;$$
$$, A_{qx}^2 - A_{px}^2, A_{qy}^2 - A_{py}^2, A_{qz}^2 - A_{pz}^2]$$

$$\lambda = \left[C_x, C_y, C_z, \Delta_x, \Delta_y, \Delta_z\right]^T \ ; \ p \neq q;$$

$$p = 1 \div 6; \qquad A_i = \left(A_p^2 - A_q^2\right)0.5; \qquad i = 1 \div 15;$$

$$q = 1 \div 6; \ j = 1 \div 15.$$

An itera tive algor ithm is used to f ind the least squares solution of system (6):

$$\hat{\lambda} = \left[\hat{C}_x, \hat{C}_y, \hat{C}_z, \hat{\Delta}_x, \hat{\Delta}_y, \hat{\Delta}_z, \right]. \quad (7)$$

Using (7) the bias and scale facto rs are obtained:

$$\hat{b}_x = \frac{\hat{C}_x}{1+\hat{\Delta}_x}, \hat{b}_y = \frac{\hat{C}_y}{1+\hat{\Delta}_y}, \hat{b}_z = \frac{\hat{C}_z}{1+\hat{\Delta}_z}. \quad (8)$$

$$\hat{S}_x = \sqrt{\frac{1}{1+\hat{\Delta}_x}}, \hat{S}_y = \sqrt{\frac{1}{1+\hat{\Delta}_y}}, \hat{S}_z = \sqrt{\frac{1}{1+\hat{\Delta}_z}}. \quad (9)$$

The proposed m ethod allows obtaining the bias and scale factor s without requiring a perfect orientation of accelerometers along the Earth gravity.

3. TEST RESULTS

The data from MMA8451Q is read using a device d escribed in [2]. The accelerom eter is set up to: 14 bits of resolution; $\pm$ 2 g full scale; 100 Hz output data rate. The accelerom eter was placed in six different pos itions and in each positio n the data was collected for 50 seconds. Collected accelerations are shown in figures from 1 to 6.

The proposed method is applied to estimate bias and scale facto rs of m easurement. The obtained values of six parameters are:

$$\hat{b}_x = -16.1\,mg; \ \hat{b}_y = 4.7\,mg; \ \hat{b}_z = 4.6\,mg;$$

$$\hat{S}_x = 0.9961; \ \hat{S}_y = 1.0023; \ \hat{S}_z = 1.0019$$

"HENRI COANDA"
AIR FORCE ACADEMY
ROMANIA

"GENERAL M.R. STEFANIK"
ARMED FORCES ACADEMY
SLOVAK REPUBLIC

INTERNATIONAL CONFERENCE of SCIENTIFIC PAPER
AFASES 2014
Brasov, 22-24 May 2014
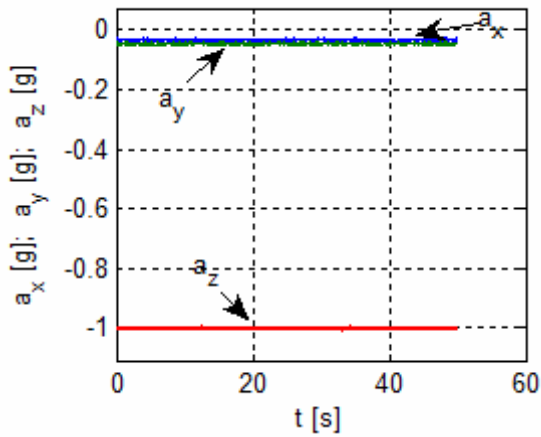
Figure 1. Accelerometer output data in position 1.
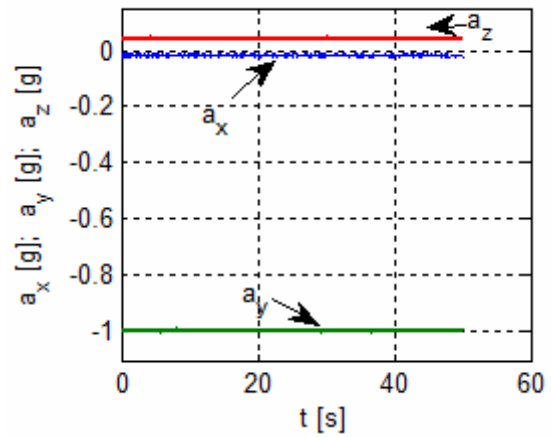
Figure 4. Accelerometer output data in position 4.
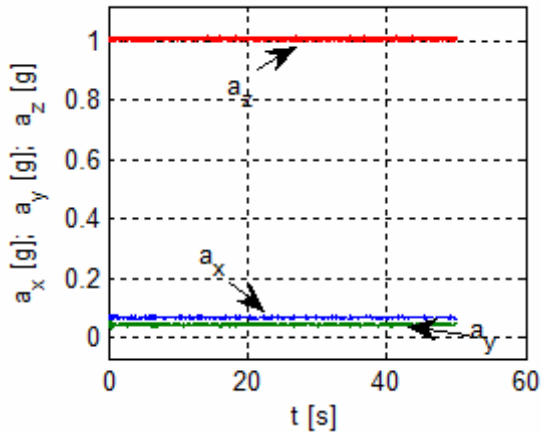
Figure 2. Accelerometer output data in position 2.
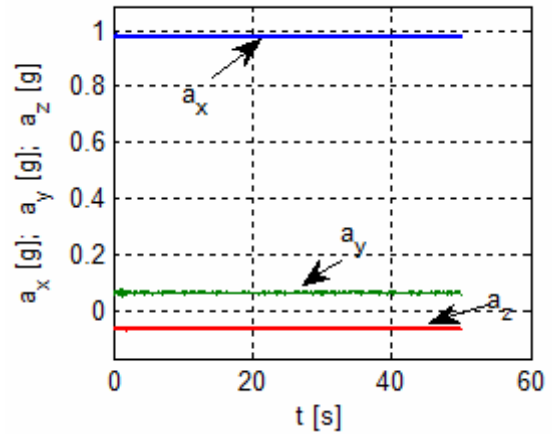
Figure 5. Accelerometer output data in position 5.
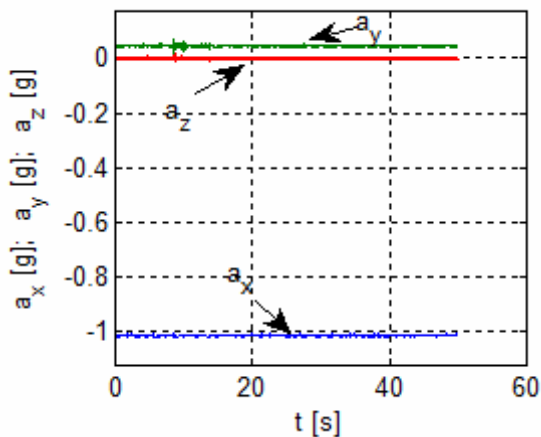
Figure 3. Accelerometer output data in position 3.
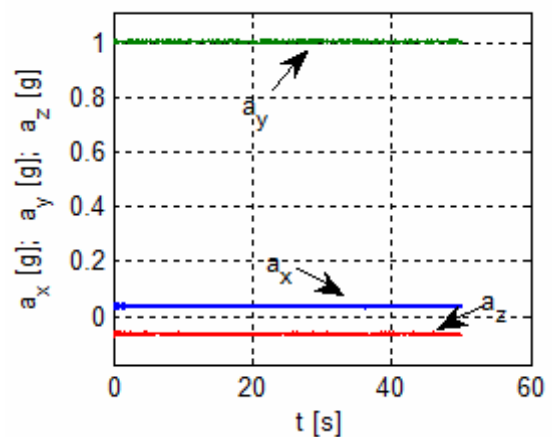
Figure 6. Accelerometer output data in position 6.

To verify proposed approach som e data is collected when accelerom eter is arbitrary orientated. Using m easurements from each axis th e relative Earth acceleration is calculated ("a" on fig.7). The relative Earth acceleration is also calc ulated after calib ration of measurements ("a_{cal}" on fig.7).
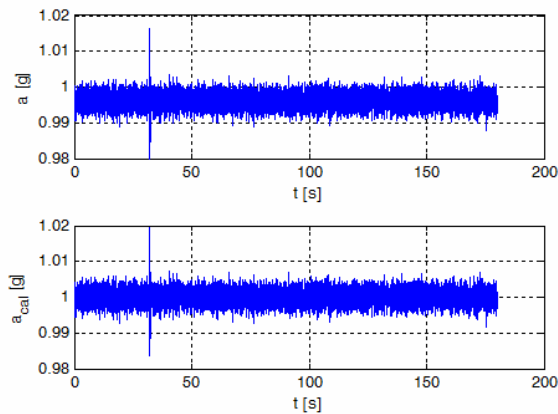
Figure 7. Accelerometer output calibration.

Figure 7 shows that calculated relative Earth acceleration is closer to 1g, when calibration is used.   T his prov es tha t th e proposed approach could be used to elim inate bias from measurement.

4. CONCLUSIONS

This paper proposes the Accelerom eter static calibration m ethod using six param eters. The method is accurate, easy to implement and doesn't require additional equipment.

The bias and scale factors of MEMS accelerometer MMA8451Q are estim ated. The results show that the x-axis bias is the biggest whereas y-axis and z- axis bias are alm ost the same.

The obtained experim ental results prove the validity of the method.

REFERENCES

1. Pedley M. *High Precision Calibration of aThree-Axis Accelerometer,* AN4399, Rev. 1, Freescale Semiconductor, (01/2013)
2. *Petrov Zh., Marinov M., Dimitrov D.,3-axis digital accelerometer data transfer controller, Scientific conference , Aviation Faculty, D. Mitropolia, Bulgaria (2013).*
3. Tuck K., *Offset Calibration of the MMA8451, 2, 3Q*, AN4069, Rev. 1, Freescale Semiconductor, (03/2012)
4. Umeda A., Onoe M., Sakata K., Fukushia T., Kanari K., Iioka H., Kobaya shi T., *Calibration of three-axis accelerometers using a three-dimensional vibration generator and three laser interferometers*, Sensors and Actuators A: Physical, Volume 114, Issue 1, (2004)
5. Won P., Golnaraghi F., *A trail Accelerometer Calibration Method Using a Mathematical Model*, IEEE Trans actions on Instrumentation and Measurement, Vol. 59, NO.8, (2010)
6. Zhang L., Li W ., Liu H., *Accelerometer Static Calibration based on the PSO algorithm,* 2nd International Conference on Electron ic & Mech anical Engineerin g and Information Technology (2012)

ALLAN VARIANCE ANALYSIS ON ERROR CHARACTERS OF LOW-COST MEMS ACCELEROMETER MMA8451Q

Marin MARINOV*, Zhivo PETROV*

*Aviation Faculty, NVU "V. Levski", Dolna Mitropolia, Bulgaria

Abstract: *This paper gives an evaluation of low-cost MEMS digital accelerometer errors. Such evaluation is required to construct an appropriate model of the accelerometer. Allan Variance is a simple and efficient method for verifying and modelling the errors by representing the root mean square random drift error as a function of averaging time.*

In this paper the characteristics of MEMS accelerometers stochastic errors are identified and quantified, using Allan variance. The derived error model can be applied further to navigation systems of small aircraft.

Keywords: *accelerometer, Allan variance, bias instability, error, random walk, rate random walk.*

1. INTRODUCTION

Advances in the Micro-Electromechanical Systems (MEMS) technology combined with the miniaturization of electronics, have made possible to introduce light-weight, low-cost and low-power chip based inertial sensors for use in measuring of angular velocity and acceleration [9].

MEMS accelerometers output the aircraft acceleration which is used to obtain the position and velocity. The accuracy of accelerometer measurements usually depend on different types of error sources, such as bias, bias instability, velocity random walk, rate random walk, etc. By integrating these measurements in the navigation algorithm, these errors will lead to a significant drift in the position and velocity. To improve the accuracy of aircraft navigation system, different kinds of algorithms are used,

integrating accelerometer measurements with other sensors such as GPS receivers [8]. To achieve an accurate estimation of aircraft navigation parameters a good model of sensors' errors is required.

The errors are caused by noise sources which are statically independent, and many approaches for modeling noise are developed. The frequency-domain approach is based on the power spectral density (PSD) [7]. Several time-domain methods have been devised for stochastic modeling [4,14].The simplest and most used is the Allan variance time-domain-analysis technique, originally developed in the mid-1960s to study the frequency stability of precision oscillators [1, 2, 3, 5, 6, 12]. Allan variance is a directly measurable quantity and can provide information on the types and magnitude of various noise terms. The method has been adapted to random-drift

characterization of a variety of devices including MEMS accelerometers [15, 16].

In this paper, the Allan variance time-domain-analysis technique is used to characterize the 3-axis, 14-bit/8-bit digital accelerometer MMA8451Q.

2. ALLAN VARIANCE METHOD

If the instantaneous output of the accelerometer is $a(t)$, the cluster average is defined as:

$$\bar{a}_k(\tau) = \frac{1}{\tau} \int_{t_k}^{t_k+\tau} a(t)dt , \qquad (1)$$

where $\bar{a}_k(\tau)$ represents the cluster average of the output acceleration for a cluster which starts from the k-th data point. The definition of the subsequent cluster average is:

$$\bar{a}_{k+\tau}(\tau) = \frac{1}{\tau} \int_{t_k+\tau}^{t_k+2\tau} a(t)dt . \qquad (2)$$

The difference between the two cluster averages $d_k(\tau)$ is:

$$d_k(\tau) = \bar{a}_{k+\tau}(\tau) - \bar{a}_k(\tau). \qquad (3)$$

The variance of differences between every two adjacent cluster averages $\sigma_d^2(\tau)$ is given by:

$$\sigma_d^2(\tau) = \left\langle \left(d_k(\tau) - \mu_k\right)^2 \right\rangle , \qquad (4)$$

where: μ_k is the mean of $d_k(\tau)$; $\langle \ \rangle$ is the ensemble average.

The Allan variance as function of averaging time is defined as:

$$\sigma^2(\tau) = \frac{\sigma_d^2(\tau)}{2} . \qquad (5)$$

Since in digital accelerometers the output data are available in discrete form (5) becomes:

$$\sigma_d^2(nT) = \frac{1}{2(K-1)} \sum_{k=1}^{K-1} \left(d_k(nT) - \mu_k\right)^2 , \qquad (6)$$

where: n is the number of samples in one cluster; K is number of clusters; T is sample time.

It can be shown that the percentage error δ, in estimating the Allan standard deviation of the cluster due to the finiteness of the number of clusters is given by [10]:

$$\delta = \frac{1}{\sqrt{2\left(\frac{N}{n} - 1\right)}} , \qquad (7)$$

where N is the number of samples in the data set.

To ensure percentage error less than 25% the following expression is obtained from (7):

$$\frac{N}{n} \geq 9 \ \Rightarrow \ n \leq \frac{N}{9} \qquad (8).$$

Consequently the number of clusters has to be not less than nine.

Different types of random processes cause slopes with different gradients to appear on the log-log plot of Allan standard deviation [11], as shown in Figure 1. Furthermore, different processes usually appear in different regions of τ, allowing their presence to be easily identified [16].
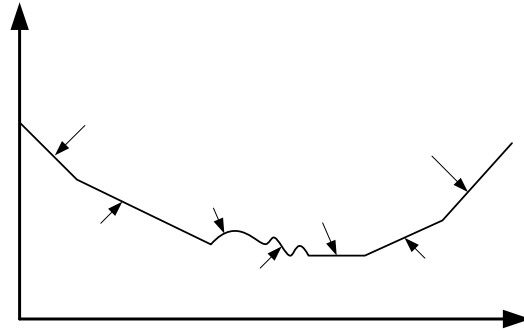
Figure 1. A possible log-log plot of Allan Deviation analysis results

The values of the parameters could be obtained directly from the plot. For a MEMS device such as MMA8451Q the important processes that have to be measured are random walk, bias instability and rate random walk.

The random walk is white noise and appears on the plot with a slope −0.5. The deviation of random walk is obtained by the following expression [11]:

$$\sigma_{rw} = \sigma(\tau_0)\sqrt{\tau_0} , \qquad (9)$$

where the plot of $\sigma(\tau)$ has the slope of −0.5 for $\tau = \tau_0$.

The bias instability appears on the plot as a flat region around the minimum. The deviation of bias instability is given by [11]:

$$\sigma_{bi} = \sigma(\tau_1)\sqrt{\frac{\pi}{2\ln(2)}} , \qquad (10)$$

"HENRI COANDA"
AIR FORCE ACADEMY
ROMANIA

"GENERAL M.R. STEFANIK"
ARMED FORCES ACADEMY
SLOVAK REPUBLIC

INTERNATIONAL CONFERENCE of SCIENTIFIC PAPER
AFASES 2014
Brasov, 22-24 May 2014

where τ_1 is chosen around the minimum of the plot.

The rate random walk is represented by a slope of +0.5 on a log-log plot of $\sigma(\tau)$ and its deviation is given by [11]:

$$\sigma_{rrw} = \sigma(\tau_2)\sqrt{\frac{3}{\tau_2}}, \qquad (11)$$

where the plot of $\sigma(\tau)$ has the slope of +0.5 for $\tau = \tau_2$.

3. RESULTS

The data from MMA8451Q is read using a device described in [13]. The accelerometer is set up to: 14 bits of resolution; ± 2 g full scale; 100 Hz output data rate. The data was collected for eight hours. Collected accelerations for each axis (x,y,z) are shown in figures from 2 to 4.
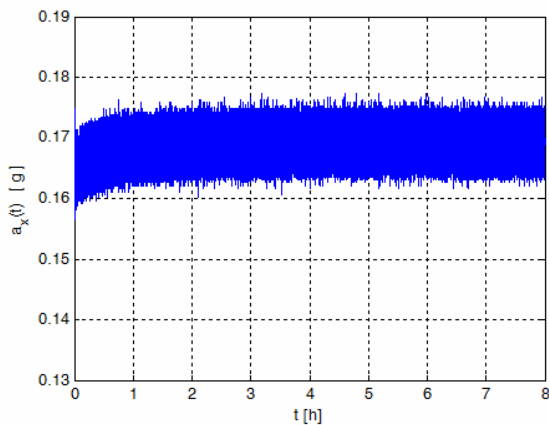
Figure 2. Measured acceleration in x-axis.
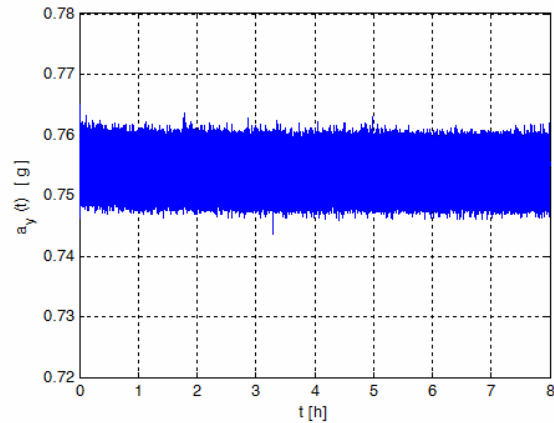
Figure 3. Measured acceleration in y-axis.
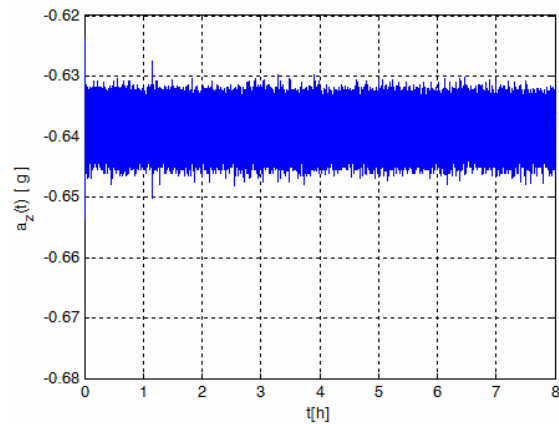
Figure 4. Measured acceleration in z-axis.

The orientation of the accelerometer was such that none of the axes was aligned with Earth gravity. The alteration of acceleration in each axis is of different character, consequently the accelerometer errors are different too.

Allan standard deviations for each axis (x,y,z) are presented in figures from 5 to 7.
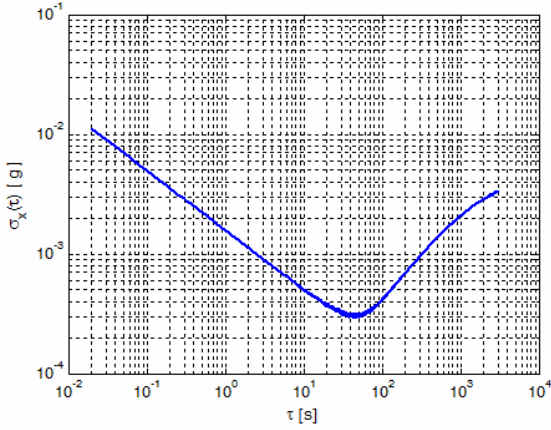
Figure 5. Allan standard deviation for x-axis.

Figure 5 shows that the slope of Allan Deviation curve for $\tau = 0.1 \div 1\,s$ is -0.5002. The value of $\sigma_{rw} = 1.5742\ mg$ is obtained for deviation of random walk, using equation (9) with $\tau_0 = 1s$. For the deviation of bias instability is measured $\sigma_{bi} = 0.46508\ mg$ at $\tau_1 = 45s$. The slope of Allan Deviation curve for $\tau = 70 \div 80\,s$ is +0.4928. Deviation of rate random walk is obtained from (11) at $\tau_2 = 75s$ and it is $\sigma_{rrw} = 0.0692\,mg\big/\sqrt{s}$.
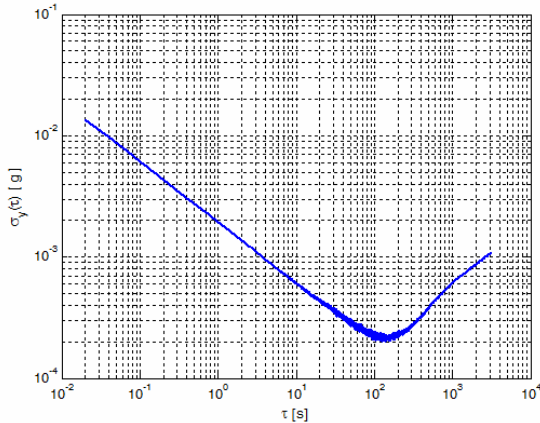
Figure 6 Allan standard deviation for y-axis.

Figure 6 shows that the slope of Allan Deviation curve for $\tau = 0.1 \div 1\,s$ is -0.4978. The value of $\sigma_{rw} = 1.9408\ mg$ is obtained for deviation of random walk, using equation (9) with $\tau_0 = 1s$. For the deviation of bias instability is measured $\sigma_{bi} = 0.3158\ mg$ at $\tau_1 = 142s$. The slope of Allan Deviation curve for $\tau = 280 \div 320\,s$ is +0.4970. Deviation of

rate random walk is obtained from (11) at $\tau_2 = 300s$ and it is $\sigma_{rrw} = 0.0930\,mg\big/\sqrt{s}$.
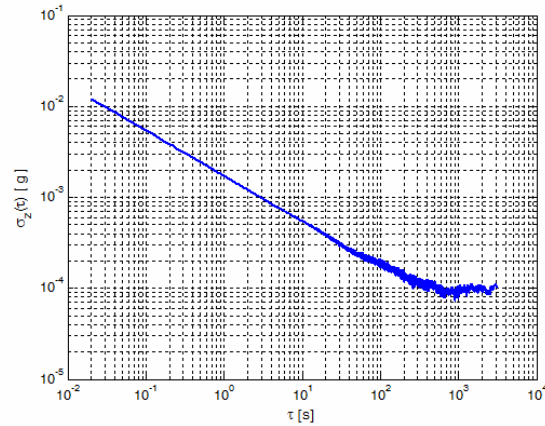
Figure 7. Allan standard deviation for z-axis.

Figure 7 shows that the slope of Allan Deviation curve for $\tau = 0.1 \div 1\,s$ is -0.5019. The value of $\sigma_{rw} = 1.7118\ mg$ is obtained for deviation of random walk, using equation (9) with $\tau_0 = 1s$. For the deviation of bias instability is measured $\sigma_{bi} = 0.1266\ mg$ at $\tau_1 = 940s$.   There isn't slope of Allan Deviation curve for obtaining the rate random walk.

According to MMA8451Q technical data the square root of power spectral density is $126\ \dfrac{\mu g}{\sqrt{Hz}}$ for output data rate (ODR) of 400 Hz. The minimum and maximum value of output data bandwidth is $\Delta f_{min} = \dfrac{ODR}{3}$ and $\Delta f_{max} = \dfrac{ODR}{2}$. Using these parameters a following range of random walk is obtained $\sigma_{rw} = 1.4549 \div 1.7819$ mg .

The relative Earth acceleration is calculated, using the following equation:

$$a = \sqrt{a_x^2 + a_y^2 + a_z^2}\ . \tag{12}$$

The calculated relative Earth acceleration is shown on figure 8.

"HENRI COANDA"
AIR FORCE ACADEMY
ROMANIA

"GENERAL M.R. STEFANIK"
ARMED FORCES ACADEMY
SLOVAK REPUBLIC

INTERNATIONAL CONFERENCE of SCIENTIFIC PAPER
AFASES 2014
Brasov, 22-24 May 2014
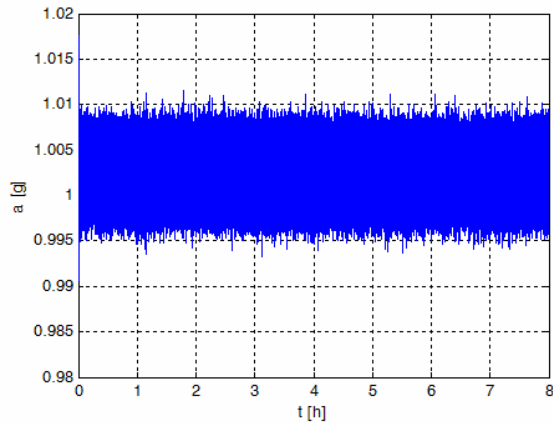
Figure 8. Relative Earth acceleration.

Allan standard deviations for measured Earth acceleration is presented in figure 9.
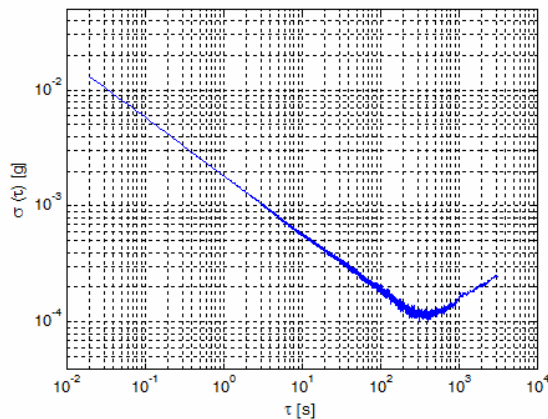
Figure 9. Allan standard deviation for measured Earth acceleration.

Figure 9 shows that the slope of Allan Deviation curve for $\tau = 0.1 \div 1\,s$ is -0.4991. The value of $\sigma_{rw} = 1.8390\,mg$ is obtained for deviation of random walk, using equation (9) with $\tau_0 = 1s$. For the deviation of bias instability is measured $\sigma_{bi} = 0.1746\,mg$ at $\tau_1 = 400s$.

4. CONCLUSIONS

The Allan-variance technique presented in this paper allows a systematic characterization of the various random errors in the output data of the digital accelerometer. The characteristic curves are obtained and different types and magnitude of error terms existing in the accelerometer MMA8451Q are determined.

The eight-hour static data from the MMA8451Q were investigated. Most of the results from the Allan-variance analysis are close to the manufacturers' claim, which proves that the method presented in this paper is valid.

There isn't a slope of -1 on plot of Allan standard deviations (Fig.5-7). Consequently the quantization errors are much less than other errors and can be ignored.

The results of the MMA8451Q clearly indicate that the random walk is the dominant error term in the short cluster time, whereas the bias instability and rate random walk terms are the dominant errors in the long cluster time.

The experimental results have provided a useful evaluation of a low-cost accelerometer MMA8451Q.

REFERENCES

1. Allan D. W., *"Statistics of atomic frequency standards,"* Proc. IEEE, vol. 54, no. 2, (1966).
2. Allan D. W., *"Time and frequency (time-domain) characterization, estimation, and prediction of precision clocks and oscillators"*, IEEE Trans. Ultrason., Ferroelectr., Freq. Control, vol. UFFC-34, no. 6, (1987).

3. Allan D. W., Barnes J. A., *"A modified "Allan Variance" with increased oscillator characterization ability"*, in Proc. 35th Annu. Freq. Control Symp., (May 1981,).

4. Bendat J. S., Piersol A. G., *Measurement and Analysis of Random Data*, New York: John Wiley and Sons, (1966).

5. Chaffee J.W., *"Relating the Allan variance to the diffusion coefficients of a linear stochastic differential equation model for precision oscillators"*, IEEE Trans. Ultrason., Ferroelectr., Freq. Control, vol. UFFC-34, no. 6, (1987).

6. Conroy B. L., Le D., *"Measurement of Allan variance and phase noise at fractions of a millihertz"*, Rev. Sci. Instrum., vol. 61, no. 6, (1990).

7. EI-Sheimy N., *Analysis and Modeling of Inertial Sensors Using AV*, IEEE Transaction on instrumentation and measurement, vol. 57, No.1, (2008).

8. Grewal M. S., Weil L. R., Andrews A. P., *Global positioning systems, inertial navigation, and integration*, Wiley, (2007).

9. Hulsing R., *"MEMS Inertial Rate and Acceleration Sensor"*, IEEE Position Location and Navigation Symposium, (1998).

10. IEEE Std 952-1997, IEEE Standard *Specification Format Guide and Test Procedure for Single Axis Interferometric Fiber Optic*, 16 (1997)

11. IEEE Std 962-1997 (R2003) *Standard Specification Format Guide and Test Procedure for Single-Axis Interferometric Fiber Optic Gyros,* Annex C. IEEE, (2003).

12. Lesage P., Audoin C., *"Characterization of frequency stability: Uncertainty due to the finite number of measurement"*, IEEE Trans. Instrum. Meas., vol. IM-22, no. 2, (1973).

13. Petrov Zh., Marinov M., Dimitrov D.,*3-axis digital accelerometer data transfer controller,* Scientific conference , Aviation Faculty, D. Mitropolia, Bulgaria (2013).

14. Sinha N., Kuszta K., B., *Modeling and Identification of Dynamic Systems*, New York: Van Nostrand Reinhold, (1983).

15. Titterton D.H., Weston J.L., *Strapdown inertial navigation technology* -2nd ed, Institution of electrical engineers, UK, (2004)

16. Woodman *O.J., An introduction to inertial navigation*, Cambridge, (2007)

.

“HENRI COANDA”
AIR FORCE ACADEMY
ROMANIA

“GENERAL M.R. STEFANIK”
ARMED FORCES ACADEMY
SLOVAK REPUBLIC

ON BOARD DIAGNOSIS IMPLICATIONS ON THE VIABILITY OF MILITARY PATROL AND INTERVENTION VEHICLES

Marian MITROI*, Cornel ARAMĂ**

*Faculty of Mechanical Engineering,”Transilvania” University of Braşov, Braşov, Romania
**”Henri Coandă” Air Force Academy, Braşov, Romania

Abstract: The constant uses of sensors, high performance actuators, as well as informatics have imposed an upward trend to the hardware and software electronics auto. In these situations the control and the management of the vehicles is very important, mainly for those which have a military purpose. The need of an on board computer diagnosis of military intervention vehicles is very useful and necessary, due, at first, to the accoutrement of any kind of vehicle equipped with a lot of electronics equipment. Secondly, the on board display of the operating parameters also offers the possibility to improve the vehicles operating in order to succeed in the combat missions.

Keywords: viability, reliability, diagnosis equipment, experimental determinations.

1. VIABILITY/RELIABILITY

The viability is the reliability of the military technique assets to which a practical and tactical assembly of measures and preoccupations is added (the capacity of military technique assets and people to avoid the wastage, to avoid in time the enemy's gun strikes and their ability to fast recover their strike, fire, maneuvers and protection capacities) that guarantee the fulfillment of the intervention [1].

The reliability studies need to be done in order to:

a) freely operate the systems on which the vehicle depends to travel safety;
b) ensure a level of reliability suitable for relatively simple devices, but whose failure could attract major faults;
c) plan maintenance activities;
d) increase the efficiency of transport by reducing turnaround times.
e) spare inventory planning;
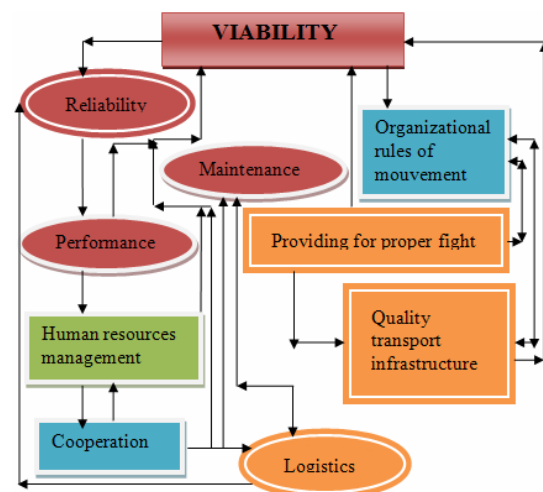
Fig.1 Interdependency of viability factors [1]

Analyzing the expenses incurred, the reliability of a device can be represented according to the schedule:
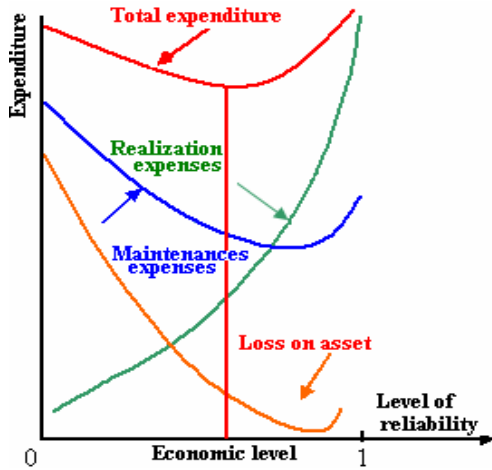
Fig. 2 Economic level of reliability[2]

Characteristic situations:
* the technical criteria prevail $\Rightarrow R \rightarrow 1$;
* the prevailing economic criteria $\Rightarrow R_{economic.}$
Take account of: the destination vehicle, the user possibilities.

The viability factors of military vehicles:

1. reliability;
2. vehicles performance;
3. efficiency of the maintainability and maintenance works;
4. rules providing the movement;
5. combat service;
6. combat service support;
7. the quality of transport infrastructure;
8. human resources management;
9. cooperation and collaboration for support.

From the qualitative point of view, *reliability* is the ability of a device found in given conditions of use, to perform specific functions for a certain period of time [2].
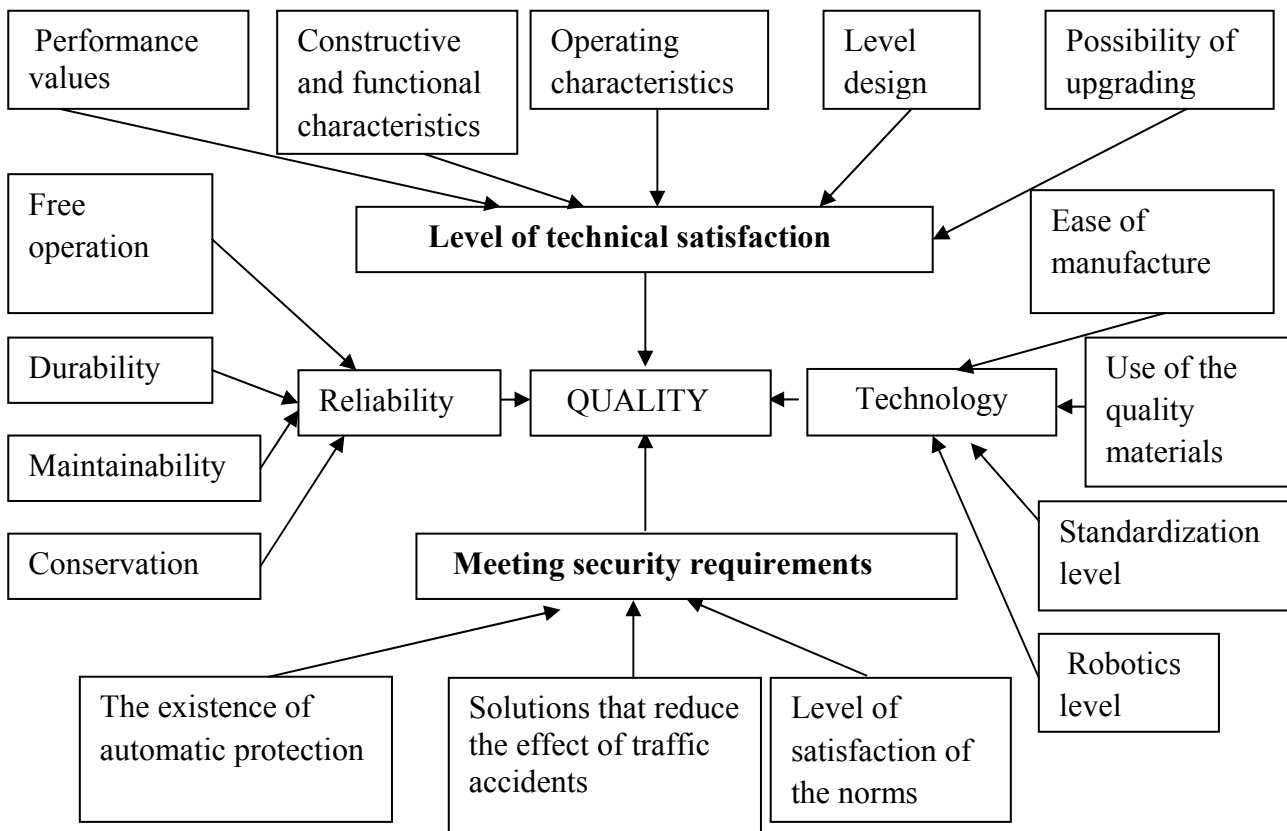
Fig. 3 Report of reliability, quality and technology[2]

"HENRI COANDA"
AIR FORCE ACADEMY
ROMANIA

"GENERAL M.R. STEFANIK"
ARMED FORCES ACADEMY
SLOVAK REPUBLIC

INTERNATIONAL CONFERENCE of SCIENTIFIC PAPER
AFASES 2014
Brasov, 22-24 May 2014

The approach of reliability, maintenance motor performance as well as human resources management, is mostly similar in military and civil field.

The reliability and durability of engines, as well as the other assemblies, depend largely on the quality of maintenance work carried out for every season, as well as the quality of materials and supplies used for this purpose. Also, the time and the quality of intervention, how this takes place has a special role.

Maintenance represents all the organizational and technical activities done in order to maintain and re-establish the technical state of a product so that this product could fulfill all the functions it was created forǎ[3].

Depending on the technical condition and the time they are performed, maintenance can be:
- predictive;
- preventive;
- corrective;
- planned;
- based on diagnosis;
- based on state.

In the current conditions of military actions, when the reaction rate has an important role, and the possibilities of unannounced interventions taken to the extreme are also present, the use of viable vehicles that meet successfully the imposed requirements is impetuously needed.

The ability of technical systems of patrol and intervention cars to function optimally can decrease from a mission to another by the occurrence of abnormal functioning. They are found stored as codes in the vehicle management system.

Errors generated on computer boards about the engine system operation, broken security, as well as ABS or ESP, can be managed using electronic "On-Board" Diagnosis (OBD).

Diagnostic work currently occupies a very important position within the terotechnical system. Early detection of any malfunction during operation could reduce the consequences arising from their timely remedy as well as the subsequent intervention cost.

Pattern of asset maintenance system design vehicles may be shown as follows:
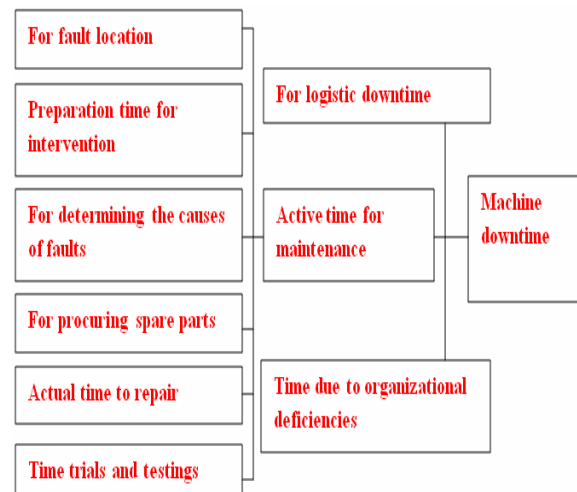
Fig. 4 Pattern of maintenance[3]

The diagnosis in vehicles can monitor in real time, but it can also identify in useful time the problems which occur to the entire management system of the vehicle.

The exploitation and the operation optimization are very important problems and need to maintain focus on the responsible factors because this is the key to maintain a high level for a good intervention and combat capacity.

2. DIAGNOSIS EQUIPMENT

The equipment for diagnosis are designed to optimize maintenance activity for

different electric, electronic, electromechanic or hydraulic systems existing in each vehicle component by reducing the time allocated to intervention on their operations.

An example of OBD system is shown in the following figure:

Fig. 5 ELM327 BLUETOOTH MICRO [6]

Very small size: 5 x 4.5 x 2.5 cm

Weight: 32 g

High baud rate: 38400 bps

Bluetooth 3.0

Reads:

- engine parameters;
- probes;
- flowmeters ;
- fuel intake : l/h and l/100km ;
- power calculation ;
- time calculation from /to 100km ;
- clear the error message.

It supports the following communication protocols:

ISO15765-4 (CAN)

ISO14230-4 (KWP2000)

ISO 9141-2

J1850 VPW

J1850 PWM

It can diagnose almost any type of car mode after 1996 which plug s type is OBD II.

It supports the functional operating systems:

- Windows XP, Vista, Windows 7;
- Mac;
- Symbian;
- ANDROID[6].

Because its operating system is ANDROID, this device is very practical and it can easily be used before every mission by all the drivers by simply using a cellphone soft named: "**Torque**".
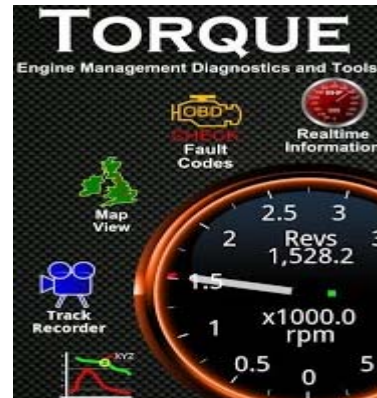
Fig.6 Display of program [6]

A part of technical fault codes which can be read by this OBD system is presented on the point 2.1 and the understanding of them on the 2.2 point.

2.1 Technical fault code (DTC)

17965 – Overload control – positive deviation:
P1557 - 35-10 - - - intermittent;
01039 – Temperature transducer-G2-
30-10 – open or short circuit to plus –
intermittent;
00930 – Closing overall - F222- block left
27-00 - implausible signal;
01312 - Bus date drivetrain
37-10 - Defect – intermittent;
00778 – Steering angle sensor -G85-
49-10 – No communication-
intermittent;
00516 - Contact closed throttle idle-F60-
30-10 - Open or short circuit to B+
– intermittent;
01249 - Cylinder injector 1.-N30-
31-10 – Open circuit or short to ground
– intermittent;
00532 – Power supply B+
- low signal – intermittent;
1316 - Control module ABS
49-10   –No communication
intermittent [5].

2.2 The understanding of fault codes

Positive deviation load: the signal comes from the air inlet circuit. It can be a problem at the pressure regulator or at the valve that makes the turbine not to work property;

"HENRI COANDA"
AIR FORCE ACADEMY
ROMANIA

"GENERAL M.R. STEFANIK"
ARMED FORCES ACADEMY
SLOVAK REPUBLIC

INTERNATIONAL CONFERENCE of SCIENTIFIC PAPER
AFASES 2014
Brasov, 22-24 May 2014

Open circuit or short to plus (B+)-intermittent: sensor fault occur after cooling circuit located on the cylinder head;

Implausible Signal: error occurs when closing door system detects continuity in the electrical signal;

Bus date drivetrain: failure occurs due to lock of electrical signal on one of the relay that sends tension to the ECU;

Open or short circuit to ground – intermittent: the code is generated due to a short circuit to ground or to the control circuit of the given circuit;

Low signal– intermittent: in this case it is a low voltage on the positive < 11,5v;

No communication –intermittent: due to an inappropriate tension, the command mode of the system can not send date to ECU.

3. EXPERIMENTAL DETERMINATIONS

Monday, 25th , February, 2014,15:12:19:55062
   Data version: 20100326
   Addresses scanned: 01 02 03 08 15 16 17 19   35 36 37 46 47 55 56 57 58 75 76 77
   Controlled composition: 1,9l R4 EDC G000AG 1464
   Workshop: WSC 02410
         Determinations were made on intervention and patrol vehicles type VW Transporter Syncro. The diagnose equipment used was: ELM 327 Blue Tooth, VCDS 12.12, and software Torque, Vital Scan, Vag-Com ROJ 12.12.

3.1. Functional parameters

   Group 001: Quantity Injection
  882 /min Engine Speed (G28)
  8.2 mg/race Quantity Injection
  7.1*KW Injection Duration Magnetic Valve

62.1*C Antifreeze - Temperature (G62)
   Group 003: Gas Recirculation (EGR)
861 /min Engine Speed (G28)
285.0 mg/race Air Mass Absorbed (req.)
416.5mg/race Air Mass Absorbed (meas.)
4.8 % Activity EGR-Valve
   Group 004: Aquator Valve for Pump/Duse
861 /min Engine Speed (G28)
-0.0 *DPMS Start Injection TEOR-Wert
7.7*KW Duration Injection TEOR-Wert
1.7*KW Sync - Angle
   Group 005: Start Conditions (last start)
4641 /min Engine Speed (G28)
9.1 mg/race Quantity Start
48.0 Start - Sync
52.2*C Antifreeze - Temperature (G62)
   Group 007: Sensor Temperature (engine warm)
69.3*C Energy - Temperature (G81)
0.0 %   Fuel cooling status
49.5*C   Manifold   Admission-Temperature (G42)
62.1*C Antifreeze - Temperature (G62)
   Group 010: Mass air
426.3 mg/race Absorbed - Mass air
999.6 mbar Atmospheric Pressure
994.5 Pressure Adm.
0.0 % Accelerator Position Pedal
   Group 011: Turbo Pressure Control
882 /min Engine Speed (G28)
1091.4 mbar Turbo Pressure (pres.)
994.5 Turbo Pressure (meas.)
19.9 % Activity Solenoid Valve
   Group 013: Idle Adjustment
0.71 mg/race Cylinder 1
-0.26 mg/race Cylinder 2
0.05 mg/race Cylinder 3
-0.54 mg/race Cylinder 4
   Group 015: Fuel Consumption
882 /min Engine Speed
8.2 mg/race Quantity Injection (meas.)

1.00 l/h Fuel - Consumer
0.0 mg/race Injection Quantity (desire)
[7].

3.2. Diagnostic interpretation

Group 003

It can be seen the fault of the air received by the engine. This is mainly due to the peacemaker valve which does not come back to the normal position after leaving the circuit in order to open the admission circuit.

Group 004

Injection occurs immediately after TDC and creates a mismatch between the angle of camshaft timing that normally has a value up to 1,5 KW. Situation occurs due to the change of distribution or some operation where the camshaft sprocket was at the beginning.

Group 011

The lock of adequate pressure on the blower at a small value creates a negative deviation and it is caused by some air leakage on the hoses path or connections, but it can also be generated by the malfunction of the turbocharger geometry.

Group 013

The injectors from the 1-st and/or 3-rd cylinder work on unsuitable parameters. The 1-st injector shows a light un-calibration distributing a larger amount of diesel fuel or it compensates the 3-rd injector that seems to be stifled.

Group 015

It can be noticed that although the vehicle is running at idle and the consumption is above normal. This is due to the function of the injection above normal parameters.

4. CONCLUSIONS

A simple On-Board Diagnosis, which usually takes between 7-10 minutes, may highlight certain aspects of operation of military vehicles patrol on response, manager issues that can make it hard or impossible to accomplish the mission given. The On-Board Diagnosis operation significantly reduces maintenance time spent from the military vehicles without being operational and it can improve their viability.

So, we can say that the possibility of a vehicle to execute the mission in the best conditions can be expressed best by viability factors and a lot of them are directly and significantly influenced by OBD systems.

REFERENCES

1. Aramă, C., *Investigation of Possibilities to Improve the Performances of Special Vehicles*, "Transilvania" University of Braşov, Doctoral degree thesis, 2006;
2. *University" POLITEHNICA"of Bucharest Reliability Vehicles Courses*
3. Pomazan, N., *Termotechnica Car Guide*, Publishing House: "Ovidius " University of Constanța, 2006;
4. Mitroi, Marian, *University Courses*, Publishing House: "Ovidius " University of Constanța, 2013;
5. Mitroi, Marian, *Individual Tests and Measurements,* Constanța, 2014
6. http://www.elm327.net
7. http://www.Ross-Tech.com

EXPERIMENTAL RESEARCH CONCERNING THE INFLUENCE OF THE ON-BOARD HYDROGEN SUPPLY EQUIPMENT ON THE ENGINES COMBUSTION

Marius Nicolae MOLDOVEANU*, Cornel ARAMĂ**

*Sunrise Technology Co. Ltd, Jiaxing, Zhejiang, China,
** "Henri Coandă" Air Force Academy, Brasov, Romania

Abstract: *The rational use of fuels and the decreasing of IC (Internal Combustion) engines pollution are fundamental requirements which were globally emphasized by the traffic authorities. As a transition solution to the propulsion system which is nowadays named "unconventional" but, at the same time, as a viable possibility to improve the IC engines performances of the future HV's (Hybrid Vehicles), some researchers suggest the solution of Semy-Hybrid hydrogen fuelling system. This study is included in the same activity area but it has to be mentioned that the researchers have begun from a different idea: the hydrogen is not "the real culprit" for the positive results which were sometimes reported. The key of problem is a substance which is fully presented but it was neglected by the majority: the nitrogen.*

Keywords: *Semy-Hybrid vehicle, nitrogen, nitro-hydrogen additivation, Pre-Combustion Treatment Technology (PCTT)*

1. INTRODUCTION

The rational use of fuels and the decreasing of IC (Internal Combustion) engines pollution are fundamental requirements which were globally emphasized by the traffic authorities. Due to these, the OEM's invest more and more resources. The HV's (Hybrid Vehicles) and first of all the EV's (Electric Vehicles) are remarkable developing in the last years. Unfortunately the global economic crisis influenced this process negatively and partly stopped it before some aspects (which had decreased the costumer's interests: the acquisition price, the limited range, the technological constructive difficulties etc.) to be solved.

As a transition solution to the propulsion system which is nowadays named "unconventional" but, at the same time, as a viable possibility to improve the IC engines performances of the future HV's, some researchers suggest the solution of Semy-Hybrid fuelling system. These fuelling systems are based on the on board hydrogen supply equipment. All of them insist on the unquestionable positive effects of the hydrogen use together with conventional fuels (first of all, gasoline and diesel fuel).

Unfortunately, the researchers who were interested in the scientific study of these kinds of fuelling systems (which are sometimes named Semi-Hybrid) have noticed that the results from the tests were contradictory in too many situations and in the end, the energy balance was a negative one.

The aim of this paper is to explain why this phenomenon is happening and to try to explain

how it is possible that the use of hydrogen does not have a positive effect on the fuel consumption and on the IC engines pollution for all the working conditions…

2. GENERAL RESEARCHES TRENDS IN THIS DOMAIN

Hydrogen as a fuel for automotive IC engines has had a long history of study in the academic and industry area. The properties that contribute to its use as a combustible fuel are well known: wide range of flammability, low ignition energy, small quenching distance, high auto ignition temperature, high flame speed at stoichiometric ratios, high diffusivity and very low density. Nowadays, the main researches are focused on using it as independent fuel or in developing the fuel cells. In this paper it is going to be discussed the situation of the IC engines which are using the conventional fuel enriched with hydrogen.

The use of hydrogen as an additional fuel to gasoline has been considered since the early '70, the alternative to the full hydrogen powered engine. Relying on its characteristics, all the producers or commercial firms advertise for their on-board hydrogen system gadgets because, from their points of view the Oxy-Hydrogen gas (the mixture called HHO, Aguygen gas, Brown gas, Hydroxy or EEW-Electrically Expanded Water) obtained from water electrolysis may improve the combustion's chemicals reaction and also increase the water formation as by product of combustion.

This work, which was performed at JIAXING SUNRISE TECHNOLOGY CO. LTD is included in the same activity area but it has to be mentioned that the researchers have begun from a different idea: the hydrogen is not "the real culprit" for the positive results which were sometimes reported. **The key of problem is a substance which is fully presented but it was neglected by the majority: the nitrogen**.

3. EXPERIMENTAL DETAILS/ NITRO-HYDROGEN ADDITIVATION

For our situation, the IC Engine seen as a thermodynamic and thermochemistry system looks as in figure 3.1.

Note: the other components from the air were neglected because of lower percentage and the low influence on the combustion.

Nitrogen is essentially chemically neutral and does not react in the combustion process. Its presence, however, does affect the temperature and pressure in the combustion chamber. This is a general statement of the researchers in the IC engines. But, in case of On-board electrolyzers the situation could change radically.

The nowadays situation:

The lean-burning nature of diesel engines and the high temperatures and pressures of the combustion process result in significant production of Nitrogen oxides, and provide a unique challenge in reducing these compounds. Modern on-road diesel engines typically must use selective catalytic reduction to meet emissions laws, as other methods such as exhaust gas recirculation cannot adequately reduce NO_x to meet newer standards in many jurisdictions. However, the fine particulate matter (sometimes visible as opaque dark-colour smoke) has traditionally been of greater concern in the realm of diesel exhaust.

Actual pollution reduction technologies are sophisticated (and expensive): electronic injection systems correlated to various sensors and coordinated by ECU (Electronic Computer Unit) corroborated with EGR (Exhaust Gas Recirculation) systems, DPF (Diesel Particulate Filters), catalysts systems and DEF (Diesel Exhaust Fluid) (commonly referred to it as AdBlue).

A new approach of the emissions problem was highlighted by US Department of Transportation report from 2007: "*Onboard electrolyzers are used with hydrogen injection systems for diesel engines. In this case, only a small amount of hydrogen and oxygen is produced to supplement, not replace, the diesel fuel used in the engine. The electricity to operate the electrolyzer is typically supplied by the engine's alternator or 12/24-VDC electrical system*".

"HENRI COANDA"
AIR FORCE ACADEMY
ROMANIA

"GENERAL M.R. STEFANIK"
ARMED FORCES ACADEMY
SLOVAK REPUBLIC

INTERNATIONAL CONFERENCE of SCIENTIFIC PAPER
AFASES 2014
Brasov, 22-24 May 2014
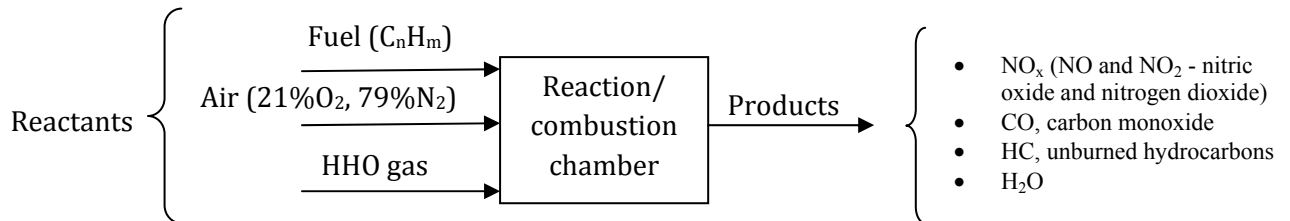
Fig. 3.1 The IC Engine seen as a thermodynamic and thermochemistry system
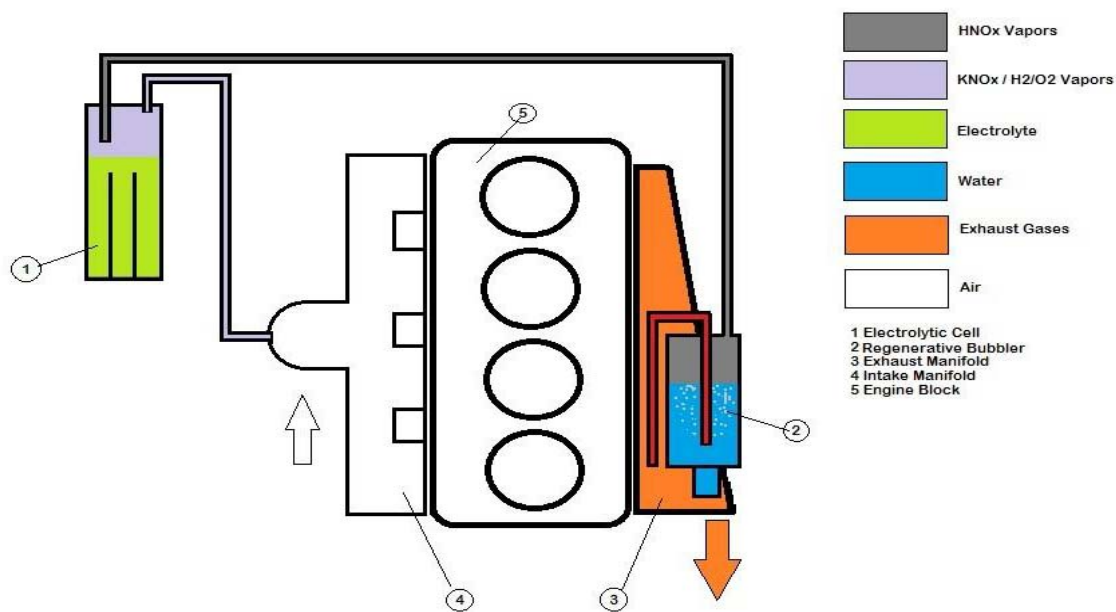
Fig. 3.2 The Pre-Combustion Treatment Technology (PCTT)

Oxy-Hydrogen (the mixture called HHO) obtained from water electrolysis may improve the combustion's chemicals reaction and also increase the water formation as by product of combustion. Water will be converted into steam and that act as carbon deposits cleaner and enhance the pressure on the explosion stroke. The addition of HHO is effective technology but is limited to efficiency of the system, the type of engine and operational parameters.

In conclusion, all the technologies in use are applied as a post combustion phase as passive methods or involve extra energy to operate (in case of HHO methods). Post combustion methods are expensive and resource consuming. NO_x and unburned particulates generation and reduction mechanisms are opposite and achieving both

results require a complex system. None of them are designed to solve the main pollution problem: actual engines park!

The Pre-Combustion Treatment Technology (PCTT):

Considering the facts that diesel engines already produce Nitrogen Oxides and the addition of HHO increases the temperature and this fact creates conditions to produce NOx, an active method called **Pre-Combustion Treatment Technology** (PCTT) was developed in order to reduce both NO_x and soot – particulate matters - from exhaust gases. A combination between HHO generator and a regenerative bubbler (RB) were used as it can be seen in figure 3.2.

The RB is fixed to exhaust manifold and use the EG (Exhaust Gas) temperature to warm up the water content where a small amount of EG is bubbled then transferred to HHO cell. The alkaline type Oxy-Hydrogen generator (an electrolytic cell) produces the HHO gas and water vapors, contaminated with electrolyte (usually KOH).

The Regenerative Bubbler contains water which is bubbled a small amount of EG in order to produce HNO_3 (nitric acid). As it is well known, the nitric acid is one of the strongest inorganic (mineral) acids. It is, at the same time, in pure state or concentrated, a very powerful oxidant. The nitric acid is very toxic, very corrosive and it can destroy different materials which get in contact with it (from the weaves to the metals). The nitric acid is very used in explosive industry where it is one of the most important substances. An example: the nitro-glycerine and other explosive substances are obtained by nitration.

Combined, the oxidant KNO_2/HNO_3 and extra H_2 and, in some conditions, ammonia, NH_3, is generated in a Oxy-Hydrogen rich flow of mixed steam. In terms of energy conservation our technology is synergetic and regenerative since the use of the elevated exhaust gases temperature to increase water temperature, induces the conditions of NO_x reaction and produces supplemental steam, then using a chemical reaction to neutralize both KOH and HNO_x vapors to almost neutral pH salt KNO_x. Oxy-Hydrogen positive effect is enhanced by Nitrogen's chemical reaction

and the presence of extra volumes of water in the form of steam.

In short, for this situation, the chemical reactions are:

$$2H_2O = 2H_2 + O_2$$
$$2H_2O = H_3O + OH$$
$$3NO_2 + H_2O = 2HNO_3 + NO$$
$$4NO + 6H_2O = 4NH_3 + 5O_2$$
$$2NO + 2KOH = 2KNO_2 + H_2$$
$$HNO_3 + KOH = H_2O + KNO_3$$
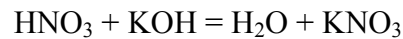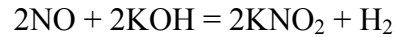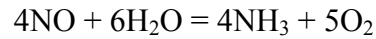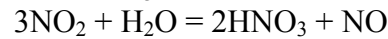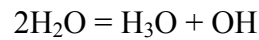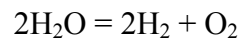
The bubbler is shown in figure 3.3 and the electrolytic cell in figure 3.4.

Fig. 3.3 The bubbler

Fig. 3.4 The electrolytic cell

Preliminary results/conclusions:

The equipment based on the water ionization/electrolysing in order to produce the HHO gas and which has been made so far for decreasing the fuel consumption and pollution are not the final solution. The effects sometimes positive are due to some complicated chemical reactions which are produced (or they should be produced) in the combustion chamber as a result of captive fire gases (which resulted from the former

"HENRI COANDA"
AIR FORCE ACADEMY
ROMANIA

"GENERAL M.R. STEFANIK"
ARMED FORCES ACADEMY
SLOVAK REPUBLIC

INTERNATIONAL CONFERENCE of SCIENTIFIC PAPER
AFASES 2014
Brasov, 22-24 May 2014

combustion cycle or captured with the support of EGR) and mainly due to the different forms of water which followed the electrolyse gas. This is the reason why the dry electrolyse gas does not have significant effects.

The oxy-hydrogen which was produced by the used generator provides steam and gases with ammonia smell due to some volumes of the reactive nitrogen which are in the exhaust gases. When salt water (NaCl) was introduced in equation, powerful explosions appeared into bubbler despite of lack of ignition source which could explain the phenomenon (note: into the bubbler is a mixture of oxygen and hydrogen which is flammable but with the condition of existence of ignition source). These explosions destroyed the bubbler. A possible explanation: it is known that the gaseous ammonia has sometimes a violent reaction with the chlorine. In this situation, the gaseous ammonia inflames and the result is a fog consisting of ammonium chloride as it can be seen in the next chemical equations:

$$2NH_3 + 3Cl_2 = N_2 + 6HCl$$
$$6NH_3 + 6HCl = 6NH_4Cl$$
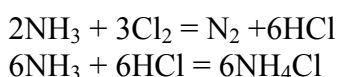
Another possibility to create a supplementary engine torque is forming ANFO mixtures (*ammonium nitrate-fuel oil* - blasting agents representing the largest industrial explosive manufactured, in terms of quantity, in the United States) by nitration of engine lube oil and the ANFO detonation with the support of hydrogen produced by the electrolysing on-board equipment.

4. CONCLUSIONS: POSSIBILITIES TO DEVELOPE THE ON-BOARD HYDROGEN SUPPLY EQUIPMENT TOGETHER WITH SOME ORIGINAL AUXILIARY INSTALLATIONS

Briefly, the main developing directions for this area are shown in Table 4.1.

The situations 2, 3, 4 and 8 are the current on-board hydrogen supply equipment. In this case A, B, E and G are obtained. The former HHO supply plants are shown in 1, 3 and 8 cases. These had a lower efficiency to produce hydrogen but they had high water volumes. In these situations A, B, C, E, F and G can be obtained. Nowadays, the situations 2, 3, 6 and 8 are tested. The water injection system (situation 9) has good results and it can work with the possibilities 2 ,3 and 6.

The hydrogen cannot be used as a simple engine fuel only if it is in high volumes which are impossible to be produced on-board. Moreover, it is not more efficient than classic hydrocarbons (because of generation difficulties) and it is very dangerous in exploitation. It is unlikely for a distribution network to be realised soon in order to solve the problem of "hydrogen economy".

As a final conclusion, the fundamental paradigm (general conception) changing, the use of nitrogen from the environment air, of the water and some chemical substances cheap and abundant as ingredients in the combustion chamber in order to obtain explosive substances could ensure a slower and more efficient transition to "electrical economy".

Table 4.1

	Possibilities:		It could be obtained:
1	The water electrolysing with acid electrolyte	A	Ionized water
2	The water electrolysing with alkaline electrolyte	B	Oxygenated water
3	The combustion chamber residual EG use	C	Nitrogen acids
4	The EGR (if it exists) exhaust gas use – without bubbling	D	Ammonia
5	The EG use by building of EGR type route – without bubbling	E	Nitrogen salts
6	Using of a bubbler for the recovered EG	F	Hydrocarbon nitrates
7	The using of additives or fuel mixtures or/and lube oil which could be nitrated	G	Gas hydrogen, gas oxygen – HHO (the name adopted in this situation)
8	The water injection into combustion chamber		
9	The water and different additives injection		

REFERENCES

1. Apostolescu, N., Chiriac, R., *A study of combustion of hydrogen – enriched gasoline in a spark ignition engine*, SAE Paper 960603, (1996).
2. Conte, E., Boulouchos, K., *Influence of hydrogen – rich – gas addition on combustion, pollutant formation and efficiency of a IC–SI engine*, SAE Paper 2004-01-0972, (2004).
3. Shinagawa, T., Okomura, T., *Effects of hydrogen addition to SI engine on knock behavior*, SAE Paper 2004-01-1851, (2004).
4. Wiseman, G. *Proof that On Board Brown's Gas (BG) Generation and Supplementation Works,* Available: http://www.eagle-research.com/cms/node/443 (March, 2011).
5. Thomas G., Parks G., *Potential Roles of Ammonia in a Hydrogen Economy, A Study of Issues Related to the Use Ammonia for On-Board Vehicular Hydrogen Storage*, U.S. Department of Energy (December, 2006).
6. Müllera I., Cederbaum L., *Ionization and double ionization of small water clusters,* The Journal of Chemical Physics 125, (November, 2006).

"HENRI COANDA"
AIR FORCE ACADEMY
ROMANIA

"GENERAL M.R. STEFANIK"
ARMED FORCES ACADEMY
SLOVAK REPUBLIC

INTERNATIONAL CONFERENCE of SCIENTIFIC PAPER
AFASES 2013
Brasov, 23-25 May 2013

ASPECTS OF THE POWER BALANCE FOR LASER CUTTING PROCESS

Mihaela NISTORAN-BOTIŞ*, Remus BOBOESCU**,

*Mechanical Faculty, University Politehnica, Timişoara, Romania, ** Engineering, Faculty, University Ioan Slavici, Timişoara, Romania

Abstract:.*Oxidation of iron in oxygen is an important power source for cutting steel through thermal processes.For oxygen-assisted laser cutting of steel plates energy to melt the material is given by the oxidation reaction and the laser beam radiation.It provides a way to assess the contribution to material melting of two physical phenomena.The material is removed in the molten state.On the basis of the cut shape are calculated power consumed to start the oxidation reaction and power given by reaction.The efficiency of the cutting process is expressed as dimensionless fractions.*

Keywords: *laser oxygen cutting,steel, specific energy.*

1. INTRODUCTION

The cutting of materials by a thermal process can be helped by the presence of reactive gas which together with material removal effect support a chemical exotherm reaction which brings energy to the erosion front [1],[2]. Using oxygen to cutting by melting of iron base materials is due to a favorable conjuncture of situations that make this possible. Thus the combustion of iron from steel in oxygen liberates sufficient calories to compensate heat losses by conduction, convection and radiation and heated the reaction products so as to keep the local temperature of workpiece to iron ignition.

Temperature for ignition of the reaction should be close to the melting temperature of the metal. Also, the melting temperature of the formed oxides` should be close to the melting temperature of the metal so that all the reaction products are liquid and can be removed by the kinetic effect of the gas as they are formed.

At forming temperature oxides can be, solid, liquid or gas. For solid oxides forms a layer which prevents contact between oxygen and metal stops metal burning. This is the case of alumina is formed on the surface of the aluminum for thermal cutting of aluminum. The formation of a reaction product gas, such as carbon monoxide, is an obstacle. Gas layer produced adheres to the melt metal surface by absorption and hinder the access of oxygen.

Contaminate the oxygen which will slow down the combustion. Liquid oxide formation is favorable to reaction propagation. They have a catalytic role. The liquid oxides can be removed simultaneously with liquid molten metal. To maintain the oxidation reaction is important contact between the reactants at the molecular level.

2. OXIDATION REACTION

Metals and gases that satisfy these conditions to enable the use of a reactive gas for machining are limited:

- iron in oxygen:

$$2Fe + 2O_2 = Fe_3O_4 + 270.8 \text{ Btu}; \qquad (1)$$

- copper in chloro:

$$2Cu + 2Cl = Cu_2Cl_2 + 70.8 \text{ Btu} \qquad (2)$$
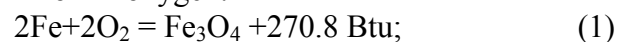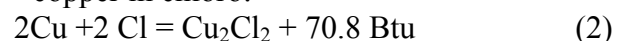
(Cu_2Cl_2 melts at $420^{o}C$);
- tin in chloro:

$$Sn + 4Cl = SnCl_4 + 129.6 \, Btu \qquad (3)$$
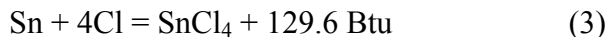
($SnCl_4$ is liquid at ambient temperature).

Cutting copper and tin with chloro in the role of reactive gas may not be made because chloro is a toxic gas.

In the presence of oxygen and iron from the steel oxidizes slowly to ambient temperature. As the temperature increases the oxidation is accelerated. For temperature of $1300^{o}C$ reaction becomes quasi-instantaneously. This temperature is called the ignition temperature.The ignition temperature depends also on the material. It is known that over the temperature of $1000^{o}C$ and the oxidation reaction becomes significant at temperatures of $1350^{o}C$ or $1400^{o}C$ is almost instantaneous [5] [6] .In some cases it is considered the temperature of $1200^{o}C$[5]. Following iron oxides are formed FeO, Fe_2O_3, Fe_3O_4. All these oxides are formed by a strong exothermic reaction while reaction is fast. For each atom of oxygen fixed in the form of iron oxidation emit 66 calories.

The chemical reactions of oxidation of iron have the following form: [6]:

$$Fe + O \rightarrow FeO + 267 kJ \qquad (4)$$

$$3Fe + 2O_2 \rightarrow Fe_3O_4 + 1120 kJ \qquad (5)$$

$$2Fe + 1{,}5O_2 \rightarrow Fe_2O_3 + 825 kJ \qquad (6)$$
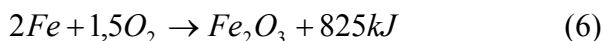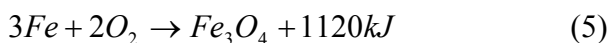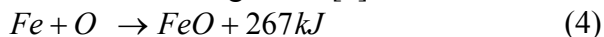
For laser cutting showed that importance has only formation of FeO. It is estimated that the temperature of cutting front is between the 1950-$2250^{o}C$. The oxidation reaction for 1mol of Fe requires a temperature of $1400^{o}C$ to initiate the reaction and the heat to boot reaction is 275 J/g. It is noted that this is much lower than that obtained from the chemical reactions. These values are given relative to amount expressed in moles of reactants. The chemical oxidation reaction of iron takes place with both reactants in excess.

In reality, the quantities of reactants vary because iron can burn faster than laser source heat the material.

From the existing alloy elements especially in alloy steels and stainless steel which give additional heat at erosion front by oxidation noted:[6]

$$Cr + 3O_2 \rightarrow 2Cr_2O_3 + 1163.67 kJ \qquad (7)$$

$$Ni + 1.5O_2 \rightarrow NiO + 248 kJ \qquad (8)$$
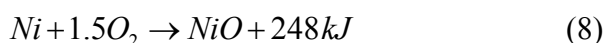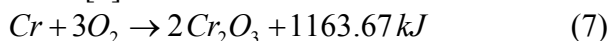
3. EXPERIMENTS

In experiments was used a CO_2 laser MAZAC 1500. Maximum average power emitted is 1500 W. In experiments using carbon steel sheet cold rolled SR EN 10025 (OL 37 - STAS 500/2, S235), with a thickness of 3 mm [3], [4].

In the experiments have varied the following parameters:

-Oxygen pressure pO_2 [bar]. Oxygen pressure is a process parameter that was measured at the outlet of the gas tank. It has a direct influence on the gas speed in the cut and as result in chemical reaction of burning material.

- Average power P[W]. Average power is the energy emitted by the laser oscillator in a long time. Average power is directly adjustable on the machine control.

- Cutting speed v [mm/min]. Cutting speed is the relative speed of movement between the laser head and the workpiece. Its influence is considerable both in general cutting process and particularly for irradiation conditions. Cutting speed is adjustable directly on the machine control.

- Pulse frequency f [Hz]. Pulse frequency is the number of pulses per unit time. Pulse frequency is adjustable directly on the machine control.

- Cycle η [%] cycle (or duty cycle) is the ratio of pulse duration (or pulse time) and total duration of the between two pulses (period). Cycle is adjustable directly on a machine command.

Upper and lower levels influence factors are given in Table 1.Was measured cut width on top of workpiece w_s [mm] and bottom of workpiece w_i[mm]. The top piece is considered that direct irradiated by laser beam. In the calculations was used the average cut width:

$$w_m = \frac{w_s + w_i}{2} \, [mm] \qquad (9)$$

Energy evaluation of laser cutting process was done by identifying a type power size a associated with physical phenomenon. Thus, similar to the average power of the laser beam material is considered power necessary to melt the material a power consumed to start oxidation reaction and power released as a

"HENRI COANDA"
AIR FORCE ACADEMY
ROMANIA

"GENERAL M.R. STEFANIK"
ARMED FORCES ACADEMY
SLOVAK REPUBLIC

INTERNATIONAL CONFERENCE of SCIENTIFIC PAPER
AFASES 2013
Brasov, 23-25 May 2013

result of oxidation. These were calculated by the ratio of energy and time.

Table 1: Levels of influence factors

influence factor	Lower level	Higher level
Average power P [W]	800	1500
Cutting speed v [mm/min]	1300	3000
Cycle η [%]	50	85
Frequency f [Hz]	150	400
Oxygen pressure pO_2 [bar]	0.8	2

As a general assumption is considered that the shape of the cut is kept constant during the process and the material is removed only in the molten state at the melting temperature. Cross section of the cut is considered the shape of a trapezoid. It neglects the removal of material as vapors. The process of cutting is uniformly and stable.

To appreciate the area in which the oxidation takes place was considered cutting front surface. This is slightly larger than the cross-section area through cut. Material removal in laser cutting process is considered relative to the cross-section area of cut.

2. SPECIFIC ENERGY

The specific energy to material removal of in molten state Q is defined as the ratio of the linear energy E_l consumed in the process and cut cross section area A_s.

$$Q = \frac{linear\,energy}{cut\,cross\,section} = \frac{E_l}{w_m\,e} \left[\frac{J}{mm^3} \right] (10)$$

Where:

e –sheet thickness, e= 3mm.

- linear energy $E_l = \frac{P}{v}$ [J/mm](11)

Specific energy to removing material characterized cutting process relative to change of influence factors. Although the calculations are based on values for a cut already achieved efficiency helps when you want to determine the linear energy for other processes of laser cutting. From the technological point of view, it is intended situation that the specific energyf or material removal is to minimal value.

Minimum specific energy expressed as minimum energy consumption as a quantity expressed in J to remove the maximum of material expressed in mm³.

The reduction in the values specific energy may be associated with the oxidation reaction contribution. The oxidation reaction increases cut cros-section area through without changing the linear energy.

Figure 1 shows the Pareto diagram for specific energy Q. Decreased specific energy Q means lower energy consumption to remove unit volume of material. It is observed that the higher effect is the speed, followed by the power effect. Speed effect is a decreasing effect and the power is increasing effect.
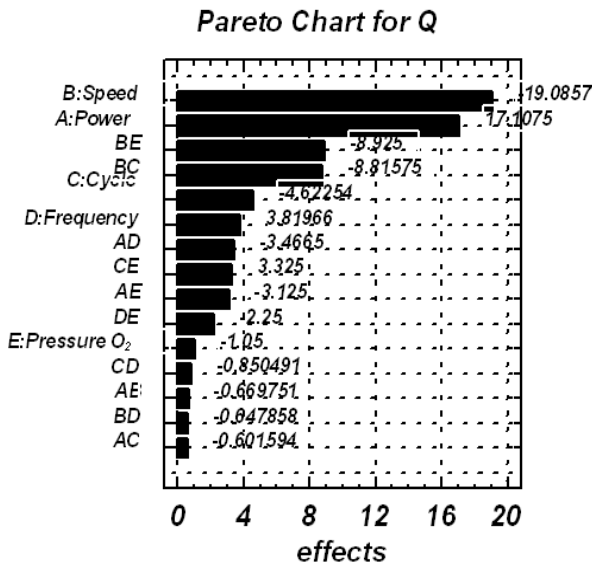
Figure 1 Pareto chart for specific energy

The following effects are cycle and frequency efects. It is noted that the oxygen pressure and its interactions have little effect. Increasing energy put to workpiece by increasing power level increase specific energy Q.

It shows that some additional energy is used for vaporization and not in useful physical phenomenon of melting material.

3. POWER FOR MELTING AND OXIDATION

In the following we will analyze the cutting process in terms of energy, using experimental results. It is considered that cutting takes place continuously and the process is stable. It is characterized by the following powers:

- P – time average power of the laser beam;
- P_u –useful power; the power needed to ensure the material melting;
- P_{in} –the power needed to provide the necessary heat to initiate the oxidation reaction;
- P_{out} –power resulting from the oxidation reaction.

The useful power is determined by the relation:

$$P_u = \frac{energy\ for\ melting}{time} = \rho \cdot A_s \cdot v \cdot L_0 \, [\text{W}] \quad (12)$$

where :
- ρ=7.85 g/cm^3, density of the material;

- L_0 –the heat required to bring the material to the melting temperature and to melt the material to be processed. $L_0 = 2396 \, J/g$

- cut cross-section area

$$A_s = \frac{w_s + w_i}{2} e = w_m \cdot e \, [\text{mm}^2] \quad (13)$$

Based on the similar reasoning, the calculated power required to initiate the oxidation reaction. is:

$$P_{in} = \frac{energy\ for\ preheating}{time} \, [\text{W}] \quad (14)$$
$$= \rho \cdot A_f \cdot v \cdot L_{in}$$

- where the cutting front area is:

$$A_f = \frac{1}{2}\frac{w_s + w_i}{2}\pi \cdot \sqrt{(\frac{w_s - w_i}{2})^2 + e^2} \, [\text{mm}^2] \quad (15)$$

Heating occurs at the front of erosion. In order to activate the oxidation reaction is necessary to heat the material more than1000^{o}C. Was considered to L$_{in}$=550J/g value.

At the cutting front takes place a heat release after oxidation:

$$P_{out} = \frac{energy\ from\ oxydation}{time} \quad (16)$$
$$= \rho \cdot A_f \cdot v \cdot L_{out} \, [\text{W}]$$

L$_{out}$ value was considered: L$_{out}$=4600J/g

Figure 2 shows the Pareto chart for useful power. It is noted that for this highest effect is speed effect. This effect is increasing effect. Thus, it is shown that the increase in speed favors melting and reduces vaporization of the material. Continuous irradiation given by cycle favors the melting and discontinuous irradiation given by frequency favors vaporization losses of heat by conduction. Power has significant effects by its interactions. Highest effects have parameters that control the interaction time between laser radiation and material. Oxygen pressure has little effect.

"HENRI COANDA"
AIR FORCE ACADEMY
ROMANIA

"GENERAL M.R. STEFANIK"
ARMED FORCES ACADEMY
SLOVAK REPUBLIC

INTERNATIONAL CONFERENCE of SCIENTIFIC PAPER
AFASES 2013
Brasov, 23-25 May 2013
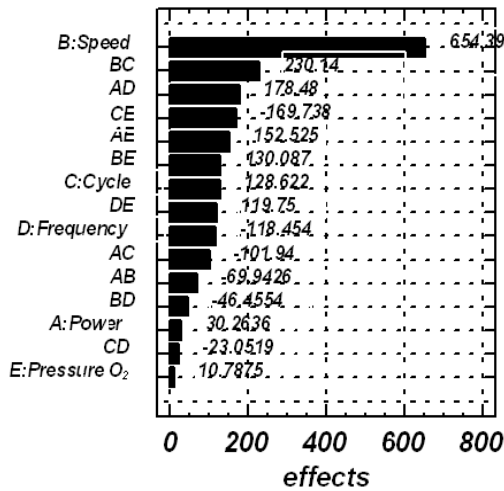
Figure 2 Pareto chart for useful power

Figure 3 shows the Pareto chart for the power required to initiate the oxidation reaction.
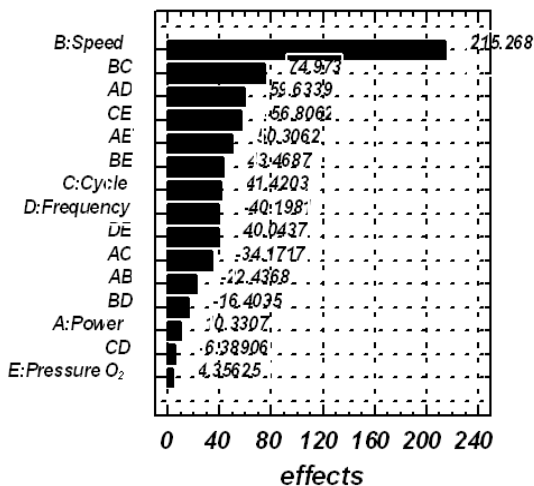
Figure 3 Pareto chart for the power required to initiate the oxidation reaction

The highest effect is speed effect. This a increasing effect is. The second effect is the interaction between the speed and cycle. The interaction between cycle and oxygen pressure has high effect.

Figure 4 shows the Pareto chart for the power given by the oxidation reaction. It is noted that the highest effect is the speed effect.
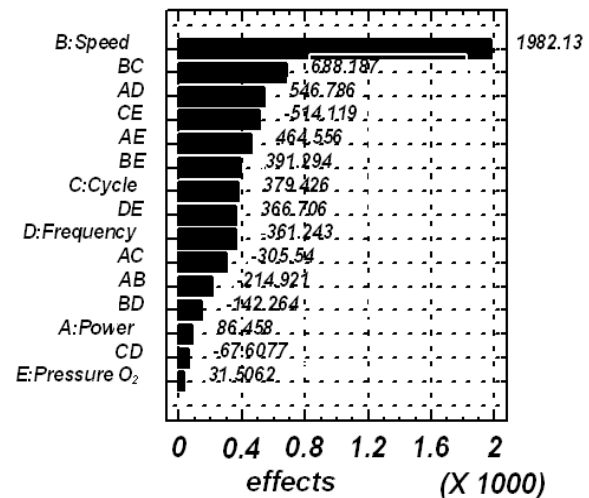
Figure 4 Pareto chart for the power given by the oxidation reaction

Hierarchy of factors influence for three powers considered is similar because the difference that appears in calculus formula is only for amount of latent heat.

4. ENERGY EFFICIENCY

Are defined the following cutting process yields:

a) *efficiency for erosion front ε_1*

$$\varepsilon_1 = \frac{power\ for\ melting}{average\ laser\ power} = \frac{P_u}{P}\,[\%] \qquad (17)$$

The yield for the erosion front shows the cut obtained by melting with laser beam irradiation and ignore presence of the oxidation reaction. Yield ε_1 can have supraunitary values just due to oxidation reactions.

b) **efficiency for initiation of the oxidation reaction** ε_2

$$\varepsilon_2 = \frac{power\ to\ i\ ntiate\ oxidation}{average\ laser\ power} = \frac{P_{in}}{P}\,[\%] \quad (18)$$

In defining for this ratio was considered that the laser beam have one role that of initiation the oxidation reaction.

c) **overall efficiency of the process** ε_3

$$\varepsilon_3 = \frac{power\ for\ melting}{laser\ power + power\ from\ oxidation}\ [\%](19)$$

The efficiency of the cutting process ε_3 takes into account the energy given by the laser beam energy and the oxidation reaction.

Figure 5 shows the Pareto chart for efficiency e1. It is observed that the speed effect is the highest.
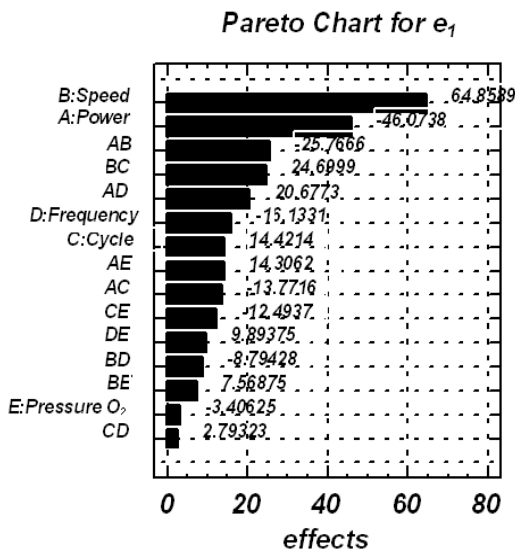
Figure 5 Pareto chart for efficiency for erosion front

This effect is increasing effect. The second effect is the power effect. This effect is a decreasing effect. Thus, it shows that increasing speed has a positive effect for material melting while increasing power favoring vaporization. The effects of the higher are the parameters that control the irradiation. Under thats are located effect of oxygen pressure and interactions in which it participates.

Figure 6 shows the Pareto chart for efficiency e2. It is noted that the highest effects are speed and power effects.The hierarchy of effects is similar to that for fraction e1 due to the calculation method.It shows that the main energy balance is between power and speed.

Figure 7 shows the Pareto chart for efficiency e3.It shows that highest effect is the speed effect. This effect is a increasing effect. The second effect is that of power effect. This effect is a decreasing effect. The difference

between the two effects is reduced compared to previous cases.
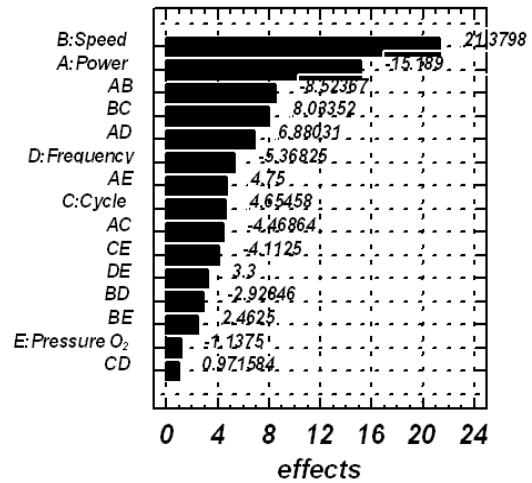
Figure 6 Pareto chart for initiation of the oxidation reaction efficiency
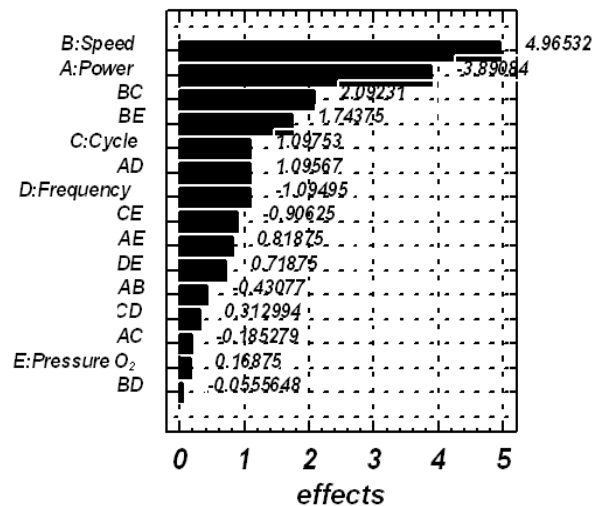
Figure 7 Pareto chart for overall efficiency of the process

We notice the high effects of speed, cycle and interactions between speed and oxygen pressure. It shows increasing the oxygen pressure effect for overall efficiency of laser cutting process.

5. CONCLUSIONS

Modeling performed on quantities which characterize energy for laser cutting process showed that:
- Cutting speed has a high effect on the analyzed quantities.
On the experimental field studied, cutting process optimization is possible by increasing

"HENRI COANDA"
AIR FORCE ACADEMY
ROMANIA

"GENERAL M.R. STEFANIK"
ARMED FORCES ACADEMY
SLOVAK REPUBLIC

INTERNATIONAL CONFERENCE of SCIENTIFIC PAPER
AFASES 2013
Brasov, 23-25 May 2013

the cutting speed. This means lower energy transmitted to the workpiece to get the same volume of material eroded.

Power and cutting speed provides the main energy balance of laser cutting process.

REFERENCES

1. J Powell, D Petring, R V Kumar, S O Al-Mashikhi, A F H Kaplan, and K. T. Voisey, Laser–oxygen cutting of mild steel: the thermodynamics of the oxidation reaction J. *Phys. D: Appl. Phys*. 42 (2009) 015504 (11pp).
2. Koji Hirano, Remy Fabbro, Experimental Observation of Hydrodynamics of Melt Layer and Striation Generation during Laser Cutting of Steel *Physics Procedia* 12 (2011) , pp:555–564.
3. Valentin Glod, Remus Boboescu "Experimental study on the oxygen flow in oxygen assisted laser cutting" *Proceedings of the 21st International Conference NAV-MAR-EDU2009* Editura Academiei Navale „Mircea cel Bătrân" Constanța p: 411-416,
4. Valentin Glod "Effects of Oxygen pressure in Laser Cutting", Metalurgia Internațional nr. 1/ 2011
5. J.F.Chaussier, A.B. Vannes, *La decoupe par procedes „haut energes"*,Universite de Bourgogne 2003
6. K. Abdel Ghany, M. Newishy "Cutting of 1,2mm thick austenitic stainless steel sheet using pulsed and CW Nd:YAG laser", *Journal of Materials Processing Technology* 168 (2005) p:438–447

ENGINEERING SCIENCES

STRUCTURED DESCRIPTION FOR OXYGEN ASSISTED LASER CUTTING PROCESS

Mihaela NISTORAN-BOTIŞ*, Remus BOBOESCU**,

Mechanical Faculty, University Politehnica, Timişoara, Romania, ** Engineering, Faculty, University Ioan Slavici, Timişoara, Romania

Abstract: Oxygen assisted laser cutting is carried out by penetration of the material followed by stabilizing and movement of the cutting front. Pulsed irradiation can be expressed as peak power and ratio spot overlap indepndente sizes.Using a factorial experiment allowed the evaluation of the effects of varied parameters on the cut width. It followed the correlation between varied parameters and physical phenomena for laser cutting.

Keywords: laser oxygen cutting, pulse wave regime, spot overlap ratio, cut shape.

1. INTRODUCTION

The oxygen-assisted laser cutting is a process having a complexity of the physical phenomena that take place.

From the physical point of view the it is noted study of individual physical phenomena such as absorption of laser radiation, material melting, oxidation reaction, heat losses by conduction and gas dynamics to cutting front.

From the technological point of view it is preferred approach as a model of type inputs (influence factors or varied parameters) - output (objective functions sizes directly measured or calculated on the basis of measurements).

There are important differences between the two approaches. Physical exclusive approach leads to detailed consideration of issues ignoring the overall context, and technological approach ignores the basic physical aspects associated with the variation of parameters.

This paper proposes a rapprochement between the two approaches. It will consider a tiered approach to physical phenomena in laser cutting process. This takes into account grouping of physical phenomena for laser cutting in the form of steps and associating variable parameters with sizes that have physical independent effects.

2. LASER CUTTING STAGES

To estimate the effect of influence factors controllable the process of cutting is recommended sequential developmental approach to laser cutting process. The laser cutting process has three important stages:
- material penetration;
- stabilizing cutting front;
- cutting front propagation;
These steps are shown in the figures 1-3.

In the first stage irradiation conditions ensure material melting and its penetration by melting and vaporization. This is expressed by the intensity of the laser beam and laser-material interaction time. In the second stage oxidation reaction and removal of molten material creates an unstable cutting front.
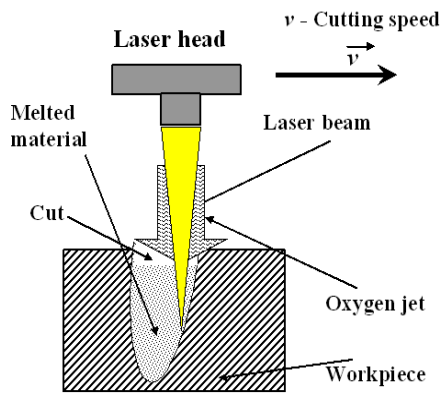
Figure 1 Material penetration
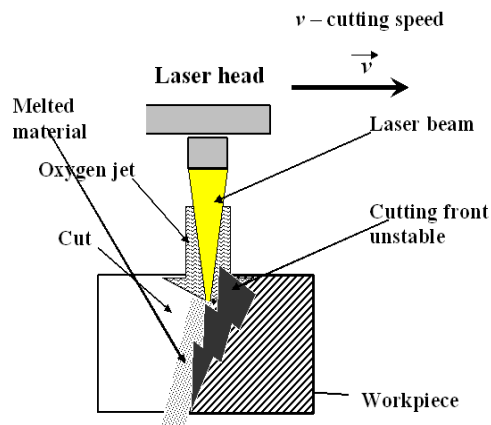
Figure 2 Stabilizing cutting front
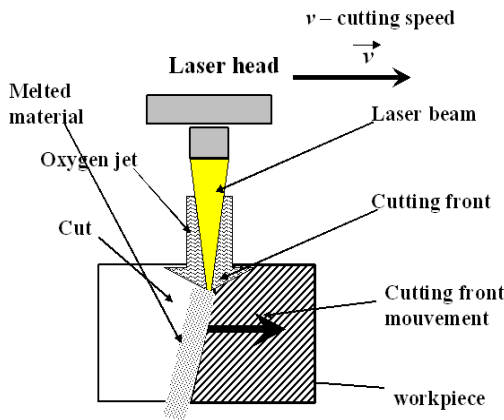
Figure 3 Propagation of cutting front

In the third stage by adjusting the cutting speed ensure the cutting front stabilization, and its movement in the cutting direction.

The advantages of a sequential approach to laser cutting process are that each parameter takes effect only at a certain stage. Action of a parameter is considered in the context of existing action of other parameters. The last stage is the laser cutting process in the development.

3. IRRADIATION CONDITIONS

Pulsed irradiation is specific of many technological laser systems. This is a characteristic design of technological laser systems allow that peak power to be much higher that average power. To laser materials processing submitted advantage stands in the possibility that in relaxation time to dissipate heat into material. Pulsed irradiation increases the number of quantities characterizing the the irradiation.

Thus, it is necessary to understand the relationship between them. A simplified scheme (rectangular pulses) for pulsed irradiation is shown in Figure 4.
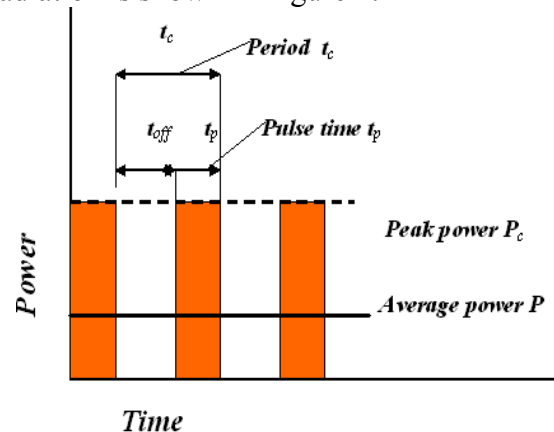
Figure 4 Sizes for pulsed irradiation

Period time t_c[s], represents a full cycle repetition pulses composed by pulse time and pause time between successive pulses. Period is calculated as the inverse of the frequency of pulsation.

$$t_c = \frac{1}{f} \text{ [s]} \qquad (1)$$

The pulse time t_p[s], is the time in which the laser light emission takes place. Depending on the cycle and frequency, the pulse time is given by the following relationship:

$$t_p = \frac{\eta}{f} \text{[s]} \qquad (2)$$

Length of the interval between pulses t_{off}[s], is that time during laser oscillator does not emit radiation. In relation (2) intervenes coefficien η (cycle or filling ratio for irradiation), which can be calculated from the relationship:

$$\eta = \frac{t_p}{t_p + t_{off}} = t_p \, f \text{ [%]} \qquad (3)$$

where:

"HENRI COANDA"
AIR FORCE ACADEMY
ROMANIA

"GENERAL M.R. STEFANIK"
ARMED FORCES ACADEMY
SLOVAK REPUBLIC

INTERNATIONAL CONFERENCE of SCIENTIFIC PAPER
AFASES 2013
Brasov, 23-25 May 2013

$$t_p + t_{off} = \frac{1}{f} \, [\text{s}] \qquad (4)$$

For technological equipment used in experiments directly adjusts cycle and frequency, pulse duration is a derived quantity from them. On the other technological systems laser pulse duration is controlled directly. Knowledge of two sizes in relations (2), (3) or (4) defines the pulse irradiation regime used.

The average power P [W] is the power emitted from laser oscillator in a long time and is equivalent to the power emitted continuously.

The peak power Pp[W] represents the maximum laser power. To a rectangular pulse shape peak power is related to the duration of the pulse. The peak power is calculated based on its relationship with average power.

$$P_p = \frac{P}{\eta} \quad [\text{W}] \qquad (5)$$

Pulse energy Ep [J] is the energy emitted during the pulse and is calculated as the ratio of average power and frequency.

$$E_p = P_p \cdot t_p = \frac{P}{f} \, [\text{J}] \qquad (6)$$

In experiments performed was directly set the average power and frequency of pulsation, pulse energy is determined by them.

Understanding how that can be driven pulse wave irradiation for technological laser system is a first step for ensuring controllability of interaction process laser – substance.

Laser beam intensity I[W/cm^2] is defined as the ratio between the peak power and the laser beam cross-section area.

$$I = \frac{E_p}{t_p \cdot (\pi \frac{D^2}{4})} = \frac{P_p}{\pi \frac{D^2}{4}} \, [\text{W/cm}^2] \qquad (7)$$

D - laser beam focal spot diameter

The laser beam intensity present relativity in definition because variation of the time that the peak power is kept constant and the considered surface. To assess the effects of irradiation, laser beam intensity should be defined to define relative to the workpiece surface. It is considered the area of intersection between the laser beam and workpiece.Laser beam intensity is not adjusted directly, but can be evaluated from the experimental conditions. It is important to evaluate the maximum intensity of the laser beam.

Laser beam intensity values will show if that irradiation can cause some physical phenomenon such as melting, vaporization or burning.

Linear energy E$_l$ [J/cm] is the ratio between the average laser power and cutting speed:

$$E_l = \frac{P}{v} \, [\text{J/cm}]$$

(8)

Linear energy is used to describe irradiation both for continuous CW and the pulse regime PW. This size ignores the characteristics of pulsed regime. It will be useful for characterization of physical phenomena that are less sensitive to temporal and spatial differences in irradiation for pulsed regime. It should be material melting and the heat affected area of material.

Irradiation in pulsed regime PW produces spatial differences on the workpiece surface.

Laser spot on the surface of the workpiece is considered to be circular, and is identified for his center point or either through one of its ends.

Regardless of how the laser spot is identified and his dimensions, spot moving over a period is given by:

$$d = v \cdot t_c = \frac{v}{f} \, [\text{mm}] \qquad (9)$$

The movement of the laser spot is shown in Figure 5. To characterize the spatial irradiation is introduced as a criterion the way in which the irradiated laser area by one spot covers an area irradiated by the previous spot.
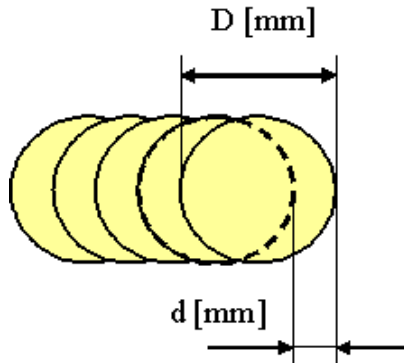
Figure 5 Moving of laser spot. D[mm] - diameter of the spot; d[mm] - moving of spot

Ratio spo (spot overlap) represents the ratio between difference of spot diameter and the distance d traveled during a period and the laser beam diameter.

$$spo = \frac{D-d}{D} \ [\text{-}] \tag{10}$$

Depending on the speed and frequency is obtained the following relation:

$$1 - spo = \frac{v}{D \cdot f} \tag{11}$$

Ratio "spo" has values lower than 1. A value of 1 means there is not displacement. Successive spots are overlap. A value of 0 for ratio "spo" means that successive spots are side by side. Negative values mean that successive spots acting individually and distant each other on the piece surface. The distance between spots is increasing as the ratio spo is smaller, with negative values. Relation (11) plays a role in practical establishment to the cutting speed.

There are cases where when the discussion is confined to positive values of the ratio "spo" it is expressed as a percentage.

Parameters that characterize irradiation plus the laser spot diameter can be grouped so as to use only two independent quantities:
- Peak power (depending on cycle and average power);
- Ratio spo (dependent on speed, frequency and spot diameter).

To express irradiation time differences fpr one point on piece surface is considered continuous irradiation model. Thus, a point on the surface of the material to interact with the laser beam during the interaction time:

$$t_{ic} = \frac{D}{v} [\text{s}] \tag{12}.$$

This is defined as the ratio between the diameter of the laser beam and speed. It represents the maximum duration that a point on the material surface can be irradiated and is independent of pulse time, duty cycle and frequency, quantities characterizing the pulsed regime. During the interaction time several laser pulses can be produced. To establish a link between the characteristics of pulsed regime and interaction time is introduced ratio:

$$r = \frac{t_{ic}}{t_c} [\text{-}] \tag{13}$$

The ratio r indicates how many pulsation periods was included in the time during a point on the workpiece.surface was seen in the area of the laser beam. Integer part of the ratio r (exception value 0) indicates the number of consecutive pulses radiating a point on the workpiece surface.

The fractional part of the fraction r indicates that the differences for irradiation times for different points on the workpiece surface are lower than pulse time.

4. EXPERIMENTAL APPLICATION

In the experiments was used a laser with CO_2 with maxim power 2kW of type MAZAK, the operation were in pulsated regime PW. The sheet cold rolled OL 37 3mm thick was used [4] [5]. Cuts were made without completely separated parts named as cut or kerf. For cuts performed have been measured cut width at the top L_s [mm] and at bottom of the workpiece L_i[mm]. Each of these measurements was the average of three different measurements equally spaced along the cut. The cut width L_m[mm] was calculated as the average between the cut width at the workpiece top surface (irradiated by the laser beam) and one at the bottom.

$$L_m = \frac{L_s + L_i}{2} [\text{mm}] \tag{14}$$

To describe the shape of the cut was introduced cut shape ratio given by:

$$R_p = 1 - \frac{L_i}{L_s} [\text{-}] \tag{15}$$

"HENRI COANDA"
AIR FORCE ACADEMY
ROMANIA

"GENERAL M.R. STEFANIK"
ARMED FORCES ACADEMY
SLOVAK REPUBLIC

INTERNATIONAL CONFERENCE of SCIENTIFIC PAPER
AFASES 2013
Brasov, 23-25 May 2013

Parameter variation was performed according to a factorial full factorial design type 25. Values in central point were: average power P=1150 W, cutting speed v=2150 [mm/min] cycle η=67.5% frequency f= 275Hz, oxygen pressure pO_2 =1.4 bar.

Figure 6 shows the Pareto chart for top cut width.Parameters effects and second order and interactions between them were considered. The most high is the frequency, it is followed by the interaction between power and cycle. Although speed has low effect is noted that the interaction between speed and power has a high effect. Thus, the higher effects are the parameters effects that control the irradiation. Frequency dependence of top cut width shows that the pulse time has a great importance. It is shown that repeated pulses favor evaporation. The qualitative aspect for possibility of material penetration is given to the power. It is noted that there are three interactions of power in the first three effects. It is shown that increase irradiation by increasing power, frequency and cycle has the effect of decreasing the cut width of the at the top piece surface by increasing the vaporization. It is noted that the effect of oxygen pressure is greater than the interactions effects in which it participate. The oxygen pressure has a increasing effect that is less than the parameters effects that control the irradiation.
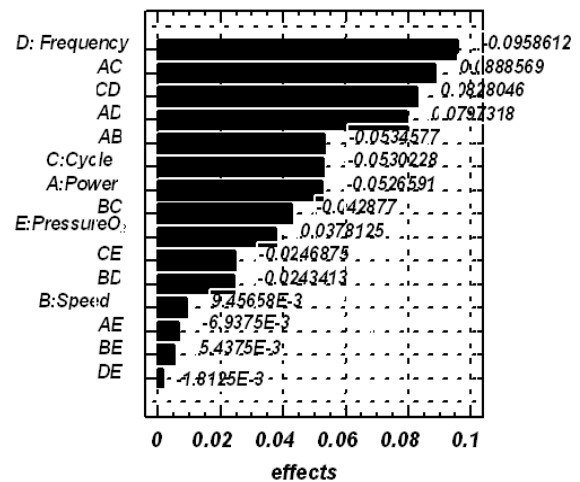
Figure 6 Pareto chart for top cut width

Figure 7 shows the Pareto chart for bottom cut width of the piece. It is noted that the highest effect is the interaction effect between speed and cycle. Power and its interaction with the cycle have the following effects.Effect of oxygen pressure is high by its interaction with frequency. It is shown that the bottom cut width is much more dependent on the speed and oxygen pressure than the top cut width. It is shown that within five effects are found all parameters. Effect of oxygen pressure is low and weaker than the interactions effects in which it participates. It is shown that by increasing the pressure of oxygen favors the the removal of the material in the molten state. This leads to a decrease for contribution of the oxidation reaction and thus decrease the bottom cut width.

Pareto Chart for Bottom kerf width L_i
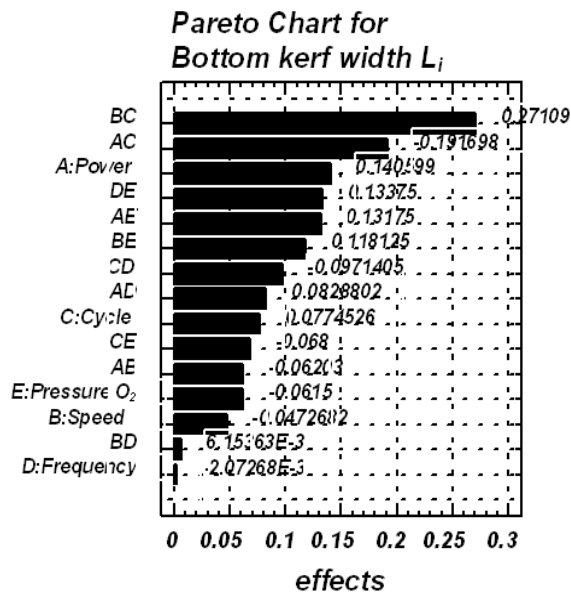
Figure 7 Pareto chart for bottom cut width

Figure 8 shows the Pareto chart for the average cut width. It is noted that the highest effect is the interaction between speed and cycle.

Pareto Chart for Average kerf width L_m
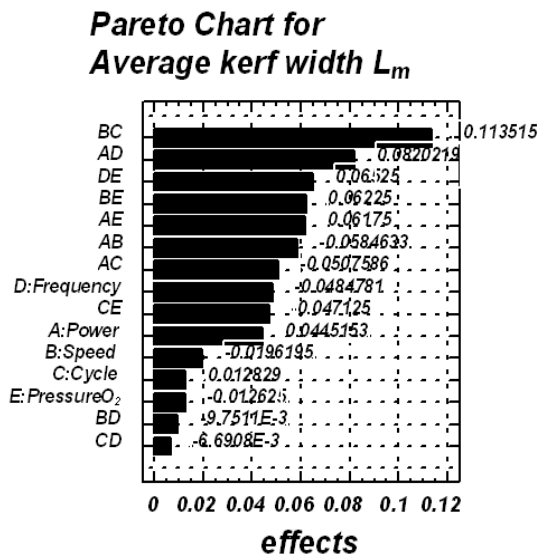
Figure 8 Pareto chart for average cut width

The second and third effect is the frequency interactions with power and oxygen pressure. It is observed so that into the first three effects are included all parameters. It is noted that the effects of interactions between parameters are higher than their parameters effects.It is noted that more interaction of oxygen pressure have high and close together effects.It is shown that pulse time setting by duty cycle and frequency has a significant effect on the average cut width. In determining time interaction time between laser radiation and material also cutting speed contributes. Pareto diagram

show that the time interaction between laser radiation and material has the most importance.

Figure 9 shows the Pareto chart for the cut shape ratio.This shows the deformation of the kerf. It is shown that the high effect is the interaction between speed and cycle. It is noted that interactions have higher effects than parameters.

Pareto Chart for Cut shape ratio R_p
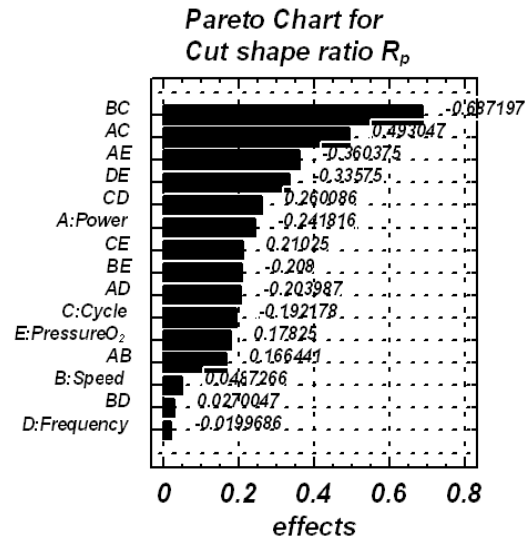
Figure 9 Pareto chart for cut shape ratio

It is noted that the highest effects contain all parameters and decreases frequency role in determining the shape of the cut. For parameters their own effects is observed that the higher effectis the power effect. Power effect of can be directly associated with the penetration of the material. In this case, this effect is related to the deformation of the cut.

3. CONCLUSIONS

The work was carried out a structured description of the steps to achieve oxygen assisted laser cutting. The work was done a time separation of the laser cutting process steps.

For evaporation laser cutting elements physical of cutting front were presented in [1].Here were identified areas of cutting front.

From the physical point of view irradiation is expressed by laser beam intensity and time of interaction between laser radiation and material.

Sizes that characterize irradiation regime for pulse wave PW were presented in [2] and [3]. For pulsed irradiation regime peak power

"HENRI COANDA"
AIR FORCE ACADEMY
ROMANIA

"GENERAL M.R. STEFANIK"
ARMED FORCES ACADEMY
SLOVAK REPUBLIC

INTERNATIONAL CONFERENCE of SCIENTIFIC PAPER
AFASES 2013
Brasov, 23-25 May 2013

is an expression of the intensity of the laser beam. Interaction time between laser radiation and material has a continuous component and a repetitive component. There are differences between the times of irradiation at different points on the workpiece surface.

For cuts made on steel plate was put in evidence the high effects of frequency for top cut width the piece and the speed for bottom cut width.

REFERENCES

1. H.Abakians, M.F.Modest, Evaporative Cutting of a Semitransparent Body With a Moving CW Laser, *Transaction of the ASME,* Vol. 110 November 1988 p.924-930.

2. Unitek Miyachi Lasers *Understanding Laser Parameters for Weld Development* Technical Aplication Brief Volume 1 no.3 2003 .

3. Yih-Fong Tzeng Effects of operating parameters on surface quality for the pulsed laser welding of zinc-coated steel *Journal of Materials Processing Technology* 100 (2000)pp: 163-170.

4. Valentin Glod, Remus Boboescu, "Experimental study on the oxygen flow in oxygen assisted laser cutting*" Proceedings of the 21st International Conference NAV-MAR-EDU2009* Editura Academiei Navale „Mircea cel Bătrân" Constanța p: 411-416.

5. Valentin Glod *"Effects of Oxygen pressure in Laser Cutting"*, Metalurgia Internațional nr. 1/ 2011.

ENGINEERING SCIENCES

WOOD PROCESSING BY LASER TOOLS

Adrian PETRU, Aurel LUNGULEASA

Faculty of Wood Engineering, Transilvania University, Brasov, Romania

Abstract: *Nowadays the laser is used more and more in industrial application. This gains more and more uses in wood industry. Operations which cannot makes with traditional technology can be made by laser technology. This paper is a study about laser using in the wood industry. The paper is a synthesis about scientific literature and papers from this domain. It shows an approach of the processing as wood cutting, burning and engraving. This study brings together all processing parameters found in literature. Some particular characteristics of the wood processing by laser are also presented. Advantages and disadvantages of the laser working are presented, as well. The most used woody species are presented, too.*

Keywords: *laser, wood processing, cutting, pyrography, engraving*

1. INTRODUCTION

Wood processing by laser is less developed than other similar areas. The laser machining for metal working has developed enhanced because of high power lasers which can cut high density materials. High costs of producing laser effect are offset by the reduced costs due to premature wear of the tool.

In the medical field the laser has imposed, because it has high accuracy than conventional processes, but also due to the fact that the side effects are greatly diminishes. Lasers have very precise control of the working parameters.

The advantages listed above do not have shown interest in woodworking because this material does not have a density comparable to metals. The species with the highest density wood is Lignum-vitae wood (*Guajacum officinale* L.). The density of this is $1400kg/m^3$

[12]. Metals can reach to $22570kg/m^3$ densities [7], which is the osmium density.

Regarding to the woodworking precision, it should not be very high due to swelling and shrinkage by varying moisture content. These natural phenomena are permanent.

Laser beam machining has several advantages over conventional methods.

Because it is a non-contact process, laser beam machining it well suited for advanced cutting of engineering materials such as difficult to be cut, brittle materials, electric and non-electric conductors, and soft and thin materials [2].

Laser beam machining is a thermal process and materials with favourable thermal properties can be successfully processed, regardless of their mechanical properties. Laser beam machining is a flexible process [15].

Other advantages include narrow slot width (minimum material lost), straight cut edges,

low roughness of cut surfaces, easy integration with computer numerically controlled (CNC) machines for cutting complex profiles [18].

By combining the laser beam and the machine providing motion, in addition to the applied numerically controlled system, it is possible to provide for a continual sheet cutting along the pre-determined contour.

A laser beam is a high intensity beam of light that can be tightly focused onto a spot only 0.1...0.2mm in diameter [17].

About researches in this domain, there were studied more articles about CO_2 laser cut quality from year 1996 till 2011 [17]. This paper confirm the great interest about laser using in metal domain and low interest about other domains that including the wood engineering.

The laser is use to cutting, etching, pyrography in the woodworking.

2. WOOD CUTTING BY LASER

The main reason that laser are used in the wood industry is the technological flexibility and speed with which good results are obtained. Wood processing industry puts particular emphasis on design. Repeating an ornament or a shape decreases the value of the item.

An example of wood cutting by laser beam is shown in Figure 1.

As a particularity, in the case of the wood behaves differently depending on the direction of the cutting plane.

This operation is suitable for intarsia jobs, where it needs precision cutting for decorative veneers. This technology is preferred because of the relatively small thickness of the veneer, and its low density, it does not require high-power lasers, all thus reducing the processing costs. The second reason for preferring this technology is that it presents great flexibility, being virtually eliminated costs of production patterns and dies and the processing time, while increasing the accuracy of execution. Execution time decreases by eliminating design and implementation templates and moulds. The preparation time of manufacture is not eliminated because execution patterns and dies is replaced with achieving control

programs, but this time is much less than the time required for preparing the classical technology. It done and saves material by using the laser cutting for intarsia veneers because it is not necessary that the veneers to be cut in package.

Cutting photonics is based on the wood influence of light rays with high power ($10^6...10^9$ W/cm^2) [5], which it heats the material to the burning temperatures.

The most common lasers, both as applications and as manufacturing, are that with gas. The advantage is that the emitted wavelengths can be determined with precision, are set up and remain independent of environmental conditions. These lasers use a gas mixture of CO_2, He and H_2 [5].

Figure 1: Wood cutting by laser [1].

CO_2 lasers dominate this application due to their good-quality beam combined to high output power [19].

When using high power lasers, the feed rate is closer to the industrial speed, this depends essentially by thickness of wood pieces, density, moisture content and adhesives.

Feed rate for beech and spruce is 0.31...0.43m/min and laser power range is from 150 to 500W [5].

The cut width is 0.1mm, the distance of the timber from the slot 1.5mm, and the lens focal length of 12.7cm [5].

About quality of surfaces obtained by laser cutting there have made a series of photographs of surfaces by electron microscopy and then were compared with photographs of the surfaces cut by conventional methods. It was thus evident that

"HENRI COANDA"
AIR FORCE ACADEMY
ROMANIA

"GENERAL M.R. STEFANIK"
ARMED FORCES ACADEMY
SLOVAK REPUBLIC

INTERNATIONAL CONFERENCE of SCIENTIFIC PAPER
AFASES 2014
Brasov, 22-24 May 2014

laser cut surfaces are smoother than the sawing. By sawing, it results cut surface of beams tracheid. It also results deep traces of tooth setting, especially of its unevenness. At the laser cutting, it was observed small damage of the wood cutting area.

The roughness of the cut surface can be compared to the milled surface.

The laser cut is a narrow, accurate and right cut. The edges are straight and sharp. The width cut decreases with increasing cutting feed rate and it is higher at the entrance than at the exit to the material, the difference being visible to increase the feed rate. By increasing the density of the wood, the cutting width is reduced.

Using laser for the wood cutting offers a number of advantages over conventional machining process: does not produce sawdust; provides the ability to cut complex profiles; surfaces are cut very fine; not cutting forces acting on the parts clipped; very small width of cut; no tool wear occurs and there is no question of their maintenance; the noise is reduced.

With respect to various other cutting processes (such as oxy-fuel cutting, plasma cutting, sawing and punching), its advantages are numerous, namely, minimal area subjected to heat, a proper cut profile, minimal deformation of a work piece, the possibility of applying high cutting speed and fast adaptation to changes in manufacturing programs.

The disadvantages using laser for cutting wood are: cut surfaces are burned, it is difficult to know the density for calculating the laser power for cutting because wood is a heterogeneous material.

Evaluation of laser cut quality bases on: geometry of cut, surface of cut, burr formation and characteristics of material in zone of cut.

The cut geometry comprises the following: kerf (kerf profile and kerf width), perpendicularity and slant tolerance, and rounding out of the cut edges.

Kerf is an important characteristic of the laser cutting. That ensures the advantage in regard to other contour cutting processes. Kerf profile by laser cutting has form of taper. The channel effect of a focused beam minimizes taper of the kerf.

The perpendicularity and slant tolerance determine the cut quality also.

The side inclination of cut angle increases along with the sheet thickness, but it decreases with increasing of the laser power.

The cut edges at the laser beam entrance side are rounded out due to the Gauss distribution of radiation intensity over the laser beam cross-section. The rounding-out of the edges is very small [17].

About woody species which can be cut by laser there is no ban. However have to an attention about the wood density. A low laser power cannot cut all material thickness and a high-power of the laser burns the wood. Studied woody species cut by laser are shown in Table 2.

3. WOOD COLOURING BY LASER (PYROGRAPHY)

Wood surfaces treatment has two goals:
- increases wood resistance (especially resistance against the pest attacks) and dimensional stability;
- obtaining the decorations.

These two goals cannot be separate because they are complementary.

Wood treatment by laser darks the colour surface. This is one of the reasons that the laser did not developed in the woodworking.

This drawback will be minimized if the colouring makes through artistic pyrography.

In a short action at a constant and relatively low energy laser on wood a charring of the material decorative shapes occurs.

An example of wood burning by laser is shown in Figure 2.
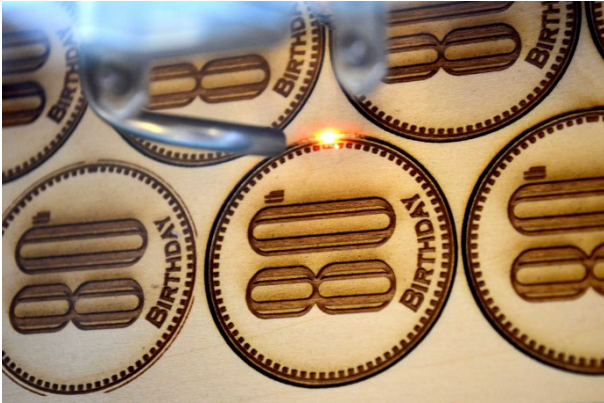
Figure 2: Wood burning by laser [6].

For decoration it uses especially CO_2 [4] [14,21] He [4], oxygen and nitrogen [3] lasers.

Colouring of the wood surface is influenced by the species of wood burned, by the laser power, the feed rate, the material thickness and the energy flow density. The colour varies from pale brown to black. The colour changes will be more pronounced if feed rate is reduced.

The carbonized depth of the wood is equal to the width of tracheid or fibres, i.e. 30...60µm [5].

By decreasing the feed rate, the wood has more time to carbonize itself, it increases the energy expended per unit length of cut, also. Increasing the moisture content decreases the carbonization effect; the excess energy is used for evaporation of water from the wood.

Wood treating by laser technology is in laboratory stage due to high costs of implementation at industrial scale. However this technology even in the laboratory opens new perspectives in research phenomena occurring in wood.

The advantages of wood colouring by laser are: surfaces can be differently coloured; it can be obtained images with high resolution.

The disadvantages are: uneven colouring due to heterogeneity of wood, increases the surface roughness, the lines are drawn too strict. The last one will be a disadvantage just if it wants to make an artistic pyrography.

A criteria for choosing of the material is its homogeneity. A homogeneous wood will be treated uniform; the colour will be without hue sudden change and properties will be uniformly distributed.

Woody species funded in literature are shown in Table 2.

4. WOOD ENGRAVING BY LASERS

The laser beam is used to detach a large proportion of wood, following pre-set patterns.

Sculpture is obtained through repeating this process for each thin layer successively.

An example of wood engraving is shown in Figure 3.

It has already shown that the laser treatment the wood areas are burned, but the laser can also be used for making ornaments in relief.

The free carbon formed on the surface can easily be removed with a jet of air or light brushing, only faint brown remaining.

MDF is the most used wood material for engraving. This has the advantage that consisting of wood fibres (small anatomical elements), the surface is cleaned against free carbon very well.

The Q-switched diode-pumped frequency-doubled Nd:YAG green laser can be successfully used to machine different types of wood, obtaining decorative drawing and 3D engraved geometries without burning [10].

The advantages of engraving by laser are: high work precision, it is eliminated the risk of fibre pull-out.

The disadvantages are: surfaces are burned, that will be removed it is necessary; it increases the number of passes because the power decreases.

Another aspect is about heterogeneity of the wood; the laser should be variable power or a high enough power to cut the maximum density of the material but, sufficiently low to does not burn the minimum density area.

Studied woody species engraved by laser are shown in Table 2.

"HENRI COANDA"
AIR FORCE ACADEMY
ROMANIA

"GENERAL M.R. STEFANIK"
ARMED FORCES ACADEMY
SLOVAK REPUBLIC

INTERNATIONAL CONFERENCE of SCIENTIFIC PAPER
AFASES 2014
Brasov, 22-24 May 2014
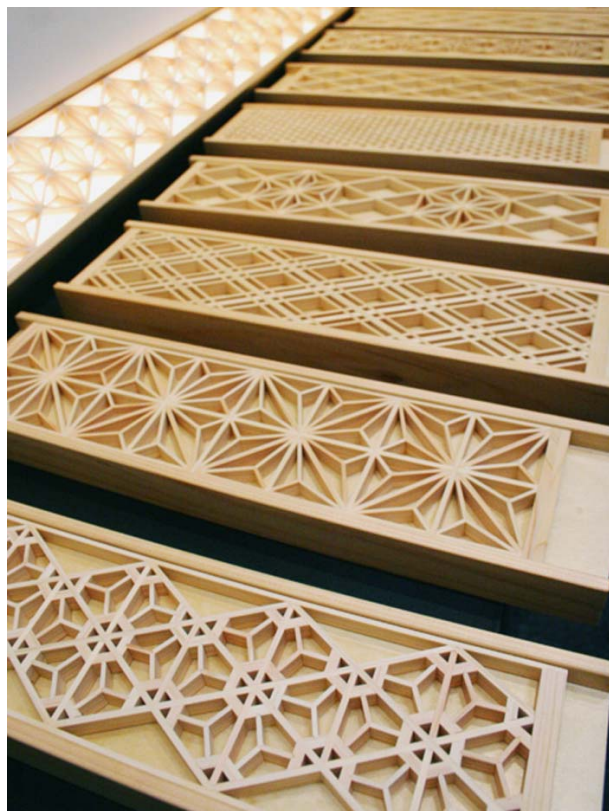
Figure 3: Wood engraving by laser [20].

5. CONCLUSIONS

Woodworking by laser is a domain unexploited at the maximum in this moment and it has some aspects unknown.

Because the relatively costs of production are high, especially for lasers pumping, they are very little used in the wood industry.

The woodworking by lasers creates new prospects in terms of phenomena research that occur during and after wood processing.

Wood surfaces treatments by laser can be controlled in small details. It is possible to study wood burning mechanisms (especially chemical wood degradation). Also it is possible to isolate insoluble wood components.

Usually just a single machine can do all these three operations.

Generally, woodworking by lasers has a number of advantages over the conventional processing: decreases working time, increases working precision, can be make complex operations, for all these operations it is need just one machine, the operations are automates.

Generally, the disadvantages are: high costs of the equipments, high cost for production of the laser effect.

The production costs can be reduced using other lasers instead lasers with gas. Q-switched diode-pumped frequency-doubled Nd:YAG green laser reduces the cost but increase the working time. It is possible because wood density is low and a high laser power is not necessary. The material with high density can be processed trough more passes.

The parameters for lasers used in wood industry are shown in Table 1.

Table 1. Main parameters for woodworking by laser.

	Cutting	Pyro-graphy	Engraving
Laser type	Gas CO_2, He and H_2 [5]	Gas CO_2, He [4], O_2 and N_2 [3]	Q-switched diode-pumped frequency-doubled Nd:YAG [10]
Power	$10^6...10^9$ W/cm^2 [5]		
Speed	50800 mm/min	91500 mm/min	

In wood industry the lasers are not used just for woodworking. They are used for:

dimensional and roughness measuring, marking etc. Among these, the lasers are used the most at the timber working, where it is difficult to determine the volume of log. That because the log shape is irregular.

Table 2. The woody species and materials processed by lasers, found in literature.

Cutting	Beech, Spruce, Douglas, Particleboards [4]
Pyrography	Black locust [3], Beech [8,14,16,21,13], Lime [14], Spruce [14,16,21], Ash [14,16], Scots pine [16], Pine [13], Maple [9], Sapelli [21], Moso bamboo [11]
Engraving	MDF, Walnut, Mahogany, Chestnut Oak, Poplar, Pine [10]

REFERENCES

1. American woodworker, *Tool Talk - Epilog CNC Lasers*. [online]. Available: http://www.americanwoodworker.com/blogs/tools/archive/2010/07/13/tool-talk-epilog-cnc-lasers.aspx (March, 2014)

2. Chen, M., Ho, Y., Hsiao, W., Wu, T., Tseng, S., Huang, K., *Optimized laser cutting on light guide plates using grey relational analysis*. Optics and Lasers in Engineering. 49 (2011)

3. Chen, Y. , Gao, J. , Fan, Y. , Tshabalala, M. A. , Stark, N. M., *Heat-induced chemical and color changes of extractive-free Black Locust (Robinia Pseudoacacia) wood*. BioResources. 7(2) (2012)

4. Dogaru V., *Aşchierea lemnului şi scule aşchietoare*. Bucureşti: Editura Didactică şi Pedagogică (1981)

5. Dogaru, V., *Bazele tăierii lemnului şi a materialelor lemnoase*. Bucureşti: Editura Tehnică (1985)

6. Grathio Labs, *Making Wooden Nickels. With Lasers*. [online]. Available: http://grathio.com/2011/06/making-wooden-nickles-with-lasers/ (March, 2014)

7. Gugnin, A. A. , L'vov, S. N. , Mal'ko, P. I., Nemchenko, V. F., Starodubov, I. P., *Electrical and thermal conductivities of rhenium, osmium, and iridium and some of their alloys with thorium and lanthanum in a wide temperature range*. Soviet Powder Metallurgy and Metal Ceramics. 11 (1972)

8. Kacík, F. , Kubovsky, I., *Chemical changes of beech wood due to CO_2 laser irradiation*. Journal of Photochemistry and Photobiology A: Chemistry. 222 (2011)

9. Kubovsky, I. , Kacík, F., *FT-IR study of maple wood changes due to CO_2 laser irradiation*. Cellulose Chemistry and Technology. 43 (2009)

10. Leone, C. , Lopresto, V., De Iorio, I. , *Wood engraving by Q-switched diode-pumped frequency-doubled Nd:YAG green laser*. Optics and Lasers in Engineering. 47 (2009)

11. Lin, C.-J. , Wang, Y.-C. , Lin, L.-D. , Chiou, C.-R. , Wang, Y.-N. and Tsai M.-J., *Effects of feed speed ratio and laser power on engraved depth and color difference of Moso bamboo lamina*. Journal of Materials Processing Technology. 198, no. 1-3 (2008)

12. Lunguleasa, A., *Wood physics and mechanics*. Braşov: Editura Universităţii Transilvania (2007)

13. Panzner, M. , Wiedemann, G. , Henneberg, K. , Fischer, R. , Wittke, T. and Dietsch, R., *Experimental investigation of the laser ablation process on wood surfaces*. Applied Surface Science. 127-129 (1998)

14. Petutschnigg, A. , Stöckler, M. , Steinwendner, F. , Schnepps, J. , Gütler, H. , Blinzer, J. , Holzer, H. and Schnabel, T., *Laser Treatment of Wood Surfaces for Ski Cores:*

"HENRI COANDA"
AIR FORCE ACADEMY
ROMANIA

"GENERAL M.R. STEFANIK"
ARMED FORCES ACADEMY
SLOVAK REPUBLIC

INTERNATIONAL CONFERENCE of SCIENTIFIC PAPER
AFASES 2014
Brasov, 22-24 May 2014

An Experimental Parameter Study. Advances in Materials Science and Engineering. 2013 (2013)

15. Prasad, G., Siores, E., Wong, W.,, *Laser cutting of metallic coated sheet steels*. Journal of Materials Processing Technology. 74 (1998)

16. Preklet, E. , Papp, G. , Barta, E. , Tolvaj, L. , Berkesi, O. , Bohus, J. , Szatmári, S. , *Changes in DRIFT spectra of wood irradiated by lasers of different wavelength*. Journal of Photochemistry and Photobiology B: Biology. 112 (2012)

17. Radovanovic, M. , Madic, M., *Experimental investigations of CO2 laser cut quality: a review*. Nonconventional Technologies Review. 4 (2011)

18. Rao, T. , Kaul, R. , Tiwari, P. , Nath, A., *Inert gas cutting of titanium sheet with pulsed mode CO2 laser*. Optics and Lasers in Engineering. 43 (2005)

19. Riveiro, A. , Quintero, F. , Lusquinos, F. , Comesana, R. , Pou J., *Parametric investigation of CO2 laser cutting of 2024-T3 alloy*. Journal of Materials Processing Technology. 210 (2010)

20. Thompson, J., *Kumiko Pattern*. [online]. Available: http://www.jeffreythompson.org/blog/tag/wood/ (March, 2014)

21. Wust, H. , Haller, P. and Wiedemann, G., *Experimental study of the effect of a Laser beam on the morphology of wood surfaces*. In Proceedings of the 3rd International Symposium on Wood Machining, Lausanne, Switzerland: (2007)

ENGINEERING SCIENCES

"HENRI COANDA"
AIR FORCE ACADEMY
ROMANIA

"GENERAL M.R. STEFANIK"
ARMED FORCES ACADEMY
SLOVAK REPUBLIC

INTERNATIONAL CONFERENCE of SCIENTIFIC PAPER
AFASES 2014
Brasov, 22-24 May 2014

COLOUR MEASUREMENT USING DIGITAL IMAGE ANALYSIS

Adrian PETRU, Aurel LUNGULEASA

Faculty of Wood Engineering, Transilvania University, Braşov, România

Abstract: *This paper presents an original colour measuring method using an assembly consisting of a computer system equipped with a scanner. One of the advantages of this method is that one it can determine the colour on small surfaces just of 1x1pixels using a common equipment. This means that the errors resulting when measuring the colour on larger surfaces (when actually an average colour of the surface is assessed) are avoided. Transforming from RGB colour system to CIEL*a*b* system is also presented. The CIEL*a*b* system was elected because it is the most widely used colour system. A measuring example is presented.*

Keywords: *measuring, colour, wood, pyrography, Lazarus, Pascal.*

1. INTRODUCTION

Colour holds an important role in human life and activity. In nature and science, colour represents an essential clue for defining species of plants, animals, minerals etc.

Colour is defined as "the property possessed by an object of producing different sensations on the eye as a result of the way the object reflects or emits light" [6].

Colour is an important wood property when evaluating its aesthetically potential and especially when it is going to be used for decorative purposes.

The wood colour varies within very large limits from white for Sycamore (*Acer pseudoplatanus* L.) to black for Ebony (*Diospyros ebenum* Koenig.) [4]. It is characteristic for each species. It meets many hues which vary around a basic value at the same wood species. Different species have different base colours.

The colour of the one and the same species can be uniform or with different nuances. The wood of the species from Romania and, generally, from the temperate climate area, has moderate colours as in contrast to the species in tropical areas.

The colour of wood is an important parameter, taken into account in several stages of wood processing, such as timber steaming, drying and dyeing.

Likewise, the measurement of wood colour is very important in the pyrography refining process of wood. To this end the present research has been conducted.

Colour instrumentation has experienced a tremendous advancement in technology during the past 40 years. During this time, the instruments have become more accurate, reliable, flexible, smaller, and faster than their predecessors, at significantly lower cost to the user.

The most important devices for colour measurement are:

- colorimeter;
- spectrocolorimeters;
- spectrophotometers;

- portables.

Colorimeter is a device of fairly simple design based upon the visual concepts of colour. The sample is illuminated at a 45° angle relative to the perpendicular line to the plane of the mounted sample. The method of the trichromatic colorimeter allows for the quick obtaining of the trichromatic components X, Y and Z.

Spectrocolorimeters are somewhat of a hybrid instrument which is capable of providing colorimetric data such as X,Y,Z or CIEL*a*b* values for various standard illuminations.

Spectrophotometers provided wavelength by wavelength measurement and data collection at each 1nm or lower if is desired. The spectral method of determining the trichromatic components is based on the spectrophotometric raise of the curve of radiance spectral factors; this is a relatively laborious method.

Micro-processors are capable of calculating colour differences, pass/fail, shade sorting, whiteness, grades of fastness, and many other shows of colour and appearance. A colour is expressed through different intensities of the system basic colours depending on the chosen colorimetric system.

Many portables do not meet the same performance specifications as bench-top models in areas such as spectral resolution, bandwidth, and large-to-small viewing areas.

The main disadvantage of the measuring apparatus is that they do not have possibility to modify measuring area.

It studied measuring wood colour by means of the CorelDraw program [8]. This method presents a disadvantage that read data need transfer to other software for processing. Another disadvantage is that the surfaces can be only by 1x1pixels, 2x2pixels and 5x5pixels.

2. MEASURING METHOD AND APPARATUS

The present study used the computerized method for measuring the wood colour, through an original procedure by means of original software named Colour Manager, developed in to Lazarus programming environment [3]. That use Pascal programming language [2].

Using a PC system can measure the colour of the scanned surfaces in different colorimetric systems, such as:

- RGB: Red (R); Green (G); Blue (B). Colour is expressed through values varying from 0, for black, to 255, for white, for each component.
- hexadecimal code. Colour is expressed through values varying from 000000 for black, to FFFFFF for white.
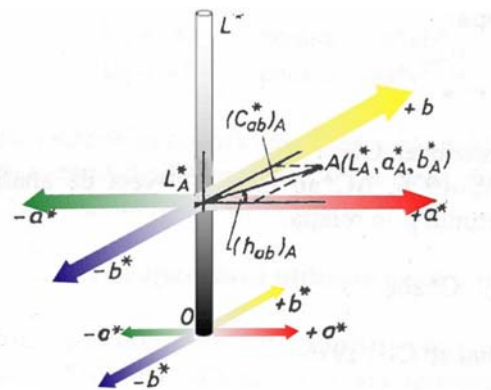
Figure 1: Colour characterization through brightness (L*), chrome or satiation (C*ab) and hue angle (hab).

The colorimetric system CIEL*a*b*, defined by the International Commission of illumination (CIE) in 1976, is widely used in colorimetry. It is standardised in Romania [9]. Within this system, a colour is featured through the rectangular proportions L*a*b* (Figure 1), where:

- L* represents the brightness of the colour. L*= 0 yields black and L*= 100 indicates diffuse white; specular white may be higher;
- a* negative values indicate green while positive values indicate magenta;
- b* negative values indicate blue and positive values indicate yellow.

"HENRI COANDA"
AIR FORCE ACADEMY
ROMANIA

"GENERAL M.R. STEFANIK"
ARMED FORCES ACADEMY
SLOVAK REPUBLIC

INTERNATIONAL CONFERENCE of SCIENTIFIC PAPER
AFASES 2014
Brasov, 22-24 May 2014

Using the rectangular coordinates L*, a* and b*, the chroma (C*ab) and the hue angle of the colour (hab) with values ranging between 0° and 360° can be determined, according to the following relations:

$$C^*ab = (a^{*2} + b^{*2})^{1/2}$$

(1)

$$hab = arctg(\frac{b^*}{a^*})$$

(2)

The colour characterization by means of the brightness (L*), the chrome (C*ab) and the hue angle (hab) according to is shown in Figure 1 [9] , in which the measured sample is represented as A point of coordinates L*$_A$; a*$_A$, b*$_A$. The L*$_A$, value (which is the brightness of the respective sample) is on the L* axis at the cross-section of this axis with the a*b* plane where is A point.

The device used for the colour measurement consisted of a PC-scanner-screen assembly.

Before starting the measurements, this assembly was calibrated so the values read by the PC, for the R, G, B trichromatic components, to be as close as possible to the ones given by the colour specimen. The assembly was calibrated with white standard specimen. To this end, the colour specimen have been scanned and the R, G, B values were determined.

Calibration is made in computer software. Measured values of the specimen are entered as a correction factors in calibration group box. These values are entered separately for each parameter (R, G or B). This tool is shown to Figure 3.

The images were scanned by means of a Pentium 4 computer and a HP LaserJet 3055 all-in-one printer, fax, copier, scanner type.

The technical characteristics of the employed computer are:
- Processor: Genuine Intel(R) CPU 2140 @ 1.60GHz;
- 0.99GB of RAM memory;
- Video in board;
- Hard disk: 80GB;
- Monitor: Acer AL1716s.

The technical characteristics of the HP LaserJet 3055 all-in-one printer, fax, copier, scanner type for scanning are:
- supported file types: JPEG, TIF, BMP, GIF, PDF, PNG;
- Resolution: 1200 ppi, 24-bit full-colour scanning from letter/A4-size scanner glass;
- Hi-Speed USB 2.0 port and port for connecting to a 10/100 Base-T network
- 64-MB RAM.
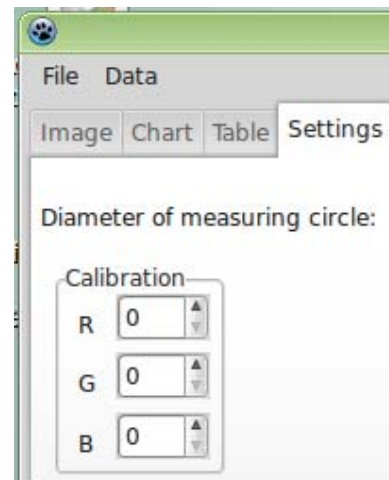
Figure 2: The Settings tab with Calibration tool.

It can scan the samples after calibration. Images need save in to BMP format.

The saved images are open into program. After image is loaded, the program determines the dimensions of the image. This is an

important parameter because it defines the measuring area limits.

Before analysing image, it sets the diameter of measuring circle from Settings tab. This is a main advantage of this method because it can set the surface area. Others apparatus use for colour measuring, especially portable apparatus do not have this possibility.

After a point is selected, the computer defines a circular surface defined by centre in the selected point and diameter defined by the specified diameter of measuring point. The measuring surface shape is similar with surfaces defined by the other apparatus.

This surface is analysed with computer pixel by pixel and colour value for each point is split into three values; for red, green and blue.

The selected areas are stamped with white colour. It does not affect the original image file in any way.

A measurement example is shown in Figure 3.

- the position of the pixel on X axis;
- the position of the pixel on Y axis;
- R value in the RGB measuring system;
- G value in the RGB measuring system;
- B value in the RGB measuring system;
- X value in the XYZ measuring system;
- Y value in the XYZ measuring system;
- Z value in the XYZ measuring system;
- L* value in the CIEL*a*b* measuring system;
- a* value in the CIEL*a*b* measuring system;
- b* value in the CIEL*a*b* measuring system;
- C*ab value in the CIEL*a*b* measuring system;
- hab value in the CIEL*a*b* measuring system.

The software determines the minimum value, the maximum value, average value and standard deviation for each parameter, as well.

Average value is calculates by formula [1].

Figure 3: Image tab with selected point.

Figure 4: Table tab with read data.

Afterwards, the colour, represented by RGB system, is converts to XYZ system using proper formulae [7].

Next step is to convert values from XYZ system to CIEL*a*b* system. It uses formulae provided for this the purpose [9].

In the Table tab are shown the measured data for each pixel. Data recoded in this table are:

Standard deviation in calculates by formula [10].

These values are shown in Table tab, also. The values can be saved and exported to other application.

An example of measured data is shown in Figure 4.

The graphical representation of measured data variations are shown in the Chart tab. The

"HENRI COANDA"
AIR FORCE ACADEMY
ROMANIA

"GENERAL M.R. STEFANIK"
ARMED FORCES ACADEMY
SLOVAK REPUBLIC

INTERNATIONAL CONFERENCE of SCIENTIFIC PAPER
AFASES 2014
Brasov, 22-24 May 2014

chart has on X axis the measured pixel and on Y axis the colour values of pixel. Y axis has values from -100 (for CIEL*a*b* measuring system) to 255 (for RGB measuring system).

Values for XYZ colour system is not show for clarity of representation.

The purpose of this representation is to show the dispersion data. A dispersed representation means the measuring is failed (average value is not represent the global colour).

An example of measured data representation is shown in Figure 5.
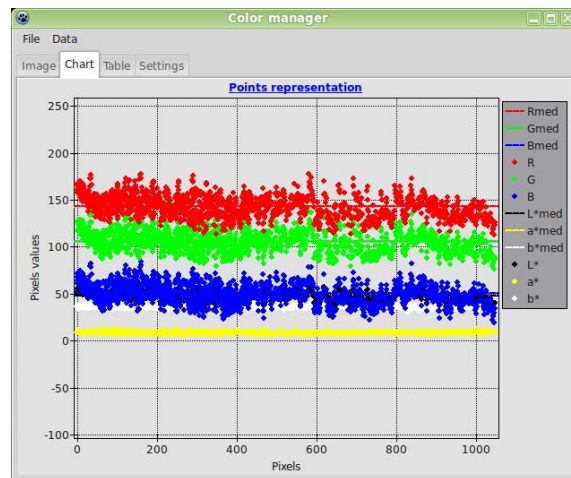
Figure 5: Chart tab with values representation.

3. CONCLUSIONS

It is made measuring on some wood samples. It can notice the measured values are dispersed but still closed (especially for CIEL*a*b* series). That means the measurement accuracy is good.

In the most cases it is necessary to measurement the colour difference of two or more measurement in same place. For that it needs to know the exact location of the measurement surface. Usually, it use surface marking with a pencil, but this method affects the results. Another method uses a template from Plexiglas, but this method is expensive [5]. It needs to make a template for each sample. The method presented in this paper does not need any devices or marks. The coordinates of the points from first measuring can be saved and they are ready for use to next measurement session. It saves money and time and measures are not affected in this case.

This is an easy and accessible method. The devices used for this purpose is at hand for every user. A particularly important advantage of employing this method is that the program enables the colour measuring for very small surfaces. This is not possible as regards the use of the colorimeter, which makes the average of the colour for a larger surface.

The method has the advantage of being cheap, it uses available equipments.

This method presents an advantage that read data do not need transfer to other program for processing.

Another advantage is that the surfaces can be larger than 1x1pixels.

The measuring precision is less than professional apparatus but, it is reasonable for a material heterogeneous like as wood.

Even if the method is designed to measure the colour of the wood, it can be used for any material.

The measurement is influenced by scanner properties. The scan resolution influence measurement but not significant because between pixels are not empty spaces.

Because the colour is a sensation it is difficult to quantify that.

REFERENCES

1. Brenci, Luminiţa-Maria, *Programarea calculatoarelor şi limbaje de programare în industria lemnului - Statistică matematică aplicată, internet şi limbajul HTML*. Braşov: Editura Universităţii Transilvania (2010)

2. Laurenzi, W., *Intoducere în programarea vizuală în Delphi*. Braşov: Editura Universităţii Transilvania (2012)

3. Lazarus, *Homepage*. [online]. Available: http://www.lazarus.freepascal.org/ (January, 2014)

4. Lunguleasa, A., *Stiinta lemnului*. Braşov: Editura Universităţii Transilvania (2001)

5. Millis, M. S., *Understanding pyrography, the photochemistry of 'scorched' decoration*. Pro Ligno. Vol. 9 / No. 4 (2013)

6. Oxford dictionaries, *Color: definition of color in Oxford dictionary (American English)*. [online]. Available: http://www.oxforddictionaries.com/us/definition/american_english/color (March, 2014)

7. Popa, E. , Popa, V., *Lemnul de anin, plop, salcâm. Proprietăţi, colorare (Alder, Poplar, Robinia Wood. Properties, Coloration)*. Braşov: Editura Universităţii Transilvania (2004)

8. Popa, E. , Popa, V., *Măsurarea culorii lemnului cu ajutorul programului CorelDraw / Measuring Wood Color by Means of the CorelDraw Program*. Pro Ligno. Vol.4 / No. 2 (2008)

9. STAS 6880/1-88, *Colorimetrie. Colorimetrie de reflexie. Noţiuni generale.*, Bucuresti: ASRO (1988)

10. , *Parametri descriptivi*. [online]. Available: http://statisticasociala.tripod.com/parametri.htm (February, 2014)

“HENRI COANDA”
AIR FORCE ACADEMY
ROMANIA

“GENERAL M.R. STEFANIK”
ARMED FORCES ACADEMY
SLOVAK REPUBLIC

INTERNATIONAL CONFERENCE of SCIENTIFIC PAPER
AFASES 2014
Brasov, 22-24 May 2014

THE INFLUENCE OF HEAT AND SURFACE TREATMENT ON THE WEAR RESISTANCE OF TITANIUM ALLOYS

Camelia PITULICE, Ioan GIACOMELLI, Maria STOICANESCU

Transilvania University of Braşov, Romania

Abstract: Titanium and titanium alloys are on the full rise in their fields of use and, as a consequence, the studies related to them enjoy a growing attention. The wear, one of the common applications in practice can be improved through changes in structure and through the composition and nature of the superficial layers. This paper examines both the opportunities provided by heat treatments on the structural changes of the mass of alloy, respectively the surface treatments on the durability in the abrasive friction. Among the thermal treatments that have been applied there are: hardening and annealing in air atmosphere and in vacuum installations; the surface treatments is consisted by nitriding and laser pulsed process coating. Wear tests have established the hierarchy of the efficiency of these processes.

Keywords: titanium, heat treatment, surface treatment, wear, nitriding, resistance

1. GENERAL CONSIDERATION

Titanium alloys with wide applications in various fields, from manufacturing to aviation, electrotechnics, electronics, medicine, present multiple structural systems, possibilities offered by their polymorphism. Various structural compositions can be obtained through heat and thermo chemical treatment operations. In titanium alloys, there are typically three types of layers, as in the Ti-Al system (figure 1).
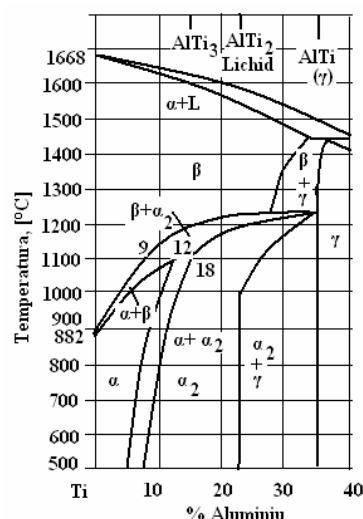
Figure 1. The Ti-Al equilibrium diagram [1]

Also, both in binary alloys of titanium, but especially in the polynary alloys, more complex structures can be found through the presence of intermetallic compounds.

These structures give produce different sets of extremely different properties.

Various structural aspects may be obtained both though chemical composition, but also through heat treatment, treatment that can be efficient due to allotropic transformation of titanium: the α allotropic form under 882°C with hexagonal compact lattice (h.c.), respective the β allotropic form above this temperature, with centered cubic volume lattice (c.c.v.). The alloying elements, extremely numerous in the case of titanium, may cause stabilization for α phase Al, Ge, C, N, O, Ca) or for β phase (V, Mo, Cr, Si, Mn) as in figure 2.
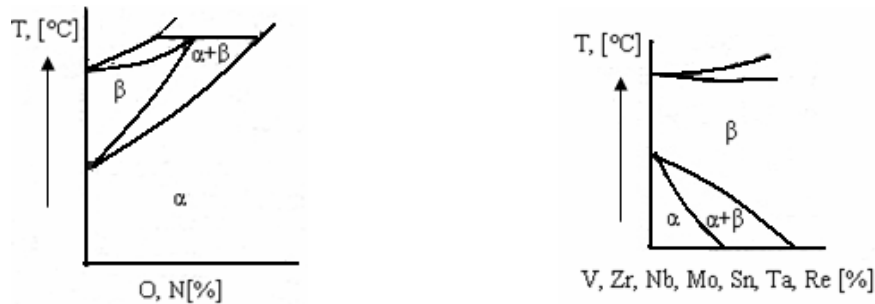
Figure 2. The Ti-X equilibrium diagram for alphagene (a) and betagene (b) alloy elements [2]

In addition, the alloying elements form, as it has been shown, defined Ti_mX_n type compounds and out of balance phases (through thermal treatments) such as:

- the α′ phase: supersaturated in betagene elements solid solution with deformed hexagonal lattice;
- the α″ phase: the martensitic solid solution with rhombic lattice;
- the $β_{sem}$ phase: supersaturated solid solution;
- the ω phase: solid solution with hexagonal lattice.

Each of these phases, with their own properties, imprints features included in a wide range of values to the alloy in equilibrium or heat-treated, according to the quantitative ratio of them.

1. EXPERIMENTAL TESTS

For the experimental tests, it has been chosen the Ti6Al4V titanium alloy, which can be found in applications from many areas. The standardized and the experimentally determined chemical compositions are provided in table 1.

Table 1. The chemical composition for Ti6Al4V titanium alloy

No.	Values	Chemical composition [%]								
		Al	V	Fe	C	N	O	H	Ti	Residual elements
1	after AS9100 ISO 14001	5,5-6,75	3,5-4,5	≤0,4	≤0,08	≤0,05	≤0,2	≤0,015	rest	≤0,4
2	measured	6,23	4,14	0,2	0,02	0,02	0,19	0,003	rest	<0,4

"HENRI COANDA"
AIR FORCE ACADEMY
ROMANIA

"GENERAL M.R. STEFANIK"
ARMED FORCES ACADEMY
SLOVAK REPUBLIC

INTERNATIONAL CONFERENCE of SCIENTIFIC PAPER
AFASES 2014
Brasov, 22-24 May 2014

A large number of specimens for the wear tests have been produced from the material with the composition given above, delivered by the supplier in the form of a 20 mm diameter bar. These were distributed in three for each type of treatment. The treatments applied, the technological parameters as well as some mechanical properties obtained are shown in table 2.

Table 2. Treatments applied to the samples for wear tests [3]

No.	Kinds of material	The treatment applied	The technological parameters			Hardness [HRC]	Resilience KCU [J / cm^2]
			Temp. [°C]	Time [min]	Quenching medium		
1		Delivery status	-	-	-	42,56	55,30
2		Hardening in the furnace with controlled atmosphere	850	60	water	53,46	36,58
3		Hardening in vacuum	1020	90	nitrogen ventilated	56,56	37,17
4	Ti6Al4V	Hardening and annealing	500	60	air	54,63	40,42
5		Hardening in vacuum and annealing	500	30	air	58,13	46,33
6		Hardening, annealing and nitriding	520	240	air	844,56 [HV 0,3]	-
7		Hardening, annealing and nitriding	540	240	air	881,06 [HV 0,3]	-

The samples that had been taken were tested for resistance to wear. It was used a TRIBOMETER device with a SUBTRONIC 25 TAYLOR HOBSON PRECISION component, to determine the profile of the wear surface (figure 3).

a)   b)
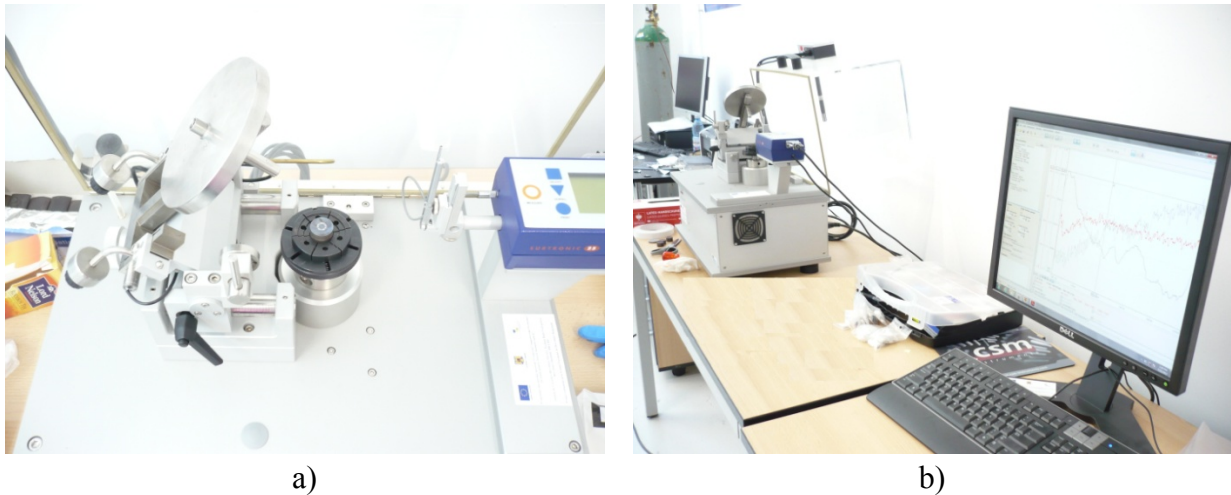
Figure 3. The tribometer device to determinate the wear resistance:
a) the test facility; b) connecting the tribometer to a PC

The tests were carried out by pressing a sphere with a diameter of 6 mm on the surface of the sample, with a force of 10N, a linear speed of 10cm/s and a stop after 5000 laps. The wear rate is provided directly after measuring the surface of the wear trace with the help of the tribometer surface analyser, the specialized software is the one that provides the test results.

In table 3, there are presented the average wear rates of the samples with different structures, coming from the heat treatments previously applied.

Table 3. The wear rate

No.	Kinds of material	The treatment applied	The metallographic structure of samples	The wear rate $[10^{-6}\ cm^3/\ N{\cdot}m]$
1		Delivery status	$\alpha+\beta$	0,934
2		Hardening in the furnace with controlled atmosphere	$\alpha+\alpha'+\beta$	0,561
3		Hardening in vacuum	$\alpha''+\beta_x+\omega$	0,729
4		Hardening and annealing	$\alpha+Ti_mXn+\beta$	0,472
5	Ti6Al4V	Hardening in vacuum and annealing	$\alpha+\beta_x+\omega$	0,314
6		Hardening, annealing and nitriding	nitrogen	0,522
7		Hardening, annealing and nitriding	nitrogen	0,336

During the series of trials, there have also been done the measurements of the volumes of material lost through wear, at different periods of time. The test conditions were the same as above. The table 4 and figure 4 show this aspect of the wear process.

“HENRI COANDA”
AIR FORCE ACADEMY
ROMANIA

“GENERAL M.R. STEFANIK”
ARMED FORCES ACADEMY
SLOVAK REPUBLIC

INTERNATIONAL CONFERENCE of SCIENTIFIC PAPER
AFASES 2014
Brasov, 22-24 May 2014

Table 4. The volume losses during the trials

Time [min]	The lost volume, $[10^{-6} \text{ mm}^3]$			
	Sample in delivery status	Sample hardened from 850°C	Sample hardened from 850°C, annealed to 500°C, 60 min	Sample hardened from 850°C, annealed to 500°C, 120 min
5	0,05553838	0,04801529	0,07312854	0,06000434
10	0,1319666	0,115608	0,1475726	0,1824015
15	0,2070887	0,1999108	0,1818821	0,150185
20	0,3082072	0,2079159	0,2743207	0,1758861
25	0,3866197	0,3643489	0,3383027	0,2352871
30	0,4385598	0,3898323	0,3658791	0,2675284
35	0,4730372	0,3924167	0,4068844	0,3590557
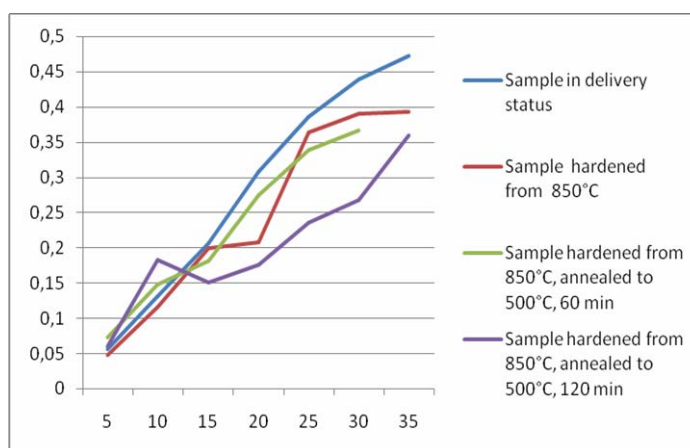
Figure 4. The variation of loss wear volume in the samples analyzed

The above mentioned ideas prove that there are notable differences in wear resistance, depending on the treatment.

Based on the sample values in as-annealed (delivery) status, there can be obtained significant increases of them, determined by the metallographic structure.

An increase of the hardness and the decrease of the wear rate can be achieved through the hardening; the annealing can be achieved through the precipitation of ω phase; the hardness further increases with favorable effects on durability. Good results can also be obtained through thermo chemical treatment (respective nitriding). In all the analyzed variants, the resilience is being kept relatively high, with good effects on shock resistance.

2. CONCLUSION

The experimental tests have demonstrated the capability of the titanium alloys to respond to the heat treatments through structural changes. This layout allows modifications of certain mechanic features depending on the necessities.

It has been proven that there is a significant correlation among the structure, the mechanic properties and the wear resistance.

Also, it has been demonstrated that there are advantages of vacuum heat treatment, especially after annealing, over the one in air atmosphere or atmosphere controlled.

The nitriding thermo chemical treatment proved to be more effective at 540°C, when the diffusing layer proved to be more consistent.

REFERENCES

[1] Dumitrescu, C., Şerban, R., *Metalurgie fizică şi tratamente termice*, Ed. Fair Partners, Bucureşti, vol. II, 2001

[2] Fătu, S., Tudoran, P., *Studiul materialelor metalice. Tratamente termice. Oţeluri aliate. Aliaje neferoase. Materiale noi*, Vol. II, Editura Libris, Braşov, 1997, pag. 74-75, 80-82, 99-111

[3] Pitulice, C., Giacomelli, I., Stoicănescu, M., *Studii privind modificări structurale în aliaje de titan prin tratamente termice*, susţinută la sesiunea ştiinţifică a ASTR

[4] Pitulice, C., Veţeleanu A., Giacomelli, I., *Influenţa tratamentului termic asupra biocompatibilităţii aliajului Ti6Al4V*, Cercetări metalurgice şi de noi materiale, Institutul de Cercetări metalurgice, Camera de comerţ şi industrie a municipiului Bucureşti şi Universitatea Transilvania Braşov, vol. XXII, nr. 1, 2014

"HENRI COANDA"
AIR FORCE ACADEMY
ROMANIA

"GENERAL M.R. STEFANIK"
ARMED FORCES ACADEMY
SLOVAK REPUBLIC

ESEM AND X-RAY EMISSION SPECTRA OF TITANIUM ALLOY IN DIFFERENT STRUCTURAL STATUS

Camelia PITULICE, Adriana ZARA, Nicoleta TORODOC, George VASILE

TRANSILVANIA UNIVERSITY OF BRASOV

Abstract : *Upon Ti6Al4V titanium alloy there were effectuated different heat treatment operations. The results obtained were tested by numerous processes such as optical microscopy, mechanical and technological attempts, and also ESEM - Enviromental Scanning Electron Microscopy investigation and X-ray analysis , respectively. The latter are the objectiv of this paper. Trough these observations there has been highlighted a series of aspects regarding the composition and internal structure of the alloy in different states obtained by heat treatment . There has been also establish the proportion between the structural phases. These analyzes come to complete the data necessary for an accurate assessment of the influence of thermal treatment concerning use characteristics. Thus, it can be chosen the structural state according to practical necessites. There are presented in this paper, some of this investigations.*

Keywords: *titanium alloy, metallographic structure, hardening and tempering, ESEM- Enviromental Scanning Electron Microscopy , X-ray spectra.*

1. INTRODUCTION

Titanium alloys, they benefit from numerous advantages concerning the properties, as compared with other metallic materials, such as low density (about 4.5 g/cm^3), high refractoriness, corrosion resistance, good weldability, mechanical properties appreciable. Meanwhile, the two allotropes Ti α compact hexagonal lattice and Ti β with volume centered cubic lattice, offers them application availability of many heat treatment operations. [1, 3]. Among the addition elements of titanium, the most common are aluminum, vanadium, molybdenum, chromium. The titanium alloys, with properties that can appear in a wide range of value found accordingly and varied utility such as in aeronautics, marine, chemical energy, chemical industry, in medical prostheses, etc.[2]. For the present research it has been chosen Ti6Al4V titanium alloy whose chemical composition is given in Table 1.

Table 1. Chemical composition of the alloy Ti6Al4V

Sort of alloy	Chemical composition, [%]							
	Al	V	Fe	C	N	O	H	Ti

Ti6Al4V	6,23	4,14	0,20	0,02	0,02	0,19	0,003	rest

2. APPLIED THERMAL TREATMENTS

From the above composition of semi-finished, there were made attemps specimens required. These were subjected to heat treatments given in Table 2.

Table 2. Thermal treatments applied titanium alloy Ti6Al4V

Nr. crt.	Applied Treatments	Temp. [°C]	Time [min]	Cooling Medium	Hardness [HRC]	Resilience [KCU]
1	Delivery status	-	-	-	42,56	55,30
2	Hardening	850	60	apă	53,46	36,58
3	Tempering (aging)	500	60	apă	54,63	40,42

The heating temperature was set to 850 ° C, found in the stability domain of the α phase. Maintanance duration it was determined so that to be realized both, the temperature uniformity on section and also the development time needed to make structural changes. Considering the increase in hardness after heating at 500 ° C subsequent hardening, it appears that this operation is actually an artificial aging. Successively the samples treated, they had structures such as:

$$\text{inițial } \alpha+\beta \xrightarrow{\text{hardening from } 850°C} \alpha+\alpha''+\beta \xrightarrow{\text{aging at } 500°C} \alpha+Ti_mX_n+\beta \ [2]$$
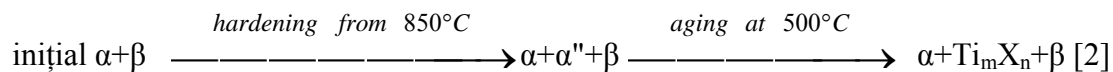
in which: - α" - has a martensitic structure with a rhombic chrystalline lattice; - Ti_mX_n - an intermetallic phase which precipitates during cooling and maintaining from 500 ° C.

3. THE RESULTS OF ANALYSIS BY ESEM AND SPECTRAL X

Enviromental Scanning Electron Microscope - ESEM - is a method for investigating of surfaces studied micro and nano scale. On the analyzed area it is sent an electron beam that scans an certain area; it will generate more signals, which received and processed generates information regarding on the chemical composition of the samples and structure. Investigations revealed the following:
- For sample in delivery status. Figure 1 shows the micrograph of the existence of two main constituents, one with an aspect compact α and another with a cvasilamelar aspect, a mixture of α + β.

"HENRI COANDA"
AIR FORCE ACADEMY
ROMANIA

"GENERAL M.R. STEFANIK"
ARMED FORCES ACADEMY
SLOVAK REPUBLIC

INTERNATIONAL CONFERENCE of SCIENTIFIC PAPER
AFASES 2014
Brasov, 22-24 May 2014
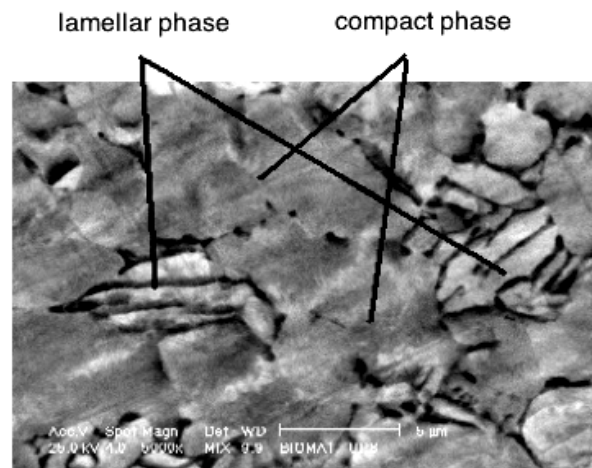
Figure 1. Micrograph alloy Ti6Al4V in delivery status obtained by ESEM .

The emission spectrum of compact phase of solid solution α, identifies an content of titanium and aluminum. In the lamellar phase was identified among titanium and aluminum also vanadium in addition rate of 3.25%. The X-ray emission spectra for these two constituents and the chemical composition are shown in Figures 2 and 3.
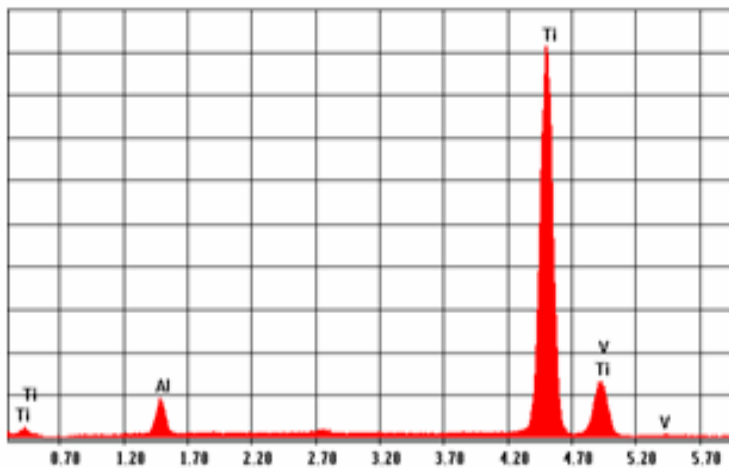
Element	Percent by weight Wt [%]
Al	7.91
Ti	92.09
V	0
Total	100

Figure 2. The X-ray emission spectrum of the compact phase. Ti6Al4V alloy. Delivery status.

.
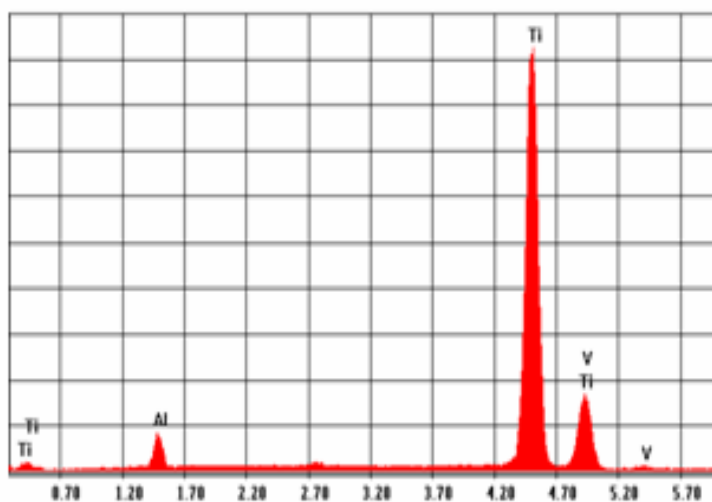
Element	Percent by weight Wt [%]
Al	6.92
Ti	89.82
V	3.25
Total	100

Figure 3. Ray emission spectrum in the lamellar phase.

According to program ImageJ analysis resulted a 62% proportion of compact phase and 38% lamellar phase. - for the sample water hardening from 850° C. For this case also there have been effectuated ESEM analysis and X-ray emission spectrum. Metallographic structure (fig. 4) reveals o radical change compared with the previous , the two constituents being more accurate delimited. The compact phase of solid solution reduced quantitatively; the constituent on mechanic mixture type gained an acicular aspect with a higher share.
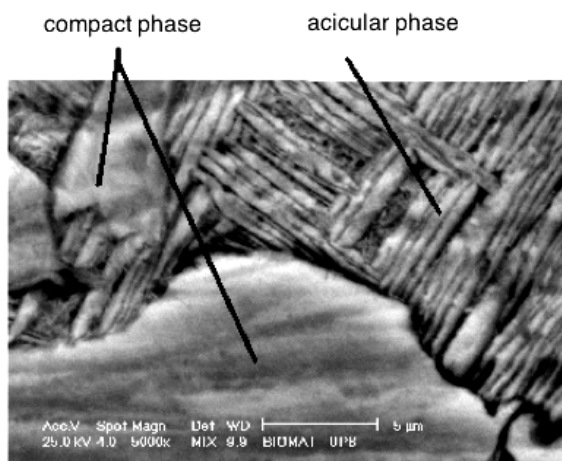
Figure 4. ESEM micrograph for Ti6Al4V alloy, hardened in water at 850 ° C.

This is composed of a mixture of phases α "+ β + Ti_mX_n. Changing the quantitatively report between constituents, as well as finely dispersed structure and qualitatively different from the original mixture phases (acicular phase) explains the differences measured of some mechanical properties.

"HENRI COANDA"
AIR FORCE ACADEMY
ROMANIA

"GENERAL M.R. STEFANIK"
ARMED FORCES ACADEMY
SLOVAK REPUBLIC

INTERNATIONAL CONFERENCE of SCIENTIFIC PAPER
AFASES 2014
Brasov, 22-24 May 2014
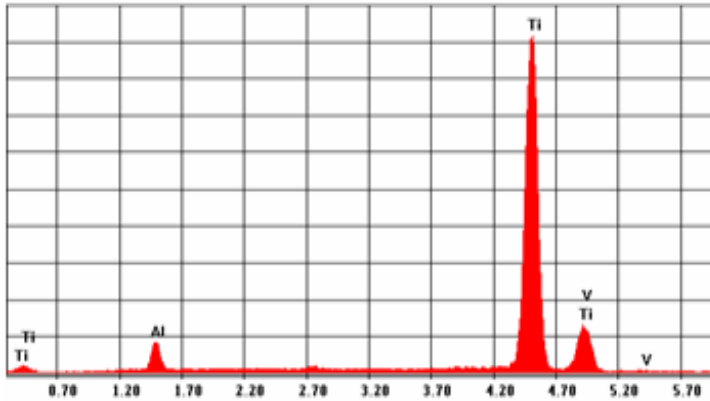
Element	Percent by weight Wt [%]
Al	7.37
Ti	92.63
V	0.00
Total	100

Figure 5. X-ray emission spectrum in the compact phase. Ti6Al4V alloy. Hardening in water from 850 ° C.
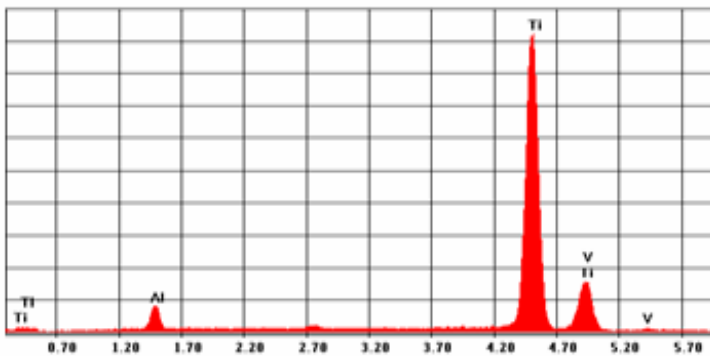
Element	Percent by weight Wt [%]
Al	6.94
Ti	90.97
V	2.09
Total	100

Figure 6. X-ray emission spectrum in the acicular phase. Ti6Al4V alloy. Hardening in water from 850 ° C.

The quantitatively report of constituents in this state is 38,6% compact phase and 61,4% acicular phase : - for sample hardening from 850° C and aging at 500° C. After hardening from 850°C effectuated with a higher speed in water, on some samples it has been applied a one hour reheating at 500° C. As was shown this heating , by its effects is an aging ; more specifically this is an artificial aging, which place the alloy in second stadium of this process. During the heating occurs an complete process of precipitation of a secondary phase Ti_mX_n .
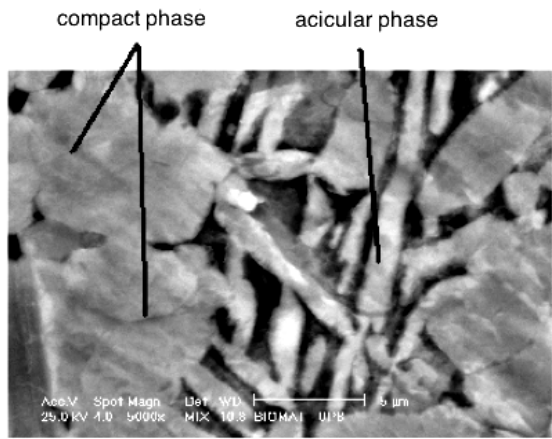
Figure 7. ESEM image of Ti6Al4V alloy, water hardened from 850 ° C and aged at 500 ° C.

Emission spectrum of the compact phase found the presence of titanium and aluminum components   (see Figure 8). Emission spectrum of the mechanical mixture with acicular aspect indicates also the presence in a proportion of 4.81% of vanadium (Figure 9).
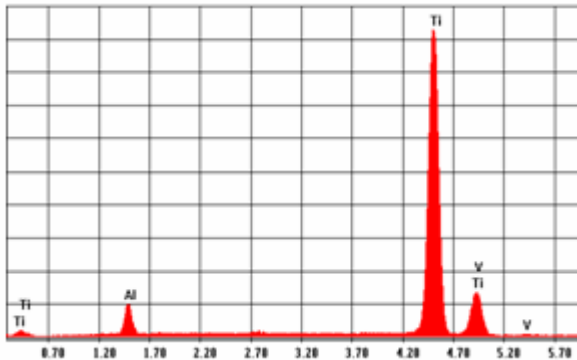
Element	Percent by weight Wt [%]
AlK	8.36
TiK	91.64
V K	0.00
Total	100

Figure 8. Emission spectrum in the compact phase. Ti6Al4V alloy. Tempering and aging at 850 ° C to 500 ° C
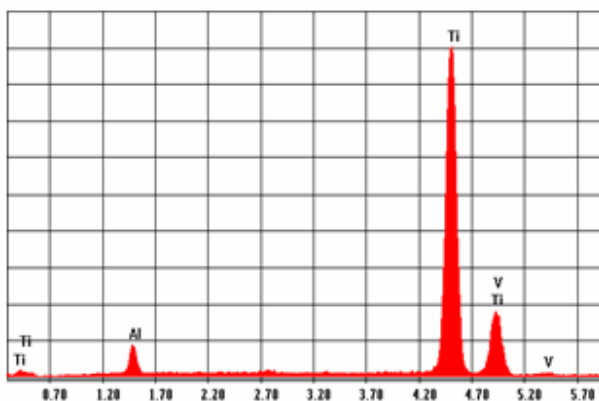
Element	Percent by weight Wt [%]
AlK	7.06
TiK	88.12
V K	4.81
Total	100

Figure 9. Emission spectrum in the RX acicular phase . Ti6Al4V alloy. tempering and aging at 850 ° C to 500 ° C.

In this case, the quantitatively report of   constituents is 65.5% compact phase and 34.5% acicular phase .

"HENRI COANDA"
AIR FORCE ACADEMY
ROMANIA

"GENERAL M.R. STEFANIK"
ARMED FORCES ACADEMY
SLOVAK REPUBLIC

INTERNATIONAL CONFERENCE of SCIENTIFIC PAPER
AFASES 2014
Brasov, 22-24 May 2014

4. CONCLUSIONS

Thermal treatments aim to change some physical-mechanical characteristics in order to obtain the necessary properties for further processing or use. These properties are determined by the structural composition of alloy and the quantitatively report of the phases.

Experimental attempts of the present work were able to produce significant changes in the structural aspect of Ti6Al4V alloy, supported also by mechanical properties (density, resilience).

Through investigations effectuated by electron microscopy and X-ray it was revealed internal structure of the alloy in three different status, refering to the size and shape of the grains, the nature of the phases of the structure, their reciprocally arrangement also quantitatively report of phases.

All this is fully consistent both with the sequence of thermal operations but also with performed properties. Also, it is concluded that in the case of the present alloys and thermal parameters used, the heating subsequently hardening could be enclose in the artificial aging. The temperature of 500 ° C places the alloy in stage II of the aging process.

5. REFERENCES

1. Collings, EW, Boyer, R., Welsch, G., *Materials properties handbook. Titanium Alloys,* ASM International, pp. 3-170, 483-609, (1994).aaaaaaaaaaaaaaaaaaaaa aaa
2. Dumitrescu, C., Serban, R., *Physical metallurgy and heat treatment*, Ed. Fair Partners, Bucharest, vol. II, (2001).
3. Fatu, S., Tudoran, P., *Study of metallic materials. Thermal treatments. Alloy steels. Alloys. New Materials*, Vol. II, Ed. Libris, Braşov, pp. 74-75, 80-82, 99-111, (1997).
4. Pitulice, C., - *Studies and research on biocompatible materials used in prosthetics*, Thesis - Transilvania University of Brasov, (2013).

ENGINEERING SCIENCES

"HENRI COANDA"
AIR FORCE ACADEMY
ROMANIA

"GENERAL M.R. STEFANIK"
ARMED FORCES ACADEMY
SLOVAK REPUBLIC

INTERNATIONAL CONFERENCE of SCIENTIFIC PAPER
AFASES 2014
Brasov, 22-24 May 2014

EVALUATION OF STRESS-STRAIN PROPERTIES OF SOME NEW POLYMER-CLAY NANOCOMPOSITES FOR AEROSPACE AND DEFENCE APPLICATIONS

Fulga TANASĂ, Mădălina ZĂNOAGĂ, Raluca DARIE

"Petru Poni" Institute of Macromolecular Chemistry, Iaşi, România

Paper dedicated to the 65th anniversary of the
"Petru Poni" Institute of Macromolecular Chemistry of Romanian Academy, Iaşi, România

Abstract: *This paper presents the effects of three different types of layered silicates, namely bentonite (Btn), Montmorillonite K10 (K10) and Nanomer I.30P (I.30P), on the performance of some new hybrid materials based on a commercial polypropylene. The study evaluated the dependence of mechanical properties on the clay nature and particle size. Low volume additions (≈5%) of clay nanoparticles have influenced differently the interfacial adhesion between matrix and filler, yielding in modified stress-strain properties. Experimental data indicated that Btn and I.30P acted as reinforcing fillers, whereas K10 behaved as a plasticizer.*

Keywords: *polymer-clay nanocomposites, mechanical properties, interfacial adhesion*

1. INTRODUCTION

Starting from the Toyota Research Group first polymer-clay nanocomposite, the improvement of properties of this new class of materials intended for structural applications was demonstrated. They rapidly enjoyed a spectacular success in military and commercial aircraft equipment, the automotive industry and even sporting goods and health care products.

Polymer-clay nanocomposites have been considered as matrices for fiber-reinforced composites for aerospace components, since the aerospace industry requires lightweight materials with high strength and stiffness, among other qualities. These enhanced polymer systems provide opportunities to address material limitations in advanced system concepts: impact resistance, control over the coefficient of thermal expansion, enhanced fire retardancy, superior barrier properties against gas and vapor transmission (for military rations in defence industry, for barrier liners in storage tanks and fuel lines for cryogenic fuels in aerospace systems), suppression of microcracking and increased modulus, enhanced scratch resistance and ballistic performance, etc. [1-3]. The use of such composites as structural materials in both commercial and general aviation aircraft has been increasing, primarily because of the advantages composites offer over metals (*e.g.*, lower weight, better fatigue performance, corrosion resistance, tailorable mechanical properties, better design flexibility, lower assembly costs) [3]. While most of the Airbus A 380 fuselage is aluminum, composite materials comprise more than 20% of its airframe. Boeing 787 Dreamliner is 80%

composite by volume and each 787 contains approximately 35 short tons of carbon fiber reinforced plastics (CFRPs), made with 23 tons of carbon fiber.

Ongoing research and studies have shown that, in general, polymer-clay nanocomposites exhibit great improvement in mechanical properties, such as strength and stiffness, compared to pure polymers upon addition of minimal amount of nanosize clay particles. Since the use of nanoscale fillers in polymers has granted the possibility to design new materials with significantly improved performance and multifunctionality, numerous polymers have been investigated: poly-propylene, polyethylene, polystryrene, poly-caprolactone, polyimides, polycarbonates, poly(ethylene oxide) and epoxydic resins [2].

Polypropylene (PP) is one of the most widely used polyolefins and one of the most interesting thermoplastic materials due to its low cost, low density, high heat distortion temperature, processability and extraordinary versatility in terms of tailored properties and applications [4].

Huge consumption of polypropylene in hi-tech industries motivates the scientific community to find new approaches to improve mechanical properties of this polymer, so they don`t negatively affect other required performance properties like impact resistance, controlled crystallinity, toughness and shrinkage. In order to improve polypropylene competitiveness in engineering applications, it is desirable to increase dimensional stability, heat distortion temperature, stiffness, strength, barrier properties, and impact resistance without sacrificing the processability.

Nowadays, clay nanoparticles play a key role in improving the mechanical, surface and barrier properties of PP. The most commonly used clays are from the smectite mineral group, such as monmorillonite (MMT), hectorite and saponite [5]. Montmorillonite belongs to the layered silicates nanoclays class, consisting of nanoparticles with anisotropic, plate-like, high aspect-ratio morphology, which leads to an improved permeation barrier. Using montmorillonite, the matrix polymer is expected to display increased dimensional stability at low reinforcement loading, characteristic that

makes it useful in aerospace and automotive industry. MMT has the widest acceptability for use in polymer-clay nanocomposites because of its availability, well known intercalation and/or exfoliation chemistry, high surface area and high surface reactivity. The layer aspect ratio can be in the range 1000 in well dispersed state without breaking of layers (although, during preparation process of nanocomposite, the breaking of clay layers into small plates occurs and the aspect ratio decreases to about 300-500) and surface area is about 750 m^2/g [6].

Despite of its advantages, MMT is incompatible with polymers, since it is a hydrophilic compound, as all nanoclays from its class. Therefore, it is recommendable to use organically modified clays in order to improve the matrix-filler compatibility which strongly affects the interface adhesion properties of nanocomposites. Even more, a compatibilizing agent, such as maleic anhydride grafted polypropylene (PP-g-MA), in the case of PP-clay nanocomposites, may be used during preparation [7,8].

Melt intercalation by twin-screw extrusion is the main method to obtain polymer-clay nanocomposites. The success of the exfoliation by melt blending is associated with the presence of strong interactions between clay and polymer chains, as well as the diffusion of polymeric chains among clay layers. The process efficiency depends on the temperature, processing time, and screw shear profile. Moderate processing intervals, low process temperature, and medium shear rates were proven to be the best experimental conditions to obtain the dispersion of the clay in exfoliated and intercalated structures. Melt-mixing or compounding is the preferred processing method in the case of PP-clay nanocomposites because it is generally more attractive than solution preparation (or, in other cases, *in situ* polymerization), due to the better commercial feasibility and lower costs [9,10].

This paper presents a study on the variation of mechanical properties of a series of new polypropylene-clay hybrid nanocomposites obtained by the melt compounding technique, starting from a commercial grade PP and using three different types of nanoclays, namely:

bentonite (Btn), a Romanian native clay from Valea Chioarului (Maramures), containing 70% MMT; Montmorillonite K10 (K10); Nanomer I.30P (I.30P), an organically modified MMT. The use of the Romanian native bentonite as filler for hybrid composites was investigated as a viable alternate option to other clays, because it is less expensive than commercial MMT. The comparative evaluation of these new nanocomposites was performed in order to estimate their competitiveness and to envisage the range of applications.

2. EXPERIMENTAL

2.1 Materials. The *polypropylene* used in experiments was an isotactic polypropylene (Malen-PF 401), a product supplied by Petrochemia Plock S.A. Poland. Polymer has a melt temperature of 170°C; decomposition temperature range 250–430°C, Vicat softening point 148°C; melt flow index (2.16 kg/230°C) 2.4–3.2 g/10min; volatile matter 0.3%wt.; isotactic index 95%.

Commercial additive agents, *viz.* Na-bentonite, Montmorillonite K10 and Nanomer I.30P were used as received.

Na-Bentonite was provided by S.C. Mateo S.R.L. It was collected at the site Valea Chioarului (Maramures County, Romania) [11]. Main characteristics of bentonite: powder, light cream colored, specific surface area = 25-30 m^2/g; apparent specific weight = 260-300 g/L; particle size 9-20μm.

Montmorillonite K10 is a sodium mont-morillonite (MMT) clay, with a high-purity grade, supplied by Sigma Aldrich Co. (USA). Main characteristics: specific surface area of 220–270 m^2/g; white powder; bulk density = 300-370g/L; particle size 5-10 μm.

Nanomer I.30P is an organically modified montmorillonite, was donated by Nanocor Inc., USA. Main characteristics: natural montmorillonite (MMT) modified by octadecylamine (70-75% montmorillonite and 25-30% octadecylamine), white powder; density 1.7 g/cm^3; mean dry particle size 10-25 μm, specific surface area of 9.51 m^2/g and interlayer distance 2.10 nm.

2.2 Hybrid nanocomposites preparation

2.2.1 Melt processing. The hybrid organic-inorganic composite samples with different clay types, added in the same amount (5%), were prepared by melt mixing in a HAAKE RHEOCORD 9000 mixer (equipped with two internal roller mixers and a capacity of mixing chamber of 48.3 cm^3; fill factor 0.8).

Before compounding, PP and clays were thoroughly dispersed in acetone for 1 h and dried, first in air and then at 80°C in a vacuum oven for 24 h to remove moisture and to enable uniform distribution of PP pellets and clay particles, which will subsequently influence the nanocomposites homogeneity. Samples composition is listed in Table 1.

Table 1.
Composition of the nanocomposite samples

Sample	Clay	Clay particle size, μm	Composition, %	
			PP	Clay
PP	–	–	100	–
PP-Btn	Bentonite	9-20	95	5
PP-MMT	Montmorillonite K10	5-10	95	5
PP-I.30P	Nanomer I.30P	15-25	95	5

Processing parameters were chosen as to minimize possible degradation of the matrix polymer and the inorganic filler. The mixing temperature was maintained at 190°C, the rotor speed was set at 100 rpm and the time was 7 min. After processing, samples were removed from the mixer and cooled down to room temperature.

2.2.2 Test samples preparation. For the mechanical tests, composites were cut into small chips or granules, which were then dried. In order to prepare films of desirable dimensions, the composite chips were pressed between Teflon sheets (12 MPa at 200°C for 5 min) in a laboratory heated press. The samples were then cooled in the press to room temperature. Films with thickness of about 1.0 mm were obtained. Specimens were finally cut in the usual dumb bell shape.

2.2.3 Mechanical testing. Tensile measurements, tensile strength, $\sigma = F/A_0$ *vs.* elongation ε (%) = $(l - l_0)/l_0$, were performed at room temperature using a tensile test machine TIRA-TEST 2200 Germany, according to ASTM D-638-08. Measurements were made to a crosshead speed of 10 mm/min. Bone-shaped test specimens were cut from a single test bar using a hydraulic knife along the same direction. Five specimens of each sample were tested to establish testing reproducibility and average values are given with the standard deviations. The deviation of the data around mean values was less than 5%.

3. RESULTS AND DISCUSSION

3.1 Influence of the clay nature on the stress-strain relationship in nanocomposites. Mechanical properties of polymer-clay nanocomposites can be altered by various factors: properties of the polymer matrix, clay particle size and morphology (anisotropic, platelet-like, high aspect-ratio), particle loading and distribution, interfacial adhesion between clay and matrix, etc. Mechanical properties of hybrid composites are strongly related to the interfacial adhesion between clay particles and matrix, as known. The interactions in the polypropylene–clay systems are responsible for significant changes in mechanical properties. A strong interfacial adhesion leads to high tensile strength and low elongation, whereas a weak interfacial adhesion leads to low strength and relatively high elongation [12]. Table 2 shows experimental data obtained for some mechanical properties of the hybrid composites.

It was observed that the clay nature had critical effects on the mechanical properties of samples. Of primary importance for our study are Young's modulus, strength at the yield point and tensile strength.

The Young's modulus (elastic modulus) of a clay–polymer composite is generally determined by the elastic properties of its components (filler and matrix), particle loading and aspect ratio [13]. As known, the elastic modulus is a stiffness parameter which governs by the size and amount of the dispersed phase. In the light of the fact that the

Table 2. Mechanical properties of the nanocomposites samples

SAMPLE	Young modulus (MPa)	Yield strength (MPa)	Elongation at yield (%)	Tensile strength (MPa)	Elongation at break (%)
PP	1512	31.97	5.06	26.11	8.20
95PP/5 Btn	2198	30.35	3.96	27.83	5.06
95PP/5 K10	1159	18.21	8.69	18.00	10.77
95PP/5 I.30P	2146	28.27	3.61	26.43	4.29

inorganic particles are rigid and have a much

higher stiffness than the thermoplastic matrix,

the composite modulus can be readily improved by adding either micro- or nanoparticles. In our case, the Young's modulus, determined from the slope of the initial elastic region, was 1512 MPa for neat PP, whereas its values for PP-Btn and PP-I.30P nanocomposites increased with 42-45% upon addition of 5% clay, as compared to pure polymer matrix. At the same time, it was observed that Young's modulus for samples with K10 decreased with approx. 25%.

This variation depends mainly on the microstructure and the interface morphology of the polymer-clay composites (including the interfacial bonding, the form, size and spatial distribution of the clay particles into the matrix, as well as the thickness of the interface) [14]. When there is a poor binding between the matrix and clay, the composite becomes brittle because the applied load may not be transferred to the clay [15]. Therefore, considering the nature of clays, it is obvious

"HENRI COANDA"
AIR FORCE ACADEMY
ROMANIA

"GENERAL M.R. STEFANIK"
ARMED FORCES ACADEMY
SLOVAK REPUBLIC

INTERNATIONAL CONFERENCE of SCIENTIFIC PAPER
AFASES 2014
Brasov, 22-24 May 2014

that I.30P had a beneficial effect on the nanocomposites elastic modulus than K10, due to the presence of the aliphatic segments (belonging to the organic modifier, octadecyl-ammonium) in its structure which acts as a compatibilizing agent. An interesting behavior was recorded for the Romanian native bentonite: at the same clay content, the corresponding nanocomposite samples showed the highest value of Young's modulus. As Btn is not organically modified and despite the low polarity of PP, we presume that its strengthening effect, as result of adhesion forces at the interface, may be exclusively due to its particular composition and particle size, as well as particles distribution in the matrix as resulted from processing.

On the other hand, the yield strength of the PP-Btn nanocomposites decreased about 5%, 12% for PP-I.30P and 43% for PP-K10, respectively, compared with neat PP. Concerning the tensile strength, values slightly increased for PP-Btn (6.6%) and PP-I.30P (1.2%), but for PP-K10 the tensile strength registered a dramatic decrease of about 31%.

The strength of nanocomposites relies on the effectiveness of stress transfer between matrix and filler [13]. Factors like particles-matrix interfacial bonding strength and particle loading, as well as particle size, significantly affect the composite stress-strain behavior. For well-bonded particles, the applied stress can be efficiently transferred to the particles in the matrix, which clearly improves the strength (Btn and I.30P). However, for poorly bonded particles (K10), the strength decrease occurs upon adding particles because the adhesion is still weak at the interface, despite the increase of the interfacial layer volume on the expenses of the overall matrix volume. This explains data we obtained for all our PP-clay nanocomposites.

Nanoclay particles are stiff materials with no elongation properties; therefore, their addition can lower composites elongation [16]. The elongation at yield for PP-Btn and PP-I.30P decreased, as expected, with approx. 22% and 28.5%, respectively, whilst for PP-K10 increased with 55%. Concerning the elongation at break, samples PP-Btn and PP-I.30P displayed a decrease of 38% and 48%, respectively, but samples PP-K10 showed an increase of 31%. This behavior of hybrid composites, consistent with data for elastic modulus and upholding our hypothesis, was induced by the stiffness of clays and caused by the clay-polymer interface adhesion.

A geometric model to correlate the interfacial adhesion and the fracture mechanism (Figure 1) is already available [17] and it takes into consideration the voids formation and their evolution during stress.
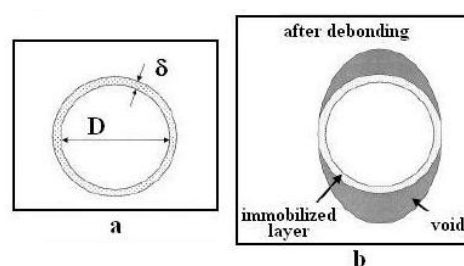
Figure 1. A geometric model
that correlates the interfacial adhesion and the
voids formation mechanism
(D=particle diameter; δ=interfacial layer thickness)

It has been shown [17] that clay particles can facilitate the development of microvoids and activate dilatational yielding in the deformed zone close to the fracture surface. It is generally agreed that for toughening to occur in rigid filler systems, the particles must debond from the matrix, creating voids around the particles and allowing the interparticle ligaments to deform plastically [18]. The voids reduce the macroscopic plastic resistance of

the material, and thereby potentially increase the fracture strain and the overall toughness. Ideally, the voids are not likely to form immediately upon application of stress as this may reduce the elastic modulus.

A schematic illustration of the fracture mechanism in PP-clay nanocomposites is presented in Figure 2 [19]. For samples with poor interfacial adhesion (Figure 2a), the cracks start from the pole of the filler surface and form a huge number of microvoids between the filler and matrix.
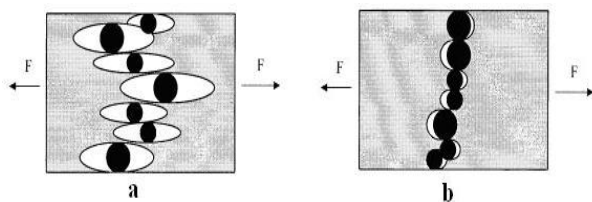
Figure 2. Schematic illustration of fracture mechanism in polymer-clay composites with (a) poor and (b) good interfacial adhesion

The microvoids are dragged along the direction of the stress. This fracture mechanism leads to a low tensile strength and relatively high elongation (PP-K10). On the other hand, in samples with good interfacial adhesion (Figure 2b), the cracks start from the equator of the filler and develop in the matrix or along the interface. Such fracture mechanism leads to a high tensile strength and low elongation (PP-Btn and PP-I.30P). Experimental data presented herein are consistent with the theoretical model, with a special mention for PP-Btn samples that proved to have the best mechanical properties in the series. Further confirmation will be obtained by comparative SEM analysis which is currently underway.

3.2 Effect of particle size on the stress-strain relationship in nanocomposites. The effect of particle size on the nanocomposites mechanical properties has recently attracted much attention. The particles restrict the mobility and deformation of the matrix by introducing a mechanical restraint. The restriction in polymeric molecular diffusion in the presence of solid particles occurs because of an effective attraction potential between segments of the chain and the repulsive potential that the polymer is subjected to when it is close to solid particles. The degree of the particle restriction depends on the properties of the filler and matrix [20].

Interfacial interaction strongly influences properties of polymer composites. In PP-clay composites only van der Waals forces act between polymer and filler. They are, however, sufficient to attach the polymer to the filler. Adsorption of the polymer on the filler surface leads to the formation of an interphase in which molecules have decreased mobility. The existence of the interphase is proved by the increased composite viscosity with increasing specific surface area of the filler and by the similarly changing yield stress and strength (see Table 2). The effect of interaction depends on the size of the contacting surfaces (specific surface area of the filler) and the interaction strength. Smaller particles have larger surface area, leading to increased yield stress. Differences in the strength of the interaction are less significant than that of the specific surface area [18]. Two important structural phenomena must be considered: (1) small particles tend to form aggregates, which deteriorate properties; for particles having specific surface area over $5 m^2/g$, the aggregation tendency becomes significant; (2) orientation of anisotropic particles determines their reinforcing effect.

Despite some assumptions of conventional micromechanics for rigid clay systems (*e.g.*, the zero thickness assumption for interfaces), numerous studies have offered mathematical support for models which include the interface effect by taking into account an interphase region between the matrix and particles [21], such as the self-consistent scheme based on a "particle-interphase-matrix" three-phase unit cell model [22].

As recorded in many other studies, the stress-strain relationship in nanocomposites significantly exceeds classical micromechanics predictions. Another possible explanation, apart from the contribution of the interphase, might be considered the natural trend of particles to aggregate. Therefore, in some systems, the primary nanoparticles aggregation (resulted from particles preparation prior to melt mixing in the presence of the matrix polymer) rather than polymer–nanoparticle interactions at the interface is mainly

"HENRI COANDA"
AIR FORCE ACADEMY
ROMANIA

"GENERAL M.R. STEFANIK"
ARMED FORCES ACADEMY
SLOVAK REPUBLIC

INTERNATIONAL CONFERENCE of SCIENTIFIC PAPER
AFASES 2014
Brasov, 22-24 May 2014

responsible for the observed reinforcement effect [23].

For the series of PP-clay nanocomposites we studied, the experimental data obtained for clays with different particle size, presented in Table 2, are consistent with theories available in the literature [24]. First observation is the opposite effect of K10 platelet-shape nanoparticles, compared with the other clays, despite its low value of particle size (5-10 μm) and narrow size distribution. The micrometric dimensions of particles are given by the primary agglomeration, but the smaller the particle size, the thicker the interphase layer on the expenses of the total volume of matrix, the component that actually contributes to energy adsorption. Therefore, the sample had a lower resistance and the deformation increased by 55% at yield and by 31% at break. For Btn (9-20 μm) and I.30P (15-25 μm) containing samples, the clay particles had a reinforcing effect, although their particle size is higher and have a wider size distribution. By this, the secondary aggregation (caused by composite preparation) occurs in a lower measure.

Both the larger (I.30P) and the smaller (K10) particles had a negative effect on the stress-strain relationship due to the presence of large individual particles (I.30P) or agglomerates (K10), which act as stress-concentrators that trigger the fracture mechanisms. The effect in the K10 containing samples was the result of particle–matrix debonding and plastic stretch of the interparticle ligaments [25]. Composites made with smaller particles would exhibit a larger reduction in the amount of deformable matrix because, at certain filler content, the interfacial area between filler and polymer is larger. This causes the composites made with K10 to exhibit lower fracture resistance (18 MPa) than those made with larger particles, I.30P (26.43

MPa), or medium size particles, Btn (27.83 MPa), regardless of the presence of the primary agglomerates. This effect depends on the compatibility at the filler–matrix interface, which determines the thickness and the mobility of the interphase layer.

3. CONCLUSIONS

This study is focused on the comparative evaluation of mechanical properties of a series of new PP-based nanocomposites, prepared by melt mixing method, using as fillers three different types of clay, in order to establish the level of competitiveness of a Romanian native bentonite to be used as an alternative to commercially available clays.

Experimental results proved that clay addition strongly affects the stress-strain dependence in the new composites. Thus, it was found that Young's modulus and tensile strength increased, whilst elongation at yield and break decreased for composites with Btn and I.30P. For composites with K10, Young's modulus and stress at break decreased, while elongation at yield and break increased. Therefore, K10 acted more as a plasticizer, in opposition with Btn and I.30P which effectively reinforced the matrix. The best results were obtained for samples containing Btn, the natural unmodified filler having an average particle size and size distribution.

For rigid clay systems, delamination of the clay layers occurs and results in a moderately increased toughness. Hence, it was suggested that extensive matrix shear yielding, activated by full debonding of the clay-matrix interfaces, leads to improvements in toughness. The relationship between the toughness of composites and the particle size becomes a competition of two effects: (1) a negative stress concentrating effect of particles

that increases with larger particles and agglomerates, and (2) a reduction in the amount of deformable polymer matrix that dominates in composites with smaller particles. However, due to the low polarity of PP, it is difficult to obtain nanocomposites with homogeneous dispersion of the silicates at the nanometer level inside the polymer. Organoclay containing layered silicates modified by nonpolar long alkyl groups are still relatively more polar than PP and may act as compatibilizing agents between matrix and clay particles.

Considering this study results, we have concluded that enhancement in mechanical properties might be achieved through two approaches used simultaneously: (a) optimization of processing parameters, the kinetic criterion being of major importance for clay layers debonding; (b) enhancement of the compatibility of the matrix-filler system by using both the organically modified clays and the modified PP, namely maleic anhydride grafted polypropylene (PP-*g*-MA), as matrix compatibilizing agent. This will be the subject of an upcoming study.

REFERENCES

1. Bokhari, W., Srivastava, D. Polymer-Clay Nano-composite materials for Thermal/Radiation shielding and Load Bearing Structural Applications in Aerospace/Defence. Available:http://www.caneus.org/materials/downloads/A5-A6%20Final%20Report.pdf (March, 2014).
2. Bayar, S., Delale, F., Liaw, B. M. Effect of temperature on mechanical properties of nanoclay reinforced polymeric nanocomposites – Part I: Experimental results. *Journal of Aerospace Engineering*. 26 (2013).
3. Dinca, I., Ban, C., Stefan, A., Pelin G. Nanocomposites as advanced materials for aerospace industry. *INCAS Bulletin*. 4(4) (2012).
4. Ghugare, S.V., Govindaiah, P., Avadhani, C.V. Polypropylene/organo-clay nanocomposites containing nucleating agents. *Polymer Bulletin*. 63(6) (2009).
5. Olad, A. Polymer/Clay Nanocomposites. In B. Reddy, *Advances in Diverse Industrial Applications of Nanocomposites*, InTech Open. Available: http://www.intechopen.com/books/advances-in-diverse-industrial-applications-of-nanocomposites/polymerclay-nanocomposites (March 2014).
6. Pavlidou, S., Papaspyrides, C.D. A review on polymer-layered silicate nanocomposites. *Progress in Polymer Science*. 32 (2008).
7. Paul, D.R., Robeson, L.M. Polymer nanotechnology: Nanocomposites. *Polymer*. 49 (2008).
8. Pérez, M.A., Rivas, B.L., Rodríguez, S.M., Maldonado, Á., Venegas, C. Polypropylene/clay nanocomposites. Synthesis and characterization. *Journal of the Chilean Chemical Society*. 55 (2010).
9. Sinha, R.S., Okamoto, M. Polymer-layered silicate nanocomposites: a review from preparation to processing. *Progress in Polymer Science*. 28 (2003).
10. Lertwimolnun, W., Vergnes, B. Influence of compatibilizer and processing conditions on the dispersion of nanoclay in a polypropylene matrix. *Polymer*. 46 (2005).
11. Humelnicu, D., Olariu, R.I., Arsene, C., Bertescu, M., Burghele, B.D. A comparative study on the removal of uranyl ions from artificially enriched radioactive waters using clays from Romania. *Analele Ştiinţifice ale Universităţii „Al. I. Cuza" Iaşi. Geologie*. LVI (2010).
12. Dibaei, A.H., Abdouss, M., Angaji, M.T., Haji, A. Surface and mechanical properties of polypropylene/clay nanocomposites. *Chemical Industry & Chemical Engineering Quarterly*. 19(3) (2013).
13. Fu, S.Y., Feng, X.Q., Lauke, B., Mai, Y.W. Effects of particle size, particle/matrix interface adhesion and particle loading on mechanical

"HENRI COANDA"
AIR FORCE ACADEMY
ROMANIA

"GENERAL M.R. STEFANIK"
ARMED FORCES ACADEMY
SLOVAK REPUBLIC

INTERNATIONAL CONFERENCE of SCIENTIFIC PAPER
AFASES 2014
Brasov, 22-24 May 2014

properties of particulate–polymer composites. *Composites: Part B*. 39 (2008).

14. Ghugare, S.V., Govindaiah, P., Avadhani, C.V. Polypropylene-organo-clay nanocomposites containing nucleating agents. *Polymer Bulletin*. 63 (2009).

15. Bikiaris, D.N., Vassiliou, A., Pavlidou, E., Karayannidis, G.P. Compatibilization of PP-*g*-MA copolymer on *i*PP/SiO₂ nanocomposites prepared by melt mixing. *European Polymer Journal.* 41 (2005).

16. Selver, E., Adanur, S. Processing and property relationship of polypropylene monofilaments containing nanoclay. *Journal of Industrial Textiles*. 40 (2010).

17. Lazzeri, A., Bucknall, C.B. Applications of a dilatational yielding model to rubber-toughened polymers. *Polymer*. 36 (1995).

18. Pukanszky, B. Particulate filled polypropylene composites. In J. Karger-Kocsis, *Polypropylene: An A-Z Reference*, Dordrecht: Kluwer Publishers (1999).

19. Fang, Z., Hu, Q. Influence of interfacial adhesion on stress-strain properties of highly filled polyethylene. *Die Angewandte Makromolekulare Chemie*. 265 (1999).

20. Drozdov, A.D., Dorfmann, A. The stress–strain response and ultimate strength of filled elastomers. *Computational Material Science*. 21 (2001).

21. Dasari, A., Yu, Z.Z., Mai, Y.-W. Transcrystalline regions in the vicinity of nanofillers in polyamide-6. *Macromolecules*. 40 (2007).

22. Colombini, D., Hassander, H., Karlsson, O.J., Maurer, F.H.J. Influence of the particle size and particle size ratio on the morphology and viscoelastic properties of bimodal hard/soft latex blends. *Macromolecules*. 37 (2004).

23. Dorigato, A., Dzenis, Y., Pegoretti, A. Filler aggregation as a reinforcement mechanism in polymer nanocomposites. *Mechanics of Materials*. 61 (2013).

24. Lazzeri, A., Thio, Y.S., Cohen, R.E. Volume strain measurements on CaCO3/polypropylene particulate composites: the effect of particle size. *Journal of Applied Polymer Science*. 91 (2004).

25. Thio, Y.S., Argon, A.S., Cohen, R.E., Weinberg, M. Toughening of isotactic polypropylene with CaCO₃ particles. *Polymer*. 43 (2002).

ENGINEERING SCIENCES

MATHEMATICAL MODEL FOR A JET ENGINE
WITH COOLING FLUID INJECTION INTO ITS COMPRESSOR

Alexandru-Nicolae TUDOSIE*

*Department of Electrical, Power Systems and Aerospace Engineering, University of Craiova, Craiova, Romania

Abstract: *The paper deals with an aircraft jet engine with cooling fluid injection in its compressor, meant to temporarily increase its thrust, treated as controlled object. The author has established system's motion equations, consecutive to the new gas-dynamic and fluid mechanics conditions. Using the equation system, the author has obtained engine's new structure matrix description, as well as its transfer function. A study concerning its time behavior, for two different fluids, was eventually performed (about its speed, combustor temperature and thrust) and some conclusions were presented. The paper is useful for students and researchers in their jet engine automation studies and may be improved by considering the flight regime influence, where possible.*

Keywords: *engine, control, cooling, injection, compressor, thrust augmentation, step response.*

1. INTRODUCTION

One of the aircraft jet engines' thrust increasing methods consists of fluid injection in the front of its compressor. The phenomena are described in [3,4,5] and thermo-dynamically explained and grounded in [5].

From the practical point of view, the aircraft engine may be overboosted using afterburning systems or alternative thrust augmentation methods. The afterburning is the most efficient thrust augmentation method, but in the same time, it is the most expensive-one, because of its fuel consumption increasing, as well as because of its mandatory constructive modifications and automatic control schemes implementation. Meanwhile, the afterburning isn't an appropriate thrust augmentation system for turboprop engines, nor for twin-jet turbofan engines. Especially for turboprops, the lack of air and the presence of the propeller

make impossible the afterburning adapting as well as a high flight speed achieving.

For these propulsion systems, alternative thrust augmentation methods are: a) fluid injection into the engine's compressor; b) fluid injection into the engine's combustor. Both these methods are meant to increase the exhaust nozzle enthalpy fall, by reducing the turbine enthalpy fall, consecutive to a smaller compressor mechanical work necessity.

The first method consists of the injection of a special volatile fluid (water, ammonia, methanol, water-methanol mixture etc) into the front of the engine's axial compressor. During the air compression evolution the temperature grows; the injected fluid vaporizes itself and extracts an important part of the resulted heat, which cools the compressed air and grows its mass air flow rate, keeping constant the volume flow rate. The extraction of that heat from the compressed air transforms the

adiabatic (isentropic) com pression evolution into a polytropic one and determ ines a mechanical work necessity decreasing.

It results an im portant thrust augmentation, caused by both the mass airflow increasing and the exhaust nozzle burned gases' speed increasing.

2. THERMODYNAMIC EFFECTS OF THE FLUID INJECTION

2.1 Compression evolution. The heat extraction through the fluid injection transforms the adiabatic com pression evolution into a polytropic one, the polytropic exponent being sm aller than 1.4 (which is the adiabatic exponent fo r air, denoted as k). The greater th e injected fluid flow rate $\dot{m}_l$ is, th e lower the polytropic exponent is, tending to 1 (which corresponds to the ideal isotherm ic evolution), as figure 1 shows.

The curve in f igure 1 was o btained applying the following algorithm [5]. Firstly, one consid ers the irr eversible adiabatic air evolution in the com pressor as a polytropic one, which leads to

$$i_1^* \frac{\left(\pi_c^*\right)^{\frac{k-1}{k}}-1}{\eta_c} = i_1^* \frac{k-1}{k} \frac{a}{a-1}\left[\left(\pi_c^*\right)^{\frac{a-1}{a}}-1\right], \quad (1)$$

where i_1^* is the air specific enthalpy in the front of the com pressor, π_c^* – compressor's pressure ratio, η_c – compressor's randament, a – polytropic exponent of the equivalent evolution. This non-linear equation's solving gives the equivalent n – value.

The injected fluid may extract the heat

$$Q_i = \dot{m}_l r_f, \quad (2)$$

where r_f is fluid's vaporizat ion latent heat, which means, for the air flow rate $\dot{m}_a$, that

$$q_i = \frac{Q_i}{\dot{m}_a} = \frac{\dot{m}_l}{\dot{m}_a} r_f \quad (3)$$

and the specific m echanical work of the compressor diminishes exactly with this va lue. Consequently, the new polytropic evolution (by a_i exponent) should have the sam e mechanical work value, so

$$\frac{a}{a-1}\left[\left(\pi_c^*\right)^{\frac{a-1}{a}}-1\right] = \frac{a_i}{a_i-1}\left[\left(\pi_{c_i}^*\right)^{\frac{a_i-1}{a_i}}-1\right], \quad (4)$$

$$i_1^* \frac{a_i}{a_i-1}\left[\left(\pi_{c_i}^*\right)^{\frac{a_i-1}{a_i}}-1\right] = i_1^*\left[\frac{\left(\pi_c^*\right)^{\frac{k-1}{k}}-1}{\eta_c}\right] - q_i \quad (5)$$

where $\pi_{c_i}^*$ is th e new compressor's pressure ratio (when the fluid injection is active)

$$\pi_{c_i}^* = \left\{1 + \frac{a_i-1}{a_i}\frac{a}{a-1}\left[\left(\pi_c^*\right)^{\frac{a-1}{a}}-1\right]\right\}^{\frac{a_i}{a_i-1}}. \quad (6)$$

From Eqs. (5) and (6) one obtains the relation between $\dot{m}_i$ and a_i

$$\frac{\left(\pi_c^*\right)^{\frac{k-1}{k}}-1}{\eta_c} = \frac{a_i-1}{a_i}\frac{a}{a-1}\left[\left(\pi_c^*\right)^{\frac{a-1}{a}}-1\right] + \frac{\dot{m}_l}{\dot{m}_a}\frac{r_f}{i_1^*}$$

$$(7)$$

which is the reason of the graphics in figure 1.

The dete rmined valu e for a_i, used by the formula (6) leads to the new valu e of $\pi_{c_i}^*$, so one can obtain the new operation line position on the compressor characteristic.

2.2 Flow rate. Most of the nowadays operational jet engines ha ve cr itical f low in their turb ines [5], so the f low param eter $\dfrac{\dot{m}_g \sqrt{T_3^*}}{p_3^*}$ remains constant even if one uses the fluid injection, where $\dot{m}_g$ is the burned gas flow rat e, T_3^* – gas tem perature before the
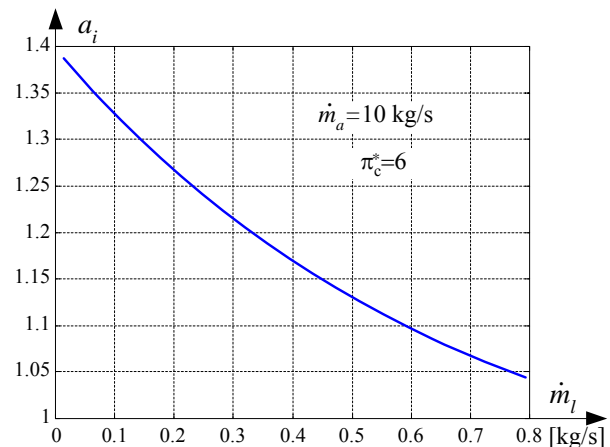
Figure 1. Polytropic exponent with respect to the injected fluid flow rate

“HENRI COANDA”
AIR FORCE ACADEMY
ROMANIA

“GENERAL M.R. STEFANIK”
ARMED FORCES ACADEMY
SLOVAK REPUBLIC

INTERNATIONAL CONFERENCE of SCIENTIFIC PAPER
AFASES 2014
Brasov, 22-24 May 2014

turbine, p_3^* – gas pressure before the turbine, proportional to the air pressure after the compressor $\left(p_3^* = \sigma_{CA}^* p_2^*\right)$. Consequently, the air/gases flow rate th rough the engine m ust satisfy it, as follows

$$\frac{\dot{m}_g \sqrt{T_3^*}}{p_3^*} = \frac{\dot{m}_a \sqrt{T_3^*}}{\sigma_{CA}^* p_2^*} = \frac{\dot{m}_{a_i} \sqrt{T_3^*}}{\sigma_{CA}^* p_{2_i}^*}, \qquad (8)$$

so the air f low rate w ith f luid inje ction $\dot{m}_{a_i}$ becomes proportional to $\dot{m}_a$

$$\dot{m}_{a_i} = \dot{m}_a \frac{\pi_{c_i}^*}{\pi_c^*}. \qquad (9)$$

The burned gases flow rate becomes, if one considers the fuel flow rate $\dot{m}_c$,

$$\dot{m}_{g_i} = \dot{m}_{a_i} + \dot{m}_l + \dot{m}_c. \qquad (10)$$

3. ENGINE'S PERFORMANCES

Engine's thrust will, obviously, grow (as figure 2 shows), both because of the flow rate $\dot{m}_{g_i}$ increasing and the specific thru st F_{sp_i} increasing

$$F_i = \dot{m}_{g_i} C_{5_i} - \dot{m}_{a_i} V = \dot{m}_{a_i}\left(\xi_g C_{5_i} - V\right), \qquad (11)$$

where C_{5_i} – exhaust gases velocity, V – air-speed, ξ_g – gases mass fraction.

Assuming that the flu id injection is used a t low flight speed (only for short tim e periods during the aircraft take-off maneuver), one can neglect the V – term, so it results

$$F_i = \dot{m}_{a_i} \xi_g C_{5_i} = \dot{m}_{a_i} F_{sp_i} = \dot{m}_a \frac{\pi_{c_i}^*}{\pi_c^*} F_{sp_i}. \qquad (11)$$

If the injected fluid is pure (dis tilled) water its flow rate being at most 4% of the air flow rate, engine's perfor mances (thrust and specific fuel consum ption) versus w ater flow
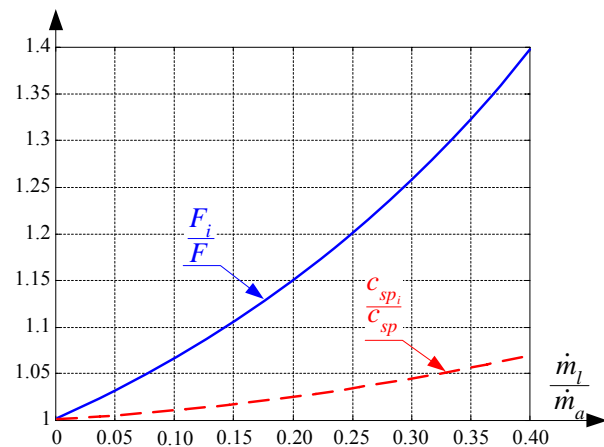
Figure 2. Engine's performances with respect to the injected fluid flow rate

rate fraction are presente d in figure 2 [5]. One can observe that for an injected water fractio n $\xi_l = \dfrac{\dot{m}_l}{\dot{m}_a} \le 0.04$, engine's thrust increases up to 40%, which is a real success of the method.

Specific fuel consum ption grows too, but moderately, no m ore than 8%, because of the T_2^* temperature, which decreases an d engine's fuel system has to com pensate th is loss by supplementary fuel injection, in order to restore the requested T_3^* burner's temperature.

If the in jection f luid is a com bustible substance, such as m ethanol, or a water-methanol mixture, T_2^* tem perature's d ecrea-sing and the supplem entary need f or fuel are partly c ompensated by t he fl uid's bur ning, which bring s its ow n heat into th e engine's combustor; consequently, the supplem entary fuel injection becom es m uch sm aller than when the injected fluid is pure water.

The described thrust augm entation method is very effective when the engine operates at high atmospheric temperatures (m ore than 25 $^{\circ}$C), low atm ospheric pressures and low

humidity (b ecause it faci litates th e injected fluid's vaporizing).

One of the m ethod's disadvantage is related to the possibility of air intake's and compressor's blades icing, as well as to th e suction of ice lumps into the compressor.

Fluid injection running time is the one who limits the fluid necessary m ass to be boarded, so, one has to optim ize the on-board fluid supplies, ac cording to the air craft take-of f needs and the atmospheric conditions.

4. ENGINE'S NEW MOTION EQUATIONS

Engine's mathematical model consists of:
- engine's spool motion equation;
- compressor's and turbine's characteristics;
- combustor's energy equation;
- air/gases flow rate's equation.

These equations are stu died in [8] for a basic engine; a matrix description is also given

$$[A] \times (u) = (b), \tag{12}$$

where $[A]$ is engine's m atrix, (u) – output parameters vector and (b) – input parameters vector:

$$A = \begin{bmatrix} T_1 s + \rho_1 & -k_{1T3} & 0 & -k_{1p2} & k_{1p4} \\ k_{2n} & -k_{2T3} & 0 & k_{2p2} & 0 \\ 0 & -1 & 1 & -k_{3p2} & -k_{3p4} \\ 0 & k_{4T3} & k_{4T4} & k_{4p2} & k_{4p4} \\ k_{5n} & k_{5T3} & 0 & k_{5p2} & 0 \end{bmatrix} \tag{13}$$

$$u^T = \left(\overline{n} \quad \overline{T_3^*} \quad \overline{T_4^*} \quad \overline{p_2^*} \quad \overline{p_4^*} \right), \tag{14}$$

$$b^T = \left(0 \quad 0 \quad 0 \quad 0 \quad k_{5Qc}\overline{Q_c} \right). \tag{15}$$

The involved co-efficient are used with their expressions, described in [8].

Based on previous chapters therm odyna-mic considerations, one can affir m that the fluid injection has influence on the com pres-sor's characteristics, as well as on the air/gases flow rate balan ce along the engine. Consequently, one has to modify the equations involving the com pressor's pressure ratio, the pressure and tem perature b ehind the compressor, the tem perature b ehind the engine's combustor, as well as the equation of flow rate's continuity.

One has to study two cases: a) neutral

injected f luid (pur e w ater); b) c ombustible injected fluid (methanol).

One can observe that the flow rate equation is the sam e for both of these cases, t he di ffe-rence being given by the other equations.

4.1 Flow rate equation. The exhaust gases flow rate is given by Eq. (10), where the fuel flow rate is the smallest and can be neglected

$$\dot{m}_{g_i}\left(p_3^*, T_3^*\right) = \dot{m}_{a_i}\left(p_2^*, n\right) + \dot{m}_l . \tag{16}$$

The above equation should be linearised, using the finite differences m ethod, in order to be used into the mathematical model

$$\left(\frac{\partial \dot{m}_{g_i}}{\partial p_3^*}\right)_0 \Delta p_3^* + \left(\frac{\partial \dot{m}_{g_i}}{\partial T_3^*}\right)_0 \Delta T_3^* = \left(\frac{\partial \dot{m}_{a_i}}{\partial p_2^*}\right)_0 \Delta p_2^* +$$

$$+ \left(\frac{\partial \dot{m}_{a_i}}{\partial n}\right)_0 \Delta n + \Delta \dot{m}_l . \tag{17}$$

Assuming that $p_3^* = \sigma_{CA}^* p_2^*, \sigma_{CA}^* = \text{const.}$, the above equation becomes

$$\left[\left(\frac{\partial \dot{m}_{g_i}}{\partial p_2^*}\right)_0 \sigma_{CA}^* - \left(\frac{\partial \dot{m}_{a_i}}{\partial p_2^*}\right)_0\right] \Delta p_2^* + \left(\frac{\partial \dot{m}_{g_i}}{\partial T_3^*}\right)_0 \Delta T_3^* -$$

$$- \left(\frac{\partial \dot{m}_{a_i}}{\partial n}\right)_0 \Delta n = \Delta \dot{m}_l , \tag{18}$$

or

$$\frac{p_{2_0}^*}{(\dot{m}_{a_i})_0} \left[\left(\frac{\partial \dot{m}_{g_i}}{\partial p_2^*}\right)_0 \sigma_{CA}^* - \left(\frac{\partial \dot{m}_{a_i}}{\partial p_2^*}\right)_0\right] \frac{\Delta p_2^*}{p_{2_0}^*} +$$

$$\frac{T_{3_0}^*}{(\dot{m}_{a_i})_0} \left(\frac{\partial \dot{m}_{g_i}}{\partial T_3^*}\right)_0 \frac{\Delta T_3^*}{T_{3_0}^*} - \frac{n_0}{(\dot{m}_{a_i})_0} \left(\frac{\partial \dot{m}_{a_i}}{\partial n}\right)_0 \frac{\Delta n}{n_0} =$$

$$= \frac{(\dot{m}_l)_0}{(\dot{m}_{a_i})_0} \frac{\Delta \dot{m}_l}{(\dot{m}_l)_0} = \xi_l \frac{\Delta \dot{m}_l}{(\dot{m}_l)_0} . \tag{19}$$

Assuming the for mal annotation $\overline{X} = \dfrac{\Delta X}{X_0}$ the above equation becomes

$$k_{2n}' \overline{n} - k_{2T3}' \overline{T_3^*} + k_{2p2}' \overline{p_2^*} = \xi_l \overline{\dot{m}_l} ; \tag{20}$$

one can observe that the second line in m atrix $[A]$ should be replaced by the new values of the co-efficient. M eanwhile, on e has to complete the second elem ent in the input vector (b) with the term in the right member of Eq. (20).

4.2 Combustor's energy equation. The fifth equation in the m athematical m odel is based on the com bustor's energy equation,

a)

b)
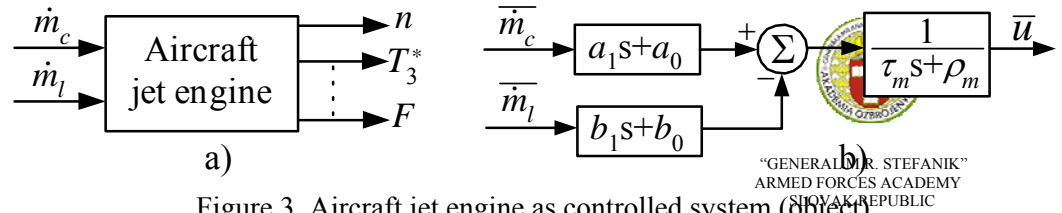
Figure 3. Aircraft jet engine as controlled system (object)

which may have different forms, according to the injected fluid's nature:

$$\dot{m}_{g_i} c_{P_g} T_3^* - \dot{m}_{a_i} c_{p_a} T_2^* = \dot{m}_c \zeta_{CA} P_c + \dot{m}_l \zeta_{CA} P_l, \quad (21)$$

where c_{P_g}, c_{p_a} − specific isobar heat of the burned gases and air (assumed as equal), ζ_{CA} − burning process' perfection co-efficient, P_c, P_l − chemical energy of the fuel, respectively of the injected fluid.

Meanwhile, the term T_2^* should be expressed with respect to p_2^*

$$\Delta T_2^* = \left(\frac{\partial T_2^*}{\partial \pi_c^*}\right)_0 \Delta \pi_c^* = \left(\frac{\partial T_2^*}{\partial \pi_c^*}\right)_0 \left(\frac{\partial \pi_c^*}{\partial p_2^*}\right)_0 \Delta p_2^*, \quad (22)$$

or as $\quad \overline{T_2^*} = \frac{p_{2_0}^*}{T_{2_0}^*} \left(\frac{\partial T_2^*}{\partial \pi_c^*}\right)_0 \left(\frac{\partial \pi_c^*}{\partial p_2^*}\right)_0 \overline{p_2^*}. \quad (23)$

a) If the injected fluid is a neutral-one, the term $\dot{m}_l \zeta_{CA} P_l$ becomes null. Consequently, Eq. (21) becomes

$$\dot{m}_{g_i} c_p T_3^* - \dot{m}_{a_i} c_p T_2^* = \dot{m}_c \zeta_{CA} P_c. \quad (24)$$

Considering Eqs. (16), (17), (18) and (23), one obtains from (24)

$$\frac{c_p\left(T_{3_0}^* - T_{2_0}^*\right) n_0}{\dot{m}_{c_0} \zeta_{CA} P_c} \left(\frac{\partial \dot{m}_a}{\partial n}\right)_0 \overline{n} + \frac{c_p\left(\dot{m}_{a_0} - \dot{m}_{l_0}\right) T_{3_0}^*}{\dot{m}_{c_0} \zeta_{CA} P_c} \overline{T_3^*}$$
$$+ \left[\frac{c_p\left(T_{3_0}^* - T_{2_0}^*\right) p_{2_0}^*}{\dot{m}_{c_0} \zeta_{CA} P_c} \left(\frac{\partial \dot{m}_a}{\partial p_2^*}\right)_0 - \frac{c_p\left(\dot{m}_{a_0} - \dot{m}_{l_0}\right)}{\dot{m}_{c_0} \zeta_{CA} P_c} \times\right.$$
$$\left.\times p_{2_0}^* \left(\frac{\partial T_2^*}{\partial \pi_c^*}\right)_0 \left(\frac{\partial \pi_c^*}{\partial p_2^*}\right)_0 \right] \overline{p_2^*} = \overline{\dot{m}_c} - \frac{\dot{m}_{l_0}}{\dot{m}_{c_0} \zeta_{CA} P_c} \overline{\dot{m}_l}. \quad (25)$$

One can observe that the co-efficient $\dfrac{\dot{m}_{l_0}}{\dot{m}_{c_0} \zeta_{CA} P_c}$ of the injected fluid flow rate parameter $\overline{\dot{m}_l}$ has a very small value comparing

to 1, the value of the co-efficient of $\overline{\dot{m}_c}$, so it may be neglected. Consequently, the above-determined equation may be re-written as

$$k_{5n}\overline{n} + k_{5T3}'\overline{T_3^*} + k_{5p2}'\overline{p_2^*} = \overline{\dot{m}_c} \quad (26)$$

and the last line in matrix $[A]$ should be appropriate restored.

b) If the injected fluid is a combustible-one, the Eq. (21) must be entirely considered. Consequently, the quantity $\dot{m}_l \zeta_{CA} P_l$ adds a new term to Eq. (25) and modifies the co-efficient of $\overline{\dot{m}_c}$, so the right member of the above-mentioned equation becomes

$$\left(1 - \frac{P_l}{P_c} \frac{\dot{m}_{l_0}}{\dot{m}_{c_0}}\right)\overline{\dot{m}_c} - \frac{\dot{m}_{l_0} c_p \left(T_{3_0}^* - T_{2_0}^*\right)}{\dot{m}_{c_0} \zeta_{CA} P_c}\overline{\dot{m}_l} =$$
$$= k_{5c}'\overline{\dot{m}_c} - k_{5l}'\overline{\dot{m}_l}. \quad (27)$$

The fifth line's new form is

$$k_{5n}\overline{n} + k_{5T3}'\overline{T_3^*} + k_{5p2}'\overline{p_2^*} = k_{5c}'\overline{\dot{m}_c} - k_{5l}'\overline{\dot{m}_l} \quad , (28)$$

so, the mathematical model should be completed. If the second line is multiplied by $\dfrac{k_{5l}'}{\xi_l}$, then added to the fifth line, one obtains for this one the form

$$\left(k_{2n}' \frac{k_{5l}'}{\xi_l} + k_{5n}\right)\overline{n} + \left(k_{2T3}' \frac{k_{5l}'}{\xi_l} + k_{5T3}\right)\overline{T_3^*} +$$
$$+ \left(k_{2p2}' \frac{k_{5l}'}{\xi_l} + k_{5p2}\right)\overline{p_2^*} = k_{5c}'\overline{\dot{m}_c}. \quad (29)$$

The $[A]$-matrix, as well as the (b)-vector should be modified in appropriate modes, with respect to the injected fluid nature.

5. SYSTEM'S QUALITY

Jet engine's behavior, as controlled object (system), should be studied for the new conditions. System's quality consists of

engine's step response (its tim e behavior for step input or inputs).

An aircraft engine with com pressor fluid injection can be represented, as controlled object, by a system with two inputs (fuel flow rate and injected flui d flow rate) and m ore outputs (engine speed, co mbustor temperature, thrust etc), as figure 3.a shows.

Following the algorithm described in [6,7,8], each one of the outpu ts u can b e expressed w ith respect to the above-m ention-ned inputs, as formally shown in figure 3.b.

As m ain outputs were considered the next three: a) engine's speed non-dim ensional parameter $\overline{n}$; b) engine's com bustor tempera-ture param eter $\overline{T_3^*}$; c) en gine's to tal thrus t parameter $\overline{F}$.

One has chosen, for a quantitative study, a VK-1A-type jet engine, with constant area exhaust nozzle, having in mind only the engine as possible controlled object, w ithout its control system s (without the speed controller and the temperature limiter).

Output param eters' expressions for the VK-1A basic engine are

$$\overline{n}(s) = \frac{1.2606}{2.0859s + 5.1015}\overline{m_c}, \qquad (30)$$

$$\overline{T_3^*}(s) = \frac{1.3799s + 2.3888}{2.0859s + 5.1015}\overline{m_c}, \qquad (31)$$

$$\overline{F}(s) = \frac{1.3762s + 4.762}{2.0859s + 5.1015}\overline{m_c}, \qquad (32)$$

depicted w ith con tinuous lin es f or ste p responses in figures 4, 5 and 6.

Figure 4 shows the engine's speed parameters step response, while figure 5 shows the sam e response of the com bustor tem pe-rature parameter and figure 6 contains engine's thrust behavior for the same conditions.

The case of the injectio n of a neutral fluid (pure water) into the compressor brings next mathematical model modifications

$$\overline{n}(s) = \frac{1}{1.6348s + 4.5158}\left(1.283\overline{m_c} - 0.092\overline{m_l}\right), \qquad (33)$$

$$\overline{T_3^*}(s) = \frac{1}{1.6348s + 4.5158}\left[(1.474s + 2.748)\overline{m_c} - (0.047s + 0.034)\overline{m_l}\right], \qquad (34)$$

$$\overline{F}(s) = \frac{1}{1.6348s + 4.5158}\left[(1.385s + 4.516)\overline{m_c} - (0.089s + 0.315)\overline{m_l}\right], \qquad (35)$$

depicted with dash lines in figures 4, 5 and 6.

The case of the injec tion of a com bustible fluid (m ethanol) into the com pressor brings similar m athematical m odel m odifications, as follows

$$\overline{n}(s) = \frac{1}{2.161s + 4.7973}\left(1.43\overline{m_c} - 0.184\overline{m_l}\right), \qquad (36)$$

$$\overline{T_3^*}(s) = \frac{1}{2.161s + 4.7973}\left[(1.816s + 2.467)\overline{m_c} - (0.053s + 0.047)\overline{m_l}\right], \qquad (37)$$

$$\overline{F}(s) = \frac{1}{2.161s + 4.7973}\left[(1.584s + 6.317)\overline{m_c} - (0.113s + 0.803)\overline{m_l}\right], \qquad (38)$$

depicted with dash-dot lines in figures 4, 5, 6.
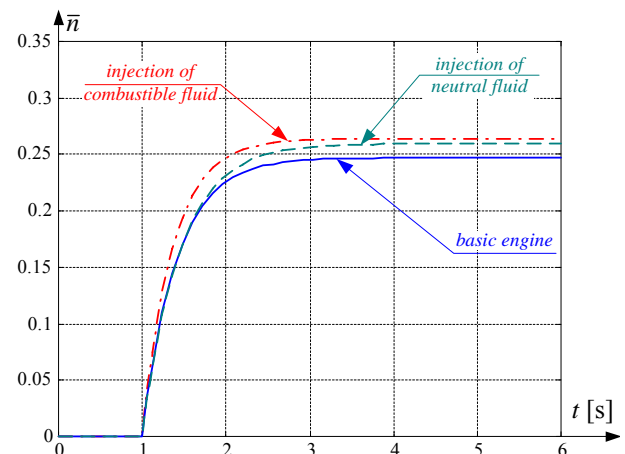
Figure 4. Engine's speed parameter step response

“HENRI COANDA”
AIR FORCE ACADEMY
ROMANIA

“GENERAL M.R. STEFANIK”
ARMED FORCES ACADEMY
SLOVAK REPUBLIC

INTERNATIONAL CONFERENCE of SCIENTIFIC PAPER
AFASES 2014
Brasov, 22-24 May 2014
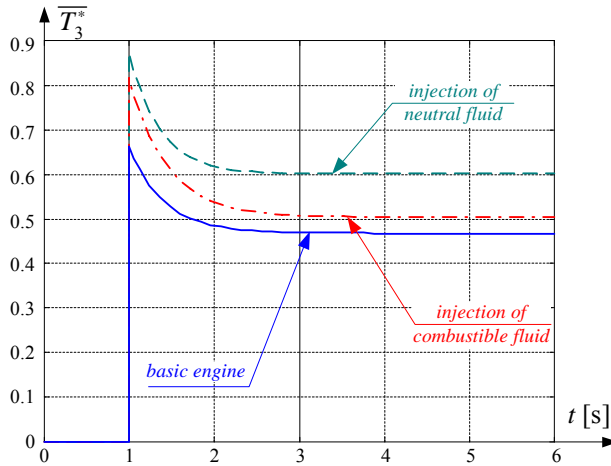
Figure 5. Engine's combustor temperature parameter step response
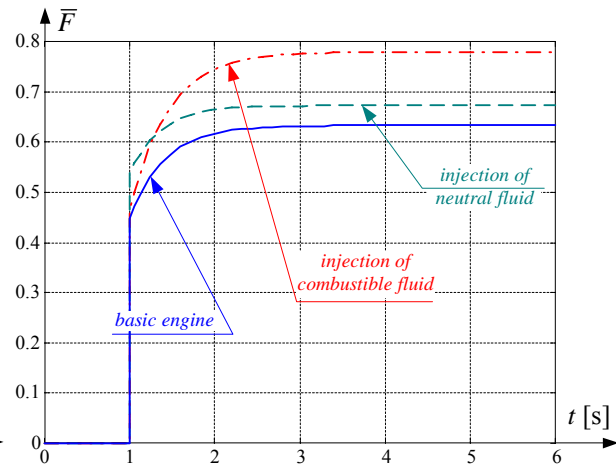
Figure 6. Engine's total thrust parameter step response

6. CONCLUSIONS

Cooling fluid injection into the jet engine's compressor determ ines gas-dynam ic and performance m odifications, injected fluid's nature having a very important contribution.

As the te chnical liter ature show s, the described method of thru st augm entation is a very effective one, especially for turboprops, thrust increasing being significant; meanwhile, the specific fuel cons umption has a moderate growing (u nder 15%), definitely acceptable because of the thrust augmentation advantages.

Gas-dynamic changes entail both jet engine's mathematical model changes, as well as performances improvements.

Mathematical m odel's equation w ere modified because of the air/gases flow rate 's balance changes, as well as because of the new energy b alance of the com bustor, when a combustible cooling fluid is involved.

Whatever th e cooling fluid were, engine's speed is less influenced (as figure 4 shows), small $\overline{n}$ – parameter's increasing being observed, especially wh en the cooling injected fluid is a co mbustible-one (obviously, because its supplementary contri bution to the engine's

combustor's burning process and supple-mentary heat transfer).

From the temperature's parameter behavior point of v iew (see figure 5), when the in jected cooling fluid is a neutral one (e.g. distilled water), one can observe the sam e trend as for the basic engine, but also a significant growing of $\overline{T_3^*}$ – parameter's va lue. T his is the c onse-quence of the air m ass flow rate growing, followed by a supplementary fuel injection.

When the cooling injected fluid is a com -bustible-one, the initial temperature growing is nearly the sam e (as for a neutral fluid), but, because of its own heat inpu t, the necessary fuel inje ction is less than bef ore, so the temperature's param eter tends to restore th e basic engine's behavior.

From the thrust-p arameter poin t o f view, whatever the injected cooling fluid were, thrust is growing. As figure 6 shows, the combustible cooling f luid inje ction gives th e most significant th rust increase, th at because both of air flow rate increase and th e specific thrust increase (due to the supplem entary heat input). Neutral cooling fluid injection assures thrust increase too, but moderate.

From the engine's tim e constant point of view, this value r emains near ly the sam e; whatever the m ethod we re, stabilization tim e values are kept around (2.5÷3.0) sec.

One has perfor med the study for an engine VK-1A-type, for sea level conditions. This study could be extended for other flight conditions (low altitu de and take-off air speed), g iven tha t this thru st au gmentation method is useful for airplane's (aircraft) taking-off, being a re store thrust method (when the atm ospheric tem perature exceeds a conventionally determ ined critical value for each engine).

REFERENCES

1. B erbente, C ., C onstantinescu, N . V . *Gases Dynamics*, vol. I, II. Politehnica University in Bucharest Inprint (1985).
2. H ill, P. G ., Peterso n, C . *Mechanics and Thermodinamics of Propulsion*. Addison - Wesley Publications, New York (1993).
3. Ispas, St. *The Turbo-Jet Engine*. Technica Publishing House (1985).
4. Mattingly, J. D. *Elements of gas turbine propulsion*. McG raw-Hill, N ew Y ork (1996).
5. Pim sner, V. *Air-breathing Jet Engines. Processes and Characteristics*, Bucharest, Didactic and Pedagogic Publishing (1983).
6. Stoenciu, D. *Aircraft Engine Automation. Aircraft Engines as Controlled Objects*. Bucharest, Milita ry Technical Academ y Inprint (1977).
7. Stoicescu, M., Rotaru, C. *Turbo-Jet Engines. Characteristics and Control Methods*. Bucharest, Military Technica l Academy Inprint (1999).
8. Tudosie, A. N. *Aerospace Propulsion Systems Automation.* University of Craiova Inprint (2005).
9. Tudosie, A. Aircraft Gas-Turbine Engine's Control Based on the Fuel Injection Control. In Max Mulder *Aeronautics and astronautics.* Intech Open Acces Publishe r (2011).

MATHEMATICAL MODEL FOR A JET ENGINE
WITH COOLING FLUID INJECTION INTO ITS COMBUSTOR

Alexandru-Nicolae TUDOSIE*

*Department of Electrical, Power Systems and Aerospace Engineering, University of Craiova, Craiova, Romania

Abstract: *The paper deals with an aircraft jet engine with cooling fluid injection into the rear part of its combustor, meant to temporarily increase its thrust, treated as controlled object. The author has established system's motion equations, consecutive to the new gas-dynamic and fluid mechanics conditions. Using the equation system, the author has obtained engine's new structure matrix description, as well as its transfer functions. A study concerning its time behavior was performed (about its speed, combustor temperature and thrust) and some conclusions were presented, comparing to other cooling fluid injection methods results. The paper is useful for students and researchers in their jet engine automation studies and may be improved by considering the flight regime influence.*

Keywords: *engine, cooling fluid, injection, combustor, thrust augmentation, flow rate.*

1. INTRODUCTION

One of the aircraft jet engines' thrust increasing methods consists of fluid injection in the rear part of its combustor, in the mixing area. The phenomena are described in [3,4,5] and thermo-dynamically explained and grounded in [5].

The aircraft engine may be overboosted using afterburning systems or alternative thrust augmentation methods. The afterburning is the most efficient thrust augmentation method, but in the same time, it is the most expensive-one, because of its fuel consumption increasing, as well as because of its mandatory constructive modifications and automatic control schemes implementation. Meanwhile, the afterburning isn't an appropriate thrust augmentation system for turboprop engines, nor for twin-jet turbofan engines in their outer jet. Especially

for turboprops, the lack of air and the presence of the propeller make impossible the afterburning adapting as well as a high flight speed achieving.

For these propulsion systems, alternative thrust augmentation methods are: a) fluid injection into the engine's compressor [5,10]; b) fluid injection into the engine's combustor, in its rear part (as figure 1 shows). Both these methods are meant to increase the exhaust nozzle enthalpy fall, by reducing the turbine enthalpy fall, consecutive to a smaller compressor mechanical work necessity.

The first method was described in [5] and engine's new mathematical model was determined and studied in [10].

The second method is the subject of this paper, which intends to establish the new mathematical model of the engine, as well as to study engine's time behavior (by studying
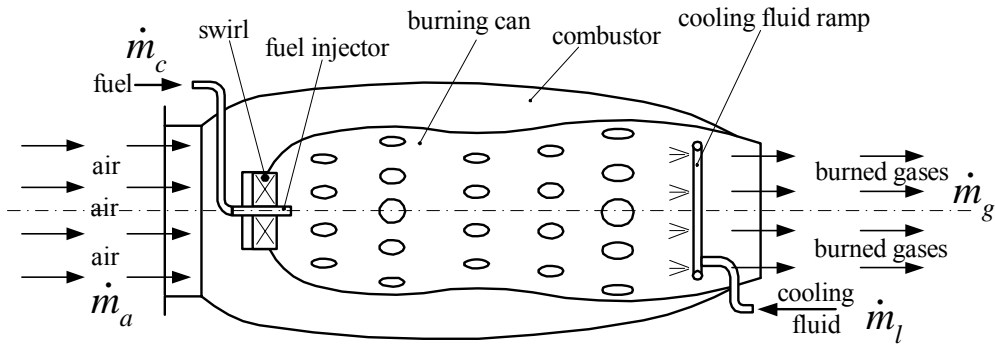
Figure 1. Aircraft jet engine's combustor with cooling fluid injection facility

the step response of th e engine concerning its speed, temperature and thrust).

In both of the above-m entioned cases, it results an im portant thrust au gmentation, caused by both the m ass airflow increasing and the exhaust nozzle burned gases' speed increasing, until 60% for the first m ethod and until 25% for the second m ethod, corresponding to a cooling fluid flow rate f raction of 5% of the engines ai r flow rate. Figure 2 shows thrust and specific fuel consum ption growing percen tages with respe ct to the injected fuel fraction. Fuel consumption is bigger than in the cas e studied in [10] (that means in the case of cooling f luid injec tion into the engine's compressor).

One can observe that engine's perfor-mances are a little sma ller than in the f irst case, but this m ethod offers som e a dvantages, such as constructive simplicity, the elimination of the ic ing possib ilities, a s we ll a s th e elimination of the blades corrosion. A m ajor disadvantage is th at an uncontrolled fluid injection could obstruct an appropriate burning deployment and it could even extinguish the combustor's flam e; that is the reaso n why the
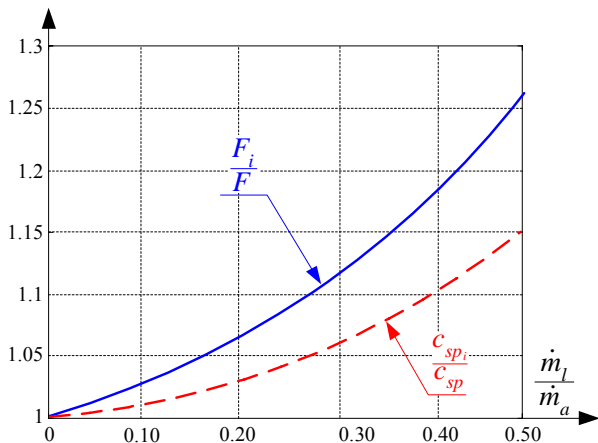
injection is done at the rear part of the burner can, near its wall, in order to assure a supplementary cooling of the burner's wal l and, meanwhile, to facilitate the m ixing of the burned gases with the vaporized cooling fluid.

In most of the practica l situa tions the used cooling f luid is the water, which m eans a neutral fluid, the injec tion of a com bustible fluid being unnecessary, even prohibited.

In some situations an a ir flow rate b y-pas-sing is necessary (see figure 3), when the compressor's air flo w rate ex ceeds the necessary, in order to prevent an unstable engine operation (stall).

2. THERMODYNAMIC EFFECTS OF THE FLUID INJECTION

2.1 Flow rate balance. The fluid injection brings into the combustor (and into the general flow) an extra flow rate $\dot{m}_l$.

Most of the nowadays operational jet engines have critical flo w in their tu rbines [5], so the flow param eter $\dfrac{\dot{m}_g \sqrt{T_3^*}}{p_3^*}$ rem ains co n-stant even if one uses the fluid injection, where $\dot{m}_g$ is the burned gases flow rate, $T_3^* -$ gas temperature before th e turbine, $p_3^* -$ gas pres-sure before the turbine, proportional to the air pressure after the compressor $\left(p_3^* = \sigma_{CA}^* p_2^*\right)$.

Figure 2. Engine's performances with respect to the injected fluid flow rate

“HENRI COANDA”
AIR FORCE ACADEMY
ROMANIA

“GENERAL M.R. STEFANIK”
ARMED FORCES ACADEMY
SLOVAK REPUBLIC

INTERNATIONAL CONFERENCE of SCIENTIFIC PAPER
AFASES 2014
Brasov, 22-24 May 2014

The greater the injected fluid flow rate $\dot{m}_l$, the less the compressor air flow $\dot{m}_a$ rate must be and it leads to an important pressure increasing (both p_2^* and p_3^*); meanwhile, the operating regime becomes closer to the stall limit, which is an undesirable phenomenon. Consequently, the burned gases flow rate must keep its value and becomes

fuel, which is a supplementary propulsion system, offering its own thrust.

Obviously, as long as the extracted $\dot{m}_{ap}$ air flow rate value depends on the cooling fluid flow rate $\dot{m}_l$ value, the presence of an appropriate fuel control system for this new combustor is compulsory, in order to correlate the fuel flow rate injection to the air flow rate.

Meanwhile, the main fuel flow rate control
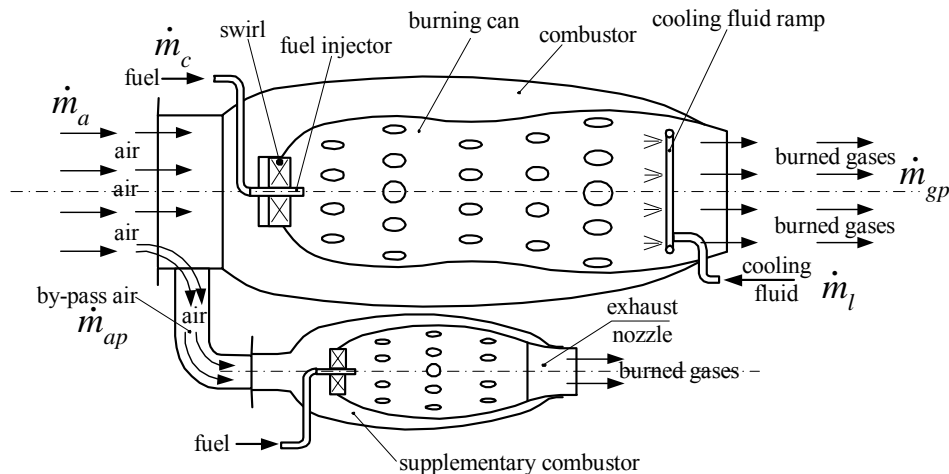
Figure 3. Jet engine's combustor with cooling fluid injection, air by-pass and supplementary combustor

$$\dot{m}_g = \dot{m}_{ai} + \dot{m}_l + \dot{m}_c , \qquad (1)$$

where $\dot{m}_{ai}$ is the new air flow rate value, smaller than the initial value $\dot{m}_a$.

In order to avoid unstable regimes, even when the cooling fluid injection is operational, a combined thrust augmentation method can be implemented. This method is meant to keep constant the compressor's air flow rate and, meanwhile, to extract (by-pass) an air flow rate $\dot{m}_{ap}$ before the engine's combustor, in order to keep the flow rate balance

$$\dot{m}_{gp} = \dot{m}_a - \dot{m}_{ap} + \dot{m}_l + \dot{m}_c \equiv \dot{m}_g . \qquad (2)$$

The extracted air flow rate is not a loss for the system; it can be used into another combustor (an external, independent, supple-mentary combustor), provided with its own exhaust nozzle and separately supplied with

system must be reset for the new conditions.

The flow rate balance must be kept in both of situations, without cooling fluid injection (basic engine) or with cooling fluid injection.

For the basic engine

$$\dot{m}_g = \mu A_{3'_{cr}} \frac{p_3^*}{\sqrt{T_3^*}} \sqrt{\frac{\chi_g}{R_g}\left(\frac{2}{\chi_g + 1}\right)^{\frac{\chi_g + 1}{\chi_g - 1}}} , \qquad (3)$$

while for the engine with fluid injection

$$\dot{m}_{gp} = \mu A_{3'_{cr}} \frac{p_3^*}{\sqrt{T_3^*}} \sqrt{\frac{\chi_{gp}}{R_{gp}}\left(\frac{2}{\chi_{gp} + 1}\right)^{\frac{\chi_{gp} + 1}{\chi_{gp} - 1}}} , \qquad (4)$$

where μ is the flow rate co-efficient, $A_{3'_{cr}}$ – turbine's stator critical area, χ_g, χ_{gp} – adiaba-tic exponents of the burned gases, R_g, R_{gp} –

gas constants of the burned gases (for both situations).

Considering the formal annotation for flow rate fractions (with respect to the $\dot{m}_a$ air flow rate) as $\xi_x = \dfrac{\dot{m}_x}{\dot{m}_a}$, from Eqs. (2), (3) and (4) one obtains

$$\frac{(1 - \xi_{ap})(1 + \xi_l + \xi_c)}{(1 - \xi_{ci})} = \sqrt{\frac{R_g}{R_{gp}} \frac{\left(\dfrac{2}{\chi_{gp} + 1}\right)^{\frac{\chi_{gp} + 1}{\chi_{gp} - 1}}}{\left(\dfrac{2}{\chi_g + 1}\right)^{\frac{\chi_g + 1}{\chi_g - 1}}}},$$

(5)

where ξ_c, ξ_{ci} – fuel flow rate fractions for the basic engine, respectively for the engine with cooling fluid injection (determined as $\xi_c = \dfrac{1}{\lambda_{CA} \min L}$), $\min L$ – stoechiometric minimum air value for 1 kg of fuel, λ_{CA} – air excess co-efficient in engine's combustor, ξ_{ap} – extracted air flow fraction and ξ_l – injected fluid fraction.

Assuming that burned gases properties are nearly the same for both of situations, the right member in Eq. (5) becomes equal to 1, so

$$\xi_{ci} = \xi_c - \xi_l + \xi_{ap}(1 + \xi_l). \qquad (6)$$

2.2 Main combustor's energy balance.
Energy balance equation for the combustor must be written in both situations (without and with cooling fluid injection).

For the basic engine the equation is

$$\dot{m}_a i_2^* + \dot{m}_c(\zeta_{CA} P_{ci} + i_c) = \dot{m}_g i_3^* = \dot{m}_a(1 + \xi_c)i_3^*,$$

(7)

while for the engine with fluid injection

$$\dot{m}_{ai} i_2^* + \dot{m}_{ci}(\zeta_{CA} P_{ci} + i_c) + \dot{m}_l i_l = \dot{m}_{gp} i_{3i}^*. \qquad (8)$$

Given the formulas (1), (2) and (6), after dividing Eqs. (7) and (8) by $\dot{m}_a$, one obtains

$$i_2^* + \xi_c(\zeta_{CA} P_{ci} + i_c) = (1 + \xi_c)i_3^*, \qquad (9)$$

$$i_2^* + \xi_{ci}(\zeta_{CA} P_{ci} + i_c) + \xi_l i_l = (1 - \xi_{ap} + \xi_l + \xi_c)i_{3i}^*$$

(10)

where i_c, i_l are fuel's and injected liquid's specific enthalpy, i_2^*, i_3^*, i_{3i}^* – air/burned gases

specific enthalpy, P_{ci} – fuel's chemical energy, ζ_{CA} – combustor's burning perfection co-efficient.

Assuming that burned gases enthalpy must remain constant and, meanwhile, assuming that fuel's enthalpy is very small, negligible compared to fuel's chemical energy (P_{ci}) and that burning perfection co-efficient (ζ_{CA}) remains constant (with or without cooling fluid injection), from the above-determined equation one can express the fluid injection fraction as

$$\xi_l = \frac{1}{i_3^* - i_l}\left[\left(1 + \frac{1}{\lambda_{CA} \min L}\right)i_{3i}^* - i_2^* - \right.$$
$$\left. - \frac{\zeta_{CA} P_{ci} + i_l}{\lambda_{CA} \min L}\right]. \qquad (11)$$

Eqs. (6) and (11) may determine the extracted air fraction, with respect to the injected cooling fluid fraction.

3. ENGINE'S NEW MOTION EQUATIONS

Engine's mathematical model consists of:
- engine's spool motion equation;
- compressor's and turbine's characteristics;
- combustor's energy equation;
- air/gases flow rate's equation.

These equations are studied in [8] for a basic engine; a matrix description is also given

$$[A] \times (u) = (b), \qquad (12)$$

where $[A]$ is engine's matrix, (u) – output parameters vector and (b) – input parameters vector:

$$A = \begin{bmatrix} T_1 s + \rho_1 & -k_{1T3} & 0 & -k_{1p2} & k_{1p4} \\ k_{2n} & -k_{2T3} & 0 & k_{2p2} & 0 \\ 0 & -1 & 1 & -k_{3p2} & -k_{3p4} \\ 0 & k_{4T3} & k_{4T4} & k_{4p2} & k_{4p4} \\ k_{5n} & k_{5T3} & 0 & k_{5p2} & 0 \end{bmatrix}$$

(13)

$$u^T = \left(\overline{n} \quad \overline{T_3^*} \quad \overline{T_4^*} \quad \overline{p_2^*} \quad \overline{p_4^*}\right), \qquad (14)$$

$$b^T = \left(0 \quad 0 \quad 0 \quad 0 \quad k_{5Qc}\overline{Q}_c\right). \qquad (15)$$

The involved co-efficient are used with their expressions, described in [8].

Based on previous chapter thermodynamic considerations, one can affirm that the fluid

"HENRI COANDA"
AIR FORCE ACADEMY
ROMANIA

"GENERAL M.R. STEFANIK"
ARMED FORCES ACADEMY
SLOVAK REPUBLIC

INTERNATIONAL CONFERENCE of SCIENTIFIC PAPER
AFASES 2014
Brasov, 22-24 May 2014

injection has influence on the air/gases flow rate balance along the engine, as well as on the energy b alance in th e engine's com bustor. Consequently, one has to m odify the equations involving the tem perature behind the engine's combustor, as well as the equation of flow rate's continuity.

One has to neglect the new propulsion system (supplem entary com bustor), which operates together with the basic engine, because it has no influence above th e mathematical m odel; it m ay only be considered as a th rust augmentation factor and it m ust be included, if possible, o nly in th e global thrust calculation.

3.1 Flow rate equation. The exhaust gases flow rate is given by Eq . (10), where the fuel flow rate is the smallest and can be neglected

$$\dot{m}_{g_i}\left(p_3^*, T_3^*\right) = \dot{m}_{a_i}\left(p_2^*, n\right) + \dot{m}_l . \qquad (16)$$

The above equation should be linearised, using the finite differences m ethod, in order to be used into the mathematical model

$$\left(\frac{\partial \dot{m}_{g_i}}{\partial p_3^*}\right)_0 \Delta p_3^* + \left(\frac{\partial \dot{m}_{g_i}}{\partial T_3^*}\right)_0 \Delta T_3^* = \left(\frac{\partial \dot{m}_{a_i}}{\partial p_2^*}\right)_0 \Delta p_2^* +$$

$$+ \left(\frac{\partial \dot{m}_{a_i}}{\partial n}\right)_0 \Delta n + \Delta \dot{m}_l . \qquad (17)$$

Assuming that $p_3^* = \sigma_{CA}^* p_2^*, \sigma_{CA}^* = \text{const.}$, the above equation becomes

$$\left[\left(\frac{\partial \dot{m}_{g_i}}{\partial p_2^*}\right)_0 \sigma_{CA}^* - \left(\frac{\partial \dot{m}_{a_i}}{\partial p_2^*}\right)_0\right]\Delta p_2^* + \left(\frac{\partial \dot{m}_{g_i}}{\partial T_3^*}\right)_0 \Delta T_3^* -$$

$$- \left(\frac{\partial \dot{m}_{a_i}}{\partial n}\right)_0 \Delta n = \Delta \dot{m}_l , \qquad (18)$$

or $\quad \dfrac{p_{2_0}^*}{\left(\dot{m}_{a_i}\right)_0}\left[\left(\dfrac{\partial \dot{m}_{g_i}}{\partial p_2^*}\right)_0 \sigma_{CA}^* - \left(\dfrac{\partial \dot{m}_{a_i}}{\partial p_2^*}\right)_0\right]\dfrac{\Delta p_2^*}{p_{2_0}^*} +$

$$\frac{T_{3_0}^*}{\left(\dot{m}_{a_i}\right)_0}\left(\frac{\partial \dot{m}_{g_i}}{\partial T_3^*}\right)_0 \frac{\Delta T_3^*}{T_{3_0}^*} - \frac{n_0}{\left(\dot{m}_{a_i}\right)_0}\left(\frac{\partial \dot{m}_{a_i}}{\partial n}\right)_0 \frac{\Delta n}{n_0} =$$

$$= \frac{\left(\dot{m}_l\right)_0}{\left(\dot{m}_{a_i}\right)_0}\frac{\Delta \dot{m}_l}{\left(\dot{m}_l\right)_0} = \xi_l \frac{\Delta \dot{m}_l}{\left(\dot{m}_{a_i}\right)_0} . \qquad (19)$$

Assuming the form al annotation $\overline{X} = \dfrac{\Delta X}{X_0}$

the above equation becomes

$$k_{2n}' \overline{n} - k_{2T3}' \overline{T_3^*} + k_{2p2}' \overline{p_2^*} = \xi_l \overline{\dot{m}_l} ; \qquad (20)$$

one can observe that the second line in m atrix [*A*] should be replaced by the new values of the co -efficient. Meanwhile, on e has to complete the second elem ent in the input vector (*b*) with the term in the right member of Eq. (20).

3.2 Combustor's energy equation. The fifth equation in the m athematical m odel is based on the com bustor's energy equation, which m ay have different form s, according to the injected fluid's nature:

$$\dot{m}_{g_i} c_{p_g} T_3^* - \dot{m}_{a_i} c_{p_a} T_2^* = \dot{m}_c \zeta_{CA} P_c + \dot{m}_l \zeta_{CA} P_l ,$$
$$(21)$$

where c_{p_g}, c_{p_a} – specific isobar heat of the burned gases and air (assum ed as equal), ζ_{CA} – burning process' perfection co-efficient, P_c, P_l – chemical energy of the fuel, respectively of the injected fluid.

Meanwhile, the te rm T_2^* should be expres- sed with respect to p_2^*

$$\Delta T_2^* = \left(\frac{\partial T_2^*}{\partial \pi_c^*}\right)_0 \Delta \pi_c^* = \left(\frac{\partial T_2^*}{\partial \pi_c^*}\right)_0 \left(\frac{\partial \pi_c^*}{\partial p_2^*}\right)_0 \Delta p_2^* , \quad (22)$$

or as $\quad \overline{T_2^*} = \dfrac{p_{2_0}^*}{T_{2_0}^*}\left(\dfrac{\partial T_2^*}{\partial \pi_c^*}\right)_0 \left(\dfrac{\partial \pi_c^*}{\partial p_2^*}\right)_0 \overline{p_2^*} . \qquad (23)$

The cooling f luid, which is injecte d into the rear part of the co mbustor is a neutral-one and doesn't participate at the burning reaction
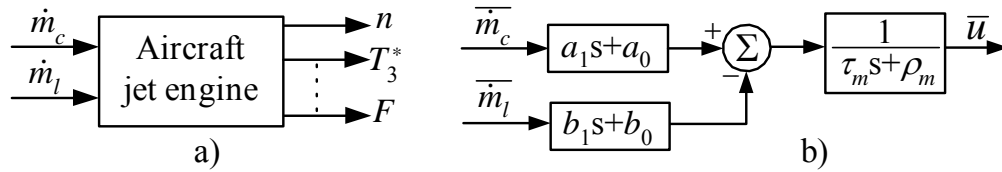
Figure 4. Aircraft jet engine as controlled system (object)

(as flamm able substance). Consequently, Eq. (21) becomes

$$\dot{m}_{g_i} c_p T_3^* - \dot{m}_{a_i} c_p T_2^* = \dot{m}_c \zeta_{CA} P_c . \qquad (24)$$

Considering Eqs. (16), (17), (18) and (23), one obtains from (24)

$$\frac{c_p\left(T_{3_0}^* - T_{2_0}^*\right)n_0}{\dot{m}_{c_0}\zeta_{CA}P_c}\left(\frac{\partial \dot{m}_a}{\partial n}\right)_0 \bar{n} + \frac{c_p\left(\dot{m}_{a_0} - \dot{m}_{l_0}\right)T_{3_0}^*}{\dot{m}_{c_0}\zeta_{CA}P_c}\overline{T_3^*}$$

$$+\left[\frac{c_p\left(T_{3_0}^* - T_{2_0}^*\right)p_{2_0}^*}{\dot{m}_{c_0}\zeta_{CA}P_c}\left(\frac{\partial \dot{m}_a}{\partial p_2^*}\right)_0 - \frac{c_p\left(\dot{m}_{a_0} - \dot{m}_{l_0}\right)}{\dot{m}_{c_0}\zeta_{CA}P_{ci}} \times\right.$$

$$\left. \times p_{2_0}^*\left(\frac{\partial T_2^*}{\partial \pi_c^*}\right)_0\left(\frac{\partial \pi_c^*}{\partial p_2^*}\right)_0\right]\overline{p_2^*} = \dot{m}_c - \frac{\dot{m}_{l_0}}{\dot{m}_{c_0}\zeta_{CA}P_{ci}}\overline{\dot{m}_l}$$

(25)

One can observe th at the co-efficient

$$\frac{\dot{m}_{l_0}}{\dot{m}_{c_0}\zeta_{CA}P_{ci}}$$ of the in jected fluid flow rate

parameter $\overline{\dot{m}_l}$ has a very small value comparing to 1, th e value of the co -efficient of $\overline{\dot{m}_c}$, so it may be neglected. Consequently, the above-determined equation may be re-written as

$$k_{5n}\bar{n} + k'_{5T3}\overline{T_3^*} + k'_{5p2}\overline{p_2^*} = \overline{\dot{m}_c} \qquad (26)$$

and the las t line in m atrix [A] should be appropriate restored.

The [A]-matrix, as well as th e (b)-vector should be modified in appropriate modes, with respect to the injected fluid nature.

4. SYSTEM'S QUALITY

Jet engine's behavior , as controlled object (system), should be studied for the new conditions. System 's quality consists of engine's step response (its tim e behavior for step input or inputs).

An aircraft engine with com bustor fluid injection can be repr esented, as controlled object, by a system with two inputs (fuel flow rate and in jected flu id flow rate) and m ore

outputs (engine speed, co mbustor temperature, thrust etc), as figure 4.a shows.

Following the algorithm described in [6,7,8], each one of the outputs *u* can be expressed w ith respect to the above-m ention-ned inputs, as formally shown in figure 4.b.

As m ain outputs the next three were considered: a) engine's speed non-dim ensional parameter $\bar{n}$; b) eng ine's combustor tempera-ture p arameter $\overline{T_3^*}$; c) engine's thrust para-meter $\overline{F}$.

One has chosen, for a quantitative study, a VK-1A-type jet engine, with constant area exhaust nozzle, having in mind only the engine as possible controlled object, without its control system s (without the speed controller and the temperatu re lim iter). Its f light regim e is conventionally chos en as stationary (airspeed *V*=0) at sea level (altitude *H*=0).

Output param eters' expressions for the VK-1A basic engine are

$$\bar{n}(s) = \frac{1.2606}{2.0859s + 5.1015}\overline{\dot{m}_c} , \qquad (30)$$

$$\overline{T_3^*}(s) = \frac{1.3799s + 2.3888}{2.0859s + 5.1015}\overline{\dot{m}_c} , \qquad (31)$$

$$\overline{F}(s) = \frac{1.3762s + 4.762}{2.0859s + 5.1015}\overline{\dot{m}_c} , \qquad (32)$$

depicted with dashed lines for step responses in figures 5, 6 and 7.

Figure 5 sh ows the en gine's speed para-meters step response, w hile figure 6 shows the same response of the com bustor tem perature parameter and figure 7 contains engine's thrust behavior for the same conditions.

The case of the injection of a neutral cooling f luid (wate r) in to th e r ear part of the engine's combustor brings next mathem atical model modifications

$$\bar{n}(s) = \frac{1}{2.3761s + 4.817}\left(1.411\overline{\dot{m}_c} - 0.167\overline{\dot{m}_l}\right),$$

(33)
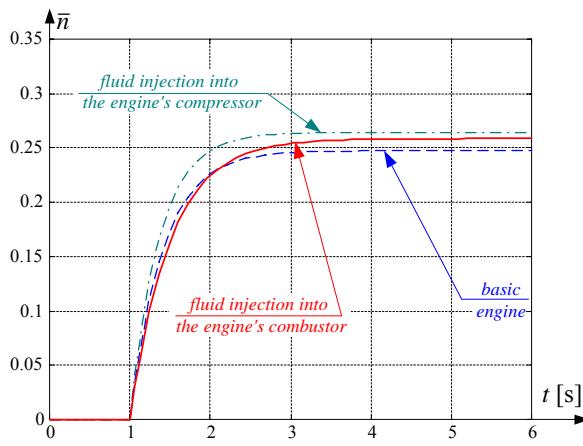
Figure 5. Engine's speed parameter
step response
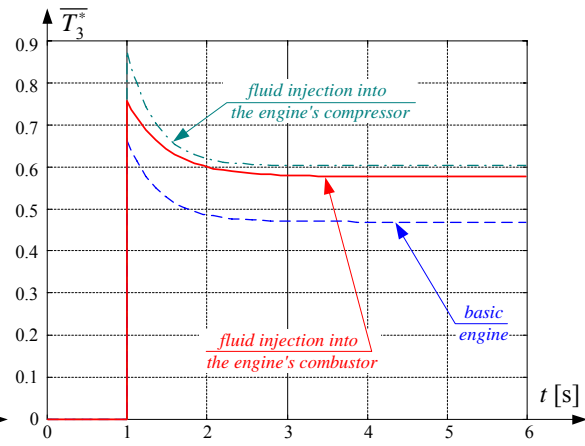
Figure 6. Engine's combustor temperature
parameter step response
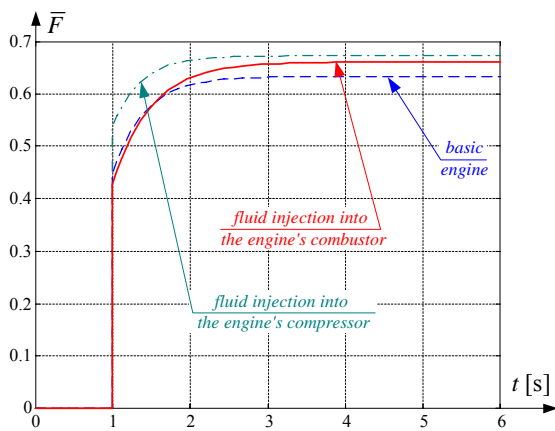
Figure 7. Engine's thrust parameter step response

$$\overline{T_3^*}(s) = \frac{1}{2.3761s + 4.817}\left[(1.8732s + 2.847)\overline{\dot{m}_c} - \right.$$
$$\left. - (0.0823s + 0.0764)\overline{\dot{m}_l}\right]$$

(34)

$$\overline{F}(s) = \frac{1}{2.3761s + 4.817}\left[(1.583s + 5.167)\overline{\dot{m}_c} - \right.$$
$$\left. - (0.0834s + 0.4725)\overline{\dot{m}_l}\right]$$

(35)

In orde r to realize a comparison between th e performances of the f luid injection thrust augmentation m ethods, the results of the compressor fluid injection method in [10] were taken and in serted into the diagrams in figures 5, 7 and 7 (dash-dot lines).

5. CONCLUSIONS

Cooling fluid injection into the jet engine's combustor determ ines gas-dynam ic m odify-cations and performances improvement.

As the tec hnical lite rature shows, the described m ethod of thrust augm entation through fluid injection in to the com bustor is a very effective one, especially for high altitudes flights, thrust increasing being significant (until 25%, as figure 2 shows); m eanwhile, the specific fuel consum ption has a m oderate growing (u nder 15%), definitely acceptable because of the thrust augmentation advantages.

Gas-dynamic changes have as consequen-ces both jet engine's m athematical m odel changes, as well as perform ances im prove-ments.

Mathematical m odel's equation was modified because of the air/g ases flow rate's balance changes, as well as because of the new energy balance of the com bustor, when a combustible cooling fluid is involved. In order to keep the engine stable , a sm all air flow rate is extracted before the com bustor and used into a supplem entary combustor (with its own exhaust nozzle, which oper ates as an auxiliary propulsion system).

Whatever the coo ling fluid injection method were, engine's speed is less influenced (as figure 5 shows), sm all $\overline{n}$ – parameter's increasing being observed. Moreover, the injection in to the co mbustor in volves less speed modifications than the injection into the compressor, but one has observed, in this case, a sm all response tim e growing (about 0.5 s), which m eans that the engine has becom e somewhat s lower than the basic engine. The injection into the compressor makes the engine a little, bu t insignif icant, f aster, f rom the response time point of view.

279

From the temperature's parameter behavior point of view (see figure 6), whatever the injection method were, one can observe the same trend as for the basic engine. H owever, a significant growing of $\overline{T_3^*}$ – parameter's v alue is observed when the in jection is used, as a consequence of the supplem entary fuel injection, in order to com pensate the air exceeding flow rate, so the temperatu re's parameter tends to restore the basic engine's behavior.

From the thrust-p arameter poin t o f view, whatever the injection m ethod is, thrust presents moderate increase (becau se of the neutral injected fluids , which doesn't assure supplementary heat input and the thrust augmentation is realized by the air flow and gases speed increas e). As figure 7 shows, thrust augmentation is more rapid when the compressor injec tion is used, but the growing percentage is com parable for both o f the used methods.

Engine's time constant is about 15% bigger than for the basic engine; whatever the method were, stabilization time values are kept around (2.5÷3.5) sec, which is accep table from the practical point of view.

One has perfor med the study for an engine VK-1A-type, for sea level conditions. This study could be extended for other flight conditions (low altitude and take-off air speed, as well as f or high altitudes and cruise a ir speed), given that the com bustor fluid injection thrust augm entation method is useful for airplane's (aircraft) b oth for tak ing-off and for medium-high altitude thrust restore.

REFERENCES

1. Berbente, C., Consta ntinescu, N. V. *Gases Dynamics*, vol. I, II. Politehnica University in Bucharest Inprint (1985).
2. Hill, P. G., Peterso n, C. *Mechanics and Thermodinamics of Propulsion*. Addison - Wesley Publications, New York (1993).
3. Ispas, S t. *The Turbo-Jet Engine*. Technica Publishing House (1985).
4. Mattingly, J. D. *Elements of gas turbine propulsion*. McGraw-Hill, New York (1996).
5. Pim sner, V. *Air-breathing Jet Engines. Processes and Characteristics*, Bucharest, Didactic and Pedagogic Publishing (1983).
6. Stoenciu, D. *Aircraft Engine Automation. Aircraft Engines as Controlled Objects*. Bucharest, Milita ry Technical Academ y Inprint (1977).
7. Stoicescu, M., Rotaru, C. *Turbo-Jet Engines. Characteristics and Control Methods*. Buchares t, Military Technical Academy Inprint (1999).
8. Tudosie, A. N. *Aerospace Propulsion Systems Automation.* University of Craiova Inprint (2005).
9. Tudosie, A. Aircraft Gas-Turbine Engine's Control Based on the Fuel Injection Control. In Max Mulder *Aeronautics and astronautics.* Intech Open Acces Publisher (2011).
10. Tudosie, A. Mathematical Model For A Jet Engine W ith Cooling Fluid In jection Into Its Com pressor. *Proceedings of International Conference of Scientific Paper "Scientific Research and Education in AirForce" AFASES 2014.*

COMPLEX TEXTILE STRUCTURES AS REINFORCEMENT FOR ADVANCED COMPOSITE MATERIALS

Mădălina ZĂNOAGĂ, Fulga TANASĂ

"Petru Poni" Institute of Macromolecular Chemistry, Iaşi, România

Abstract: *Fiber reinforced composites were primary developed for aerospace and defense applications. High performance materials were designed and obtained exploiting the fibers high strength-to-weight ratio. The well known complex textile structures used as reinforcements for advanced composites are 2D and 3D woven fabrics and nonwoven fiber mats, but the knitted fabrics (weft knitted structures, as well as warp knitted) are of high interest in last decades due to their properties and development potential. There are three main types of 3D knitted structures: multiaxial fabrics (multilayer), knitted fabrics with spatial geometry (spatial fashioned) and sandwich/spacer fabrics. Their characteristics and applications are summarized herein.*

Keywords: *fiber reinforced composites, 3D knitted structures, aerospace applications*

1. INTRODUCTION

The history of textiles can be traced back to the prehistoric times. Current applications of textiles have crossed many barriers and reached limits beyond expectations. Fields like sports and leisure, healthcare and wellness, energy generation and storage, electronics and IT, automotive and aerospace, just to give a few examples, are using hi-tech textile reinforced composite materials. Fiber reinforced composites were primary developed for aerospace and defense applications. In these industries, high performance considerations overbalance cost efficiency criteria. High performance materials were, therefore, designed and obtained exploiting the fibers high strength-to-weight ratio. Textile reinforced composites proved to be competitive materials due to certain advantages, in addition to their strength (given by the fiber/yarn structure) and unity and ability to transmit strains (ensured by the polymeric matrix):

➢ controlled anisotropy (due to textile reinforcement) - their structure can be designed so that fibers are oriented in preferential directions, depending on the maximum strain;

➢ textile reinforcements allow to obtain composites with a better weight-to-strength ratio in comparison with steel and other classic materials used for such applications;

➢ textiles maintain their integrity and behavior under extreme conditions: they are not susceptible to corrosion in outdoor applications, display dimensional stability under significant

temperature gradient, are not sensitive to electromagnetic fields;

➢ these composites have an improved fatigue resistance.

Advanced composites based on technical textiles can be found in many industrial applications as storage and transport structures (tanks, pipes, hoses, etc.) [1]. The automotive industry uses them for car frames and other automobile parts (manifold, wheels), whilst in aeronautics composites developed from the 1st level to 2nd level applications (it refers to structural elements) [2] and the future aircraft trend is to build them using exclusively composites. One application of great interest nowadays is the energy production management, especially when it comes to wind energy (wind mills) [3]. Sport equipment industry is employing high amounts of textile reinforced composites in the production of sporting goods and protective equipment (helmets, etc.). An interesting application is in civil buildings, as walls reinforcement, aiming to obtain strengthened structures with reduced thickness and, subsequently, low production costs [4].

2. COMPLEX TEXTILE STRUCTURES

2.1 Types of complex textile structures.

An introduction in complex textile structures used as reinforcement in advanced composites has to take into account two basic criteria: (1) textiles geometry (structure) and (2) the processing [5].

Considering the significant dimension of the textile material and its specific geometry [6], it is possible to define such structures as: unidimensional (non-axial – roving yarns), bidimensional (monoaxial – chopped strand mats; non-axial – sheets; biaxial – plain weave; triaxial – triaxial weave; multiaxial) and tridimensional (liniar element – 3D solid braiding, multiple weave, triaxial and multiaxial 3D weave; plane element – laminates, beams, honeycombs). In this classification, the preset fibers directions used in the material structure was also allowed for.

Depending on their architecture [7], textile reinforcements can be assorted into 4 groups,

as follows: discrete, continuous, with plane and spatial geometry, as presented in Scheme 1. The textile component may be represented by short fibers, filaments or yarns, fabrics or complex structures, continuous or not, with (un)controlled orientation.
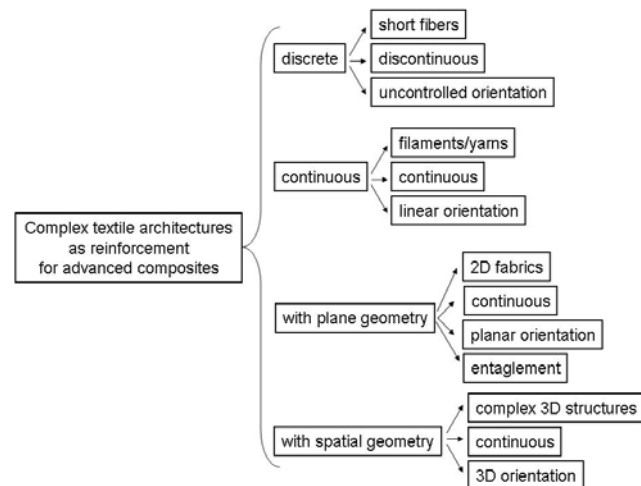
Scheme 1. Classification of textile reinforcements according to their architecture

In terms of technology, all specific processes from textile industries may be used to produce complex structures, but, due to their chacracteristics and the material geometry that results, they lead to different behavior and recommend materials for various applications. The main production processes employed in textile reinforcements are weaving, braiding, knitting and non-wovens production. Other processes, such as filament winding and poltrusion, which process filaments, are also applied. The selection of a specific technological process takes into account its architectural capabilities, the material characteristics and behavior (dimensional stability, mechanic strength, drapability and formability, etc.), as well as its suitability for the composite processing and application.

2.2 Fibers used for complex textile structures. Textile reinforcements are using high performance fibers such as glass, carbon/graphite, aromatic polyamides (aramides – Kevlar), polyesters (HM/HT PES), ceramic fibers, boron and silicon carbide fibers, etc. They have superior mechanical characteristics, as presented in Table 1, so that can meet the specific demands of advanced

"HENRI COANDA"
AIR FORCE ACADEMY
ROMANIA

"GENERAL M.R. STEFANIK"
ARMED FORCES ACADEMY
SLOVAK REPUBLIC

INTERNATIONAL CONFERENCE of SCIENTIFIC PAPER
AFASES 2014
Brasov, 22-24 May 2014

composite applications. Their high bending rigidity and other properties that affect the knitting process must be taken into consideration when designing a knitted structure as reinforcement for composite materials [2].

Table 1. Main characteristics of fibers used in textile reinforcements

Fiber	Relative density (g/cm^3)	Young`s modulus (GPa)	Tensile strength (GPa)
Carbon	2.0	400	2.0-2.5
Boron	2.6	400	3.4
E-glass	2.5	70	1.5-2.0
S-glass	2.6	84	4.6
Kevlar 29	1.44	60	2.7
Kevlar 49	1.45	60	2.7

Glass fibers (yarns, rovings) are the most common high performance fibers used to reinforce composite materials. They are characterized by hardness, resistance to chemical agents, stability and inertness, low weight and processability [4]. There are more types of glass fibers depending on their chemical composition: E-glass, with good strength and high electrical resistivity, most common in composite materials; S-glass, with high tensile strength, used mainly in military applications; and C-glass, characterized by chemical stability and corrosion resistance. The glass fibers possess high strength, low elongation, high bending rigidity and brittleness. It was shown that glass fibers can resist when bent around the needle hook and, therefore, can be processed through knitting [8,9]. Due to their brittleness and low resistance to friction, the glass yarns are easily damaged, thus affecting the knitting process and, subsequently, the real strength of the reinforcement. Therefore, it is required to identify optimal processing parameters prior to

knitting glass fibers. The fabric density and the amount of damaged fibers strongly affect the performance of the final composite. So, a high fiber fraction volume is mandatory for advanced composite materials.

2.3 Knitted fabrics. The most used composite reinforcements are 2D and 3D woven fabrics and nonwoven fiber materials, but the knitted fabrics (weft knitted structures, as well as warp knitted) are of high interest in last decades due to their properties and development potential. The main advantages of knitted fabrics for composite reinforcement are:

➤ they allow knitted fabrics with complex tridimensional shapes;

➤ it is possible to improve the fabric handling and plastic injection during composite processing;

➤ acceptable processability of high performance fibers (glass, aramid, PES HT or HM);

➤ short intervals of production;

➤ controlled anisotropy (yarn in-laid under preferential angles).

Compared to other textiles (woven, braiding, non-crimp materials), knitted fabrics display lower values for in-plane strength and stiffness. Another issue limiting their use is the low volume fraction, due to their specific geometry of knitted stitches, characterized by areas without yarns.

Mechanical properties are controlled by fabric structure and characteristics, yarn properties and process parameters. Using float stitches and in-laid straight yarns placed under certain angles it is possible to improve material characteristics by controlling its structure. Stitch density also affects the tensile behavior and fabric stiffness. Yarns influence the material behavior, their properties being transferred to the final structure. The bending

strength and rigidity of the knitted fabrics essentially depend on the process specific parameters, considering that high performance fibers are rigid and, therefore, they must be processed carefully. The use of in-laid straight yarns eliminates the problem of fiber damage and also increases the volume fraction [4].

Warp knitted fabrics (Figure 1) are resistant to runs and relatively easy to sew. Among their advantages, there are higher productivity rates than weaving, the variety of fabric constructions, large working widths and low stress rate on the yarn (that enable it for rigid fibers such as glass, aramide and carbon), etc.
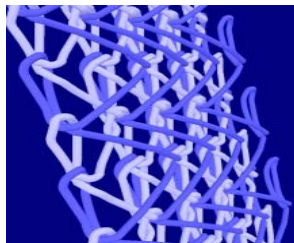
Figure 1. A warp knitted structure

Stitch-bonding is a special form of warp knitting and is commonly used for the production of composite materials and technical textiles (Figure 2). It is an efficient process and one of the most modern ways to create textiles reinforced composite materials for industrial use. The advantages of the stitch-bonding process include high transverse stability and resistance to tearing, low stretch that enables an enhanced transfer of yarn properties, as well as high productivity rate and the scope it offers for functional design of textiles, such as fiber-reinforced plastics [10].

Figure 2. Illustration of a stitch-bonded fabric

Weft knitting is commonly used for garments, such as socks or T-shirts, because the resulting materials may fit shapes. This structure (Figure 3) makes the material elastic whatever the fiber.
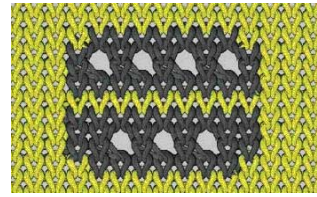
Figure 3. Example of a carbon-Kevlar weft-knitted structure

This feature may be of great use in order to produce composite reinforcements for different aircraft parts, such as cabin equipment. Still, these techniques have some disadvantages: (1) there are almost no finite element models to predict the behavior of the knitted materials; (2) the elasticity of the preform does not allow the manufacturing of high-performance parts. Weft knits are produced with circular and flat machines and most types of yarns can be used, it is even possible to mix different yarns in various areas using the intarsia technique (for instance, it is possible to knit a Kevlar zone inside a carbon part to bring cutting resistance) [11].

3. TRIDIMENSIONAL KNITTED STRUCTURES

Knitted fabrics can easily achieve 3D architectures due to their high extensibility and formability that allow complex shapes. This is the reason why the knitted fabrics are regarded as a viable option for preforms for advanced composite materials [4].

The main advantages of the 3D knitted structures are, as follows:
➢ fabrics high formability due especially to their drapability;
➢ shapes high complexity and wide variety;
➢ the use of the already existing technology, without major modifications;
➢ good impact resistance.

Specific properties of these textile structures are given by their complexity. Knitted 3D performs are currently under study and the development of these fabrics, yet at laboratory stage, still needs a significant input from the R&D community in terms of improving their characteristics, developing up-graded production protocols (for example, impregnation with resin yields in an uneven behavior of the composite due to fibers

"HENRI COANDA"
AIR FORCE ACADEMY
ROMANIA

"GENERAL M.R. STEFANIK"
ARMED FORCES ACADEMY
SLOVAK REPUBLIC

INTERNATIONAL CONFERENCE of SCIENTIFIC PAPER
AFASES 2014
Brasov, 22-24 May 2014

migration in stitches), as well as prediction models.

There are three main types of 3D knitted structures: multiaxial fabrics (multilayer), knitted fabrics with spatial geometry (spatial fashioned) and sandwich/spacer fabrics.

3.1 Multiaxial fabrics (multilayer). The multiaxial fabrics are characterized by multiple layers of yarns arranged under certain angles that are finally assembled into knitted fabrics (Figure 4). These fabrics are produced on special warp knitting machines using glass or carbon fibers for layers.

The different layers in the multiaxial warp knitted fabrics are independent and the yarns are fed under preset angles corresponding to the directions requiring higher strength during use, criterion imposed by the application.
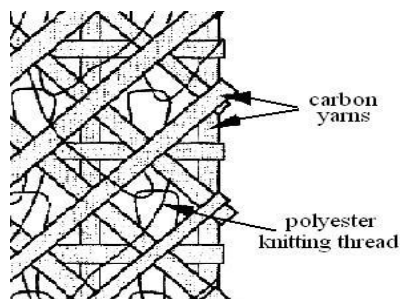
Figure 4. Typical multiaxial knitted structure (carbon and polyester yarns)

The layers are connected within the knitted fabric, by the means of pillars or tricot stitches. By using warp knitting techniques in conjunction with fiber placement concepts, multilayer structures containing straight and relatively uncrimped fibers stacked in the required orientations can be produced. The warp knitting technology is best suited for this kind of structures with in-laid yarns. These fabrics have excellent dimensional stability and outstanding in-plane shear resistance in all directions, show higher elastic modulus compared to woven fabrics, and their tear strength is higher than that of wovens (probably due to the shifting of yarn layers under force and bunch together to resist tearing). Multiaxial fabrics are used mainly as composites reinforcement (HM or HT polymer filaments, such as polyester, nylon and PEEK, and glass, aramid or carbon fibers/yarns) [12,13].

3.2 Spatial fashioned knitted fabrics. The spatial fashioning of the knitted fabrics is based on the need to produce fabrics with complex shapes that are similar to the final product shape. Even if a certain degree of spatial geometry can be obtained by using modules of structures with different patterns or by dynamic stitch length, this technique is the only one that allows textile component parts of great variety in shape and diverse degrees of complexity [4]. Spatial fashioned knitting (also known as "flechage") is based on two different types of knitting courses, on all working needles and on a variable number of needles, determining zones with different geometry. Areas with the highest amount of stitches will have, in the end, a spatial geometry (Figure 5A and B) [14].
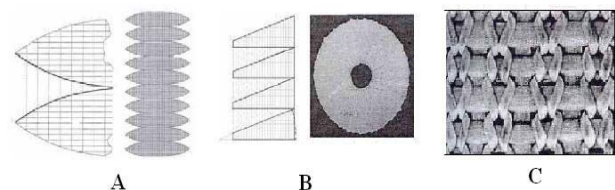
Figure 5. Spatial fashioned knitted fabrics:
A – sphere; B – disc; C - jersey fabric with warp and weft yarns inserted in the structure

One issue connected to the use of preforms made of fashioned fabrics refers to their relatively low strength which can be improved by inserting both warp and weft yarns within the structure (Figure 5C). Apart from increasing the fabric strength, this technique also improves the volume fraction of the

material, with beneficial effects on the properties of the final composites.

3.3 Sandwich/spacer fabrics. A sandwich or a spacer structure is a 3D assembly made of two separate fabrics, interconnected through simple yarns or knitted layers. The fabric thickness is determined by length of the connecting yarns/layers [4].

When produced on warp machines, these fabrics are known as spacers and thickness depends on the distance between two consecutive layers (spacer distance). An interesting application of such spacer fabrics are the textile reinforced concrete panels is used in buildings.

In the case of weft knitting, the fabrics are known as sandwich structures. The connection can be generated through yarns fed on both beds or by knitted layers. In the first case, there are limitations in terms of shape complexity and fabric thickness. The second approach implies to separately knit the two beds and, at a certain point, to stop and knit the connection layer only on selected needles [4]. Examples are given in Figure 6.

(a)

(b)

Figure 6. Spacer fabric made of glass fibers (a) and a sandwich structure (b)

3. CONCLUSION

By combining textile processing techniques with advanced materials characterization methods and prediction models, it it possible nowadays to obtain advanced composites with outstanding properties using complex textile structures as reinforcement.

Knitted fabrics are well known for their applications in the field of technical textiles, including composite materials with polymer matrices. Both weft and warp knitting technologies can be used to produce such reinforcements. Warp knitted fabrics are best suited for structures with in-laid straight yarns (multiaxial fabrics), whilst weft knitted ones allow structures with tridimensional architecture, used as preforms for advanced composite materials. The complex 3D textile systems are being used mostly in defense and aerospace applications (for example, glider wings), where they can effectively replace conventional materials.

A better understanding of the mechanism of fibers reinforcement in composite materials enables the design and production of new high performance textile-based composites for a wide range of applications. Technology optimization will yield in reduced production costs, while geometrical modeling and predictive calculations of the physical and structural properties of textile complex structures will result in preforms with tailored properties.

REFERENCES

1. Mallick, P. *Composites Engineering Handbook*. New York: Marcel Dekker, Inc. (1997).
2. Miller, D. M. Glass Fibers. In ASM International Handbook Committee, *Engineered Material Handbook*, Vol. I – Composites (1989).
3. Mouritz, A.P., Bannister, M.K., Falzon, P.J., Leong, K.H. Review of applications for advanced three-dimensional fibre textile composites. *Composites Part A: Applied Science and Manufacturing*. 30 (2000).
4. Ciobanu, L. Development of 3D Knitted Fabrics for Advanced Composite Materials. In Dr. Brahim Attaf, *Advances in Composite Materials - Ecodesign and Analysis*, InTechOpen. Available:

"HENRI COANDA"
AIR FORCE ACADEMY
ROMANIA

"GENERAL M.R. STEFANIK"
ARMED FORCES ACADEMY
SLOVAK REPUBLIC

INTERNATIONAL CONFERENCE of SCIENTIFIC PAPER
AFASES 2014
Brasov, 22-24 May 2014

http://www.intechopen.com/books/advances-in-composite-materials-ecodesign-andanalysis/development-of-3d-knitted-fabrics-for-advanced-composite-materials (January 2014).

5. Hu, J. Introduction to three-dimensional fibrous assemblies. In J. Hu, *3-D fibrous assemblies Properties, applications and modelling of three-dimensional textile structures*, Cambridge: Woodhead Publishing (2008).

6. Fukuta, K., Onooka, R., Aoki, E., Nagatsuka, Y. In S. Kawabata, *15th Textile Research Symposium*. Osaka: The Textile Machinery Society of Japan (1984).

7. Scardino, F. An introduction to textile structures and their behaviour. In T.W. Chou, F.K. Ko, *Textile Structural Composites, Composite Materials Series*, vol. 3. Amsterdam: Elsevier Science Publishers B.V. (1989).

8. Lau, K.W., Dias, T. Knittability of High – Modulus Yarns. In M.L. Scott, *Proceedings of the 11th International Conference on Composite Materials (6 volumes) JTI*. Cambridge: Woodhead Publishing (1994).

9. Savci, S., Curiskis, J.I., Pailthorpe, M.T. Knittability of Glass Fiber Weft – Knitted Preforms for Composites. *Textile Research Journal*. 71 (2001).

10. Gokarneshan, N., Varadarajan, B., Sentilkumar, C.B., Balamurugan, K., Rachel, A. Engineering knits for versatile technical applications: Some insights on recent researches. *Journal of the Textile Institute*. 102 (2011).

11. Van De Casteele, L. Weft knitting for composite aircraft parts. *JEC Magazine*. 24 (2006).

12. Ogale V., Alagirusamy, R. Textile preforms for advanced composites. IJFTR 29(2004). Available: http://www.niscair.res.in/sciencecommunication/researchjournals/rejour/ijftr (March 2014).

13. Chun, H.J., Kim, H.W., Byun, J.H. Elastic behaviors of stitched multiaxial warp knit fabric composites. *Key Engineering Materials*. 306-308 (2006). Available: www.scientific.net (March 2014).

14. Cebulla, H., Diestel, O., Offerman, P. Modelling and Production of Fully Fashioned Biaxial Weft Knitted Fabrics. In M.D. Araujo, *Proceedings of the 1st Autex Conference: Tecnitex 2001: designing textiles for technical applications (vol. I)*. Braga: Williams (2001).

ENGINEERING SCIENCES

STUDYING ENVIRONMENTAL PROBLEMATICS AND HAZARDS WITH HELP OF INFORMATICS APPLICATIONS (SEPHIA)

Bogdan CIORUȚA*, Mirela COMAN**, Andrei-Alin CIORUȚA*

*Faculty of Science, North University Center Baia Mare, Technical University of Cluj-Napoca
**Faculty of Mineral Resources and Environment, North University Center Baia Mare, Technical University of Cluj-Napoca

Abstract: During recent decades the stirring up of the processes of globalization, practically in all spheres of present day civilization, has aggravated and brought numerous problems resulting from nature-society interactions. To overcome these problems, it is necessary to develop and adopt new concepts and techniques to study and evaluate the changes occurring on the earth ecosystem. For this, application of information technology via Environmental Information Systems is the best option. Much more, understanding this complexity through interactive applications will develop new strategies and ideas to manage and protect ecosystem. This paper deals with new and interactive approach to process, analysis and synthesis of environmental systems using various models and IT applications, so we could underline that environmental science and technology are therefore a vital component of productive knowledge and thus a high priority for the mankind sustainable fraternity with nature. Since years, environmental scientists and computer experts are working on different and innovative computer-based modeling techniques to study the environmental problematic and hazards system and to provide the maximum accuracy in decision making or in elaborating sustainable strategies of community development. This kind of innovative techniques, some of them exemplified in the present paper (GeoGebra, AutoCAD, G.S. Surfer, ArcView GIS etc), can become the answer to question in those cases where the early warning, maximum accuracy in prediction and emergency is taken in account.

Keywords: Environmental Informatics, IT applications, innovative

1. INTRODUCTION

The modern society (information society) in accordance with the actual changes and preocupations in the environment domain has provided various types of informatics resources (tools, methodologies, procedures) to manage and support the ideas and actions related to the environmental issues.

Population grows over time as well as the modern technology implication in everyday life. Informatics become essential for all the fields related to technology and environment protection. Informatics resources are becoming nowadays more and more important for environmental management, planning and decision-making. An exhaustive analysis of the environmental hazards in terms of physical, chemical, biological, geological, hydro-meteorological processes and their interactions is becoming critical, and not so extraordinary maded without the support offered by the environmental information systems (EISs) and environmental informatics.

2. ENVIRONMENTAL INFORMATICS METHODS AND TECHNIQUES

Nowadays, significant efforts are required to analyze relevant data and environment information, simulate related processes, evaluate resulting impacts or scenarios and generate viable decision alternatives.

The informatics resources developed in the last 3-4 decades have enabled and help us to investigate the complex interactions between the natural systems and engineered ecosystem, and also to search for sustainable strategies for a harmonious development.

In figure 1 are mentioned the general steps necessary to define, analyse and solve the problems related to obtaining environmental information with help of EISs.
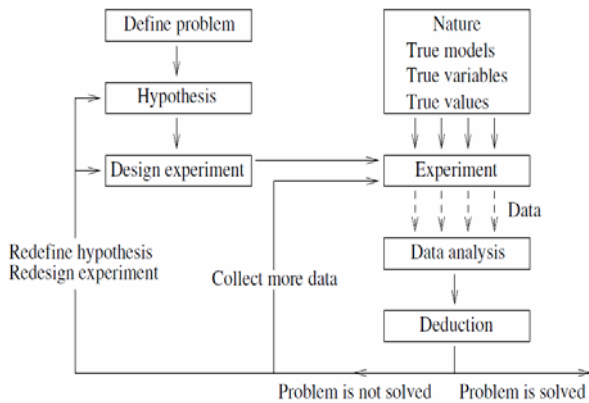
Fig. 1. *Specific steps for developing EISs and obtaining environmental information*

There can be mentioned a few important scientific contributions in the domain of informatics applied to environmental sciences (knowed as Environmental Informatics) as:
- traditional mathematical simulation models - tools for the forecasting of environmental phenomena;
- optimization techniques - used in the field of environmental pollution control and management;
- environmental evaluation applications;
- modeling systems for different environment study regimes.

All the resources presented above are used for defining environmental problems, archiving and processing environmental data with obtaining environmental information and adequate enviromatics knowledge.

The advent of the informatics systems had affected the access of the public to large and diverse environmental databases.

Collecting, storing and retrieving environmental data performed thanks to database techniques, make the processing of environmental data to the field of modeling very interesting: data are used to generate information, and information to generate knowledge. Figure 2 present in this sense the specific steps for obtaining adequate environmental knowledge starting from environmental data.
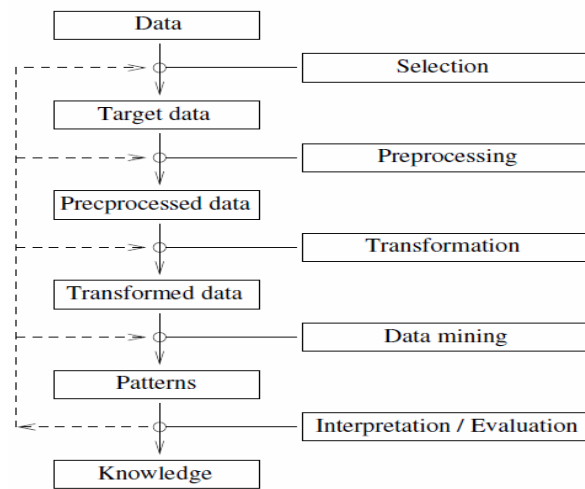
Fig. 2. *Specific steps for obtaining adequate environmental knowledge using EISs*

As we mentioned above, the techniques developed in the environmental informatics field are implemented and find their incarnation in an array of different software tools, platforms and environments (data storage software, data processing software, end-user applications etc).

The main tools that facilitate the environmental data storage are databases, which contains scientific the results of observing (monitoring) natural phenomena.

Environmental data that are stored in environmental database are different from other data because they have a specific attribute: spatio-temporallity.

Figure 3 illustrate a specific way for getting information and knowledge (data output - maps and reports) using EISs from data that are spatio-temporally referenced (data input).

"HENRI COANDA"
AIR FORCE ACADEMY
ROMANIA

"GENERAL M.R. STEFANIK"
ARMED FORCES ACADEMY
SLOVAK REPUBLIC

INTERNATIONAL CONFERENCE of SCIENTIFIC PAPER
AFASES 2014
Brasov, 22-24 May 2014
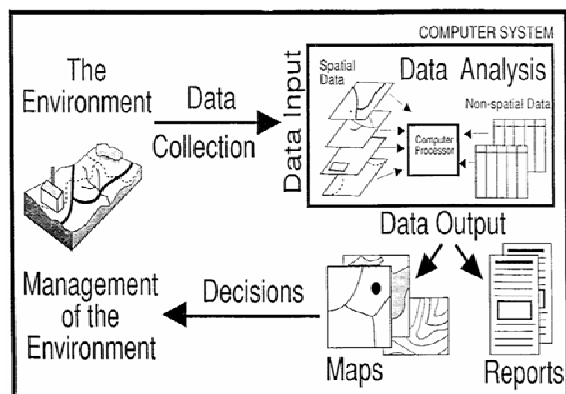
Fig. 3. *A specific way for getting information and knowledge using common environmental info-interactive applications or EISs*

This particularity give a different meaning and let us to define Environmental Informatics and Environmental Information Systems by the expression "info-diversity in ecological diversity".

Figure 4 illustrate according to the last 3-4 decades the perception related to development timeline phases of the info-diversity resources considered to be an integrated part of the Environmental Informatics.
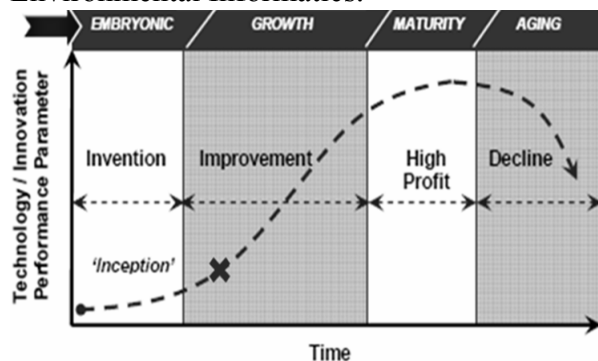
Fig. 4. *Environmental Informatics - delimited by the technology-time scale*

As we observe Environmental Informatics delimited by the technology (software development) and time scale is still in the 2nd

phase (growth) were improvement measures and strategies are necessary.

The traditional environmental systems - models, technologies, methodologies and applications - have been challenged by the difficulties in handling dynamic and uncertain features of real-world environmental systems. Conditions for environmental management will keep changing with time, demanding periodically updated decision support.

Advance in information technology area has been in extraordinarily rapid pace. There will be continuous attempt to apply new techniques and tools to environmental management, also to use the environmental informatics resources associated with artificial intelligence techniques to promote the long-term viability of the environmental informatics and connected applications in everyday's environmental-society problems.
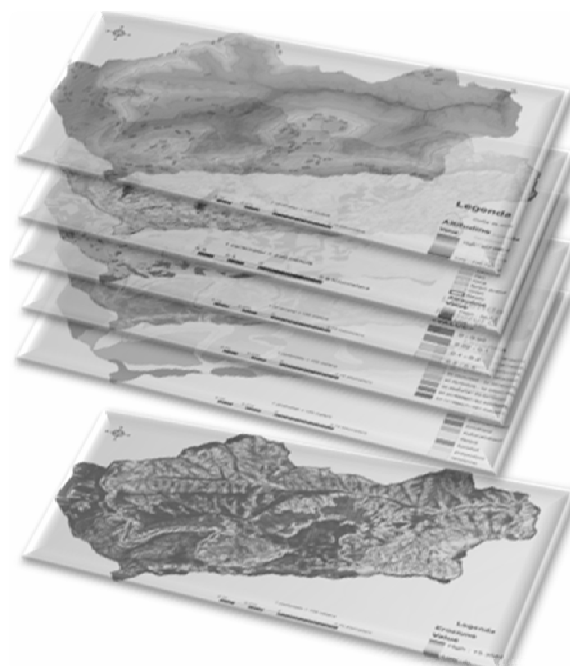
Fig. 5. *The perspective of getting multidisciplinary information using as EISs the GIS products*

Figure 5 introduce a new methodology perspective of getting multidisciplinary information (as multi-thematic maps) using for example the GIS products as an EIS.

The magnitude universe of informational activities, many forms of expression, diversity of instruments and information environment technologies have produced major changes in the way people communicate, learn, do business, solve various problems and to relate to others and the environment. With the recent vision we have formatted and gained from studying the multi-disciplinary area of Environmental Informatics and Environmental Information Systems, we consider that in near future in all the countries are imperious necessary informatics systems for environmental research and protection.

3. CONCLUSIONS

Information and communications technologies have produced unprecedented changes in society in all its aspects. Nowadays, Artificial Intelligence via interactive computational applications plays a specific and well defined role in all areas or activity domains: production, service, management, monitoring, research, public involvement in decision making, and in almost all countries.

Environmental systems are based on the above considerations binding instruments in environmental science, can be defined as a collection of packet data and information, described by a series of specific indicators relevant for studying, monitoring and exhaustive exploration of the field and environmental issues.

As a conclusion, it can be said that modern data analysis methods are useful tools in environmental informatics and environmental statistics. Good methods are understandable for the environmental scientists and at the same time reliable, robust and helpful for discovering important relationships in the data. In cooperation between environmental scientists and information scientists, what makes the relationship flourish is the knowledge of both sides about their field and efficient communication concerning the specific needs of a certain problem and the properties of the methods. Without these ingredients, the results of cooperation projects may not be satisfactory.

REFERENCES

1. Avouris, N. M., Page, B. (1995) *Environmental Informatics: Methodology and Applications of Environmental Information Processing,* Kluwer Academic, Dordrecht, Boston
2. Checkland, P. and Holwell, S. (1998) *Information, Systems and Information System -Making Sense of the Field,* John Wiley & Sons Ltd., Chichester
3. Cioruța, B., Coman, M. (2011) *A forey in modern scientific research of the environment. From SIM to Environmental Informatics*, Ecoterra no. 29/2011
4. Coman, M., Cioruța, B. (2011) *The evolution, definition and role of EIS in the development of environmental protection strategies*, Ecoterra no. 27/2011
5. Gunter, O. (1998) *Environmental Information Systems,* Springer, Berlin
6. Page, B. (1996): Environmental Informatics - Towards a new Discipline in Applied Computer Science for Environmental Protection and Research, Pennsylvania State University, Malvern, London
7. Page, B., Hilty, L. M. (1995). Trends in Environmental Information Processing. In Brunnstein, K., and Raubold (Eds.). *Applications and Impacts. IFIP Transactions A-52*, Amsterdam
8. Porter, J. H. and Callahan, J. T. (1994) Circumventing a Dilemma: Historical Approaches to Data Sharing in Ecological Research, In *Environmental Information Management and Analysis: Ecosystem to global Scale* (Eds. Michener, W. K., Brunt, J. W. and Stafford, S. G.), Taylor & Francis, London
9. Tomlinson, R. F. (1970) *Environment Information Systems,* International Geographical Union, Ottawa, Canada.

THE IDEA OF IMPLEMENTING A MATHEMATICS PLATFORM FOR ANDROID DEVICES WITH HELP OF APP INVENTOR

Bogdan CIORUȚA*, Mirela COMAN**

*Faculty of Science, North University Center Baia Mare, Technical University of Cluj-Napoca
**Faculty of Mineral Resources and Environment, North University Center Baia Mare, Technical University of Cluj-Napoca

Abstract: *App Inventor for the Android platform is a powerful visual and drag-and-drop tool that lets anyone build and design games and other mobile apps with 2D graphics and animation, create multimedia quizzes and guides, design complex apps that control robots, apps that inform and educate or learn computer sciences - with no programming experience required. App Inventor is freely available for anyone to use, runs online and is accessible from any browser, so the users can design the app interface using a web-based graphical user interface builder only by piecing together blocks like in a puzzle.*
In this paperwork we try to give some basic ideas of how everyone using App Inventor could build a specific mathematic application similar to Microsoft Mathematics v. 4.0 - a very powerful software that provides a set of mathematical tools that help students get school work done quickly and easily.

Keywords: *Environmental Informatics, IT applications, innovative*

1. INTRODUCTION

People have been doing personal computing since the 1980s, but today's mobile applications are making computing personal as never before [3]. Today, we carry com puters with us constantly, as sm art-phones and pads and the new devices that are regularly emerging.

More significantly, today's personal computing is increasingly about us: where we live, where we work, who our friends are, what we buy, what we like, whom we talk with, and what we talk about. This personal computing is linked to global data services and information sources in a way that fundamentally transform s our experience and our perception of our world.
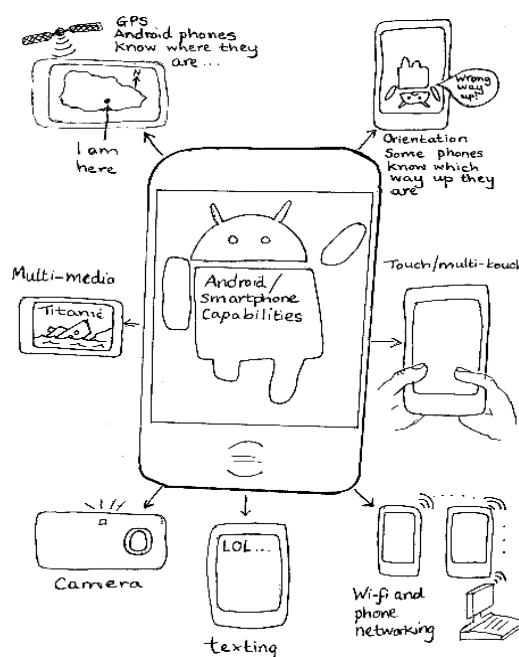
Fig. 1. *Android devices - using perspectives*

Our consumer culture gives us all sorts of opportunities for entertainm ent, pleasure and sometimes even learning. The high-tech objects (cell phones, tablet com puters, TVs, etc) that we use today to consume entertainment and information are black boxes to most of us [3]. In other words, most people can't create the apps that run on these gadgets . What if we could chan ge that? W hat if we could take creative co ntrol of our everyday gadgets, like cell phones?

2. APP INVENTOR FOR ANDROID - BACKGROUND AND MAIN ISSUES

When App Inventor sof tware was created at Google, the team who did this work was motivated by the vision that mobile computing could be personal com puting technology that anyone can actually personalize, by creating applications f or pers onal use, with n o programming experience required [1].
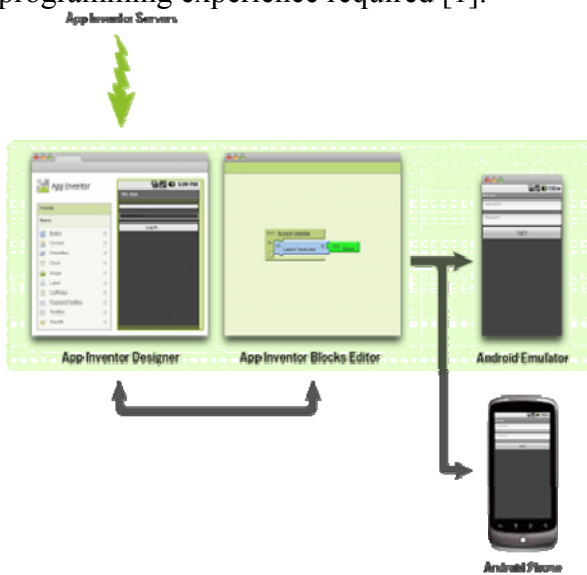
Fig. 2. *App Inventor for the Android platform*

Even if App Inventor is still a be ta system under development - Google team is working to m ake it more powerful and easier to use - there is already a growing comm unity of App Inventor users of all ages who are exploring and experiencing what it's like to m ake applications for themselves [10,12].

Design processes help take your awesom e ideas and m ake them r eality. There is nothing mysterious about a de sign process, although frequently developers give them fearsome and

magical-sounding names such as waterfall model, spiral m odel, and agile developm ent. These all refer to the s ame thing: lo gical steps that developers and programm ers use to m ove an idea f rom a dream to a f ully f unctional program [2,6].
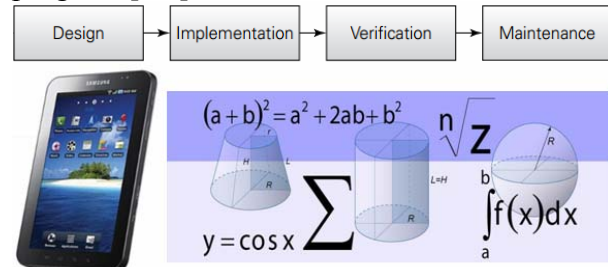
Fig. 3. *The development process of every apps - clarifying the Design Idea*

When it co mes to the develope r tool App Inventor and even the mobile operating system Android, it is dif ficult to talk abo ut histo ry, given that this history is still rather young.

Since Android was fi rst r eleased in October 2008, the Linux-based operating system for different mobile devices that was initiated by the Open Handset Alliance (OHA) and marketed by Google has developed from a niche product to a market leader [4,5].

App Inventor for the Android platform is a blocks language for mobile phones and a powerful visual and drag-and-drop tool that lets anyone build and design gam es and other mobile apps with 2D graphics and anim ation, create cus tom m ultimedia quizze s, design complex apps that control robots or communicate with the we b, build apps that inform and educate or learn com puter sciences - with no programm ing experince required [9,10].
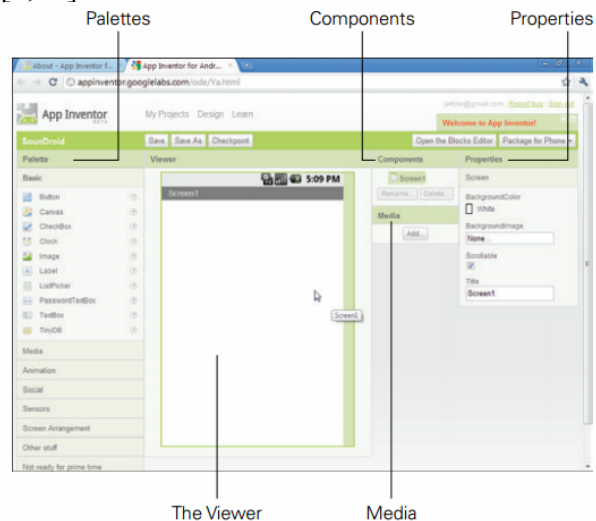
Fig. 4. *The Design view for App Inventor*

"HENRI COANDA"
AIR FORCE ACADEMY
ROMANIA

"GENERAL M.R. STEFANIK"
ARMED FORCES ACADEMY
SLOVAK REPUBLIC

INTERNATIONAL CONFERENCE of SCIENTIFIC PAPER
AFASES 2014
Brasov, 22-24 May 2014

The Design window should appear in your browser once you enter th e name of your app and click O K. The Des ign window is where you begin creating how app will look, the user interface (UI)[12].
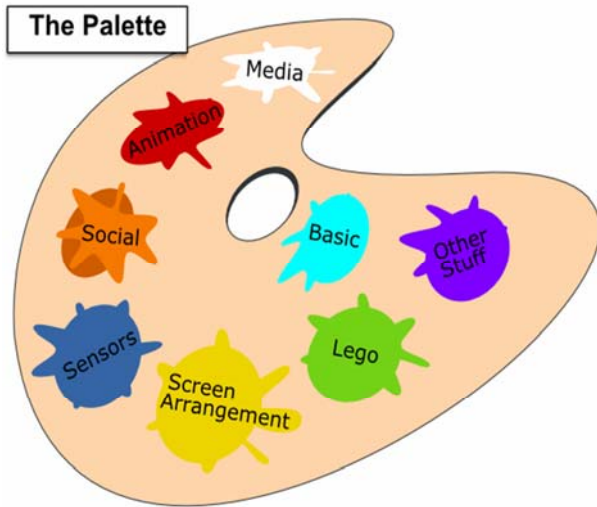
Fig. 5. *App Inventor - the Palette of components*

Accessing the Blocks Editor is realized with Open the Blocks Editor butto n near th e top right corner of the Design window [11,13].

Accessing the Emulator is realized with the New e mulator button at the top of the Blocks Editor window. This will open an emulation of an Android device. Back in the Blocks Editor, with the Connect to Device... button we can establish the connection with the app and also be able to see the project in the emulator.

3. RESULTS AND DISCUSSIONS

With an applic ation like Microsof t Mathematics for android students can learn to solve equ ations step -by-step while gaining a better understanding of f undamental concepts in algebra, calculus, geom etry, text recognition, trigonom etry, physics, and m uch more [8].

Fig. 6. *Microsoft Mathematics - specific apps*

Our results working with App Inventor were determined in accordance with our skills, our determination and our interest in graphics, animation and educational software.
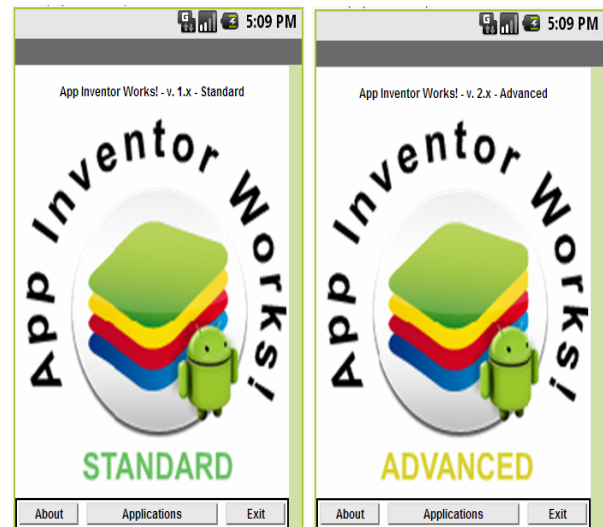
Fig. 7. *Results - different types of apps integrated into educational mathematics platform*

295

We present a few res ults that co uld b e develop by any students even if they have no programming experien ce lik e most of us everyday entertainm ent and infor mation consumers. As you can see is possible to represent, in an in teresting way (design , animation), different types of m athematics fundamental concepts (like in the firs t emulator im age), for mulas, equ ation and triangle solver apps, and much more:

- App Inventor Works - Standard version - 5 different apps: *Calculator*, *Formulas*, *Equation Solver*, *Geometry Solver* a nd *Unit Converter*.
- App Inventor W orks - Advanced - 5 different apps: *Glossary*, *Financial Calculus*, *Statistics*, *Grapher* (2D) and *Surfer* (3D geometry creator).
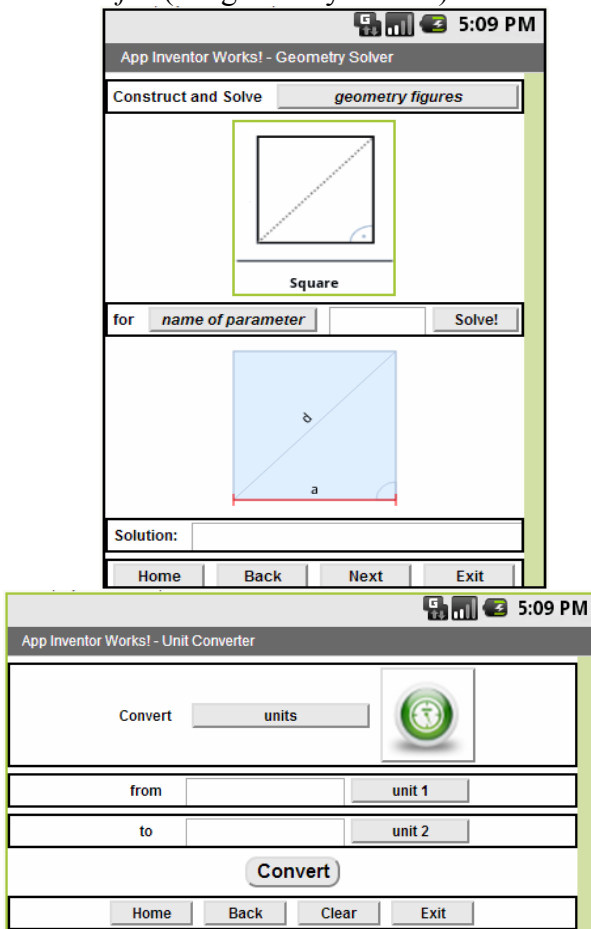
Fig. 8. *Geometry Solver* and *Unit Converter*

All the apps are based on various palette of components (basic, m edia, anim ation, social, sensor, screen arrangem ent etc) and blocks (definition, tex t, lis t, m ath, logic, contro l, color) whic h f acilitate the pro ject d esign and functionality.

4. CONCLUSIONS

Information and comm unications tools and methodologies have pro duced unprecedented changes in our society in all its as pects, bu t especially in mobile devices environment.

According to this tren d, in the present workpaper, we try to help everyone who use App Inventor for Android and are interested in mathematics to dev elop specif ic e ducational applications.

REFERENCES

1. Burnette E. , *Hello Android: introducing Google mobile development platform*, The Pragmatic Bookshelf, USA, 2010
2. Kirk A., *Data Visualization: a successful design process*, Packt P ublishing Ltd., UK, 2012
3. Kloss, Jorg H., *Android Apps with App Inventor: the fast and easy way to build android apps*, Pearson Education Inc., USA, 2012
4. Marinacci J., *Building Mobile Applications with Java*, O'Reilly M edia Inc., Canada, 2012
5. Mednieks Z., Dornin L., Nakamura M., *Programming Android*, O' Reilly Media Inc., Canada, 2011
6. Segaran T., *Beautiful Data - the stories behind elegant data solutions*, O'Reilly Media Inc., Canada, 2009
7. Steele J., Iliin sky N., *Beautiful Visualization - looking at data through the eyes of experts*, O'Reilly Me dia In c., Canada, 2010
8. Svirin A., *1300 Math Formulas*, The Pragmatic Bookshelf, USA, 2004
9. Tyler J., *App Inventor for Android: build your own apps - no experience required!*, John Wiley Ltd., USA, 2011
10. Wolber D., Abelson H., Spertus E., Looney L., *App Inventor - create your own Android apps*, O'Reilly Med ia, Inc., Canada, 2011
11. http://appinventor.mit.edu
12. www.appinventor.org
13. www.it-ebooks.info

“HENRI COANDA”
AIR FORCE ACADEMY
ROMANIA

“GENERAL M.R. STEFANIK”
ARMED FORCES ACADEMY
SLOVAK REPUBLIC

INTERNATIONAL CONFERENCE of SCIENTIFIC PAPER
AFASES 2014
Brasov, 22-24 May 2014

ECONOMICS CONSIDERATION ON WOODEN BIOMASS CONSUMPTION

Tatiana GRÎU *, Aurel LUNGULEASA **

*Wood Engineering Faculty, Transylvania University, Brasov, Romania, ** Wood Engineering Faculty, Transylvania University, Brasov, Romania

Abstract: Energy is the important element that ensures the economic and social development level in the world. According to the research made in this field a lot of researches are orientated to the development of the alternative source of energy. The importance to ensure the necessary energy will be observed from the moment when will start to exhaust the fossil combustible. This paper describes the efficiency use of the fossil combustible and renewable source of energy (SRE) on Romanian energetically market. The accessibility of the renewable energy source in the world directed the economical and social increase in the developing state. Energy is a source that generates the progress of the state. The main objectives of the paper are the accessibility of the energetically source in Romania and the fuel consumption for heating. Important obtained results in the research describes the biomass (pellets, briquettes and wood) as an accessibility solid combustible for producing energy in the world, being widely spread and the cheapest on the energetically market.

Keywords: biomass, combustible produce, energy, fuels, heat

1. INTRODUCTION

In present all researches in Romania and Europe try to exploit the alternative field in energy production and bringing a lot of new scientifically date about the renewable source of energy, especially about the production of energy from the biomass. Energy represents an important point for all the developing countries because energy offers comfort on social and economical plan.

In this moment, main energetically source are the fossil fuels like oil, coal, natural gas, nuclear energy and a low percent from the SRE (Source of Renewable Energy) contributes in European Union (EU) with about 10% to the energy production in 2010. According to statistics, the field of the energy production from fossil combustible will touch the peak point in 2020, after which the chart of

availability will decrease [6, 12]. The importance to research the energetically market in the SRE production has a significant and actual role for the population. Countries like Germany, Finland and Sweden ensure 30% for their energy consumption from the SRE production and especially from biomass.

In the 2006, the biomass contribution to the production of the energy in EU was about 86.6 Mtoe (Millions tone equivalent oil) from firewood, briquettes and pellets [19]. The prognoses show that the biomass will cover 60% from the total energy consumption compare with others SRE, with a production of 190-200 PJ/an (1J=10^{15} PJ) [3].

In present, firewood is the principal energy source for producing energy for about 2 billons of people in rural areas and provides more than 14 % from the all energy consumption in the world, comparable with

coal (12%), gas (15%) and electricity (14%) [1, 2, 6]. A major problem with which a lot of researches are confronting is that the consumers use all kinds of thermal furnaces with lower yield for producing energy heat [15].

In the last years according to researches, there were recorded significant increases in imports of the fossil combustible (natural gas) in EU, which were used to produce heat energy. In the energetically field, there were made a lot of research about the efficiency of the thermal furnaces [5, 7, 9, 10, 16, 18]. The thermal furnace in present has a yield of 92% for natural gas use and 85-90% for biomass fuel use.

The amount of released heat from the biomass is influenced by a series of factors as moisture content from the material that absorbs energy in the burning process, the volatile substance, the chemical composition (C, H, O and N) etc.

In Serbia, there are found about 40.9 % of the consumers that use renewable combustible as firewood, briquettes and pellets to produce heat [7]. In Romania the major parts of the consumer use firewood for heating in the rural areas, but these thermal furnaces have a lower yield about 10-15% or natural gas with a higher yield of 90%. The biomass in Romania is the most used combustible in the rural areas.

An important aspect in the use of wooden biomass to produce heat is that that biomass is an ecologically material with lower CO_2 emission in the burning process. The exploitation of the SRE in the entire world can ensure the necessary energy for life and to contribute to the environment protection.

The paper presents a theoretical and experimental research based on a study made to determine the most accessible fuel for producing the heat. The energetically market in Romania knows a lot of combustible materials. In the process of the determination which is the best combustible for heating process were taken in consideration the ecologically aspects and the economical ones.

The main objectives of the paper consist in highlighting the most effective and ecologically solid combustible to produce thermal energy (heat) for the housing and the cost for this energy. The motivation of the

necessity of this research occurs from the aspects of the highest costs on the fossil combustible which increased five times since 2000 and in the future it expects to still increase and the availability of them will decrease.

2. MATERIALS AND METHOD

2.1. Materials. Investigating the energetically market were founded a lot of materials which can be used in thermal furnace as ecologically combustible. These materials are firewood, briquettes and pellets from different kinds of species. The pellets/ briquettes are obtained from the forest waste and are considerate energetically products which are used to produce heat in residential and industrial buildings [20].

Table 1.
Chemical characteristics of the solid fuels

Species	Energetically characteristic, %				
	C	H	O	N	A
Firewood					
Willow	51.7	6.1	41.1	0.9	0.48
Beech	49.9	8.2	37.1	0.7	0.5
Spruce	49.1	9.2	38.9	0.6	0.32
Poplar	49.1	9.2	38.9	0.6	0.32
Ash	50.7	8.0	37.5	0.6	0.51
Briquettes					
Beech	50.2	8.1	37.1	0.7	0.41
Willow	51.8	6.1	41.1	0.9	0.72
Spruce	49.9	8.2	38.1	0.6	0.5
Straw	45.6	5.8	42.4	0.5	5.7
Pellets					
Beech	50.2	8.1	37.1	0.6	0.5
Willow	51.7	6.1	41.1	0.9	0.48
Fossils combustible					
Pit coal	65.9	4.6	23.0	0.7	1.2
Natural gas	75	25	-	-	-

In this paper where analysed five energetically species. The raw materials were taken from Willow (*Salix alba* L.), Spruce (*Picea abies* Karrsten.), Beech (*Fagus sylvatica* L.), Ash (*Fraxinus excelsior* L.) and Poplar (*Populus tremula* L.), (Table 1) species. The results were compared with the fossils combustible as gas and pit coal. These species are considerate as energetically species because they have higher calorific power, quickly grow and are widely spread in Europe.

"HENRI COANDA"
AIR FORCE ACADEMY
ROMANIA

"GENERAL M.R. STEFANIK"
ARMED FORCES ACADEMY
SLOVAK REPUBLIC

INTERNATIONAL CONFERENCE of SCIENTIFIC PAPER
AFASES 2014
Brasov, 22-24 May 2014

The raw materials were analysed in laboratory to investigate the calorific power of the species.

The chemical composition (Table 1) of the materials is considerate as another important energetically characteristic that are described in others scientifically papers [17, 21]. These elements are presented in different quantity in all kind of combustible materials.

2.2. Method. Experimental method used consists of the determination of the calorific power of wood species and briquettes/pellets with the calorimeter with explosive burning OXY-1C [8]. The amount of the moisture content was determinate through the drying method with the laboratory oven at the temperature of $103^{o}C$.

Economical aspects were made on the Romanian energetically market taking in consideration the cost of the combustible displayed by the suppliers.

2.3. Case study. The economically parts were made for a house with a surface of 100 m^2 and the ceiling height is 2.65 m. It is a house for a family with four members. The obtained results from experimental research there were studied in theoretical way. In account were taken the necessary of heat (1) for the houses surface, the quantity of combustible consumption (2) for this surface [13] and was determinate the kWh cost for every type of combustible.

$$Q = Q_T \left(1 + \frac{\Sigma A}{100}\right) + Q_i \ [W] \tag{1}$$

where:
Q – Necessary of heating, in W;
Q_T – Released heat flux through transmission, in W;
Q_i – Thermal load for heating the interior air, in W;

ΣA – Sum of the additions of the affected thermal flux released through transmission, in %.

$$B = \frac{Q}{c_i} \ \left[\frac{kg}{h}\right] \tag{2}$$

where:
B - Consumption of combustible, in kg/h;
Q - Necessary of heating, in W;
C_i – Lower calorific power, in kJ/kg.

In case, the consumer wants to replace the existing heating system it is necessary to determinate what elements need to be replaced (pipe, valves, thermal furnace, accessories, etc). These elements need to be described in a draft plan. The main aspect in this part is to determinate the economical ones like the investment costs, maintenance costs and how much costs the thermal furnace for different kinds of combustible.

The chosen combustible materials were selected from the energetically market in Romania. These species present energetically character with higher calorific power and there are most used materials to produce briquettes and pellets [11, 14, 18].

3. RESULTS AND DISCUSSIONS

The heat amount released by biomass described by Kausley et al [15] in their research is calculated like sum of heat released by the elements that compound the burning process: like time of burning, the heat of flame released and temperature of ignition. The obtained experimental results yield the Lower Calorific Power (LCP) that was used in accounting process. In practice wood materials present the higher calorific power that cannot be used effectively. This amount of heat in the burning process is evaporated with formed volatile substance through the chimney.

The moisture content used for determination was 20% for wood and 10% for pellets and briquettes. The moisture degree in the material is an important element from which depends the amount of heat released in a burning process. These are the limit of the moisture contents for the sold combustible materials by the suppliers. The calorific power resulted in the experimental research (Figure 1 and 2) are determinate for moisture content of 20% for wood samples and 10% for briquettes and pellets samples. An analysis of the received results shows that the briquettes and pellets have a higher calorific power in compare with the wood sample. The pellets have calorific power about 18,299 kJ/kg (4.685 kWh/kg) and briquettes about 16,868 kJ/kg (4.227 kWh/kg) at the moisture content of 10%. The compare fossil combustibles have a LCP of 35,500 kJ/m^3 (9.861 kWh/m^3) for gas and 29,000 kJ/kg (8.055 kWh/kg) for pit coal.
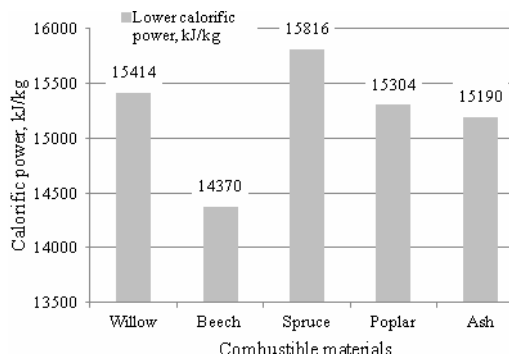
Figure 1.
Lower calorific power of wood species, kJ/kg
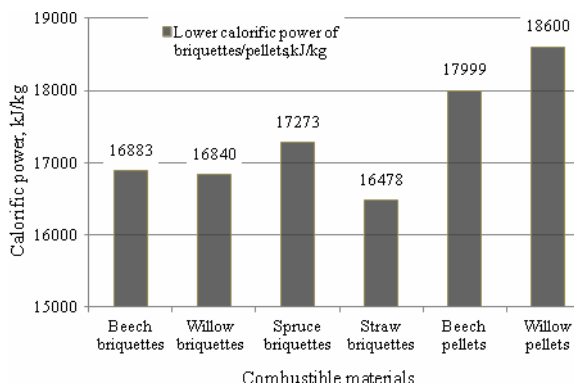
Figure 2.
Lower calorific power of the briquettes and pellets, kJ/kg

The experimental results are described in table 2. The Beech specie (11.63 kJ/cm^3) like firewood presents a bigger energy density than the Willow specie (11.56 kJ/cm^3). An appreciable energy density was obtained for the Spruce (11.78 kJ/cm^3) and Ash (12.91 kJ/cm^3) species. The highest energy density from all the SRE combustible materials has the Spruce briquettes (13.47 kJ/cm^3)The burning rate means the degree of maintenance of the heat released from the woody species in the burning process. Taking in consideration this aspect the biggest burning rate presents the Beech (0.392 kJ/min) and Willow (0.351 kJ/min) species. Compare firewood with the briquettes and pellets sample, the biggest burning rate present the Beech (0.428 kJ/min) and Spruce (0.435 kJ/min) briquettes. This is way a lot of products have 70% percent Beech sawdust and 30% Spruce sawdust. From the pellets materials the biggest burning rate presents Willow (0.419 kJ/min) pellets. This aspect is important when consumers want to heat a house and to maintain it, and to have a lower combustible consumption.

Table 2.
Energetically characteristics of the solid fuel

Species	Mass, g	Density, g/cm^3	Burning time, min	Burning rate, kJ/min	Energy density, kJ/cm^3
Firewood					
Willow	0.639	0.75	28	0.351	11.56
Beech	0.683	0.81	25	0.392	11.63
Spruce	0.546	0.77	28	0.308	11.78
Poplar	0.539	0.69	29	0.285	10.55
Ash	0.618	0.85	31	0.303	12.91
Briquettes					
Beech	0.634	0.54	25	0.428	9.11
Willow	0.645	0.65	29	0.374	10.94
Spruce	0.681	0.78	27	0.435	13.47
Straw	0.632	0.72	27	0.362	11.14
Pellets					
Beech	0.560	0.45	26	0.398	8.32
Willow	0.580	0.56	28	0.419	10.41
Fossil combustible					
Pit coal	1.0	1.30	42	0.692	37.83
Natural gas	1.0	0.717	38	0.921	25.09

"HENRI COANDA"
AIR FORCE ACADEMY
ROMANIA

"GENERAL M.R. STEFANIK"
ARMED FORCES ACADEMY
SLOVAK REPUBLIC

INTERNATIONAL CONFERENCE of SCIENTIFIC PAPER
AFASES 2014
Brasov, 22-24 May 2014

In present the energetically market of the SRE will encourage the consumers through the governmental programs to orient to the alternative source of energy because these are ecologically and cheap fuels that can be used by everyone. From the 2007 in European Union is accessible a lot of grant programs for producing energy from the alternative source of energy, and till 2020 is trying to reduce the noxious emissions comparative with the 1990 and to increase the effectiveness of the alternative energy [17].

Table 3.
The account of the necessary of the heat and consumption of the combustible

Surface, mp	Heat necessary, kW	Consumption of: kg/h				
		Firewood	Briquettes	Pellets	Coal	Gas
100	18.2	1.2	1.1	0.98	0.5	0.3

The necessary heat for 100 m^2 from the accounted procedure results 18.2 kW in the winter season for about 100 days (Table 3).

Considering this heat necessary is determinate the consumption of the combustible in thermal furnace for different kind of fuels. The producing necessary energy from firewood consumes about 700 kg by the wooden thermal installation with a yield of 80%. The briquettes and pellets installation will consume in cold season about 550-650 kg with a yield of 85-90%. From the lasts research [4] and taking in account the investment cost, the pellets are the expensive fuels for producing heat than firewood.

Table 4.
Cost of the solid combustible in Romania

Combustible	Firewood	Briquette	Pellet	Coal	Gas
Unit price, €/kg; €/m^3	0.04	0.2	0.2	0.1	0.3
Price €/kWh	0.009	0.04	0.01	0.01	0.03
Energy consumption, kWh/year	10800				
Annual cost for energy, €/year	97.2	432	108	108	324
Cost thermal furnace, €	1000	2700	4700	1800	955
Total costs, €	1000	2700	4700	1800	955
Maintenance costs, €/year	110	110	110	110	40
Current repairs, €/year	45	45	45	45	25

The costs of the combustible materials displayed by the Romanian suppliers (Table 4) were used to determinate the cost for a kg or m^3 of combustible. In this case the energy consumption for a year will be 10,800 kWh. According to this the cheapest fuel for heating the house is firewood (97.2 euro/year) (Table 4). The expensive fuels are the briquettes and pellets and natural gas for heating the house. These are because of two aspects. One is because the thermal installation is expensive and another one is because the costs of the material. Analysing the maintenance costs and the investment costs the firewood furnace with higher yields are not so cheap. Costs of amortization will achieve evident in a longer period of time from 7 to 10 years.

The energy represented by heat touch about 50% from the final energy consumption in a lot of developing countries [20]. Biomass will became a priority in energy producing from the moment when the fossil combustible will decrease.

3. CONCLUSIONS

The necessity to ensure the quantity of heat in the cold season is an important factor and from the results it is evident that biomass products are the cheapest combustible.

Important aspect results in this paper that firewood is a cheap form to produce energy and save about thrice compares with the gas form. Combustion with solid biomass is the most important sector for bio energy production, being the efficiency in the heat production process.

ACKNOWLEDGEMENTS

REFERENCES

1. Ashton, S., Cassidy, P.. Sustainable forestry for bioenergy and bio-based products. *Energy Basics.* (2007).
2. Barbu, M.C.. Actual developments of the forestry and wood industry. *International Conference Preceding "Wood Science and Engineering in the Third Millennium".* Nov, Brasov (2011).
3. Braga, I., Frosin, D., Ghincioiu, N.. Technologies of biomass energy wood. *The National Conference of Wood Science and Engineering in the Third Millennium.* Brasov (2003).
4. Chau, J., Sowlati, T., Sokhansanj, S., Preto, F., Melin, S., Bi, X.. Economic sensitivity of wood biomass utilization for greenhouse heating application. *Applied Energy.* 86 (2009).
5. Ciganas, N., Raila, A.. Analysis of heating value variations in stored wood. *Engineering for rural development.* (2010).
6. Demibras A.. *Biorefineries-for biomass upgrading facilities.* London: Publishing Springer. (2010).
7. Glavonjic, D.B.. Consumption of Wood Fuels in Households in Serbia – Present state and possible contribution to the climate change mitigation. *Thermal Science.* 15 (3) (2011).
8. Griu, T., Lunguleasa, A.. Salix a renewable source of energy. *The 14th Intenetional Conference of AFASES.* May, Brasov (2012).
9. Guerra-Santin, O., Itard, L.. The effect of energy performance regulations on energy consumption. *Energy Efficiency.* 5 (2012).
10. Guerra-Santin, O.. Occupant behaviour in energy efficient dwellings: evidence of a rebound effect. *J Hous and the Built Environ.* (2012).
11. Gunther, B., Gebauer, K., Barkowski, R., Rosenthal, M., Bues, C.-T.. Calorific value of selected wood species and wood products. *European Journal of Wood and Wood Products.* 70 (5) (2012).
12. IEA. International Energy Agency – Bioenergy Project Development and Biomass Supply. *IEA ORG.* [online]. Available:http://www.iea.org/weo/2007.asp (January, 2012).
13. Ilina, M., Berbecaru, D., Stan, G., Georgescu, M., Popescu, M., Cocora, O., Hera, D., Gabreanu, R., Iordache, F., Brandabur, C., Stanescu, D.P., Antonescu, N., Caluianu, V., Draganescu, T., Ivanescu, G., Craciun, M., Dabela, G., Frunzulica, R., Toropoc, M.S., Beldiman, M., Costachel, A., Cimpoia, A.. *Heating Handbook.* Bucharest: Artecno Publising House (2002).
14. Karp, A., Hanley, S.J., Trybush, S.O., Macalpine, W., Pei, M., Shield, I.. Genetic Improvement of willow for bioenergy and bio fuels. *Journal of Interative Plant Biology.* 53(2) (2011).
15. Kausley, B.S., Pandit, A.B.. Modelling of solid fuels stoves. *Fuel.* 89 (2010).
16. Kim, E., Barle, S.. The energy consumption of Paris and its supply areas from the eighteenth century to the present. *Reg Environ Change.* 12 (2012).
17. Li, J., Yang, W., Blasiak, W., Ponzio, A.. Volumetric combustion of biomass for

“HENRI COANDA”
AIR FORCE ACADEMY
ROMANIA

“GENERAL M.R. STEFANIK”
ARMED FORCES ACADEMY
SLOVAK REPUBLIC

INTERNATIONAL CONFERENCE of SCIENTIFIC PAPER
AFASES 2014
Brasov, 22-24 May 2014

CO_2 and NO_x reduction in coal-fired boilers. *Fuel*. 102 (2012).

18. Lunguleasa, A., Panayotov, P.. Ecological briquette obtained from wooden biomass. *Journal Recent*. 9 (1) (2008).

19. Panoutsou, C.. *Solid Biofuels for Energy - Supply of solid biofuels: Potential Feedstock, Cost and sustainability issues in EU27*. London: Publishing Springer. (2011).

20. Serrano, C., Portero, H., Monedero, E.. Pine chips combustion in a 50 kW domestic biomass boiler. *Fuel*. 111 (2013).

21. Stolarski, J.M., Szczukowski, S., Tworkowski, J., Krzyzaniak, M.. Cost of heat energy generation from willow biomass. *Renewable Energy*. 59 (2013).

ENGINEERING SCIENCES

“HENRI COANDA”
AIR FORCE ACADEMY
ROMANIA

“GENERAL M.R. STEFANIK”
ARMED FORCES ACADEMY
SLOVAK REPUBLIC

INTERNATIONAL CONFERENCE of SCIENTIFIC PAPER
AFASES 2014
Brasov, 22-24 May 2014

HYGROSCOPICITY OF CHIPBOARD VERSUS SOLID WOOD

Aurel LUNGULEASA

Faculty of Wood Engineering, Transylvania University, Brasov, Romania

Abstract: *The paper presents some aspects referring to water absorbtion and thickness swelling for solid wood and chipboard (with and without melamine film for protection). There is made a comparison between the two wooden materials in terms of hygroscopicity. A similar methodology was used in order to obtain all results in the same conditions. Also, it was taken into account that wood has a different swelling in tangential and radial direction and in the case of film covered chipboard the large swelling was near the cuts and very small to the center of the specimen. Results have showed that swelling of covered chipboard was lower than on solid wood.*

Keywords*: higroscopicity, chipboard, composite, solid wood, swelling*

1. INTRODUCTION

Hygroscopicity of solid wood and other wooden products as chipboard is an important property because in the range of saturation moisture content the dimensional changes (swelling and shrinkage) are produced. Beyond of certain limit of moisture content (fiber saturation point, FSP) and certain time the woody semi-product will be destroyed. When water mass that is absorbed in woody products will be reported to its initial mass the phenomenon can be name the water absorption and is specific for wooden panels as chipboard, fiberboard, plywood, laminated wood and so on. The same term is for solid wood [1, 2, 3]. Consequently, the water absorption, specific for both solid wood and boards, is calculated with the next relationship (Eq. 1):

$$A_w = \frac{m_i - m_f}{m_i} \cdot 100 \quad [\%] \qquad (1)$$

Where there are: A_w –water absorption, in %; m_i - initial mass of wooden sample before immersion, in g; m_f – final mass of wooden sample after immersion in water, in g.

More important from the point of view of hygroscopicity is thickness swelling, for solid wood and wooden panels, even is a consequence of the first phenomenon, but only in the range of bound water from wood (up to FSP). This hygroscopical property has name the thickness swelling and is determined on the base of initial and final wooden dimensions, as follow (Eq. 2):

$$\alpha_t = \frac{t_f - t_i}{t_i} \cdot 100 \quad [\%], \qquad (2)$$

Where there are:
β_t- thickness swelling, in %;
t_f is final thickness if woody sample, in mm;
t_i – initial thickness of woody sample, in mm.

The wooden boards as chipboards, fiberboards, laminated products and plywood present different properties of hygroscopicity related to solid wood, usually higher because of destroying of wooden integrity in particles or sheets. Behavior related to water of wooden materials could hardly be changed because of

adhesive quantity and type. Therefore when there are used phenol-formaldehyde adhesive the hygroscopic properties will be improved, because these adhesives are themselves to water resistant and a part of these will penetrate superficial area of wooden products. In this way it can say that wooden boards with phenol-formaldehyde adhesive will be use in medium with great air humidity as plywood for constructions. Even mechanical strengths are higher but also the cost prices in this case are higher.

For chipboard the both properties of hygroscopicity depend also if their surfaces are covered or not with protection films. Therefore for comparison it must took samples with protection film and others without protection films. The samples for solid wood used for comparison will have different values of higroscopicity on radial and tangential directions, reason for what it should determine the both properties on radial and tangential directions and after that, it made the average of these values.

Also, because the wooden specie influences very much the hygroscopical properties of boards in the work-paper it should use only beech specie both for solid wood and for wooden panels (chipboard with and without film coating).

The main objective of this paper is to find out how water or high humidity affects the swelling and water absorbtion properties of solid wood (in the tangential and radial direction) and non-covered or melamine–covered chipboard (in thickness), in order to use them corespondingly.

2. METHODIC AND MATERIALS

Before of actually experiments all wooden samples were conditioned into atmosphere with constant parameters up to all samples reached a constant moisture constant about 10 %. Form of all wooden samples were prismatic, the samples from solid wood having dimension $100\times20\times20$ mm and the samples from chipboard having $50\times50\times18$ mm (Fig 1). These different dimenssion are adopted for obtaining a similar outside surfaces for both categories of the sample types, namely about

$86 - 88$ cm^2, the delection from both type of samples being only 2,3 % [4], respectively in resonable limits.

Wooden samples were introduced grouped (5 pieces) into water down to about 2 cm under superior level of liquid, for a time of 2 hours and a constant temperature 18 ^{0}C [5, 6]. Before immersion of wooden samples it should make the next determinations:

- For wooden panel (chipboard with and without coated films), there are determined the initial mass with 0.1 g accuracy and initial thickness of all samples with 0.01 mm acuracy;
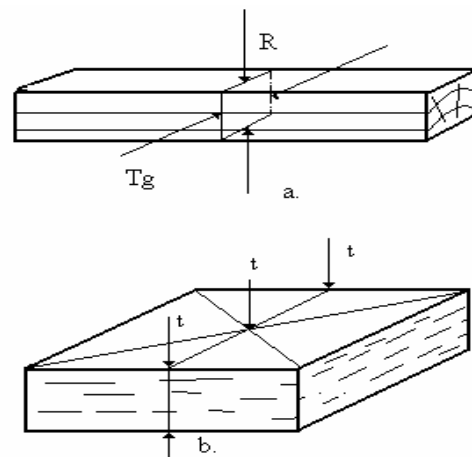
Fig 1. Form and dimensions of woody samples: a-for solid wood; b-for chipboards; R-radial; Tg-tangential; t-thickness of panel boards

- For all solid wood samples there are determined the initial mass, with the same accuracy 0.1 g;
- For all solid wood samples the dimensions on radial and tangential directions are determined with an accuracy of 0.01 mm;
- For water it must carry out and keeping the temperature to regime one (temperature 18 ^{0}C, PH neutral, cleaness and without carbonates etc).

The same determinations referring to wooden samples were make after testing, namely in the moment of sample evacuation from water. Also it keep into account the water adsorbent to sample surfaces that might to eliminate by low pressing with absorbent paper. Time of weighing and measuring must be very short because water can be rapidly evaporated. For covered panels with decorative and protection

“HENRI COANDA”
AIR FORCE ACADEMY
ROMANIA

“GENERAL M.R. STEFANIK”
ARMED FORCES ACADEMY
SLOVAK REPUBLIC

INTERNATIONAL CONFERENCE of SCIENTIFIC PAPER
AFASES 2014
Brasov, 22-24 May 2014

films it keeps into account that the thickness of wooden samples after immersion will be better in outside zone and the lowest in the middle zone of sample, determining both values of thicknesses. Therefore if the solid wood is use two specific relationships are necessary.

Table 1
Hygroscopical results for solid wood

$$\alpha_{tt} = \frac{t_{ft} - t_{it}}{t_{it}} \cdot 100 \quad [\%]$$

$$\alpha_{tr} = \frac{t_{fr} - t_{ir}}{t_{ir}} \cdot 100 \quad [\%]$$

(3)

N	Mass, g		Thickness, mm		α_{tr}	α_{tt}	A_w, %	α, %
	m_i	m_f	r_i/r_f	t_i/t_f				
1	32,6	33,3	19,7 20,0	20,4 20,9	1.5	2.4	2.4	1.95
2	32,4	32,9	19,8 20,1	20,4 20,9	1.5	2.4	4.6	1.95
3	32,8	32,9	19,9 20,1	20,4 20,9	1.0	2.3	3.3	1.65
4	31,6	32,3	19,8 20,1	20,4 20,9	1.5	2.3	2.2	1.94
5	30,2	30,9	19,7 19,9	20,9 21.8	1.0	2.4	2.3	1.70
Mean							2.5	1.83

Where there are: α_{tt} is swelling coefficient of solid wood on tangential direction, in %; α_{tr} is swelling coefficient of solid wood on radial direction, in %; t_{fr}, t_{ft} – final thickness of solid wood on radial and tangential direction after imersion, in mm; t_{ir}, t_{it} – initial thickness of solid wood on radial and tangential direction before imersion, in mm;

Keeping into consideration that chipboard has not radial and tangential direction, in order to make a good comparision between solid wood and chipboard there was take a medium value of radial and tangential values, namely:

$$\alpha_t = \frac{\alpha_{tr} + \alpha_{tt}}{2}$$

(4)

Results of hygroscopical tests was centralized in a lot of tables separated for each type of sample (solid wood and chipboard).

3. RESULTS AND DISCUSSION

On the base of measurements that are made for each type of wooden products it may realize a lot of tables, from what it can extract water absorption and thickness swelling as an medium value for entire testing, as it sees for instance in the Table 1 for uncovered chipboard or in the Table 2 for solid wood.

Table 2
Hygroscopical results for composites

No	Mass, g		Thickness, mm		A_w, %	α_t, %
	m_i	m_f	t_i	t_f		
1	32.2	62.2	17.3	22.2	93.1	28.3
2	32.3	62.0	17.2	22.4	91.9	30.2
3	32.3	62.8	17.4	22.4	94.4	28.7
4	32.4	63.0	17.4	22.2	94.4	27.5
5	34.1	64.3	17.2	21.8	88.5	26.7
	----	----	----	-------	92.4	28.2

For solid wood there is a radial and tangential swelling, reason for what for obtaining the thickness swelling it may do the average of above values from Table 2.

Because there were made a lot of tests for each type of wooden products after finishing of tests it takes data from many tests and put together in the centralized Table 3, for obtaining the main tendency parameter as arithmetic average of these.

Table 3.
Hygroscopicity for different wooden materials

No.	Assortments	A_w, %	α_t %
1	Solid wood	2.5	1.8
2	Melamine chipboard	9.1	(1.0+3.7)/2=2.3
3	Chipboard	92.4	28.2

On the base of these value it may do two graphs for visualizing the tendency of wooden products, as it sees in Fig 2 for water absorption and Fig 3 for thickness swelling.
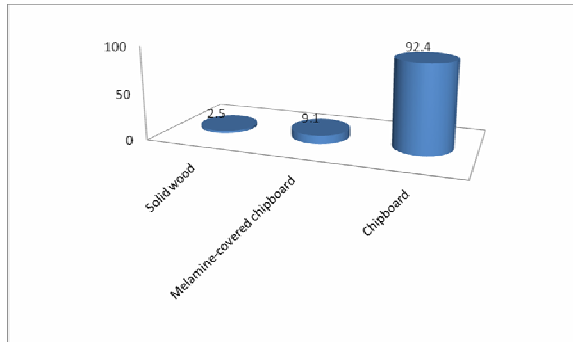
Fig 2. Water absorption for woody materials

It can observe from Table 3 that the best lower water absortion are for solid wood (with 2.5%), the next being melamine-covered chipboard (with 9.1%) and the lowest water absortion is for non-covered chipboard, with 92.4 %.
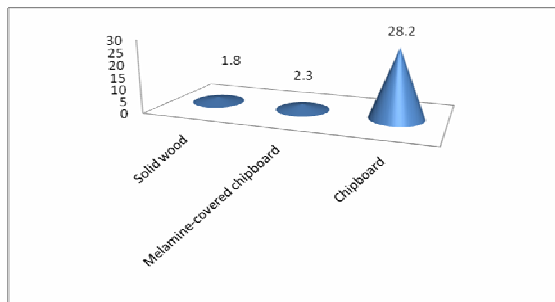
Fig 3. Swelling of woody materials

The same considerations are exposed in Fig 3 related to thickness swelling for different types of wooden materials. As general rule, the classification is the same as for the water absorption, namely: on the first place is solid wood with 1.8 %, on the second place is melamine-covered chipboard with 2.3% on average and last position remains to non-covered chipboard with 28.2 %.

Refering to thickness swelling of melamine-covered chipboard it has two different values, namely in the middle of sample with 1.0% (obtaining the first place, before the solid wood that has 1.8%) and the thickness swelling on the edge with 3.7% (placing the melamine-covered chipboard on the second place). Therefore it can conclude that in terms of thickness swelling, the melamine-coated chipboards are superior even than solid wood.

Additionally, in the paper, several measurements were made on water absorption and thickness swelling of wood-plastic composite. The results (water absorption of 0.3% and 0.2% thickness swelling) showed that this compound is different from the other two materials taken into consideration in the paper. There are no terms of comparison between these types of materials related higroscopicity.

4. CONCLUSION

Study about hygroscopicity of wooden products as agglomerate wooden products versus solid wood was a constant problems of researches from all countries all over of world for finding certain methods for improving this property, the last frontier being the obtaining of wooden products without higroscopicity. Nearby of these two materials the wooden material from plastics and wood fiber is taken in consideration for what hygroscopical properties are very low, about inexistent.

From experimental studies it can observe that the melamine-covered wooden panels have a low higroscopicity related to un-covered boards and even related to solid wood. From this point of view a good covered board is better than solid wood as timber could be, beside other currently features of these boards as low cost, broad dimensions, uniform thickness and plainly.

All studies made in the paper about higroscopy of woody materials have the aim of water absortion and thickness swelling, in order to use them corespondingly.

REFERENCES

1. Kollmann, F., Coté W., *Principles of wood science and technology. I Solid wood*, Springer Heidelberg, New York (1968).
2. Rimbu I. *Wood technology,* vol II, Technical Print House, Bucharest (1980).
3. A. Lunguleasa, *Wood physics and mechanics*, Transylvania University Press, Brasov (2007).

"HENRI COANDA"
AIR FORCE ACADEMY
ROMANIA

"GENERAL M.R. STEFANIK"
ARMED FORCES ACADEMY
SLOVAK REPUBLIC

INTERNATIONAL CONFERENCE of SCIENTIFIC PAPER
AFASES 2014
Brasov, 22-24 May 2014

4. A. Lunguleasa, *Study and contribution about chipboard manufacturing with high adessive surface*, Ph. Doctoral Thesis, Transylvania University, Brasov (1999).

5. Wood Fuels Handbook, *Biomass Trade Center*, Available: http://nuke. biomasstrade centres.eu/Portals/0/D2.1.1 %20%20wood%20fuels%20handbook_btc_ en.pdf, (January, 2013).

6. P. Bekhta, P. Niemz, J. Sedliacik Effect of pre-pressing of veneer on the glueability and properties of veneer-based products. Eur J Wood Wood Prod 70(1-3):99-106 (2012).

ENGINEERING SCIENCES

“HENRI COANDA”
AIR FORCE ACADEMY
ROMANIA

“GENERAL M.R. STEFANIK”
ARMED FORCES ACADEMY
SLOVAK REPUBLIC

INTERNATIONAL CONFERENCE of SCIENTIFIC PAPER
AFASES 2014
Brasov, 22-24 May 2014

UTILIZATION OF TECHNICAL INNOVATION ON A NEW PRODUCT

Raluca NICOLAE (MANESCU), Anisor NEDELCU

Transilvania University of Brasov, Romania, Manufacturing Engineering Department.

Abstract: *This paper aims to show the role of innovation capitalizing on a new technical product, which can lead to modernization and economic development. We analyzed the essential characteristics of the new product, given its origin and manifestation of a technical and economic context.Also this paper aims to shed light on the degree of implementation for each phase of said sequence which will depend on the specific product and the state of its complexity. Last was ultimately leads to awareness by companies, customer feedback from bringing useful suggestions on this basis were identified opportunities*

Keywords: *technical product, production process, product development flow.*

1. INTRODUCTION

It capitalized on the technical pro duct concept ag ain, which is m aterialized as a prototype.

Verifying a technical product is used in consumer testing. Determ ined the essential characteristics of the new product, prepare samples produced in sm all quantities to consumers targeted testi ng to obtain feedback from them.

Constructive and technical refinement phase, the developm ent of product and production process, is developed the new product execution docum entation: technical specifications, drawings, for mulas, patterns and instructions. The new product is experienced pilot or test stations, depending on the nature of the product.[1]

.

Sales m arket are exp erimental tests performed to determine product acceptance by customers.

Thus the ne w product i s launched i nto production o n a calendar scheduling appropriate marketing.

2. ANALYSES

One of the essential foundations for creating a successful new product over the long term is to identif y technological trends from an ear ly st age and to exploit the opportunities that new t echnologies offer for product innovations.

However, factors such as th e hu gely dynamic nature of technological progres s make it increas ingly dif ficult f or the new product to com prehensively identify technology-related opportunities and to harness them in a goal-oriented manner.

A key prerequis ite for success ful technology developm ent therefore lies in the ability of an organization to rapidly and efficiently align the requirements of the market with the potential offered by new te chnologies and to integrate the resu lts in its ow n products and processes.

A funda mental contribution to the development and design of technical products were teachers and Wolfgang Gerhard Pahl Beitz, whose book serves worldwide as basic manual for students and researchers. In their

systematic conception, definition o f technica l objects is decom posed into four success ive phases:[2]

-        definition phase function: allows to specify the functionality you need to ensure their subject and ach ieve functional m odeling needs;

-        conceptual definition phase: specify what physical principles will be used to ensure functional requirements;

-        physico-morphological definition phase one takes the natural and organic elements necessary to achieve physical principles retained;

-        detailed definition phase: describes the interactions between co mponent parts of the product and how to produce the parts.

In an ideal situation, each stage m ay be carried out as independent as possible of the next stage, in order to ensure the freedom of action in each level.

In a newer edition of their book [3], Pahl and Beitz, propose a m   ore advanced procedure, under which the developm ent and design of technical system s and technical products consists of 5 phases:

-        clarifying and defining them e (design) is proposing the produc t is - clear them   e, elaborate list of requirements, the result of this phase is a list of requirem   ents (design specifications);

-        development principle solution: determining the   struc   ture f   unctions, identifying working principles and working structures, com bining the choice of concepts. The result of this step is a solution in principle (a concept);

-        building structu   re develo   pment: Preliminary form design, m aterial selection and calculation, choosing prelim   inary configurations, refining and im   proving configuration. The resu lt of th is p hase is a configuration or confor   mation (layout) preliminary;

-        finalizing the structure construction: eliminating weaknesses, erro rs control f or th e influence of disturbances and m   inimal costs, preparing prelim   inary list of parts and production and assem bly docum ents. Result phase: configuration (conformation) final;

-        preparing docum ents for production and exploitation: th   ey develop   deta   iled

drawings, parts lists,   i   nstructions for manufacturing, assem   bly, transport and operation, check all docum ents. The result of steps: production of t   he product documentation.

In the 2007 edition, the process is completed with a final phase: m arketing. With the introduction of m   arket life cycle begins (commercial) product.[4]

The application rate for each phase of said sequ ence will   depend on the specific product, the state of its com   plexity and the degree of departure from its predecessors.

The m   ethods and organizational solutions developed in the technology and tehnical innovation unit to improve and synchronize research, innovation and technology developm ent processes have been shown success in the tehnical fields: products whose technology developm   ent capabilities have been properly orga nized ach ieve high er growth, increased pr   ofitability and an enhanced competitive edge.
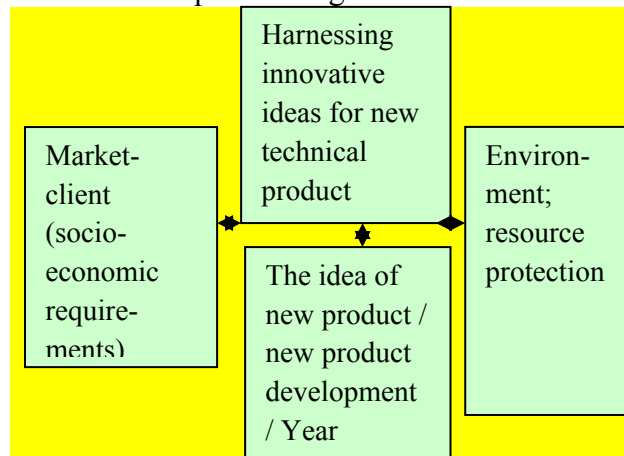
Figura 1. Criteria for growth of innovative development of a new product

Identification and evaluation of significant risks should be done with consideration of interna l factors an d external factors.

The innovation must be widely adopted in order to self-susta   in. W hen a technology goes through a major transformation phase and yields a successful i nnovation then it becom es a great learning experience, not only for the parent industry but for other industries as well. Big innovations are generally the outcom e of intra- and interdisci plinary networking a mong technological sectors along with combination of implicit and explicit knowledge.

"HENRI COANDA"
AIR FORCE ACADEMY
ROMANIA

"GENERAL M.R. STEFANIK"
ARMED FORCES ACADEMY
SLOVAK REPUBLIC
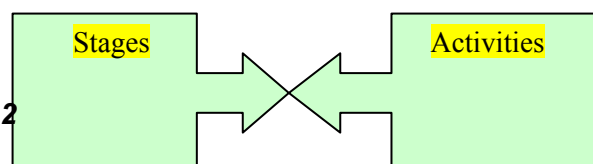
INTERNATIONAL CONFERENCE of SCIENTIFIC PAPER
AFASES 2014
Brasov, 22-24 May 2014

THE TEXT OF THE PAPER

- Fundamental Research - Industrial research (applied) - Experimental Development / Technology - Technology Transfer - Recovery results	- The idea and theme for a new product. Clarifying and elucidating the basis. - Development concepts, studies, methods, procedures, technical and economic analyzes, plans, diagrams, documents on products and technologies. - Design, implementation, testing prototype / prototype plant pilot. Validation / pilot plant. - Advice and technical assistance. Development documentation for technical and economic analysis. Dissemination of information. - Design number zero. Preparation Manufacturing. Implementation, testing and certificate number zero. Start manufacturing.

Figure 2. Steps and key activities capitalize innovative new technical products.

The company acknowledges a problem, feedback from customer brings it useful suggestions on this basis are idendificate opportunities. Further, creative teams intervene to support businesses in the process of identifying the idea.
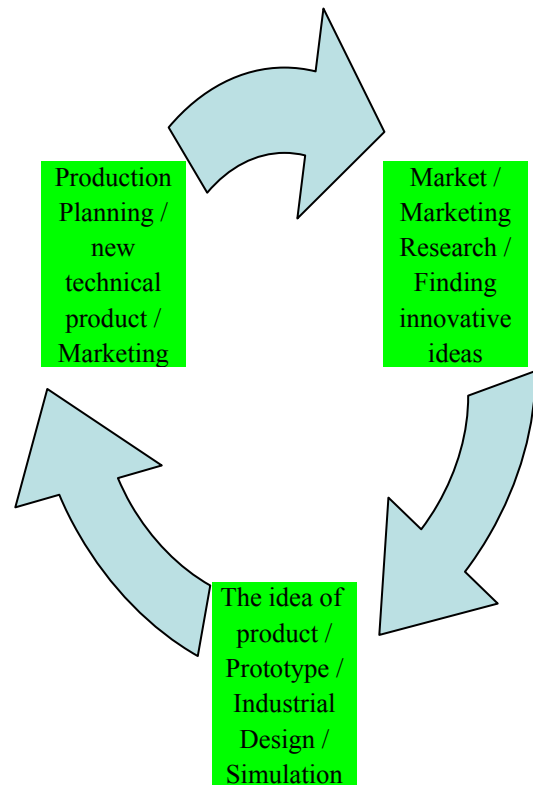
Figure 3. - The flow of new technical development new product

3. CONCLUSIONS & ACKNOWLEDGMENT

The result o f this stage is the idea of the product, which is subj ect to the assessm ent process in order to develop new useful products.

The suggestions and inform ation received from m arket leading on the initiativ e of finding a new idea. The processes used in this study are m ore exploratory and less custom er driven than the typical, tehnical innovation.

Utilization of tehnical in novation on a new product will always be a high risk undertaking, but m uch c an be learned about effective new product m anagement from a review of the

experiences in past ne w product projects and in other companies.

The im petus f or a ll th e pro jects in this study com es from the convergence of developing technologies, va rious contextual or environmental factors and a new product champion or visionary.

The econom ic efficiency of investm ents allocated technology intern ational transfer is dependent, first, the essential features of any investment (profit, time, risk), plus specific elements of the cross-border nature of international investment.

It is necessary to use efficiency ind icators to high light a ll p ossible correlations. Construction of indi cators system requires careful work to identify and quantify all resources allocated or co nsumed and the types of effects generated.

ACKNOWLEDGMENT

REFERENCES

1   Constantin, R., Ioan, D., F., Anton, H., Alexandru, M., Dan, C., B., *Fundamentals of management innovation and technological transfer, Bucharest*, 2012.
2   Pahl, G., Beitz, W., *Konstruktionslehre, Springer Verlag*, 1977.
3   Pahl, G., Beitz, W., *Engineering Design A Systematic Approach 3rd Ed., Springer-Verlag, London Limited 2007. Translation from the German Language: Konstruktionslehre, Springer-Verlag, Berlin, Heidelberg*, 2003.
4 Gerhard   P., *Konstruktionslehre. Grundlagen erfolgreicher Produktentwicklung. Methoden und Anwendung. 7 Aufl., Springer, Berlin*, 2007.

MANAGEMENT CONCEPTS TO SUPPORT FLEXIBLE MANUFACTURING SYSTEMS DEVELOPMENT IN ECONOMIC ENVIRONMENT

Raluca NICOLAE (MANESCU), Anisor NEDELCU

Transilvania University of Brasov, Romania, Manufacturing Engineering Department.

Abstract: Information and management concepts has focused on how available knowledge is exploited to improve organizational performance especially in flexible manufacturing systems or activities. There is limited information on how concepts acquired during flexible manufacturing systems development can be utilized the product life cycle to provide decision support. Existing management systems knowledge do not seem to provide information on well-known manufacturing constraints and product attributes identified during product development. Some flexible manufacturing systems do not provide the means of identify and utilise tacit knowledge which have a major impact on some flexible manufacturing systems development process. An organized transfer of knowledge from previous systems will no doubt enhance the management quality, efficiency, cost and time to market of new flexible manufacturing system in economical field. The study shows that has developed a knowledge management framework to support flexible manufacturing systems development in economic environment.

Keywords: Management concepts, Product development, Framework, flexible manufacturing system

1. INTRODUCTION

To im   prove an effective knowled   ge management of flexible manufacturing systems the strategy is that realize t   he benefit i n order to support decision-making process   and thereb y remain sustainable in economic field.

Management concept has increasingl   y become sought; however, many organis ations are still unable t o develop and improve knowledge to enhance economic performance.

Knowledge is frag   mented, som etimes difficult to locate and therefore to i   mprove or to share. There is a need therefore to develop decision support s ystems to im   prove, store, share   and capture data, information and knowledge. Decision support s ystems is   enable the transfo rmation of tacit to im   plicit knowle dge to be   shared and improved for decision making. They   will also enable the conversion of   explicit   to   implicit knowledge a process of internalisation.[1]

2. ANALYSES

Consequently knowledge and experiences are so metimes poorl y documented and therefore are not available for reinstate in future projects. In figure 1 shows the co   ncept of   knowledge regarding fle xible m aufacturing s ystem derived from theory , information and experience   and, which is im   portant in nature and   could be described as successfully applied knowledge.

When a co mpany are   checked flex ible manufacturing sy stems ar e i mplemented available information theor y a nd applied   knowledge experience so lead to a guaranteed success.
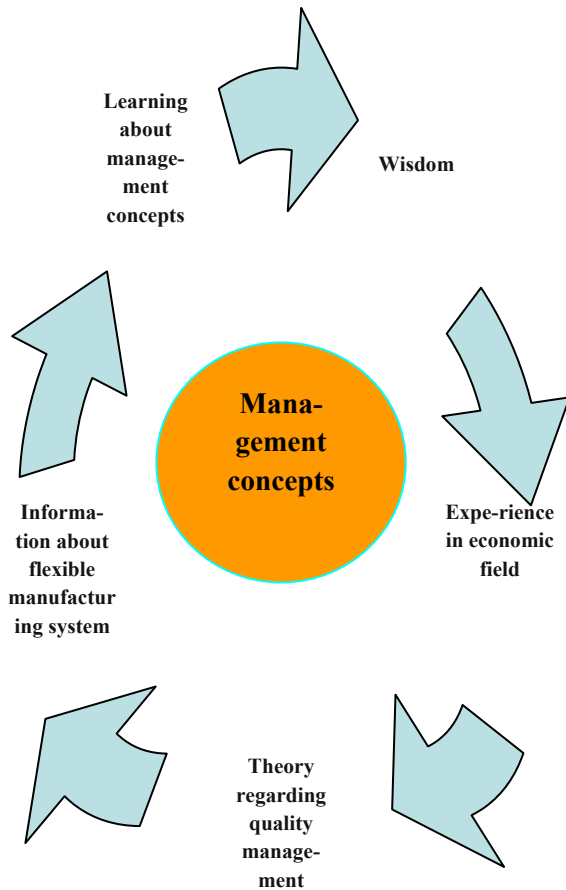
Figure 1. Knowledge derived from theory, information and experience to develop economic field.

When experim ental data are class ified as premium items, they are shaped so that they become available.

When rules or heuristics are app lied to information, knowledge is then created as actionable infor mation for producing som e benefit value. The knowledge that is created and shared am ongst organisational m embers can be categorized into two typical for ms of knowledge—tacit and explicit [1].

Knowledge in product developm ent environment is considered to consist of four activities.[1]

1. Identif ication; th e id entification of knowledge required to develop new flexible manufacturing system s, including product specifications, proces s, tooling and m aterial capabilities.

2. Capture; how the knowledge is captured stored and retrieved.

3. For malise and present; how knowledge can be for malized and presented to

ensure its u se in existing and f uture f lexible manufacturing system.

4. Utilisation; how the knowledge identified, captured and for malised can be integrated into products and decisions, and applied in other flexible m anufacturing system.[2]
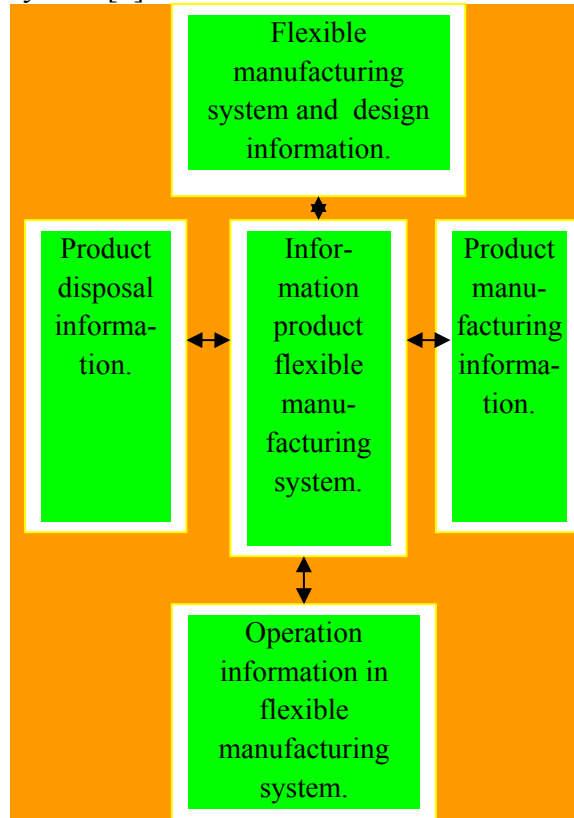
Figure 2 . Information and knowledge framework in product life cycle

In figure 2 shows the concepts about information and knowledge managem ent framework for a flexible m anufacturing system life cycle by showing all the sources and information about the product can be derived.

Each of the phases has data and knowledge that describe the characteristics of that stage in the product life cycle.

Such inform ation are useful to the product and m anufacture flexible manufacturing system and also to the customer who would need a full understanding of product attributes to enable optim al design, manufacture and guar anteed production performance.

Also an flexible m anufacturing system would be m ade awar e of all re levant information including data on product functionality, durability , efficiency, energy

"HENRI COANDA"
AIR FORCE ACADEMY
ROMANIA

"GENERAL M.R. STEFANIK"
ARMED FORCES ACADEMY
SLOVAK REPUBLIC

INTERNATIONAL CONFERENCE of SCIENTIFIC PAPER
AFASES 2014
Brasov, 22-24 May 2014

requirement, while the industries will product specification and requirem ents, m ode of operation, value added, cost price, delivery due date, maintenance requirem ents. The sales department working in collaboration with the design and production departm ent will also establish th at they c an delive r what has bee n promised to the institu tion within the due date. This will involve m aterial requirem ent planning, supplier m anagement, production scheduling and planning, outsourcing requirement, quality assurance. An order is confirmed only when there is an contract established between custom er and the enterprise.

All the product inf ormation or discerned elem ents, are patterned in a certain way, that data is transform ed into information. As rules or heuristics ar e applied to product, knowledge is then created as actionable information for producing some benefit value.

All the process involves the identification, captu re, form alisation and presentation of knowledge and its utiliza tion, support effective decision m aking within a flexible m anufacturing system and product development environment.

Extraordinarily, however, th e development of project to support flexible manufacturing system , has barely intersected with studies on com mercial new product development, which co nsider the com parable problem of achievin g efficiency whils t attaining consumer satisfaction.

Engineers engaging in new product development bring to their work the form al and articu lated expe rtise of their discip lines that have been socia lly constructed through time by particular professional or academ ic communities. [3] Mohrman et al., explains that an organisation striving to der ive co mpetitive advantage from knowledge management needs

to understand which elem ents of the organisation's proc esses af fects its ability to acquire, create and apply knowledge.[3] Knowledge helps to achieve im proved business perform ance through product and process, and in this sense knowledge can be classified not only from the knowledge type (tacit and explic it) but also f rom the knowledge dom ain (product related and process related) [4].

Using this definition, knowledge has four classifications:
- Tacit-product related; know-how (human brain)
- Tac it-process related; hu man capability (human brain and culture),
- Explicit-product related; knowledge base (knowledge repository),
- Explicit-p rocess re lated; workflo w (workflow system).
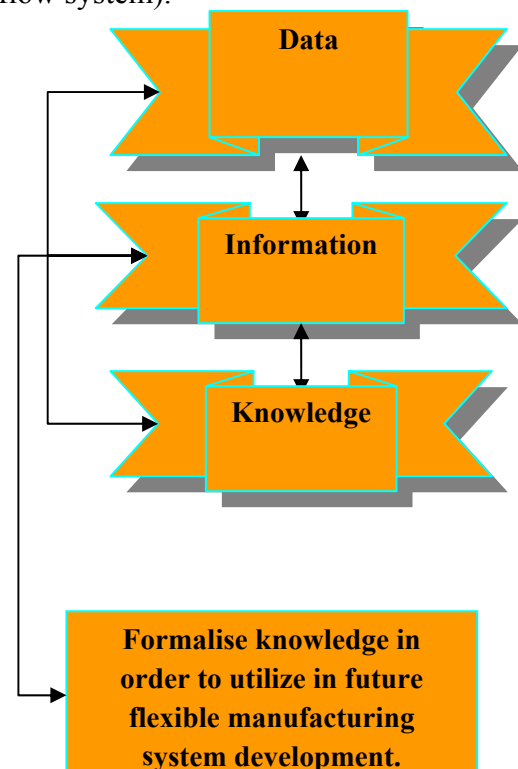
Figure 3. Formalise interactions

3. CONCLUSIONS & ACKNOWLEDGMENT

In this paper has developed a knowledge-based m anagement in flexible m anufacturing system that adapts knowledge managem   ent concepts into product developm ent where the major objective s were to prov ide decisio n support to h elp economic field, according the utilisation of best-know knowledge, m inimise costs, ach ieve quality assuranc e a nd shorten time to product. Product developm   ent activities must be structured in such a way that any engineering decisi ons taken are based on proven knowledge and experience. Any failure to apply knowledge and experience could result in product and process redesign, which would be seen as non-value process and waste of valuable resource. There is a need for a knowledge-based fram   ework to support flexible m anufacturing system developm ent, which includes a knowledge-based system developed f rom an organisation's knowledge and past experience captur   ed in a database. This process involves   the identification, capture, form alisation and presentation of knowledge and its utilisation to support effective decision m   aking within a product development environment.

REFERENCES

1   Chike, F., O., Alan, H.,   *Knowledge management to support product development in cold roll-forming environment,* 2011.
2 Polanyi,   M., *The tacit dimension. Routledge and Kegan Paul, London* , 1996.
3   Mohrman, SA., Finegold, D., Mohrman, AM., *An empirical model of the organization knowledge system in new product development firms. J Eng Technol. Manag* 20(1–2):7–38, 2003.
4   Ahna, JH., Chang, SG., *Assessing the contribution of knowledge to business performance: the KP3 methodology. Decis Support Syst 36(2004):403–4162007,* 2004.

"HENRI COANDA"
AIR FORCE ACADEMY
ROMANIA

"GENERAL M.R. STEFANIK"
ARMED FORCES ACADEMY
SLOVAK REPUBLIC

QUALITY MANAGEMENT APPLIED THROUGH QFD METHOD

Ramona PAKOCS

Romania, Transylvania University of Brasov, Engineering and Management Department,
ramona.pakocs@unitbv.ro

Abstract: *The purpose of this paper is based on the analysis between the interests of the company and customers' requirements achieved by using QFD method.*
I have started with a few notions related to the method in order to understand exactly how it applies continuing with a brief overview of the company, and finally the proper analysis and conclusions about this.

Keywords: *quality, improvement, performance, product, control.*

1. INTRODUCTION

This study represents a national and international concern about quality management for companies. For this, an analysis was made using the QFD method for the company S.C. BETA S.R.L., where the following six basic steps were emphasized: identifying customer's needs, identifying technical needs, the relationship between customer's needs and technical needs, competitive assessment and sales key points, assessment of the technical needs of competing product and services, setting targets and selecting the technical needs that are to be modified in the process.

2. QFD METHODOLOGY

QFD concept is a methodology for systematizing the information obtained from the user in order to get / to define the characteristics of the product / service, market adaptation.

QFD objectives provide information on aspects of the product / improvement service.

The objective is to achieve a design quality of an excellence product / service by transforming customer's needs into quality of product characteristics, without omissions or unnecessary items. [1]

The QFD method is based on the **House of Quality** a set of matrices used to link the voice of the customer and technical requirements of a product, process control plans and manufacturing operations. [3]

3. CASE STUDY USING QFD METHOD AT S.C. BETA S.R.L.

SC. BETA SRL., is a Romanian company, having the legal form of a limited liability company.

The main activity of the company is providing translation and interpretation services from and into any language, under the best conditions.

The company works both locally and nationally, based on cooperation agreements with other leading companies in the same industry. The need for concluding such agreements with other companies in the same field comes due to the fact that in Braşov there

are no authorized translators for strange languages (Flemish, Japanese, Arabic, Swedish, etc..).

The company's activity is of about 3000 pages translated per month, and references from our customers from various areas including national and international companies represent the company's business card.

3.1. The current situation of S.C. BETA S.R.L.

Currently the company does not have documents showing irregularities concerning deadlines. [2]

Reasons for non compliance with deadlines are related to the following aspects:
- large volume of work;
- incorrect communication of the real time to the customer;
- stress at work;
- emergencies.

The aim of the process is to avoid delaying the works from the time agreed with the client.

Strengths that the company owns are:

- Provides application of the Hague Apostille;
- The company collaborates with national translators for translating documents into strange languages (Chinese, Arabic, Swedish, etc.).
- Tutoring at reasonable prices;
- Emergencies are not a problem;
- No work is refused.

Weaknesses of the company:

- disagreements between the time set for making the work and their delivery time;
- duties from the job description do not always correspond to the tasks that employees have;
- some complaints about quality.

3.2. Process mapping for S.C. BETA S.R.L.

✦ Analysis and improvement

Map of processes at S.C. BETA S.R.L.
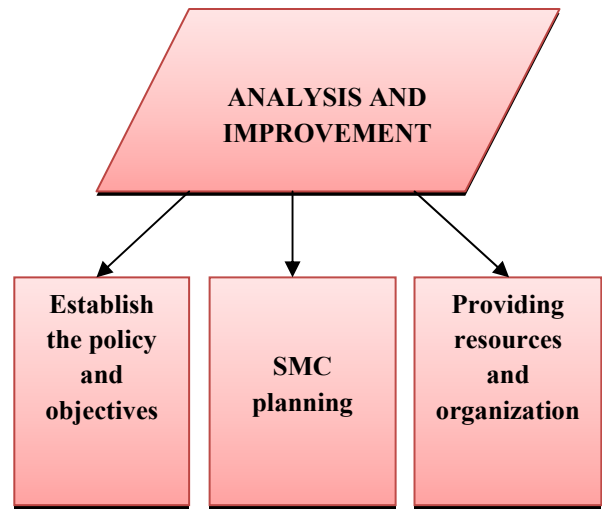
Figure 1. Management processes
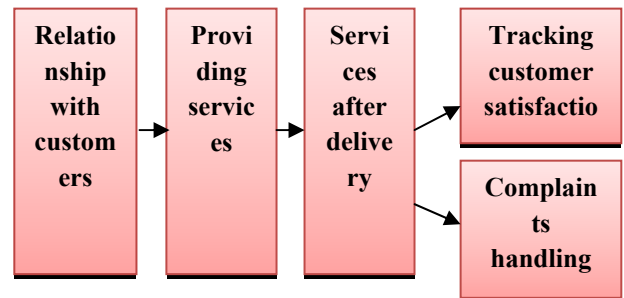
Figure 2. Processes of value creation
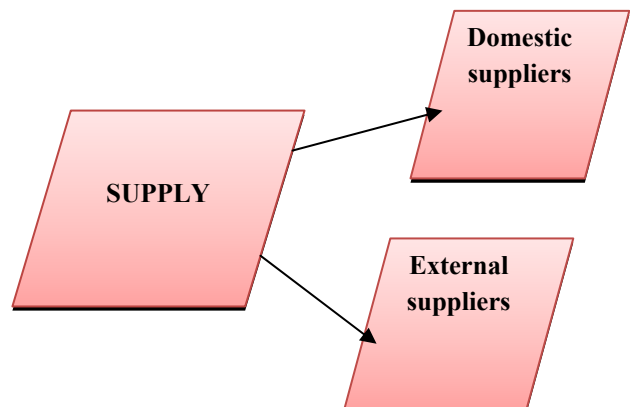
Figure. 3. Support processes

“HENRI COANDA”
AIR FORCE ACADEMY
ROMANIA

“GENERAL M.R. STEFANIK”
ARMED FORCES ACADEMY
SLOVAK REPUBLIC

INTERNATIONAL CONFERENCE of SCIENTIFIC PAPER
AFASES 2014
Brasov, 22-24 May 2014

Process sheet at S.C. BETA S.R.L.

Service name: performing services.

SERVICE	INPUTS	ACTIVITY	OUTPUTS
Translations	Marketing study; - Rebates; -Offers for customers;	- Taking orders (works) from customer; - Translating works; - Correction; - Delivering works;	- Delivering works; - Promotion; - Participation to national fairs.
Interpretations	-Offers to existing customers and potential customers.	- Made by telephone, at the request of customers; - Choosing the translator for the required language; - Documents are interpreted; - Payment is made by the customer.	Addressing customer requirements by the company.
Tutoring	-Through advertising.	Individually/ in groups; -At the office or address of the customer.	-Certificate of linguistic competence

Table 1. Process sheet at S.C. BETA
S.R.L.

Responsible person: the secretary-PR
Performance Indicators:
- Customer's satisfaction;
- Number of complaints;
- Delays;
- Economic indicators.

Relationship with customers

Customer orientation is an important point for the success and for maintaining S.C. BETA S.R.L. on the market.

The company focuses on customers orientation, identification and analysis of their needs, transposed in products and services on the progress of the interaction with customers, with the aim of developing and maintaining long-term and economically advantageous relationships.

This procedure aims to highlight the relationship with customers, customer's requirements definition, broadening the portfolio of customers, customer satisfaction, efficient document translation process, feed-back from customers.

In translation department work translators who translate documents by taking into consideration the deadline and quality of work.

In customer department, the company's PR responsible has the following responsibilities: taking orders, recording and distributing documents to translators, respecting deadline of works, cash responsible, complaints handling.

In management department duties correspond to the general manager who has to role of organizing business activities through regulations and internal order, establishing company strategies aimed to proper functioning of the company.

In order to make translations, translators must be registered on the website of the Ministry of Justice; this gives them the right to make translations on their own name being responsible for each document translated.

The company operates by internal regulations that are set by the manager of the company; they all aim proper function within the company. [2]

These regulations contain information on how the documents should be saved, time, quality of works, tasks that each employee has.

Order note is a reference document that is prepared for a specific number of pages (over 100 pages) and contains translation company data and customer data, term, number of pages and language it must be translated into. This document represents an additional certainty regarding the order.

⬥ Workflow consists of:

- Identification;
- Translation;
- Requirements definition;
- Drafting contracts;
- Settlement;
- Satisfaction assessment.

⬥ Registrations

- Registration / update of customer database;
- Registration of accounting documents;
- Registration of customer requirements;
- Registration of order notes.

⬥ Deviations

The main deviation in this company is the lack of effective communication. The message is often distorted due to the fact that messages are not transmitted properly.

Improving product performance process

Process subject to improvement is the process of time achievement so as to meet the deadlines set by the order.

We want to improve this process because we don't want disagreements between the time set for carrying out the works and the delivery time. It often happens to fail to comply with the time set because of the large volume of work, the emergencies that have priority and wrong estimation of the execution time.

⬥ Proper analysis:

The analysis begins by studying the process - customer relationship.

Currently the company does not have documents showing irregularities concerning time-limits.

Reasons for not complying with deadlines are related to following aspects:

- The big volume of work;
- Incorrect communication of the real time to the customer;
- Stress at work;
- Emergencies.

All these irregularities are due to company policy "no work is refused, emergencies are not a problem." Responsible for all these is the general manager.

The aim is to avoid delaying the works as regards the time agreed with the customer. For this it was proposed to apply the method "Deming's Wheel" as follows:
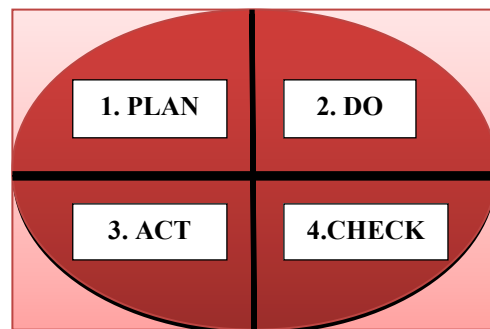
Figure. 4. Improvement - Deming's wheel method [4]

1. PLAN	2. DO
• Respect the time allocated to each department; • Consider a higher period of time for the works that are not "urgent"; • "Emergencies" remain a priority; • Record orders in the database;	• Interior regulations on departments • Incentives/ penalties;

"HENRI COANDA"
AIR FORCE ACADEMY
ROMANIA

"GENERAL M.R. STEFANIK"
ARMED FORCES ACADEMY
SLOVAK REPUBLIC

INTERNATIONAL CONFERENCE of SCIENTIFIC PAPER
AFASES 2014
Brasov, 22-24 May 2014

3. ACT	4. CHECK
• Application of internal order regulations on Departments. ✓ *Incentives:* • Bonus by the end of the month; • Team-building; • Flexible schedule. ✓ *Punishment:* • Overtime; • Not giving any incentive; • Compliance with the time allocated to each department; • Record orders in the database; • "Emergencies" remained a priority.	• Evaluation of actual results; • Comparing these results with the targets set in previous planning.

Table 2. Improvement through the method of Deming's Wheel - details

After applying this method significant improvements resulted on how to perform works and timely completion. Streamlining this process entailed not only an ease of process, but also a better relationship between employees and the company thus leading to satisfying customer needs.

Quality assessment by using the EFQM system of S.C. BETA S.R.L.

Orientation to employees

The company puts forward the employees' potential through the experience gained in the field, studies and documents that certify their training.

Issues examined:

- the way human resources are planned and improved;
- the way employees' skills are developed;
- the way employees are involved in setting goals and evaluating results;
- the way employees are involved in improvement actions;
- the way they deal with safety and health at work.

In order to relax and develop relationships between employees, the company organizes monthly team-building and different events.

Next we made **QFD matrix that highlights the correspondence between customer requirements and business interests:**

Competitor evaluation matrix (S.C. ALFA S.R.L.):

	CS	MC	SC	C	EN	IMS	IIT	
	4 ▲			4 ▲				CS
		3 ▲						MC
					4 ▲	4 ▲		SC
								C
					3 ▲			EN
	3 ▲	4 ▲						IMS
				3 ▲				IIT
IMPROVING	⇩	⇩		⇩				

Company interests / Requirements	CS	MC	SC	C	EN	IMS	IIT
LP	♣	♣	♣	♥	♥	♥	♣
Q	♣	♣	♦	♣	♣	♣	♣
STW	♣	♦	♥	♣	♣	♦	♠
P	♦	♥	♥	♦	♠	♠	♠
MPC	♥	♥	♠	♠	♣	♥	♠
PC	♦	♥	♠	♠	♠	♣	♠
TOTAL	26	23	17	19	20	21	14

Table 3. QFD matrix- Correspondence between customer requirements and business interests

Were:
CS - customer satisfaction;
MC - maintain clients;
SC - signing contracts;
C - complaints;
EN - expanding nationally;
IMS - increasing market share;
IIT - increase in turnover;
LP - low prices;
Q - quality;
STW - Short- time working;
P - privacy;
MPC - market position of the company;
PC - prestige company.

Marking way as regards the analysis for the company S.C. BETA S.R.L.:
♣ - very important   1♣ = 5 p
♦ - important   1♦ = 4 p
♥ - less important   1♥ = 3 p
♠ - not important   1♠ = 1 p

Marking way in the analysis for the competing company S.C. ALFA S.R.L.
1 ▲ = **less important**
2 …
3 …
4 ▲ = **very important**

3. CONCLUSIONS

Following the analysis made using QFD, a correlation has been achieved, between customer requirements and business interests.

From QFD matrix we have found that the most important criteria for the company S.C BETA S.R.L. are customer satisfaction and maintaining it. Competitor, S.C. ALFA S.R.L., besides customer satisfaction focuses on broadening the database (signing agreements).

The company wants to improve the criteria listed in the table in order to be able to achieve its objectives on everything related to service quality, improving customer relationships and possible national expansion.

REFERENCES

1. Ciurea, Sorin; Nicolae, Dragulanescu, (1995), *Total Quality Management,* Economica Publishing House, Brasov, Romania.
2. Company data *S.C. BETA S.R.L.*
3. Deaconescu, Tudor. (1998), *Fundamentals of engineering quality*, Transilvania eds., Brasov, Romania.
4. Popescu, Maria. (2011), *Quality Management,* Transilvania eds., Brasov, Romania.

RISK MANAGEMENT AND RISK TYPE ANALYSIS SPECIFIC TO INTELLECTUAL PROPERTY IN INDUSTRIAL PROFILE COMPANIES

Ramona PAKOCS, Nouraş Barbu LUPULESCU

Romania, Transylvania University of Brasov, Engineering and Management Department,
ramona.pakocs@unitbv.ro
nouras@unitbv.ro

Abstract: Before being marketed, any product has been conceived, designed, manufactured, based on schemes, drawings protected against internal and external theft of intellectual copyright or by documents / certificates / patents. After being marketed, the product becomes the source for copying, denigration etc. All these actions are risk sources. Risk management helps us identify, analyze and treat the specific risks of intellectual property. To overcome these specific risks of intellectual property it is necessary and obligatory to make an analysis of the types of risks within industrial profile companies in order to minimize the possible disastrous effects in research and production activities.

Keywords: creation, product risk, protection, analysis, identification, minimization.

1. INTRODUCTION

In accordance with ISO / IEC Guide 73:2002, risk can be defined as the combination of the probability of an event to happen and its consequences. [3]

In the industrial profile companies in all types of activities, there are events and consequences that could generate opportunities for gain or threats leading to loss.

Although in most cases are taken into account only the negative consequences of risk, risk management includes both positive and negative aspects of risk, and methods of prevention and reduction of its effects.

Adverse effects of the different types of intellectual property risks in the industrial profile companies can be disastrous, but the application of an efficient risk management, aims to identifying factors that could affect the proper functioning of the organization.

2. RISK MANAGEMENT AND RISK ANALYSIS OF SPECIFIC TYPES OF INTELLECTUAL PROPERTY RISKS

2.1. Risk management

In the general context of management, knowledge, risk management is the systematic approach to risk within an organization, understanding by organization the broad sense of the term as defined by international standards in quality. Considering, however, the management as an "art" when the risk management can be defined as "**Art of keeping uncertainty under control**." [1]

Risk management is a key component of strategic management of any organization, ensuring effective management of potential opportunities and adverse effects of different types of risks.

By **risk management process** the organization consistently applies policies,

procedures and practices for the identification, analysis and treatment of risk. [2]

In the category of **intellectual property risks**, internal / external **risk factors** that can act are mainly represented by:

- failure to supervise the market, (A)
- cession, licensing contracts and, in general, transfer of rights agreements, and contracts with employees wrongly drawn or negotiated, (B)
- unfair competition acts from the company towards the competing market or from competing market towards the company, (C)
- undervaluation or overvaluation of negotiable intangible assets that can lead to large losses in either the percentage of participation in the joint venture contracts or the failure to sign them (D)
- infringement (piracy) of copyright by the company against competing market either by representatives or individuals from competing market towards the company, (E)
- counterfeit of trademark or products / services, (F)
- counterfeit of patented inventions, (G)
- counterfeit of industrial design, etc., (H) as follows in Figure 1:
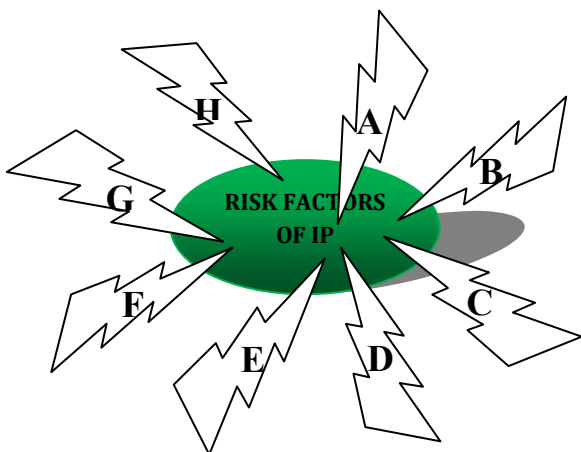
Figure 1. Risk Factors of IP

2.2. Analysis of the specific risk of intellectual property

From studying the sources of risk in the strategy of industrial profile companies, intellectual property they be divided into the following important types of risk:

- ➢ Risks of conception / creation;
- ➢ Specific assumed IP production risks;
- ➢ Marketing risks;
- ➢ Management risks;
- ➢ Social risks. [2]

In industrial engineering we can express each risk by the following formulas:

$$R = P \times C \qquad (1)$$

Or

$$R = F \times C \qquad (2)$$

Where:

P – Is the probability of a negative event to happen.

C - Is the consequence of occurrence of that event.

F - Is the frequency with which the event can happen.

Both relations are equivalent and will be expressed by value units divided by time units: USD / year USD / month etc.

Risk management at the company level is designed to identify potential events that may affect the organization.

Risk management process in the company consists in seven related components that are integrated into the general management of the organization and are represented in the following diagram: [1]

“HENRI COANDA”
AIR FORCE ACADEMY
ROMANIA

“GENERAL M.R. STEFANIK”
ARMED FORCES ACADEMY
SLOVAK REPUBLIC

INTERNATIONAL CONFERENCE of SCIENTIFIC PAPER
AFASES 2014
Brasov, 22-24 May 2014
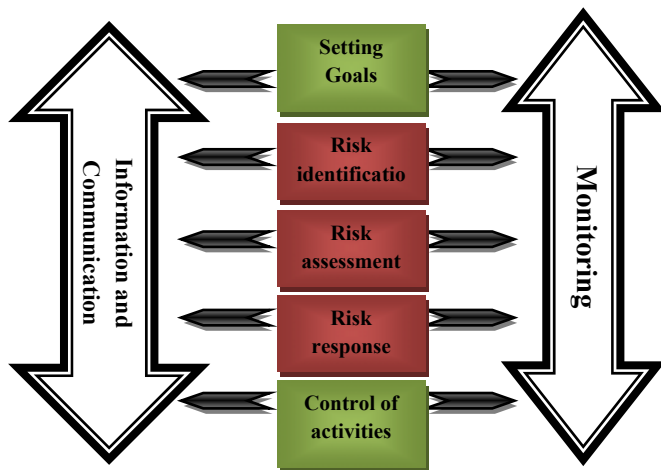
Figure 2. Risk management process at the company level

To demonstrate the need to implement a management strategy for the prevention of risk in intellectual property, we will analyze a case study on the risks of conception / creation.

For reasons of confidentiality the company was named S.C. ALFA S.A., then changing its name to S.C. BETA S.A.

2.3. Case study on the analysis of conception / creation risk and non-contractual abuse at S.C. ALFA S.A.

This case study approaches the development and extent of the rights on the scientific engineering work on the route "project - patented invention - technical work" as a result of revocation of a patented invention.

Analysis of the case study is made based on the expertise in industrial property, namely on the patent no. 79533 of 26.04.1982 - **Hydraulic control block** (Figure 3), Holder: the company S.C. ALFA S.A. and provides solutions that can be applied within large companies in machinery industry, formerly state companies, but avoided for unknown reasons. [2]
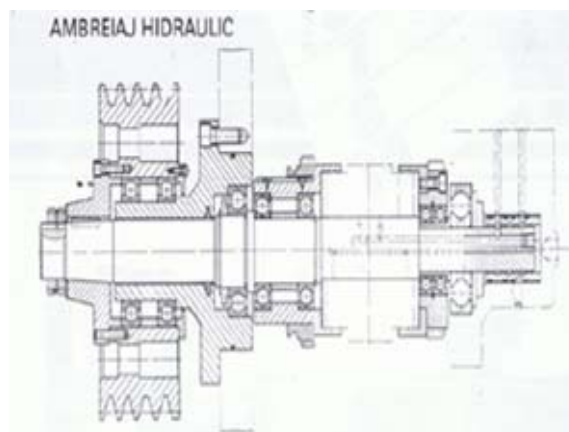
Figure 3. Hydraulic clutch subject of patent no. 79 533 - Hydraulic control block

It was analyzed step by step the protection evolution of the invention subject, and the transition from paid protection under special law to unpaid protection as a result of the general law, as it follows:

- 18.06.1956 – Decree no. 321 on copyright

- 30.10.1974 – Law No. 62 on inventions and innovations

21.09.1981 – Beginning of the protection period regarding the patent no. 79533. Filing date of the patent.

- 01.04.1983–The period covered by the lawsuit no. 8/1995

- 31.03.1987- at this time there is no one agreement on the payment way.

PERIOD OF UNPAID PROTECTION

- 21.09.1988 - The final date the invention object was protected by Patent under Law no. 62/74.
- 22.09.1988 -The date the invention object was not longer protected by law no. 62/74 on inventions and innovations.

Neither the provision imposed by law no. 64/91 on invention patent, on partly of totally unpaid rewards. Revocation is due to non-payment of fees for maintenance in force. Inventors were not announced. Revocation is enforced.

- 21.01.1992 - Entry into force of the Law no. 64/1991 on patents. Repeal of Law no. 62/1974 on inventions and innovations.

- 24.06.1996 - Entry into force of the Law no. 8/March 14, 1996 on Copyright and Related Rights (promulgated on 21/09/1996. Entry into force was made 90 days after its publication in the Official Gazette. No. 60 on March 26, 1996). Repeal Decree no. 321/56 on copyright.

On 09.21.1981 the company ALFA S.A. requires OSIM urgent patenting of an invention that the authors, two engineers had designed and then assigned under law No. 62 of 1974 on inventions and innovations. **Under the law, it was assigned the patent, not the right to use the object of the patent.**

Until 01/04/1983, inventors are paid according to the law in force then.

Between 01.04.1983 - 2002, the invention is applied by S.C. ALFA S.A., either as general assembly (**Figure 4**) or as spare parts.
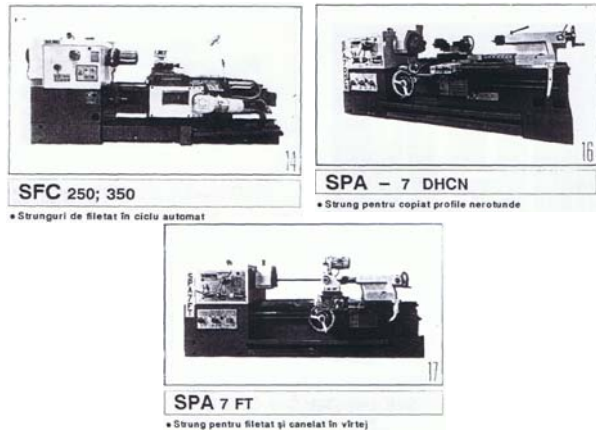
Figure 4. Three of ALFA's lathes patented under no. 79533 of 26.4.1982 - Hydraulic control block.

From 31.03.1987, S.C. ALFA S.A., now, S.C. BETA S.A. has not paid taxes to OSIM the invention being cancelled.

S.C. BETA S.A. did not announce inventors that it was no longer interested in paying annual taxes for maintaining invention protection. From this time there is no agreement on payment.

However S.C. BETA S.A. continues to apply the former invention. Financial rights of inventors have NOT been negotiated between the inventor and the unit that applied the invention. The unit had to notify because, according to Article 41/L64-91 "The holder may waive, in whole or in part, the patent, based on a written statement filed with the State Office for Inventions and Trademarks. In case of inventions referred to in art. 5 paragraph 1 a) and paragraph 2 and the inventions assigned according to art. 5 paragraph 1 b) the patent holder is obliged to notify the inventor about his waiver intention, upon the request of the inventor; the holder is required to transfer his patent rights." **Therefore, it is an illegal usage.**

S.C. BETA S.A. stood on the provision of art. 41/L64-91 "*Invention or part thereof, whose protection was waived, can be freely exploited by third parties***." But prevalence was made illegal because it cannot be taken from the context of the whole article 41**.

Without settling accounts with inventors, fraudulently applying Part 4 of art. 41/L.64-91,

"HENRI COANDA"
AIR FORCE ACADEMY
ROMANIA

"GENERAL M.R. STEFANIK"
ARMED FORCES ACADEMY
SLOVAK REPUBLIC

INTERNATIONAL CONFERENCE of SCIENTIFIC PAPER
AFASES 2014
Brasov, 22-24 May 2014

S.C. BETA S.A. still applies the technical work, former invention. As a result, the inventors summon to court S.C. BETA S.A., this time for failure to comply with the Supreme Court decision to stop producing the invention object, and for additional damage. For this second period S.C. BETA S.A. has not concluded a license agreement or assignment with the holders of the rights.

Defendant's lawyers invoked the statute of limitations, according to Decree no. 167/58, [*** 58] recognizing that there is a right to claim, but just to show that it is prescribed.

3. CONCLUSIONS

The most important aspects and conclusions analyzed are:

1. A first issue concerns the validity of the patent and, related to this, to whom belongs the duty to inform on the progress of the invention, and thus of the operation as a result of the holder's payment obligation to the inventor under the contract, the legal provisions related to the monies dues, and the transfer of the right over the patent from holder to the inventor.

2. A second issue relates to the forfeiture of holder's rights due to non-payment of annual fees to maintain the patent in force

3. A third issue is that the author of the work enjoys rights throughout his life.

4. A fourth issue related to this case is the exclusive right of exploitation of the patent and work.

5. The author has the right to patrimonial repair in case of using his work without right.

6. Sixthly, copyright is exercised over scientific works: plans, drawings, i.e. projects and scientific documentation. The employed author of a work is the owner of his creation and has the exclusive right to exploit it.

7. As long as the scientific work has the character of an invention, it is not protected by Law no. 8/1996, only by Law no. 64/91. When the novelty feature disappears, the scientific work will be protected under Law no. 8/1996.

8. If the holder is no longer interested in applying the invention, he must notify both the inventor to take it and OSIM. Exploitation of an invention in case of article 5, b) / L.64-91 without a contract is a counterfeit.

REFERENCES

1. Bârsan- Pipu, N., Popescu I., *Risk Management.Concepts.Methods. Applications.* Braşov: "Transilvania" Publishing House (2003).

2. Fântână, R.S., *Research on integrated quality - risk management of technical - economic intellectual property*, PhD Thesis, "Transilvania" University. Brasov Faculty of Technological Engineering (2008).

3. Patriche C. F., *Research on integrated quality – risk management in technical and economic restructuring of companies, PhD Thesis, "Transilvania" University of Brasov, Brasov (2007).*

4. Law no. 64 from October 11, 1991 (*(republished) *) on patents *) ISSUER: PARLIAMENT; Published in Official Gazette no. 541 of August 8, 2007.

ACKNOWLEDGMENT

ENGINEERING SCIENCES

INVESTIGATION OF SWEEP APPLIED TO ROTATING AXIAL CASCADES AND NUMERICAL SIMULATIONS OF FLOW

Irina Carmen ANDREI

"Elie Carafoli" National Institute for Aerospace Research   – INCAS, Bucharest, Romania

Abstract: *This paper presents an original approach regarding the application of sweep to rotating blade cascades. The justification for swept blades is given by its consequence, i.e. a reduction of local velocity (usually from supersonic/ transonic to subsonic regimes) such that the losses due to shock waves and/or boundary layer displacement and/or followed by reattachment are minimized. As study cases were considered a cascade blade, as well as forward and backward sweep of span-wise cross sections. The RANS model was used to describe the flow and a comparative study was conducted by using four turbulence models, i.e. Spalart-Allmaras, k-ε, k-ω and Reynolds Stress RST models. The CFD analysis was done with the FLUENT solver, with the settings for 2D case, implicit equations and double precision. The convergence was monitored such that the residuals should be minimized. The results of the numerical simulations of the flow are expressed as the distributions of Mach number (in relative flow, since it is a rotational frame), static pressure, static temperature and entropy, which have been presented comparatively, for each turbulence model and sweep study case, corresponding to the design rotational speed of 275 [m/s].*

Keywords: *aerodynamics, rotating axial blade cascades, sweep, numerical simulation, CFD analysis.*
MSC2010: _____

1. INTRODUCTION

The design of the modern aircraft engines is targeted to the achievement of new standards for performance and reliability, as well as the satisfying of the environmental friendly demands, i.e. tough limits for aircraft noise and emissions level.

Among the assets of the propulsion technology that produce a quieter engine are the advanced aerodynamics together with composite fans. High speed flow at tip blade, in particular for large diameter fans, is responsible for noise and blade loss induced by the occurrence of shock waves, boundary layer separation and/ or re-attachment.

On the other hand, high blade loading enables a more compact construction of compressors and fan, and therefore weight reduction; nevertheless, the higher the blade loading, the higher the rotational speed and the velocities at tip blade. The sound level of the jet engines can be reduced by the new design of the larger fan blades; as larger fans turn slower than the smaller ones, then the velocity of air is reduced and therefore the noise is lowered. But larger fans involve larger diameters and the velocity at blade tip can be transonic up

to supersonic unless the rotational speed diminishes.

The engine thrust can be increased with larger compressor pressure ratios and more stages.

By the design of highly loaded cascades, the number of the compressor stages is reduced, as well as the parts weight. The fewer the compressor stages, then fewer parts and fewer costs. On the other hand, by lowering the flow velocity at tip blade from supersonic to transonic and/or subsonic, blade loss due to shock waves, boundary layer separation and /or re-attachment can be significantly reduced.

Therefore, the use of sweep to the design of blades for the axial flow compressor and fan is advantageous for reducing noise level and blade loss, and hence performance improvement via optimized construction.

2. BASICS OF BLADE STACKING

2.1 Justification for th e use of sweep to transonic cascades

Blade *sweep* has been used in transonic compressor design with the intent of reducing shock losses, analogous to the use of swept wings in external aerodynamic applications. Under certain circumstances it is beneficial to align the blade leading and/or trailing edges LE/ TE more closely with the local flow direction. Sweep and dihedral define the stacking line modifications (which are also referred as 3D stacking, [5]) do change the blade surface, such that the blade edges are aligned more closely to the local direction of flow. The 3D stacking is important for both *technology manufacturing* **reasons** (with regard to the flow of mechanical operations that allows to obtaining the blade surface) and *functional*, since it influences the multi staged axial flow compressor's cascades through flow pattern, within blade tip areas and at off-design regimes in a higher extent. From CFD and experiment has been shown that the movement of the boundary layer at blade tip has a large influence upon the rotor flow pattern. For instance, no matter that at the design regime the reverse flow is absent (i.e. the design regime free of local

stall), with the decay of the flow coefficient at off-design regimes, the tip blade area (wherein the boundary layer has been detached) becomes larger. The use of *3D stacking* has been the source of a large number of experimental and numerical investigations over recent years, and consequently it came up the need to define carefully the conventions. Considering an axis placed on the LE/ TE lines, Zero-lift airfoil axis or any other particular shape and airfoil movement, can generate the 3D stacking. In Fig. 1 are explained the sweep and dihedral movements.

Both the dihedral & sweep have been introduced and used for the rotor 3D blade design into the core compressors for the Rolls-Royce Trent family engines and Joint Engine Alliance of the GE & PW for the GP7000 series.

According to Gallimore [9-10], Neubert and Weingold [13], Golub, Rawls and Russell [11], theory would suggest that the reduction in shock losses would be achieved by either positive or negative sweep, but tests of various transonic rotors demonstrate the advantage of positive sweep in achieving both improved efficiency and flow range.
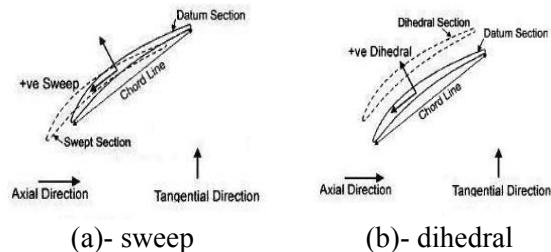
(a)- sweep (b)- dihedral
Fig. 1- Basic stacking line modifications, [5]

Near the hub the *positive sweep* reduces the region of low axial velocity towards the TE while the *negative sweep* causes a separation to occur. The positive sweep near the hub moves the front part of the suction surface into a higher-pressure region, which reduces the effective incidence and peak velocity along the airfoil chord at the expense of increasing the blade force near the trailing edge. A similar trend is observed near the rotor tip while the opposite trend is observed at mid-height. *Positively swept* end-wall sections increase the leading edge blade force and reduce the trailing edge blade force near mid-

"HENRI COANDA"
AIR FORCE ACADEMY
ROMANIA

"GENERAL M.R. STEFANIK"
ARMED FORCES ACADEMY
SLOVAK REPUBLIC

INTERNATIONAL CONFERENCE of SCIENTIFIC PAPER
AFASES 2014
Brasov, 22-24 May 2014

height. The **_negative sweep_** leads to the creating of favorable conditions for boundary layer separation. The **_positive dihedral_** reduces the hub corner and tip clearance losses, leading to a fuller velocity profile near the end-walls, but at the expense of increasing the losses near the mid-height region. The use of *positive dihedral* has been calculated to be beneficial for both fixed and free ends of blades. It provides a method of introducing a rapid reduction in blade force local to the end-walls and alleviates high suction surface deceleration rates in these regions at the expense of increased blade force at mid-span.

2.2 Sw ept blade constructions and study cases

Blade loss and noise level are significantly lowered by using the airfoil sweep into 3D line stacking, since the velocity at tip blade is reduced, which means construction optimization for performance improvement.

With respect to the aircraft's flight direction and the air velocity at inlet, the sweep movements are **Forward *FWD* Sweep** (i.e. *positive sweep*) and **Backward *BCK* Sweep** (i.e. *negative sweep*), as indicated in fig. 1. With referrence to the axial flow compressor blade, there are 5 significant blade spanwise sections, equally distanced located, as follows: blade hub **B**, midspan **M**, blade tip V, and BM – at bottom half midspan, MV – at top half midspan. Constructions of positive and negative swept blades with respect to the study case rotor blade and swept rotor blade are compared in fig. 2.

(a)- forward sweep   (b)- backward sweep

(c)- combination of   (d)- combination of
FWD & BCK sweep   FWD & BCK sweep
Fig. 2- Constructions of swept blades, [1]
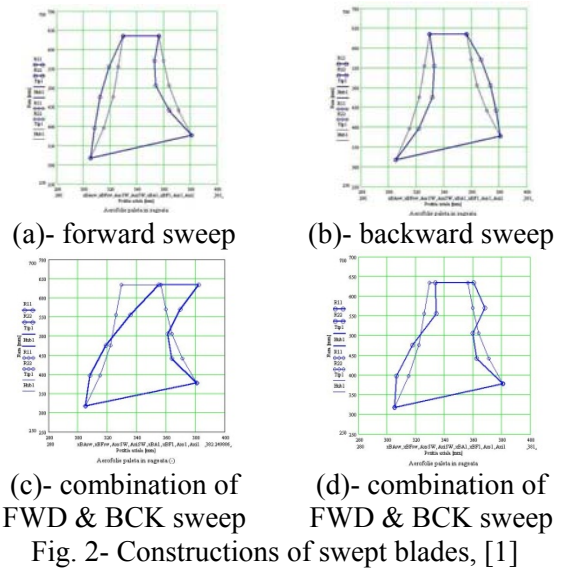
Note that the solutions obtained by the author after applng various sweep angles at different blade span-wise cross sections, are very similar with actual fan blade constructions; e.g. fig. 2-c is likewise the fan blade of the *GE Unducted Fan UDF* engine, and fig. 2-d features the fan blades of the *PW&GE GP7200, GEnX* and *RR Trent 1000* engines.
The span-wise distributions of the sweep angle $\chi[°]$ for each case are listed in Table 1.

Table 1 Values of the sweep angle $\chi[°]$

Blade cross section	B Bottom	BM	M Mid-span	MV	V Top
Case #1	0	5	7	5	0
Case #2	0	-5	-7	-5	0
Case #3	0	5	2	-7	-18
Case #4	0	6	3	-6	-3

3. MATHEMATICAL SUPPORT

3.1 Flow model

The Reynolds Averaged Navier-Stokes RANS equations system (1) has been used for modeling the main flow.

$$\begin{cases} \dfrac{\partial U}{\partial t} + \nabla F = Q \\[2mm] \dfrac{\partial T}{\partial t} + \nabla G = S \end{cases} \tag{1}$$

The vectors U (2) and T (3) contain the conservative variables:

$$U = \begin{bmatrix} \rho \\ \rho V \\ \rho E \end{bmatrix} \tag{2}$$

The turbulent kynetic energy k and the turbulent dissipation ε define the vector T.

$$T = \begin{bmatrix} \rho k \\ \rho \varepsilon \end{bmatrix} \tag{3}$$

The flux vector F (4):

$$F = \begin{bmatrix} \rho V \\ \rho V \otimes V + p\bar{\bar{I}} - \bar{\bar{\tau}}^{t} \\ \rho H V - \rho(\alpha_t + \alpha)\nabla T - \bar{\bar{\tau}}V \end{bmatrix} \tag{4}$$

The source vector Q (5):

$$Q = \begin{bmatrix} 0 \\ \rho f \\ \rho f V + q_v \end{bmatrix} \tag{5}$$

The source term S (6):

$$S = \begin{bmatrix} S_k \\ S_\varepsilon \end{bmatrix} \tag{6}$$

The viscous flux G (7):

$$G = \begin{bmatrix} \rho k V - \left(\mu + \dfrac{\mu_t}{\sigma_k} \right)\nabla k \\[3mm] \rho k \varepsilon - \left(\mu + \dfrac{\mu_t}{\sigma_k} \right)\nabla k \end{bmatrix} \tag{7}$$

The RANS model, unllike the Navier-Stokes model, contains within the expression of the flux F (4) the tensor of the total stresses $\bar{\bar{\tau}}^{t}$ (8) and the effective viscosity μ_{ef} (9), which replaces the molecular viscosity μ.

$$\bar{\bar{\tau}}^{t} = 2(\mu + \mu_t)\bar{\bar{d}} - \frac{2}{3}(\mu + \mu_t)\nabla V \bar{\bar{I}} \tag{8}$$

$$\mu_{ef} = \mu + \mu_t \tag{9}$$

More details about the RANS model and CFD techniques are provided in the papers of Fletcher [3], Chung [4], Hirsch [5], Berbente [6] and others [7, 8].

3.2 Turbulence models

In purpose of closing the equations system, one has to include a turbulence model also; for a thorough analysis, there have been considered four turbulence models: Spalart-Allmaras, $k-\epsilon$, $k-\omega$ and RST model.

4. NUMERICAL RESULTS

In this paper a 2D study has been carried out; there has been considered the reference blade [1], defined by NACA 65(20)10 airfoils, customized blade span-wisely for the specific conditions of a rotating cascade.

(a)- no sweep effect
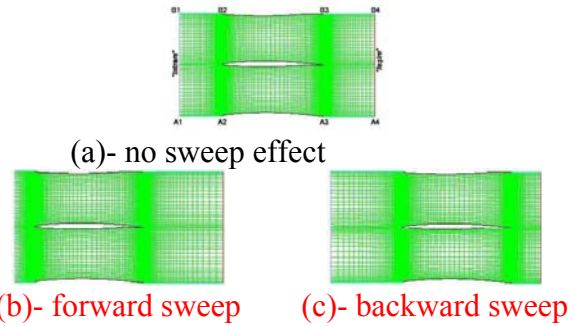
(b)- forward sweep   (c)- backward sweep
Fig. 3 Computational grid

The airfoil at mid-span has been considered for the 2D study, as well as the boundary conditions and other limitations due to the neighboring cascades and the given geometry of a multi-staged axial-compressor, [1].

There have been computed the solutions (i.e. the flow parameters) of the RANS model in association with the turbulence models, for the mid-span airfoil, without sweep effect (fig. 3-a) and with forward sweep (fig. 3-b) and backward sweep (fig. 3-c) respectively. The convergence of the solutions has been monitored for different values of the rotational speed, i.e. 0, 100, 200 and 275 [m/s].

(a)- Spalart-Allmaras   (b)- $k-\epsilon$

(c)- $k-\omega$ (d)- RST
Fig. 4 Mach number of the relative flow,

"HENRI COANDA"
AIR FORCE ACADEMY
ROMANIA

"GENERAL M.R. STEFANIK"
ARMED FORCES ACADEMY
SLOVAK REPUBLIC

INTERNATIONAL CONFERENCE of SCIENTIFIC PAPER
AFASES 2014
Brasov, 22-24 May 2014

/ Spalart-Allmaras, $k - \epsilon$, $k - \omega$ and RST turbulence models/ no sweep effects

(a)- Spalart-Allmaras (b)- $k - \epsilon$

(c)- $k - \omega$ (d)- RST
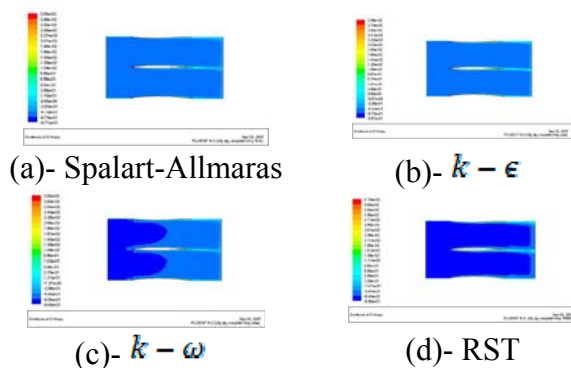
Fig. 5 Entropy distributions,
/ Spalart-Allmaras, $k - \epsilon$, $k - \omega$ and RST turbulence models/ no sweep effects
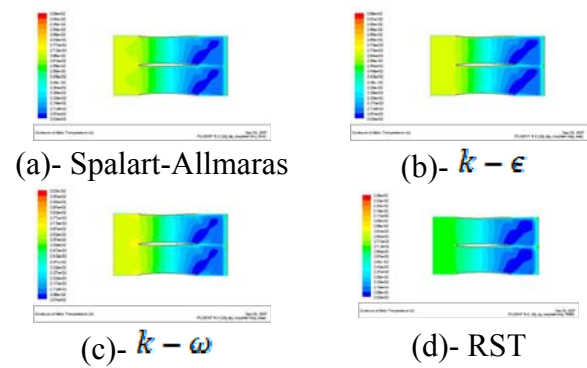
As one can notice from figs. 4-7, the numerical results and the computational accuracy are influenced in greater extent by the turbulence model. For the cascades of multistage turbomachinery, the Spalart-Allmaras model it is convenient to use due to its fast convergence velocity and it is simpler, since it is described by one equation. The $k - \epsilon$ turbulence model is rather suited to capture wall-effects, while for the main flow the other models are more accurate. The more equations used to describe the turbulence model, the greater the number of iterations to achieve a convenient computational accuracy.

(a)- Spalart-Allmaras (b)- $k - \epsilon$

(c)- $k - \omega$ (d)- RST

Fig. 6 Pressure distributions,

/ Spalart-Allmaras, $k - \epsilon$, $k - \omega$ and RST turbulence models/ no sweep effects

(a)- Spalart-Allmaras (b)- $k - \epsilon$

(c)- $k - \omega$ (d)- RST

Fig. 7 Temperature distributions,
/ Spalart-Allmaras, $k - \epsilon$, $k - \omega$ and RST turbulence models/ no sweep effects

For the study case, the results obtained by using the Spalart-Allmaras SA turbulence model are in accordance with experimental data; the highest percent of recommendations that can be found in literature [14-32] points out that for the flow in (axial) cascades the Spalart-Allmaras model is the best option to describe the turbulence.

Table 2 – The number of iterations necessary for obtaining the convergence

Turbu-lence model	Number of iterations		
	No-sweep	Forward sweep	Backward sweep
S-A	3160	2781	4072
$k - \epsilon$	2923	2348	4255
$k - \omega$	5115	5172	4020
RST	3308	2339	4972

In the following, there are highlighted the effects of both forward and backward sweep of the study case airfoil; a thorough computational analysis was performed, after considering four turbulence models.

The results depicted in figs. 8-11 refer to the computations carried on with the Spalart-Allmaras turbulence model.

(a)- no sweep effect

(b)- forward sweep   (c)- backward sweep

Fig. 8 Effect of sweep on Mach number

(a)- no sweep effect

(b)- forward sweep   (c)- backward sweep

Fig. 9 Effect of sweep on static pressure

(a)- no sweep effect

(b)- forward sweep   (c)- backward sweep

Fig. 10 Effect of sweep on static temperature

(a)- no sweep effect

(b)- forward sweep   (c)- backward sweep

Fig. 11 Effect of sweep on entropy
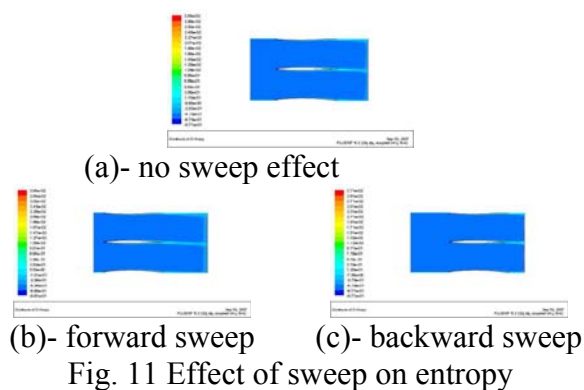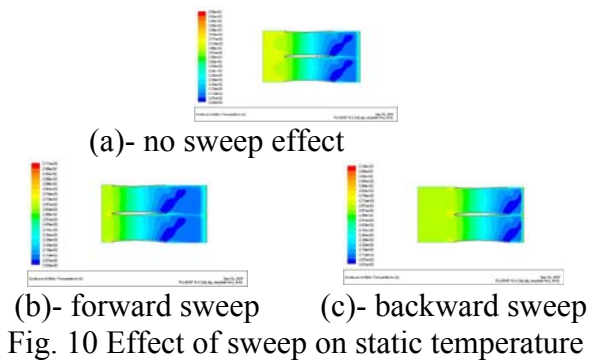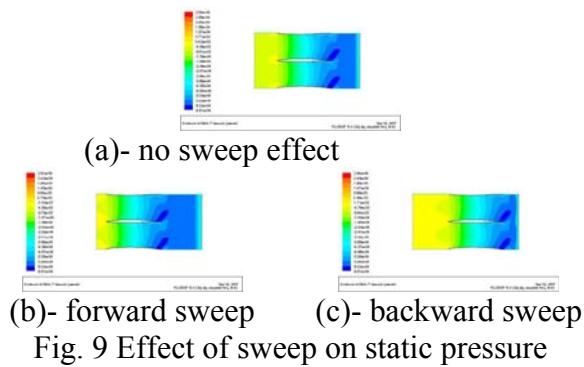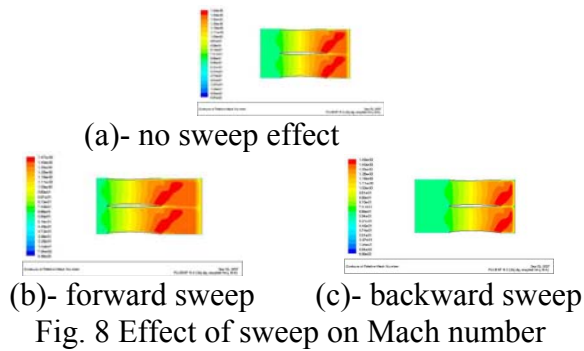
5. CONCLUSIONS

This paper presents a thorough investigation regarding the application of sweep to rotating axial blade cascades.

The author develops an original approach with regard to the obtaining of swept blade constructions, as derivatives of a basic cascade blade configuration.

As study cases were considered cascade blades, with forward and backward sweep versus no-sweep configurations.

The RANS model was used to describe the flow and a comparative study was conducted by using four turbulence models, i.e. Spalart-Allmaras S-A, $k-\varepsilon$, $k-\varpi$ and Reynolds Stress RST models. The CFD analysis was done with the FLUENT solver, with the settings for 2D case, implicit equations and double precision. The convergence was monitored such that the residuals should be minimized; the number of iterations required for obtaining the convergence is listed in Table 2.

The results of the numerical simulations of the flow are expressed as the distributions of Mach number (in relative flow, since it is a rotational frame), static pressure, static temperature and entropy, which have been presented comparatively, for each turbulence model and sweep study case, corresponding to the design rotational speed of 275 [m/s]. In accordance with the experiment and literature [14-32], it came out that the Spalart-Allmaras model represents a good option for modeling the turbulence within blade cascades.

In figs. 8-11 it has been shown the effect of forward and backward sweep versus no-sweep, for the flow parameters, such as the relative Mach number, static pressure, static temperature and entropy.

Concluding remarks:

- Forward sweep allows to reduce the local velocity at blade tip and expands the area downstream the airfoil such that the losses are minimized (which is beneficial for obtaining uniform flow at the next stage cascade inlet), since the variation of the entropy is the least; thus, the optimization of blade cascades with minimum losses is enabled.
- S-A turbulence model is more suited for the CFD analysis of cascades.
- the solution is obtained faster for forward swept blade, while far much greater
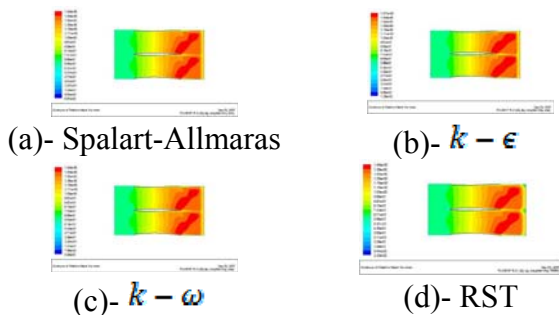
"HENRI COANDA"
AIR FORCE ACADEMY
ROMANIA

"GENERAL M.R. STEFANIK"
ARMED FORCES ACADEMY
SLOVAK REPUBLIC

INTERNATIONAL CONFERENCE of SCIENTIFIC PAPER
AFASES 2014
Brasov, 22-24 May 2014

number of iterations are required for backward swept blade.

- Combinations of forward and backward sweep can be used for highly loaded wide span fan blades, fig. 2-c, 2-d, [1].

REFERENCES

1. ANDREI I. C., *Researches with Regard to Studying the Flow Through Axial Compressor Cascades and Potential Means in Purpose to Performance Improvement, with Applications to the Jet Engines*, Ph. D. Thesis, University „POLITEHNICA" of Bucharest, (2007), Central Library index: 043/3219, 533.6(043.2) 621.51.001, 5(043.2) 621.45(043.2) B-UP 1).

2. Ferziger J. H., Perić M., *Computational Methods for Fluid Dynamics*, 3rd Edition, Springer Verlag, (2002).

3. Srinivas K., Fletcher C. A. J., *Computational Techniques for Fluid Dynamics*, Volume 1, Fundamental and General Techniques, Second Edition, Springer Series in Computational Physics, Springer Verlag, (1991), ISSN 0172-5726, ISBN 3-540-53058-4.

4. Chung T. J., *Computational Fluid Dynamics*, Cambridge University Press, (2002), ISBN 0-521-59416-2.

5. Hirsch C.A.: *Numerical Computation of Internal and External Flows*, Wiley and Sons, (1990).

6. Dănăilă S., Berbente C., *Metode numerice în dinamica fluidelor*, Ed. Academiei Române, București, (2003).

7. (***), *Notes on Numerical Fluid Mechanics*, volume 52, Flow Simulation with High-Performance Computers II, Edited by Ernst Heinrich Hirschel, Vieweg (1996).

8. (***), *Applied Computational Aerodynamics*, vol. 125, Progress in Astronautics and Aeronautics, editor Henne P. A., John Wiley & sons, (1990).

9. Gallimore Simon J., Bolger John J., Cumpsty Nicholas A., Taylor Mark J., Wright Peter I., Place James M. M., *The Use of Sweep and Dihedral in Multistage Axial Flow Compressor Blading – Part I: University Research and Methods Development*, Jl. of Turbomachinery, October (2002), vol. 124, pp. 521-532.

10. Gallimore Simon J., Bolger John J., Cumpsty Nicholas A., Taylor Mark J., Wright Peter I., Place James M. M., *The Use of Sweep and Dihedral in Multistage Axial Flow Compressor Blading – Part II: Low and High-Speed Designs and Test Verification*, Jl. of Turbomachinery, October (2002), vol. 124, pp. 533-541.

11. Golub A. R., Rawls J. W., Russell J. W., *Evaluation of the Advanced Subsonic Technology Program Noise Reduction Benefits*, TM-212144, (2005).

12. Gostelow J. P., *Cascade Aerodynamics*, Pergamon Press, New York, NY, (1984).

13. Neubert R. J., Hobbs D. E., Weingold H. D., *Application of Sweep to Improve the Efficiency of a Transonic Fan Part I: Design*, Journal of Power and Propulsion, vol. 11, nr. 1, January-February, (1995), pp. 49-54.

14. Adamczyk John J., *Aerodynamic Analysis of Multistage Turbomachinery Flows in Support of Aerodynamic Design*, ASME Journal of Turbomachinery, April (2000), vol. 122, pp. 189-217.

15. Anton Weber, Heinz-Adolf Schreiber, Reinhold Fuchs, Wolfgang Steinert, *3-D Transonic Flow in a Compressor Cascade With Shock-Induced Corner Stall*, Jl. of

Turbomachinery, July (2002), vol. 124, pp. 358-366.

16. Árpád Veress, Imre Santa, *A 2D mathematical model on transonic axial compressor rotor flow*, Periodica Polytechnica, series of Transportation Engineering, vol. 30, nr. 1-2, pp. 53-67, (2002), BUTE, Budapest.

17. Cherrett M. A., Bryce J.D., Ginder R.B., *Unsteady Three-Dimensional Flow in a Single Stage Transonic Fan: Part I – Unsteady Rotor Exit Flow Field*, Journal of Turbomachinery, vol. 117, Oct., pp. 506-513, (1995).

18. Clark William S., Hall Kenneth C., A *Time-Linearized Navier–Stokes Analysis of Stall Flutter*, Jl. of Turbomachinery, July (2000), vol. 122, pp. 467-476.

19. Ehrich F. F., Spakovszky Z. S., Martinez-Sanchez M., Song S. J., Wisler D. C., Storace A. F., Shin H.-W., Beacher B. F., *Unsteady Flow and Whirl-Inducing Forces in Axial-Flow Compressors: Part II – Analysis*, Journal of Turbomachinery, July (2001), vol. 123, pp. 446-452.

20. Gerolymos G. A., Neubauer J., Sharma V. C., Vallet I., *Improved Prediction of Turbomachinery Flows Using Near Wall Reynolds Stress Model*, Jl. of Turbomachinery, vol. 124, Jan. (2002), pp. 86-99.

21. Helming K., *Numerical Analysis of Sweep Effects in Shrouded Propfan Rotors*, Journal of Propulsion and Power, vol. 12, no. 1, pp. 139-145, (1996).

22. Hobbs D. E., Weingold H. D., *Development of Controlled Diffusion Airfoils for Multistage Compressor Applications*, Jl. of Engineering for Gas Turbine and Power, vol. 106, April (1984), pp. 271-278.

23. Küsters Bernhardt, Schreiber Heinz-Adolf, Köller Ulf, Mönig Reinhardt, *Development of Advanced Compressor Airfoils for Heavy-Duty Gas Turbines–Part II: Experimental and Theoretical Analysis*,

Jl.of Turbomachine., July (2000), vol. 122, pp. 406-415.

24. L. He, T. Chen, R. G. Wells, Y. S. Li, W. Ning, *Analysis of Rotor-Rotor and Stator-Stator Interferences in Multi-Stage Turbomachines*, Jl. of Turbomachinery, October (2002), vol. 124, pp. 564-571.

25. L. Sbardella, M. Imregun, Linearized *Unsteady Viscous Turbomachinery Flows Using Hybrid Grids*, Jl. of Turbomachinery, July (2001), vol. 123, pp. 568-582.

26. Leroy H. Smith, Jr., *Axial Compressor Aero-design Evolution at General Electric*, Journal of Turbomachinery, July (2002), vol. 124, pp. 321-330.

27. Ng W. F., Epstein A. H., *Unsteady Losses in Transonic Compressors*, Journal of Engineering for Gas Turbines and Power, vol. 107, pp. 345-353, (1985).

28. Ning W., Li Y. S., Wells R. G., *Predicting Blade Row Interactions Using a Multistage Time-Linearized Navier-Stokes Solver*, Journal of Turbomachinery, January (2003), vol. 125, pp. 25-32.

29. Ottavy Xavier, Trébinjac Isabelle, Vouillarmet André, *Analysis of the Interrow Flow Field within a Transonic Axial Compressor: Part 1 – Experimental Investigation*, Jl. of Turbomachinery, January (2001), vol. 123, pp. 49-56.

30. Ottavy Xavier, Trébinjac Isabelle, Vouillarmet André, *Analysis of the Interrow Flow Field within a Transonic Axial Compressor: Part 2 – Unsteady Flow Analysis*, Jl. of Turbomachinery, January (2001), vol. 123, pp. 57-63.

31. Rodrick V. Chima, Meng-Sing Liou, *Comparison of the AUSM+ and H-CUSP Schemes for Turbomachinery Applications*, TM—2003-212457, June (2003), Glenn Research Center, Cleveland, Ohio, USA.

32. Shan Peng, *Kinematic Analysis of 3-D swept Shock Surfaces in Axial Flow Compressors*, Jl. of Turbomachinery, July (2001), vol. 123, pp. 490-500.

AN APPLICATION TO Mastroianni OPERATORS

Cristina Sanda CISMAŞIU

Abstract. *A new linear positive operator is defined and studied resorting to the method of Mastroianni [2], [3].*

1. Introduction

Motiveted by the Mastroianni′s operators [2],[3] which were studied by O. Agratini, B. Della Vechia [1], we consider the sequence $\left(\Phi_{n,c}\right)_{n\in N}$, $c>0$ of real valued functions defined on [0, +∞) as

$$\Phi_{n,c}\left(x\right)=\left(\frac{c}{1+c}\right)^{ncx}, \ \ c>0, \ x\geq 0, \ n\in N$$

.

These functions satisfy the following conditions, for each $n\in N$ and $c>0$:

(i). $\Phi_{n,c}\left(0\right)=1,$

(ii). $\Phi_{n,c}\in C^{\infty}\left[0,\infty\right),$

(iii). $\Phi_{n,c}\left(x\right)$ is completely monotone, so that $\left(-1\right)^{k}\Phi^{(k)}_{n,c}\left(x\right)\geq 0, \ x\geq 0,$

(iv). $\Phi^{(k)}_{n,c}\left(x\right)=\left(nc\ln\frac{c}{1+c}\right)^{k}\Phi_{n,c}\left(x\right),$

(v). $\lim\limits_{x\to\infty}x^{r}\Phi^{(k)}_{n,c}\left(x\right)=0, \ r\in N_0.$

Let

$$E_2\left[0,\infty\right):=\left\{ f\in C\left[0,\infty\right) \mid \left(\exists\right) \lim\limits_{x\to\infty}\frac{\left|f\left(x\right)\right|}{1+x^2} <\infty \right\}$$

be the space endowed with the norm

$$\left\|f\right\|_*=\sup\left\{\frac{\left|f\left(x\right)\right|}{1+x^2}, \ x\geq 0\right\}$$ which is a Banach space.

We define the operator
$$L_{n,c}:E_2\left[0,\infty\right)\to C\left[0,\infty\right) \ \text{as}$$

$$L_{n,c}\ (f;x) = \sum_{k=0}^{\infty} p_{n,k,c}(x) f\left(\frac{k}{n}\right) \text{ with} \qquad (1.1)$$

$$p_{n,k,c}(x) = \frac{(-1)^k\, x^k \Phi_{n,c}^{(k)}(x)}{k!} = \frac{(-1)^k\, x^k \left(nc\ln\dfrac{c}{1+c}\right)^k \Phi_{n,c}(x)}{k!} . \qquad (1.2)$$

Because

$$\sum_{k=0}^{\infty} p_{n,k,c}(x) = \Phi_{n,c}(x) \sum_{k=0}^{\infty} \frac{\left(-ncx\ln\dfrac{c}{1+c}\right)^k}{k!} = \Phi_{n,c}(x)\exp\left(-ncx\ln\frac{c}{1+c}\right) = 1\,,$$

these operators preserve constant functions. Our aim is to find some approximation properties.

2. Main results

Lemma 1. *The moments of the operators* $L_{n,c}\ (f;x)$ *for* $e_r(x) = x^r, r = 0,1,2$, $x \geq 0$ *are given as*

$$L_{n,c}\ (e_0;x) = 1,$$

$$L_{n,c}\ (e_1;x) = -\frac{\Phi_{n,c}{}'(0)}{n} e_1(x) = -cx\ln\frac{c}{1+c}, \qquad (2.1)$$

$$L_{n,c}\ (e_2;x) = \frac{\Phi_{n,c}{}''(0)}{n^2} e_2(x) - \frac{\Phi_{n,c}{}'(0)}{n^2} e_1(x) = x^2 c^2 \ln^2\frac{c}{1+c} - \frac{x}{n} c\ln\frac{c}{1+c}.$$

Proof. By a sim ple computation it can easily be verified the identities of the lemma.

Theorem 2.1. *If* $c = c(n) \to \infty$, $n \to \infty$ *then* $\lim_{n\to\infty} L_{n,\ c(n)} f = f$ *uniformly on compact subsets of* $[0,\infty)$ *for any* $(\forall) f \in E_2[0,\infty)$.

Indeed, taking $c = c(n) \to \infty$, $n \to \infty$ according to the well-known Bohm ann-Korovkin theorem , relations of the lem ma guarantee that $\lim_{n\to\infty} L_{n,\ c(n)} f = f$ uniformly on compact subsets of $[0,\infty)$.

Remark. If $c \to \infty$ the o perators (1.1) converge to classical Szasz-M irakjan operators

$$S_n(f;x) = \sum_{k=0}^{\infty} e^{-nx} \frac{(nx)^k}{k!} f\left(\frac{k}{n}\right), x \geq 0 .$$

Applying a classical result due to Shisha O. and Mond B. [4] we obtain the pointwise estimate

“HENRI COANDA”
AIR FORCE ACADEMY
ROMANIA

“GENERAL M.R. STEFANIK”
ARMED FORCES ACADEMY
SLOVAK REPUBLIC

INTERNATIONAL CONFERENCE of SCIENTIFIC PAPER
AFASES 2014
Brasov, 22-24 May 2014

$$\left| L_{n,c}\left(f;x\right) - f\left(x\right)\right| \le \left(1 + \delta^{-1}\sqrt{L_{n,c}\left(\left(e_1 - xe_0\right)^2;x\right)}\right)\omega\left(f,\delta\right), x \ge 0$$

with

$$L_{n,c}\left(\left(e_1 - xe_0\right)^2;x\right) = x^2(1 + 2\frac{\Phi_n'\left(0\right)}{n} + \frac{\Phi_n''\left(0\right)}{n^2}) - \frac{\Phi_n'\left(0\right)}{n^2}x =$$

$$= x^2(1 + 2c\ln\frac{c}{1+c} + c^2\ln^2\frac{c}{1+c}) - x\frac{c}{n}\ln\frac{c}{1+c}.$$

These operators admitte a generalization of Durrmeyer type, because

$$\int_0^\infty p_{n,k}\left(x\right)dx = \int_0^\infty \frac{\left(-nxc\ln\frac{c}{1+c}\right)^k}{k!}\left(\frac{c}{1+c}\right)^{ncx}dx = \frac{\left(-nc\ln\frac{c}{1+c}\right)^k}{k!}\int_0^\infty x^k\left(\frac{c}{1+c}\right)^{ncx}dx =$$

$$= \frac{\left(-nc\ln\frac{c}{1+c}\right)^k}{k!}\cdot\frac{\left(-1\right)^k k!}{\left(nc\ln\frac{c}{1+c}\right)^k}\int_0^\infty\left(\frac{c}{1+c}\right)^{ncx}dx = -\frac{1}{nc\ln\frac{c}{1+c}}.$$

The Durrmeyer type operator asociated with the operator (1.1)-(1.2) become:

$$DL_{n,c}\left(f;x\right) = -\left(nc\ln\frac{c}{1+c}\right)\sum_{k=0}^\infty p_{n,k,c}\left(x\right)\int_0^\infty p_{n,k,c}\left(t\right)f\left(t\right)\,dt.$$

For these operators we have

$$DL_{n,\,c}\left(e_0;x\right)=1,$$

$$DL_{n,\,c}\left(e_1;x\right)=\left(-nc\ln\frac{c}{1+c}\right)\sum_{k=0}^{\infty}p_{n,k}\left(x\right)\int_0^{\infty}\frac{\left(-nct\ln\frac{c}{1+c}\right)^k\Phi_{n,c}\left(t\right)}{k!}\,t\,dt=$$

$$=\left(-nc\ln\frac{c}{1+c}\right)\sum_{k=0}^{\infty}p_{n,k}\left(x\right)\frac{\left(-nc\ln\frac{c}{1+c}\right)^k}{k!}\int_0^{\infty}t^{k+1}\Phi_{n,c}\left(t\right)dt=$$

$$=\left(-nc\ln\frac{c}{1+c}\right)\sum_{k=0}^{\infty}p_{n,k}\left(x\right)\frac{\left(-nc\ln\frac{c}{1+c}\right)^k}{k!}\cdot\frac{\left(k+1\right)!}{\left(-nc\ln\frac{c}{1+c}\right)^{k+2}}=$$

$$=\left(-nc\ln\frac{c}{1+c}\right)\sum_{k=0}^{\infty}p_{n,k}\left(x\right)\frac{k+1}{\left(-nc\ln\frac{c}{1+c}\right)^2}=\frac{1}{-nc\ln\frac{c}{1+c}}\sum_{k=0}^{\infty}\left(k+1\right)p_{n,k,c}\left(x\right)=$$

$$=-\frac{1}{nc\ln\frac{c}{1+c}}nL_{n,c}\left(e_1;x\right)-\frac{1}{nc\ln\frac{c}{1+c}}=x-\frac{1}{nc\ln\frac{c}{1+c}}.$$

$$DL_{n,\,c}\left(e_2;x\right)=\left(-nc\ln\frac{c}{1+c}\right)\sum_{k=0}^{\infty}p_{n,k}\left(x\right)\int_0^{\infty}\frac{\left(-nct\ln\frac{c}{1+c}\right)^k\Phi_{n,c}\left(t\right)}{k!}\,t^2dt=$$

$$=\left(-nc\ln\frac{c}{1+c}\right)\sum_{k=0}^{\infty}p_{n,k}\left(x\right)\frac{\left(-nc\ln\frac{c}{1+c}\right)^k}{k!}\int_0^{\infty}t^{k+2}\Phi_{n,c}\left(t\right)dt=$$

$$=\left(-nc\ln\frac{c}{1+c}\right)\sum_{k=0}^{\infty}p_{n,k}\left(x\right)\frac{\left(-nc\ln\frac{c}{1+c}\right)^k}{k!}\cdot\frac{\left(k+2\right)!}{\left(-nc\ln\frac{c}{1+c}\right)^{k+3}}=\left(-nc\ln\frac{c}{1+c}\right)\sum_{k=0}^{\infty}p_{n,k}\left(x\right)\frac{\left(k+2\right)\left(k+1\right)}{\left(-nc\ln\frac{c}{1+c}\right)^3}=$$

$$=\frac{1}{\left(-nc\ln\frac{c}{1+c}\right)^2}\sum_{k=0}^{\infty}\left(k+1\right)\left(k+2\right)p_{n,k,c}\left(x\right)=\frac{1}{\left(nc\ln\frac{c}{1+c}\right)^2}\left\{n^2L_{n,c}\left(e_2;x\right)+3nL_{n,c}\left(e_1;x\right)+2\right\}=$$

$$=x^2-\frac{4x}{nc\ln\frac{c}{1+c}}+\frac{2}{\left(nc\ln\frac{c}{1+c}\right)^2}.$$

References

If $c=c(n)\to\infty$, $n\to\infty$ then

$$\lim_{n\to\infty}DL_{n,\,c(n)}\left(f\right)=f,\ \left(\forall\right)f\in E_2\left[0,\infty\right)$$

uniformly on compact subsets of $\left[0,\infty\right)$.

1. O. Agratini, B. Della Vechia, *Mastroianni operators revisited,* Facta Universitatis (Nis), Ser. Math. Inform. 19 (2004), 53-63.

"HENRI COANDA"
AIR FORCE ACADEMY
ROMANIA

"GENERAL M.R. STEFANIK"
ARMED FORCES ACADEMY
SLOVAK REPUBLIC

INTERNATIONAL CONFERENCE of SCIENTIFIC PAPER
AFASES 2014
Brasov, 22-24 May 2014

2. G. Mastroianni, *Su un operatore lineare e positivo*, Rend. Acc. Sc. Fis. Mat., Napoli (4) 46 (1979), 161-176.

3. G. Mastroianni, *Su una classe di operatori e positivi,* Rend. Acc. Sc. Fis. Mat., Napoli (4) 48 (1980), 217-235.

4.O. Shisha, B. Mond, *The degree of convergence of linear positive operators*, Proc. Nat. Acad. Sci. U.S.A. 60 (1968), 1196-1200.

Applied Mathematics,IT&C

THE EQUATION OF DISPERSION AND THE DISPLACEMENT VECTOR IN THE SYMMETRIC CASE

Mihaela DUMITRACHE, Camelia GHELDIU

Faculty of Mathematics and Computer Science, University of Pitesti, Piteşti, Romania,

Abstract: *In this paper we study the propagation of the symmetric Lamb waves and we find the equation of dispersion and the equations of the displacement vector in the symmetric case.*

Keywords: *35L05, 35L10, 35P30.*

1. INTRODUCTION

In this paper we consider an elastic, isotropic, continuous and homogeneous medium and we study the propagation of the Lamb waves through it. Using the results from [1], [2] and [3], we obtain the equation of dispersion and the equations of the displacement vector in the symmetric case.

2. PROBLEM FORMULATION

In the following we consider the normal guided Lamb waves. These waves appear in a plate of thickness 2*h* comparable with the wavelength, due to coupling between the components longitudinal *L* and the transverse components of the wave *TV*. Thus, two types of wave Lamb can be produced, but, in this parer, we study just the symmetric waves which are depicted in Figure 1, where for each side of the middle of the plate, the longitudinal components are equal and the transverse components are opposite.

We assume homogeneous and isotropic elastic plate bounded by two parallel planes located at a short distance *2h*, and we want to find the equation of dispersion and the equations of the displacement vector.
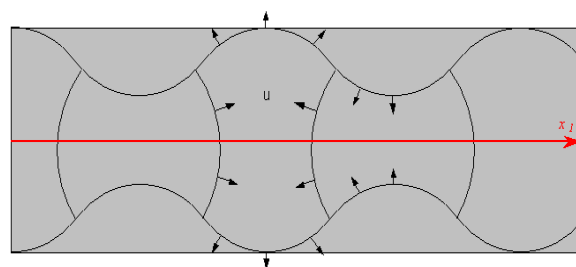
Figura 1: The symmetric Lamb waves

3. PROBLEM SOLUTION

In the article [1] we started from the equation of the displacement vector ***u*** for a material point

$$\mathbf{u} = \nabla \varphi + \nabla \times \psi \qquad (1)$$

where φ is a scalar potential and ψ is a vectorial potential. In expression (1) the two potentials should verify the following two equations of wave

$$\nabla^2 \varphi - \frac{1}{v_L^2} \frac{\partial^2 \varphi}{\partial t^2} = 0, \qquad (2)$$

where v_L is the phase velocity of the longitudinal waves and

$$\nabla^2 \psi - \frac{1}{v_T^2} \frac{\partial^2 \psi}{\partial t^2} = 0, \qquad (3)$$

where v_T is the phase velocity of the longitudinal waves.

The scalar and the vectorial potentials are trigonometric functions of time t, with the same frequency ω. However, they can be expressed as follows, with the wave number k:

$$\phi = \phi_0(x_2) e^{i(\omega t - kx_1)},$$
$$\psi = \psi_{0j}(x_2) e^{i(\omega t - kx_1)}, \quad j = 1, 2, 3. \qquad (4)$$

The equation of dispersion has the following relation:

$$\frac{\tan(qh + \alpha)}{\tan(ph + \alpha)} = -\frac{4k^2 pq}{(q^2 - k^2)^2} \qquad (5)$$

with $\alpha = 0$ and $\alpha = \frac{\pi}{2}$, where the constants p and q are defined as follows:

$$p^2 = \frac{\omega^2}{v_L^2} - k^2, \qquad q^2 = \frac{\omega^2}{v_T^2} - k^2, \qquad (6)$$

and the constant angle α can take the values 0 and $\frac{\pi}{2}$ depending on the type of symmetry of the wave.

Further, using the results from [3], we know that we have three regions with respect to the phase velocity. So, we write the equation of dispersion (5) and the equations of the displacement vector for each subdomain of wave number k taking into account the type of values that can be taken the constants p and q, for the case $\alpha = 0$ (the symmetric case) .

The first case is for $k < \frac{\omega}{v_L}$. We have p and q real numbers, so the dispersion equation is

$$\frac{\tan(qh + \alpha)}{\tan(ph + \alpha)} = -\frac{4k^2 pq}{(q^2 - k^2)^2}, \qquad (7)$$

and the equations of the displacement vector are:

$$u_1 = qA\left[\cos(qx_2) - \frac{2k^2}{k^2 - q^2} \cdot \frac{\cos(qh)}{\cos(ph)} \cdot \cos(px_2) \right]$$
$$\cdot \cos(\omega t - kx_1),$$
$$u_2 = -kA\left[\sin(qx_2) + \frac{2pq}{k^2 - q^2} \frac{\cos(qh)}{\cos(ph)} \cdot \sin(px_2) \right]$$
$$\cdot \sin(\omega t - kx_1). \qquad (8)$$

The second case is for $\frac{\omega}{v_L} < k < \frac{\omega}{v_T}$. We have p an imaginar number, i.e. $p = ip$ and q a real number, so the dispersion equation has the form:

$$\frac{\tan(qh + \alpha)}{\tan(ph + \alpha)} = \frac{4k^2 pq}{(q^2 - k^2)^2}, \qquad (9)$$

and the equations of the displacement vector are:

$$u_1 = qA\left[\cos(qx_2) - \frac{2k^2}{k^2 - q^2} \frac{\cos(qh)}{\cosh(ph)} \cosh(px_2) \right]$$
$$\cdot \cos(\omega t - kx_1),$$
$$u_2 = -kA\left[\sin(qx_2) - \frac{2pq}{k^2 - q^2} \frac{\cos(qh)}{\cosh(ph)} \sinh(px_2) \right]$$
$$\cdot \sin(\omega t - kx_1). \qquad (10)$$

The third case is for $\frac{\omega}{v_L} < \frac{\omega}{v_T} < k$. We have p and q imaginare numbers, i.e. $p = ip$ and $q = iq$, so the dispersion equation is

$$\frac{\tan(qh + \alpha)}{\tan(ph + \alpha)} = \frac{4k^2 pq}{(q^2 + k^2)^2} \qquad (11)$$

and the equations of the displacement vector are the following form:

"HENRI COANDA"
AIR FORCE ACADEMY
ROMANIA

"GENERAL M.R. STEFANIK"
ARMED FORCES ACADEMY
SLOVAK REPUBLIC

INTERNATIONAL CONFERENCE of SCIENTIFIC PAPER
AFASES 2014
Brasov, 22-24 May 2014

$$u_1 = qA\left[\cosh(qx_2) - \frac{2k^2}{k^2+q^2} \cdot \frac{\cosh(qh)}{\cosh(ph)} \cdot\right.$$
$$\left.\cdot \cosh(px_2)\right]\cos(\omega t - kx_1),$$

$$u_2 = -kA\left[\sinh(qx_2) + \frac{2pq}{k^2+q^2} \cdot \frac{\cosh(qh)}{\cosh(ph)} \cdot\right.$$
$$\left.\cdot \sinh(px_2)\right]\cos(\omega t - kx_1),$$

$$(12)$$

where A is a constant factor.

3. CONCLUSIONS

In this paper we use the symmetric Lamb waves in an elastic, isotropic, continuous and homogeneous medium and we find the equation of dispersion and the equations of the displacement vector for every subdomain of the wave number k in the symmetric case.

REFERENCES

1. Dumitrache, M., Gheldiu C, *High-frequency waves. The equation of the displacement vector*. The Proceedings of the International Session of 15-th Scientific Papers "Scientific Research and Education in the Air Force", AFASES 2013, 23-25 mai Braşov, ISSN, ISSN-L 2247- 3173, pg. 329-332.
2. Dumitrache, M., Gheldiu C, *High frequency waves and the equation of dispersion*. International Scientific Conference "Mathematics & IT: Research and Education (MITRE-2013)" Chisinau, August 18-22, 2013, at the Moldova State University (MSU), Faculty of Mathematics and Computer Science.
3. Dumitrache, M., Gheldiu C, *The curve of dispersion in the plane* (ω, k), Buletin Ştiinţific-Universitatea din Piteşti, Seria Matematică şi Informatică, Nr. 19 (2013).

Applied Mathematics,IT&C

BUILDING A HYBRID SECURE SOCKET LAYER PROTOCOL

Gabriela MOGOS*

* Facultad de Informatica y Electronica, Escuela Superior Politecnica de Chimborazo, Riobamba, Ecuador

Abstract: Randomness is an essential resource for cryptography and random number generators are, at the same time, very important for the most cryptographic systems. Using these weak random values may lead to vulnerabilities of the systems, causing the adversary to easily break the system, as demonstrated by breaking the implementation of Secure Socket Layer.

This paper presents a hybrid Secure Socket Layer that includes together a Quantum Random Number Generator (QRNG), to generate the random numbers, and, an Elliptical Curve Cryptography (ECC) algorithm, to encrypt the data.

1. INTRODUCTION

Secure Socket Layer uses a combination of public key and symm etric-key encryption. Symmetric-key encryption is much faster than public-key encrypti on, but public-key encryption provides better authentication techniques.

The Secure Socket Layer han dshake allows th e s erver to au thenticate its elf to th e client using public-key techniques, then allows the client and the server to cooperate in the creation of symm etric keys used for rapid encryption, decryption, and tam per detection during the session that follows.

In our paper, we present a theoretical demonstration of how to im prove the secur ity of Secure Socket Layer protocol by replacing Random Num ber Generato r with Quantum Random Num ber Generato r and the *Rivest, Shamir, Adleman* (RSA) cryptographic algorithm, currently used, with *Elliptic Curve Cryptography* (ECC) algorithm.

In first part of paper, we present *Random Number Generator* (RNG) and *Quantum Random Number Generator* (QRNG), and, advantages of using QRNG in generating a sequence of true random bits.

To motivate the need for replacing the *RSA cryptosystem* (existing in SSL 3.0) with *ECC cryptosystem*, in the second part of the paper, we present a com parative analysis of those cryptosystems and in the last part, we present the hybrid Secure Socket Layer protocol.

2. HYBRID SECURE SOCKET LAYER PROTOCOL

2.1 Random Number Generators vs. Quantum Random Number Generators.

Random numbers seem to be of an ever increasing im portance in cryptography,

various stochastic num erical sim ulations and calculations, statistical research, various randomized or stochastic algorithm s, etc. and the need for them is spa nning a wide range of fields from engineering to physics to bioinformatics.

The applications usually put constraints on properties of input random num bers (probability distribut ion, bias, correlation, entropy, determ inism, s equence repeatability, etc.).

Random number generators based on quantum physics are true random num ber generators as quantum physical phenom ena are intrinsically random.

Our paper is based on the study done by researchers [11] f rom the Joint Quantu m Institute (JQI), in partnership with European quantum infor mation scientists, who have found a method of producing a certifiably random string of num bers based on fundamental principles of quantum mechanics.

They repor t their re sults in th e 15 April 2010 issue of *Nature* [12].

What is the ration ale f or that quantum randomness is a better form of random ness than, classic randomness?

Quantum hardware random num ber generators produce sequences of numbers that are not p redictable, and therefore p rovide th e greatest security when used to encrypt data.

Three principal types of quantum indeterminism underlying to realize a QRNG:

(i) The indeterm inacy of individual outcomes of single events as proposed by Born and Dirac;

(ii) Quantum com plementarity (du e to the use of conjugate variables), as put forward by Heisenberg, Pauli and Bohr;

(iii)Value indefiniteness due to Bell, Ko chen & Specker, and Greenberger, Horne & Zeilinger).

A simple design for a Q RNG is based on a construction with a photon source, a 50/50 beam-splitter and two identical sin gle photo n detectors. This construction ensures a random and balanced probability of detection of the photon at each detector.

Meanwhile, commercial Quantum Random Number Ge nerators hav e already appeared on the m arket. In 2001, *ID Quantique* [3] introduced the f irst commercial quantum

random number genera tor, which generated a strong interest.

Seeing that, the Quantum Random Number Generator is idea l f or applic ations requirin g very high rates of true random numbers, our aim is to replace exis ting the classic Random Number Ge nerator (RNG) used by Secure Socket Layer protocols, with quantum one (QRNG).
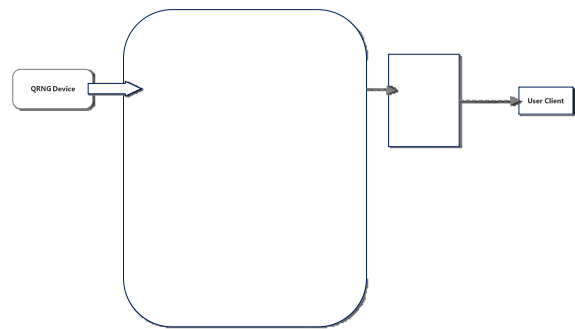
Figure 1. Connect a Quantum Random Number Generator to a computer

The Quantum Random Number Ge nerator is used for cryptographic purposes and other applications requ iring the h ighest leve ls of security and randomness properties.

The Quantum Random Number Ge nerator device connects to a co mputer via PCI or USB interface.

Advantages of Quantum Random Number Generator on Secure Socket Layer:

The *Quantum Random Number Generator* offers the best option for strong security in the long term , especially if the technologies are based on the use of algorithm s. Photons and entangled photons of the sort used in quantum cryptography and communication have a form of tam per evidence an d protection built into the technology at the level of quantum - mechanical processes. At the m oment, it is widely believed that this technology cannot be defeated.

Quantum Random Number Generators (QRNGs) have the advantage over conventional random ness sources of being invulnerable to enviro nmental perturbations and of allowing live status verification.

Quantum Random Number Generator (QRNG) ca n generate t ruly random numbers from the f undamentally probabilistic nature of quantum processes.

"HENRI COANDA"
AIR FORCE ACADEMY
ROMANIA

"GENERAL M.R. STEFANIK"
ARMED FORCES ACADEMY
SLOVAK REPUBLIC

INTERNATIONAL CONFERENCE of SCIENTIFIC PAPER
AFASES 2014
Brasov, 22-24 May 2014

Generating large num bers using QRNG, lead to a "chain reaction" of i mproving the security SSL protocol.
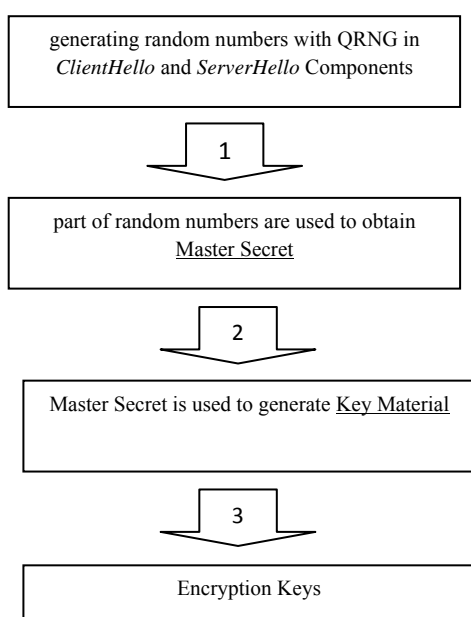
2.2 Elliptical Curve Cryptography (ECC) vs. Rivest, Shamir, Adleman (RSA) cryptosystem.

Every Secu re Socket Layer conn ection begins with a handshake, during which the two parties com municate th eir capabilities to the other side, perform aut hentication, and agree on their session keys. The session keys are then used to encry pt the rest of the conversation, possib ly spanning m ultiple connections. They are d eleted afterwards. The goal of the key exchange phase is to enable the two parties to negotiate the keys securely, to prevent anyone else from learning these keys.

Several key exchange m echanisms exist, but, at the mom ent, by far the most commonly used one is based on RSA [9], where the

server's private key is used to protect the session keys.

Elliptic Curve Cryptography (E CC) algorithm [5] relies on the diff iculty of solving the Elliptic Curve Discrete Logarithm Problem (ECDLP) in much the same w ay that R SA depends on the difficulty of factori ng the product of two large pri mes. The be st known method for solving ECDLP is fully e xponential, whereas t he fa ctoring proble m is sub-exponential.

Starting from the data set [1], we have realized a com parative analysis between thes e two algorithms:
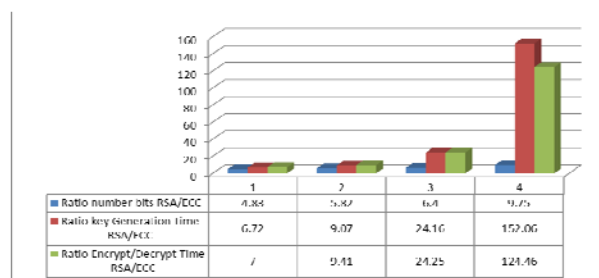
Figure 2. Comparative analysis RSA/ECC

Advantage of Elliptic Curve Cryptography on Secure Socket Layer:

- ECC is an em erging public-key cryptosystem that offe rs equ ivalent secu rity with smaller keys sizes.
- Augments end to end encryption for data in flight by he lping to m aintain data privacy and prevent data leakag e of sensitive infor mation particularly when providing the next generation of security level requirements.
- We can red uce the tran smission cost during handshake.
- Can be used to i mplement encryption on small, mobile devices with limited resources in terms of power, CPU and memory.
- Can be used for large web servers to handling many encrypted sessions.

2.3 Secure Socket Layer a hybrid protocol

Speculating weaknesses of the current SSL version 3.0, we propose an im provement of it in term s of perfor mance, security and space requirements.

In the following we present our reasons to replace the classical random number generator currently u sed by S ecure Sock et Layer protocol with quantum random generator, and, RSA algorithm with ECC.
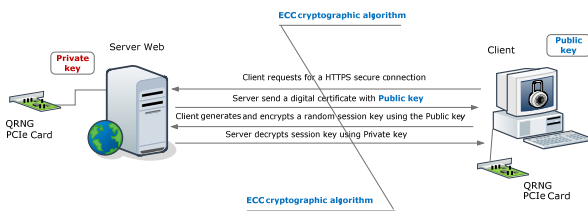
Figure 4. Schematic diagram of the protocol

I. Replace the Random Number Generator (RNG) with quantum one (QRNG) **-** the obtained key is very safe and we can get an increase of the num ber of bits that should be a "cryptographically secure" random number.

Due to indeterm inism (Bohr and Heisenberg) and exclusi on principles (Pauli) from quantum physics, the opportunity of attackers to "guess" the numbers is zero, which makes the generated num bers to be truly random. Since the data will be encrypted using asymmetric cryptographic algorithms, key size is essential in ensuring the security an d integrity of encrypted information.

II. Replace RSA cryptographic algorithm with ECC algorithm **-** we will provide the same security protocol, however, the sm aller key sizes lead to faster processing, which is very useful to im plementing encryption on small, mobile devices with limited resources in terms of power, CPU and memory.

3. CONCLUSIONS & ACKNOWLEDGMENT

We can conclude th at the *Hybrid Secure Socket Layer* can offer security advantages over conventional alternatives, can be used for large web s ervers that will be han dling m any encrypted s essions and its perform ances are better than the class ic Secure Socket Laye r protocol.

This th eoretical study is part of a larger project [13] that we will be de veloped b y *Facultad de Informatica y Electronica, Riobamba, Ecuador*.

REFERENCES

1. Kancheti S., *Comparative Study of Elliptic Curve Cryptography and RSA in Constrained Environment*, (2010).
2. Lofberg J., *Yalmip: A toolbox for modeling and optimization in MATLAB.*
3. http://www.idquantique.com
4. Navascues M., Pironio S., and Acin A.. *Bounding the set of quantum correlations*, Physical Review Letters, 98:010401, (2007).
5. NIST, Recomm endation for Key Management – Part 1: General (Revised). *National Institute of Standards and Technology.* NIST Special Publication 800-57, (2007).
6. Pironio S., Navascues M., Acin A., *Convergent relaxations of polynomial optimization problems with non-commuting variables*, arXiv:0903.4368, (2009).
7. Pironio S., Acin A ., Brunner N., Gisin M., Massar S., and Scarani V., *Device-independent quantum key distribution secure against collective attacks*, Ne w Journal of Physics, 11:045021, (2009).
8. In the second edition of *Numerical Recipes in C: The Art of Scientific Computing* (Cambridge Univers ity Press, 1992), p. 277. Chapter 7 includes a thorough (and sobering) discussion of random num ber generation.
9. Rivest R.L., Sham ir A., & Adlem an, L., *A Method for Obtaining Digital Signatures and Public-Key Cryptosystem*, Retrieved from http://people.csail.mit.edu/rivest/Rsapaper.pdf , (1978).

"HENRI COANDA"
AIR FORCE ACADEMY
ROMANIA

"GENERAL M.R. STEFANIK"
ARMED FORCES ACADEMY
SLOVAK REPUBLIC

INTERNATIONAL CONFERENCE of SCIENTIFIC PAPER
AFASES 2014
Brasov, 22-24 May 2014

10. Sturm J .F., SeDuMi, *a MATLAB toolbox for optimization over symmetric cones*, http://sedumi.mcmaster.ca.
11. http://jqi.umd.edu/sites/default/files/newsletters/feb_2010_newsletter.pdf.
12. Pironio S., Acín A., Massar S., Boyer A. de la Giroday, Matsukevich D. N., Maunz P., Olm schenk S., Hayes D., Luo L., Manning T. A. & Monroe C., *Random numbers certified by Bell's theorem*, Nature, 2010; 464 (7291): 1021 DOI: 10.1038/nature09008.
13. Mogos G., Radu Gh., *Hybrid Secure Socket Layer protocol*, Review of the Air Force Academy, Vol. XII, No. 2(26), pp. /2014, http://www.afahc.ro/revista/Nr_2_2014/91_MOGOS_RADU.pdf.

Applied Mathematics,IT&C

ON THE MAX PARETO POWER SERIES DISTRIBUTION

Bogdan Gheorghe MUNTEANU

The "Henri Coanda" Air Force Academy, Brasov, Romania

Abstract: *This paper presents a new distribution wich unitary treated through the family of the power series distributions, resulting in a new distribution which we called a Max Pareto power series (MaxParPS) distribution. Some properties and reliability characteristics (e.g. survival function, hazard rate) are studied. It also shows that in some conditions a Poisson limit theorem for this type of distribution takes place.*

Keywords: *distribution of the maximum, limit theorem, Pareto distribution, power series distribution.*
MSC2010: 60K10, 62N05.

1. INTRODUCTION

Together the most common reliability distributions (exponential, Erlang, Weibull), there was also Pareto distribution which has applications not only in the economy (e.g. income of the population), but also to the study of lifetime of the systems k of n, as well as in field of quality assurance [5].

Pareto at the end XIXth century, formulated the principle of 80/20, of the unbalanced distributions, which postulates that 80% of the effects are generated by 20% of the cases.

This is the reason for introducing this new class of MaxParPS distribution with the aim of study the probability behavior of the most complicated processes.

The methodology and techniques of working are presented and analyzed in [2], which allows the study of the distribution of the maximum of a random sample of size Z of the statistical population that has Pareto distribution. Random variable (r.v.) Z has a distribution that is part of the power series distributions class (PSD, [1]).

The general problem of determining the distribution of the maximum and minimum of a random sequence will was solved by Louzada et al. in [3], with working tool of the generate function composing of the number of the r.v. of sequence with the survival function of the r.v. components of the sequence.

Instead, in this paper is approached, in a unitary manner, the distribution of the maximum of a sequence of independent Pareto distributed r.v. through the PSD class, distribution enjoyed by the number of the r.v. of the sequence.

The case of the minim was analyzed in [4] when it was discussed about the lifetime Min Pareto power series (MinParPS) distribution.

2. THE MAXPARPS DISTRIBUTION

We consider the r.v. $X_i \sim Par(\mu,\alpha)$, $\mu,\alpha > 0$, where $(X_i)_{i\geq 1}$ are independent and identically distributed random variables (i.i.d.r.v.), with the distribution function (d.f.)

$$F_{X_i}(x) = F_{Par}(x) = 1 - \left(\frac{\mu}{x}\right)^\alpha, \quad x \geq \mu \quad \text{and the}$$

probability density function (p.d.f.)

$$f_{X_i}(x) = f_{Par}(x) = \frac{\alpha\mu^\alpha}{x^{\alpha+1}}, \; x \geq \mu.$$

Also, we note by $U_{Par} = \max\{X_1, X_2,...,X_N\}$, where the r.v. $N \in PSD$, [1,2].

Proposition 2.1. *If r.v.* $U_{Par} = \max\{X_1, X_2,...,X_N\}$, *where* $(X_i)_{i\geq 1}$ *are i.i.d.r.v.,* $X_i \sim Par(\mu,\alpha)$, $\mu,\alpha > 0$ *and* $N \in PSD$, *with*

$$P(N = n) = \frac{a_n\theta^n}{A(\theta)}, n = 1,2,..., \quad \theta \in (0,\tau), \tau > 0,$$

r.v. $(X_i)_{i\geq 1}$ *and N being independent, then the d.f. of the r.v.* U_{Par} *is given by:*

$$U_{Par}(x) = \frac{A\left[\theta - \theta\left(\frac{\mu}{x}\right)^\alpha\right]}{A(\theta)}, x \geq \mu. \quad (2.1)$$

We note that r.v. U_{Par} following the MaxParPS distribution of parameters μ,α and θ by $U_{Par} \sim MaxParPS(\mu,\alpha,\theta)$.

Consquence 2.1. *The survival function of the r.v.* U_{Par} *is the following:*

$$S_{U_{Par}}(x) = \frac{A(\theta) - A\left[\theta - \theta\left(\frac{\mu}{x}\right)^\alpha\right]}{A(\theta)}, \quad x \geq \mu.$$

Consequence 2.2. *P.d.f. of the r.v.* U_{Par} *is characterized by the relationship:*

$$u_{Par}(x) = \frac{\alpha\theta\mu^\alpha A'\left[\theta - \theta\left(\frac{\mu}{x}\right)^\alpha\right]}{x^{\alpha+1} A(\theta)}, \quad (2.2)$$

for any $x \geq \mu$.

Proposition 2.2. *Hazard rate of the r.v.* U_{Par} *is given by:*

$$h_{U_{Par}}(x) = \frac{u_{Par}(x)}{1 - U_{Par}(x)}$$

$$= \frac{\alpha\theta\mu^\alpha A'\left[\theta - \theta\left(\frac{\mu}{x}\right)^\alpha\right]}{x^{\alpha+1}\left[A(\theta) - A\left[\theta - \theta\left(\frac{\mu}{x}\right)^\alpha\right]\right]}, \quad x \geq \mu.$$

Proposition 2.3. *If* $(X_i)_{i\geq 1}$ *is a sequence of independent Pareto distributed r.v., nonnegative, absolutely continous type, with the d.f.* F_{Par} *and* $N \in PSD$,

$$P(N = n) = \frac{a_n\theta^n}{A(\theta)}, n = 1,2,..., \; (a_n)_{n\geq 1} \qquad a$$

sequence of nonnegative real number,

$$A(\theta) = \sum_{n\geq 1} a_n\theta^n, \quad \forall \; \theta \in (0,\tau), \tau > 0, \text{ then:}$$

$$\lim_{\theta\to 0^+} U_{Par}(x) = (F_{Par}(x))^k, \quad x \geq \mu,$$

where $k = \min\{n \in N^*, a_n > 0\}$.

Proof: By applying the l'Hospital rule k-time, we have:

"HENRI COANDA"
AIR FORCE ACADEMY
ROMANIA

"GENERAL M.R. STEFANIK"
ARMED FORCES ACADEMY
SLOVAK REPUBLIC

INTERNATIONAL CONFERENCE of SCIENTIFIC PAPER
AFASES 2014
Brasov, 22-24 May 2014

$$\lim_{\theta \to 0^+} U_{Par}(x) = \lim_{\theta \to 0^+} \frac{A\left[\theta - \theta\left(\frac{\mu}{x}\right)^\alpha\right]}{A(\theta)}$$

$$\overset{\frac{0}{0}}{=} \lim_{\theta \to 0^+} \frac{\left(1 - \left(\frac{\mu}{x}\right)^\alpha\right)^k A^{(k)}\left[\theta - \theta\left(\frac{\mu}{x}\right)^\alpha\right]}{A^{(k)}(\theta)}$$

$$= \frac{\left(1 - \left(\frac{\mu}{x}\right)^\alpha\right)^k k! a_k}{k! a_k} = \left(1 - \left(\frac{\mu}{x}\right)^\alpha\right)^k, \quad x \geq \mu.$$

□

Consequence 2.3. *The rth moments, $r \in N$, $r \geq 1$ of the r.v. $U_{Par} \sim MaxParPS(\mu, \alpha, \theta)$ is the following:*

$$EU_{Par}^r =$$

$$= \sum_{n \geq 1} \frac{a_n \theta^n}{A(\theta)} \cdot E[\max\{X_1, X_2, ..., X_N\}]^r, \quad (2.3)$$

where p.d.f. of the r.v. $\max\{X_1, X_2, ..., X_N\}$ is given by

$$f_{\max\{X_1, X_2, ..., X_N\}}(x) = z f_{Par}(x)(F_{Par}(x))^{n-1}.$$

Proof: It is known that the distribution function of the maximum of a sample of size $N = n$ which has the d.f. F_{Par} is $U_n(x) = (F_{Par}(x))^n$.

With total probability formula, a d.f. of the maximum of a sequence of i.i.d.r.v. in a random number, has the expression:

$$U_{Par}(x) = \sum_{n \geq 1} U_n(x) \cdot P(N = n)$$

$$= \sum_{n \geq 1} (F_{Par}(x))^n \cdot P(N = n).$$

By determining the derivative of the latter relation in connection with x, we obtain:

$$u_{Par}(x) =$$

$$= \sum_{n \geq 1} n f_{Par}(x)(F_{Par}(x))^{n-1} \cdot P(N = n) \quad (2.4)$$

where $z f_{Par}(x)(F_{Par}(x))^{n-1}$ is the p.d.f. of the r.v. $\max\{X_1, X_2, ..., X_N\}$. By applying the mean of the relationship (2.4), the relationship (2.3) is obtained.

□

3. POISSON LIMIT THEOREM FOR MAXPARPS DISTRIBUTION

The study of special cases of distributions MaxParPS is necessary for this section because we want to study under what conditions the Max-Pareto-Binomial zero truncated (MaxParB) distribution, respectively, Max-Pareto-Poisson zero truncated (MaxParP) distribution are approximate.

The d.f. of the MaxParB is defined by (2.1), where $N \sim Binom^*(n, p) \in PSD$, $n \in \{1, 2, ...\}$, $p \in (0, 1)$ and $A(\theta) = (1 + \theta)^n - 1$, where $\theta = \frac{p}{1-p}$, namely:

$$U_{ParB}(x) = \frac{\left(1 - p\left(\frac{\mu}{x}\right)^\alpha\right)^n - (1-p)^n}{1 - (1-p)^n}, \quad (2.5)$$

for any $x \geq \mu$.

A r.v. which admits the d.f. according to the relationship (2.5), is denoted by

"HENRI COANDA"
AIR FORCE ACADEMY
ROMANIA

"GENERAL M.R. STEFANIK"
ARMED FORCES ACADEMY
SLOVAK REPUBLIC

INTERNATIONAL CONFERENCE of SCIENTIFIC PAPER
AFASES 2014
Brasov, 22-24 May 2014

$U_{ParB} \sim MaxParB(\mu, \alpha, n, p)$, $\qquad \mu, \alpha > 0$, $n \in \{1,2,...\}$, and $p \in (0,1)$.

P.d.f. of the r.v. U_{ParB} is defined according to the relationship (2.2), so that :

$$u_{ParB}(x) = \frac{np\alpha\mu^{\alpha}\left(1 - p\left(\frac{\mu}{x}\right)^{\alpha}\right)^{n-1}}{x^{\alpha+1}\left(1 - (1-p)^n\right)}, \quad (2.6)$$

for any $x \ge \mu$.

At the same time, the MaxParP distribution is characterized by the d.f. defined by the relationship (2.1), where $N \sim Poisson*(\lambda) \in PSD$, $\lambda > 0$ and $A(\theta^*) = e^{\theta^*} - 1$, with $\theta^* = \lambda$:

$$U_{ParP}(x) = \frac{e^{-\lambda\left(\frac{\mu}{x}\right)^{\alpha}} - e^{-\lambda}}{1 - e^{-\lambda}}, x \ge \mu. \quad (2.7)$$

and p.d.f.. according to the relationship (2.2):

$$u_{ParP}(x) = \frac{\alpha\lambda\mu^{\alpha}e^{-\lambda\left(\frac{\mu}{x}\right)^{\alpha}}}{x^{\alpha+1}\left(1 - e^{-\lambda}\right)}, x \ge \mu. \quad (2.8)$$

D.f. of (2.7) characterizes the distribution of the r.v. will we note thus: $U_{ParP} \sim MaxParP(\mu, \alpha, \lambda)$, $\mu, \alpha, \lambda > 0$.

Under the above conditions, takes place the following result:

Theorem 3.1. (Poisson Limit Theorem) *If r.v.* $U_{ParB} \sim MaxParB(\mu, \alpha, n, p)$, *with* $n \to \infty$ *and* $p \to 0^+$ *such that* $n \cdot p \to \lambda$, $\lambda > 0$, *then:*

$$\lim_{\substack{n \to \infty \\ p \to 0^+}} U_{ParB}(x) = U_{ParP}(x), \forall x \ge \mu,$$

where $U_{ParB}(x)$, *respectively* $U_{ParP}(x)$, $x \ge \mu$ *are d.f. of the r.v.* $U_{ParB} \sim MaxParB(\mu, \alpha, n, p)$, *respectively* $U_{ParP} \sim MaxParP(\mu, \alpha, \lambda)$, *defined by the relationship (2.5) and (2.7).*

Proof. By calculating separately two elementary limits:

$$\lim_{\substack{n \to \infty \\ p \to 0^+}} (1 - p)^n = \lim_{\substack{n \to \infty \\ p \to 0^+}} \left[(1-p)^{-1/p}\right]^{-pn} = e^{-\lambda}$$

and

$$\lim_{\substack{n \to \infty \\ p \to 0^+}} \left(1 - p\left(\frac{\mu}{x}\right)^{\alpha}\right)^n = e^{-\lim_{\substack{n \to \infty \\ p \to 0^+}} p\left(\frac{\mu}{x}\right)^{\alpha} n} = e^{-\lambda\left(\frac{\mu}{x}\right)^{\alpha}},$$

we have the following final limit:

$$\lim_{\substack{n \to \infty \\ p \to 0^+}} U_{ParB}(x) =$$

$$= \lim_{\substack{n \to \infty \\ p \to 0^+}} \frac{\left(1 - p\left(\frac{\mu}{x}\right)^{\alpha}\right)^n - (1-p)^n}{1 - (1-p)^n}$$

$$= \frac{e^{-\lambda\left(\frac{\mu}{x}\right)^{\alpha}} - e^{-\lambda}}{1 - e^{-\lambda}} = U_{ParP}(x), \ \forall x \ge \mu.$$

$\square$

Remark 3.1. Poisson limit theorem for the distribution MaxParPS is confirmed visually of the plot in Figure 1, where they are presented p.d.f. of the MaxParB and MaxParP

"HENRI COANDA"
AIR FORCE ACADEMY
ROMANIA

"GENERAL M.R. STEFANIK"
ARMED FORCES ACADEMY
SLOVAK REPUBLIC

INTERNATIONAL CONFERENCE of SCIENTIFIC PAPER
AFASES 2014
Brasov, 22-24 May 2014

distributions for the following parameters:
$\mu = \alpha = 1$, $n = 20$, $\lambda = 10$ and $p = 1/2$.
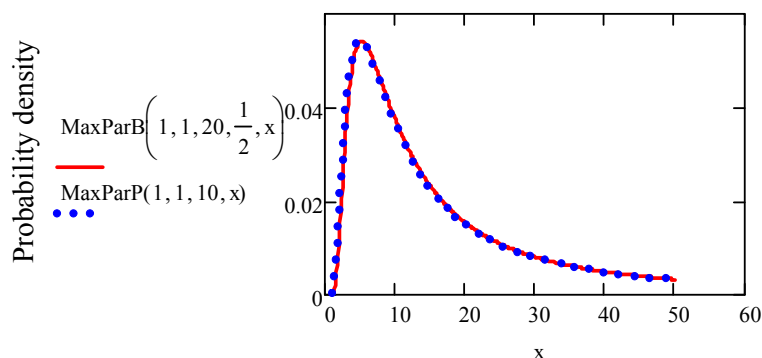
Fig.1. P.d.f. of the MaxParB and MaxParP distributions

REFERENCES

1. Johnson, N.L., Kemp, A.W. Kotz, S. (2005) .*Univariate Discrete Distribution*, New Jersey.
2. Leahu, A., Munteanu, B. Gh., Cataranciuc S. (2013). *On the lifetime as the maximum or minimum of the sample with power series distributed size,* Romai J., Vol. 9, No.2, 119 -128 .
3. Louzada, F., Bereta, M. P.E., Franco, M.A.P. (2012). *On the Distribution of the Minimum or Maximium of a Random Number of i.i.d. Lifetime Random Variables,* Applied Mathematics, 3, 4(2012), p. 350-353.
4. Munteanu, B. Gh. (2014). *Distribuția duratei de viată Min-Pareto,* Conferința Științifică Internațională Modelare matematică, optimizare și tehnologii informaționale, MMOTI 2014, Chișinau, p. 147-153 .
5. *** http://www.e-birouvirtual.ro/node/3813 (aprilie 2014).

Applied Mathematics,IT&C

USER AUTHENTICATION TO A WEB SITE USING FINGERPRINTS

Mihai Lica PURA

Faculty of Military Electronic and Information Systems, Military Technical Academy, Bucharest, Romania

Abstract: *Nowadays, authenticated access to web sites becomes more and more important. Usernames and passwords are one of the easiest ways to accomplish it. But a more secure approach is to use biometrics. This article presents a very simple modality to use fingerprints to control the access to a web site. The client component of the proposed architecture is an ActiveX control that communicates with the fingerprint reader and sends data back to the web server. The server component is an ISAPI Server that processes the requests of the client regarding authentication and does or does not grant access to the web site. The ActiveX is integrated in the web page with the help of Java Script.*

Keywords: *web site authentication, biometrics, fingerprint*

1. INTRODUCTION

Since its creation, Word W ide W eb (WWW) ha s continued to grow and to im pact the everyday life of pe ople ([1]). News, m ail, banking, storage, and so on, are all provided as web services through some web sites. But such important services can be used with confidence only if they also provide the necessary security. The five m ost im portant security objectives are authenticatio n, confidentiality, integrity, non-repudiation, and availability. For the web servers and for the communication between the client applications and the web servers, all these ob jectives (web server au thentication by the user, confidentiality and integ rity of the e xchanged data, availability of the server) were addressed and accomplished mainly by using Public Key Infrastructure (PKI) and cryptographic operations through protocols like TL S (Trusted L ayer Secu rity) o r SSL (Secure

Sockets Layer) ([2]). But so far, authentication of the users is still m ostly based on c redentials of type username and password.

While this type of authentica tion can assure the n eeded confidence, still it has som e disadvantages that can dr astically diminish the provided security. In this article we present the use of biometrics to pro vide authen tication to critical web sites like the one described above, with the purpose of eliminating the disadvantages of using passwords. The idea is not new. But the solutions that can be found are only a few ([3, 4, 5]), and all of the m are proprietary solutions. This means that they ar e not free, and that they have to be integrated in the web s ite that will u se them, which is no t always easy to do. So we have proposed to develop an open source web site authentication solution based on fingerpri nts, and to use it to provide authentication add-ons to the m ost common CMSs (Content Management Framework) that are used for publishing web

content, like Joomla, Silverstipe and Drupal, in order to simplify their use and to ease their spreading.

The rest o f the paper is o rganized as follows. In the second section we present the disadvantages of using password based authentication, the advantages of using biometrics and th e arch itecture of our authentication solution. The third section gives some im plementation details f or the components of our solution. The last section contains the conclusions and our future work directions.

2. THE ARCHITECTURE OF THE AUTHENTICATION SYSTEM

We will sta rt b y presen ting the disadvantages of using username/password pairs for user authentic ation. The first obvious disadvantage is th e fact that the pas sword has to be remembered by the user, because writing it down would be insecure, so the users tend to choose easy to rem ember strings of characters that can be guessed by attackers or can be subject to dictionary attacks. One solution to this problem would be the use of password management applications ([6]), but few people have the necessary knowledge and training to manage and use this kind of software. Also, many of such applications have been proved error prone, so using them is not necessary the best choice.

The second disadvantage of using usernames and passwords is the fact that any person who knows the usernam e and the password of a user can authenticate to the web server. For the legitim ate user it is dif ficult to realize that som eone el se has the password, until unw anted ope rations ar e alr eady performed by the m alicious part, when, of course, it is too late. C ountermeasures to this issue ex ist. They consist in e nforcing a password change policy by the web server, and/or the use of user activity logs. Changing the password on a regular basis will assure that if a m alicious pa rt has entere d in th e possession of a password, it will not have tim e to use it. Also, by consulting the a ctivity lo g for his own account, the legitim ate user can see if so meone else has su ccessfully

authenticated to the server from a different location, or at a different moment of tim e. Of course, this m eans that the legitim ate user has to keep track of the IP she uses, and of the times it has authentica ted to the s erver. But most of the users are not trained to perform these actions, or they n eglect them because of the extra operations involved.

The use of biom etrics in general and of fingerprints in particul ar addresses both of these problem s. First of all, the user does not have to remem ber anything that is to be kept secret. A usernam e is still being used, but it is public inf ormation. Second, only the legitimate user will be authenticated to the web server, because no one else can have her biometric data.

We will now continue with the presentation of our proposed authentication framework. In a typical scenario for access ing a web site there are two com ponents: the web server and the client application. The client component is usually a web browser and it runs on the client m achine, which is the personal computer of any user who wants to access the web site. T he server com ponent runs on a rem ote m achine and answers the client's req uests. For an authenticated acces s to a web site, the client, prior to accessing the web pages served by the server, needs to transmit to the serv er a secret on ly knew by the two of them, that uniquely ide ntifies he r. Typically, this secret is a usernam e-password pair. Based on the c lient's identity established in this way by the w eb server, the server knows wha t pages the c lient is entitled to request.

The password is entered by the client in a text box of the sign up page and then transmitted to the server as any othe r information from a web for m. But when using fingerprints, we need one m ore c omponent. That is because the fingerprint reader has to be accessed b y the web page to get the information it generate s about the fingerprint that it has scanned. This com ponent has to run on the clien t m achine, because the fingerprin t reader is attached to it, but also needs to communicate with th e serve r to send th e credentials of the clien t who wants to authenticate.

"HENRI COANDA"
AIR FORCE ACADEMY
ROMANIA

"GENERAL M.R. STEFANIK"
ARMED FORCES ACADEMY
SLOVAK REPUBLIC

INTERNATIONAL CONFERENCE of SCIENTIFIC PAPER
AFASES 2014
Brasov, 22-24 May 2014

In conclusion, the proposed authentication framework has three com ponents: the web server, the web page that runs in a browser and the client application accessing the fingerprints reader. W e will p resent all thes e com ponents in the following sections.

2.1 The Ac tiveX client component. The technology that we have chosen to create the client side component responsible of accessing the fingerp rints read er is ActiveX. Presenting the ActiveX technology and the developm ent of ActiveX com ponents is out of the scope of this paper. For more information on this please see ([7]).

We have defined a single m ethod for our ActiveX component. This m ethod displays a modal window. The window has an edit box component for entering the usernam e, a label for displaying the error or the success messages and three buttons. One of the buttons is for exiting. The other tw o buttons correspond to the two actions necessary for a biometric authenticatio n. The firs t step is th e enrollment of the user. For this we have settled the *Enroll* button. T his operation is only required to be taken one tim e, and one tim e only. That is at the re gistration of the user. Then, every tim e the user wants to authenticate, he has to use the *Verify* button.

In the enro ll ope ration, the fingerprints reader gets a tem plate of the user's f ingerprint that will be store in th e database of the server. Then, each tim e the authentication process takes place, the fingerp rint take n by the read er is ve rified agains t th e tem plate sto red in th e database. If they m atch, the user is authenticated with th e ente red us ername. If they do not m atch, the verification fails. After performing verification, the m odal window returns 0 or 1, depending on the success of the operation (0 if verification failed and 1 if it was succes sful). The scrip t that uses th is

ActiveX will use the result to g rant access to the web site or not.

2.2 The web page.
To use this ActiveX component, it has to be placed on the login page of the target web site. This is done by using the HTML tag *object*.

Here is an example:

```
<object
    id="BioAuthCtrl"          name="BC"
classid="clsid:9F1EAE3D-C2E8-4171-BB80-
D62B91F5B0FE"              height="300"
VIEWASTEXT style="width: 530px">
</object>
```

After this, the objec t c an be used in the JavaScript f rom the page through its nam e, "*BC*" in our example.

Let us p resume that w e have asso ciated a function *f()* with the *onclick* event for a sign up button on a login web page of a web site. To use our ActiveX f or fingerprint authentication, the JavaScript code would be:

```
function f(){
    var x=BC.enroll();
    if(x == 1)
        // grant access to the site
    ...
    if(x==0)
        // forbid access to site
        ...
}
```

2.3 The server component. The serve r side component was build using IS API Server technology (Internet Server Application Programming Interface). The communicatio n between the two com ponents wa s implemented using *CGatwayInterface* implementation of the *WinInet API* provided in

[8]. Presenting the ISAPI Server technology and its programming is out of the scope of this paper. For f urther inform ation please consult [9].

The ISAPI Server we have im plemented can process the following three requests: *storeTemplate*, *saveTemp* and *performVerify*.

The prototypes of th e three reque sts a re provided below, using a hypothetical exam ple for the URL of the target web site:

http://my.site.com/BioAuthServer.dll?saveTem p&template="string_template_part1"&usern ame="string_username"

http://my.site.com/BioAuthServer.dll?perform Verify&template="string_template_part2"&u sername="string_username"

http://my.site.com/BioAuthServer.dll?storeTem plate&template="string_template"&usernam e="string_username"

The *storeTemplate* request sav es the template of the user's f ingerprint in th e database of the server, associating it with the corresponding usernam e, also sent by the client. It is used in the user enrollment phase.

The other two requests, *saveTemp* and *performVerify*, are used in the user authentication phase. T he verification process has been broken into two parts. This was necessary because of the maximum data length that can be tr ansmitted in a *WinInet* communication, which is 1024 kilobytes. The fingerprint's data nece ssary for v erification against th e tem plate exceed this m aximum size. That is why the data are sent in two parts: *saveTemp* request sends the f irst 1024 kilobytes of the fingerprint's data, and *performVerify* sends th e las t kilob ytes of it. When handling a *performVerify* request, the web server concaten ates the two parts of the data of the fingerprint and perfor ms verification. It then a nswers to the c lient telling it if the ver ification was successful or not.

3. IMPLEMENTATION DETAILS

To sim plify our implem entation, the database of the users' f ingerprints tem plates was constructed as a directory of files. At the enrollment phase, a file is created for each user, using the corresp onding usernam e sent by the client. This file contains the template of the fingerprint received from the fingerprint reader.

When the *saveTemp* request is perfor med, the ISAPI Server save s the first part of the fingerprint's tem plate a s a tem porary f ile. If *storeTemplate* request follows, the final template f ile is build f rom the temporary f ile and the second part of the tem plate. W hen *performVerify* request is perform ed, the username passed to the server is used to search for the f ile that s tores the respective tem plate. If the f ile does not exis t, the verif ication fails. If the f ile exists, it is o pened and the tem plate is read f rom it. Then the tem plate rec eived from the client is ve rified aga inst the tem plate stored by the web server. If they match, the verification is succe ssful. Other wise, th e verification fails.

One thing that we have to have in m ind is that these three requests are in form of strings. This m eans that the template s (tha t are bina ry data) are first serialized by the clie nt ActiveX and only after that they are sent to the server as HTTP requests. At the server side th e deserialization takes place, obtaining the binary data.

To protect the data exchanged between the client and the web server, th e serialized fingerprints data are fi rst encrypted with a session key previously com puted by the two parts. To e liminate the possib ility of reply attacks, th e salted en cryption is used. Of course, at the server sid e de cryption is performed prior to a ny other processing. Because of the fact that encrypted data is binary data, it is enc oded as a BASE64 string. The use of HTTPS is also highly recommended.

The ActiveX com ponent needs to have access to th e local reso urces of the com puter the web browser is running on. Only this way it will be able to c ommunicate with th e fingerprints read er. To authen ticate th e ActiveX component to the user, it will be digitally signed. This way the use r will be able to check if the applica tion that tr ies to ac cess

"HENRI COANDA"
AIR FORCE ACADEMY
ROMANIA

"GENERAL M.R. STEFANIK"
ARMED FORCES ACADEMY
SLOVAK REPUBLIC

INTERNATIONAL CONFERENCE of SCIENTIFIC PAPER
AFASES 2014
Brasov, 22-24 May 2014

the fingerprints reader is really the one used in the web server authentication process.

So far we did not m ention anything about the biom etric specific f unctions. We will skip this information becau se these functions are highly dependent to the fingerprint reader. But, generally, these functions are part of an API that com es toge ther with th e dr iver of the reader. The im portant thing is that it is ver y easy to configure the ActiveX component to use the fingerprints reader desired by the user.

4. CONCLUSIONS

In this paper we have presented a web site authentication framework based on fingerprints. We have described the need for an alternative to clas sical password based authentication, at least regarding critical web sites like the ones used for e-banking, and e-mail. We also highlighted the advantages of using biom etric credentia ls in ge neral, and fingerprints in particular.

The presented fram ework has som e drawbacks that we inten d to solve in the near future. The most obvious one is the fact that the tem plate's da tabase is pr imitive. This aspect can be im proved by using a relational database server, like Mi crosoft SQL Server, or MySQL. Regarding hum an-computer interaction, the ActiveX window must be split in two separate windows: one for the enrollment phase, and one for the verifica tion phase. The two operations have total separate flows, so the separation of the windows is necessary.

Another possible im provement is the replacement of the ISAPI Server with an ISAPI Filter. This way the configuration of the authentication process at the serve r leve l will be easier to make.

After addres sing all th ese aspects, w e will develop fingerprint auth entication add-ons for the most used web content CMSs, like Joom la, Silverstripe and Drupa l, and we will m ake them available on the corresponding web pages of these tools. This way, fingerprint authentication will be e asy to add to any web site created with one of them.

We would like to thank to engineer Florin Panta who participa ted to the im plementation of the presented framework by the work he has done for his diploma paper.

REFERENCES

1. Ti m Berners-Lee, *Information Management: A Proposal*, CERN, 1989, [online]. Available: http://info.cern.ch/Proposal.html (F ebruary 2014).
2. The Tr ansport Layer Security (TLS) Protocol Version 1.2 RFC 5246, [online]. Available: http://datatracker.ietf.org/doc/rfc5246/ (February 2014).
3. BIO-Key, W EB-KEY, [online]. Available: http://www.bio-key.com/products/overview-2/web-key (February 2014).
4. Plurilo ck Security Solutio ns Inc. , FINGERPASS, [online]. Availab le: http://plurilock.com/products/fingerpass (February 2014).
5. DigitalPersona, DIGITALPERSONA ONLINE, [online]. Available: http://www.digitalpersona.com/Authenticat ion-Solutions/DigitalPersona-Online/DigitalPersona-Online/ (February 2014).

6. Gaw, Shirley, Edward W. Felten, *Password management strategies for online accounts,* Proceedings of the second symposium on Usable privacy and security, ACM, 2006.

7. Kedar Gore, *A Complete Web ActiveX Control*, [online]. Available: http://geekduo.com/geekduo/2011/11/a-complete-web-activex-control-part-i/ (February 2014).

8. Steve Zimmer man, *Designing ActiveX Components Part II: Implementing Internet Communication with WinInet*, Microsoft Interactive Developer, 1997.

9. The ISAPI Developer's Site, [online]. Available: http://www.genusa.com/isapi/isapitut.htm (March 2014).

"HENRI COANDA"
AIR FORCE ACADEMY
ROMANIA

"GENERAL M.R. STEFANIK"
ARMED FORCES ACADEMY
SLOVAK REPUBLIC

INTERNATIONAL CONFERENCE of SCIENTIFIC PAPER
AFASES 2014
Brasov, 22-24 May 2014

IDENTITY-BASED CHRYPTOGRAPHY: FROM PROPOSALS TO EVERYDAY USE

Mihai Lica PURA, Victor Valeriu PATRICIU

Faculty of Military Electronic and Information Systems, Military Technical Academy, Bucharest, Romania

Abstract: Since the invention of public key cryptographic algorithms, researchers have also proposed what will later be known as identity based cryptography: the use of identities as public keys. Over the years, different identity based encryption and signature algorithms were developed, making possible what others only predicted some 30 years ago. This paper is a survey over what identity based cryptography is, what advantages it has over classical PKI, what success stories of its use already exists, and on how can one benefit from it, in different civilian and even military scenarios. The purpose of the paper is to set a background for latter research on developing an identity base cryptographic scheme for military use.

Keywords: identity based encryption, identity based cryptography, public key cryptography

1. INTRODUCTION

Identity-based cryptography is a particular case of public key cryptography that in certain conditions offers implementation and utilization advantages, without reducing the security degree. In a conventional public key security scheme, the generation of the two keys (the private key and the public key) starts from an unpredictable randomly chose large number. This leads to two random keys mathematically bounded. Given the random character of the public key, it cannot be given as is to the interested users because it would be very difficult to store and to use. That is why the certificates are use to bind the key to the user and to the issuing certification authority. The necessity of the certificates determines, prior to any communication, the need to search for the qualified certificate of the person someone would like to securely communicate with and to validate this certificate in order to make sure that it belongs to the other party.

But what if the public key can be chosen? This is the determinant characteristic of identity-based cryptography (IBC): the public key is no longer random, but a piece of information regarding the identity of the user ([1]). For example, the whole name, the e-mail address or the home address can all be use as a public key. The chosen information should comply with some rules like: the information should be uniquely bound to a user, the information should be bound in such a way that the users cannot later deny, and, of course, this information should be publicly available.

In this paper we will present the general problematic of identity based cryptography, with an emphasis on its possible applications, especially in military organizations. The rest of the paper is organized as follows. The second section presents the mathematical backgrounds of identity based cryptography.

In the third section the curren t state of the art of IBC is described, based on the published RFCs. The fourth s ection presents the costs of using such schem es, de monstrating the superiority of IBC over classical PKI. The fifth section dis cuses th e security of the IBC schemes, taking into consideration the possible attacks and countermeasures. The sixth section presents som e possible applications of IBC, and also the m ilitary relev ance of such schemes. The last section con tains som e conclusions and future work directions.

2. CHARACTERISTICS OF IDENTITY-BASED CRYPTOGRAPHY

The users of an identity-based cryptography schem e can derive their public key star ting f rom the value of an identity element, which, m ost of the tim e, is an ASCII value ([1]). After the public key is chosen, the corresponding private key m ust be generated. If a user could generate they own private key for the public key they have chosen, then they could generate the priv ate key for any other user of the s ame security schem e, because the public keys are public. If this would happen, the security would be compromised. T hat i s why the private key can only be generated by a specially designated key generation centre (KGC). The KGC has also a pair of keys: a public and a priv ate o ne. Starting from the identity of a user (which is also the user's public key) and using its private key, the KGC computes the private key of every user.

From a m athematical point of view, identity-based cryptography is a particular form of pairing based cryptography. The IBC cryptosystem is build based on pairing between elem ents of a group to a s econd group. The pairing can be regarded also as a mapping from elements from the first group to elements from the second group. This way, a hard problem in one gr oup is reduced to an easier problem in the other.

An identity -based cryp tographic schem e consists out of four algorithms ([2]):

• Setup algorithm is run only one tim e by the KGC. In this step the private and public key pair of the KGC is created along with the others parameters of the scheme.

• Key generation algorithm is run by the KGC for e very user that asks for its private key. The re sult is the p rivate key o f this use r and it is transmitted to it.

• Encryption algor ithm uses the iden tity of a node (its public key) to encrypt a m essage for this node.

• Decryption step is perform ed at the receiving node: using its private key the node decrypts the encrypted m essage and obtains the clear message.

Besides these four algorithm s, others aspects sho uld be take n into cons ideration. When a user asks for a private key, the KGC must authenticate the us er to be sur e that they are not im personating another one in order to find out they private key. If the authentication succeeds, th e priva te ke y m ust be transm itted to the u ser on a secu re channel in order to avoid eavesdropping by a m alicious user ([3]). Such secure side channels can be Bluetooth of Infrared channels.

We will now present the advantages of IBC schemes. The first and the m ost obvious advantage o f this secu rity schem e is that the users can securely communicate by encrypting and/or signing messages without the prior need of exchanging public keys through the exchange of certificates ([4]). This way, there is no longer need for a certificate distribution infrastructure (PKI). Another advan tage is th at if the certificates are no longer needed, th e certificate validation step is als o m issing because there is no need to check if the public key really belongs to the user by checking the signature of the c ertification author ity ([4]). This is an im portant advantage because the validation of the user's certificate would imply the validation of the whole certificate path.

IBC schem es ha ve also som e disadvantages. We will briefly present them in the following paragraphs.

The m ain disadvantage of the schem e is that the KGC knows (can compute) the private keys of all de users ([5]). If it is com promised, the security of communications can be questioned. This m eans that the users should trust the KGC that their keys will no t be made available to others. This disadvantage can be eliminated in m any m anners. If all the users are known prior to the start of the communication and no other user will be

"HENRI COANDA"
AIR FORCE ACADEMY
ROMANIA

"GENERAL M.R. STEFANIK"
ARMED FORCES ACADEMY
SLOVAK REPUBLIC

INTERNATIONAL CONFERENCE of SCIENTIFIC PAPER
AFASES 2014
Brasov, 22-24 May 2014

joining after, than the KGC is no longer needed. If there is no need for a private key revocation m echanism than the KGC can be destroyed and the private keys of the users will be safe. Another way of solving this problem is to replace a cen tralized KGC with sev eral KGC in such a way that all are needed to participate in order to generate private keys ([5]).

3. CURRENT STATE OF THE ART IN THE FIELD

In this moment there are over 400 scientific publications on IBC. IBC m athematics is being standardized in IEEE 1363.3 (6). The interest of the In ternet Comm unity in this matter and thus the belief of the sp ecialists in identity-based cryptogra phy can be also seen from the RFCs publish ed. The total number of RFCs that handle aspe cts of identity -based cryptography is four.

The first one dates from August 1995 and proposes "An identity -based Cry ptographic Protocol for Authen ticated Key Exchange" (RFC1824) ([7]). The authors of this RFC describe "the basic m echanisms and functions of an identity-b ased s ystem f or the secur e authenticated exchange of cryptographic keys, the generation of signatu res, and th e authentic distribution of public key".

The second RFC is na med "Identity-based cryptography standard (IBCS) #1: supersingular curve implementations of the BF and BB1 cryptosystem s" (RFC5091) ([8]). It was published in December 2007 and was a proposal for an Identity -Based Cryptographic Standard (IBCS#1). It describes the algorithms that im plement two kinds of id entity-based encryption: Boneh-Fran klin (BF) and Boneh-Boyen (BB1).

The third RFC is "Iden tity-Based Encryption Architecture and Supporting Data Structures" (RFC5408) ([9]) and it was published in January 2009 and describes a security architecture required to implem ent identity-based encryptio n and defines the data structures that can be used to im plement the technology.

The forth RFC "Using the Boneh-Franklin and Boneh- Boyen Iden tity-Based Encryption Algorithms with the Cryptographic Message Syntax (CMS)" (RFC5409) ([10]) was published in January 2009. It describes the conventions for using iden tity-based encryption algorithm s (BF and BB1) in the Cryptographic Message Syntax (CMS) to encrypt co ntent encry ption k eys. It also defines the object identi fiers (OIDs) and the convention for encoding a recipient's identity.

By analyzin g these RFCs one can see th at although identity-based encryption was not shown that much attention, lately it becam e a relative d ebated sub ject. It is inter esting to observe that the last three RFCs was published by e mployees of Voltage Security, a corporation that has implem ented and now offers secur ity solution s based on iden tity-based enc ryption. These id entity-based encryption solutions focus on infor mation encryption for e-m ails, files, docum ents and databases.

Another corporation that invested into identity-based cryptography is Gemalto which developed the first sm artcard im plementation of identity-based encryption. The implementation is based on the Boneh-Franklin algorithm . From the adv antages of this new so lution the most im portant aspe cts are th at th e encry ption of the confidential messages is m ore secure, m ore user-friend ly and m ore m anageable by large corporations and telecom operators. Of course, the

smartcard solution was developed in collaboration with Voltage. The advantages that identity-based en cryption b rings to th e smartcards are: more protection for the private keys, strong authenticat ion for the end-users, and sim plicity of the encryption process for users and also for telecom operators.

4. COSTS CONSIDERATION

Ferris Research conducted an analysis of IBC at the end of 2008 and observes that the interest f or identity-ba sed cryptos ystems is growing. F erris looked on the cost of the security solution proposed by Voltage and concluded that the total cost of ownership of a typical iden tity-based cryptograph ic system is one third of a typical public key system . In the same research o ther inte resting results emerged. We will briefly present some of them ([11]).

The infrastructure r equired by an identity-based encryption system is far simpler than the one needed by a PKI solution. This m eans that fewer servers are required and the installations are m uch easier. The operating costs of the Voltage IBC system were one-fifth of those of public key s ystems, and the use rs o f identity-based encryption system s wer e m ore productive that the users of typical cryptographic systems.

These consideration su ggest th at identity based cryptography is a good candidate for extending its use becaus e not only that it leads to higher profit for the providing com panies, but it also determ ines higher productivity for the users. W e believe that th is win-win situation will conduct to a high spread f IBC cryptosystems. The only difficulty so far is the lack of regulations on this matter.

5. SECURITY CONSIDERATIONS

Boneh and Franklin gave the first for mal definition of security f or identity -based encryption ([12, 13]). In an attack defined by them, the malicious user can choose the target identity in an adaptive m anner, based on the master public key and any other keys that they had already obtained. These schem es are

called "fully secure". Another notion was introduced by Canetti. It is ca lled selec tive-identity sec urity bec ause it requ ires f or the malicious user to spec ify the targe t identity in advanced, before the m aster public key is published. This last schem e is considered weaker by the research comm unity ([13]). Based on these definitions of security as countermeasures for different kinds of attacks, the researchers proposed satisfying identity-based encryption schemes.

Another way to form alize notions of security for the cryptographic schem es in general and f or the identity-bas ed cryptography in particul ar is con sidering the combinations between various security goals and possible attack m odels ([13, 14]). There are four es sential secu rity goals and three important attacks that should be taken into consideration:
• The security goals are: "one-wayness", "indistinguishability", s emantic security an d non-malleability.
• The attack models are: chosen plaintext attack, non-adaptive chosen cipher text attack and adaptive chosen cipher text attack.

From the rela tions b etween a ll these security objectiv es and attack m odels ra ise different se curity scena rios th at we re stud ied by the researchers.

If the alg orithms are im plemented on cryptographic devices th ere are a num ber of specific attacks like the power analysis attack ([15]). This kind of at tack con sists in two phases: data acquisition phase and data analysis pha se. In the f irst phase th e atta cker collects data of the power consum ption of the devices while it operates. The second phase consists in analyz ing the collec ted data in order to retrieve secr et inform ation. Another attack specific when using cryptographic devices is fault attack ([15]). In this attack th e malicious user disrupts in som e way the normal execution of the device in order to obtain faulty output.

An aspect more closely related to the identity-based cryptogr aphy is the efficient implementation of pairings ([16, 17]). This is important both from t he point of view of security (p airing bein g a central part of identity-based re lated algo rithms) and applications (pairing should be efficiently

"HENRI COANDA"
AIR FORCE ACADEMY
ROMANIA

"GENERAL M.R. STEFANIK"
ARMED FORCES ACADEMY
SLOVAK REPUBLIC

INTERNATIONAL CONFERENCE of SCIENTIFIC PAPER
AFASES 2014
Brasov, 22-24 May 2014

computable on resource constrained devices). Attackers can adapt the us ed attacks to pairin g ([15]). Research showed that it is possible to obtain important information this way, but has also showed specific counterm easures. Researchers have also highlight som e open problems is this field : curve param eterization attacks, sp ecial poin t attacks and high-order power attacks. They were called open problems because th ey were not s ufficiently researched or were not researched at all. So their real destructive potential is unknown.

6. APPLICATIONS OF IBC

6.1 General applications. From a practical and scientific point of view, there are some special app lications of ide ntity-based cryptography. The m ost common one is the identity-based encryp tion. All of th e prev ious examples were based on it. The possible applications of identity-b ased encryption would have to be in dom ains that can profit out of its advantages over public key system s and do not m ind or can overcom e the disadvantages. The m ost obvious system s that can be secu re with th e help of iden tity-based encryption are the system s in with communication are based on identity. In an e-mail system the m essages target a s ingle recipient. The e-mail address is unique and its owner should be the only one that receives the message. So, using it as a public key in an identity-based encrypti on schem e would be a natural thing to do. Th e m essage is sent directly (the sender doe s not have to look for or valid ate the certificate of the recipient) th e software does the encryption in a user transparent m anner. The sam e discussion can be applied to GSM co mmunication system s. The telepho ne num ber of each user is unique

in the whole world. So it can be used as a public key in order to reach end-to -end user security. The solution implem entation would naturally d ress the ex isting inf rastructure. All the communication between devices can be encrypted this way too, using as public key the IP address of the device.

Relatively recently researchers showed that identity-based cryptogr aphy can also be used for e-signature in a schem e based on error-correcting codes, thus providing m eans for identification ([18]).

There is another appl ication th at take s identity-based encryp tion one step further: Fuzzy Identity-b ased E ncryption ([19]). The idea is to replace the identity ASCII value used as public keys with a set of descriptiv e attributes (o f a certain biometric: fingerprint, iris, v oice, f ace, etc). T his attributes are us ed as a public key in orde r to encryp t m essages for the respective user. The main difference of this solution is that the priva te key is de rived from that b iometric to o. The erro r-tolerance property of Fuzzy-Ide ntity-based encryption allows for a private key (derived from a measurement of the same biometric) to decrypt that m essage even if it was encryp ted with a slightly different measurem ent of the biometric.

Another interesting concept is attribute-based encryption ([20]). In this schem e the users' keys and the cipher text are labeled with sets of descript ive attributes. So a particular key can decrypt a particul ar cipher text only if the attributes of the key match the attributes of the cipher text. This attributes take the for m of an access structure that specifies what type of text the key can decryp t. From the attribu te-based encryption point of view, identity -based encryption is only a particular case.

6.2 Military relevan ce. Iden tity-based cryptography is a new e merging technology

that prom ises to reduce costs and overhead time and to provide security in a more natural way (for the users). Benefits of IBC - high system usability, h ighly scalable architecture, low opera tional im pact, f ully statele ss operation- a re all ve ry im portant in m ilitary applications. Milita ry communications ca n also benefit from it, if used in proper scenarios, where its few i mportant disadvantages can be cancelled.

Here is an enum eration of other possible military a pplications of identity ba sed cryptosystems.

• Encryption applications using hybrid (symmetric-asymmetric) schem es but without the complex aspects of PKI.

• E-Signature schem es without huge problems of c ertificates generation, distribution, revocati on (no CRLs), validation ([4]).

• Possible mixing cryptography schem es and biometric attri butes, in so-called biocryptography ([19]).

• Large app lications in MANET's, where dynam ic coalition-form ing environments are very envisaged in future military networking; in this ca se, for example, two Trusted Authorities from different coalition forces m ay wish to (tem porarily or permanently) generate a common set of public parameters and a com mon m aster secret, and to issue new private keys to all entities under their joint command only for this context ([21]).

• Identity-based cryptography can be used to enable strong security with reduced bandwidth consum ption and latency, becaus e the security associations between nodes can be established without the need to exchange any other information ([22]).

• The advantages of identity-b ased cryptography can be combined with m ethods of assuring com patibility with current public key inf rastructures (like IB-m RSA Identity - Based-Mediated RSA). This way, one can assure interoperabil ity without decreasing security ([23]).

• If the initial identity -based cryptosystem is enrich ed with a hierarchical approach to KGC pr oblem, than the new cryptosystem will comply with the hierarchical characteristics of the m ilitary organization. A n

advantage is that in this way the key escrow is allowed at different levels ([21]).

• Several key agreem ent protocols based on identity-based cryptography had been developed and can be successfully used to secure communications.

• ID-based group signature schem es c an be relatively easy converted into Group Signature schemes.

• Zero knowledge proo f of identity : proving yo ur identity not with a piece of information you have (for exam ple by sending a password to a server), but with prove of your knowledge ([24]).

7. CONCLUSIONS

In this paper we have m ade a general introduction in identity based cryptography's problematic. W e have presented the key differences between it and clas sical PKI, highlighting its advantages and disadvantages. Based on these considera tions, we have given a non exhaustive list with possible applications of IBC.

Researching over thes e aspects, m ade possible to better u nderstand in which scenarios th e user cou ld really benefit from using an ide ntity bas ed cryptosys tem, and not a classical PKI scheme. So based on this survey we will con tinue ou r work by researching over the use of IBC schemes in the communication inside the Rom anian arm y, as a backup or even as an alternative to the PKI infrastructure proposed and im plemented so far.

REFERENCES

1. Adi Sham ir, *Identity-Based Cryptosystems and Signatures Schemes*, Advances in Cryptology: Proceeding s of CRYPTO'84, Lecture Notes in Com puter Science, 7:47-53, 1984.
2. Shane Balfe, Kent D. Boklan, Zev Klagsbrun, Kenneth G. Paterson, *Key Refreshing in Identity-Based Cryptography and its Applications in MANETS*, Proceedings of the Military

"HENRI COANDA"
AIR FORCE ACADEMY
ROMANIA

"GENERAL M.R. STEFANIK"
ARMED FORCES ACADEMY
SLOVAK REPUBLIC

INTERNATIONAL CONFERENCE of SCIENTIFIC PAPER
AFASES 2014
Brasov, 22-24 May 2014

Communications Conference MILCOM '07, 2007.

3. Leonardo B. Oliviera, Diego Aranha, Eduardo Morais, Felipe Daguano, Julio Lopez, Ricardo Dahab, *TinyTate: Identity-Based Encryption for Sensor Networks*, [online]. Available: http://eprint.iacr.org/2007/020.pdf (2007).

4. Sherm an S.M. Chow, *Certificateless Encryption*, Identity-Based Cryptography, IOS Press, pp. 207-225, 2009.

5. Antoine Joux, *Introduction to Identity-Based Cryptography*, Identity- Based Cryptography, IOS Press, 2009.

6. IEEE 13 63.3 Standard, [online]. Available: http://grouper.ieee.org/groups/1363/IBC/index.html (2006).

7. RFC 1824, [online]. Available: http://ietfreport.isoc.org/idref/rfc1824/ (1995).

8. RFC 5091, [online]. Available: http://www.rfc-editor.org/pipermail/rfc-dist/2007-December/001834.html (2007).

9. RFC 5408, [online]. Available: http://tools.ietf.org/html/rfc5408/ (2009).

10. RFC 5409, [online]. Available: http://www.ietf.org/rfc/rfc5409.txt (2009).

11. Ferris Research, *Report 586 – The total Cost of Ownership for Voltage Identity-Based Encryption Solution*, [online]. Available: http://www.ferris.com/2006/05/30/the-total-cost-of-ownership-for-voltage-identity-based-encryption-solutions/ (2006).

12. Dan Boneh, Matthew K. Franklin, *Identity-Based Encryption from the Weil Pairing*, Advances in Cryptology: Proceedings of CRYPTO '01, 2001.

13. Dan Boneh, Xavier Boyen, *Efficient Selective Identity-Based Encryption Without Random Oracles*, Advances in Cryptology (EUROCRYPT 2004), Lecture Notes in Com puter Science, vol. 3027, Springer, 2004.

14. David Galindo, Marina Gavrilova, Osvaldo Gervasi, Vipin Kum ar, Chih Jeng Tan, David Taniar, Antonio Lagana, Youngsong Mun, Hyunseung Choo, *A Separation Between Selective and Full-Identity Security Notions for Identity-Based Encryption*, Proceed ings of ICCSA International Conference on Computer Science an d its App lications, Lecture Notes for Com puter Science, vol. 3982, Springer, pp. 318-326, 2006.

15. Claire W helan, Dan Page, Frederik Vercauteren, Michae l Scott, W illiam Marnane, *Implementation Attacks and Countermeasures*, Identity-Based Cryptography, IOS Press, pp. 226-243, 2009.

16. Darrel Hankerson, Alfred Menezes, Michael Scott, *Software Implementation of Pairings*, Identity-Based Cryptography, IOS Press, pp. 188-206, 2009.

17. Maurice Keller, R obert Ronan, Andrew Byrne, Colin Murphy, W illiam Ma rnane, *Hardware Implementation of Pairings*, Identity-Based Crypt ography, IOS Press, pp. 207-225, 2009.

18. Pierre-Louis Cayrel, Philippe Gaborit, Marc Girault, *Identity-Based Identification and Signature Schemes using Error Correcting Codes*, Identity-Based Cryptography, IOS Press, pp. 207-225, 2009.

19. Am it Sahai, Brent Waters, *Fuzzy Identity-Based Encryption*, [online]. Availab le: http://eprint.iacr.org (2004).

20. Am it Sahai, Brent W aters, Steve Lu, *Attribute-Based Encryption*, Id entity-Based Cryptography, IOS Press, pp. 156-168, 2009.

21. Shushan Zhao, *Application of Identity-Based Cryptography in Mobile Ad Hoc Networks*, ACM   Transactions on Computational Logic, 2007.

22. D. W. Carm an, G. H. Cirincione, *Identity-Based Ramdom Key Predistribution for Army   MANETS*, [online]. Available: http://www.dtic.mil/dtic/ (2004).

23. Dan Boneh, Xuhua Ding, Gene Tsudik, *Identity-Based Mediated RSA*, Dow Jones & Company, Inc., 2002.

24. Jonathan Katz, Raf ail Ostrovsky, Michael O. Rabin, *Identity-Based Zero-Knowledge*, Security in Comm unication Networks, Lecture Notes for Computer Science, vol. 3352, Springer, pp. 180-192, 2002.

AN ASYMPTOTIC PROPERTY OF THE MERGING ALGORITHM

Paul VASILIU

Faculty of Marine Engineering, "Mircea cel Bătrân" Naval Academy, Constanta, Romania

Abstract: This paper focuses on the study of the asymptotic behavior of the medium number of comparisons from the merging algorithm on two sorted arrays, depending on the total length of the resulting array obtained by merging. This paper presents a program written in C++ that supports the theoretical result that was obtained.

1. INTRODUCTION

Let it be the following arrays sorted in ascending order $V = (v_1, v_2, \ldots, v_p)$ and $W = (w_1, w_2, \ldots, w_q)$. The result of the merging operation of two arrays sorted in ascending or descending order, V and W, is a new array, X, that contains all the elements from V and W sorted in ascending or descending order. The algorithm of merging two arrays is well known. The algorithm consists of iterating through the V and W arrays and comparing each current element v_i from V with the current element w_j from W. The minimum value between v_i and w_j is written to the resulting array, X. In the merging algorithm, one of the V or W arrays is iterated first and the elements of the other one are written to the X array.

Let it be the following merging function written in C++:

```cpp
void merge(int *v,int *w,int *x,int p,int q)
{
int i,j,k;
i=j=k=0;
while(i<p && j<q){
    if (v[i]<w[j]){
        x[k++]=v[i++];
        }
    else
        x[k++]=w[j++];
}
 while (i<p)
     x[k++]=v[i++];
 while (j<q)
     x[k++]=w[j++];
}
```

Let it be the sorted array in an ascending order $X = (x_1, x_2, \ldots, x_n)$ with $n = p + q$

elements, obtained by merging the V and W arrays. Let it be C, the medium number of comparisons, defined by the total number of comparison divided by the number of possible arrays V and W. The [1] and [2] papers present the limits of the medium required number of comparisons, C, depending on the lengths, p and q of the V and W arrays. In this paper we will prove that the medium number of comparison required for obtaining the X array sorted in ascending order can be approximated with $n-2$. It must be mentioned that this number does not depend on the lengths of V or W arrays.

The obtained result is validated with a program written in C++ language.

2. FINDING THE C NUMBER

The operation of merging the V and W arrays involves comparing the elements of these arrays and updating the X array. Also, for merging, one array will be iterated first. Obviously, the total number of comparisons required for building the X array is equal to $n-m$, where m is the number of remained elements from the array that was not iterated. The minimum number of comparisons equals to the minimum value between p and q in the following case: if all the elements of the array with the smallest number of elements, are smaller than all the elements from the array with more elements that the first one. If the elements with the greatest values from V and W will be the greatest elements from X array, then the number of comparisons is equal to $p+q-1$.

Without reducing the generality we will suppose that the V array will be iterated first. In the end, we will double the value of the number of comparisons by including the case when W will be iterated first.

It is clear that the greatest element from V will influence the value of C. Let it be the final array sorted in ascending order, with n elements $X = (x_1, x_2, \ldots, x_n)$, with $x_1 < x_2 < \cdots < x_n$. In order to compute C, we have to follow the next steps:

1. It is assumed that x_i is the greatest element from V and then there are i comparisons required;

2. Compute the number of possible arrays V for which x_i is the greatest element from V;

3. Repeat steps 1 and 2 for all the possible choices of x_i;

4. Compute the value of C.

If x_1 is the greatest element from V, than there is an array $V = (x_1)$, with no element that precede x_1, which means that only one comparison is needed, $(1 \cdot 2^{1-1})$.

If x_2 is the greatest element from V, than there are two possible array that contain this element: $V = (x_2)$ and $V = (x_1, x_2)$, where x_1 might be an element from V. For both these possible arrays, 2 comparisons are needed for each array, (x_2 with x_1 and x_2 with x_2 or with x_3), in total 4 comparisons, ($2 \cdot 2^{2-1}$).

If x_3 is the greatest element from V, then there are 2 possible values that can exists in V: x_1 and/or x_2. In this case there are 4 possible V arrays with x_3, being the greatest element, $V = (x_3)$, $V = (x_1, x_3)$ with $x_1 < x_3$, $V = (x_2, x_3)$ with $x_2 < x_3$, $V = (x_1, x_2, x_3)$ with $x_1 < x_2 < x_3$ or $x_2 < x_1 < x_3$. For each of the four arrays, 3 comparisons are needed, (x_3 wit x_1, x_3 with x_2 and x_3 with x_3 or with x_4), which makes a total of 12 comparisons, ($3 \cdot 2^{3-1}$).

In general, if x_i is the greatest element from V, there are $i-1$ possible elements that can precede it and that can be elements of V. The number of subsets with $i-1$ elements is equal to 2^{i-1}, so there are 2^{i-1} V arrays with x_i being the greatest element. The total number of comparisons equals to $i \cdot 2^{i-1}$.

Because we supposed that the V array will be first iterated, this implies that $i <= n-1$. Suppose by contradiction that $i = n$, W could be iterated first because the greatest element from X is now in V.

From the above considerations it follows that

"HENRI COANDA"
AIR FORCE ACADEMY
ROMANIA

"GENERAL M.R. STEFANIK"
ARMED FORCES ACADEMY
SLOVAK REPUBLIC

INTERNATIONAL CONFERENCE of SCIENTIFIC PAPER
AFASES 2014
Brasov, 22-24 May 2014

the total number of comparisons required for iterating first the V array, and then W is equal to:

$$\sum_{i=1}^{n-1} i \cdot 2^{i-1} \qquad (1)$$

The total number of possible V arrays is equal to:

$$\sum_{i=1}^{n-1} 2^{i-1} = 2^{n-1} - 1 \qquad (2)$$

By symmetry, supposing that W is iterated first, and after that V, it follows that the number of comparisons equals:

$$\sum_{i=1}^{n-1} i \cdot 2^{i-1} \qquad (3)$$

and the number of possible arrays W equals to:

$$\sum_{i=1}^{n-1} 2^{i-1} = 2^{n-1} - 1 \qquad (4)$$

This leads to a total number of comparisons equal to:

$$2 \cdot \sum_{i=1}^{n-1} i \cdot 2^{i-1} = \sum_{i=1}^{n-1} i \cdot 2^{i} \qquad (5)$$

and the total number of possible arrays V and W is equal to:

$$2 \cdot \left(2^{n-1} - 1\right) = 2^{n} - 2 \qquad (6)$$

From the equality:

$$1 + x + x^2 + \cdots + x^n = \frac{x^{n+1} - 1}{x - 1} \qquad (7)$$

which occurs for $x \neq 1$, through derivation, and then multiplication with x and substitution of x with 2 we have the following equality:

$$\sum_{i=1}^{n-1} i \cdot 2^{i} = (n-2) \cdot 2^{n} + 2 \qquad (8)$$

The medium number of comparisons becomes:

$$C = \frac{(n-2) \cdot 2^{n} + 2}{2^{n} - 2} \qquad (9)$$

By processing (9), we obtain:

$$C = n - 2 + \frac{2 \cdot n - 2}{2^{n} - 2} \qquad (10)$$

From the equality:

$$\lim_{n \to \infty} \frac{2 \cdot n - 2}{2^{n} - 2} = 0 \qquad (11)$$

results that for values of n big enough, C can be approximate with $n-2$.

The above chart of the function $y(x) = \frac{2 \cdot x - 2}{2^{x} - 2}$, $x \geq 0$, $x \neq 1$ and

$y(1) = \frac{1}{\ln 2}$ proves that the approximation is very good for values of $n \geq 10$.
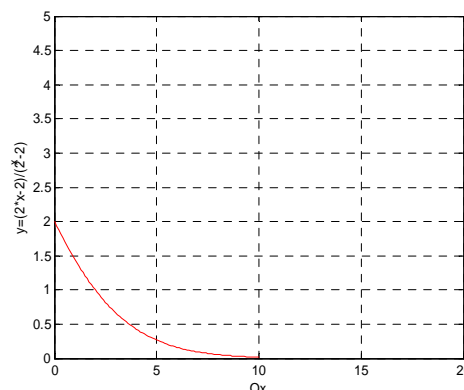

Figure 1. The optimal value of n

2.1. A VERIFICATION OF THE THEORETICAL RESULT

This theoretical result can be experimentally checked with the following C++ program :

```
#include <stdio.h>
#include <conio.h>
#include <malloc.h>
#include <math.h>
#include <stdlib.h>
int * aloc(int n)
{
```

```c
 int *p;
 p=(int *)malloc(n*sizeof(int));
 return p;
}
void sort_ascending(int *v,int n)
{
int i,j,temp;
for(i=0;i<n;i++)
for(j=i+1;j<n;j++){
if(v[i]>v[j]){
   temp=v[i];
   v[i]=v[j];
   v[j]=temp;
}}}
void gen(int *v,int n)
{
int i;
for(i=0;i<n;i++)
v[i]=rand();
}
int interclas(int *v,int *w,int *x,int p,int q)
{
int i,j,k,ncomp;
ncomp=i=j=k=0;
while(i<p && j<q){
ncomp++;
if (v[i]<w[j])
x[k++]=v[i++];
else
x[k++]=w[j++];
}
while (i<p)
x[k++]=v[i++];
while (j<q)
x[k++]=w[j++];
return ncomp;
}
int main()
{
int p,q,*V,*W,*X,nc;
printf(" Size of V = ");
scanf("%d",&p);
printf(" Size of  W = ");
scanf("%d",&q);
V=aloc(p);
W=aloc(q);
X=aloc(p+q);
gen(V,p);
gen(W,q);
sort_ascending(V,p);
sort_ascending(W,q);
nc=interclas(V,W,X,p,q);
printf(" C = %d\n",nc);
getch();}
```

The input of the program are: size p and q of the arrays $V = (v_1, v_2, \ldots, v_p)$ and $W = (w_1, w_2, \ldots, w_q)$ respectively. The program random generate the arrays, ascending sort the arrays, merge the arrays and generate $X = (x_1, x_2, \ldots, x_n)$ array with $n = p + q$ components. Are counted comparisons.

An example is:
Size of V = 78
Size of W = 67
C = 143

In the above example $p = 78$, $q = 67$, $n = p + q = 78 + 67 = 145$. The medium number of comparisons is equal with: $n - 2 = 145 - 2 = 143$.

3. CONCLUSIONS

In papers [1, 2] is determined the medium number of comparisons needed for merging the arrays $V = (v_1, v_2, \ldots, v_p)$ and $W = (w_1, w_2, \ldots, w_q)$. This number depends on the lengths, p and q, of these two arrays. In the presented paper we proved that the medium number of comparisons can be computed depending on the sum of the length of these two arrays $n = p + q$. Moreover, we showed that for $n \geq 10$, the medium number of comparisons can be approximated with $n - 2$.

REFERENCES

1. Dijkstra, E. W., *Some beautiful arguments using mathematical induction.* Acta Informatica 13(1982).
2. Knuth, D. E. *The Art of Computer Programming, Volume 3: Sorting and Searching.* Addison Wesley (1973).

"HENRI COANDA"
AIR FORCE ACADEMY
ROMANIA

"GENERAL M.R. STEFANIK"
ARMED FORCES ACADEMY
SLOVAK REPUBLIC

INTERNATIONAL CONFERENCE of SCIENTIFIC PAPER
AFASES 2014
Brasov, 22-24 May 2014

SOCIAL ROBOT IN ATTENTIONAL THERAPIES

Paulina VÉLEZ*, Antonio FERREIRO**

*Faculty of Computer and Electronics, Politecnic University of Chimborazo, Riobamba, Ecuador,
** Faculty of Health Sciences, National University of Chimborazo, Riobamba, Ecuador

Abstract: This paper describes how social robots can be used in philological therapies to improve the attentional capacities of children. A social robot is a powerful tool especially if the users are children. A social robot can be a playful tool, as a toy, but can direct some activities and gain the child interest in it.

1. INTRODUCTION

A social robot is able to interact with humans and also is able to help hum ans to do some task. In this respect there are many social robots that have been developed to help children to increase their social capacities.

Using a social robot is possible to help in a physiological way childr en, especially to stimulate their attentions in school years. It is possible to use a social robot as part of psychological therapies as a complem entary tool. In order to reach the goal of th is research is necessary define Attention Deficit and Hyperactivity Disorder (ADHD). ADHD consist in persis tent p atterns of inatten tion and/or hyperactivity and im pulsivity, which are sev ere and common in children in schoo l years in it age and level of development [1].

There are different test th at h elp to measure the attention capacity, so it is possible to establish the necessary parameters and characteristics that th e social rob ot need to have in order to deve lop the robot social abilities that can help the child.

2. ROBOT AS A FRIEND?

In our days the robots are common, there are presents I alm ost ever y industry and also in almost every daily ac tivities. Robots were tools to do som e task that were ha rd f or the men to do it, to reduce the tim e in productions processes and to do some works in dangerous environment. But, in the last years robots has been introduce not only as a tool to do hard jobs, bu t a lso as a too l to interac t, c ollaborate and assist hum ans been. The m ain idea was and is in this days is create a robot able to communicate and interact with people unti l specific task has been accomplish.

A robot that is able to interact with hum ans been is define as a "S ocial Robot". To talk about social robot is necessary to include som e concepts such as: em bodiment, social environment, and the capacity to reach it social goals [2]. A robot can be social depending on

aspects such as: it physical body, level of intelligence and behavior.

To interact with peopl e, a robot needs to have a social intelligen t, and also it body need to have a body design according with the goal of the inter action (bod y conception)[3]. To have a robot with body is im portant, but m ost important is tha t it bod y have some specific characteristic that can h elp the users to build a mental m odel that help them recognize th e robot as a partner in the interaction process.

A social robot needs to have an anthropomorphic body, which means to have a body with hum an characteris tics as head with face, arms, or hands. This body is necessary to have sensors so it can feel the environm ent, and will enable the robot interaction [4].

Talk about a social robot is talk about a robot that is able to in teract with people in a common environm ent that could be deterministic or non-determ inistic. In social robot area is possible to talk about assistive robots and collaborative robots. A n assistive robot help people to do som e task, assist people in their activities, in other aspect, a collaborative robots can participate with human doing some task together.

If the robot is able to assist people to do some task and also is able to interac t with people at the sam e ti me, is possible to define two kinds of classification, Socially Interactive Robot and Socially A ssitive Robots [5, 17]. These kinds of robot us e the interaction and also provide assistance by combine its skills.

2.1 Embodiment and Antropomorphi ze. To create a social robot is necessary creating a physical body with speci fic characteristics. This process, give a body to the robot is called Embodiment [6]. The embodiment of the robot implies to give to the robot physical similarities with hum an, this m eans that the robot bod y will h ave som e hum an's characteristics and f unctionalities; thi s process is called Anthropomorphize [7].

When the embodiment is given to the robot is necessary m easure the em pathy level of th e robot with the user. Mori in his Uncanny Valley theory has def ine a curve, in this cu rve is possible to see that the em pathy will decrease un til the sim ilarity with the hum an been is been reaching [8].

2.2 Robot as a Friend? Is it possible that a robot be a "friend" w ith a hum an been? As a machine that has b een given a social intelligent and a friendly body, is possible to use it as a toy. A child has the enough imagination to play wh it it toys and convert them in his friend, esta blishing a relationship with his toy s. This give as the idea that f or the children is possible to estab lish a f riendship and confidence with a social robot. This is an advantage that can be useful in rder to use a robot in attentional ther apies with children in school age.

There are som e factors that h as to b e consider, in order to reach a good orientated anthropomorphize and they are the elicited agent knowledge, the effectance motivation and the socially motivation [9].

3. ATTENTION DEFICIT AND HYPERACTIVITY DISORDER (ADHD)

Attention is an im portant process when children are in school age, because it can help them to retain and acquisition of essential knowledge and to process the infor mation. Also is im portant in order to develop their personality and socialization.

Attention Def icit an d Hyperactiv ity Disorder (ADHD) consist on persistent pattern of inattention and/or hyperactivity and impulsivity, which are m ore severe than expected in children in school years [1].

The causes are unknown, "m any children with ADHD show no evidence o f structural damage to the central nervous system . Contrastingly, children with known neurological disorders caused by brain injury do not have attention deficit disorder and hyperactivity "[1, 15]

Children with attentional deficit are expose to stressful events and h as problems with their families [15].

4. ROBOTS IN ATTENTIONAL THERAPIES

A social rob ot can be us ed as a tool that is able to reach the child interest as a toy. This characteristic can be useful in order to use the robot as a tool assist in the attentional therapies with children in schoo l a ge, which

“HENRI COANDA”
AIR FORCE ACADEMY
ROMANIA

“GENERAL M.R. STEFANIK”
ARMED FORCES ACADEMY
SLOVAK REPUBLIC

INTERNATIONAL CONFERENCE of SCIENTIFIC PAPER
AFASES 2014
Brasov, 22-24 May 2014

means between 7 and 12 years old. The process of increase the volum e of care and attention span becom es voluntary in school age [10].

"Attentional problem s are persistent and occur frequ ently associ ated with o ther early problems" and its triggers as aggressive, shy and cognitive deficits that require t be attended by special education [11].

A social ro bot can b e used in attentional therapy by developm ent of a physiological model and the evaluation of the com plex interaction mode 1 [12]. This to things can create a robot as a powerful tool in to be use in the therapy.

The goal if the social ro bot is to accelerate the result of the child therapy, been used as a complementary tool, a nd to work with th e psychology. To reach the goal, a social assistive rob ot will be u sed, com bining at the same ti me the characteristics o f a social interface, define by Breatzel [16].

4.1 The Robot. The social robot needs to have som e specific characteristic to reach th e interaction whit the child. This is c alled peer-to-peer interaction skills, and the ch aracteristic are: [13, 15].
- Express and/or perceive emotions.
- Communicate with high level dialogue.
- Learn/recognize models of the agents.
- Establish / maintain social relationships.
- Use natural cues (gaze, gestures).
- Exhibit distinctive personality and character.
- May learn / develop social competencies.

A social robot, also needs to have verbal and nonverbal behaviors, this m eans that the robot should be able to express it "em otions" with it body language, f acial gestures, dialogs and sounds [14].

To define the robot "personality" is possible to create a co mputational m odel that describes how the robot will ans wer to the environmental s timuli. This m odel will establish tim e answer, leve ls of task accomplish and times in collaborative task [9].

4.3 Robot in the therapy. The social robot will work together with the psy chology. It is possible to do the therapy in groups and also have an individual ther apy. The activities will be f ocus in reinf orce the child a ttitude by dialogs that encourag e the ch ild when he/sh e do some task in the correct way [15].

5. CONCLUSIONS

A social ro bot with an orien tated skills and behaviors can be us eful in atten tional therapies with children in school age. The child im agination allows establishing a friendship between the robot, and the child and this help in the therapy because the confidence is gained and makes easier the interactions and the reach of the task.

The robot will assist the psychology work, and will g uide the ta sk of the child with friendly dialogs, facial and body gestures.

This research is the beginning of the project that has the co llaboration of a prim ary school, where the attentional capacities of the children will be te st an d them an atten tional therapies w ill b e acc omplish in order to measure the level of improve in each child.

REFERENCES

1. Sadoc, B., Sadoc, V., Kaplan and Sadock´s Synopsis of Psychiatry. *Behavioral Science/Clinical Psychiatry.* Phyladelphia (2003).
2. Duffy, B., Rooney, C., O´Hare, G., O´Donoghue, R. What is a Social Robot?

Source. [online]. Available:
http://www.csi.ucd.ie/prism/publications/pub1999/AICS99Duf.pdf (March, 2014).

3. Dautenhahn, K., Getting to Know each other Artif icial soc ial intelligenc e f or autonomous robots. *Robotics and Autonomous systems.* Issue (1995).

4. Ishiguro, H., Kanda, T., Hirano,T., Eaton, D., Interactive Robots as Social Partners an Peer Tutos for Children: A field Tria. *Human-Computer Interaction.* Issu e (2004).

5. Feil-Seifer, D., Matari´c, M., Defining Socially As sistive Robo tics. *Procedings of the IEEE, 9ᵗʰ International Conference on Rehabilitation Robotics.* Issue (2005).

6. Bartneck, Ch., Forlizzi, J. A Design-Centred Fram ework for Social Hum an-Robot Interaction. *Proceedings of the Ro-Man2004.* Issue (2004).

7. Duffy, B. Anthropom orphism and the social robot. *Robotics and Autonomous Systems 42.* Issue (2003).

8. Mori, M. T he Uncanny Valley. *Energy.* Issue (1970).

9. Epley, N., Waytz, A., Cacioppo, J. On Seeing Human: A Three-Factor Theory of Anthropomorphism. *Psychological Review.* Issue (2007).

10. Luria, A. Atención y memoria. Barcelona: Kairos (1984).

11. De la Barra, F., Toledo, V., Rodríguez, J. Estudio de salud mental en dos cohortes de niños escolares de Santiago Occidente. III: predictores tempranos de problemas conductuales y cognitivos. *Revista Chilena de Neuropsiquiatría.* Issue (2003).

12. Scassellati, B. Imitation and Mechanism of Joint Attention: A Developmental Structure for Building Social Skills on a Humanoid Robot. Source. [online]. Available: http://groups.csail.mit.edu/lbr/humanoid-robotics-group/cog/cog-publications/springer-final-scaz.pdf (March, 2014).

13. Fong, T., Nourbakhsh, I., Dautenhan, K. A Survey of socially interactive robots. *Robotics and Autonomous Systems 42.* Issue (2003).

14. Yan, R., Peng Tee, K., Chua, Y, Huang, Z., Li, H. An Attention-Directed Robot for Social Telepresence. *The 1ˢᵗ International Conference on Human-Agent Interaction.* Issue (2013).

15. Velez, P. Ferreiro, A. Social Robotic in Therapies to Improve Children's Attentional Capacities. *Review of the Air Force Accademy,* Vol. XII, No. 2(26)/2014, pp. 101-108, http://www.afahc.ro/revista/Nr_2_2014/101_VÉLEZ_FERREIRO.pdf.

16. Breazeal, C., Toward sociable robots. *Robotics and Autonomous Systems.* Issue (2003).